Design, Simulation and Control of a Flexible LNG Reception Terminal

by

SANDRA MARY PIRIE

Thesis submitted to the
UNIVERSITY OF STRATHCLYDE
for the degree of
DOCTOR OF PHILOSOPHY

Industrial Control Unit
Department of Electronic and Electrical Engineering
University of Strathclyde

March 1992

To Peter

ACKNOWLEDGEMENTS

There are several people to whom I am vastly indebted for their assistance and contribution to my research work and the preparation of this thesis. Firstly, I would like to thank my supervisors, Dr. M.A. Johnson and Prof. C.D. Grant for their guidance, support and expertise.

I would like to thank the London Research Station of British Gas plc for initiating and supporting the research project upon which this thesis is based. Particular thanks to Dr. R. Bird and Mr. S.C. Chauhan of British Gas plc for their assistance.

Also, I would like to thank Dr. B.E. Postlethwaite and Prof. M.J. Grimble of the University of Strathclyde for providing technical support in their specialist fields, and Prof. M.J. Grimble again for the use of departmental facilities in the Industrial Control Unit.

Finally, I would like to thank my present employer, BP Chemicals plc, and all of my former colleagues at the Industrial Control Unit for their support and encouragement.

ABSTRACT

This research is a preliminary design study relating to the importation of liquefied natural gas (LNG) in the United Kingdom, focusing on the process design, simulation and control of a flexible LNG reception terminal.

The primary operating objective of the proposed LNG reception terminal is to accept a wide variety of LNG feedstocks, and to continuously produce output with consistent specifications. This requirement to provide "feedstock flexibility" was the major influence in the development of this research. The process design was derived from the application of selection criteria to assess the impact of feedstock flexibility on process unit performance. The subsequent dynamic simulation had to represent multiple operating conditions and feedstock changeovers for a multicomponent system. This required the incorporation of an interactive physical properties database and the adoption of a pseudo-binary distillation column model in the simulation. Regulatory control loops were developed and tuned to provide stable operation for all the plant's operating conditions. In order to assess the impact of multiple feedstock conditions, control system performance was evaluated for disturbance rejection and control valve action. A changeover mechanism was developed which enabled successful dynamic simulation of feedstock changeovers. The simulation also identified significant interactions between certain process units in the flowsheet. In conclusion, the primary objective of the supervisory control system would be management of these interactions as opposed to maintenance of product specifications.

This work has provided a preliminary flowsheet and a design tool for process and control studies, for a flexible LNG reception terminal. These will enable the design engineer to investigate a range of changes to the process design and to assess their implications for the plant's overall dynamic behaviour.

PREFACE

For many processes, there is an incentive to develop a flexible process plant that is able to safely and economically accept a variety of feedstocks, whilst maintaining output product specifications.

Given the recent advances in computer technology and process control theory, can the advantages of a flexible plant be realised? Conventional process design practice in relation to plant flexibility is to identify the main feedstock, design an appropriate flowsheet to handle that feedstock and then apply regulatory control to process units. Variations from the main feedstock would usually be accommodated by selective analysis of problem areas, identified perhaps by steady state simulation, thus giving the plant some degree of feedstock flexibility. This research investigates the hypothesis that true feedstock flexibility can be achieved if each phase of the design process addresses flexibility as a primary objective.

With feedstock flexibility as a primary objective, each design phase could become more complex. However, it should be manageable using the latest computer-based design tools and advanced control theory. Steady state simulation models would be required to simulate various process designs for a variety of feedstocks in order to arrive at a flowsheet which incorporates the requisite flexibility. The best flowsheet would have to be selected on the basis of a number of criteria in addition to traditional design parameters, for example the turndown experienced in key units. Then, a dynamic simulation would need to be developed to assess the dynamic behaviour of the plant during feedstock changeover and at multiple operating conditions. This simulation could be employed as a design tool for control studies. Finally, the impact of feedstock changeovers could be assessed by incorporating the regulatory control loops into the dynamic simulation thereby indicating whether supervisory control would be required.

For British Gas plc, the UK's primary gas utility, the requirement for feedstock flexibility is potentially an important factor in petrochemical process design. Natural gas supplies in the UK are already supplemented from abroad by pipeline and to a lesser extent by LNG imports. This trend is expected to rise with the forecast increases in natural gas demand and diminishing North Sea gas reserves, and as the global market in energy supplies becomes more active. Feedstock flexibility would allow any gas utility to react to changing market conditions quickly with minimal plant redundancy.

In process design terms, this implies that the full operational envelopes of individual plant units has to be utilised with minimal impact on plant turndown. Furthermore, a major factor is the investigation and control of process unit dynamic behaviour on a plantwide basis.

This opportunity to examine process design, modelling and control implications for both individual process units and plant supervisory control, lead to British Gas plc funding a broad study of these issues. The research project would result in a preliminary flowsheet for an LNG reception terminal incorporating feedstock flexibility. This preliminary design could then be developed by British Gas plc into a detailed plant design. Obviously, commercial constraints had to be applied to the study and this has resulted in an appropriate resource and time allocation to the various phases of the work. The three and a half year project was divided into three consecutive work packages for one person of approximately equal durations. These areas were process design, dynamic simulation, and control studies and plantwide control combined.

The resultant novel aspects of the work are as follows:

Process Design:

(i) Use of selection criteria to assess feedstock flexibility.

Dynamic Simulation:

(ii) Development of a pseudo-binary distillation column model to describe a multicomponent system.

(iii) Inclusion of an interactive physical property database.

(iv) Identification of significant interaction between individual process units, during feedstock changeover.

Control Studies:

(v) Single-input single-output control loop analysis of set point performance for overshoot and rise time.

(vi) Extending the use of regulatory control loop tuning to include control signal response and disturbance rejection measures.

Plantwide Control:

(vii) Developing a changeover mechanism for smooth transition between LNG feedstocks.

Publications

The following documents have been generated as a direct result of the research reported in this thesis:

Conference Papers

S.M.Pirie (1991)
Application of WPC in the Process Industry, I.Chem.E. Process Control Subject Group, Leeds, February 21.

S.M.Pirie, Grant C.D., Johnson M.A., Postlethwaite B.E. and Grimble M.J. (1991)
Simulation and Control of a Hydrocarbon Processing Plant, ESPRIT CIM-Europe Workshop, Athens, Greece, March 14-19.

Industrial Reports

Pirie S.M. (1988)
Literature Survey - LNG Process Review. Report ICU/190/June for British Gas plc; Industrial Control Unit, University of Strathclyde.

Pirie S.M. and Chauhan S.C. (1988)
Baseload LNG Terminal Flowsheet Development. Report ICU/227/October for British Gas plc; Industrial Control Unit, University of Strathclyde.

Pirie S.M. (1989)
Process Unit Dynamic Models. Report ICU/246/March for British Gas plc; Industrial Control Unit, University of Strathclyde.

Pirie S.M. (1990)
Dynamic Simulation of LNG Reception Terminal Flowsheet. Report ICU/277/March for British Gas plc; Industrial Control Unit, University of Strathclyde.

Pirie S.M. (1990)
LNG Reception Terminal Simulation Studies. Report ICU/292/June for British Gas plc; Industrial Control Unit, University of Strathclyde.

Pirie S.M. (1990)
Control of a LNG Reception Terminal: Part 1 - Single and Multiloop Classical Control. Report ICU/310/November for British Gas plc; Industrial Control Unit, University of Strathclyde.

Pirie S.M. (1991)
Control of a LNG Reception Terminal: Part 2 - Advanced and Supervisory Control. Report ICU/322/March for British Gas plc; Industrial Control Unit, University of Strathclyde.

Pirie S.M. (1991)
LNG Reception Terminal Simulation: User Manual. Report ICU/311/March for British Gas plc; Industrial Control Unit, University of Strathclyde.

ABBREVIATIONS

ACSL	:	Advanced Continuous Simulation Language
BLT	:	biggest log-modulus tuning
CARIMA	:	controlled auto-regressive and integrated moving average
CRG	:	catalytic rich gas
C.V.	:	calorific value
GL1K, GL1Z, GL2Z	:	LNG feedstock references
GPC	:	Generalized Predictive Control
HP	:	high pressure
LNG	:	liquefied natural gas
LP	:	low pressure
LRPC	:	long-range predictive control
MIC	:	Morari Index of Integral Controllability
MIMO	:	multiple-input, multiple-output
MRI	:	Morari Resiliency Index
NG	:	natural gas
N.I.	:	Niederlinski Index
ODE	:	ordinary differential equation
ORV	:	open rack vaporiser
PDE	:	partial differential equation
P	:	proportional
PI	:	proportional-integral
PID	:	proportional-integral-derivative
PP	:	physical properties
PPD	:	physical properties database
RGA	:	realtive gain array
RKS	:	Redlich-Kwong-Soave
SISO	:	single-input, single-output
VLE	:	vapour-liquid equilibrium
WPC	:	Weighted Predictive Control

NOMENCLATURE

A	(m^2)	cross sectional area/heat transfer area
a	(m^2/m)	heat transfer area per unit length
B	(kgmol/hr)	distillation column boilup
c_p	(J/kgK)	specific heat capacity
C	(-)	constant
C_v	(%)	control valve position
d	(m)	diameter
D	(kgmol/hr)	distillate flow rate
D(s)	(-)	disturbance signal
E(s)	(-)	controller actuating error
f	(-)	degrees of freedom
F	(kgmol/hr)	molar flow rate
F	(-)	detuning factor
g	(m/s^2)	gravity
h	(kJ/kgmol)	enthalpy
h	(W/m^2K)	heat transfer coefficient
h	(m)	height
J	(-)	cost function
K_c	(-)	proportional gain
K_p	(-)	process gain
K_p	(-)	equilibrium constant
L	(kgmol/hr)	liquid phase molar flow rate/distillation reflux
L	(m)	length
L_{cm}	(dB)	closed-loop log modulus
mw	(kg/kgmol)	molecular weight
M	(kgmol)	liquid molar hold up
n	(-)	number of components/number of tubes
N	(-)	number of trays in distillation column
N_0, N_1		WPC prediction horizon
N_2		WPC control horizon
p	(bar)	pressure
P	(W)	power
q^{-1}	(-)	backward shift operator
Q	(W)	rate of heat transfer

R	(kJ/kgmolK)	Universal gas constant
R(s)	(-)	set point signal
t	(hr)(s)	time
T	(^{o}C)(K)	temperature
$T(q^{-1})$		disturbance parameter
T_r	(hr)	rise time
T_s	(hr)	sampling period
$\Delta T_{\ell m}$	(^{o}C)	logarithmic mean temperature difference
U	(W/m^2K)	overall heat transfer coefficient
U(s)	(-)	control signal
V	(kgmol/hr)	vapour molar flow rate/distillation column boilup
V	(m^3)	volume
W(s)	(-)	set point signal
W	(kg/hr)	mass flow rate
x	(-)	component concentration in liquid phase
y	(-)	component concentration in vapour phase
ψ	(kgmol/hr)	component molar flow rate in vapour phase
Y(s)	(-)	process output
Δz	(m)	spatial increment
Z	(-)	compressibility factor
α	(-)	relative volatility
α	(kgmol/hr)	CO conversion in water-gas shift reaction
β	(kgmol/hr)	CO conversion in methanation reaction
$\varepsilon(s)$	(-)	sensitivity function
γ	(-)	condition number
η	(%)	efficiency
η	(-)	complementary sensitivity function
λ	(-)	eigenvalue
λ	(-)	WPC control weighting function
λ_{ij}	(-)	relative gain element
Λ	(-)	relative gain array
ρ	(kg/m^3)	density
σ	(-)	singular value of a system
τ	(hr)	time constant
τ_I	(hr)	integral time constant
ω_{co}	(rad/hr)	cross-over frequency
ω_n	(rad/hr)	natural frequency
ζ	(-)	damping ratio

Subscripts

a	ethane
b	heavy hydrocarbon
B	base
D	distillate
f	feed stream/final value
i	component index/tray index/inlet stream/inner stream
i	intermediate value/previous time step
I	impurity
L	liquid phase
o	outlet stream/outer stream
p	product stream
rct	reactor
s	steam
ss	steady state
std	standard conditions
t	tube
v	valve
V	vapour phase
w	weir
W	water
ZN	Ziegler-Nichols
1	primary loop in cascade controller
2	secondary loop in cascade controller

CONTENTS

CHAPTER 1

INTRODUCTION

1.1 BACKGROUND

The UK natural gas industry is fundamentally changing as indigenous natural gas reserves diminish, demand increases, and the market place is deregulated. In order to address these changes, British Gas plc, the primary gas supply utility in the UK, is now actively investigating alternative sources of natural gas supply. A key alternative will be the large scale importation of LNG from a variety of exporting countries.

This thesis has the objective of establishing the process and control design fundamentals for a modern, energy efficient, flexible feedstock LNG reception terminal. However, by means of introduction, this chapter will briefly discuss the natural gas industry and describe the general principles of LNG importation.

The global supply/demand position of natural gas and the trends in relation to the UK are given in Section 1.2. A review of the complete LNG importation process, and specific operational requirements for the proposed reception terminal are described in Section 1.3. The particular design considerations for a flexible LNG reception terminal are defined in Section 1.4. Finally, Section 1.5 defines the objectives for this thesis, and Section 1.6 describes the thesis layout.

1.2 SUPPLY AND DEMAND OF NATURAL GAS

Although natural gas constitutes 25% of world energy hydrocarbon consumption, it accounts for under 10% of international oil and gas trade (BPCP, 1991). USSR and the USA are the main gas producing countries. Gas is exported either by pipeline or by tanker, in the form of LNG. As many large consumer countries have access to trans-border gas pipelines, pipeline exports are far greater than LNG shipments. In 1990, pipeline exports reached 233.5 billion cubic metres, compared with 72.3 billion cubic metres for LNG. Only Algeria exports both forms of natural gas.

LNG trade projects require large scale investment by both parties, a significant gas reserve in the exporting country and a substantial market in the importing region (Jensen, 1985). However, forecasts indicate that the trend in LNG trade is upwards. At present, Indonesia is the largest exporter of LNG, with its 38% share in the market in 1990 (BPCP, 1991) steadily increasing as new contracts are secured. Several new LNG trade negotiations are currently underway, involving such countries as Indonesia, Algeria and Norway. Australia began LNG exportation to Japan in 1989, and has a 5% share in Japanese imports with new expansion projects currently underway. As many countries export LNG, chiefly from the Asia-Pacific region, there is a wide range of possible imported LNG compositions available, which may also vary from a single supplier. This can pose problems for the importer, particularly if the reception terminal is limited in feedstock range.

Gas importation is the main source of natural gas in Spain, Japan, South Korea and Taiwan. Japan is by far the biggest importer of LNG, and receives over 66% of the world's LNG exports. This is primarily because there are no major gas reserves in East Asia. Japan imports from seven of the eight LNG exporting countries. France is the next largest importer, with just over 12%.

LNG liquefaction and storage facilities have been in operation since 1953. The first LNG liquefaction plant was brought on stream in Algeria in 1964. This coincided with the first commercial LNG

importation scheme at Canvey Island in the UK. The experience indicated that transportation of LNG by tanker was a practical and economic proposition (Hearfield, 1984).

1.2.1 Supply and Demand Trends in the UK

The UK gas supply base has moved from 93% coal and 7% oil in the 1950's, through 63% natural gas in the 1970's, to the present day where the North Sea fields constitute the major source of natural gas. In the past decade, natural gas production has increased by over 27%. In terms of 1990 production levels, the remaining gas reserves should last approximately 12 years, assuming production remains at its current level (BPCP, 1991). However, natural gas consumption is gradually increasing its share in the UK fuel market, rising to 62% in the domestic market and 33% in the industrial sector, in 1989. Natural gas is also becoming the preferred fuel in electricity generation, due to its environmental attractiveness and recent advances in combustion technology.

In 1990, the UK imported 7.5 million cubic metres of natural gas by pipeline from Norway and 0.1 million cubic metres of LNG from Algeria. It is anticipated that the UK will begin to import significant volumes of LNG to supplement other natural gas forms, and that this LNG will have a range of compositions.

1.3 THE LNG IMPORTATION PROCESS

The main advantage in liquefying natural gas is its 600:1 volume reduction achieved in the liquid state, at a temperature of -162°C and atmospheric pressure. The batch transportation and storage of LNG is feasible in this condition. The main processes in the LNG cycle are briefly discussed below; *liquefaction*, *transportation*, *storage* and *vaporisation*.

The natural gas *liquefaction* plant converts gas received from pipeline or distribution mains into liquid form, and consists of:

(i) A feed preparation or treatment section, for the removal of components which may solidify when the gas is liquefied.

(ii) A liquefaction section, which removes latent heat to condense the gas.

LNG tankers *transport* the LNG from liquefaction to reception terminals. They range in size from about 5,000 to 130,000 cubic metres - a recent comparison of natural gas transportation costs (Leibson et al., 1987) favoured larger capacity ships as they become more efficient as trading distance increases. At the reception terminal, the LNG is unloaded for *storage* in either above- or under-ground tanks, at -162°C and atmospheric pressure.

The LNG reception terminal forms the final stage in the LNG cycle, and is mainly concerned with *vaporisation*, and odorising the distribution gas. The key processes of the cycle are illustrated in Figure 1.1. Three basic types of reception terminal are described below, whose function depends on whether the combustion characteristics of the LNG match the product specifications. Calorific Value (C.V.) is the most important product specification.

1.3.1 Conventional LNG Reception Terminal

Many LNG exporters produce feedstocks which are within the permitted C.V. range defined by the distribution network in the customer country. Hence, no further processing is required and a conventional reception terminal can be employed. Figure 1.1 shows a simplistic conventional plant arrangement, without gas quality adjustment.

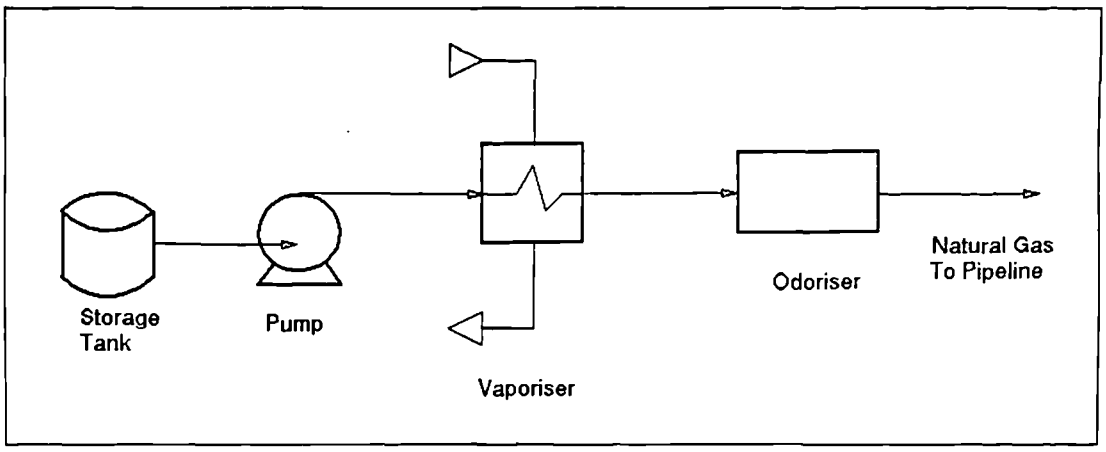

Figure 1.1 Block diagram of standard LNG reception terminal

Cove Point reception terminal in the USA is a typical example of a reception terminal with no gas quality adjustment (Van Meerbeke, 1987). This basic form of reception terminal can handle only a limited range of LNG compositions, and hence is unable to regulate C.V.. The Montoir de Bretagne terminal in France receives two types of LNG feedstock which are mixed in the storage tanks prior to vaporisation. This mixing yields a steady distribution gas which meets product specifications (Lechat and Caudron, 1986).

1.3.2 **Rich-feedstock LNG Reception Terminal**

If the LNG feedstock has too high a C.V., the LNG requires processing before distribution. Three contrasting rich-feedstock reception terminals operating in Europe are discussed below.

At Barcelona in Spain, a reception terminal separates the LNG by distillation and removes the by-products to lower the C.V. to its desired level (Keen, 1983). This process is illustrated in Figure 1.2. By contrast, La Spezia in Italy separates and processes the heavy LNG fraction, before reblending. As none of the feed is removed during the process, as illustrated in Figure 1.3, the heavy hydrocarbons are converted to produce lower C.V. components. Gasunie, in the Netherlands, imports LNG which is richer than gas from their domestic gas supply. Thus, Gasunie dilute the LNG feed with locally produced coal gas to attain product specifications (Wolfs and Hoornstra, 1982). Of these terminals, La Spezia offers the least flexibility, as it has only one feedstock and one product.

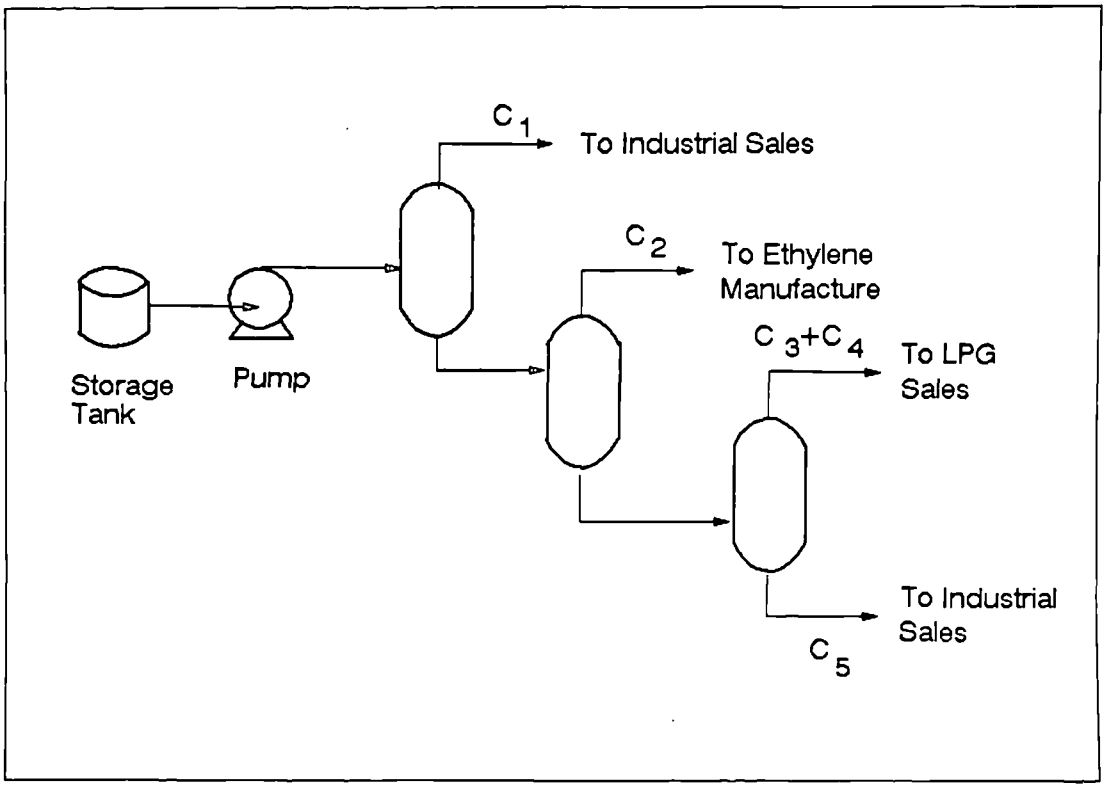

Figure 1.2 Barcelona reception terminal flowsheet

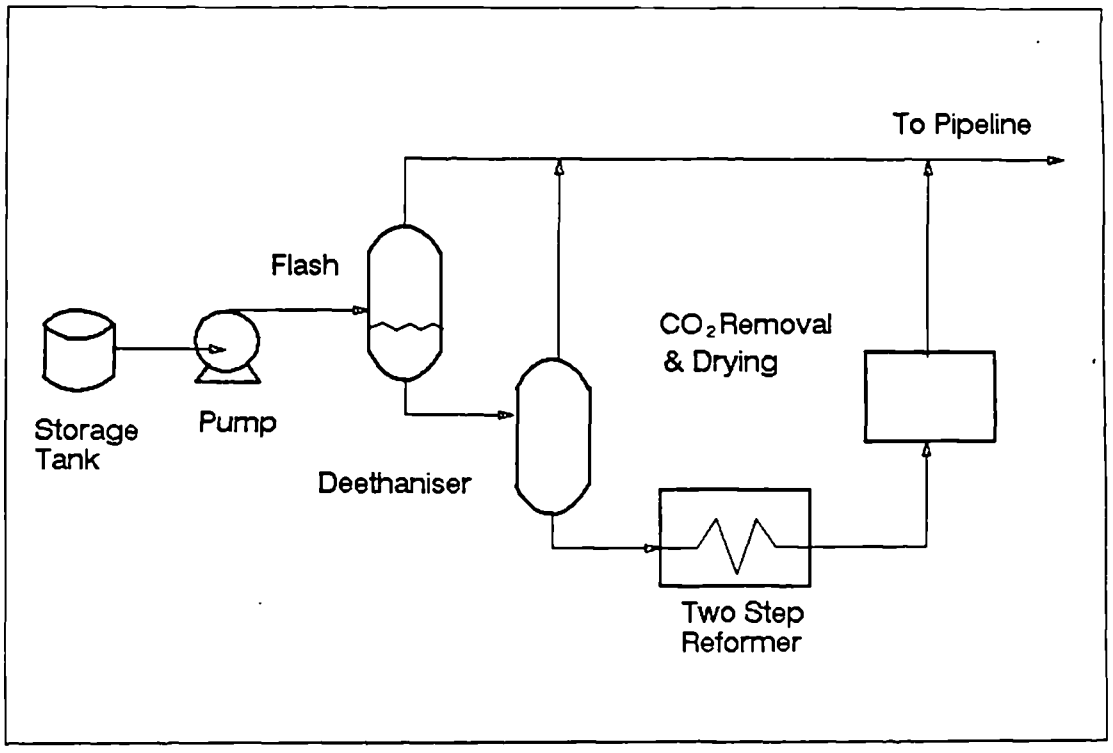

Figure 1.3 La Spezia reception terminal flowsheet

1.3.3 LNG Enrichment Reception Terminal

Much of the LNG exported to Japan requires enrichment before distribution, as the C.V. is too low. Three different LNG compositions are handled at the Sodegaura Works reception terminal. The product specifications for its numerous customers are satisfied by injecting liquefied petroleum gas (LPG), butane or propane (all of higher C.V.), to the LNG after regasification (Johnson, 1984). Hence, this process can accept a wide variation in LNG composition, provided the C.V. is lower than distribution requirements.

1.4 A FLEXIBLE LNG RECEPTION TERMINAL

To fully exploit the global LNG market, LNG reception terminals must be flexible in their ability to accept a range of LNG feedstock compositions. This thesis is primarily concerned with the achievement of feedstock flexibility for an LNG reception terminal. In particular, the process design and control systems for safe and efficient feedstock changeovers will be developed.

North Sea natural gas contains a high proportion of methane (typically in excess of 90%), and only the lightest LNG feedstocks are compatible with UK distribution gas. Three different feedstock compositions will be considered in this study, varying in hydrocarbon content and combustion characteristics, from a single Algerian supplier. The C.V. for each LNG feedstock exceeds the UK product specification. Hence, a flexible rich-feedstock reception terminal will be required, which can maintain product specifications. In addition, the operational limits of each process unit should not be exceeded, from both a safety and productivity viewpoint.

There are two different operating regimes for designing an LNG reception terminal; base load and peak shaving. A base load plant operates at a steady production rate to satisfy a base demand level. By comparison, a peak shaving plant is designed for short periods of operation to handle fluctuations in demand. This study will concentrate on a base load reception terminal only.

Feedstock flexibility will be assessed in terms of the variation in throughput, which results from different operating conditions for a change in the plant feedstock. The associated control system for the plant will have to cope with two different scenarios - disturbances during normal operation and changes in LNG feedstock. The control system will be required to maintain product specifications at all times, and to enable continuous operation during a feedstock changeover.

1.5 THESIS OBJECTIVES

The objectives of this thesis are given below, and are categorised into four main work phases.

Process Design:

(i) Design a preliminary flowsheet for an LNG reception terminal, which provides the degree of flexibility suitable for the proposed range of LNG feedstocks.

Dynamic Simulation:

(ii) Develop a mathematical model for each process unit which simulates its behaviour for the range of feedstock conditions.

(iii) Assess dynamic simulation facilities and select a suitable simulation package.

(iv) Develop an adaptable and effective simulation environment for implementing the dynamic models.

(v) Obtain a reliable dynamic simulation for the complete flowsheet that simulates its behaviour for the range of feedstock conditions.

Control Studies:

(vi) Develop and incorporate regulatory control loops to provide stable and robust unit operation, during feedstock changeover and at multiple operating conditions.

Plantwide Control:

(vii) Devise a mechanism for changing LNG feedstocks in continuous operation, which ensures stable and robust plant operation.

(viii) Simulate a range of feedstock changeovers on the flowsheet dynamic model to assess the impact on individual process units and product specifications.

(ix) Identify the requirements for a supervisory control system to handle feedstock changeovers.

1.6 THESIS LAYOUT

Process Design:

An outline of the main processes in the proposed LNG reception terminal was used to derive a series of potential flowsheet designs. Selection criteria were developed to assess and select the *best* preliminary flowsheet design on the basis of steady state simulation results, and this work is documented in Chapter 2.

Dynamic Simulation:

A library of mathematical models was developed to simulate each process unit in the preliminary flowsheet design. This is reported in Chapter 3. In Chapter 4, the individual units were modelled using a suitable simulation package. The subsequent validation in the steady and dynamic states is also discussed in this chapter. The individual models were then linked together to create a dynamic simulation of the complete flowsheet, and a series of step feedstock changeovers were introduced to assess model robustness. This is described in Chapter 5.

Control Studies and Plantwide Control:

The complete control system development is reported in Chapters 6 and 7. Individual control loops were derived for single-input single-output (SISO), multiloop and multivariable systems. The SISO and multiloop control systems are addressed in the remainder of Chapter 6. The application of an advanced control algorithm and multivariable system control are described in Chapter 7. A series of changeover mechanisms were derived which enabled dynamic simulation responses for the continuous mode changeovers to be assessed. Finally, the implications for a supervisory control system were discussed, concluding Chapter 7.

The achievements and novel aspects of the work are reported in Chapter 8, along with recommendations for further work.

CHAPTER 2

FLOWSHEET DEVELOPMENT AND SELECTION

2.1 INTRODUCTION

This chapter documents the development of a preliminary flowsheet for the proposed base load LNG reception terminal. The major design objective for this flowsheet is to provide the degree of flexibility suitable for the range of LNG feedstocks.

The full operational requirements for the LNG reception terminal are defined in Section 2.2. An outline flowsheet is derived and nine individual process routes are presented in Section 2.3.

A steady state simulation of all the proposed flowsheets was implemented by British Gas plc, in collaboration with the author. Selection criteria are developed to enable assessment of each process routes' ability to handle feedstock flexibility. Then a comparison of the steady state data for each process route is carried out. This work is documented in Section 2.4.

A final flowsheet is selected in Section 2.5, based on an upgrade of an original process route. This flowsheet will form the basis for subsequent dynamic modelling and control studies reported in the thesis.

2.2 OPERATIONAL REQUIREMENTS

The LNG reception terminal would be operated in a base load manner, with an anticipated output of 25 MMm^3/Day (standard conditions, dry). The installation would consist of three parallel trains, each producing 8.3 MMm^3/Day (st.,dry). Only one train would receive a variety of feedstocks. This train is the subject of this study to design a flexible LNG reception terminal flowsheet.

The three feedstock compositions considered in this study were based on Algerian LNG. These feedstocks, as listed in Table 2.1, illustrate the variation in composition and calorific value (C.V.) from a single supplier country. The feedstock with the highest proportion of methane has the lowest C.V., and is referred to as the GL1K feedstock. By comparison, the GL1Z feedstock has more heavy hydrocarbons and therefore a higher C.V.. The intermediate feedstock is called GL2Z. The variation between LNG supplies from different countries may be more significant (Jensen, 1985), and this can pose additional problems for the importer.

Component	LNG Feedstock		
	GL1K	GL2Z	GL1Z
CH_4	93.15	91.12	88.20
C_2H_6	5.40	5.85	7.27
C_3H_8	0.50	1.50	2.61
nC_4H_{10}	0.00	0.35	0.50
iC_4H_{10}	0.20	0.26	0.41
nC_5H_{12}	0.00	0.12	0.01
N_2	0.75	1.00	1.00
C.V. (MJ/m^3)	39.39	40.50	41.62

Table 2.1 LNG feedstock compositions (mol%)

A major objective of the LNG reception terminal is to handle the specified range of LNG feedstocks, and produce an export gas according to product specifications, at a steady rate. The British Gas region within which a terminal operates will dictate the quality of gas exported from the plant. For this study, a C.V. of 37.9 MJ/m^3 has been declared, and is thus used as a blending target for the

plant. From a profitability viewpoint, the thermal giveaway (defined as actual therms per day exported less *saleable*, or declared, therms per day exported), must be kept to a minimum.

The export gas must comply with the product specifications given in Table 2.2. In particular, the Wobbe No. is a combustion characteristic measuring gas quality and is defined as:

$$\text{Wobbe No.} = \text{C.V.}/\sqrt{(\text{specific gravity})}.$$

This parameter relates to flame height for gas appliances and hence must be maintained within a permitted range in the export gas.

A notable assumption in this plant design is that the importation terminal is constrained to operate without yielding by-products. The sole objective of the plant is to supply natural gas to the UK grid. In addition, continuous plant operation must be maintained during changeover from one LNG feedstock to another. This would allow storage tanks to be brought on stream without shutting down the plant. Hence, the individual plant units must be designed to handle different operating conditions associated with each LNG feedstock. Further constraints include a need to eliminate over-design and to operate as safely and economically as possible.

As the LNG feedstocks have a higher C.V. than the target value, then several process options are possible:

(i) Pump the LNG up to transmission pressure and vaporise. Export into the grid without processing and redeclare the C.V. periodically.

(ii) Pump the LNG up to transmission pressure. Then, process and reblend a portion of the feed to give a reblended export gas C.V. which matches the target C.V..

(iii) Mix the LNG feedstocks in the storage tanks, prior to processing. This reduces the need for plant flexibility and enables a more tightly optimised plant to be designed.

In this study, only the second approach has been considered feasible since this is the only route for which the target C.V. is met and is able to operate on a variety of imported LNG feedstocks with the least constraint. In summary, a single plant has to be developed

that can convert the LNG feedstocks to achieve a target C.V.. The export gas must satisfy product composition constraints to give a steady production rate of 347300 m^3/hr (st.,dry) at 70 bar pressure and approximately 10^0C.

Combustion Characteristics		
Wobbe No., range	47.3-51.2	MJ/m^3(st.,dry)(1)
Calorific Value, range	36.9-42.2	MJ/m^3(st.,dry)
Chemical Components		(max)
H_2S, ppmv		3.3
Total sulphur, ppmv		35.0
Oxygen, mol%		0.1
Unsaturated hydrocarbons, mol %		4.0
Carbon monoxide, mol %		1.5 (2)
Hydrogen, mol %		10.0
Carbon dioxide, mol %		2.0 (3)
NO_x, ppm		0.5 (2)
Dew Points		(max)
Water (at 70 bar), ^{o}C		-10
Hydrocarbon (at any pressure), ^{o}C		- 2
Temperature, Pressure		
Temperature, range ^{o}C		1-38
Pressure, bar		70.0
Other		
Distinctive odour		Obligatory
Solids, waxes, gums		Forbidden

Definition

m^3(st.,dry) = measured at 15^0C, 1013.25 mbar and dry

Footnotes (in brackets)

(1) The Wobbe range quoted is the full acceptable range. It is applicable only to gases containing at least 85 mol % of methane.

(2) Provisional specification.

(3) British Gas may accept gases containing more than 2% CO_2, subject to Wobbe number being within specification and subject to an economic case (showing net savings) being established.

Table 2.2 British Gas general specifications for distributed gas

2.3 FLOWSHEET ARRANGEMENT

2.3.1 Outline Flowsheet

An outline flowsheet has been derived from the operational requirements described in Section 2.2. Some form of heavies conversion process is required to convert excess heavy hydrocarbons and thus reduce the C.V. of the export gas. Also, a separation process is essential as only a portion of the heavy hydrocarbons requires processing to meet product gas specifications. Hereafter, the stream that is fed to the heavies conversion process will be called the *heavies processed* stream, and the remaining stream will be the *unprocessed* stream.

An outline flowsheet containing the main processes is given in Figure 2.1. The *pumping* process is required to raise the LNG feed stream up to transmission pressure, before the *separation* process forms the unprocessed and heavies processed streams. *Vaporisation* is accomplished by an open rack vaporiser (ORV) unit, which evaporates the LNG to produce natural gas close to distribution temperature. (The operation and control of the ORV have been studied in detail, (Muir, 1987)).

Heavies conversion is achieved by reacting the heavy hydrocarbons with steam in the presence of a catalyst. This introduces excess water into the heavies processed stream which must be totally removed to avoid corrosion and formation of ice-like hydrates which could block downstream equipment. Carbon dioxide is another reactor product which is restricted in the final export gas (see Table 2.2). Although reblending with the unprocessed stream reduces the molar content of CO_2, a CO_2-removal process may be necessary. These units form the *Drying and Clean-up* process that removes unwanted by-products of the heavies processing section.

Recompression is essential to raise the heavies processed stream to the distribution pressure of 70 bar. The final process in the outline flowsheet involves *blending* the heavies processed and unprocessed streams to form an export gas which conforms with the target C.V. and product specifications.

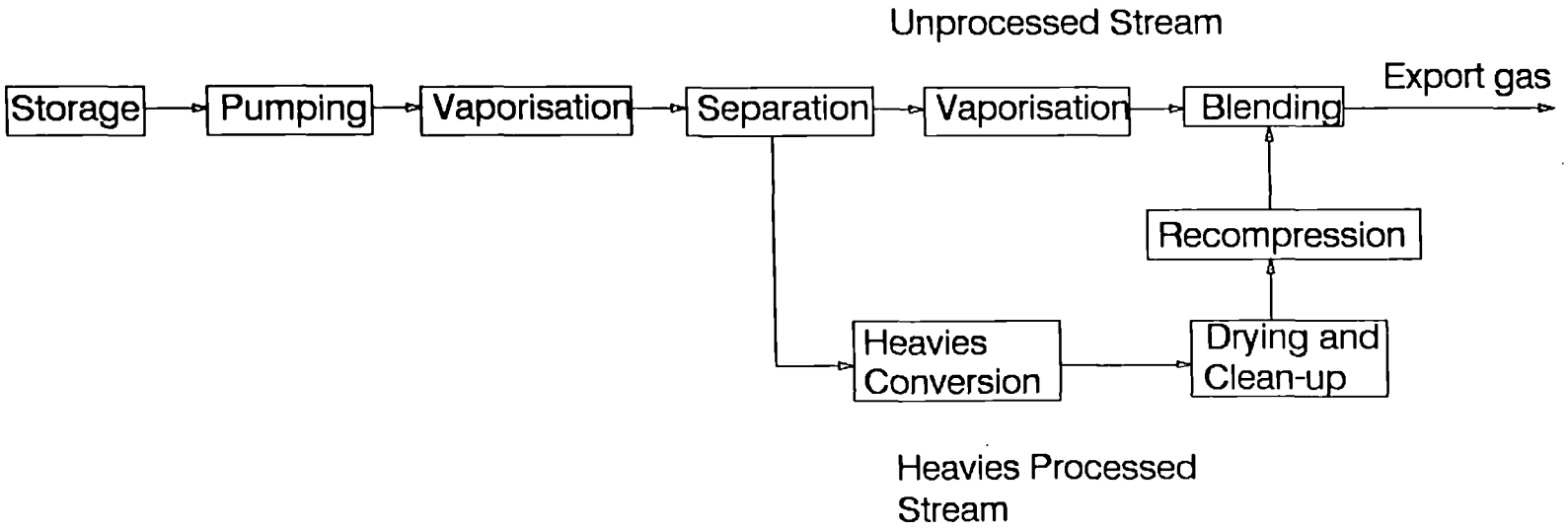

Figure 2.1 Outline flowsheet

The major items in the outline flowsheet are the heavies conversion and separation processes which can be satisfied by several different operations and arrangements. Most of the remaining processes have been derived from the stream conditions and downstream requirements. Hence, a flowsheet development and selection procedure have been undertaken to assess potential flowsheet designs. The main requirement of the preliminary flowsheet design has been to reduce the C.V. of the feedstock, and meet product specifications for a variety of LNG feeds. It should be noted that these preliminary flowsheets designs do not include heat integration and process optimisation. (In effect, each heat exchanger has been incorporated to provide a stream temperature change of up to 150°C).

There are many different forms of heavies conversion units that can be operated to convert hydrocarbons into lower C.V. products (such as methane or hydrogen-rich gas). A review of the heavies conversion process is given in Appendix 1. Three heavies conversion operations have been considered in this study:

(i) Steam Methane reformer.
(ii) High Pressure (HP) Catalytic Rich Gas (CRG) reformer.
(iii) Low Pressure (LP) CRG reformer.

The steam methane reformer normally operates at low pressure, yielding a hydrogen-rich gas. A series of operating pressures and temperatures was investigated for the reforming process, using a steady state simulation package. It was found that operating conditions of 18 bar at 500°C resulted in a high H_2 production and a low CO level. In addition, a steam to carbon (S/C) mass flow ratio of 2.43 satisfied the Boudouard reaction temperature, and thus avoided carbon formation on the catalyst surface.

The CRG reformer produces a methane-rich gas when operated at high temperature. Operating conditions for the CRG reformer were based on recommendations from British Gas plc, at operating pressures of 45 bar and 25 bar. As feed preheat must be maintained below 450°C to avoid carbon formation (BPCL, 1972), a feed temperature of 400°C and an S/C mass flow ratio of 3.0 was selected for both operating pressures.

Three operations were considered for the separation process in the outline flowsheet:

(i) Splitter - This produces two streams of variable flow rate with identical composition and phase to the feed.

(ii) Flash unit - This is a single-stage separation unit used to give a coarse separation of the light and heavy components in a stream.

(iii) Distillation column - This is a multi-stage separation unit producing high purity top, bottom or side products from a single feed.

Three fundamental separation arrangements were initially considered:

(i) Splitter only.

(ii) Flash unit then splitter.

(iii) Splitter then flash unit.

In the outline flowsheet of Figure 2.1, separation occurred after the LNG feed was pumped up to distribution pressure. As a significant drop from this pressure would incur additional pumping and/or compression costs in downstream operations, high operating pressures were preferred in the subsequent flowsheet operations.

Operating pressure was a major consideration in selecting suitable operating conditions for the flash unit. An investigation of unit performance was based on the GL2Z feedstock using a steady state simulation package. It was found that increasing the flash pressure at a constant temperature reduced the vapour fraction, increased top product purity, and reduced heat requirements. The same effect was achieved by increasing flash temperature while maintaining a constant pressure. As the main hydrocarbon components were methane and ethane, an arbitrary ethane recovery of 30% was nominated in the top product, and operating conditions in the region of 40-50 bar and -70°C were investigated. This gave suitable flash unit operating conditions of 48.09 bar at -72.82°C for the GL2Z feed. Operating conditions were similarly derived for the remaining feeds by adopting a constant pressure, and are given in Table 2.3.

LNG Feedstock	Flash Pressure (bar)	Flash Temperature (^{o}C)
GL1K	48.09	-74.95
GL2Z	48.09	-72.82
GL1Z	48.09	-69.79

Table 2.3 Flash unit operating conditions

2.3.2 Process Route Options

The options considered for the heavies conversion and separation processes have been incorporated in the outline flowsheet to produce a variety of plant arrangements. These have been grouped into three different flowsheeting families based on the reforming process, as illustrated in Figure 2.2. A description of the flowsheets in each family is given in the following subsections.

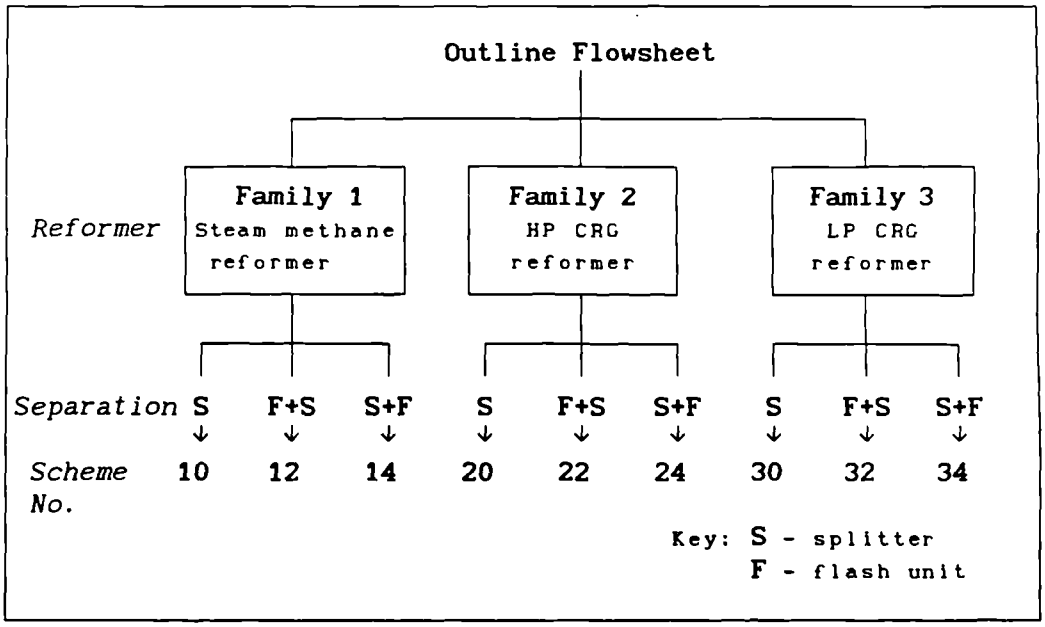

Figure 2.2 Flowsheet families

Every flowsheet arrangement was simulated in the steady state mode by British Gas plc, using an in-house simulation package. To ensure product specifications were achieved for each process route and LNG feedstock, the split ratio in the separation process was varied to give the target C.V. of the export gas. In addition, the feed flow rate was scaled up to give the required production rate, and product specifications including the Wobbe No. were monitored.

2.3.2.1 *Family 1*

The steam methane reformer family consists of three flowsheets incorporating the different separation options.

Scheme 10 Split Separation

The split operation has been initially considered for the separation stage in flowsheet development as it gives the simplest arrangement. The basic flowsheet arrangement is illustrated in Figure 2.3.

The LNG feed is pumped from storage up to distribution pressure (70 bar) and vaporised to 10°C, using an ORV unit, prior to splitting. An unprocessed stream and heavies processed stream are formed. The latter is expanded and fed through a series of heat exchangers and a fired heater to attain the steam methane reformer operating conditions of 18 bar and 500°C. Steam is added at the recommended S/C mass flow ratio of 2.43, prior to reforming.

Simulation results have shown that the reformer outlet stream contains approximately 74% H_2, 17% CO, 6% CO_2 and 2% CH_4, at 900°C (dry basis). The outlet stream is cooled and condensate is removed by intermediate knock-out pots. (The condensate accounts for approximately 19% of the total reformer product). Following CO_2-removal and drying, the heavies processed stream is compressed to distribution pressure and blended with the unprocessed stream at distribution temperature and pressure to form the export gas. Utilities streams and effluent treatment have not been modelled as these were outwith the scope of the preliminary flowsheet design.

To complete the steady state simulation, the split ratio was adjusted and feed flow rate scaled up to achieve product specifications. The split ratio has been calculated as the percentage of LNG feed sent to the heavies processing section. The following mean settings were required to obtain 347300 m^3/hr of export gas with a C.V. of 37.9 MJ/m^3:

LNG feed flow rate: 10755 kgmol/hr

Split ratio: 2.47 %

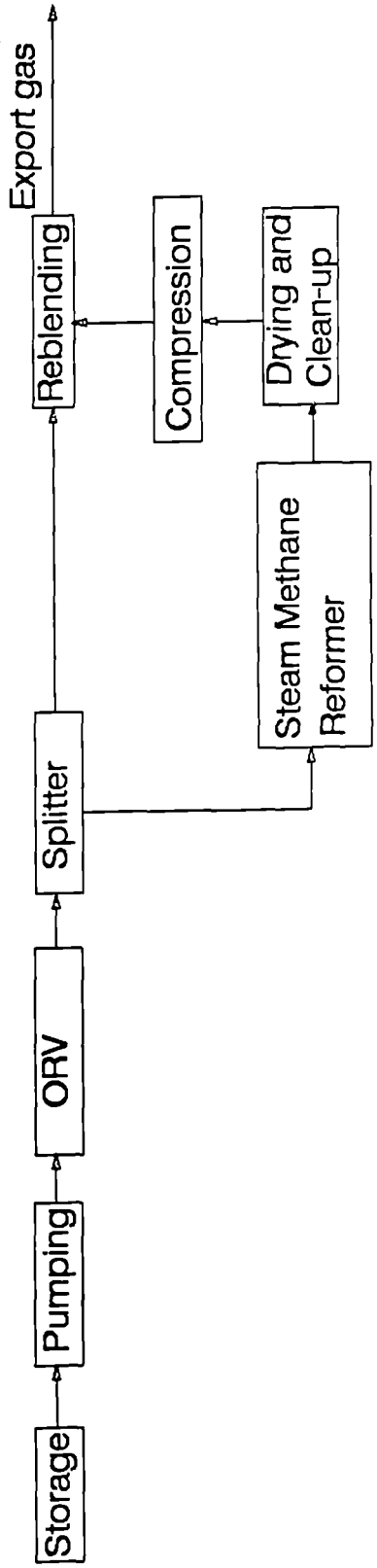

Figure 2.3 Scheme 10 flowsheet

Scheme 12 Flash then Split Separation

The addition of a flash unit to the separation process would improve the degree of separation of the LNG feedstock and therefore increase the proportion of heavy hydrocarbons in the heavies processed stream. This should enhance the performance of the steam methane reformer, as proportionally more excess hydrocarbons can be converted.

The flowsheet arrangement for Scheme 12 for a flash unit followed by a split separation process is illustrated in Figure 2.4. The LNG feed is pumped to distribution pressure before entering the flash unit at 48.09 bar. The flash unit operating conditions are described in Table 2.3. The vapour top product forms part the unprocessed stream which is heated to 10°C, then compressed to 70 bar. The bottom product is vaporised to 10°C before entering the splitter.

The smaller of the split streams is fed to the steam methane reformer with steam. The reformer product is progressively cooled and condensate is removed, prior to CO_2-removal and drying. The heavies processed stream is then mixed with the reformer by-pass stream, and compressed to distribution pressure. The final export gas is formed by blending the combined heavies processed stream with the unprocessed stream. A steady state simulation of the flowsheet required the following mean settings:

LNG feed flow rate: 10743 kgmol/hr

Split ratio: 5.4 %

Scheme 14 Split then Flash Separation

The flowsheet arrangement for the split followed by a flash unit separation is illustrated in Figure 2.5. The LNG feed is pumped to distribution pressure before splitting. One stream is then flashed at 48.09 bar. The top product is condensed and pumped to distribution pressure before blending with the other split stream. This forms the unprocessed stream, which is vaporised to 10°C.

The flash bottom product becomes the heavies processed stream and is vaporised, expanded and heated to the required inlet conditions. After reforming, the outlet stream is cooled, dried and cleaned. The heavies processed stream is then compressed to 70 bar before mixing

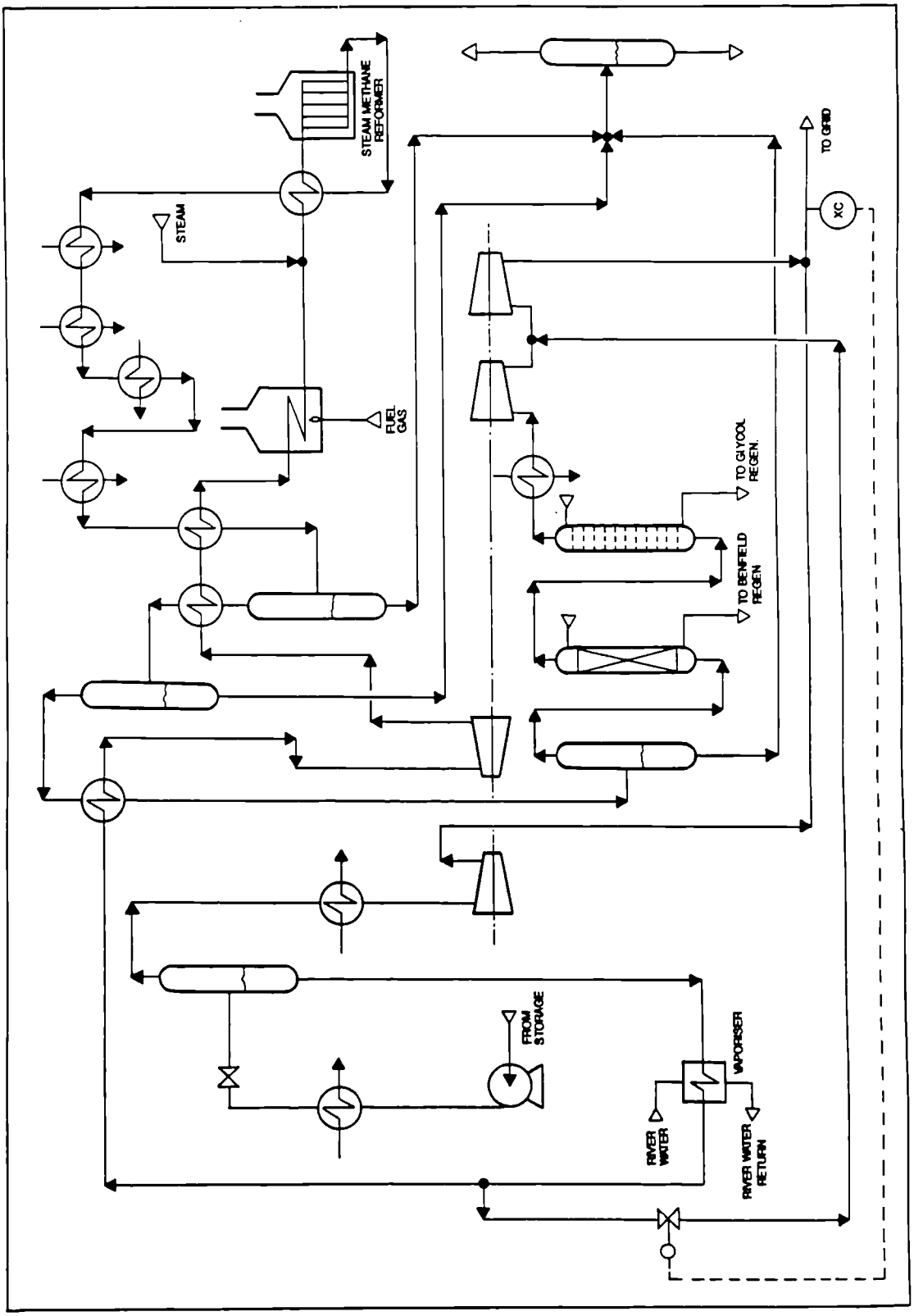

Figure 2.4 Scheme 12 flowsheet

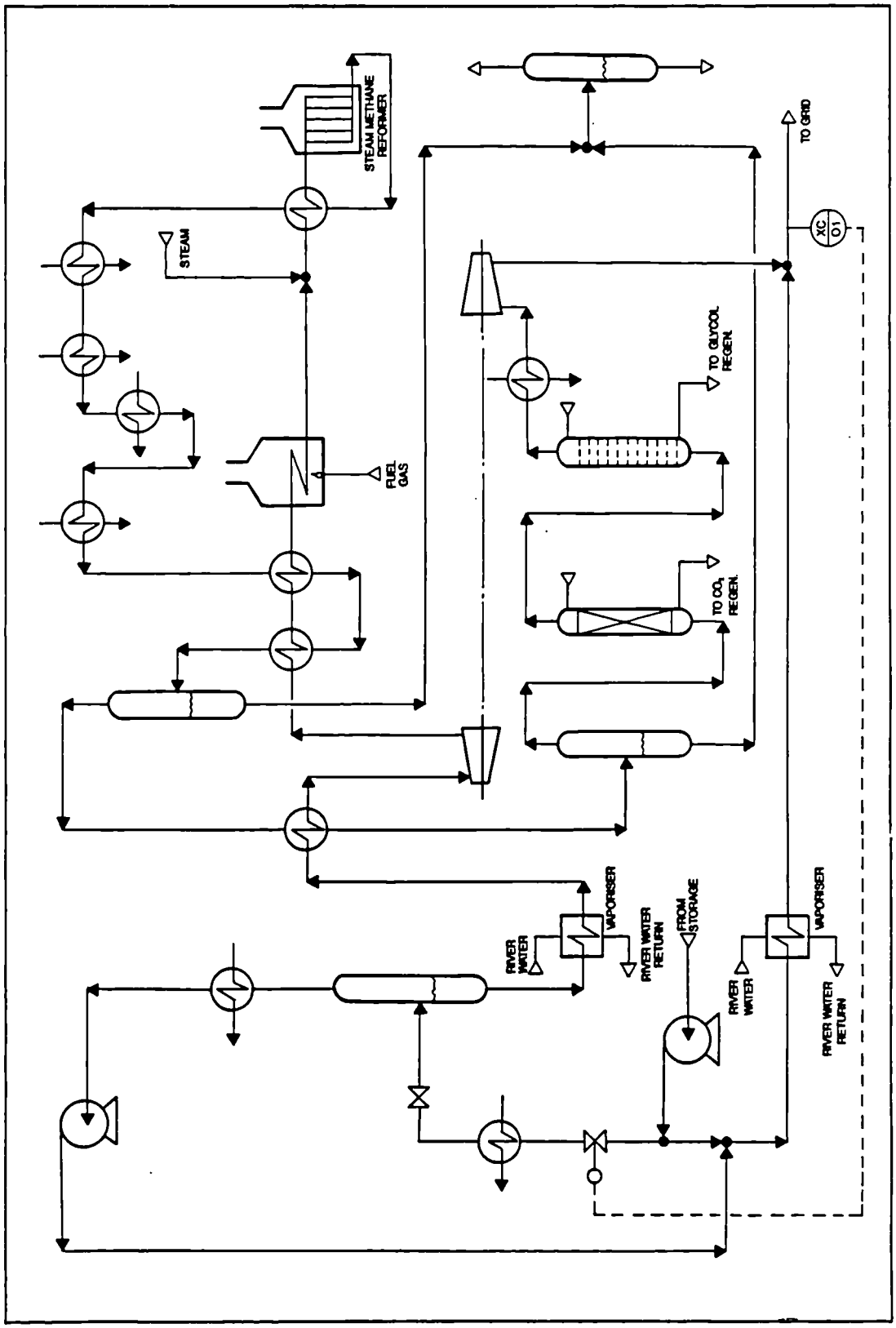

Figure 2.5 Scheme 14 flowsheet

with the unprocessed stream to form the export gas. The flowsheet simulation required the following mean settings:

LNG feed flow rate: 10746 kgmol/hr
Split ratio: 5.21 %

2.3.2.2 *Family 2*

The HP CRG reformer is the basis of the Family 2 flowsheets. A different separation arrangement is described within each process route, as in Family 1.

Scheme 20 Split Separation

This flowsheet, consisting of a split unit in the separation process, is similar to the Family 1 arrangement (Scheme 10). The complete flowsheet is illustrated in Figure 2.6.

The LNG feed is pumped from storage up to 70 bar, and vaporised to 10°C with an ORV, prior to splitting. A fired heater raises the heavies processed stream temperature to 400°C before steam is added at the prescribed S/C mass flow ratio for CRG reforming. Steady state simulation studies have shown that the reformer outlet stream contains approximately 83% CH_4, 10% H_2, 6% CO_2 and trace CO, at 395°C. The CRG reformer has lower inlet and exit gas temperatures than the steam methane reformer family. The reformer outlet stream is cooled against its inlet stream, with further cooling and condensate removal by intermediate knock-out pots. After CO_2-removal and drying, the heavies processed stream is compressed and blended with the unprocessed stream to form the export gas. The following mean settings were required to achieve product specifications:

LNG feed flow rate: 10243 kgmol/hr
Split ratio: 39.10 %

Scheme 22 Flash then Split Separation

Separation in the previous flowsheet has been improved by including a flash unit, as in Scheme 12 and Figure 2.4. The LNG feed is pumped to 70 bar, then flashed to 48.09 bar. The top product, forming the unprocessed stream, is heated and compressed to distribution conditions. The flash bottom product is vaporised to 10°C then split to form a heavies processed stream and reformer by-pass stream. This

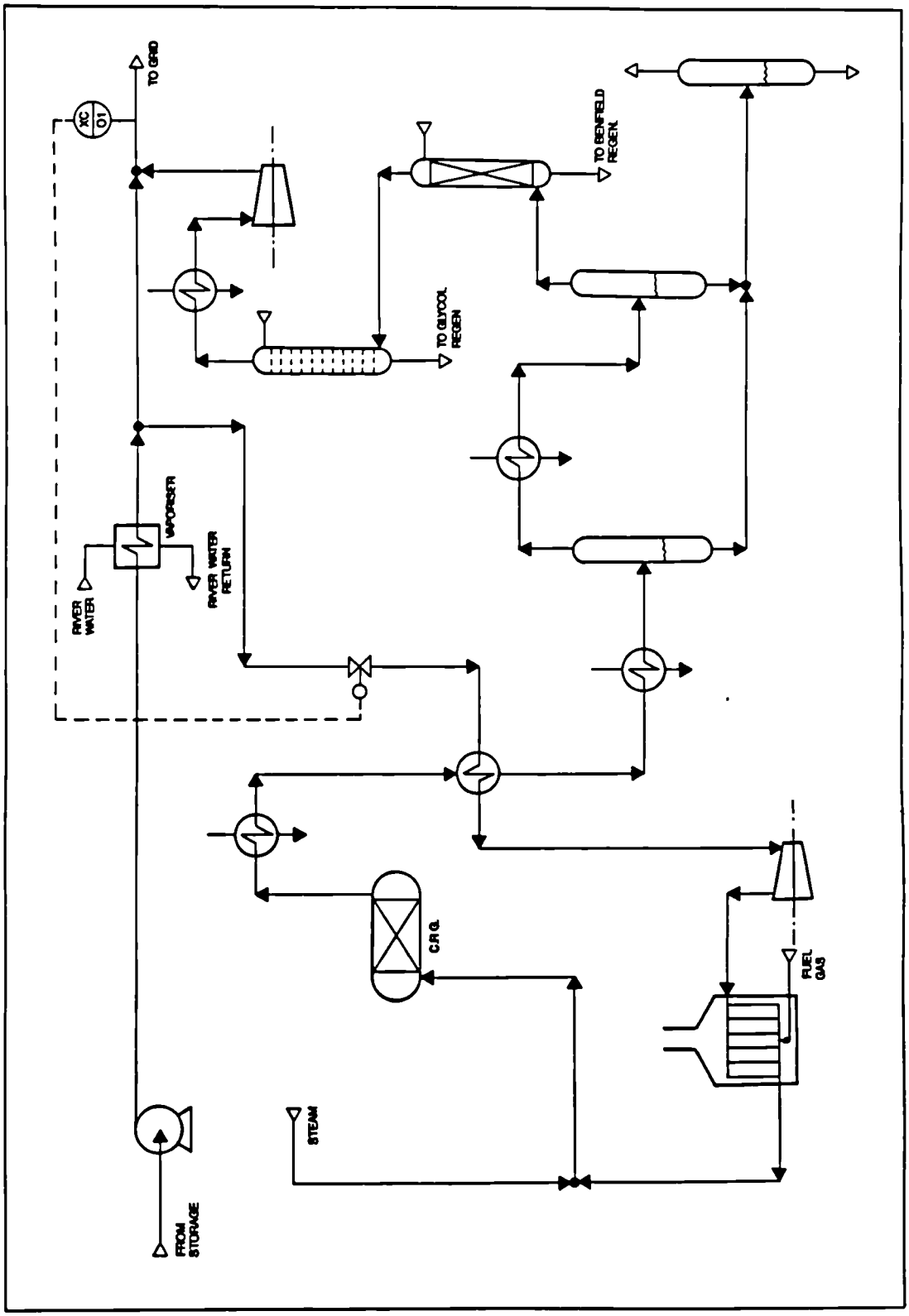

Figure 2.6 Scheme 20 flowsheet

arrangement is illustrated in Figure 2.7.

After reforming and treatment, the heavies processed stream is mixed with the reformer by-pass stream, cooled, compressed to 70 bar and finally mixed with the unprocessed stream to form export gas. The flowsheet simulation required the following mean settings:

LNG feed flow rate: 10781 kgmol/hr
Split ratio: 62.14 %

Scheme 24 Split then Flash Separation

This Family 2 flowsheet arrangement is illustrated in Figure 2.8. The LNG feed is pumped up to 70 bar before splitting, and the larger stream is then flashed. The vapour top product is cooled and pumped to distribution pressure, before blending with the smaller split stream, to form the unprocessed stream. The combined stream is then vaporised to 10°C. The flash unit bottom product becomes the heavies processed stream. After reforming and treatment, the processed and unprocessed streams are combined to form the export gas. The following mean settings were required to satisfy the product specifications:

LNG feed flow rate: 10726 kgmol/hr
Split ratio: 62.18 %

2.3.2.3 *Family 3*

The LP CRG reformer is the basis of the Family 3 flowsheets. It is introduced as a further comparison with Family 2 to investigate the effect of operating pressure on a CRG reformer. As before, the flowsheet development has been grouped into three sections.

Scheme 30 Split Separation

As with the previous family developments, the simple split separation is first considered. The flowsheet arrangement is identical to Scheme 20, as illustrated in Figure 2.6.

Due to the lower operating pressure of 25 bar in the CRG reformer, product compositions differ. The outlet stream contains approximately 81% CH_4, 12% H_2, 7% CO_2 and trace CO, at 370°C. Hence, reducing the CRG reformer pressure has an adverse effect on

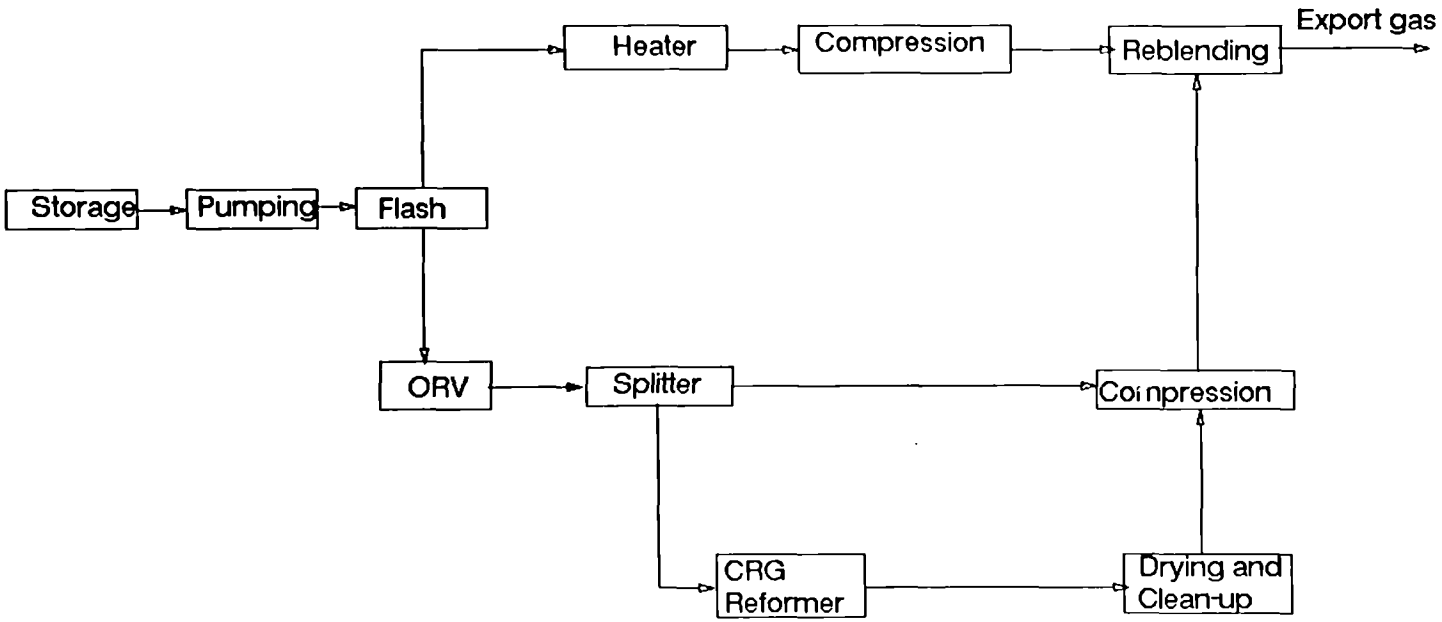

Figure 2.7 Scheme 22 flowsheet

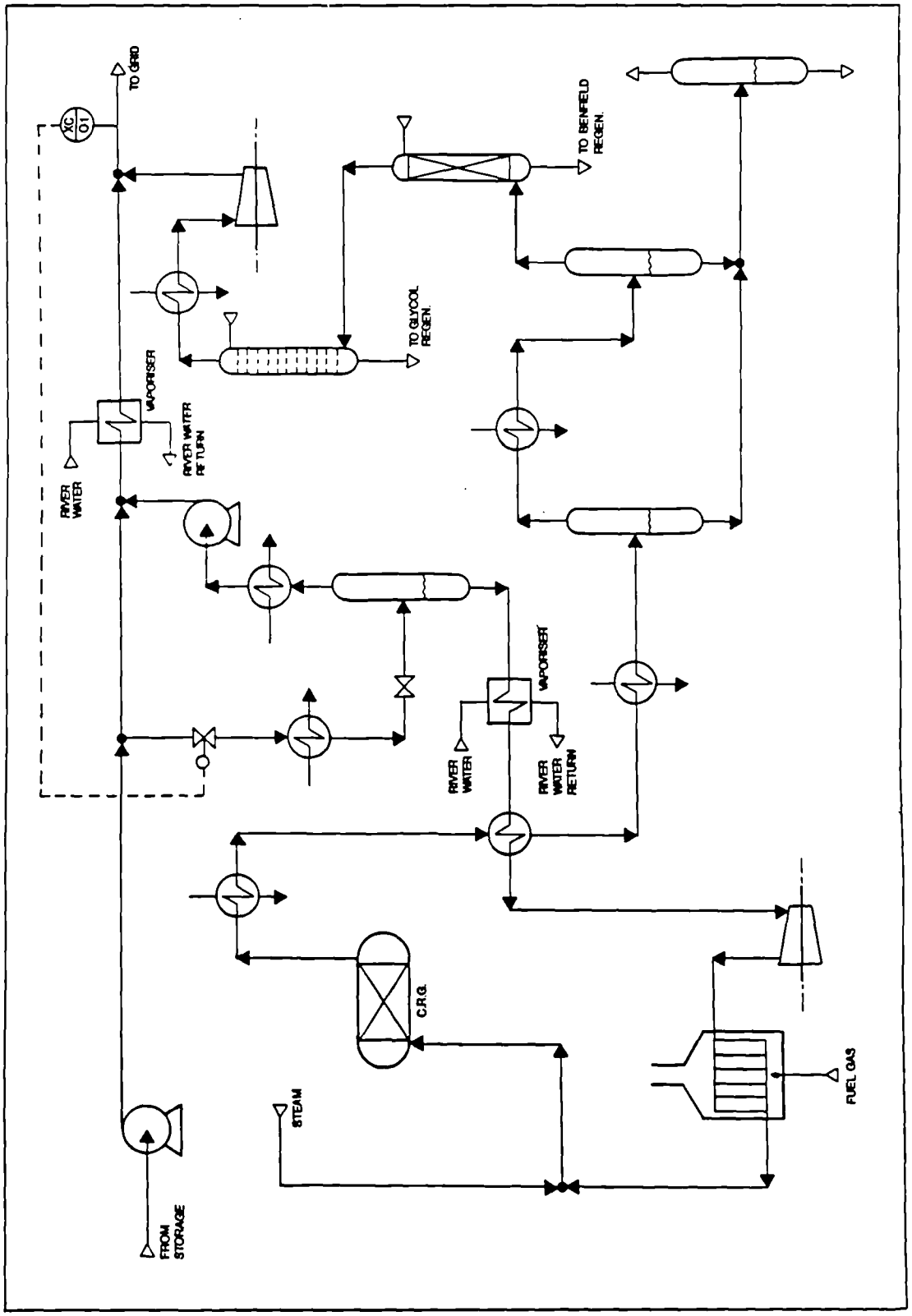

Figure 2.8 Scheme 24 flowsheet

methane-rich gas production. The steady state simulation required the following mean settings:

LNG feed flow rate: 10180 kgmol/hr
Split ratio: 36.52 %

Scheme 32 Flash then Split Separation

The process description for this flowsheet is identical to Scheme 22, except the LP CRG reformer is operated at 25 bar. The following mean settings were required for the flowsheet simulation:

LNG feed flow rate: 10731 kgmol/hr
Split ratio: 56.25 %

Scheme 34 Split then Flash Separation

The process description for this flowsheet differs from Scheme 24, illustrated in Figure 2.8, in LP CRG reformer operating pressure only. The mean settings required for simulation were:

LNG feed flow rate: 15872 kgmol/hr
Split ratio: 59.87 %

2.4 SELECTION OF THE BEST PROCESS ROUTE

Conventional factors that are normally considered in flowsheet evaluation (Ulrich, 1984) include plant operability and controllability, operating costs and capital cost. The main objective in the design of the preliminary flowsheet for an LNG reception terminal have been to attain a high degree of flexibility.

A limiting factor in feedstock flexibility is the extent of turndown in individual units. Turndown refers to the variation in a key parameter resulting from a change in the unit and/or plant feed conditions. The parameter may be concerned with throughput or duty, whichever is restricted by the physical dimensions of the unit. Hence, for small variations the unit should be capable of handling a change in feedstock, without adversely affecting its operation. If satisfactory turndown can be achieved for a process route, then designing single streams for maximum throughput and duty may be feasible. However, if the conditions change markedly, then the unit may not function in its designed manner. Thus, it may be necessary to introduce multiple streams and units to accommodate significant changes, which leads to increased capital costs. Therefore, low turndown variations are desirable for changes in the LNG feedstock condition.

The main operating costs that may vary between process routes are:

(i) Utilities, eg. power, heating and cooling requirements.
(ii) Catalyst and steam requirements for heavies conversion.
(iii) Effluent treatment.

The process route selection has been based primarily on a comparison of the above requirements, rather than actual costs, and turndown. Capital costs have only been considered in a comparative sense, as an accurate capital costing would require detailed unit designs.

Assessment of the process routes in Section 2.3 was based on a comparative study of the steady state simulation data produced for each LNG feedstock condition. Since it was impractical to consider the performance of each unit in each flowsheet, a set of criteria was developed which identified key parameters for comparison.

2.4.1 Selection Criteria

In the absence of established methods for assessing feedstock flexibility in the literature, the following approach was developed. Selection criteria were chosen to represent major cost items in the process routes and are listed in Table 2.4. Two forms of the criteria have been derived and compared for each process route; the mean value and the turndown ratio. The mean value represents an average value of the parameter for the three feed conditions. The turndown ratio is the ratio of the minimum to maximum value of a parameter for changes in the feed conditions, multiplied by 100. Hence, a high ratio value approaching 100 represents a small variation in the parameter and good feedstock flexibility. By comparison, a small value indicates a large variation between feedstock conditions and hence poor feedstock flexibility. The chosen selection parameters of Table 2.4 are described below.

The ratio of product to feed mass flow rates is an indication of the yield and relative efficiency of the flowsheet. As the product specifications in Table 2.2 impose limits on the Wobbe No., a selection criterion assesses the Wobbe No. value by its position within these limits. Therefore, a Wobbe No. on the lower or upper limit would be equivalent to a position of zero or one, respectively. Midway between the imposed limits (at 0.5) would be ideal, as this would allow maximum variation from the mean steady state value.

Mass flow rates in the heavies processing section give relative unit sizing, catalyst requirements, and utility costs. Effluent production from the knock-out pots and absorbers is important as it has associated treatment costs besides its environmental impact.

The remaining selection criteria in Table 2.4 are concerned with operating costs. Expansion power may be considered as a credit, as it could be incorporated in other plant utilities. Thus, it has not been included in the total power requirement, which consists of compression and pumping power only.

Criterion	Description
Production	
. Feed (kg/s)	. LNG feed rate
. kg Product/kg Feed	. Yield
. Wobbe No. position	. Wobbe No. of export gas relative to limiting range
Heavies Processing	
. Heavies Stream (kg/s)	. Heavies processed stream mass flow rate
. Steam Flow (kg/s)	. Steam requirement for heavies conversion process
. Effluent Flow (kg/s)	. Effluent flow rate from Drying and Clean Up process
Operating Costs	
. Total Power (kW)	. Total power requirement
. Compression Power (kW)	. Compression power requirement
. Expansion Power (kW)	. Expansion power requirement
. Nett Heating (kW)	. Total heat requirement
. Nett Cooling (kW)	. Total cooling requirement
. Cryogenic Heat (kW)	. Heat supplied to LNG below its critical point
. Fired Heat (kW)	. Heat supplied to reformer or its feed
. Process Heat (kW)	. Remaining heat requirements (excluding ORV heat)
. Cryogenic Cooling (kW)	. Cooling provided below 150 K
. Process Cooling (kW)	. Remaining process cooling requirements

Table 2.4 Selection criteria

The heating and cooling requirements have been itemised. ORV heat has not been included as a criterion because sea or river water would be used as the heating medium. Therefore, only secondary costs would arise, associated with pumping. Fired heat would be readily available if supplied by boil-off gas from the LNG storage tanks, and hence would be cheaper than most other heat forms. Cryogenic cooling is also relatively inexpensive as it is provided by refrigeration

cycles in typical LNG importation designs (Burton, 1990). Steam raised in waste heat boilers is considered a credit to the heat utilities. However, as waste heat boilers have not been modelled in every process route simulation, their results were not incorporated in the preliminary design study. Conversely, cryogenic heat represents the most expensive heat form (as it requires an intermediate cycle), and should therefore be limited. It should be noted that optimisation of the heat recovery and process integration, which might significantly reduce these preliminary utility costs, have not been considered in the process route designs.

The mean values and turndown ratios for each selection criterion were employed in two stages to select a preliminary flowsheet design from the nine original process routes. First, the *best* separation arrangement within each flowsheet family was selected; **intra-family** selection. Then, the *best* flowsheet from each family was compared; **inter-family** selection.

2.4.2 Intra-family Selection

Selection criteria data for each flowsheet and LNG feedstock condition are tabulated in Appendix 2. Each criterion was considered by comparing mean values and selected turndown ratios from the simulation results. The *best* scheme within each family demonstrated good overall performance, both in terms of competitive operating costs and feedstock flexibility.

2.4.2.1 *Family 1 Selection*

The selection criteria data for Schemes 10, 12 and 14 are listed in Table 2.5, in terms of mean and turndown values. The full results for each feedstock condition are listed in Appendix 2.

Table 2.5 indicates that the yield and Wobbe No. position are indistinguishable. Although Scheme 14 sends the least feed to heavies conversion, the low turndown ratios associated with each scheme imply poor feedstock flexibility.

Selection Criterion	Scheme		
	10	12	14
Production			
Feed (kg/s)	58.56	52.82	52.83
kg Product/kg Feed	1.016	1.016	1.016
Wobbe No. Position	0.674	0.673	0.675
Heavies Processing			
Heavies Stream (kg/s)	2.804	1.286	1.269
Turndown (%)	30.4	44.0	45.0
Steam (kg/s)	7.646	3.558	3.685
Effluent Treatment			
Waste Water (kg/s)	4.00	1.87	1.86
Waste CO_2 (kg/s)	1.73	0.83	0.83
Total Power			
Total Power (kW)	6987.	6499.	3248.
Compression Power (kW)	4715.	5393.	2173.
Nett Heating Analysis			
Cryogenic Heat (kW)	0. (0%)	29299. (44%)	1265. (2%)
Fired Heat (kW)	45841. (38%)	5212. (8%)	2752. (4%)
Process Heat (kW)	6267. (5%)	20846. (31%)	16667. (27%)
Nett Heating (kW)	136572.	66350.	61119.
Nett Cooling Analysis			
Cryogenic Cooling (kW)	0.	0.	440.
Process Cooling (kW)	35931.	23002.	18190.
Nett Cooling (kW)	35931.	23002.	18630.

Table 2.5 Family 1 selection criteria

In terms of utility requirements, Scheme 12 shows poor heat distribution, with cryogenic heat demand (most costly) representing over 40% of its total heat demand. Scheme 14 demonstrates the best heat distribution in Family 1 as it exhibits:

(i) Low nett heating requirement.

(ii) Low cryogenic heat demand.

(iii) Largest proportion of ORV heat demand.

This is also true of the low cooling demand in Scheme 14, where the cryogenic cooling is required to condense the flash unit vapour stream. This cooling can be readily supplied by heat exchange with the LNG feed stream.

As Scheme 14 showed good overall utility requirements and feedstock flexibility, it was selected as the *best* Family 1 process route.

2.4.2.2 *Family 2 Selection*

The mean and turndown values for Schemes 20, 22 and 24 are listed in Table 2.6. Results corresponding to each feedstock condition are included in Appendix 2.

Selection Criterion	Scheme		
	20	22	24
Production			
Feed (kg/s)	50.34	53.01	52.74
kg Product/kg Feed	0.990	0.990	0.990
Wobbe No. Position	0.824	0.814	0.815
Heavies Processing			
Heavies Stream (kg/s)	19.619	15.433	15.353
Turndown (%)	63.0	75.1	75.6
Steam (kg/s)	59.041	46.370	46.163
Effluent Treatment			
Waste Water (kg/s)	56.50	43.83	43.63
Waste CO_2 (kg/s)	2.91	3.08	3.06
Total Power			
Total Power (kW)	3339.	5669.	3058.
Compression Power (kW)	2294.	4569.	1791.
Nett Heating Analysis			
Cryogenic Heat (kW)	0. (0%)	31853. (53%)	15078. (24%)
Fired Heat (kW)	11638. (18%)	5473. (9%)	5448. (9%)
Process Heat (kW)	12407. (20%)	11894. (20%)	11841. (19%)
Nett Heating (kW)	63332.	60251.	63021.
Nett Cooling Analysis			
Cryogenic Cooling (kW)	0.	0.	4222.
Process Cooling (kW)	175503.	141684.	137251.
Nett Cooling (kW)	175503.	141684.	141473.

Table 2.6 Family 2 selection criteria

In Table 2.6, Schemes 22 and 24 send less feed to heavies processing and demonstrate better turndown requirements than Scheme 20. Although Scheme 20 produces the most effluent, its CO_2 contribution is least. This is because its feed to the heavies processing section contains fewer heavy hydrocarbons and hence less conversion occurs.

Scheme 24 requires the least compression and combined power of the process routes. Although Scheme 22 has the lowest nett heating demand, it demonstrates poor heat distribution, with over 50% in cryogenic heat form. Scheme 20 has the best distribution as most of its heat is derived from the ORV unit. The cooling requirement for

Scheme 24 would be less than that of Scheme 22 as cryogenic cooling is readily available using LNG cold as a refrigeration medium.

In summary, Scheme 20 shows good heat distribution, as it relies mainly on ORV heat. However, a large proportion of the feed stream is sent to heavies conversion, which leads to greater demands on the heavies processing section. Based on overall power demands and cooling requirements, Scheme 24 has been selected as the *best* Family 2 flowsheet.

2.4.2.3 *Family 3 Selection*

Family 3 flowsheets include an LP CRG reformer in the heavies conversion section. Otherwise, the process routes are identical to those in Family 2. The lower operating pressure resulted in lower methane production and higher compression costs than in Family 2 schemes. Therefore, a Family 3 flowsheet selection was not conducted as equivalent Family 2 schemes would easily out perform them.

2.4.3 **Inter-family Selection**

The *best* process routes from the intra-family selection are:

14: Splitter + Flash unit + Steam methane reformer

24: Splitter + Flash unit + HP CRG reformer

The comparison between Schemes 14 and 24 was conducted in the same style as Section 2.4.2, but with a greater emphasis on turndown for flowsheet flexibility assessment. The selection criteria results for both schemes are given in Table 2.7.

Scheme 14 has a greater yield, and its Wobbe No. position is closer to ideal. This suggests that there is more potential for variation in hydrogen content, provided the permitted hydrogen concentration is not exceeded in the export gas product specification.

Scheme 14 sends significantly less to the heavies processing section, and consequently less reacting steam is required. This represents a significant saving in reactor capital costs and effluent treatment. The smaller power required by Scheme 24 could be reduced further by increasing the operating pressure of the CRG reformer to 70 bar, as compression costs would drop considerably. By contrast, the steam

methane reformer is restricted to low pressures by materials and conversion maxima. Although the nett heating requirements are comparable in both process routes, Scheme 14 exhibits a better heat distribution by deriving more of its heat from the ORV unit, and requiring less cryogenic heat.

Selection Criterion		Scheme	
		14	24
Production	Feed (kg/s)	52.83	52.74
	kg Product/kg Feed	1.016	0.990
	Wobbe No. Position	0.675	0.815
Heavies Processing	Heavies Stream (kg/s)	1.269	15.353
	Turndown (%)	45.0	75.6
	Steam (kg/s)	3.685	46.163
Effluent Treatment	Waste Water (kg/s)	1.86	43.63
	Waste CO_2 (kg/s)	0.83	3.06
Total Power	Total Power (kW)	3248.	3058.
	Compression Power (kW)	2173.	1791.
Nett Heating Analysis	Cryogenic Heat (kW)	1265. (2%)	15078. (24%)
	Fired Heat (kW)	2752. (4%)	5448. (9%)
	Process Heat (kW)	16667. (27%)	11841. (19%)
	Nett Heating (kW)	61119.	63021.
Nett Cooling Analysis	Cryogenic Cooling (kW)	440.	4222.
	Process Cooling (kW)	18190.	137251.
	Nett Cooling (kW)	18631.	141472.

Table 2.7 Inter-family selection criteria

The turndown ratios for several selection criteria have also been considered in the inter-family selection. A turndown ratio approaching 100 represents a small variation in a parameter, and therefore good feedstock flexibility. The ratios for Schemes 14 and 24 are listed in Table 2.8. Scheme 14 shows significant turndown in the heavies processed stream. As this stream is more than halved when changing from the heavy to light LNG feedstocks (Appendix 2) this may warrant introducing parallel trains in the reformer section.

Scheme 24 has higher overall turndown ratios which implies a smaller redundant capacity when using a light feedstock. This reduces the need for parallel streams and plant units in the process route.

Selection Criterion	Scheme	
	14	24
Feed (kg/s)	99.5	99.2
kg Product/kg Feed	98.8	99.2
Wobbe No. Position	82.9	95.5
Heavies Stream (kg/s)	45.0	75.6
Steam (kg/s)	59.4	75.4
Effluent Flow (kg/s)	43.2	75.2
Total Power (kW)	60.6	84.1
Compression Power (kW)	43.4	76.3
Nett Heating (kW)	86.7	90.3
Nett Cooling (kW)	44.0	74.9

Table 2.8 Turndown ratios for Schemes 14 and 24

Inter-family Selection: Conclusions

From the above comparison, Scheme 14 has lower operating costs for most of the criteria. Its yield and Wobbe No. are better, and the proportion of feed sent to heavies conversion is significantly less, which incurs less effluent treatment downstream. In addition, the heating and cooling demands are either less or easier to provide. The power requirement of this process route is the only drawback.

However, as the key factor in the flowsheet design is feedstock flexibility, the turndown ratios are also important. As Scheme 14 does not handle feedstock changes as well as Scheme 24, certain units would either have to be over-designed, or parallel streams introduced. Either option would encroach on the need for flexibility. Therefore, as both schemes have disadvantages, they were considered for further improvement.

2.5 FURTHER IMPROVEMENTS TO BEST FLOWSHEETS

The two selected flowsheets have their individual merits, and consequently further amendments to the existing process routes were investigated to help differentiate between their performance. The LNG feedstocks contain a high proportion of methane, and both Schemes 14 and 24 passed between 35% and 49% methane (molar basis) from the LNG feed to the heavies conversion section. This gave a high proportion of methane in the heavies processed stream.

The major difference between the two process routes is in the heavies conversion section. The steam methane reformer, in Scheme 14, successfully converts most of the hydrocarbons to produce an H_2-rich gas, and therefore leaves little room for improvement. In contrast, the CRG reformer in Scheme 24 converts heavy hydrocarbons to form a methane-rich gas. Thus, any methane passed to the CRG reformer acts, for the most part, as an inert. This suggests the performance of Scheme 24 may be improved by lowering the proportion of methane in the heavies processed stream. Therefore, the addition of a separation stage to extract more methane from the heavies conversion feed has been considered as it may give a significant improvement to the performance of Scheme 24.

If an additional flash unit was employed in this capacity, the separation may include the carry-over of more ethane and propane into the unprocessed stream than desired. Steady state simulation results have shown that for each mole of ethane carried over into 10 moles of the unprocessed stream, an additional 0.8 moles of the heavies processed stream is required to meet the C.V. specification. Therefore, a distillation column was selected as a better form of separation than a flash unit.

2.5.1 Addition of a Distillation Column to Scheme 24

The objective of adding a distillation column to Scheme 24 was to minimise the methane content in the heavies conversion feed, and hence divert more methane to the unprocessed stream. The existing separation arrangement in Scheme 24 has been retained because:

(i) The flash unit reduces the separation load to the column by

about 45%.

(ii) Upon column failure, the flash unit would allow some separation to be performed.

The following design considerations were key factors in selecting a suitable distillation column arrangement and operating conditions:

I Operating Pressure

The column pressure is dictated by feed pressure (48.09 bar), and downstream pressure conditions (top product at 70 bar, and bottom product at 45 bar). The pseudo-critical pressure for all three column feeds is approximately 46 bar. This sets an upper limit of about 40 bar on column pressure.

II Product Purity

As the distillation products are intermediate in the flowsheet, high product purity is desirable but not essential.

III Reflux Ratio

There is an optimum reflux ratio associated with the distillation column, defined as the ratio of reflux to minimum reflux, R/R_m. As this ratio is typically between 1.03 to 1.3 (Douglas, 1988), an R/R_m of 1.1 has been selected.

2.5.1.1 *Distillation Column Arrangements*

Several separation arrangements were investigated for Scheme 24, by introducing the bottom product of the flash unit to a suitable distillation column arrangement. Four different arrangements were considered, and are described below:

(i) Arrangement 1 - The flash unit bottom product is fed directly to the distillation column to form a two-phase feed, as illustrated in Figure 2.9.

(ii) Arrangement 2 - An intermediate flash is introduced at column pressure, and only the bottom product is fed to the column, as a liquid feed. The top product is fed to the unprocessed stream, as illustrated in Figure 2.10.

(iii) Arrangement 3 - Both top and bottom products of the intermediate flash are fed to the distillation column, as shown in Figure 2.11. This is similar to Arrangement 1,

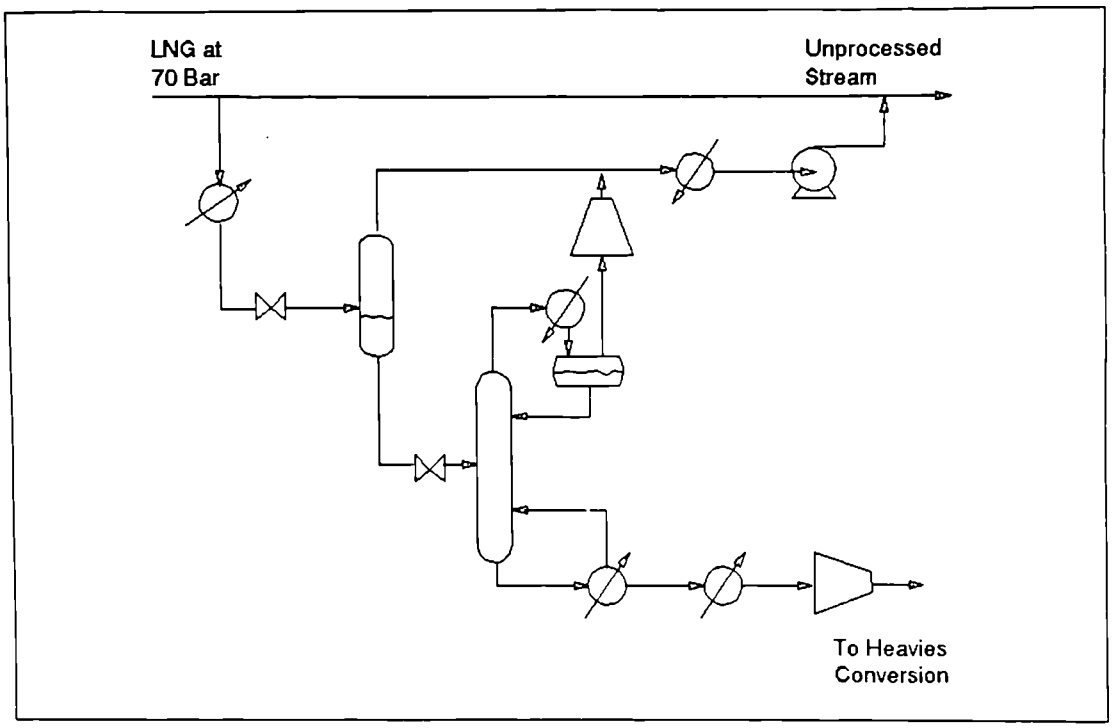

Figure 2.9 Distillation column Arrangement 1

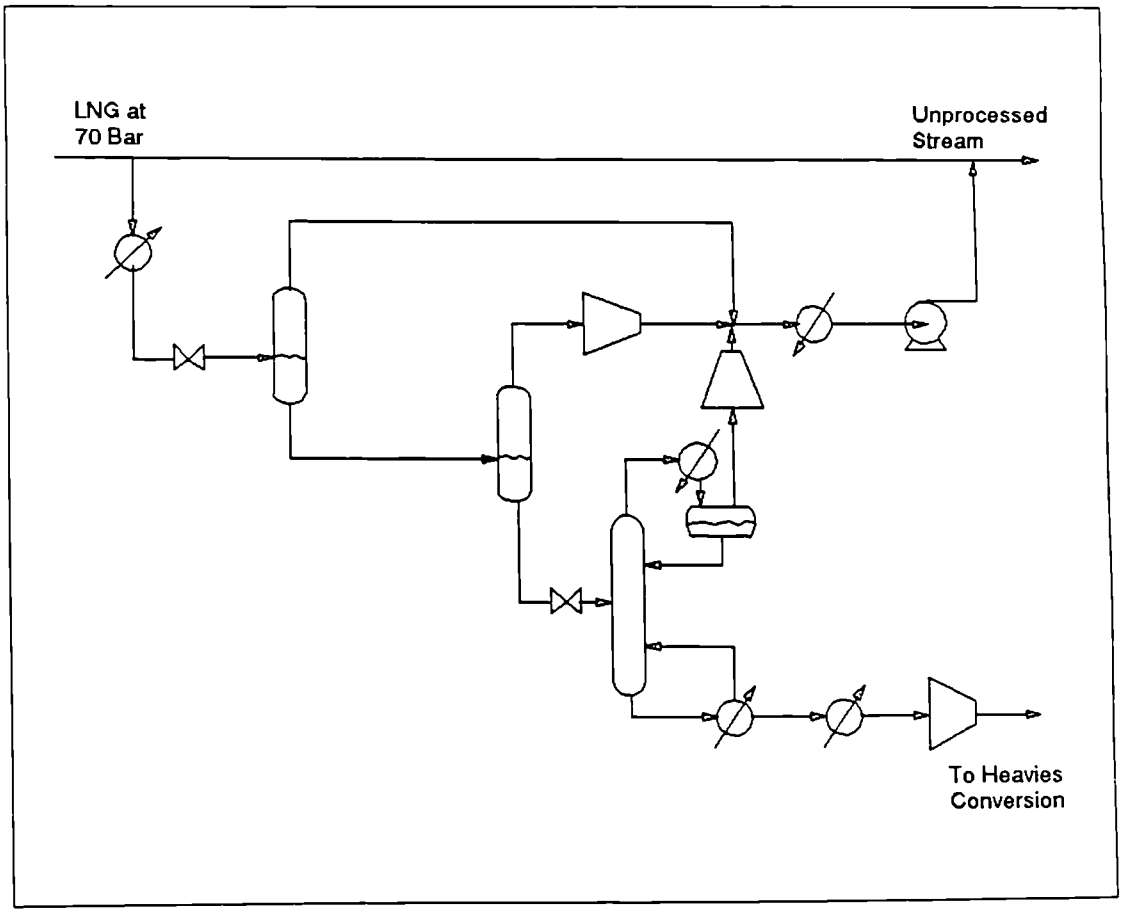

Figure 2.10 Distillation column Arrangement 2

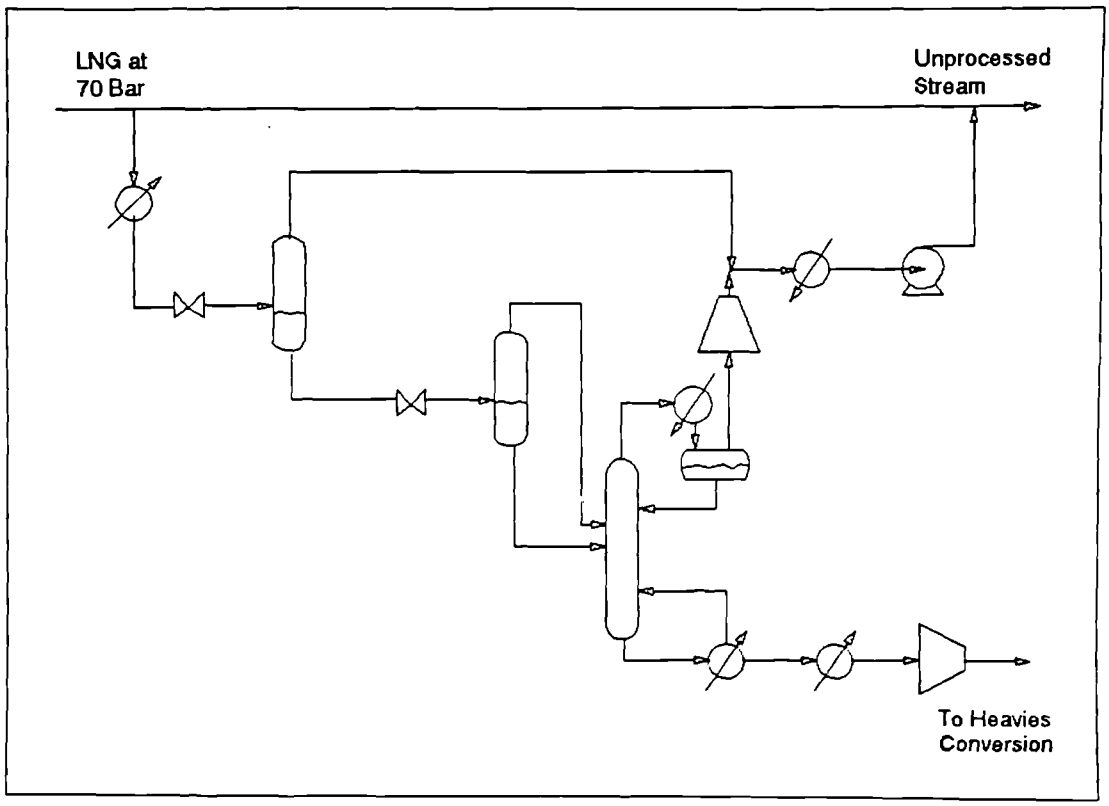

Figure 2.11 Distillation column Arrangement 3

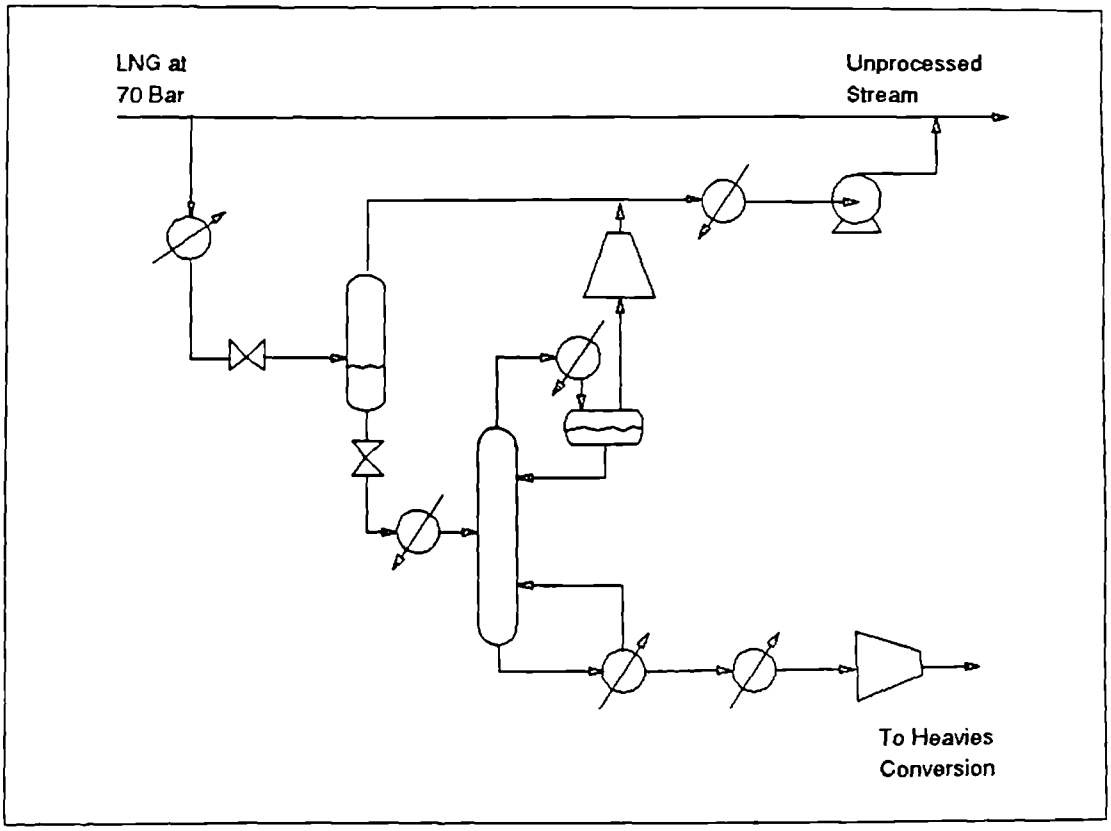

Figure 2.12 Distillation column Arrangement 4

except there are two single phase feeds (vapour and liquid), separated by one stage.

(iv) Arrangement 4 - The bottom product of the flash unit is expanded to column pressure and cooled, thus entering the column as a liquid feed. This arrangement is illustrated in Figure 2.12.

2.5.1.2 *Comparison of Distillation Column Arrangements*

The GL1Z feedstock condition was selected for distillation column modelling as previous simulation results showed that this feedstock condition, with high heavy hydrocarbon content, sent the greatest proportion of feed to the heavies processing section. Hence, this represented the most demanding operating condition for the distillation column, and formed the basis for designing maximum flows and separation requirements.

Each column arrangement was modelled in the steady state, and two column operating pressures were initially investigated: 35 and 40 bar. The splitter was ignored and as the revised split ratio was unknown at this stage, the simulation was based on a nominal GL1Z feed rate of 100 kgmol/hr in the flash unit. The corresponding bottom product stream conditions are given in Table 2.9, representing feed conditions to the distillation column arrangements.

GL1Z FEEDSTOCK	100 kgmol/hr
FLASH UNIT BOTTOM PRODUCT COMPOSITION	
CH_4	34.62
C_2H_6	5.42
C_3H_8	2.35
nC_4H_{10}	0.39
iC_4H_{10}	0.48
nC_5H_{12}	0.01
N_2	0.21
FLOW RATE (kgmol/hr)	43.49
FLASH TEMPERATURE (^{o}C)	-69.79
FLASH PRESSURE (bar)	48.09

Table 2.9 Flash unit bottom product composition

The separation arrangements were modelled to achieve a similar methane recovery in the combined unprocessed stream. Preliminary

steady state simulation results showed that reducing column pressure from 40 to 35 bar resulted in a reduced reflux ratio and smaller reboiler and condenser duties for each arrangement. However, this lead to increased heating, cooling and power requirements downstream. Nevertheless, it was decided to adopt the lower operating pressure of 35 bar, as this would be further from the critical pressure and hence provide more reliable separation. In addition, unit capital costs would reduce and a safer operating environment would be attained.

The steady state simulation results in Table 2.10 indicate that the arrangements gave similar degrees of separation. In terms of operating costs, Arrangement 2 required the lowest condenser and reboiler duties for the column. A comparison of the peripheral units suggested that the capital costs associated with Arrangements 2 and 3 would be higher as both required an additional upstream flash unit. This would also have an adverse effect on column controllability. Therefore, Arrangements 1 and 4 were preferred as they represented standard distillation column arrangements, with a smaller reflux ratio and good unit performance.

The practice of introducing a two-phase feed to a column is not recommended by leading distillation column manufacturers, as flashing within the column may dislodge lower trays. Therefore, Arrangement 4 was selected as the final distillation column for inclusion in Scheme 24.

2.5.1.3 *Conclusions on Scheme 24 Enhancement*

Several distillation arrangements were investigated to demonstrate the potential of including a distillation column in the process route for Scheme 24. Although the lower operating pressure of 35 bar was chosen, it is still rather high and this may cause additional problems at the material design, control and operation stages. Hence, it was decided to retain the existing column without attempting to optimize the design of the distillation arrangement further. Therefore, a distillation column arrangement was selected from the existing work for comparison in the inter-family selection. Arrangement 4 was considered the most suitable option for the required separation section as the column accepts a conventional

liquid feed and requires few additional units. The revised flowsheet, renamed Scheme 25, was modelled according to the previously developed process routes.

Column Conditions	ARRANGEMENT			
	1	2	3	4
COLUMN PRESSURE (bar)	35	35	35	35
REFLUX RATIO	0.382	0.449	0.450	0.235
TOTAL STAGES	10	11	10	10
FEED TRAY(S)	6	5	5,6	6
TOP PRODUCT COMPONENTS				
CH_4	33.91	10.09	33.94	33.93
C_2H_6	0.14	0.09	0.31	0.25
C_3H_8	0.00	0.00	0.00	0.00
nC_4H_{10}	0.00	0.00	0.00	0.00
iC_4H_{10}	0.00	0.00	0.00	0.00
nC_5H_{12}	0.00	0.00	0.00	0.00
N_2	0.21	0.02	0.21	0.21
FLOW RATE (kgmol/hr)	34.26	10.20	34.46	34.40
TEMPERATURE(^{o}C)	-90.71	-89.04	-89.19	-89.69
BOTTOM PRODUCT COMPONENTS				
CH_4	0.70	0.21	0.68	0.69
C_2H_6	5.29	4.23	5.11	5.16
C_3H_8	2.35	2.24	2.35	2.35
nC_4H_{10}	0.39	0.39	0.39	0.39
iC_4H_{10}	0.48	0.48	0.48	0.48
nC_5H_{12}	0.01	0.01	0.01	0.01
N_2	0.00	0.00	0.00	0.00
FLOW RATE (kgmol/hr)	9.23	7.55	9.3	9.09
TEMPERATURE (^{o}C)	21.64	38.06	22.32	22.12
CONDENSER DUTY (MJ/hr)	-52.9	-21.9	-74.8	-36.9
REBOILER DUTY (MJ/hr)	225.3	140.1	147.8	260.0
TOTAL FEED TO UNPROCESSED STREAM				
CH_4	87.50	88.00	86.46	87.52
C_2H_6	1.98	3.04	2.28	2.09
C_3H_8	0.26	0.36	0.26	0.26
nC_4H_{10}	0.02	0.02	0.02	0.02
iC_4H_{10}	0.02	0.02	0.02	0.02
nC_5H_{12}	0.00	0.00	0.00	0.00
N_2	1.00	1.00	1.00	1.00
FLOW RATE (kgmol/hr)	90.77	92.45	90.04	90.91

Table 2.10 Steady state results for distillation arrangements

2.5.2 Comparison of the Revised Flowsheets

The *best* intra-family flowsheets, Schemes 14 and 24, were compared with the most recently developed process route, Scheme 25. The simulation results for Scheme 25 are also included in Appendix 2. A comparison of the three process routes, Schemes 14, 24 and 25, was conducted using the procedure described in Section 2.4, and focusing on Scheme 25.

The results in Table 2.11 demonstrate that Scheme 25 required a greater feed rate and produced a lighter export gas, as more of the heaviest hydrocarbons were converted. The heavies processed stream in Scheme 24 was greatly reduced by including a distillation column. This has a cost benefit on equipment downstream of the column. Scheme 14 still sent the smallest proportion of its feed to heavies conversion, and thus produced the least effluent. Scheme 25 showed a reduction in waste water over Scheme 24. Although Scheme 25 required the greatest total power, its compression power requirements were significantly less, representing an improved power distribution. Scheme 25 also required the greatest proportion of cryogenic heat, which is the most expensive heat form. By comparison, its fired heat requirement was small, indicating an overall poor heat distribution. Its cooling breakdown was an improvement on that of Scheme 24.

The turndown ratios associated with LNG feed requirements and plant yield in Table 2.12 are comparable for each process route. Incorporating a distillation column in Scheme 24 has resulted in similar turndown results.

The selection criteria results have shown that the performance of Scheme 24 improved in several areas by the addition of a distillation column. The improved methane recovery in the top product separation section of Scheme 25 has enabled the split ratio to be reduced more than twofold over Scheme 24. This contributed to the lower steam requirement and effluent treatment. The power and cooling requirements have also improved. Moreover, the high turndown ratios, which indicate good feedstock flexibility, have been maintained. However, the LNG feed rate and heating requirements have increased.

Selection Criterion	Scheme		
	14	24	25
Production			
Feed (kg/s)	52.83	52.74	77.62
kg Product/kg Feed	1.016	0.990	0.990
Wobbe No. Position	0.675	0.815	0.857
Heavies Processing			
Heavies Stream (kg/s)	1.269	15.353	9.591
Turndown (%)	45.0	75.6	70.4
Steam (kg/s)	3.685	46.163	28.876
Effluent Treatment			
Waste Water (kg/s)	1.86	43.63	25.13
Waste CO_2 (kg/s)	0.83	3.06	4.44
Total Power			
Total Power (kW)	3248.	3058.	3586.
Compression Power (kW)	2173.	1791.	1101.
Nett Heating Analysis			
Cryogenic Heat (kW)	1265. (2%)	15078. (24%)	30192. (33%)
Fired Heat (kW)	2752. (4%)	5448. (9%)	2455. (3%)
Process Heat (kW)	16667. (27%)	11841. (19%)	17711. (20%)
Nett Heating (kW)	61119.	63021.	90133.
Nett Cooling Analysis			
Cryogenic Cooling (kW)	440.	4222.	19634.
Process Cooling (kW)	18190.	137251.	84507.
Nett Cooling (kW)	18631.	141472.	104141.

Table 2.11 Revised inter-family selection criteria

Selection Criteria	Scheme		
	14	24	25
Feed (kg/s)	99.5	99.2	95.9
kg Product/kg Feed	98.8	99.2	99.3
Wobbe No. Position	82.9	95.5	98.3
Heavies Stream (kg/s)	45.0	75.6	70.4
Steam (kg/s)	59.4	75.4	71.2
Effluent Flow (kg/s)	43.2	75.2	70.0
Total Power (kW)	60.6	84.1	87.4
Compression Power (kW)	43.4	76.3	71.7
Nett Heating (kW)	86.7	90.3	93.2
Nett Cooling (kW)	44.0	74.9	74.6

Table 2.12 Turndown ratios for inter-family selection

Scheme 14 still gives the best yield and export gas quality, and competitive operating costs. However, its low turndown ratios suggest that many streams may have to be operated in parallel to accommodate the significant turndown in flow rates and duties.

Therefore, as adding a distillation column to Scheme 24 does have distinct advantages, without impairing plant flexibility, Scheme 25 was selected as the *best* preliminary flowsheet design.

2.6 PRELIMINARY FLOWSHEET DESIGN

The preliminary flowsheet design was obtained from a detailed assessment of related process routes, which considered different options for the separation and heavies conversion processes. Scheme 25 was selected as the *best* process route in Section 2.5. As the flowsheet selection was based on an outline flowsheet assessment, only essential units were incorporated. As none of the individual units have been integrated or improved, the steady state simulations represented sub-optimal results for each flowsheet design.

2.6.1 Flowsheet Refinements

The comparison study in Sections 2.4 and 2.5 highlighted several areas in which overall plant performance could be further improved. These included:

(i) *Split pumping* - The initial pumping of LNG feed up to distribution pressure may be broken down into two stages. As the downstream flash pressure is 48.09 bars, the feed need only be a few bars above. Thus, with initial pumping up to say 52 bars, an additional pump may be incorporated to raise the unprocessed stream to distribution pressure after the split operation.

(ii) *Distillation column* - In Scheme 25, the distillation column top product is condensed and then compressed before mixing to form the unprocessed stream. Hence, as a liquid stream is desired, it would be appropriate to substitute the partial condenser by a total condenser. This would require an extra tray within the column to compensate for the top stage (partial condenser) tray removal.

(iii) *Nitrogen blending* - To reduce the C.V. of the export gas, the heavy hydrocarbon stream could be diluted with an inert gas such as nitrogen, which is already present in the LNG feedstocks.

The above recommendations were introduced to Scheme 25. Split pumping resulted in a 25% reduction in the total power requirement. In the distillation column, the partial condenser was replaced. Product purity was maintained by the addition of a theoretical tray, bringing the total number of trays to 11.

Nitrogen blending was also introduced to the process route, and set at a constant ratio of 3.5% of the unprocessed stream flow rate. This was added immediately before the unprocessed and processed streams were finally blended. The corresponding steady state simulation results show a marked reduction in feed stream flow rate. In addition, the total power requirement was halved and heating and cooling requirements were also reduced. However, the turndown ratios were significantly lower for most selection criteria, indicating reduced feedstock flexibility. The reduction in utilities and processed stream equipment size must, therefore, be balanced against excessive turndown. This may be overcome by tuning the nitrogen feed rate to an acceptable level for each feedstock condition. Moreover, nitrogen blending may be introduced as a final variable to maintain target C.V. and avoid further corrective action. Hence, nitrogen blending should be considered as a worthwhile addition to an LNG importation terminal design. This option was not pursued in this design study.

2.6.2 The Selected Flowsheet Arrangement: Summary

The revised process route for the LNG reception terminal, Scheme 25 Revision 1, is illustrated in Figure 2.13 and described below.

The LNG feedstock, stored at atmospheric pressure and -170°C, is initially pumped up to 52 bar before splitting. The smaller stream is then flashed at 48.09 bar, according to the flash temperatures in Table 2.3. The liquid bottom product is expanded and then cooled to between -83°C and -88°C to form a liquid at 35.1 bar. This stream enters the distillation column on tray 6. The column is operated at 35 bar with 11 theoretical trays, plus a total condenser and reboiler.

The distillation column and flash unit top products are compressed to 70 bar and combined. Blending with the other split stream forms the unprocessed stream, which is vaporised to 10°C by the ORV unit. The distillation column bottom product becomes the heavies processed stream. This stream is compressed to 46 bar and heated to 400°C, by a heat exchanger and fired heater. Steam is added at a mass flow rate set at three times that of the hydrocarbon feed, for CRG

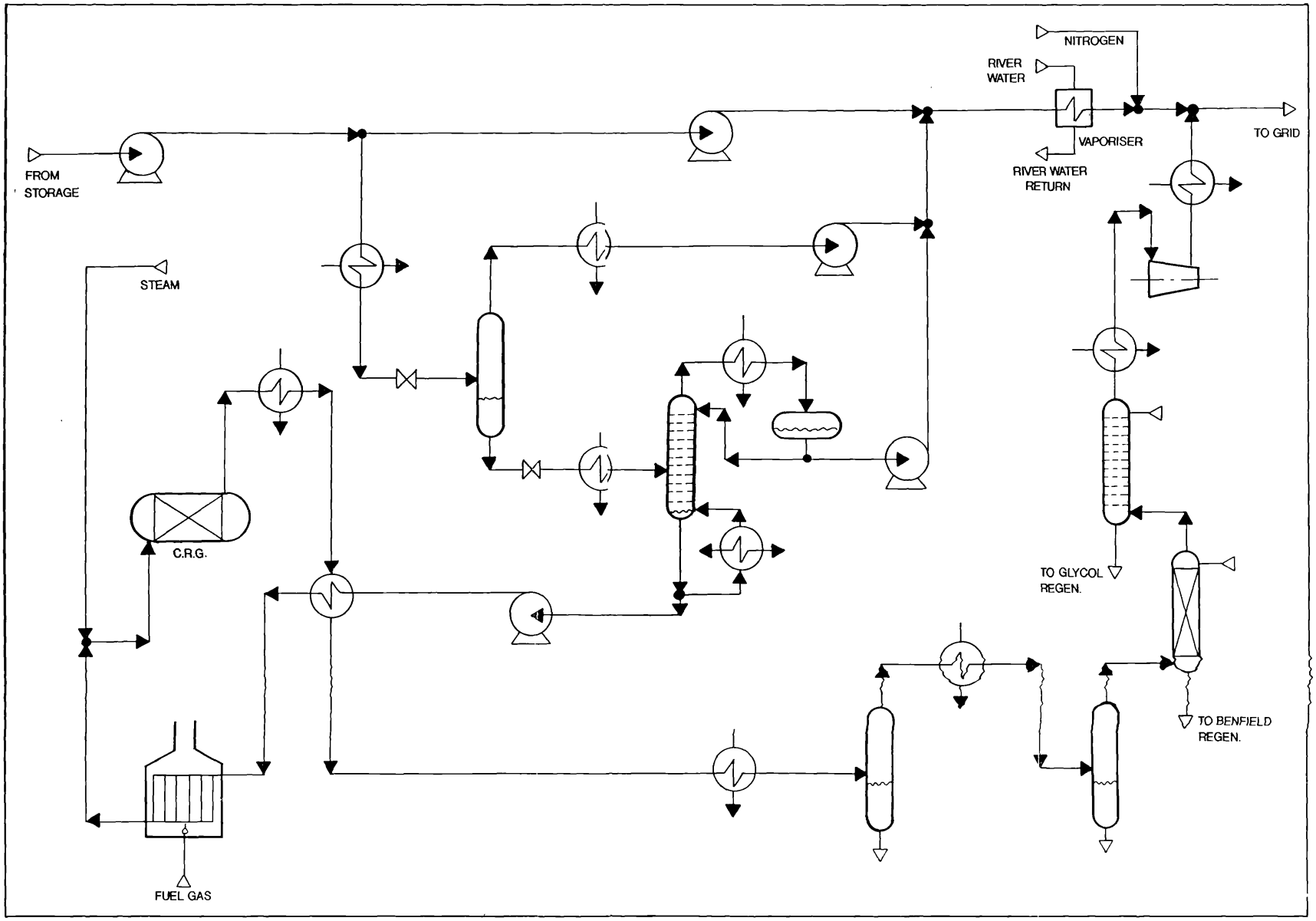

Figure 2.13 Preliminary LNG reception terminal flowsheet

reforming. The reformer outlet stream conditions for each feedstock, dry basis, are given in Table 2.13.

Condition	Feedstock		
Component (mol %)	GL1K	GL2Z	GL1Z
CH_4	78.51	72.41	71.71
CO	0.05	0.11	0.12
CO_2	10.17	15.34	15.93
H_2	11.21	12.14	12.24
N_2	0.06	0.00	0.00
Temperature (°C)	405	429	432

Table 2.13 HP CRG reformer product compositions

The reformer outlet stream is progressively cooled and condensate is removed by intermediate knock-out pots. After CO_2-removal and drying, the heavies processed stream is compressed to 70 bar and cooled to 10°C, prior to blending with the unprocessed stream to form the export gas.

The full operating conditions for the preliminary flowsheet design are tabulated in Appendix 3.

2.7 ACHIEVEMENTS AND CONCLUSIONS

In this chapter, the design of a preliminary flowsheet for the proposed LNG reception terminal was described. The final flowsheet is shown to have the required flexibility for processing the range of LNG feedstocks. However, in arriving at this flowsheet, a novel method of assessing feedstock flexibility has been developed.

Operational requirements and product specifications were used to define an outline flowsheet. This became the basis for initially identifying nine potential process routes, to investigate various separation and heavies conversion process options. An assessment of each flowsheet design was based on steady state simulation data for each LNG feedstock condition. Selection criteria were devised to extract and compare relevant simulation results. This concerned the relative values of productivity, operating costs and throughput. The turndown ratios associated with key parameters in the criteria were used to assess plant flexibility. The selection procedure was relative with greater emphasis on those utilities which were comparatively more expensive, particularly in the heat analysis. As two of the process routes satisfied the selection criteria, a means of upgrading one of the flowsheets was pursued. The upgraded flowsheet, Scheme 25, was selected as the *best* flowsheet. In selecting a final flowsheet for this plant, the actual capital and operating costs would have to be considered in more detail, as would peripheral units which provide refrigeration cycles, steam and sea/river water pumping.

The importance of feedstock flexibility as a design objective was emphasised by the equal attention paid to simulation data for each of the LNG feedstock conditions. The development of the selection criteria provided a tool for assessing the impact of process design changes on feedstock flexibility and operating costs.

The selected flowsheet represents a preliminary process route for the LNG reception terminal. However, validation of this flowsheet design during feedstock changeover can only be addressed by assessing its dynamic behaviour. This will be discussed in the following chapters.

CHAPTER 3

DYNAMIC MODELS FOR PROCESS UNITS

3.1 INTRODUCTION

Prior to embarking on the dynamic simulation of the preliminary flowsheet, mathematical models for the individual process units have to be developed from first principles. This chapter documents the search for and selection of suitable models for each process unit.

Scheme 25 was selected in Chapter 2 as the preliminary flowsheet for dynamic simulation and control studies. As the flowsheet contains many operations, a compromise has to be reached between model size, complexity and accuracy to enable the implementation of the overall dynamic simulation. Furthermore, the key design objective of feedstock flexibility has to be accurately modelled. Therefore, each operation will be modelled for multicomponent stream conditions, where practical. Finally, for those operations with relatively fast dynamics, it is likely that steady state models will be adequate. These assumptions are discussed in Section 3.2.

Of the twelve plant items, seven required development of dynamic models. Section 3.3 describes a review of available models and the development of customised models suitable for this simulation. The remaining operations were described by steady state models only, and Section 3.3 also describes these.

The models for the individual process units are essential tools for dynamic studies of plantwide operability and control, which will be described in later chapters.

3.2 DYNAMIC MODELLING

A dynamic model is a mathematical description of a real process that incorporates the key features of its dynamic behaviour. Model development must reflect the level of accuracy required, the availability of data, and the application. In this study, the dynamic simulation was primarily used to:

(i) Understand the process dynamics - by studying the plant behaviour at multiple operating conditions and during feedstock changeover.

(ii) Design the control structure - by assessing different control strategies.

(iii) Select appropriate controllers and settings - by conducting tests on the simulation that would not normally be possible on a real process.

Mathematical models may be derived either from first principles (theoretical), plant data (empirical), or a combination of both (semi-empirical models). As this study is in the preliminary design stage, the dynamic models for each operation have been based solely on theoretical models. The models for twelve different operations are presented in this chapter, and are listed in Table 3.1.

Operation	No. off	Operation	No. off
Distillation column	1	Absorber	2
CRG reformer	1	Pump	5
Flash unit	1	Knock-out pot	2
Heat exchanger	9	Compressor	1
Fired heater	1	Mixer	5
ORV	1	Splitter	1

Table 3.1 Flowsheet operations

The dynamic behaviour of process units is commonly represented in two forms. The *transfer function* model describes a linear dynamic relationship between the input and output of a system, and is usually expressed as a Laplace transform. However, the accuracy of this simplified model is limited by the degree of non-linearity in the real process. Greater accuracy can be obtained from *non-linear equation based* models that are derived from the fundamental

relationships within a system. These equations are based on the conservation of mass, energy and momentum, and describe the physical and chemical system relationships.

In the plant simulation, it would be impractical to describe each unit using rigorous mathematical models, especially when some dynamic behaviour may be so fast that it is insignificant in a plantwide context. So, those operations with relatively fast dynamics have been replaced by steady state models. Predominantly dynamic modes have been modelled using non-linear equation based models.

3.2.1 Process Stream Conditions

The distillation column represents the most complex dynamic model in the preliminary flowsheet. To reduce the modelling requirements for this operation, the feasibility of approximating multicomponent process streams by pseudo-binary streams, for multiple LNG feedstock conditions, was investigated.

For each LNG feedstock condition in the distillation column, listed in Table 3.2, the top product contains 99% methane, almost all the nitrogen, and some ethane. The bottom product contains the remaining methane and ethane, and all other heavy hydrocarbons. Therefore, it seems reasonable to equate the dominant top product component (methane) as a *light* key component and the remaining composition as a *heavy* key component, within the column. This procedure would permit a pseudo-binary operation to mimic the multicomponent model, while retaining the key features of a multicomponent stream.

Although the pseudo-binary approximation may be feasible for the separation process, difficulties arise with other units. In particular, in the CRG reformer each hydrocarbon component is converted according to a specific chemical reaction (Appendix 1). Thus, the conversion of a heavies component cannot be generalised. Similarly, the physical properties of each pseudo-binary stream in the flowsheet would have to be approximated by a weighting function on the *heavy* component, which could range from pure ethane to the heaviest hydrocarbons. Hence, the pseudo-binary process stream description has only been applied to the distillation column.

GL1K feedstock *			
Component	Feed	Top (%)	Bottom
CH_4	5957.5	5200.9 (99.0)	756.6
C_2H_6	50.2	20.6 (0.4)	481.2
C_3H_8	53.8	--	53.8
iC_4H_{10}	23.6	--	23.6
N_2	35.8	34.9 (0.6)	1.3
Total Flow (kgmol/hr)	6572.5	5256.0 (100)	1316.5

GL2Z feedstock *			
Component	Feed	Top (%)	Bottom
CH_4	5213.9	5104.4 (99.0)	109.5
C_2H_6	582.5	21.0 (0.4)	561.5
C_3H_8	178.9	--	178.9
nC_4H_{10}	46.1	--	46.1
iC_4H_{10}	33.8	--	33.8
nC_5H_{12}	15.7	--	15.7
N_2	29.1	29.1 (0.6)	--
Total Flow (kgmol/hr)	6100.0	5154.5 (100)	945.5

GL1Z feedstock *			
Component	Feed	Top (%)	Bottom
CH_4	4287.5	4248.9 (99.0)	38.6
C_2H_6	702.7	16.2 (0.4)	686.5
C_3H_8	308.3	--	308.3
nC_4H_{10}	64.9	--	64.9
iC_4H_{10}	52.8	--	52.8
nC_5H_{12}	1.5	--	1.5
N_2	27.8	27.8 (0.6)	--
Total Flow (kgmol/hr)	5445.6	4292.9 (100)	1152.7

* from Scheme 25, Rev.1

Table 3.2 Steady state distillation column results

3.2.2 General Modelling Assumptions

Several assumptions have been introduced to the dynamic simulation in trying to reduce model size. For example, a length of interconnecting pipe between units may delay the propagation of flow variations, in either direction. However, as the preliminary flowsheet design in Chapter 2 has not included pipework specifications, the dynamics of the flow processes can only be approximated. Therefore, the pipework dynamics have been assumed negligible. It should be noted that operating pressure has been externally set for most units.

The pneumatic control valve is a common form of final control element. This type of valve exhibits inherent first-order dynamics. However, fast acting control valves have been assumed for the flowsheet, with a typical stroke time of under 10 seconds. Thus, the response is so fast that the dynamics can be neglected (Stephanopoulos, 1984). In this simulation, each valve has been described by a steady state model. For a linearly installed valve, a known relationship exists between valve position and flow rate, assuming a constant pressure drop across the valve. Generally, the pressure drop is variable (Shinskey, 1988), but as the pipework dynamics have not been considered it would be inconsistent to model this effect in isolation. So, a constant pressure drop has usually been assumed.

3.3 DYNAMIC MODELS FOR INDIVIDUAL PROCESS UNITS

This section describes suitable mathematical models to simulate each unit in the preliminary flowsheet, for a multicomponent system. Each dynamic model has been selected following a literature survey of available models. Those units represented by dynamic models are described in detail. The remaining steady state model approximations are summarised at the end of this section.

An interactive physical properties database has been included in the completed flowsheet simulation, and is described in detail in Chapter 4. Therefore, the dynamic models have been developed on the basis of variable physical property values. Any deficiencies in the recommended models have been noted.

3.3.1 Distillation Column

The distillation column in the preliminary flowsheet forms the final part of the separation process. This unit is the only operation to be described by a pseudo-binary component system. The column is operated at 35 bar, with 11 theoretical trays, and a total condenser and reboiler. The top product is a methane-rich gas, and the bottom product contains mostly heavies for CRG reforming.

3.3.1.1 *Distillation Column Dynamic Models*

The dynamic model of a distillation column is generally based on a staged structure, with mathematical descriptions of the individual trays, heat exchanger elements and drums. The following review of available dynamic models describes a range in complexity from the rigorous, multicomponent form to a very simplified linearised approximation.

Rigorous multicomponent models

Each tray in the recycle structure of a column can be associated with three lags, which describe different aspects of the dynamic behaviour. The variation in component concentration on a tray is usually slow. Propagation of liquid flow changes is faster, relating to flow variations in the column. The fastest dynamics are associated with vapour flow changes, and are caused by pressure

changes. Hence, a fundamental assumption in most dynamic models is that vapour dynamics are very fast and can be neglected in the formulation of the model.

A comprehensive mathematical model of a distillation column was presented by Gani et al. (1986). The model consisted of ordinary differential equations (ODEs) representing mass, component and energy balances on each tray, and a set of algebraic equations for the thermodynamics and plate hydraulics. The following general assumptions were made:

(i) Vapour hold up is negligible.

(ii) Liquid and vapour leaving each tray are in thermal equilibrium.

(iii) Liquid and vapour are perfectly mixed, and Murphree's tray efficiency applies to the vapour composition.

Thus, for an n-component feed, (n-1) component balances, plus a total mass and energy balance would be required to describe each tray. These ODEs were based on the conservation principle for a tray model, shown in Figure 3.1, where L and V represent the liquid and vapour flows, F is the feed, and E is the entrainment flow rate. The vapour liquid equilibrium relationship, and physical property and hydraulic correlations were defined as functions of temperature, pressure, composition and tray dimensions. A solution algorithm was presented for the dynamic model such that for a given liquid phase composition and enthalpy on each tray, the vapour phase composition, temperature and pressure were derived.

A simpler model of the multicomponent distillation column was developed by Peiser and Grover (1962) that introduced additional assumptions to the tray hydraulic relationship. In this model, the Francis weir formula was adopted to relate the liquid down flow from a tray, L_i, to the liquid head using the general form:

$$L_i = c \sqrt{2g}\, \rho_{L,i}\, (h_i - h_w)^{3/2} \qquad (3.1)$$

where c is a constant, g is gravitational acceleration, ρ_L is liquid stream density and h_i and h_w represent the liquid and weir heights on a tray, respectively. The liquid level, h_i was then derived from a pressure balance over each tray.

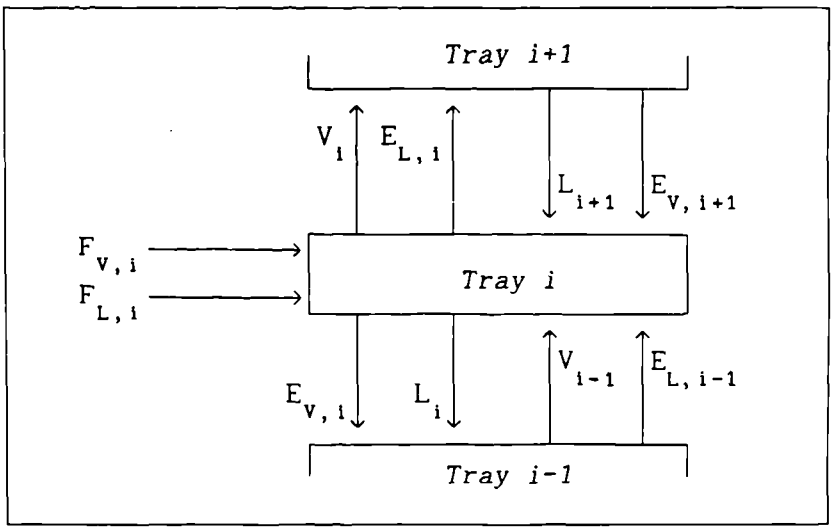

Figure 3.1 Vapour and liquid flow rates in tray i

Distillation column model reduction techniques

Cho and Joseph (1983a) developed a reduced-order dynamic model for the distillation column. The model reduction procedure approximated the column as a spatially distributed system in which the composition and flow profiles were represented as continuous variables along the length of the column.

Two approaches to reduced-order approximations were developed. The first was based on approximating the tray-by-tray differential equations. These partial differential equations (PDEs) were in turn solved by the orthogonal collocation method. In the second approach, the model reduction was achieved by a direct transition of the PDEs to polynomial representations of the composition and flow profiles in the column. On comparison with a rigorous model, the reduced-order models' results gave good accuracy with a large decrease in model dimensionality, especially for larger columns. Also, it was found that accuracy improved by placing collocation points where the nonlinearity was more pronounced.

This model reduction exercise showed that the number of equations required to describe a multicomponent distillation column could be drastically reduced and yet still produce satisfactory results. The use of polynomials to represent tray conditions was also validated (Cho and Joseph, 1983b).

Dynamic modelling assumptions

Although most dynamic models assume negligible vapour hold up, Choe and Luyben (1987) have demonstrated the inaccuracy inherent in this assumption. They recommended that vapour hold up be included in column models where the vapour density becomes significant compared to the liquid density. For most common materials, this corresponds to pressure in excess of 5-10 bar. Kinoshita (1986) also investigated this assumption, in the presence of extremely volatile components. Simulation results showed that neglecting the vapour hold up predicted faster changes in both liquid and vapour tray compositions than would occur in a rigorous model.

Thus, for high volatility component separation or high pressure conditions, both Kinoshita (1986) and Choe and Luyben (1987) recommended that vapour hold up should be included in model development. However, this feature would greatly add to the complexity of the dynamic model, as conservation equations would be required for both the liquid and vapour phases (effectively doubling the number of equations on each tray). Therefore, vapour hold up has been ignored in this study.

Simplified binary component models

A non-linear simulation model of a binary component distillation column was established by Foss (1983) for preliminary control studies. Besides the general assumptions, a constant thermal energy was assumed with negligible exchange of enthalpy between liquid and vapour streams. This eliminated an energy balance equation, and hence only two state variables remained on each tray: liquid molar hold up, and the mole fraction of light component. The liquid overflow was derived using the Francis weir formula (3.1). Vapour composition, y_i, was expressed in terms of the liquid composition, x_i, on each tray:

$$y_i = \frac{\alpha x_i}{1 - (\alpha - 1) x_i} \qquad \text{for } \alpha > 1 \qquad (3.2)$$

where the relative volatility, α, was assumed constant. As reflux dynamics from the top of the column were assumed relatively fast they were neglected. However, the reboiler dynamics were approximated by a first-order lag. The open-loop results verified that the dynamics

of the nonlinear model were governed by the hydraulic and composition modes, where the dynamics of the former are faster.

Low fidelity models

Simple analytical models of distillation column dynamic behaviour are usually derived from plant data or an accurate dynamic model, using some form of linearisation technique. Linear input-output models are often applied in transfer function form as a basis for control studies (Skogestad and Morari, 1988). However, the inherent recycle structure of the distillation column can often lead to inaccurate time constant approximations (Kapoor et al., 1986). These analytical expressions for a linearised model may be sometimes derived from steady state data and design information (Kapoor and McAvoy, 1987).

3.3.1.2 *Pseudo-binary Component System Model*

A rigorous dynamic model of the distillation column would be complex and may result in excessive runtime during simulation. Therefore, a pseudo-binary component model has been developed to represent the multicomponent system, consisting of methane (*light* key) and heavy hydrocarbon plus nitrogen (*heavy* key) components.

The recommended model is based on an ideal binary distillation column (Stephanopoulos, 1984) with the following simplifying assumptions:

(i) Vapour hold up on each tray is negligible.
(ii) Each liquid stage is well mixed, with no interstage backmixing.
(iii) Each tray is 100% efficient.
(iv) There is negligible heat exchange with the environment.
(v) The feed and reflux streams are saturated liquids.
(vi) The column operates at a single pressure which changes instantly in response to external pressure changes. So, there are no pressure dynamics and a negligible pressure gradient.
(vii) The molar flow rate of liquid leaving each tray is related to the liquid hold up on the tray.

Three state equations are required to fully describe the mass and energy transfer on each tray in a binary system. The state variables

are liquid hold up, M_i, mole fraction of the light component in the liquid phase, x_i, and liquid enthalpy, $h_{L,i}$. The following state equations account for mass transfer in the column, with the stream notation defined in Figures 3.2 and 3.3.

Reflux drum:

$$\frac{d(M_{RD})}{dt} = V_N - L - D \tag{3.3}$$

$$\frac{d(M_{RD}x_D)}{dt} = V_N y_N - (L + D) x_D \tag{3.4}$$

Top tray (i = N):

$$\frac{d(M_N)}{dt} = L + V_{N-1} - L_N - V_N \tag{3.5}$$

$$\frac{d(M_N x_N)}{dt} = Lx_D + V_{N-1}y_{N-1} - L_N x_N - V_N y_N \tag{3.6}$$

Intermediate trays (except feed):

$$\frac{d(M_i)}{dt} = L_{i+1} + V_{i-1} - L_i - V_i \tag{3.7}$$

$$\frac{d(M_i x_i)}{dt} = L_{i+1} x_{i+1} + V_{i-1}y_{i-1} - L_i x_i - V_i y_i \tag{3.8}$$

Feed tray (i = f):

$$\frac{d(M_f)}{dt} = F_f + L_{f+1} + V_{f-1} - L_f - V_f \tag{3.9}$$

$$\frac{d(M_f x_f)}{dt} = F_f x_f + L_{f+1}x_{f+1} + V_{f-1}y_{f-1} - L_f x_f - V_f y_f \tag{3.10}$$

Bottom tray (i = 1):

$$\frac{d(M_1)}{dt} = L_2 + V - L_1 - V_1 \tag{3.11}$$

$$\frac{d(M_1 x_1)}{dt} = L_2 x_2 + Vy_B - L_1 x_1 - V_1 y_1 \tag{3.12}$$

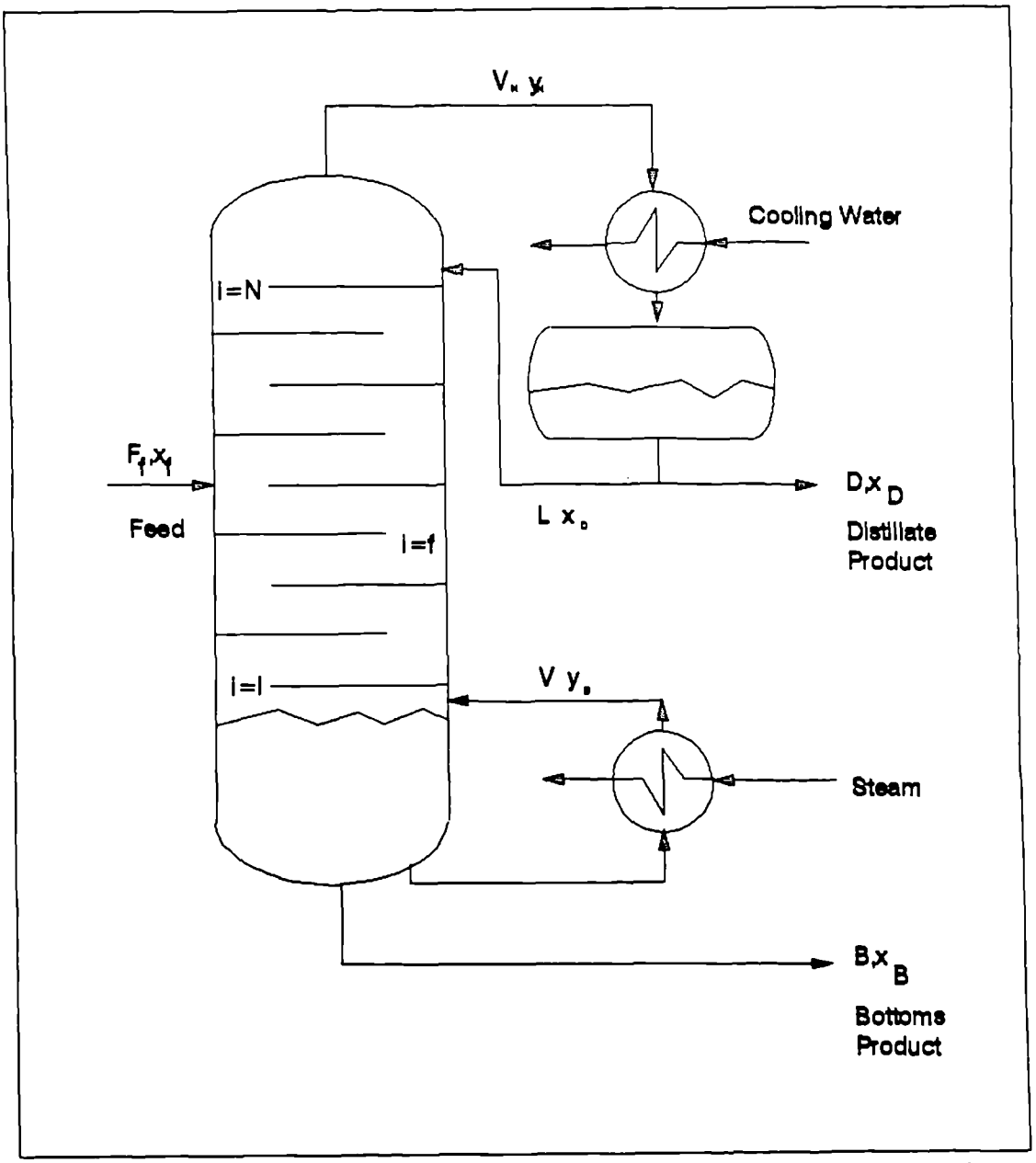

Figure 3.2 Distillation column arrangement

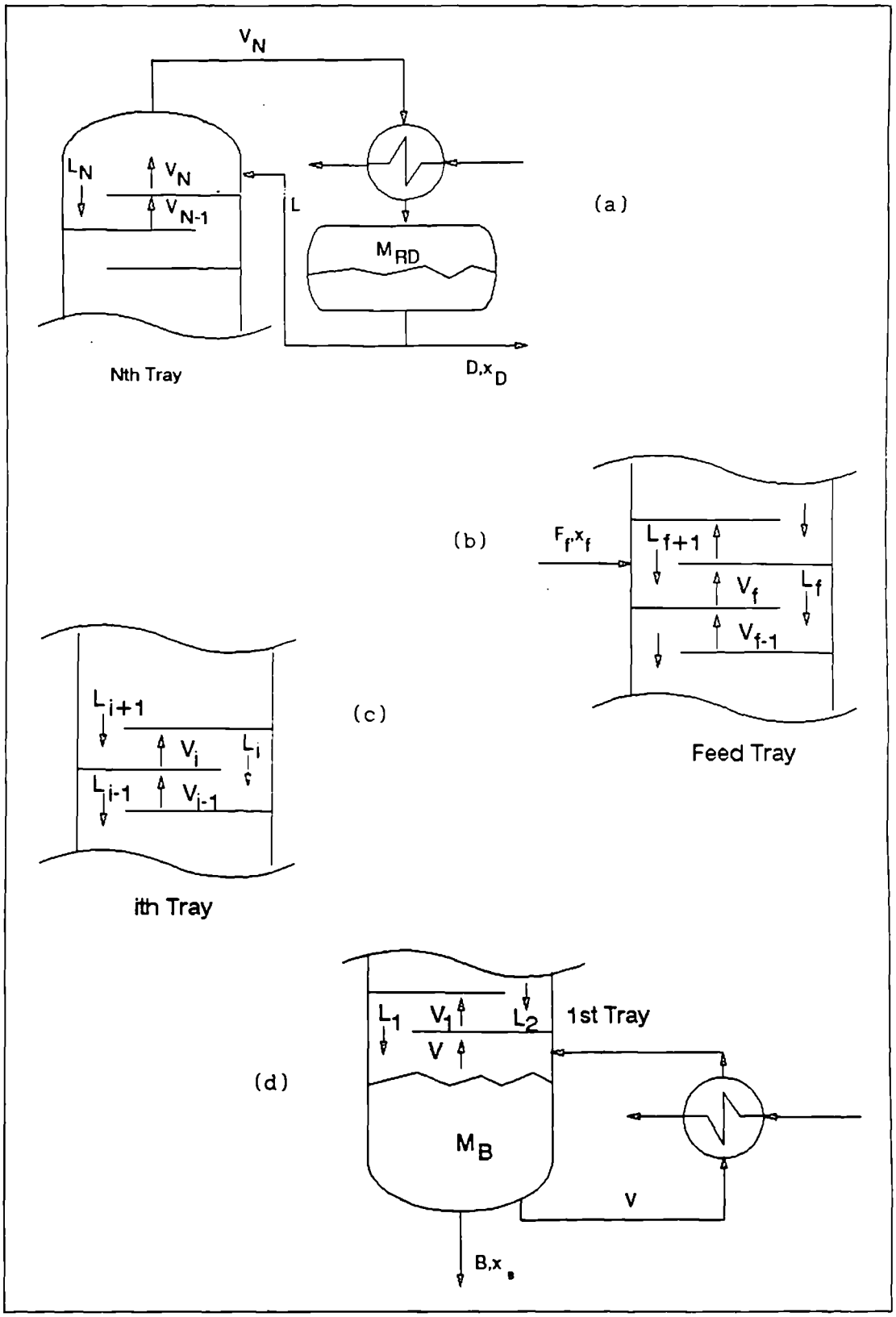

Figure 3.3 Tray modelling details for a binary distillation column
(a) top tray and condenser, (b) feed tray,
(c) intermediate tray, i, (c) bottom tray and reboiler

Column base:

$$\frac{d(M_B)}{dt} = L_1 - V - B \qquad (3.13)$$

$$\frac{d(M_B x_B)}{dt} = L_1 x_1 - V y_B - B x_B \qquad (3.14)$$

x_i and y_i refer to liquid and vapour compositions on each tray. An energy balance equation was introduced to calculate the vapour flow rates from each tray in the column (Fuentes and Luyben, 1982). Thus, for an intermediate tray i, the ODE was given by:

$$\frac{d(M_i h_{L,i})}{dt} = L_{i+1} h_{L,i+1} + V_{i-1} h_{V,i-1} - L_i h_{L,i} - V_i h_{V,i}$$

$$= M_i \left\{ \frac{d(h_{L,i})}{dx_i} \cdot \frac{d(x_i)}{dt} \right\} + h_{L,i} \frac{d(M_i)}{dt} \qquad (3.15)$$

Substituting (3.7) and (3.8) into (3.15), and rearranging, gave:

$$V_i = \left\{ \left(x_{i+1} \frac{d(h_{L,i})}{dx_i} - h_{L,i+1} \right) L_{i+1} + \left(y_{i-1} \frac{d(h_{L,i})}{dx_i} - h_{V,i-1} \right) V_{i-1} + \left\{ \left(h_{L,i} - x_i \frac{d(h_{L,i})}{dx_i} \right) \left(L_{i+1} + V_{i-1} \right) \right\} \right\} \Bigg/ \left\{ h_{L,i} - h_{V,i} + (y_i - x_i) \frac{d(h_{L,i})}{dx_i} \right\} \qquad (3.16)$$

The rate of change of enthalpy with composition for the light key in the liquid phase, $d(h_{L,i})/dx_i$, was derived from the steady state simulation results. The variation of $h_{L,i}$ is plotted in Figure 3.4. Data for each LNG feedstock condition was combined to form a single 2-dimensional look-up table, as a function of the methane composition on each tray and the feed condition. It should be noted that this derivation conflicts with the earlier assumption of constant molar overflow. Assuming a direct relationship between molar hold up and liquid down flow (assumption (vii)) allows the liquid tray hydraulics to be described by the Francis weir formula:

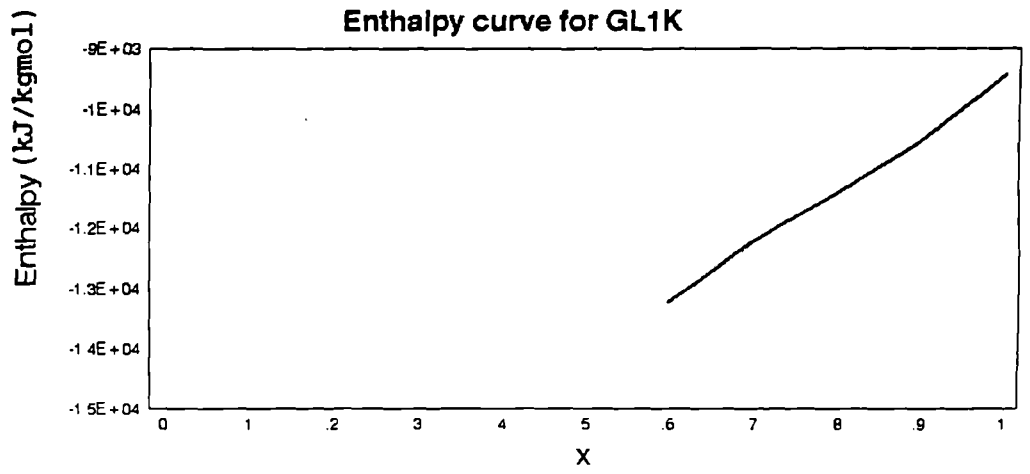

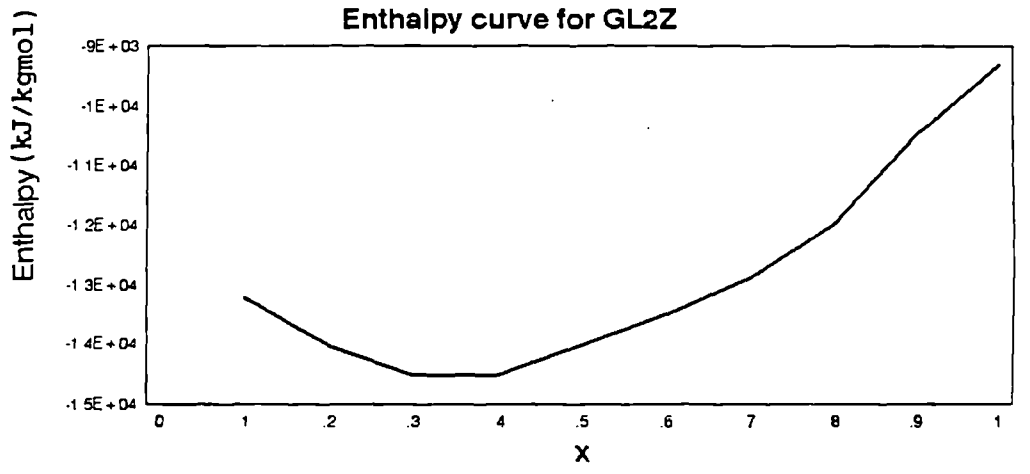

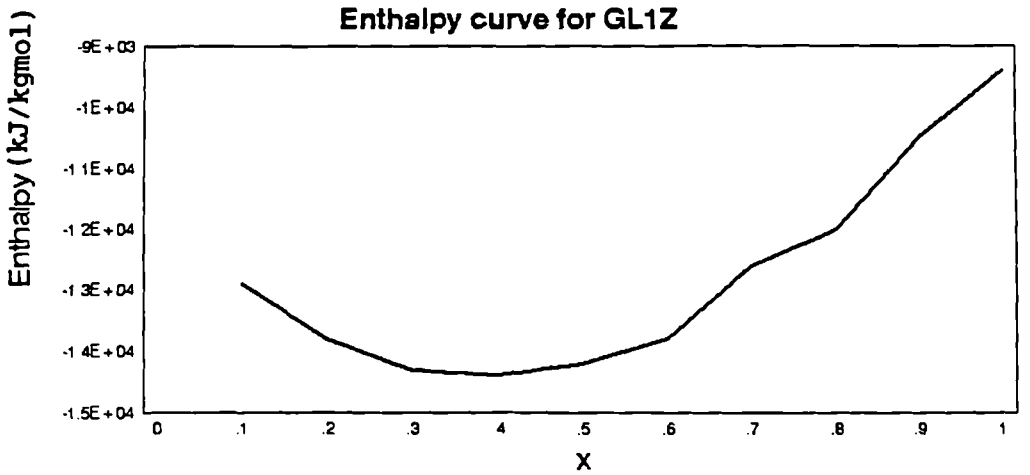

Figure 3.4 Liquid phase enthalpy curves for the distillation column

$$L_i = L_c (h_i - h_w)^{3/2} \qquad i = 1,2,..f,...,N \qquad (3.17)$$

where L_c is a constant derived interactively during development, and h_i and h_w are the liquid level and weir height, respectively.

The vapour-liquid equilibrium relationship is often simplified by adopting a constant relative volatility term, α, as in (3.2). However, greater accuracy has been achieved by deriving a relationship from existing steady state results for the three feedstock conditions, in a look-up table. The combined equilibrium curve in Figure 3.5 illustrates the similarity between the feedstock conditions. This has enabled a single relationship to be applied to both the equilibrium and temperature curves. This relates the liquid molar compositions of methane on each tray to its corresponding vapour composition and tray temperature as:

$$y_i = f_1(x_i) \qquad (3.18)$$

$$T_i = f_2(x_i) \qquad (3.19)$$

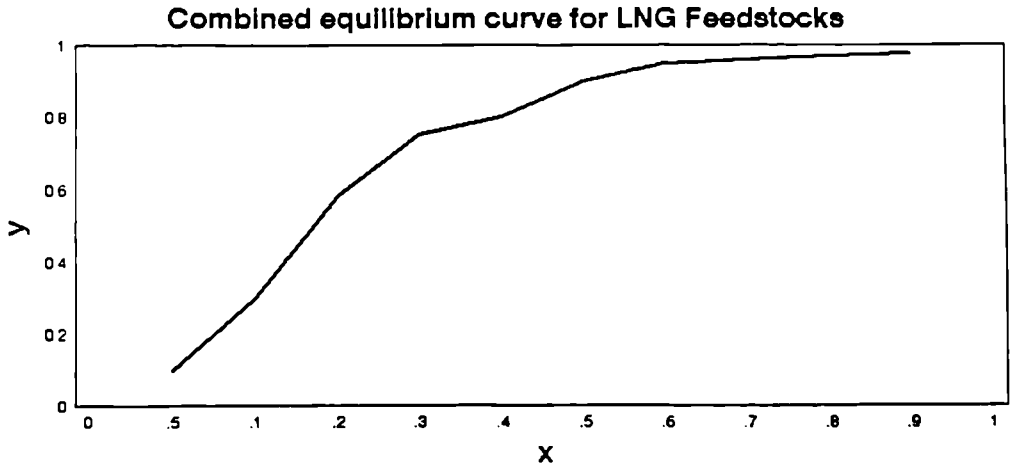

Figure 3.5 Combined equilibrium curves for LNG feedstocks

For compatibility of the plant simulation, the product streams from the pseudo-binary column must be converted back to a multicomponent system on exit. In addition, the physical properties data within the column should be based on a multicomponent composition. Although a *heavies* weighting approximation is feasible about one steady state condition, the inaccuracy would increase as a new operating condition

is approached. So, the pseudo-binary system was modified to more closely reflect the multicomponent system.

The *heavies* component on each tray was expanded to form a multicomponent composition for both phases, by extracting steady state data to form look-up tables. The look-up tables were derived for each heavy hydrocarbon, in the liquid and vapour phases, as a function of methane composition on the tray, and the proportion of the given hydrocarbon in the column feed stream. For example, the ethane ratio in the liquid phase, plotted in Figure 3.6, was given by:

$$\frac{x_{b(1),i}}{(1 - x_{a,i})}$$

where $x_{b(1),i}$ and $x_{a,i}$ are the ethane and methane compositions on tray i, respectively. Therefore, heavy hydrocarbon composition was given by:

$$x_{b(j),i} = f_3(x_{a,i}, x_{b(j),f})$$

This extension of the pseudo-binary concept allowed approximate multicomponent compositions to be obtained within the column and for the top and bottom product streams. The proportion of N_2 was derived from consistency constraints.

In summary, the look-up tables employed in the dynamic model were:

- Equilibrium curve
- Tray temperature
- Rate of change of liquid enthalpy with liquid composition
- Ratios of *heavy* components, for both phases (10 off)

The overall calculation procedure for an intermediate tray i is shown in Figure 3.7.

The reflux drum and column base were described by only two state equations - total mass and component mass balances. Reflux dynamics are generally very fast (Foss, 1983) and hence may be neglected. However, the reboiler dynamics are appreciable and have thus been approximated by first-order dynamics.

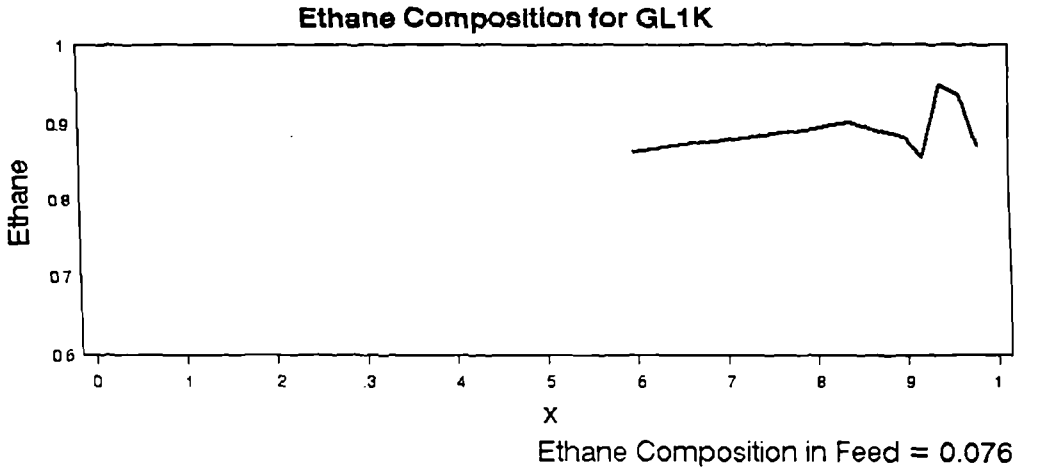

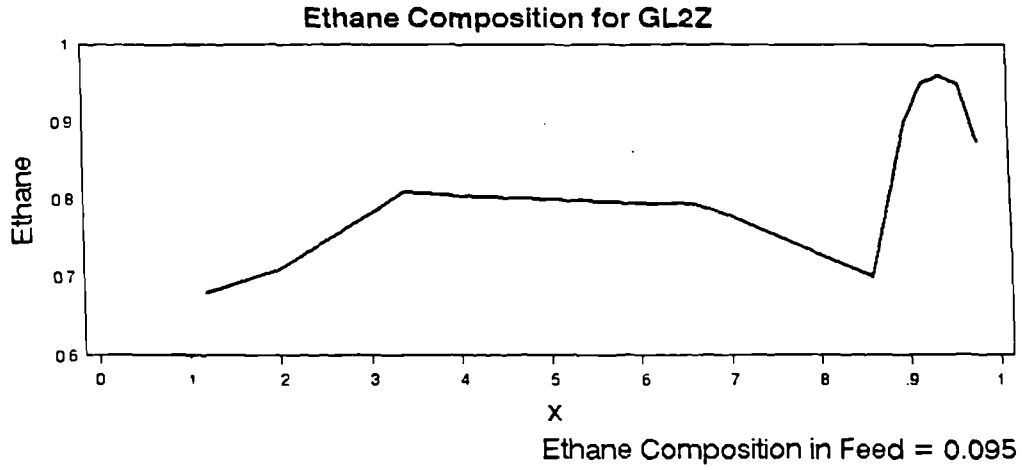

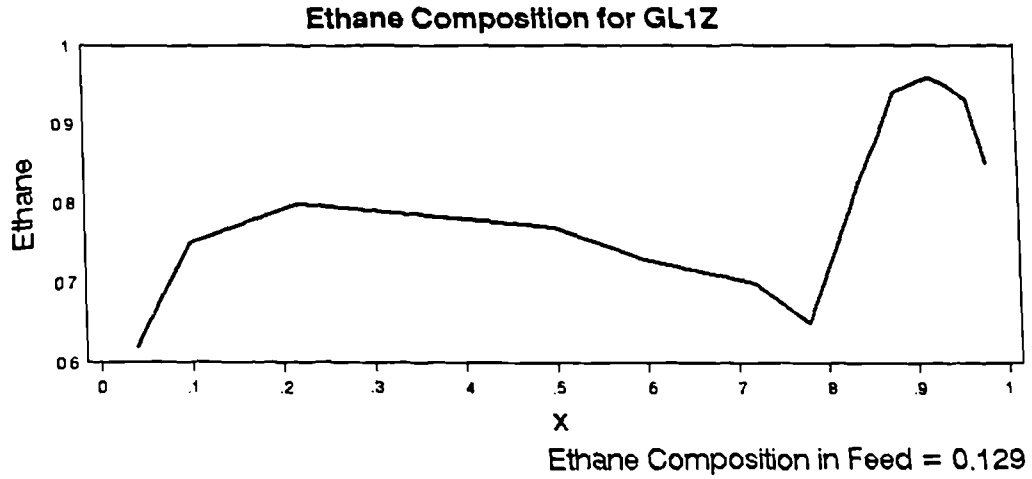

Figure 3.6 Ethane ratios for multicomponent composition in the liquid phase

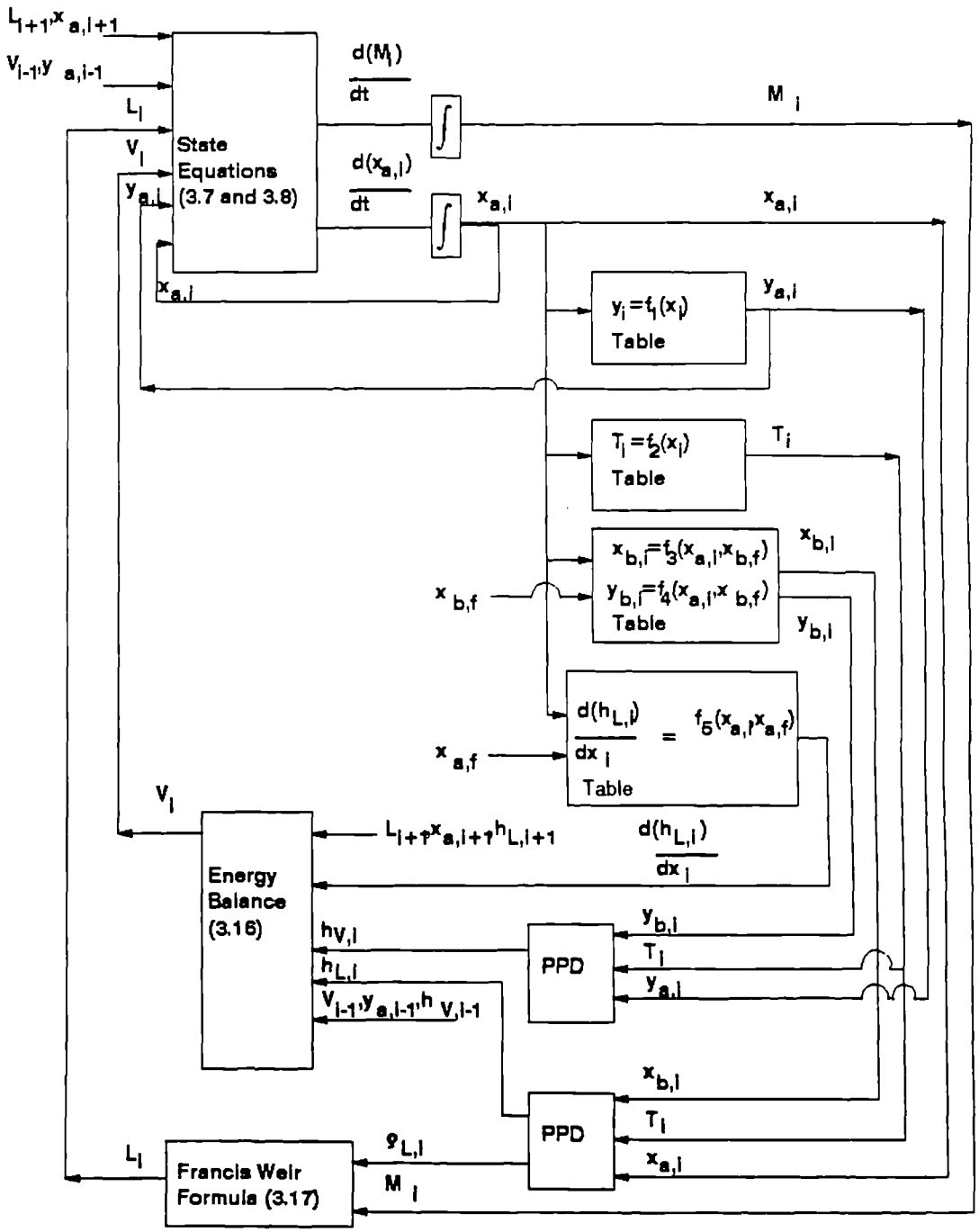

Figure 3.7 Calculation procedure for intermediate tray, i

3.3.1.3 *Pseudo-binary Model Deficiencies*

The multicomponent distillation column has been approximated by a pseudo-binary system to reduce the model size. The widely used look-up tables have been based solely on the steady state simulation results for a few feedstock conditions. Thus, the linearised data is only reliable within a limited region about each steady state condition, which imposes an artificial operating envelope. In addition, intermediate values between each point in the look-up tables are derived by linear interpolation. External values are linearly extrapolated from nearest points.

The model assumes perfect pressure control and a constant pressure throughout the column. However, the steady state simulation results are based on a column with a representative pressure drop on each tray. The effects of pressure variation have been included in the look-up tables, using the steady state simulation data.

Choe and Luyben (1987) have shown that vapour density becomes significant when the operating pressure exceeds 10 bar. However, including vapour hold up would make the calculation of tray compositions and hold ups more complex, as the vapour composition derivative, (dy_i/dt), would also have to be derived.

The vapour-liquid equilibrium relationship was approximated from an equilibrium curve. Alternatively, Fuentes and Luyben (1982) suggested a simple polynomial relationship for the VLE relationship, based on composition. This approach was investigated for the equilibrium and temperature curves, as a function of methane composition. However, up to 6^{th}-order expressions were required to ensure a reasonable level of accuracy. As this resulted in a significant increase in simulation runtime, the original look-up tables were retained.

3.3.2 **CRG Reformer**

The adiabatic CRG reformer is a fixed bed tubular reactor, operated at 44.5 bar with an inlet temperature of 400°C. Steam is added prior to reforming, at a fixed mass flow ratio of three. The outlet stream is rich in methane, with an estimated pressure drop of 1 bar and an increase in temperature to approximately 420°C.

3.3.2.1 *Review of Adiabatic Fixed Bed Reactor Models*

Catalytic reactions are generally classified as homogeneous or heterogeneous. Homogeneous reactions occur where both the catalyst and reactants are of the same phase, whereas, heterogeneous reactions refer to two-phase reactions. The CRG reformer is heterogeneous as the vapour phase process stream interacts with solid catalyst pellets.

There are several approaches to modelling heterogeneous fixed bed reactors. Heterogeneous reactions may be rigorously modelled by representing the catalyst explicitly and including mass and energy balances for each phase. If local gradients within the reactor tubes are assumed negligible, the rigorous model is reduced to a pseudo-homogeneous representation of a continuum in the reactor tubes.

Heterogeneous model

A conventional heterogeneous model of a fixed bed reactor would describe the fixed bed of solid particles as a continuum (dispersion model). It is developed from reaction rate and continuity equations describing the reactants and catalyst pellets. The resulting PDEs include spatial variables in terms of axial and radial positions, and pellet size (Carberry, 1976; Müller and Hofmann, 1987).

An alternate model was developed by Schnitzlein and Hofmann (1987), which considered the microscopic structure of the catalyst packing. The model assumed there were two types of void present between the catalyst packing, representing ideal mixing and displacement. Thus, the flow and dispersion of fluid in a packed bed was described by elementary cells regularly interconnected by channels to form a two-dimensional network. The model was successfully applied in simulating both single and multiphase reactors, and demonstrated good flexibility owing to its block structure.

Several aspects of the modelling and simulation of individual fixed bed reactors were discussed by Eigenberger and Ruppel (1986), by comparing the performance of heterogeneous and simplified models with plant data. In particular, the problems associated with maintaining steady operating conditions in and around the tubes in a multi-tubular fixed bed reactor were investigated.

Pseudo-homogeneous model

The complexity of a heterogeneous model can be reduced by simplifying the catalyst activity. If catalyst deactivation is slow then the pellet size can be assumed constant, and this removes a spatial variable from the rigorous model. Moreover, if the tube dimensions are significantly greater than those of the catalyst pellet, then axial mixing of the mass can be assumed negligible, and the bed will behave as a perfect mixer. This is termed plug flow, and reduces the rigorous model to a two-dimensional pseudo-homogeneous model, with axial and radial position variables. This condition is illustrated in Figure 3.8. Hence, the model assumes that an entering fluid element moves through the reactor as a plug of material that completely fills the reactor tube cross section.

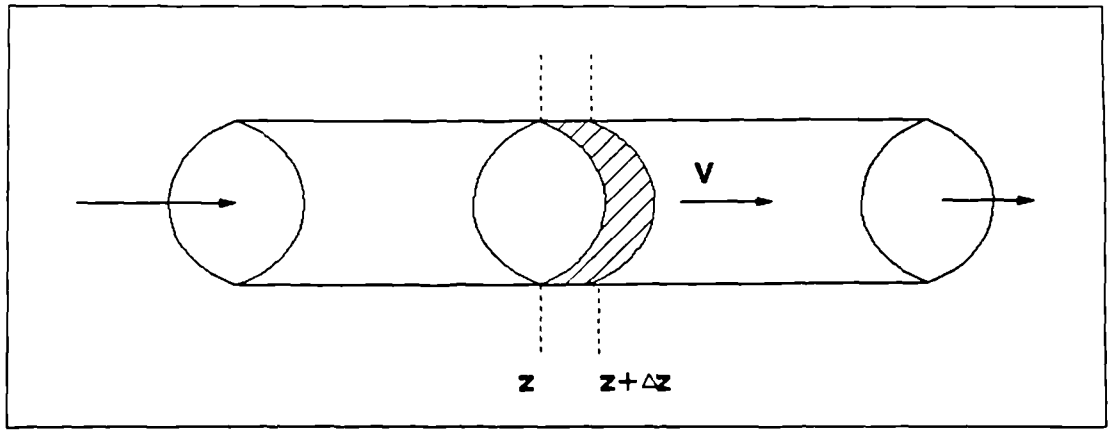

Figure 3.8 Plug flow in a tubular reactor

Vortmeyer and Schaefer (1974) derived a single phase model for an adiabatic packed bed reactor directly by transforming the differential energy balance equations for a two-phase model. They assumed that the thermal capacity of the gas phase could be neglected, and that the second derivatives of catalyst and gas temperatures were equal (equivalence condition). Experimental

results have validated the equivalence of single and two-phase models, and identified a relationship between the phases.

In the two-dimensional plug flow model, axial and radial variations in temperature and composition are derived. However, if the ratio of tube to catalyst diameter is large, then the radial gradient between the centre of the tube and the tube wall will lessen. So, the radial gradient may be assumed negligible for a large ratio, and the continuity equations become one-dimensional. The temperature and conversion profiles become functions of bed length alone. These assumptions demonstrate that plug flow and steady radial conditions depend on the dimensions of the reactor tube being long and narrow. An example of a one-dimensional pseudo-homogeneous reactor model has been used to describe an adiabatic methanator similar to the CRG reformer (Van Doesburg and de Jong, 1976).

The axial dispersion model is a further simplification of the 1-D plug flow model, which may be considered as a correction term for tubular reactor modelling. Mass transport in the axial direction is characterised by an apparent longitudinal diffusivity term, D_z, which is superimposed on the plug flow velocity (Hill, 1977). D_z is often called the mixing coefficient as its magnitude governs the degree of mixing which prevails in the axial direction. (The performance of an ideal plug flow reactor is given by $D_z = 0$).

3.3.2.2 *Simplified Model of CRG Reformer*

A simplified dynamic model has been adopted to describe the CRG reformer, as a rigorous model would require greater computing runtime and real plant data to estimate model parameters. Many simplifying assumptions have been made to reduce the model complexity:

(i) Negligible axial mixing and dispersion of heat, ie. plug flow model.

(ii) Negligible radial gradients.

(iii) The adiabatic operation assumes negligible heat interaction between the reformer contents and their surroundings, and identical behaviour in each tube.

(iv) There is sufficient catalyst for each reaction to proceed to equilibrium.

(v) A relatively small and constant pressure drop is assumed along the reactor tube.

(vi) Catalyst deactivation is negligible.

For the purposes of simulation, the reformer has been interpreted as two reactors in series: a heavy hydrocarbon conversion followed by methanation reforming. In the first reactor, methane is considered inert (as discussed in Section 2.5), and the heavy hydrocarbons are completely converted according to the general reaction:

$$C_xH_{(2x+2)} + x\,H_2O \rightarrow x\,CO + (2x+1)\,H_2 \qquad (3.20)$$

where $x = 2,\ldots,5$.

An intermediate stream composition may be calculated from this conversion reaction, consisting of CH_4, CO, H_2 and H_2O.

The second stage of reforming is described by the water-gas shift and methanation reactions (Appendix 1), respectively:

$$CO + H_2O \rightleftarrows CO_2 + H_2 \qquad (3.21)$$

$$CO + 3H_2 \rightleftarrows CH_4 + H_2O \qquad (3.22)$$

Xu and Froment (1989) described a similar process in a detailed thermodynamic analysis, based on three reactions that included (3.21) and (3.22).

The extent to which each reaction proceeds is governed by the equilibrium constant, K_p, which is defined by the partial pressure ratio of reactants to products. The K_p values are given by:

$$K_{p_1} = \frac{p(H_2)p(CO_2)}{p(CO)p(H_2O)} = \frac{\psi_{H_2}\psi_{CO_2}}{\psi_{CO}\psi_{H_2O}} \qquad (3.23)$$

$$K_{p_2} = \frac{p(CH_4)p(H_2O)}{p(CO)[p(H_2)]^3} = \frac{\psi_{CH_4}\psi_{H_2O}}{\psi_{CO}(\psi_{H_2})^3}\left(\frac{F}{p}\right)^2 \qquad (3.24)$$

for reactions (3.21) and (3.22), respectively, where ψ is the component flow rate, F is the total flow rate and p is the outlet pressure. The K_p values are functions of temperature. Thus, (3.21)

and (3.22) are governed by temperature and reactant composition. Reaction (3.22) is also influenced by operating pressure, with high pressure favouring methane-rich gas production.

The conversion of CO in the water-gas shift and methanation reactions was assumed to be α moles and β moles, respectively. By substituting α and β into the K_p expressions, the final product composition was found using a Newton-Raphson iteration method.

The product stream temperature was initially required to calculate the K_p values. However, temperature could not be derived until the product composition was known. Thus, the calculation procedure was modified by substituting the temperature obtained in the previous calculation time step to determine the current K_p values.

The enthalpy balance for the reformer included heat generated by the heavies conversion, water-gas shift and methanation reactions. As the heats of reaction referred to standard conditions, the overall enthalpy balance became:

$$\frac{d(h_p)}{dt} = \left\{ (h_f - h_{f,std})F_f - (h_p - h_{p,std})F_p + Q_{rct} \right\} \times \left\{ \frac{mw_p}{\rho_p A_t L_t} \right\} \qquad (3.25)$$

where subscripts f and p denote the feed and product streams, A_t and L_t are tube area and length, and Q_{rct} is the total heat generated.

The time delay associated with the reactants travelling through a reformer tube may be approximated by a first-order transfer function with a time constant given by:

$$\tau_r = \frac{\rho_t A_t L_t}{F_p mw_p} \qquad (3.26)$$

The value of τ_r, in the order of 1.4s for this model, was comparable to results described in a similar reformer study by Mandler et al. (1986). Their work also identified a larger time constant relating to the thermal processes within the reactor. This was attributed to the high heat capacity of the catalyst pellets, which was

significantly greater than that of the reactants. Thus, any change in the inlet conditions would gradually affect the catalyst temperature profile, which subsequently changes the gas temperature. This resulted in a marked time delay before the new steady state condition was reached. The delay was modelled as a first-order lag on the outlet stream temperature, with a time constant of 75s (Mandler et al., 1986).

The calculation procedure for the CRG reformer model is illustrated in Figure 3.9.

3.3.2.3 *Reformer Model Deficiencies*

A major assumption of the reformer model was that the heavy hydrocarbons were totally converted, and all reactions proceeded to equilibrium. This was supported by the high steam to hydrocarbon mass flow ratio in the reformer inlet. Without this simplification, a rigorous model that predicted temperature and composition profiles along the tube length would have to be considered.

Catalyst deactivation is a very real problem in the working life of any reactor. Its effect on the CRG reformer operation has not been included in the recommended model. However, suitable plant data could be incorporated as an additional term in the temperature lag.

Pressure drop along the reformer tube is assumed constant at 1 bar. This affects the methanation reaction. Therefore, if the variation in pressure drop was significant, the introduction of a pressure profile would have to be considered.

Residence time in the reformer model has been based on vapour flowing through an empty reactor tube. The actual value is probably less due to the obstruction of catalyst pellets. The time delay associated with the heat capacity of the catalyst is assumed constant and derived from a similar reactor model development (Mandler et al., 1986). So, it has been assumed that the time delay for the real process would not vary significantly due to changes in inlet conditions and catalyst performance within the operating envelope.

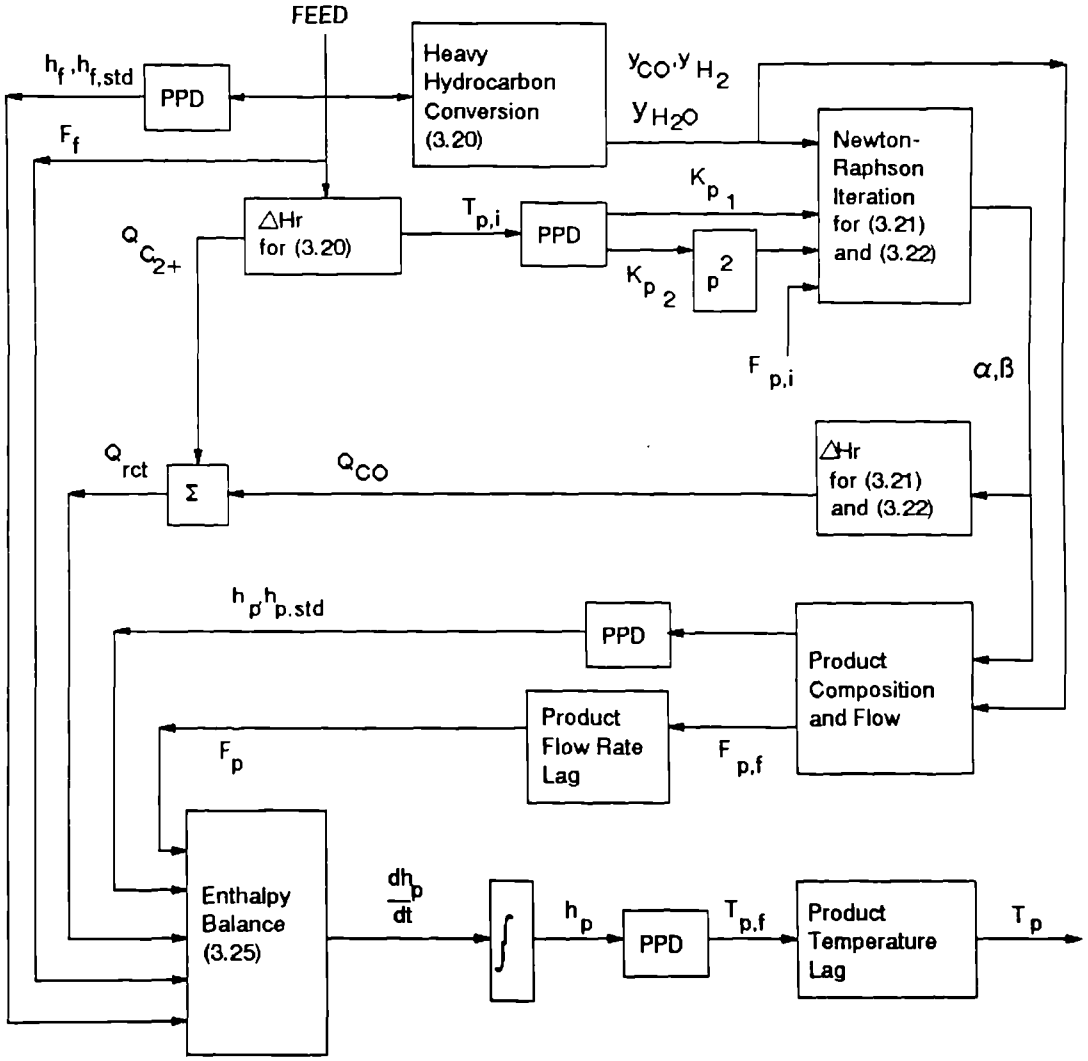

Key:

$T_{p,i}$ - product temperature from previous calculation step

$F_{p,i}$ - product flow rate from previous calculation step

PPD - Physical Properties Database

Figure 3.9 Calculation procedure for CRG reformer model

3.3.3 **Flash Unit**

The flash operation forms part of the separation process. Before entering the adiabatic flash unit, the feed stream is preheated and a pressure let-down valve reduces the stream pressure. The flash unit is operated at 48.09 bar and approximately -170°C.

3.3.3.1 *Flash Unit Modelling Simplifications*

The flash unit is essentially one stage in a distillation column. Therefore, the dynamic modelling literature is generally encompassed in the development of the more complex distillation column model.

A rigorous dynamic model of a multicomponent flash unit includes the conservation equations for both the liquid and vapour phases. It can be subdivided into three parts: the feed stream, liquid hold up and vapour hold up. An equilibrium-flash calculation is conducted on the feed stream to determine the proportion of liquid and vapour phase streams. The contributions from these streams are then introduced to their respective mass and energy balance equations describing the liquid and vapour hold ups. The liquid hold up calculations are similar to those describing the tray in a distillation column, with no vapour flows.

A well established simplification of the rigorous dynamic model is to assume that vapour phase dynamics are negligible (Luyben, 1973). The liquid and vapour phase physical properties also play an important role in the simplification of a flash unit model. Stephanopoulos (1984) described a simple dynamic model with the vapour-liquid equilibrium relationships for each component and the physical properties assumed constant. However, this represents an over-simplified model that could only reliably describe a flash unit over a limited operating envelope.

3.3.3.2 *Multicomponent Flash Unit Model*

The following assumptions have been made in developing a suitable dynamic model for the flash unit:

(i) Vapour hold up is negligible.

(ii) There is negligible heat exchange with the environment.

(iii) The vapour and liquid phases are always in equilibrium.

(iv) Both phases form ideal solutions.

These assumptions limit the conservation equations to the liquid phase in the flash drum. For the flash unit arrangement illustrated in Figure 3.10, the conservation equations are:

Total Mass Balance:

$$A\rho_L \frac{dh}{dt} = (F_f mw_f) - (F_V mw_V) - (F_L mw_L) \qquad (3.27)$$

Component Balance:

$$A\rho_L \frac{d(hx_i)}{dt} = (F_f x_f mw_f) - (F_V y_i mw_V) - (F_L x_i mw_L) \qquad (3.28)$$

where $i = 1, 2, \ldots, N-1$

Energy Balance:

$$\left(\frac{A\rho_L}{mw_L}\right) \frac{d(hh_L)}{dt} = F_f(h_f - h_L) - F_V(h_V - h_L) \qquad (3.29)$$

Consistency Constraints:

$$\sum_{i=1}^{N} x_i = 1 \qquad \sum_{i=1}^{N} y_i = 1 \qquad (3.30)$$

where h is the liquid level, h is stream enthalpy and subscripts f, V and L refer to the feed stream, vapour and liquid products, respectively.

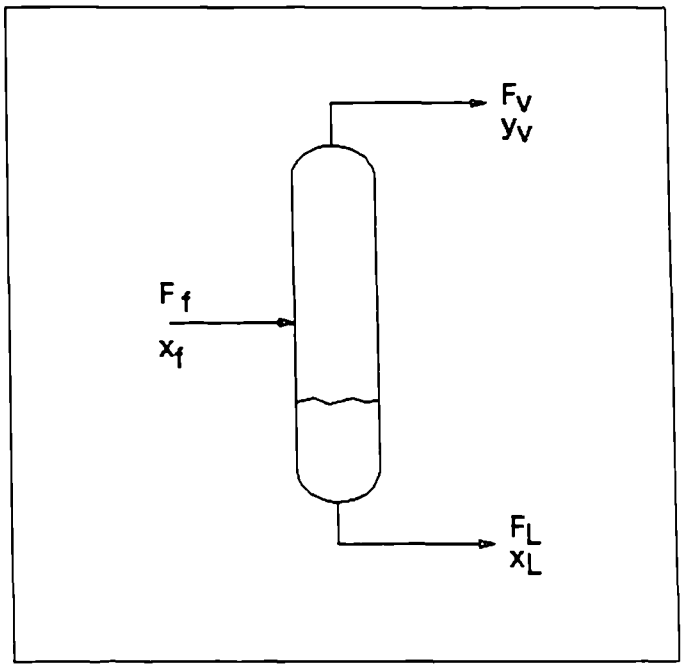

Figure 3.10 Flash unit arrangement

Only the temperature, liquid phase composition and level can be obtained from the conservation balances. The corresponding vapour composition and pressure are derived from nested iterative calculations. From initial estimates of pressure and vapour composition, the liquid and vapour phase fugacities for each component are calculated and compared. The vapour phase composition is then varied until the fugacities are equivalent, such that the phases are in equilibrium. The resulting vapour composition is checked with the consistency constraint. If the constraint is not satisfied a new estimate of pressure re-initiates the calculation, which proceeds until the fugacity and consistency conditions are both satisfied.

The overall calculation procedure for this model is illustrated in Figure 3.11.

3.3.3.3 *Flash Unit Model Deficiencies*

The dynamic behaviour associated with liquid hold up in the flash drum has been simplified by only considering the three main process streams and assuming the feed stream enters the drum as a liquid. This neglects the impact of the two phase feed stream on drum conditions, which may result in the liquid product stream having slightly faster dynamics than in the real process. This is due to the assumption of perfect mixing in the drum. The effect of a liquid feed stream on the vapour dynamics would be less as these dynamics are significantly faster.

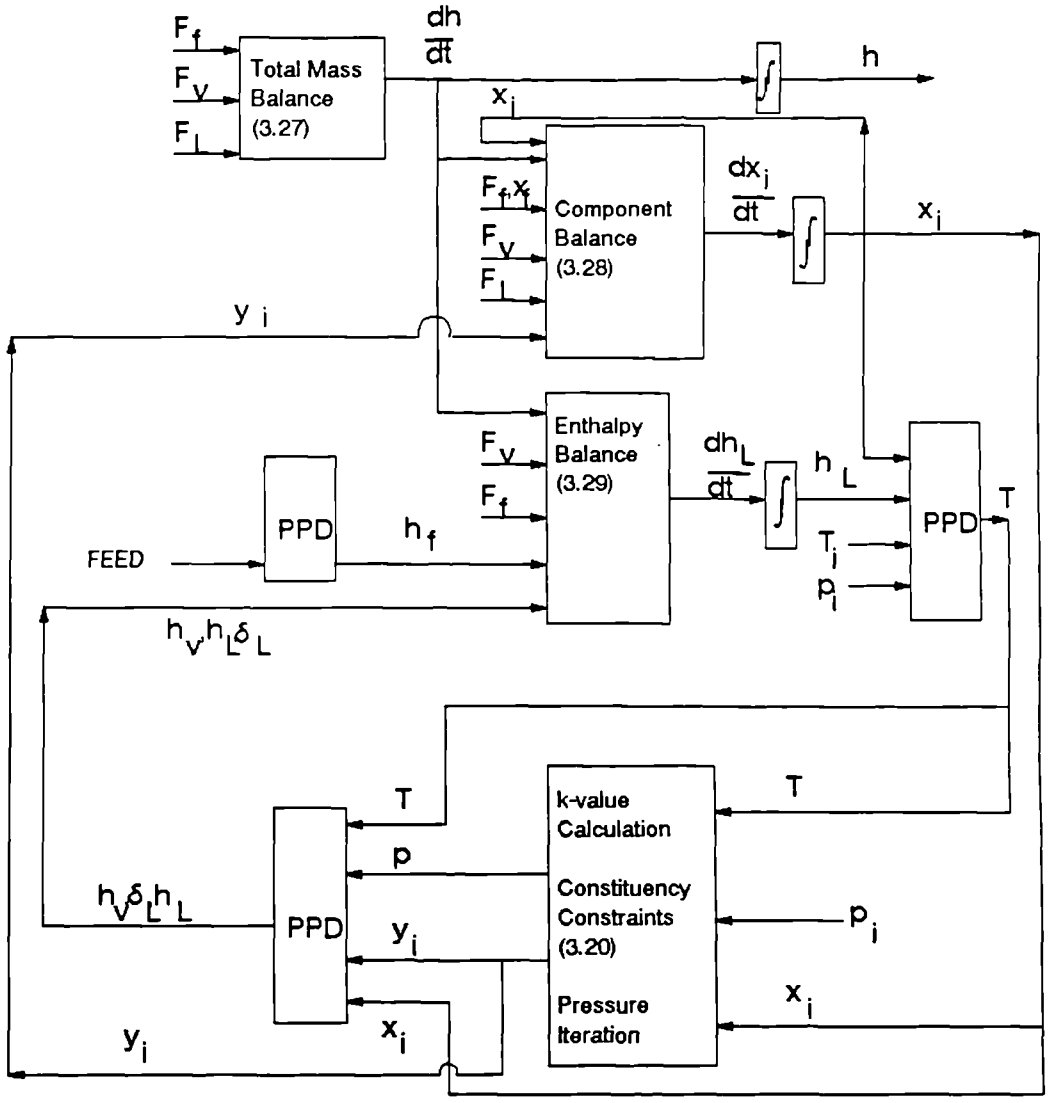

Key:
T_i - temperature from previous calculation step
p_i - pressure from previous calculation step
PPD - Physical Properties Database

Figure 3.11 Calculation procedure for the flash unit model

3.3.4 **Heat Exchanger**

There are a total of nine heat exchangers excluding those for the distillation column. Most are employed in cooling the process streams, and include single phase, condensing and vaporising heat exchangers. Only one unit involves the heat exchange of two process streams. The remaining units are served by plant utility streams.

Each unit is assumed to be a counter-current shell and tube type heat exchanger, due to the wide range of applications for this design.

3.3.4.1 *Heat Exchanger Modelling*

A rigorous dynamic model of a heat exchanger is inherently distributed parameter, where the output variables are dependent on both time and position. Therefore, the model is described by PDEs. In its most rigorous form, process fluid temperature is modelled in both the axial and radial directions. A cross section of a typical heat exchanger tube arrangement is shown in Figure 3.12. If the process fluid is compressible (ie. vapour) the model would also require a mass balance PDE to determine composition along the tube. So, the rigorous process model would represent variations in temperature and composition along and through the heat exchanger tube. An incompressible process fluid would experience no composition changes, and remove the need for a mass balance.

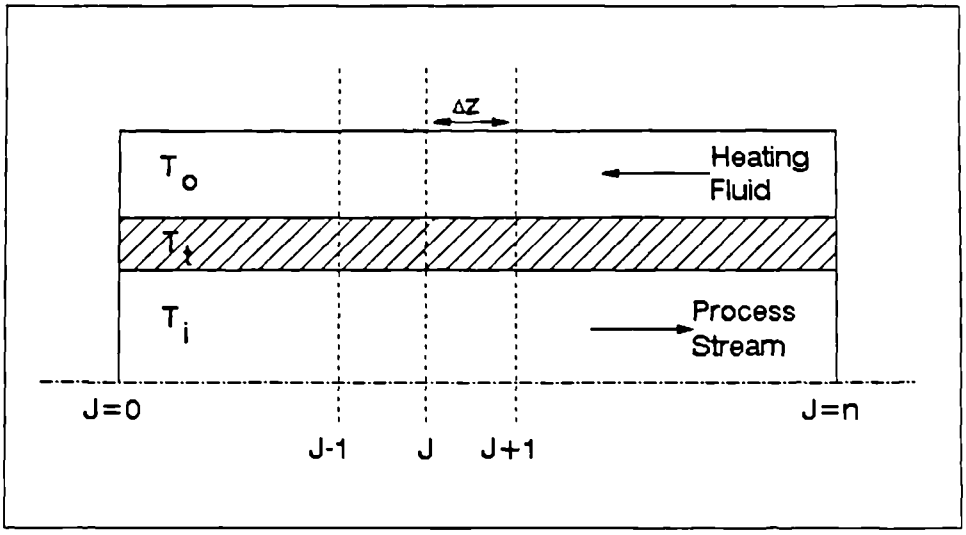

Figure 3.12 Heat exchanger arrangement

Dynamic models for shell and tube type heat exchangers are often simplified by assuming the fluid is in plug flow. Thus, temperature variations are expressed over a differential section of tube, Δz, for the process fluid, tube wall and utilities stream (Guy, 1982a, b). Where the process fluid is heated by condensing steam, the steam temperature is related to the condensation pressure, which is independent of axial position. Therefore, steam temperature, T_s, can be expressed as a lumped parameter that only varies with time. Several assumptions can be made to simplify the PDEs, including:

(i) Physical properties of the liquid remain constant, and no evaporation occurs.

(ii) The heat transfer coefficient from the steam to the tube wall is constant.

(iii) The heat transfer coefficient from the tube wall to the liquid varies only with flow rate.

Hence, the energy balance for a section of tube, Δz, is reduced to:

Tubeside:

$$\rho_i A_i c_{p,i} \frac{\partial T_i}{\partial t} = - W_i c_{p,i} \frac{\partial T_i}{\partial z} + h_i a_i (T_t - T_i) \qquad (3.31)$$

Tube Wall:

$$\rho_t A_t c_{p,t} \frac{\partial T_t}{\partial t} = \frac{h_o A_o}{\Delta z} (T_o - T_t) - h_i a_i (T_t - T_i) \qquad (3.32)$$

where

ρ	stream density
A	cross sectional area
c	specific heat capacity
W^p	mass flow rate
h	heat transfer coefficient
a	area of tube per unit length

and subscripts i, o and t denote the inner and outer fluids and tube wall, respectively. Boundary conditions are required for (3.31) and (3.32) to find the initial conditions for the unit. These expressions may then be solved numerically, by converting the PDEs into ordinary differential equations using the finite difference approximation (Seborg et al., 1989). With the exchanger model partitioned into many sections, the energy balance equations may be derived for the tube wall and process fluid, over each Δz section of the tube.

In a simplified distributed parameter model, the tube wall dynamics

are neglected (Stephanopoulos, 1984). Thus, only one state variable is required to model this system - the process fluid temperature. The energy balance equation (3.31) becomes:

$$\rho_i c_{p,i} A_i \frac{\partial T}{\partial t} = - W_i c_{p,i} \frac{\partial T}{\partial z} + \frac{A_i U (T_s - T_i)}{\Delta z} \qquad (3.33)$$

where an overall heat transfer coefficient, U, has replaced the heat transfer coefficients for inner and outer tube sides of the wall.

3.3.4.2 *Simplified Model of a Heat Exchanger*

A prerequisite for implementing any of the above dynamic models would be to determine the heat transfer properties and dimensions of the exchanger. As the heat transfer properties depend on several factors, a detailed study of each heat exchanger would be essential.

From a plantwide perspective, only significant dynamics will be important in the plant simulation. Most of the heat exchangers transfer heat using a continuous supply of heating fluid from a utilities plant (which is outside the model boundaries). As the dynamics of a heat exchanger are comparatively fast, and temperature control is effective (Shinskey, 1988), it is reasonable to assume that the required outlet temperature will be maintained. Therefore, a steady state model has been adopted for each heater and cooler, assuming perfect temperature control. Where a phase change occurs in the heat exchange unit, the dew or bubble point of the process stream has been derived to ensure that the new phase is attainable.

The counter-current heat exchanger in the heavies processing section cannot be simplified to a steady state model as both streams are process fluids. So, the outlet stream temperatures have been derived from a steady state energy balance:

$$Q = UA\Delta T_{\ell m} \qquad (3.34)$$

where Q is the total heat transfer and $\Delta T_{\ell m}$ is the logarithmic mean temperature difference. A constant value of U has been derived from steady state simulation results, corresponding to the largest heat transfer coefficient to attain design conditions (GL1Z condition). It should be noted that the energy balance (3.34) can only be applied to a change of phase when the specific heat capacity does not change

significantly between phases.

The heat balance (3.34) can also be expressed in terms of the process fluid conditions, where:

$$\begin{aligned} Q &= F_1(h_{1,i} - h_{1,o}) \\ &= F_2(h_{2,i} - h_{2,o}) \end{aligned} \qquad (3.35)$$

Thus, the above heat balances (3.34) and (3.35) have been combined to derive the outlet stream enthalpies, and temperatures, using the previously calculated temperature as an initial estimate within an iterative routine.

Rigorous dynamic models indicate that there is also a first-order lag associated with the outlet stream temperatures (Roffel and Rijnsdorp, 1982). This time constant is generally related to the fluid flow rate, heat transfer coefficient and surface area. Therefore, a time constant of 32s has been obtained from a similar heat exchanger system (Muir, 1987). The first-order lag has been incorporated in the final calculation of both process stream outlet temperatures. The assumed pressure drop across each heat exchanger is 0.3 bar.

3.3.4.3 *Heat Exchanger Model Deficiencies*

Heat exchanger dynamics are dependent on a number of variables, relating to the physical properties of the process stream. As the hold up of the process fluids are very small, dynamic behaviour has been confined to the enthalpy variations. The steady state heat balance ensures that the outlet fluid temperatures are realistic, and the first-order dynamic behaviour for enthalpy should approximate the expected temperature lags inherent in the system. Hence, this counter-current heat exchanger model was considered adequate for the overall plant simulation.

3.3.5 **Fired Heater**

The fired heater raises the process stream temperature from about 330°C to 400°C, prior to reforming. This type of direct fired heat exchanger would probably use a natural gas fuel.

3.3.5.1 *Dynamic Modelling of Furnaces*

The process fluid in a fired heater passes through banks of tubes in radiating and convection sections. The furnace burners are located immediately below the vertically mounted tubes in the radiation section, and air is continuously drawn in to support burning. There is no direct heat source in the convection section, and the tubes are arranged in horizontal banks. So, the heat transfer mechanisms comprise radiation and to a lesser extent convection. In rigorous steady state terms these may be expressed as:

$$\text{Radiation:} \quad Q_R = \sigma_F \alpha A_{cp} F_F (T_g^4 - T_t^4) \tag{3.36}$$

$$\text{Convection:} \quad Q_C = hA_t (T_g - T_t) \tag{3.37}$$

where the σ, α and h parameters would be derived from manufacturer's data. A detailed analysis of the solution of (3.36) and (3.37) is presented in the Heat Exchanger Design Handbook (1983). A simpler approach (Wimpress, 1978) given by:

$$\begin{aligned} Q &= Q_R + Q_C \\ &= \sigma_F \alpha A_{cp} F_F (T_g^4 - T_t^4) + 35\alpha_F A_t F (T_g - T_t) \end{aligned} \tag{3.38}$$

shows that the outlet temperature is a function of several factors, notably tube wall temperature, the inner heat transfer coefficient and tube wall thermal resistance.

In a rigorous dynamic model of a fired heater, each burner would be modelled with its heat distribution within the radiation section related to immediate radiating coils. The oxygen consumption level may also be simulated, as a function of the burner efficiency and heat generated. However, a model of this accuracy requires detailed design, manufacturer's and plant data. The dynamic behaviour of the heat source may be approximated by a second-order system. This would comprise the larger immediate effect of direct heat from each burner, and a secondary reflection of heat from the fired heater walls.

A simpler dynamic model of a furnace has been developed using a similar approach to heat exchanger modelling (Roffel and Rijnsdorp, 1982). The heat mechanism in the radiation section is described by distributed parameter expressions for the heat balances describing the tube wall and process fluid. The dynamic behaviour has then been approximated by a second-order transfer function relating fuel feed to outlet temperature. The smaller time constant relates radiation energy to tube temperature. The larger time constant accounts for the residence time of the process stream in the radiation section, and the lag associated with the furnace wall.

3.3.5.2 *Recommended Fired Heater Model*

Any rigorous approach to modelling a fired heater would require detailed design data on furnace material and dimensions. Moreover, as the plant utilities have not been modelled (including fuel to the fired heater) and the composition of the process fluid remains unchanged, it seems reasonable to adopt a linear dynamic model to represent this unit. Hence, the simplified transfer function model developed by Roffel and Rijnsdorp (1982) has been adopted to describe the dominant dynamic behaviour of the fired heater.

The enthalpy balance has been simplified to:

$$\rho V \frac{d(h_{2,1})}{dt} = W(h_1 - h_{2,1}) + Q \qquad (3.39)$$

where V is the tube volume of the fired heater and Q is the rate of heat transfer of the fuel. The time constant relating heat input to intermediate outlet enthalpy, $h_{2,1}$, is of the form ($\rho V/W$), which corresponds to the smaller time constant. The larger time constant has been described by a first-order transfer function relating $h_{2,1}$ to its final outlet enthalpy. This has been given an approximate value of 60s (Shinskey, 1988). As the larger time constant represents residence time in the fired heater tubes, component flow rates in the outlet process stream have also been subject to a first-order lag.

3.3.5.3 *Fired Heater Model Deficiencies*

In the recommended model, it has been assumed that the fuel gas composition remains constant. Therefore, there is no direct relationship between the C.V. of the fuel gas and the heat input to the system, and a linear relationship exists between the linearly installed valve position and heat input, Q.

Although the dominant time constant, relating to residence time in the fired heater, has been assumed constant, it would be a function of the process stream flow rate and system pressure. Hence, if the process fluid flow rate increased appreciably, this would place a greater load on the furnace, and the dynamic lags will become less significant. As the plant model operates within a specified region it is anticipated that the dynamic behaviour will be acceptable.

Shinskey (1988) suggested that the significant length of tubing in a fired heater results in dead time within the process flow. This effect has not been included in the dynamic model as the residence time has been interpreted as a fixed time constant (Roffel and Rijnsdorp, 1982).

3.3.6 **Open Rack Vaporiser (ORV) Unit**

The ORV unit in the unprocessed stream line raises the inlet stream temperature from about -110°C to a distribution temperature of 10°C at 70 bar.

3.3.6.1 *Basis for ORV Dynamic Model*

The fundamental equations used to describe the dynamic behaviour of an ORV unit are similar to the counter-current heat exchanger approach described in Section 3.3.4, with process fluid vaporisation. This unit was the subject of a study by Muir (1987), in which detailed dynamic models of two types of ORV were developed. Distributed parameter models were derived for each ORV, which varied in time and one spatial dimension.

The following PDEs describe the heat balance over a differential section of the tube (Muir, 1987):

LNG:

$$\frac{\partial}{\partial t}\left(A_L \rho_L c_{p,L} T_L\right) = -\frac{\partial}{\partial z}\left(W_L c_{p,L} T_L\right) + h_L a_L (T_t - T_L) \qquad (3.40)$$

Tube Wall:

$$\frac{\partial}{\partial t}\left(A_t \rho_t c_{p,t} T_t\right) = h_L a_L (T_L - T_t) + h_W a_W (T_W - T_t) \qquad (3.41)$$

Water:

$$\frac{\partial}{\partial t}\left(A_W \rho_W c_{p,W} T_W\right) = -\frac{\partial}{\partial z}\left(W_W c_{p,W} T_W\right) + h_W a_W (T_t - T_W) \qquad (3.42)$$

where subscripts L, t and W describe the LNG stream, tube wall and water stream, respectively, and the heat transfer coefficients, h_L and h_W, include terms for the tube wall and fouling resistances. These coefficients and the fluid properties are both functions of temperature. For control system design, the non-linear simulations were approximated by linear transfer function models about one operating point.

3.3.6.2 *ORV Model Refinement*

The ORV model adopted for dynamic simulation was based on a transfer function model developed by Muir (1987). Of the two ORV's investigated, the type B ORV model was selected as it predicts ice formation and was retained in the control study by Muir (1987).

The original transfer function matrix for each tube in the type B ORV determined the temperature and flow rate of both the process and heating fluid streams as:

$$\begin{bmatrix} T_{L,o} \\ W_{L,o} \\ T_{W,o} \\ W_{W,o} \end{bmatrix} = \mathbf{G}(s) \begin{bmatrix} T_{L,i} \\ W_{L,i} \\ T_{W,i} \\ W_{W,i} \end{bmatrix} \qquad (3.43)$$

where

$$G(s) = \begin{bmatrix} \frac{0.035\, e^{-4.7s}}{(1+32s)} & \frac{-535.8}{(1+8s)} & \frac{1.50}{(1+3s)^2} & \frac{4.86}{(1+208s)(1+2s)^2} \\ 0 & \frac{1}{(1+5s)} & 0 & 0 \\ \frac{0.029}{(1+11s)(1+2s)} & \frac{-244.7}{(1+6s)(1+s)} & \frac{0.94\, e^{-3s}}{(1+4s)} & \frac{7.64}{(1+2s)} \\ 0 & 0 & 0 & \frac{1}{(1+5s)} \end{bmatrix}$$

and W is the mass flow rate in kg/s/tube. Most time constants and dead times in (3.43) were below 10 seconds. These transfer functions would have relatively fast dynamic behaviour, and were thus neglected. For example, the transfer function relating water inlet flow rate to LNG outlet temperature, $g_{(1,4)}$, is third-order with one significant time constant. The effect of the fast dynamics can be assessed by comparing frequency response characteristics with and without the 2s time constants. A comparison of Bode plots has shown that the magnitude and phase plots are equivalent up to 0.4 and 0.02 rad/s, respectively. As only low frequency disturbances are anticipated, it is reasonable to remove the smaller time constants from G(s). Thus, the reduced transfer function represents a low frequency model approximation of the original transfer function, and the G(s) matrix was simplified to:

$$\begin{bmatrix} T_{L,o} \\ T_{W,o} \end{bmatrix} = G'(s) \begin{bmatrix} T_{L,i} \\ W_{L,i} \\ T_{W,i} \\ W_{W,i} \end{bmatrix} \qquad \begin{aligned} W_{L,o} &= W_{L,i} \\ W_{W,o} &= W_{W,i} \end{aligned} \qquad (3.44)$$

The transfer function model was then modified and scaled to comply with the overall plant simulation. The procedure and transfer function model are described in Appendix 5.

3.3.6.3 *ORV Model Deficiencies*

Two major assumptions have been made in deriving a transfer function description for the ORV unit:

(i) The dynamic behaviour is more strongly related to the tube properties and stream ratios than the operating conditions.

(ii) The feed conditions do not vary significantly for different

LNG feedstock conditions.

The original nonlinear model (Muir, 1987) raised the temperature of LNG from -162°C to 5.5°C, with a water inlet temperature of 8°C. The LNG inlet temperature is markedly higher in this study. This suggests that the tube length may be over designed for this unit and thus the final outlet temperature would be attained earlier. So, the time constants may be overestimated.

The original transfer function model was derived from variations in inlet temperatures and mass flow rates. Changes in LNG composition were not considered. Hence, a change in the feed composition would have no effect on the transfer function model, provided the mass flow rate was maintained. As the transfer function model was based on the GL2Z feedstock condition, the steady state heat balance is only satisfied for that condition, due to constant gain values. This highlights the limitations of linear model approximations, namely that they represent the output response to a specified change in input conditions. However, this model has been adopted as part of the plant simulation to demonstrate the dominant dynamic behaviour in an ORV unit.

3.3.7 **Absorber Unit**

There are two absorber units, used for CO_2-removal (acid gas), and H_2O-removal. These are required to reduce the proportion of impurities to within the product specification limits described in Table 2.2. An absorption column is similar to the rectifying section of a distillation column. Vapour hold up occurs as the stream travels up the packed or staged absorber column, and the impure component reacts and is subsequently removed from the process stream.

The acid gas removal process for CO_2 typically consists of an absorption stage in a liquid reactant or solvent medium. This medium is continuously regenerated by stripping the acid gas in a neighbouring column. The most popular process uses monoethanolamine solution (MEA) which reacts with the acid gas. The water removal unit operates similarly, except it is usually a staged as opposed to a packed absorber, to withdraw almost all traces of water.

3.3.7.1 *Absorber Unit Modelling Techniques*

Different techniques adopted in modelling the packed bed and staged absorber units are briefly discussed below.

Packed absorber unit

Two approaches have been proposed for modelling packed columns:

(i) The absorber bed is divided into sections, with each representing a tray in a staged tower.

(ii) Differential mass and energy balances are used to describe a small element of packed absorber.

In an example of the first approach (Krishnamurthy and Taylor, 1985), a packed column was approximated by a sequence of non-equilibrium stages, each representing a section of packing. Mass and energy balances were developed for both phases, with rate equations and equilibrium relations. Although this absorber was approximated by a staged system, it was flexible enough to model a staged process.

De Leye and Froment (1986) adopted the second approach to develop a rigorous simulation of a packed column in which a single irreversible reaction was considered. In this model, plug flow was assumed for both phases, and differential equations were developed for the concentration profiles in the liquid film ascending the column. Areas for model simplification included reducing the order of the kinetic equation for moderately fast reactions, such as CO_2-removal.

An absorber-stripper model for CO_2-removal (Benfield process) was developed by Suenson et al. (1985) based on a plug flow assumption with a pseudo first-order hypothesis. The model consisted of CO_2 mass balances in the packed bed sections, with boundary conditions established. The resulting PDEs were converted to ODEs, using orthogonal collocation, to give numerical solutions in the space and time variables. This modelling approach is similar to the model reduction techniques discussed in Section 3.3.3.

Staged absorber unit

The dynamic behaviour of a staged absorber unit can be more simply represented than a distillation column because impurity removal is

the most significant reaction occurring. This is demonstrated in the dynamic model developed by Seborg et al. (1989) in which only one component balance was required for each tray. Thus, an n-stage absorber was described by n ODEs. However, the deviation of the process transfer functions suggested that the model order may rise dramatically as the number of trays increase.

The number of equations required in a rigorous absorber model has been greatly reduced by an approximation procedure devised by Cho and Joseph (1983a). Several simplifications were made, including the assumption that liquid and vapour stream compositions were continuous variables of the spatial variable, z. For example, a first-order approximation yielded:

$$M\frac{\partial x}{\partial t} = V\frac{\partial y}{\partial z} - L\frac{\partial x}{\partial z}$$

$$y = Kx + \frac{\partial y}{\partial z}\Delta z$$

where Δz is the stage height. A comparison of the reduced model with a rigorous model indicated that model accuracy was not impaired, and that this type of approximation was better for larger columns.

3.3.7.2 *Simplified Absorber Model*

The proportions of CO_2 and water in the absorber feed are moderately low. Therefore, it has been assumed that under normal operating conditions sufficient impurity can be removed to satisfy the product specifications. Furthermore, detailed process design data would be required before considering any of the modelling approaches discussed in Section 3.3.7.1. Hence, the modelling requirement in plantwide terms should be to represent a reasonably accurate product stream condition and include the dominant dynamic behaviour of the system.

A low fidelity "black box" model has been adopted for the reactions occurring in the absorber, as impurity levels in the feed are low. A fixed impurity removal has been assumed in both models: 99% of CO_2 and 99.9% of H_2O.

The flow of vapour through a packed absorber column is dictated by the pressure drop over the unit. Thus, the molar hold up within a

column can be expressed in terms of pressure, where pV/RT is assumed constant for an ideal gas. Assuming temperature remains steady across the absorber, the following mass balance has been obtained:

$$\frac{d}{dt}\left(\frac{pV}{RT}\right) = F_f - (F_V + F_I)$$

$$\frac{dp}{dt} = (F_f - F_V - F_I)\left(\frac{RT}{V}\right) \qquad (3.45)$$

where F_V and F_I are vapour and impurity flow rates, respectively, and V the absorber volume. Thus, the outlet stream flow rate, F_V, can be determined as a function of the pressure difference in the downstream valve, as column pressure varies. Therefore, this low fidelity model describes the variation in pressure and vapour flow rate through the absorber as inlet stream conditions vary.

3.3.8 **Units Operating in Steady State**

The remaining units in the preliminary flowsheet have relatively fast dynamic behaviour, and have therefore been described by steady state model approximations. These are the remaining operations in Table 3.1, and include the heater/cooler units discussed in Section 3.3.4. The mass and energy balance expressions associated with these units are static, and based on a multicomponent system, according to the existing flowsheet simulation.

In this section, each operation is briefly described with the main assumptions leading to the steady state expressions.

3.3.8.1 *Compressor Unit*

The compressor unit is required to raise the pressure of the heavies processed stream to distribution pressure at 70 bar, prior to mixing with the unprocessed stream. Typical compressor operating ranges (Sinnott, 1983) suggest that the centrifugual compressor is most suitable for this application.

A compressor unit usually has a small gas content compared to the connecting pipework (Roffel and Rijnsdorp, 1982). Thus, it is reasonable to assume that the unit can be described by its static

behaviour alone. The performance characteristics associated with a given compressor unit determine the change in pressure for a given change in flow rate through the unit, and define a safe operating envelope. The ratio of inlet to discharge pressure is generally defined by:

$$\frac{p_2}{p_1} = f\ (\ W,\ N\ ) \tag{3.46}$$

where W is the mass flow rate and N is the speed of rotation, and itself a function of the performance characteristics of the specific unit. This means that the demanded discharge pressure is maintained at a certain flow rate, provided N is within the compressor speed range. As manufacturers' data relating to the actual compressor performance is not available, it has been assumed that pressure control is effective in this simulation, and a constant discharge pressure is always maintained.

As the compressor unit model maintains a constant discharge pressure, and stream composition, any variation in discharge temperature would arise from a change in the physical properties of the feed stream, given by:

$$T_2 = T_1 \left(\frac{p_2}{p_1} \right)^{\left(\frac{k-1}{k}\right)} \tag{3.47}$$

where $k = c_p / c_v$. The power requirement of the compressor is:

$$P = \frac{Z\ R\ T\ F}{\left(\frac{k-1}{k}\right)} \left\{ \left(\frac{p_2}{p_1} \right)^{\left(\frac{k-1}{k-\eta}\right)} - 1 \right\} \tag{3.48}$$

where Z is the compressibility factor, R the gas constant and η the polytropic efficiency.

Although the compressor dynamics are assumed negligible, this assumption would depend on the actual size of the unit. It may be reasonable to assume a constant discharge pressure about a given operating point. However, the turndown requirements associated with a flexible plant may exceed the safe operating limits of a unit. Thus, the desired discharge pressure may not always be attainable.

This problem would normally be addressed in the detailed design of the individual units. Therefore, in this study, it has been assumed that the unit is capable of safe and satisfactory operation for each feedstock condition.

3.3.8.2 *Pump Unit*

Each pump unit is required to handle a large turndown ratio and pressure differential. The choice of suitable pump (be it positive-displacement or centrifugal) is governed by several factors (Peters and Timmerhaus, 1968). A centrifugal pump has been selected for each application in this study as it delivers fluid at uniform pressure, without shocks or pulsations in the discharge line. This pump gives the added advantage of being able to operate safely with a partly or completely closed discharge line. Hence, a control valve may be positioned in the discharge line, to prevent cavitation, without damaging the pump. However, these advantages are offset by two factors - the unsuitability of the centrifugal pump at high heads, and the narrow operating range at maximum efficiency.

It has been assumed that the centrifugal pump can be adequately described by its static behaviour. (The liquid content within the pump is so small as to produce very fast dynamics, about the surrounding pipework). Several relationships have been developed for an ideal centrifugal pump, relating impeller speed, fluid discharge, pressure head and power requirement. However, they assume there is no frictional, leakage or recirculation losses. In practice, pump performance can best be determined from experimental data, in the form of characteristic curves supplied by the manufacturer.

The pressure rise across a pump may be described by the pump characteristics in the form:

$$\frac{\Delta p}{\rho} = k_1 N^2 - k_2 F^2 \qquad (3.49)$$

where N is the pump speed, and k_1 and k_2 are functions of the pump design (Shinskey, 1988). This relationship (3.49) indicates that outlet pressure may be controlled directly by varying the discharge flow rate. Thus, the demanded pressure will always be maintained, and it is reasonable to assume perfect pressure control.

A steady state pump description is considered adequate for the overall plant simulation, assuming each pump design is sufficient to handle a variety of operating conditions. The power requirement for a pump has been given by:

$$P = \frac{\Delta p\ W}{\rho\ \eta} \tag{3.50}$$

with an associated discharge enthalpy of:

$$h_2 = h_1 + \frac{\eta_t P}{F} \tag{3.51}$$

The rise in discharge temperature due to friction energy is assumed to be very small. However, this increase depends on the pressure rise, rather than pump size. The pump efficiency may vary according to changes in operating conditions, effected by different feedstocks, especially for the larger turndown ratio cases.

Pressure control through a pump is usually achieved by manipulating a control valve. The pump is sized to deliver maximum flow at a desired pressure with the valve fully open. At lower flows, the control valve closes to maintain the discharge pressure. Thus, a pump is normally controlled by flow rather than discharge pressure. This suggests that discharge pressure varies with changing operating conditions. However, the relationship in (3.49) has not been modelled, and discharge pressure has been assumed constant.

3.3.8.3 *Knock-out Pot*

Two knock-out pots are used to remove excess water vapour (and trace hydrocarbons) downstream of the reforming operation. A knock-out pot separates most of the liquid from a two-phase stream. The separation takes place in a vertical vessel where gravity settling allows the liquid to collect at the base. The hold up time associated with liquid collection is typically about 10 minutes (Sinnott, 1983).

The knock-out pot is similar to a flash unit, except that the mixed phase feed is separated without any change in pressure or temperature, assuming negligible heat exchange with the surroundings. Hence, only mass and component balances are required. As there is negligible vapour hold up associated with the process stream passing

through the drum, the model is reduced to a steady state simulation. The dynamics of the liquid phase can be neglected as they represent the effluent stream, which is beyond the scope of the plant model. Also, as liquid level in the knock-out pot would be maintained by manipulating the liquid product flow rate, perfect liquid level control has been assumed.

The simplified model was based on component and mass balances. The proportion of vapour to liquid streams was obtained from a steady state flash calculation of the mixed phase feed stream. Product compositions and flow rates were derived from the vapour-liquid equilibrium relationship and consistency constraints in (3.30).

3.3.8.4 *Mixer*

The five mixing operations are involved in either vapour or liquid phase mixing. Gas mixing normally occurs in a length of pipe with turbulent flow conditions, where turbulence promoters may be introduced to increase the rate of mixing. Mixing liquids is more difficult, depending on the viscosity of the liquids.

There will be negligible dynamics associated with vapour phase mixing. However, the dynamic behaviour of a liquid phase mixer depends on the type of mixer employed. Shinskey (1988) developed a first-order plus dead time model to describe the dynamic behaviour for incomplete mixing. As both mixers (M-01 and M-02) in Figure 2.13 deal with similar stream compositions, it was assumed that the fluids were fully mixed before reaching the next operation. Hence, each mixer was described by steady state equations, including the energy balance:

$$h_3 = \frac{F_1 h_1 + F_2 h_2}{F_3} \qquad (3.52)$$

where subscripts 1, 2 and 3 refer to the feed and product streams, respectively. As flow resistance in the pipework has not been included in the simulation, the lower pressure of the two incoming streams was adopted as the new outlet pressure.

3.3.8.5 *Splitter*

The splitter plays a vital role in the flowsheet as it ultimately controls the proportion of feedstock fed to heavies processing. It is used to split the LNG feed, and forms the first part of the separation process.

There are negligible dynamics associated with this operation, and no sizing data or physical properties are required. Therefore, with ratio control maintaining the split ratio on the heavies processing stream, the mass balances were expressed as:

Controlled stream	$F_2 = (\text{split ratio}) \times F_1$	(3.53)
Wild stream	$F_3 = F_1 - F_2$	(3.54)
Composition	$x_{i,1} = x_{i,2} = x_{i,3}$	(3.55)

3.3.8.6 *Concluding Steady State Model Approximations*

Those units that have been approximated by steady state models are concerned with either vapour streams or units with a small hold up. Therefore, the dynamic behaviour associated with these process streams is fast, and would be negligible compared to the dynamic responses in other sections of the plant.

Many literature examples of the dynamic models discussed in this section also included the connecting pipe dynamics in the process simulation. In certain cases, the interconnecting pipework was simulated with slower dynamics than that of the units concerned (Roffel and Rijnsdorp, 1982). However, dynamic behaviour associated with the pipework has not been simulated. This condition has established a cut off point beyond which dynamic behaviour is so fast that it becomes negligible in the overall plant simulation. Even so, it is questionable whether the combined dynamics of all the faster units would still be negligible in the plant model. From a practical viewpoint, it is reasonable to assume that the above units can be approximated by steady state models, within the scope of a large dynamic simulation.

3.4 ACHIEVEMENTS AND CONCLUSIONS

The development of appropriate mathematical models for each unit in the preliminary flowsheet has been presented in this chapter. The requirement of these models is to collectively represent the dynamic behaviour of the plant about several operating conditions, with reasonable accuracy. This requirement was addressed throughout the model development process and Chapter 4 will show that they achieved this purpose.

Due to the number and variety of process units involved in the flowsheet, it was impractical and unnecessary to model each unit rigorously. Therefore, a two-level approach was adopted with only those units with appreciably slow dynamics represented by dynamic models. The overall simulation will be formed from a collection of the steady state and dynamic models developed.

Most of the rigorous dynamic models described in the literature review were either empirical or semi-empirical, in that they relied upon real plant data to fully define the model parameters. As this work represented a preliminary design study, detailed design information was limited. Hence, the accuracy of each model was dictated by available unit data and anticipated simulation runtime.

In the case of the distillation column, a novel pseudo-binary distillation column model was developed. This model retains the key features of a multicomponent system by incorporating simplistic representations of each tray, based on data for each operating condition. This model should accommodate the requirement for accurately modelling the range of feedstock conditions without the added complications of a true multicomponent model.

The models developed in this chapter will be validated and employed in the dynamic simulation of the preliminary flowsheet. This work will be described in Chapters 4 and 5.

CHAPTER 4

DYNAMIC SIMULATION OF FLOWSHEET OPERATIONS

4.1 INTRODUCTION

The implementation and validation of dynamic models for the preliminary LNG reception terminal process units are presented in this chapter.

Firstly, appropriate dynamic simulation facilities are selected to accommodate the requirements of the industrial sponsor, British Gas plc. As the eventual complete plant simulation will represent a design tool for the analysis of feedstock changeovers, it is necessary to develop these individual models in an adaptable and effective simulation environment. Therefore, a flexible model structure and naming convention is defined for generic models. Furthermore, simulation accuracy will depend on the quality of physical properties data used for the range of feedstock conditions. This preparatory design work is described in Section 4.2.

The dimensions and parameters describing each unit are identified in Section 4.3. The dynamic model of each process unit is validated in the steady and dynamic states. This work is presented and discussed in Section 4.4.

These individual models will be used in the complete plant simulation model to be built in Chapter 5.

4.2 DYNAMIC MODEL ENVIRONMENT

The number of operations in the preliminary flowsheet, and the required level of modelling detail suggested that a powerful simulation package would be required to model the fully integrated system. Hence, an assessment of available simulation facilities was conducted to select the most appropriate package, and this assessment is described in Appendix 4. The ACSL simulation facility was finally chosen because:

(i) ACSL was available to both parties in the project.

(ii) ACSL had been successfully applied in previous research projects, and so technical expertise was available.

(iii) ACSL is FORTRAN-based, and therefore several computing tools could be employed to support the simulation.

A model structure was defined for the complete simulation that met the need for an adaptable modelling environment. It was also recognised that physical property values could not be assumed constant in this simulation, as several feedstock conditions were to be represented. Therefore, various means of deriving the physical properties were considered in the initial stages of ACSL modelling. The above requirements are addressed in the following subsections.

4.2.1 ACSL Model Structure

The preliminary flowsheet in Figure 2.13 contained many operations. Thus, a consistent and flexible model structure was devised prior to model implementation, and developed on two levels:

(i) A strict naming convention identified each variable, which could be generically applied to every process unit in the flowsheet simulation.

(ii) The flowsheet coding was segmented into discrete units, corresponding to the individual operations. This allowed each unit to be modelled independently, which simplified validation and enhanced model development.

4.2.1.1 *Parameter and Variable Naming Convention*

The process streams and units in the preliminary flowsheet were numbered using standard conventions. The labelled flowsheet is

illustrated in Figure 4.1. Each of the parameter and variable names were referenced according to a process stream number. This approach is effective as process stream conditions remain unchanged between operations, and the information relating to each stream is described by a single variable name.

Physical property names were generated in two parts; by the property condition and stream number. For example,

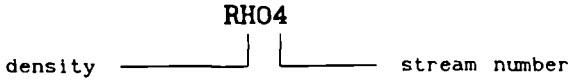

described the density of stream 4, downstream of pump **P-02**. Similarly, all parameters relating to a unit were referenced according to the inlet stream number. So, the cross sectional area of the flash unit, **F-01**, was given as:

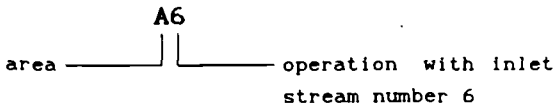

As there were a total of 11 possible components in the process route, it would be appropriate to describe the molar composition of each process stream in array form. However, the ACSL model coding convention imposed many restrictions on the use of arrays (MAGA, 1987). Therefore, only the heavy hydrocarbons were described by an array, of dimension 5. Each component was referenced according to:

(i) Stream phase.
(ii) Component identity - a letter.
(iii) Stream number.

The component names for liquid and vapour phase streams are listed in Table 4.1. A glossary of the variable names used in subsequent ACSL simulation plots is given in Table 4.2. The stream numbering convention is as defined in Figure 4.1.

4.2.1.2 *Flowsheet Model Structure*

The ACSL model structure was influenced by two factors; the need for a flexible model structure, and the multiple occurrence of many operations. As a result, a modularised approach was adopted to develop the fully integrated model, by describing each type of operation within its own ACSL-coded macro. A macro is similar to a

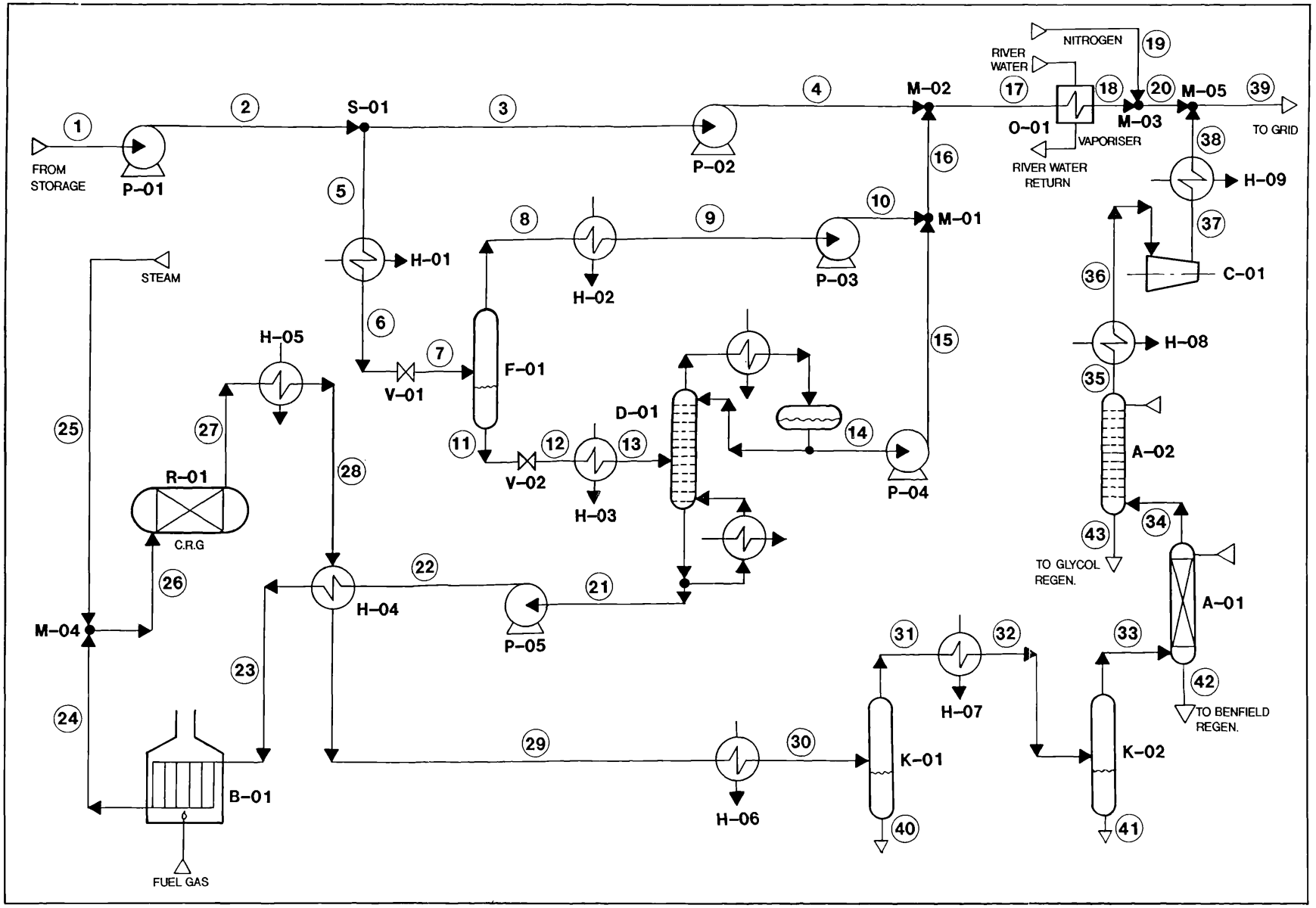

Figure 4.1 Labelled flowsheet schematic

FORTRAN subroutine - it is defined only once, but may be used many times. In addition:

(i) Variables and statement labels may be generated locally.

(ii) Macros may invoke other macros, exhibiting a hierarchical structure.

(iii) Macros may be placed anywhere in the model provided they are defined before they are invoked.

Liquid Phase	Vapour Phase	Component
XA##	YA##	CH_4
XB##(1)	YB##(1)	C_2H_6
XB##(2)	YB##(2)	C_3H_8
XB##(3)	YB##(3)	nC_4H_{10}
XB##(4)	YB##(4)	iC_4H_{10}
XB##(5)	YB##(5)	nC_5H_{12}
XC##	YC##	CO
XD##	YD##	CO_2
XE##	YE##	H_2
XF##	YF##	H_2O
XN##	YN##	N_2

= stream number

Table 4.1 ACSL stream composition

ACSL variable name	Definition
ENTH##	Stream enthalpy
F##	Molar flow rate
H##	Liquid level
L	Distillation column reflux
MW##	Stream molecular weight
P##	Pressure
RHO##	Stream density
T##	Stream temperature
V	Distillation column boilup
XA##	Proportion of methane in liquid phase
XB##(1)	Proportion of ethane in liquid phase
YA##	Proportion of methane in vapour phase
YB##(1)	Proportion of ethane in vapour phase

= stream number

Table 4.2 ACSL variable naming convention

Adopting a macro structure for the ACSL code enabled a library of unit models to be developed describing the operations. In the ACSL code, a macro call statement invoked the drive or front-end macro that was defined by its macro name and the corresponding inlet and outlet process stream numbers for the operation. For example,

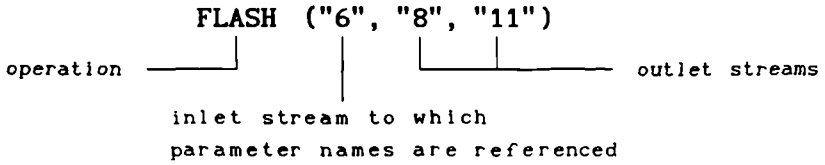

Therefore, as each operation was identified and modelled by a generic drive macro, which calls up further macros, multiples of existing units were incorporated in the flowsheet model without introducing additional ACSL code.

The flexibility of coding with this type of ACSL model structure was demonstrated by the simplicity of adding or removing process units from the original ACSL model. Provided the units already existed in the flowsheet, changes to the model could be simplified to macro call statements and parameter requirements. *Removing* a unit from the flowsheet model was achieved by removing the corresponding macro call statement. *Adding* a unit to the original flowsheet model was more involved as new parameters had to be assigned to describe that unit. However, the use of macros demonstrated that a flexible model structure could be developed for the dynamic simulation.

4.2.2 **Physical Properties Database**

To assess plant flexibility for the preliminary flowsheet design, it was imperative that the simulation mimicked each feedstock condition. Hence, most physical properties (PP) could not be assumed constant, as was assumed in simplified dynamic modelling, because the PP varied. Typical PP requirements for the flowsheet included enthalpy, density and vapour-liquid equilibrium (VLE) values.

Several approaches to deriving the physical properties were investigated. Initially, some PP values were obtained from a data package about the GL2Z feedstock condition, and linearly extrapolated for the dynamic simulation. However, values were only reasonable

when close to the original operating point, and often resulted in unacceptable errors at the other feed conditions. Some PP values were also approximated using standard correlations (Sinnott, 1983), assuming ideal vapour and liquid correlations. The results for most streams were found to be inaccurate, except in two regions:

(i) Low temperatures and pressures for the liquid phase.

(ii) High temperatures and pressures for the vapour phase, below critical conditions.

However, the accuracy of these methods deteriorated as critical conditions were approached. In the vapour phase, this was attributed to the compressibility factor, Z, being assumed constant. These results showed that Z would have to be incorporated as a variable in the PP calculations. Therefore, an analytical equation of state was considered that formed an algebraic relationship between pressure, temperature and molar volume. The Redlich-Kwong-Soave (RKS) equation-of-state was recommended for this application (PROCESS manual, 1987), as it is reliable at critical conditions, and especially for hydrocarbon mixtures (except liquid phase density). Several approaches to using the RKS method are presented by Raman (1985) and Reid et al. (1987).

Although a suitable calculation procedure was identified, source data was still required for critical properties and acentric factors. A comparison of VLE values for the flash unit, adopting the RKS method within several PP data packages, gave inconsistent results. This was due to the source data, as all other conditions were identical. As sufficiently accurate results could not be obtained using traditional methods, the physical properties database (PPD) used in the British Gas in-house simulation package, was then adopted for the dynamic simulation. This database, entitled the "British Gas Thermophysical Properties Database", enabled the reflection of the preliminary flowsheet steady state conditions derived in Chapter 2.

The PPD was written in FORTRAN, and accessed interactively in ACSL using a series of drive subroutines. The source data was limited to the 11 flowsheet components, and the calculations used a selection of recommended methods, including:

. Ideal Gas Equations

. COSTALD (liquid density)
. TRAPP (viscosity and thermal conductivity)
. LRS Equation of State (a modified form of the RKS method).

As the PP requirements for each stream differed, "drive" subroutines were developed to calculate selective groups of PP's. These drive subroutines, listed in Table 4.3, included compatibility and conversion statements for single and double precision variables, and arrays. Iteration loops were included in some drive subroutines, where an initial estimate was iterated to obtain the new PP value.

Inputs	Outputs	Application
. Stream composition . Temperature . Pressure . Phase	. Molecular weight . Density . Enthalpy . Specific heat capacity	General
. Temperature	. Chemical equilibria	CRG reformer
. Stream composition . Temperature estimate . Pressure . Enthalpy	. Temperature †	General
. Stream composition . Temperature . Pressure	. Vapour and liquid compositions . Vapour fraction	K.O. pot
. Liquid composition . Temperature . Pressure estimate	. Vapour stream composition † . Pressure †	Flash unit
. Inlet compositions . Inlet temperatures . Inlet pressures	. Outlet temperatures †	Counter-current heat exchanger

† iterative calculations

Table 4.3 Physical property subroutine calculations

4.3 MODEL IMPLEMENTATION

Each operation was modelled independently in ACSL using a generic macro structure. Certain units required additional information before they could be implemented, such as sizing data and time constants. Each dynamic model also required a preliminary control loop structure, integration algorithm and step size to be fully defined. These aspects are discussed in the following subsections.

4.3.1 Data Collection for Individual Units

Sizing and performance parameters were mainly required for the dynamic models described in Section 3.2. The sizing data was derived from three different sources:

(i) Steady state simulation data.
(ii) Recognised scaling procedures.
(iii) Literature examples.

Most of the design data for the flash unit and distillation column was based on the steady state simulation results for the three feedstock conditions. The reflux drum sizing was calculated independently and is presented in Appendix 5. The steady state simulation results for the counter-current heat exchanger gave a different heat transfer coefficient, U, for each condition as U is a function of the stream composition, flow characteristics, and stream conditions. Hence, an average of the three values was adopted for U and included as the product of heat transfer coefficient and surface area, UA.

The CRG reformer and ORV unit tube sizings were derived from scaling dimensions. The CRG reformer calculations are included in Appendix 5. Time constants and dimensions for the ORV unit were also derived in Appendix 5, as part of the transfer function model development. A summary of the key dimensions is given in Table 4.4.

The data requirements for each operation in the flowsheet are summarised in Figure 4.2.

OPERATION	DATA
Distillation Column	
Number of theoretical trays	11
Feed tray	4
Column diameter (m)	2.7
Weir height (m)	0.122
Height between trays (m)	0.6
Reflux drum area (m^2)	22.0
Downcomer (fraction of column area)(%)	12.5
Francis weir constant ($kgmol/(m^{3/2} hr)$)	422354
CRG Reformer	
Tube bundle cross sectional area (m^2)	1.478
Tube length (m)	2.4384
Heat of reaction (kJ/kgmol):	
Equation 3.20 C_2	+346955.6
C_3	+498260.0
nC_4	+651770.0
iC_4	+660500.0
nC_5	+803800.0
Equation 3.21	-41229.4
Equation 3.22	-206176.3
Flash Unit	
Diameter of drum (m)	5.79
Height of drum (m)	14.48
Initial liquid level in drum (m)	2.90
Counter-current Heat Exchanger	
UA (kJ/K hr)	583704
Temperature lag time constant (hr)	0.0089

Table 4.4 Dynamic model parameters

4.3.2 **ACSL Modelling**

Development of the generic macros for each unit was undertaken in two sections. The specific requirements addressed within each macro were:

(i) Suitable integration algorithm and time step.

(ii) Preliminary control loop structure.

(iii) Initial conditions.

The ACSL software includes eight different integration algorithms, ranging from low order, fixed step algorithms, to variable order and variable step algorithms. The lowest order of integration algorithm was adopted for the steady state models, with an arbitrary time step.

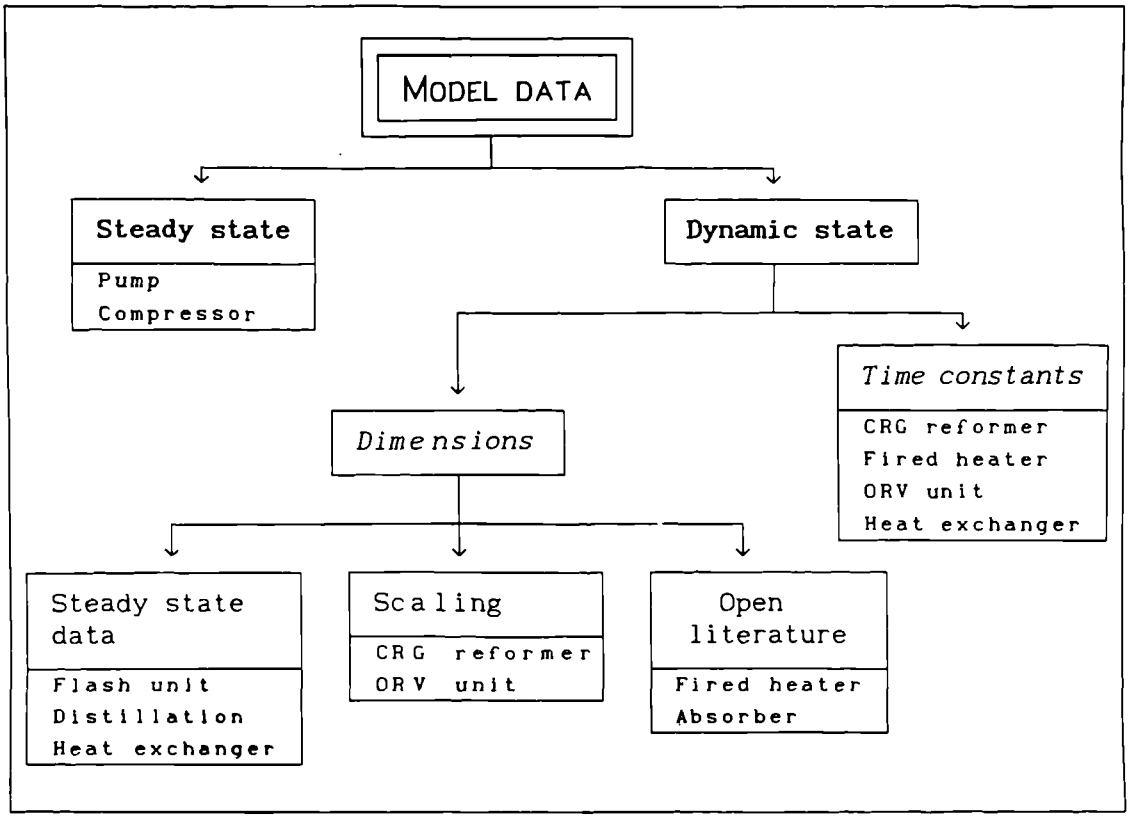

Figure 4.2 ACSL model data requirements

As the dynamic models included differential and iterative calculations, an appropriate integration algorithm and step size was determined for each dynamic model. Achieving an appropriate step size was important since a large step size would result in inaccurate and unstable results, whereas a small step size would promote unnecessarily high runtime. Two approaches were recommended (MAGA, 1987) for determining the appropriate step size:

(i) Use a variable step algorithm to initially run the model, and access information on the current step size and integration order used by the algorithm. This will suggest whether a fixed or variable step algorithm is appropriate, and recommend a suitable step size.

(ii) Calculate the smallest time constant of the system; the recommended step size should be less.

The first approach was adopted for each dynamic model. It was found that a variable step algorithm was more suitable for the distillation column as both step size and integration order varied markedly. This

model is known as a stiff system (Schwarz, 1989), where stability can be better retained by using an implicit multistep method. Hence, the Gear's Stiff method was adopted. The time step limits were selected by considering tray dynamics, using the second approach.

The 4^{th}-order Runge-Kutta integration algorithm was selected for the remaining dynamic models, with a step size of 10^{-3}hr. The use of iterative calculations in deriving the product composition for the CRG reformer made this dynamic model particularly sensitive to integration step size. In addition, there was a significantly smaller time delay associated with the flow through the catalyst tubes. So, the integration time step was less than the dominant time constant for variations in catalyst enthalpy. The remaining dynamic models in the preliminary flowsheet were adequately serviced by the 2^{nd}-order Runge-Kutta integration algorithm.

Most of the dynamic models required control valves on the inlet or product streams to be fully specified. Thus, a preliminary control loop structure was introduced to the individual units. This was later refined as part of the control studies for the complete flowsheet, and is discussed in Chapter 6.

4.4 MODEL VALIDATION

Model validation was an essential step in ensuring that sufficiently accurate and flexible models were developed. This stage preceded the fully integrated dynamic simulation of the plant and hence concentrated on individual models.

Those operations that were approximated by steady state descriptions, listed in Table 3.1, did not require validation as they were developed to comply with the existing steady state data. Hence, model validation was only concerned with the dynamic models at multiple operating conditions. The steady state and dynamic behaviour of each dynamic model was assessed and the results are reported in this section.

4.4.1 Steady State Validation

A steady state validation was conducted on the selected dynamic models for each design condition. In each case, feed and operating conditions relating to each LNG feedstock were introduced and the simulation proceeded to a new steady condition. This required the introduction of preliminary control loops to allow each model to move between operating conditions.

The dynamic models considered in this validation exercise were the distillation column, CRG reformer and flash unit. Each model could move between the operating conditions when subjected to a step change in conditions. The ACSL simulation results at each new steady state condition were compared with the steady state simulation results first employed in Chapter 2. Results for the dynamic models are presented in Appendix 6. In each case, the model was considered sufficiently accurate if the process conditions produced by ACSL agreed to within 10% of the steady state simulation data. Each model was found to satisfy this requirement.

As the look-up tables used in the dynamic model of the distillation column were developed from steady state data, the overall results compared favourably for the specified feedstocks. The maximum steady state error for any variable (see Appendix 6) was 8.5%, on reflux.

The accuracy of the *heavies* ratio look-up tables for multicomponent tray compositions was investigated at intermediate feed conditions, by introducing a series of feeds and conducting a component balance when the model reached its new steady state. The corresponding results in Table 4.5, showed good agreement for most components in the intermediate feeds I to IV, except the iC_4H_{10} and nC_4H_{10} components. This discrepancy was attributed to the look-up tables' limited data, which was based on only three feed conditions.

Feed Stream	I	II	III	IV	V	VI
Feed molar flow rate (kgmol/hr)						
C_1	5350	5246	5197	5002	5551	4636
C_2	519	565	610	689	427	854
C_3	122	168	165	274	52	366
iC_4	36	44	48	52	--	91
nC_4	31	33	37	46	15	61
nC_5	12	15	12	6	--	--
N_2	31	31	30	30	55	91
Total*	6100	6100	6100	6100	6100	6100
Product molar flow rate (kgmol/hr)						
C_1	5350	5246	5197	5002	5551	4636
C_2	521	568	605	747	409	1110
C_3	124	165	174	224	67	267
iC_4	22	31	33	42	--	26
nC_4	40	45	43	46	35	31
nC_5	10	14	12	7	--	--
N_2	33	31	30	30	38	31
Total*	6100	6100	6100	6100	6100	6100

* sum of flow rates ≠ total due to roundup errors

Table 4.5 Results for distillation column at intermediate feeds

The remaining feed conditions in Table 4.5, V and VI, were chosen outwith the LNG feed data region. Their results gave good agreement for methane component and total mass balances. However, the remaining component balances were erroneous, as the *heavies* ratio data was no longer reliable. A recommended operating envelope for the distillation column feed, specifying the look-up table boundaries, has been defined, and is given in Table 4.6. Although a selection of product compositions at intermediate feedstocks

contained component balance inaccuracies, the dynamic model was considered adequate for subsequent simulation and control studies.

Distillation column feed composition	Lower limit	Upper limit
C_1	0.7874	0.9065
C_2	0.0763	0.1290
C_3	0.0566	0.0082
iC_4	0.0000	0.0119
nC_4	0.0036	0.0097
nC_5	0.0000	0.0026

Table 4.6 Recommended operating envelope for distillation column

The dynamic model results for the flash unit compared favourably with the steady state results given in Appendix 6. The slight mass balance offset was attributed to the varying liquid level.

The results in Appendix 6 have demonstrated that the dynamic models can achieve their new steady state conditions with a reasonable level of accuracy. In addition, the models could change from one LNG feedstock condition to another, in response to a step change in conditions.

4.4.2 **Dynamic Model Validation**

The dynamic model validation has been conducted on several dynamic models, to assess their open-loop step response behaviour. These responses were obtained about an initially steady GL2Z feedstock condition, with the preliminary control loops disabled. A typical step disturbance to an inlet condition was then introduced, and the simulation proceeded until the model reached its new steady condition.

Although the control loops were disabled, the final control elements (control valves) were retained. (This was achieved in the simulation by setting controller gain to zero and the control valve bias equivalent to the valve position for the GL2Z feedstock condition). Hence, the valve characteristics were included in the open-loop step responses, as the associated molar flow rate through a linearly installed valve is governed by the following relationship:

$$F = C_v \sqrt{\frac{\Delta p}{\rho}} \quad \frac{K_v}{mw} \tag{4.1}$$

where C_v is the control valve position (fixed for no control action), and K_v is a control valve coefficient. This meant the resultant flow rate through a fixed valve was related to the pressure difference and changes in the stream's physical properties.

The dynamic behaviour of process unit models would normally be validated against corresponding plant data. However, as this project represents a preliminary design study, no suitable data was available. Therefore, trends in the open-loop transient response curves were compared with results from similar operations in the open literature.

The models studied in this validation exhibited dynamic behaviour associated with changes in state variables, or as a result of first-order lags. The results are presented in the following subsections. The variable names associated with the ACSL simulation results correspond to Figure 4.1 and Table 4.2.

4.4.2.1 *Distillation Column Validation*

The distillation column model for open-loop step responses required four control loops. The corresponding control valves were located on the top and bottom product streams, reflux and reboiler energy, as illustrated in Figure 4.3. Thus, flow rate through these valves varied in relation to stream conditions. As perfect pressure control was assumed, this variation was limited to changes in the physical properties of each stream.

Literature examples of distillation column responses are generally concerned with step changes in reflux and vapour boilup (Fuentes and Luyben, 1983; Georgiou et al., 1988). Their corresponding open-loop step responses present the transients for top and bottom product compositions. Thus, the proposed step disturbances to the distillation column model have applied similar open-loop tests, about the GL2Z feedstock condition. These are listed in Table 4.7, for the model arrangement illustrated in Figure 4.3.

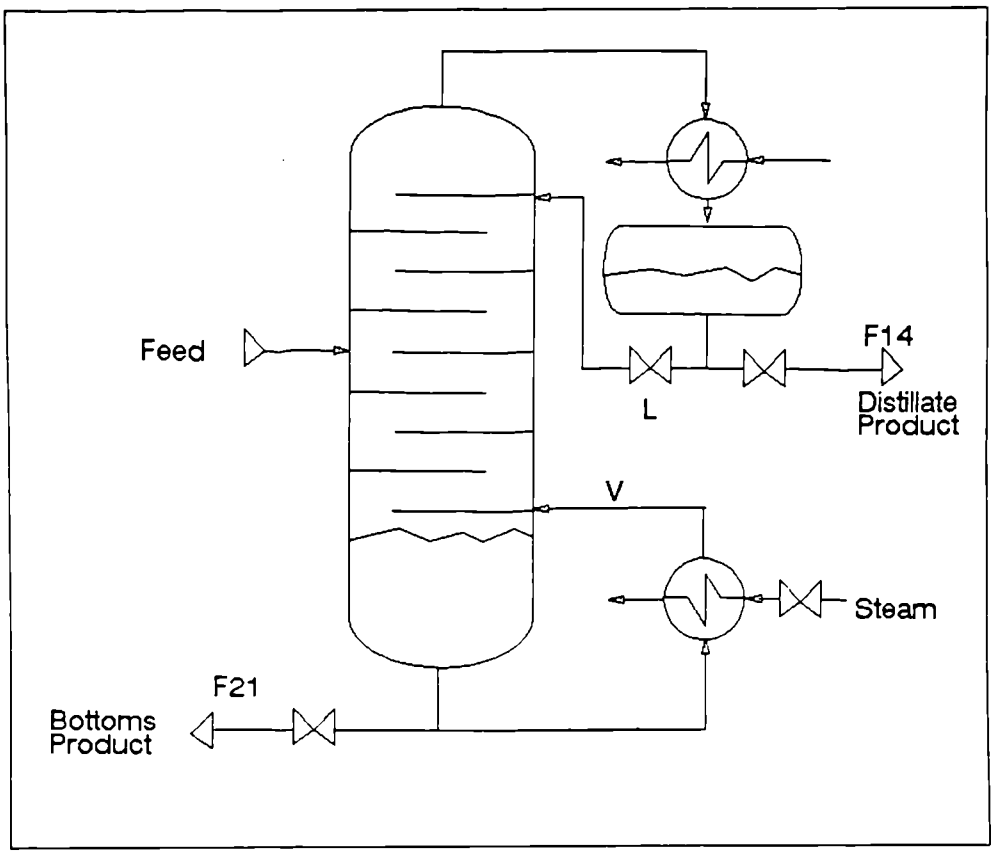

Figure 4.3 Simplified diagram of distillation column

Variable	Steady State Value	Step Value	Step Change
Reflux (kgmol/hr)	1854.38	1891.47 1817.29	+2.0% -2.0%
Boilup (kgmol/hr)	3694.81	3768.71 3620.91	+2.0% -2.0%

Table 4.7 Step disturbances to distillation column

Step change in reflux:

A 2% increase in reflux flow rate to the distillation column resulted in the reflux drum emptying before the simulation was completed. So, to allow a final steady condition to be achieved and maintained, level control was introduced. As the reflux and boilup streams were key variables in the validation exercise, the reflux drum and column base levels were controlled by manipulating top and bottom product flow rates, respectively, using proportional controllers.

The open-loop step response for an increase in reflux is shown in Figure 4.4, with level control active on the reflux drum and column base. The results showed that the increase in methane composition in the bottom product, XA21, was significantly greater than for methane composition in the top product, XA14, and were similar to those obtained by Georgio et al. (1988). The transient for XA21 was S-shaped, which suggested at least a second-order response. There was a marked undershoot in the boilup, V, which coincided with the sharply increasing gradient in XA21. This was caused by irregularities in the relative vapour enthalpies at the column base, which upset the enthalpy difference in the reboiler.

The open-loop step response for a 2% decrease in reflux flow rate are shown in Figure 4.5, with level control disabled. The composition trends were similar to those of Georgio et al. (1988) although XA21 varied to a greater extent than XA14. There was also a shorter time constant associated with these responses (approximately 0.13 hr compared with 0.60 hr for an equivalent step increase in reflux), with XA21 reacting faster than XA14.

Step change in boilup:
The open-loop step response for a 2% increase in vapour boilup is shown in Figure 4.6, with level control disabled. The trends in XA14 and XA21 were similar to those given by Fuentes and Luyben (1983). The model achieved its new steady state condition within 0.5 hr, with XA21 responding faster than XA14.

A 2% step reduction in boilup caused the reflux drum to empty before the new steady condition was achieved. So, the step response was repeated with level control active, as with the step increase in reflux. The resulting trends in top and bottom product compositions in Figure 4.7 resembled those of Fuentes and Luyben (1983), again with a smaller time constant associated with XA21 than XA14. The initial dip in boilup, originally identified in Figure 4.4, was also present in this response and was traced to a quirk in the enthalpy calculation for vapour flow. This may have resulted from the use of look-up tables to determine both multicomponent compositions and temperatures, creating a phase change and offset enthalpy value.

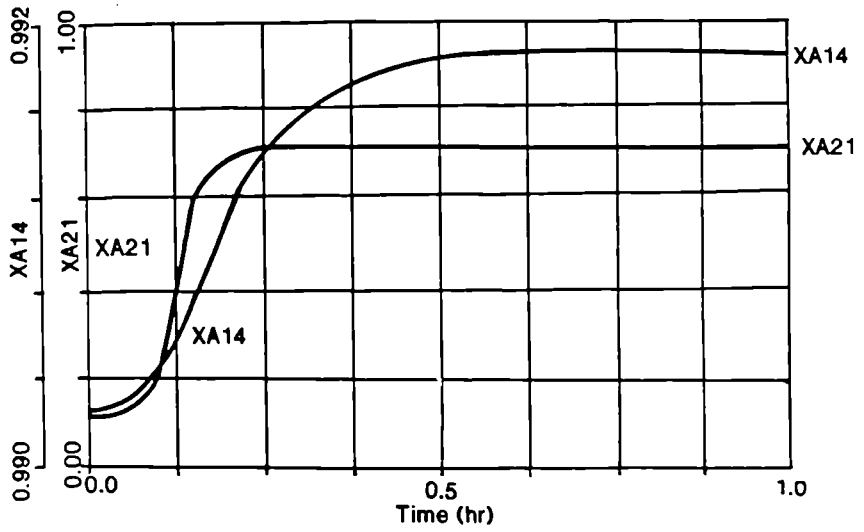

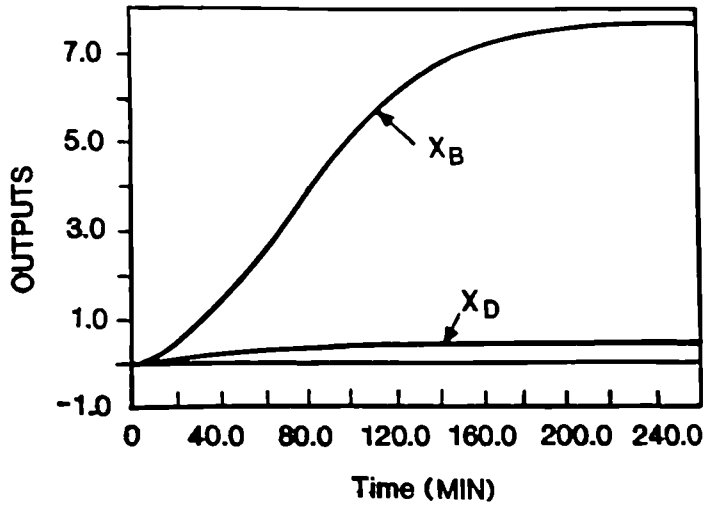

(Georgiou et al., 1988)

Figure 4.4 Open-loop step response to increase in reflux in the distillation column, with level control active

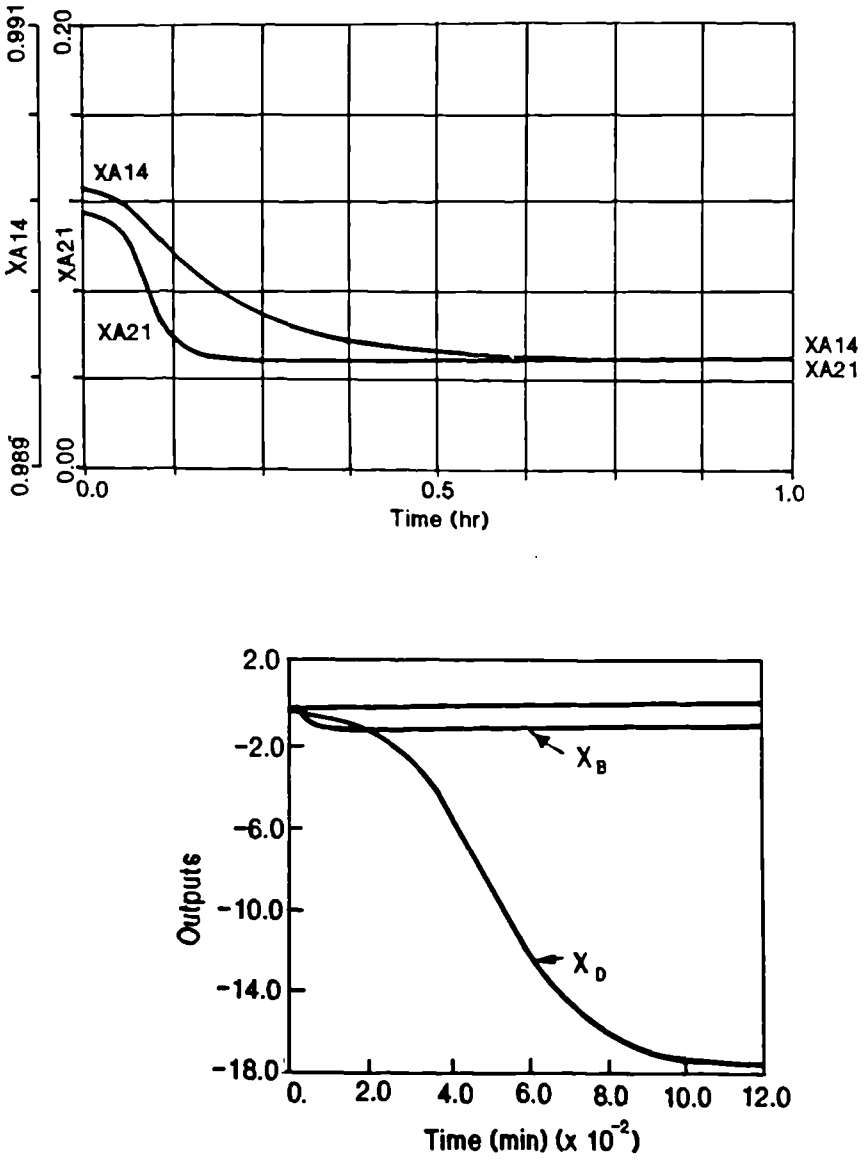

(Georgiou et al., 1988)

Figure 4.5 Open-loop step response to decrease in reflux in the distillation column

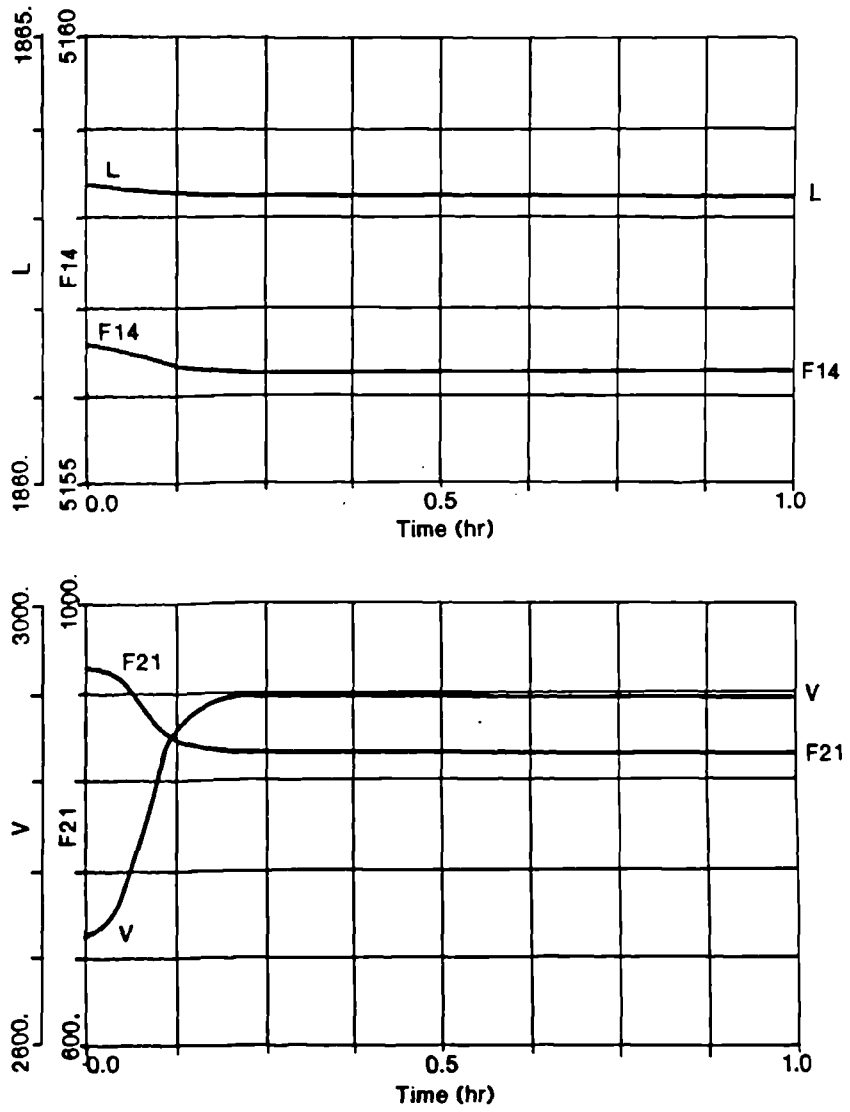

Figure 4.5 Open-loop step response to decrease in reflux in the distillation column (contd.)

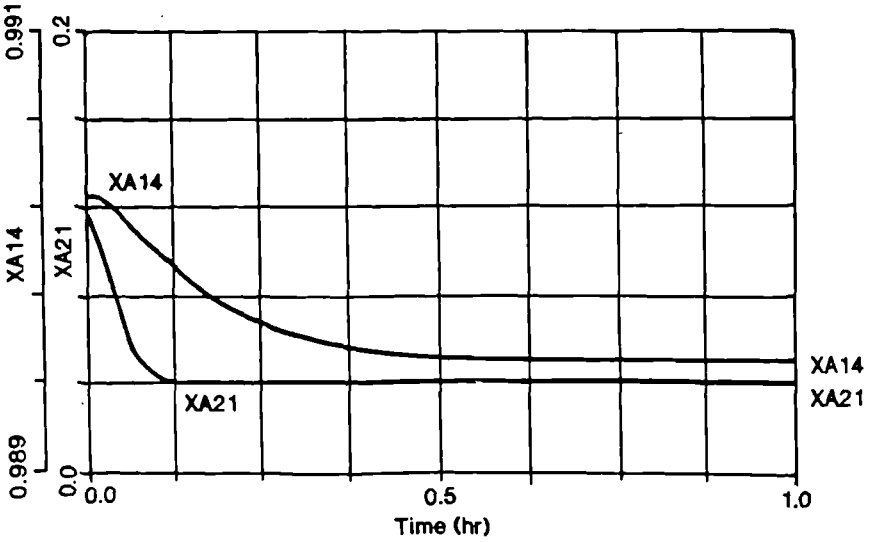

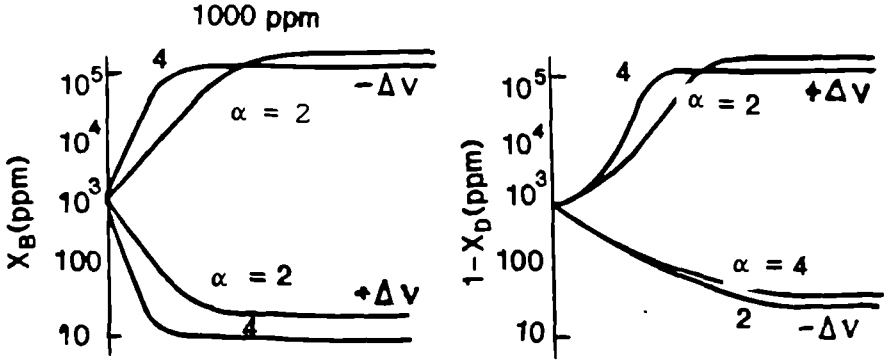

(Fuentes and Luyben, 1983)

Figure 4.6 Open-loop step response to increase in boilup in the distillation column

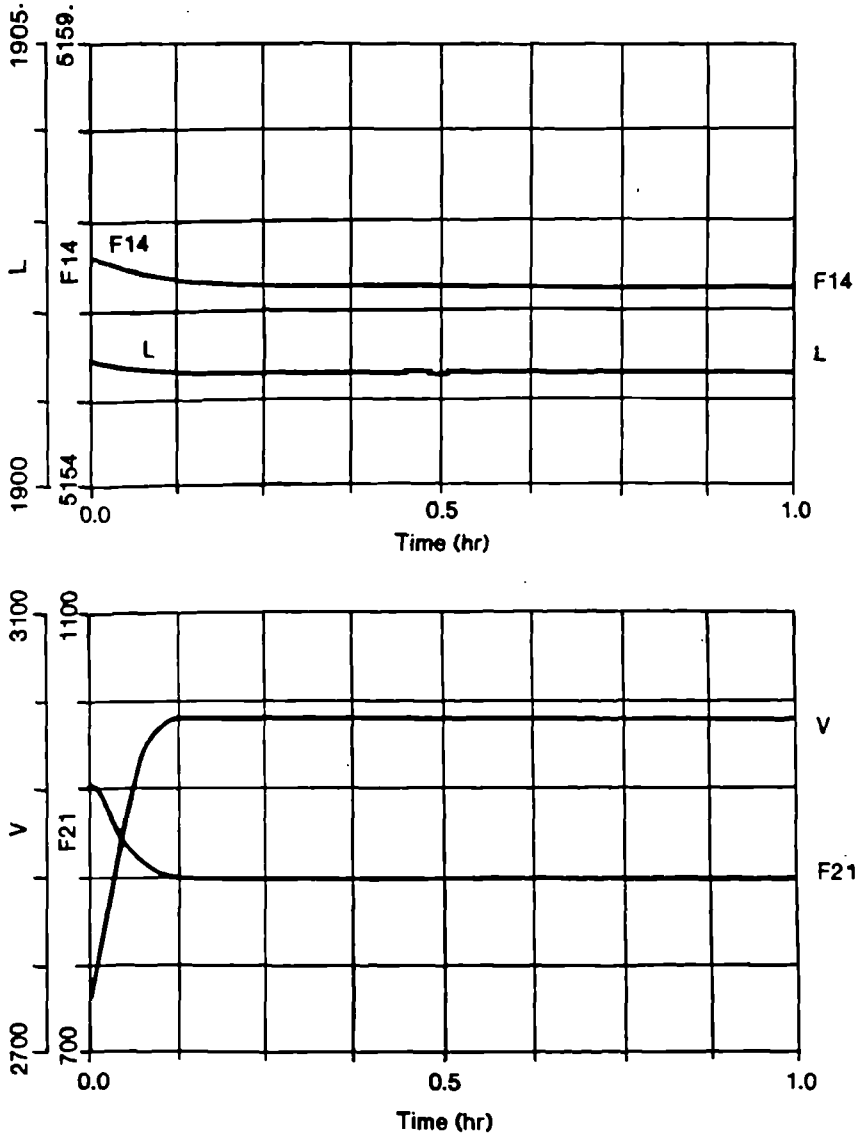

Figure 4.6 Open-loop step response to increase in boilup in the distillation column (contd.)

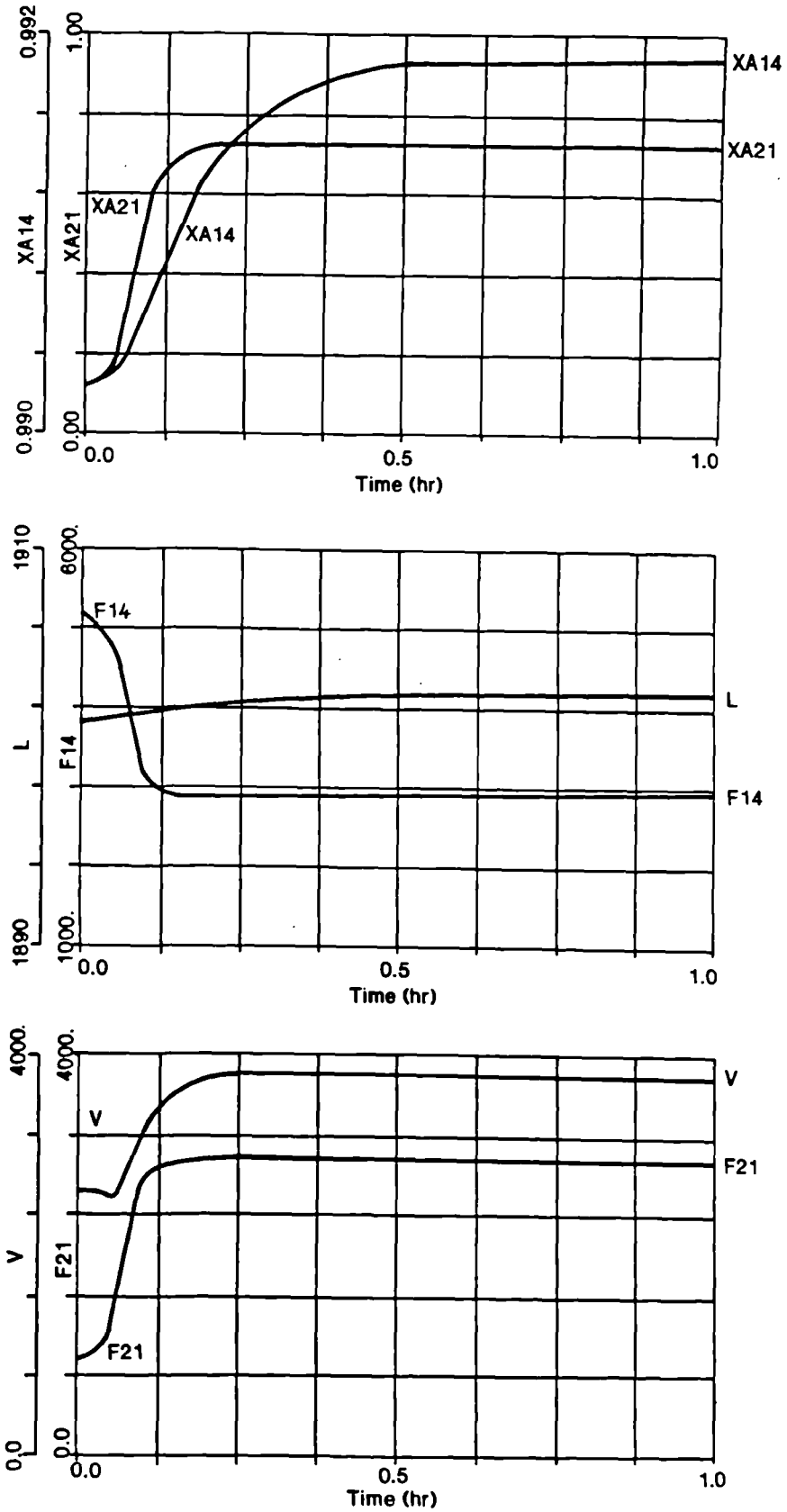

Figure 4.7 Open-loop step response to decrease in boilup in the distillation column, with level control active

Comparison with binary component distillation column model:

The above open-loop step responses for changes in reflux and boilup demonstrated the expected trends in top and bottom product compositions, and provided evidence of a satisfactory model for simulation studies. However, these responses only evolved in the later stages of model development. This has been demonstrated by comparing the current open-loop step results with those produced by the earlier version of the distillation column model. Previously, only binary components were available on each tray, and independent look-up tables were associated with each LNG feedstock condition. The corresponding open-loop step response for a 2% decrease in reflux for this binary component model is shown in Figure 4.8. Comparing this response with its upgraded equivalent in Figure 4.5, shows that the undershoots in XA21 and column base flows have been removed. This overall improvement in open-loop step responses has been attributed to two factors:

(i) Converting the *heavies* component to a multicomponent system, for calculating physical properties data.

(ii) Incorporating the *heavies* ratios in table form to allow variations in ratio values during transient conditions.

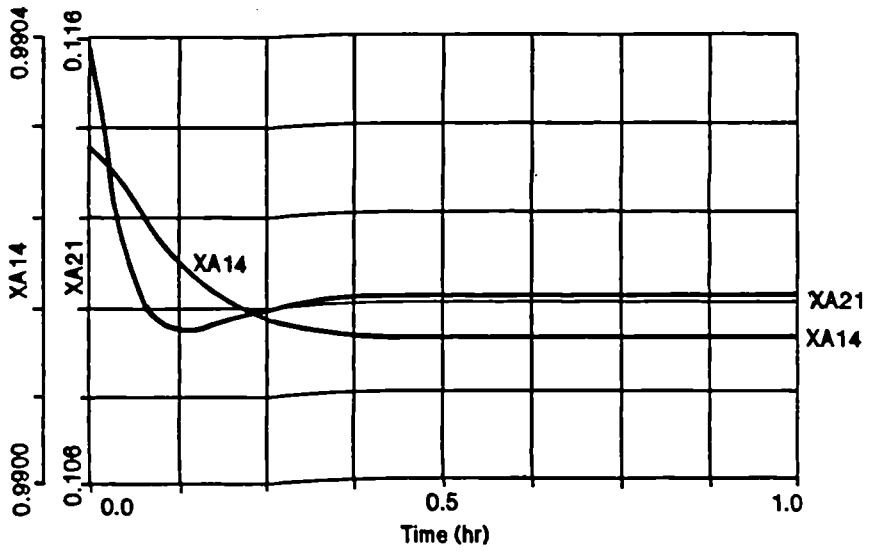

Figure 4.8 Open-loop step response to decrease in reflux in the binary distillation column model

4.4.2.2 *Heavies Processing Section Validation*

The counter-current heat exchanger, at the beginning of the heavies processing section, transfers heat from the CRG reformer outlet stream to the inlet stream. Therefore, as changes in the inlet stream conditions would affect the returning counter-current stream, the open-loop step response studies have included every operation within the heavies processing loop for the dynamic validation. This arrangement consisted of a counter-current heat exchanger, fired heater, mixer, CRG reformer and cooler. A simplified diagram of the heavies processing arrangement is shown in Figure 4.9, highlighting the important variables from streams 22 to 29.

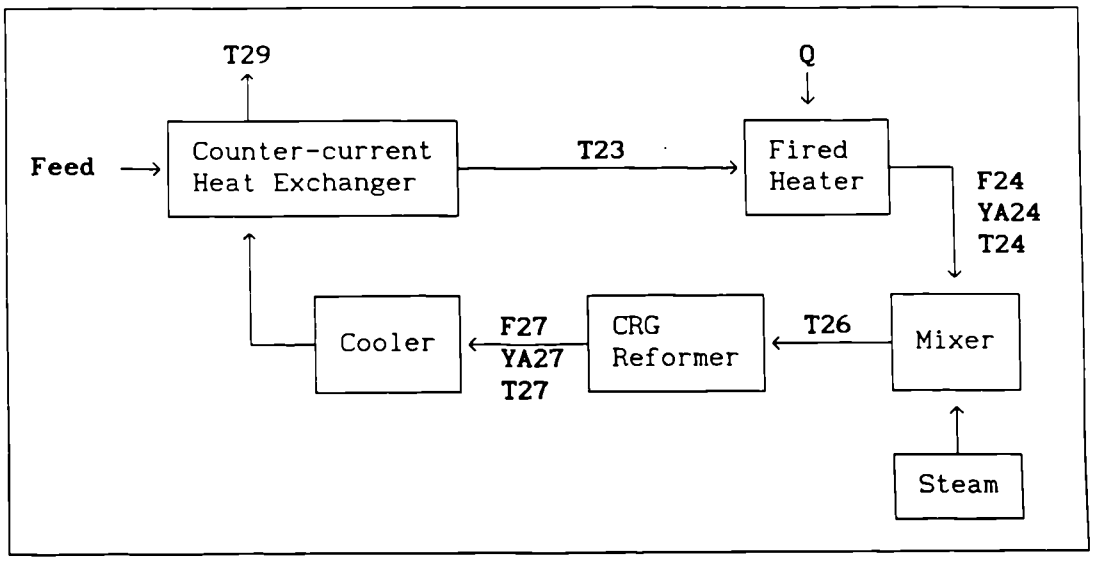

Figure 4.9 Block diagram of heavies processing section

There were potentially three manipulated variables in Figure 4.9; heat inputs to the fired heater and cooler, and steam to the reformer. Hence, this system was not modelled entirely open-loop as:

(i) Steam was added at a constant mass flow ratio.

(ii) The steady state cooler model maintained a constant outlet stream temperature.

The step disturbances are listed in Table 4.8.

Feed Stream Variable	Steady State	Step Value	Step
Flow rate (kgmol/hr)	945.50	992.78 898.23	+5% -5%
Methane composition	0.1158	0.1274 0.1042	+10% -10%
Temperature (K)	280.57	330.57 230.57	+50 K -50 K

Table 4.8 Step disturbances to heavies processing section at stream 22

Step change in flow rate:

A step increase in the feed flow rate initially decreased the heat exchanger outlet temperatures, T23 and T29, as illustrated in the corresponding open-loop responses in Figure 4.10. Time lags in the fired heater produced a gradual change in inlet conditions to the CRG reformer, in stream 24.

As the methanation reaction was exothermic, a reduced reformer inlet temperature, T26, enhanced the methane production, YA27. However, the initial rise in YA27 was cut back due to the variation in inlet conditions. The increase in feed flow rate was quickly transferred through the units to the CRG reformer, whereas the resultant change in enthalpy was significantly delayed, especially within the catalyst tubes. Only changes in flow rate and composition influenced the counter-current side of the heat exchanger, as the steady state cooler model assumed perfect temperature control. The complementary results for a 5% reduction in inlet flow rate showed a similar trend.

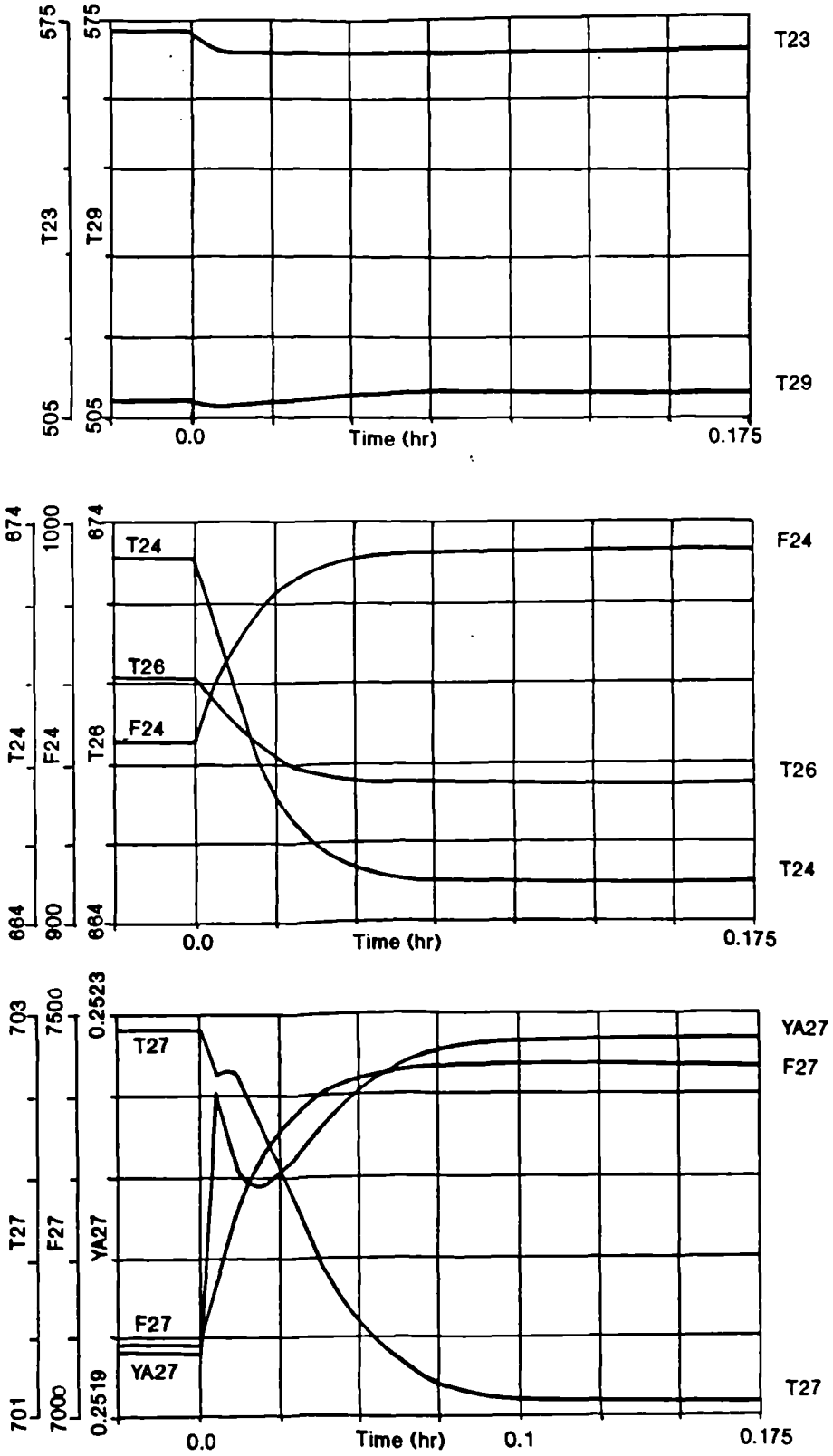

Figure 4.10 Open-loop step response to increase in feed flow to the heavies processing section

Step change in composition:

The resulting dynamic responses in Figure 4.11 showed an initial step increase in T23. This was caused by a sudden change in the product composition, which gave a different outlet temperature from the initial stream enthalpy.

The step increase in methane composition included a corresponding step decrease in the proportion of heavy hydrocarbons. So, there was less conversion of heavy hydrocarbons (endothermic reactions) resulting in a smaller reduction of intermediate tube temperature and thus an initial increase in product temperature. However, the more dominant effect of reducing intermediate CO production was to undermine final methane production, leading to a reduced product flow rate and temperature. This produced a non-minimum phase effect on both product temperature and methane composition. The increase in methane composition resulted from the methane enriched feed coupled with a greater conversion of CO. A 10% decrease in the methane composition produced complementary transients. Both open-loop step responses for the heavies processing section attained their new steady state conditions within 0.2 hr.

Step change in temperature:

A step increase in the inlet stream temperature raised both of the heat exchanger outlet stream temperatures, as illustrated in Figure 4.12. The gradual increase in T26 reduced the K-values in the methanation and water-gas shift reactions. Hence, less carbon monoxide was converted, and as the methanation reaction required 4 moles of reactant to produce 2 moles of product, the outlet molar flow rate increased as methane composition reduced. A converse transient was produced when the inlet stream temperature reduced by 50 K.

Summary of Heavies Processing Section Validation:

Following each disturbance to the heavies processing section, the CRG reformer achieved a new steady state condition. Each new condition was validated with results from a steady state simulation package, and showed good agreement.

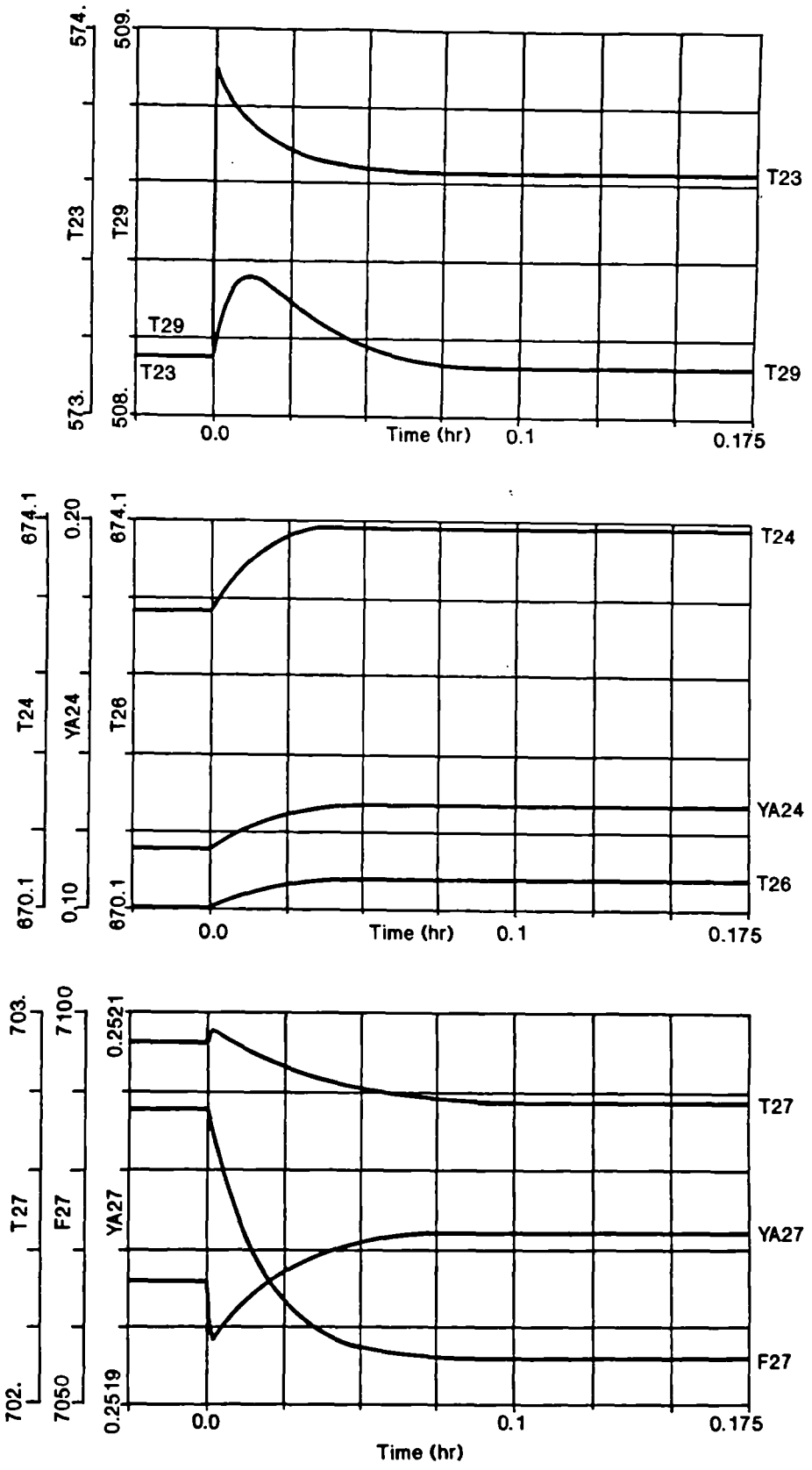

Figure 4.11 Open-loop step response to increase in methane feed to the heavies processing section

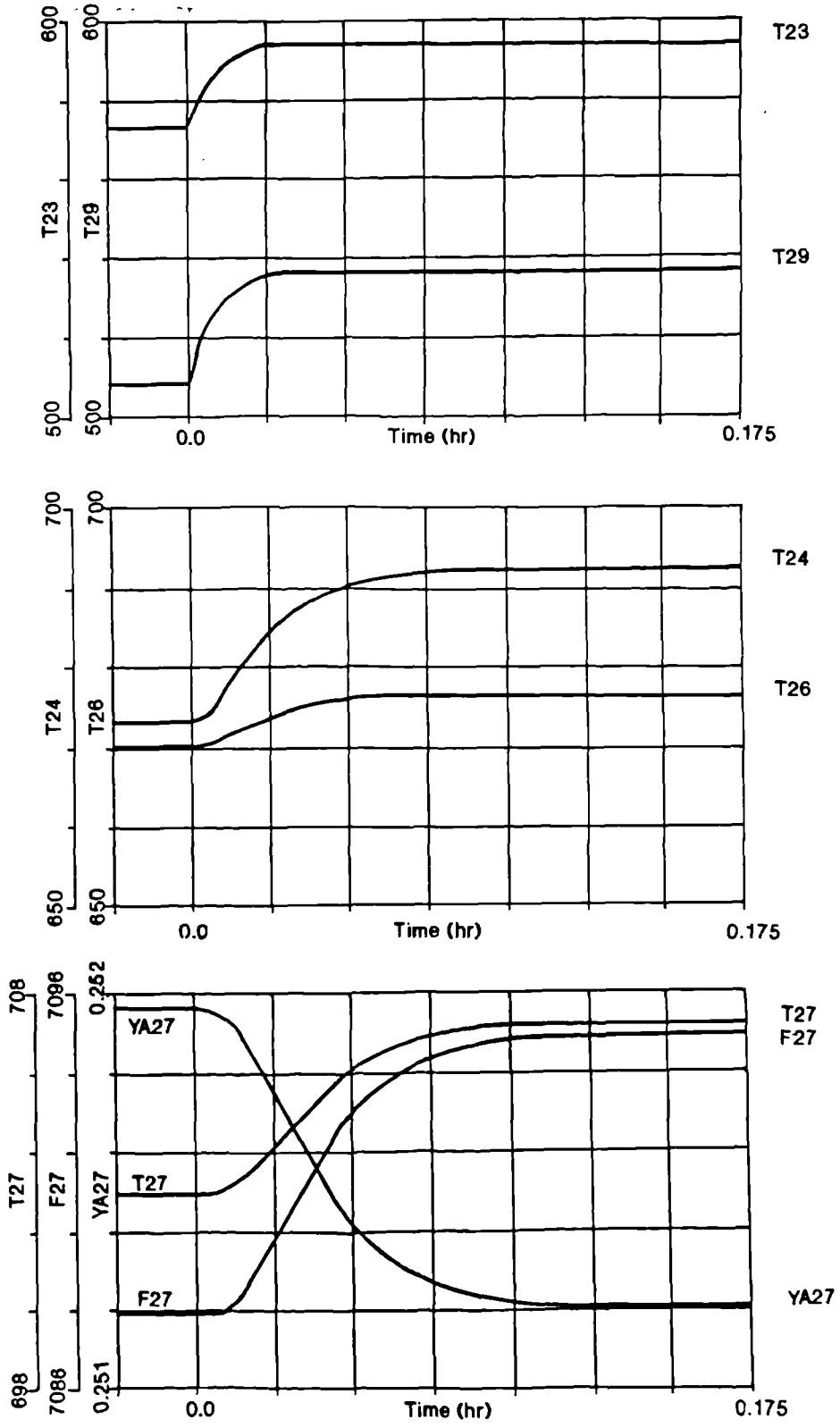

Figure 4.12 Open-loop step response to increase in temperature in the heavies processing section

4.4.2.3 *Flash Unit Validation*

The flash unit model required control valves on the top and bottom product streams to be fully specified, as illustrated in the block diagram in Figure 4.13. Therefore, a change in inlet conditions would influence the upstream valve pressure, and product flow rates. The open-loop step disturbances are listed in Table 4.9.

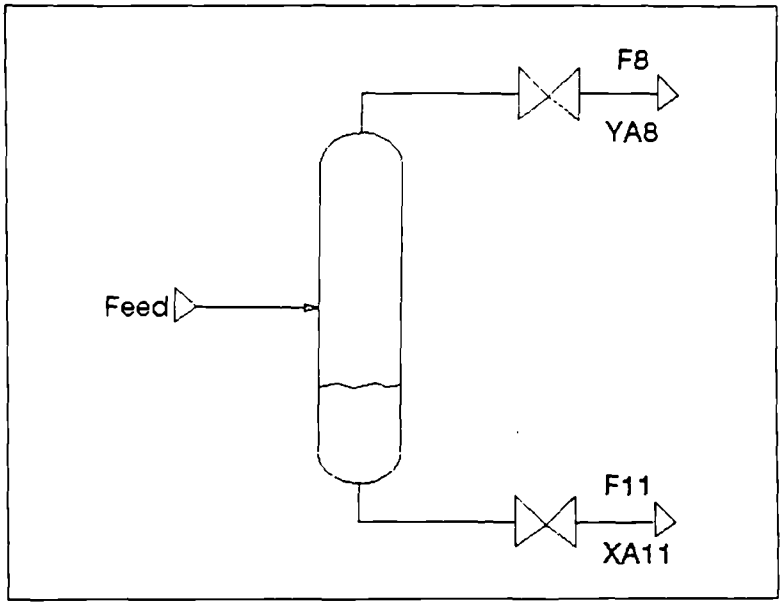

Figure 4.13 Simplified diagram of flash unit

Feed Stream Variable	Steady State Value	Step Value	Step Change
Flow rate (kgmol/hr)	13896.0	14590.8 13210.2	+5% -5%
Methane composition	0.9112	0.9567 0.8656	+5% -5%

Table 4.9 Step disturbances to flash unit

Step change in flow rate:

A step increase in the feed flow rate resulted in an immediate increase in liquid level, H11, temperature, T11, and bottom product methane composition, XA11, as shown in Figure 4.14. Hence, the drum pressure was forced to increase as methane composition in the top product reduced. The top and bottom product flow rates would also be expected to increase, due to the feed flow rate and pressure differential across the valves increasing. However, F11 initially

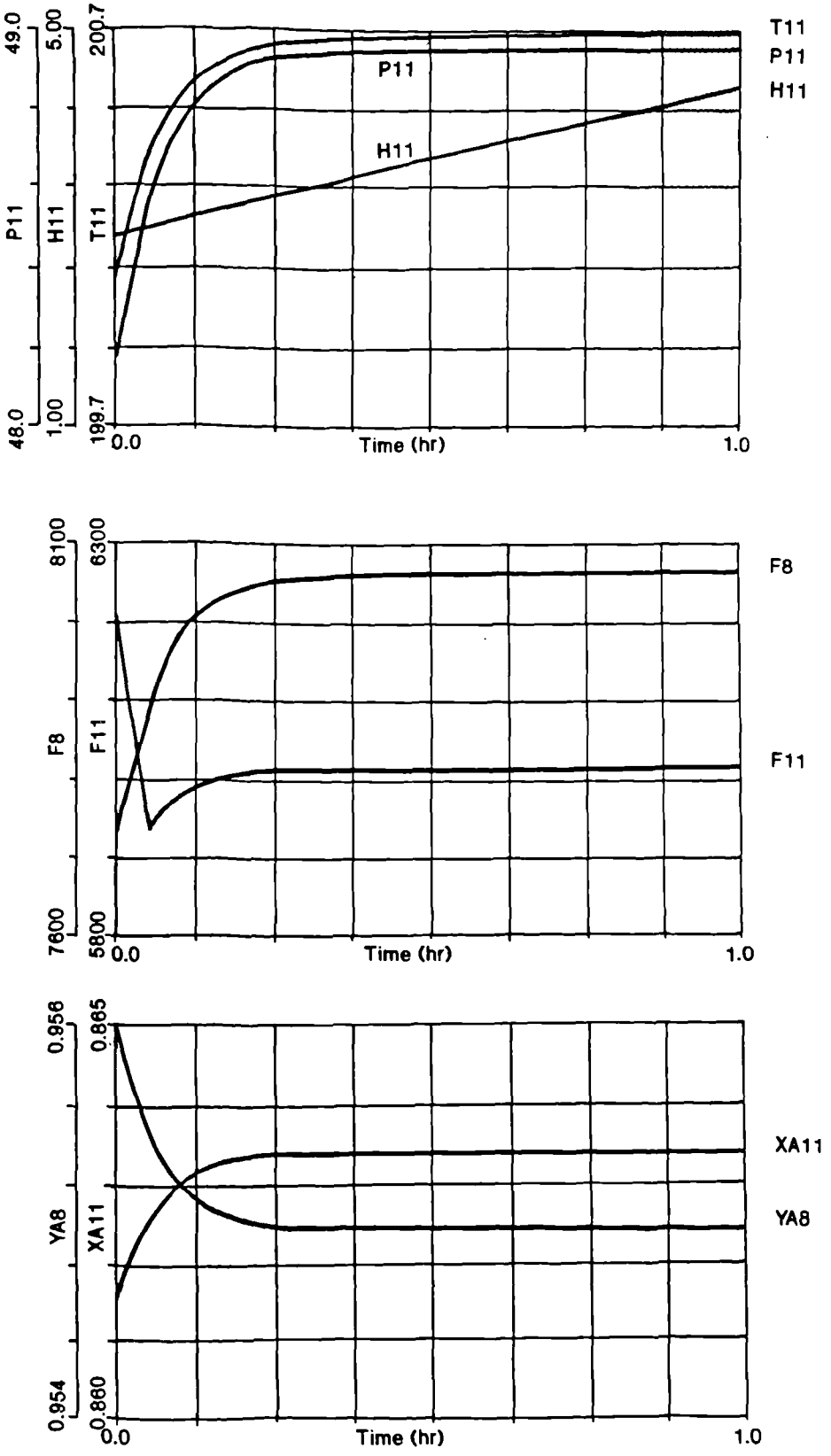

Figure 4.14 Open-loop step response to increase in feed flow to the flash unit

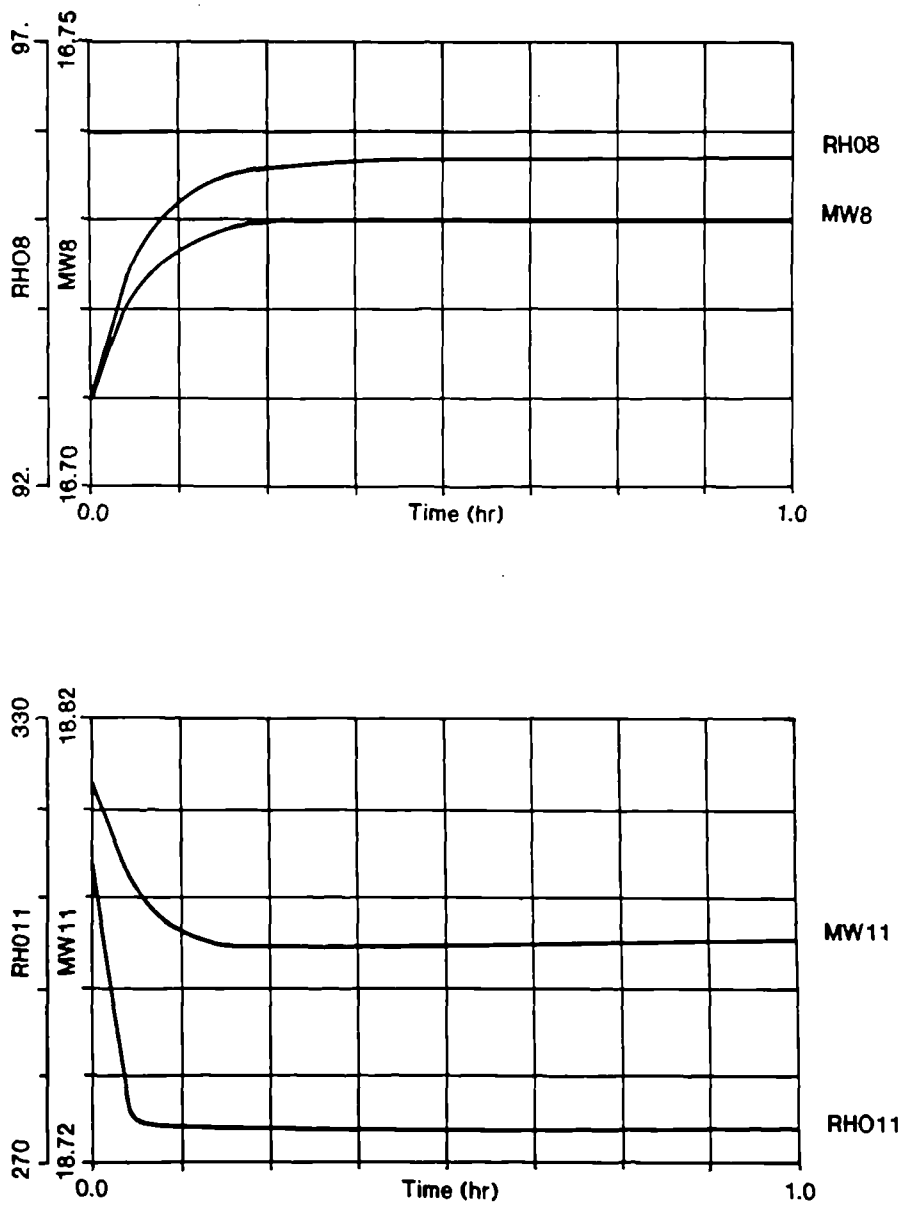

Figure 4.14 Open-loop step response to increase in feed flow to the flash unit (contd.)

reduced to a minimum value before sharply recovering to its new steady condition. This unexpected response was due to the bottom product density, RHO11. At the start of the step disturbance, RHO11 quickly dropped before levelling out, at a pressure of 48.9 bar, while the corresponding molecular weight continued to reduce gradually. These conflicting results were attributed to the unexpected behaviour of liquid stream density in the region of critical pressure, where the density calculation became less accurate. This was verified by repeating the open-loop step response at a lower operating pressure of 45 bar. The resulting plots, in Figure 4.15, showed both F8 and F11 increasing for a step increase in the feed flow rate.

It should be noted that a steady condition could not be achieved with this system because of the integrating nature of the liquid level. This produced a constant change in the liquid level for a given difference between inlet and outlet mass flow rates in the flash drum.

The complementary results for a 5% reduction in inlet flow rate compared favourably as pressure was reduced.

Step change in composition:
When a step increase of 5% in methane composition was applied to the flash unit model, drum pressure increased dramatically. As a result, the iterative calculation for top product composition failed to converge after only a few calculation steps. So, the step disturbance was reduced until the simulation could proceed. This corresponded to a step increase of 1%, with the responses plotted in Figure 4.16. The step change immediately increased temperature, pressure and the product flow rates. However, the liquid product composition behaved unpredictably, when drum pressure exceeded 51 bar. As with earlier open-loop responses, this was attributed to the pressure exceeding critical conditions. The variation in product flow rates was due to the valve characteristics in equation (4.1). (It should be noted that the simulation shown in Figure 4.16 terminated when the liquid level reached zero).

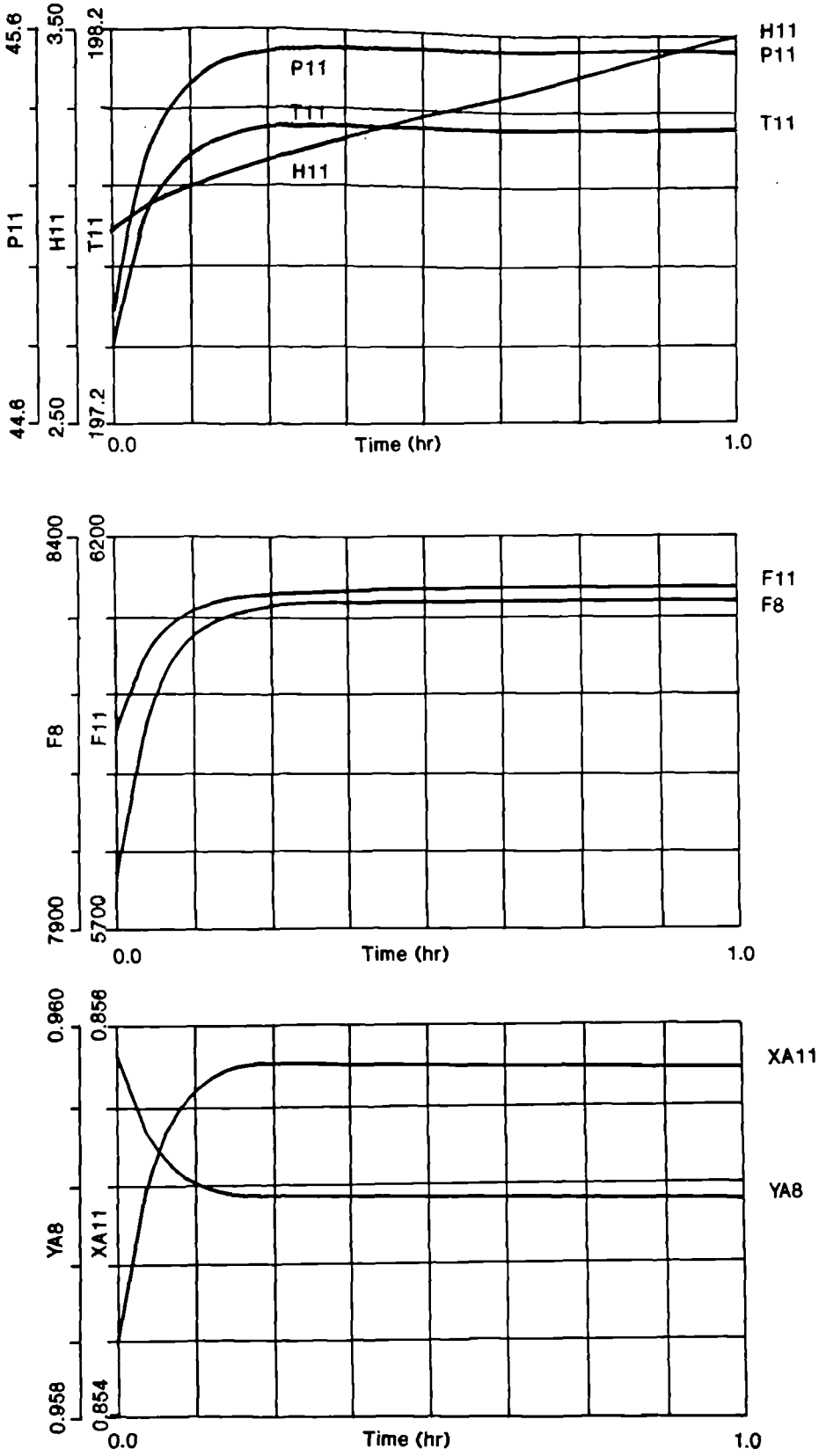

Figure 4.15 Open-loop step response to increase in feed flow to the flash unit, at a lower pressure

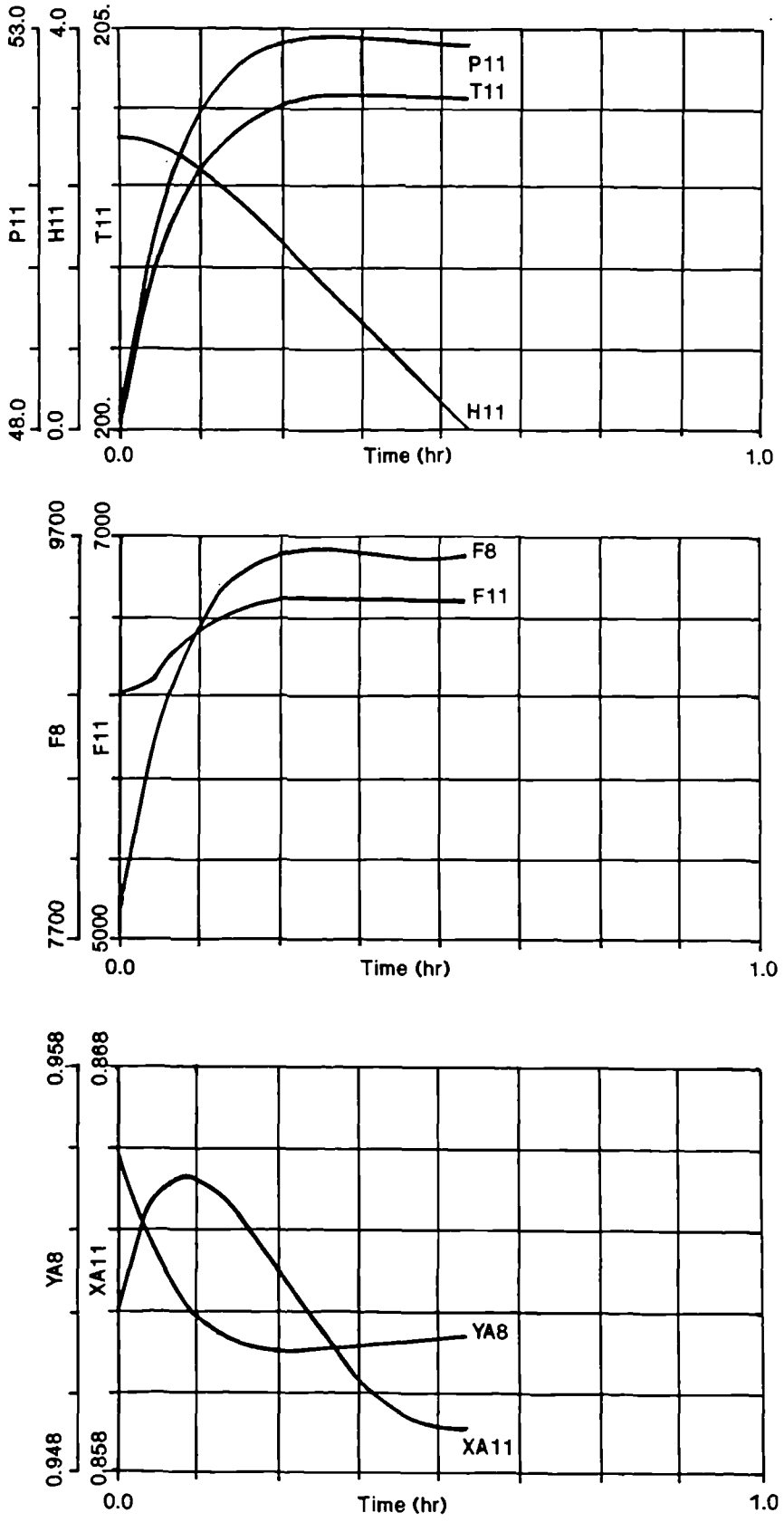

Figure 4.16 Open-loop step response to increase in methane feed to the flash unit

A 5% decrease in the methane composition produced expected responses, with a gradual reduction in temperature and pressure. This was accompanied by a steady decrease in methane composition in the bottom product. The product flow rates also reduced, with a constant increase in liquid level.

Summary of flash unit model validation:

The above open-loop step responses for the flash unit with GL2Z feedstock showed that:

(i) For a step increase in flow rate, dynamic behaviour became unreliable as the operating pressure approached 49 bar, near the critical conditions.

(ii) Small disturbances in feed composition were sufficient to produce a large variation in drum pressure, for the open-loop system.

(iii) The new steady condition was achieved within 1.0 hr, for each step response.

These observations suggested that a lower operating pressure should be considered in future design studies. Also, tight pressure control may be necessary to ensure a safe and reliable operation.

4.4.2.4 *ORV Unit Validation*

The ORV model required a control valve to maintain the water inlet stream, as illustrated in Figure 4.17. As the simulation was based on a transfer function model, the ACSL simulation results for the open-loop responses were compared with the original non-linear model results (Muir, 1987). The dynamic behaviour was plotted for two forms of inlet disturbance, listed in Table 4.10, and related to natural gas outlet temperature, in the linearised ACSL model.

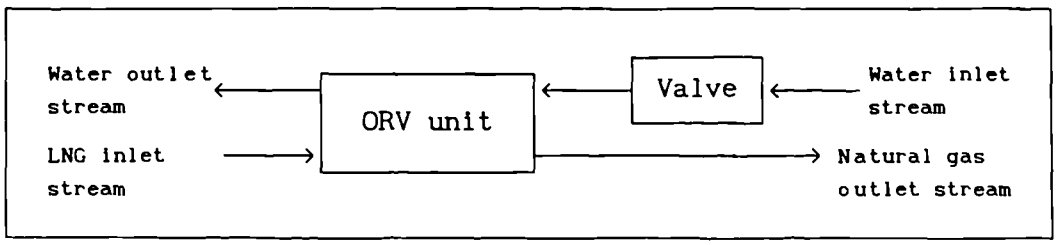

Figure 4.17 Simplified diagram of ORV unit

Variable	Steady State Value	Step Value	Step Change
Water inlet flow rate (kgmol/hr)	484780.	581736. 387824.	+20% -20%
LNG inlet temperature (kgmol/hr)	179.8	184. 174.	+5% -5%

Table 4.10 Step disturbances to ORV

The open-loop step responses for a change in water inlet flow rate, in Figure 4.18, illustrated the approximations required to represent a non-linear unit using transfer function expressions. The new steady state condition was achieved within 0.3 hr, with an overall temperature variation of approximately 1.5 K.

Step changes in the LNG inlet temperature gave similar results to the original non-linear model, and are compared in Figure 4.19. The dead time was ignored in the linearised ACSL model as it only amounted to 4 seconds, and thus would be considered negligible in the fully integrated flowsheet simulation. The response was completed within 0.03 hr, with a small variation in outlet temperature.

4.4.3 Conclusions on Model Validation

The foregoing steady and dynamic state validation studies were conducted on selected units that were described by dynamic models. The results for the steady state exercise compared favourably with those obtained in the earlier flowsheet development study, in Chapter 2, for the three LNG feedstock conditions. As the steady state validation involved changing the inlet and operating conditions to correspond with each feed condition, this study also demonstrated the models' ability to move between feedstocks.

The open-loop step responses were conducted about the GL2Z feed condition. Generally, the dynamic models' behaviour gave reasonable agreement with expected trends. However, problems arose in the physical properties calculations for the distillation column and flash unit models, creating irregular transient responses at certain stream conditions.

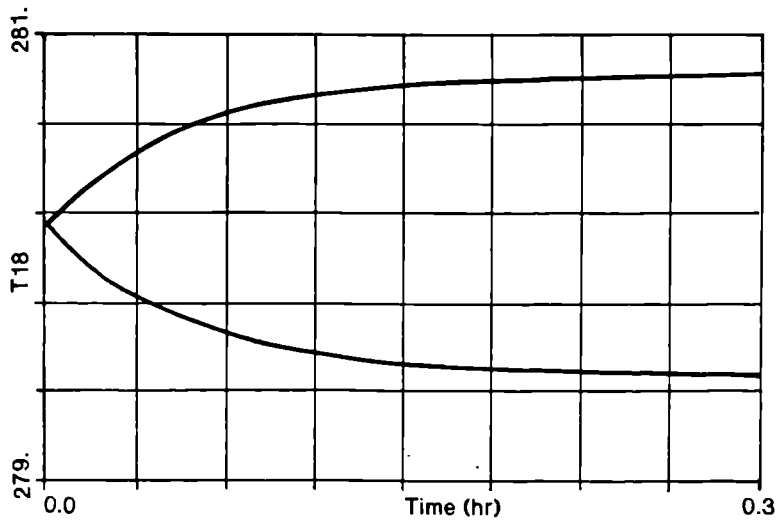

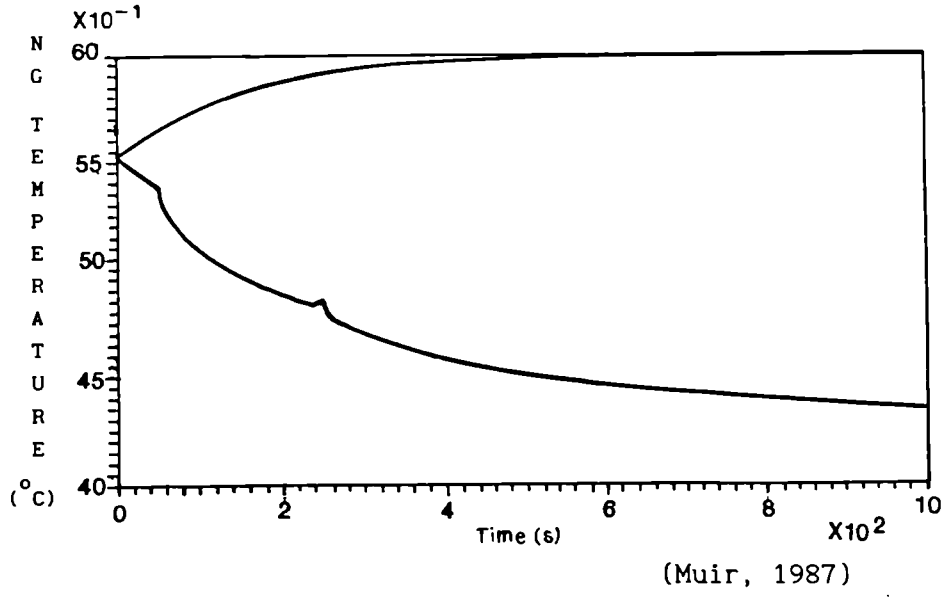

(Muir, 1987)

Figure 4.18 Open-loop step response to changes in water inlet flow rate to ORV

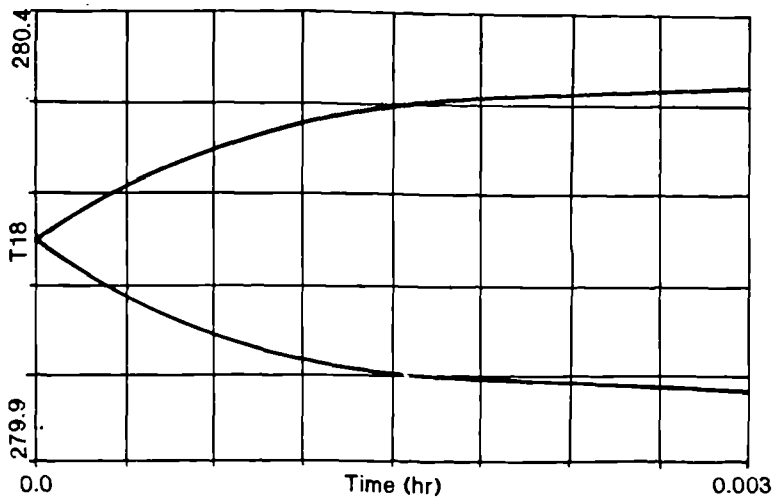

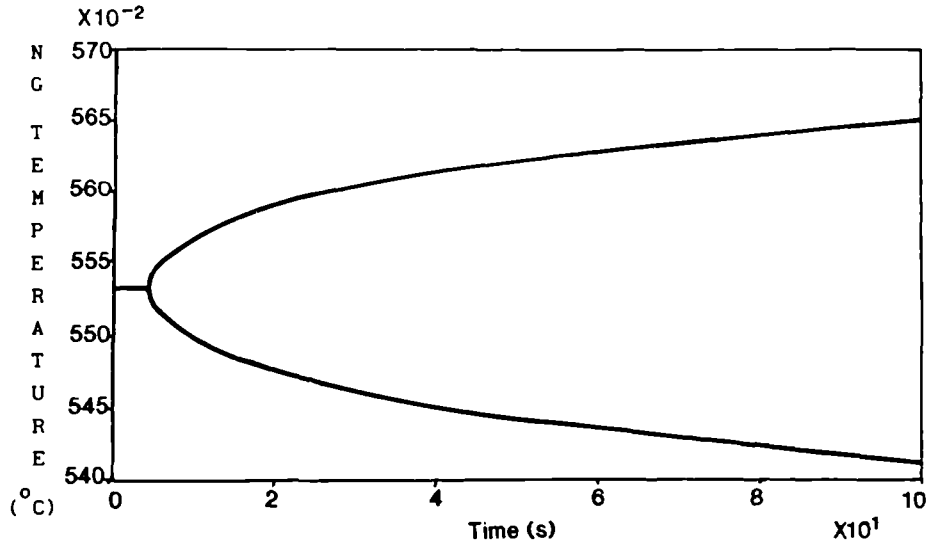

(Muir, 1987)

Figure 4.19 Open-loop step response to changes in LNG inlet temperature to ORV

The irregularities within the distillation column model were attributed to limitations in the operating envelope, which was defined by the steady state look-up tables. The feed envelope defined in Table 4.6 was not violated during the open-loop responses, as the intermediate feedstock, GL2Z, was the initial feed condition. However, at certain transient states the methane composition on a tray would move outwith the look-up tables' catchment area sufficiently to give inconsistent stream and hence physical property conditions. A comparison of the pseudo-binary model with a simpler binary component model verified that multicomponent composition data was required on each tray, to accurately represent the multicomponent system.

In the flash unit, the recommended operating pressure was near the critical conditions of the feed stream. Hence, an increase in pressure of 1 bar, as a result of increasing feed rate, was sufficiently close to the critical pressure to upset the physical properties calculations. Thus, future work on the flowsheet development should consider reducing the operating pressure of the drum. The large pressure variation resulting from a change in feed composition further emphasised the need for tight pressure control. In the present study, it was sufficient to be aware of physical properties data uncertainty in the 49 bar pressure region.

4.5 ACHIEVEMENTS AND CONCLUSIONS

In this chapter, ACSL was chosen as a suitable dynamic simulation package. As the models are required to act as a design tool for the investigation of feedstock changeovers, it was necessary to develop an adaptable and effective model structure. This included a generic naming convention and modular model structures.

The provision of accurate physical properties data for the full range of operating conditions was achieved by the development and incorporation of an interactive physical properties database.

The model validation exercise was conducted on all dynamic models. Each operation achieved a steady state condition that closely resembled the steady state simulation results. Model fidelity was to within 10% for each LNG feedstock condition. The open-loop step responses demonstrated that most of the dynamic models moved to new steady conditions with the expected trends in the transient curves.

Implementation and validation of both binary and pseudo-binary distillation column models was carried out. This clearly showed the advantages of adopting a pseudo-binary distillation column model as had been anticipated earlier in Chapter 3. However, it was also apparent during validation that an artificial operating envelope would have to be imposed on the model due to the limitations of the pseudo-binary approximations made in its development.

Also during validation of the flash unit, it was discovered that it would become unreliable as pressure rose to 49 bar, and critical conditions were approached. This suggested that future process design studies should consider a reduction in the flash unit operating pressure, and that tight pressure control will be required in subsequent control studies.

Since each model is valid and is shown to give satisfactory results both at and between LNG feedstock conditions, the complete flowsheet dynamic model can now be assembled.

CHAPTER 5

FLOWSHEET SIMULATION STUDIES

5.1 INTRODUCTION

The final stages in developing a fully integrated dynamic simulation of a flexible LNG reception terminal, in preparation for subsequent control studies, are described in this chapter.

The steady and dynamic state models will be linked together with preliminary control loops installed to form the complete flowsheet simulation. This process and the difficulties encountered in linking the models are discussed in Section 5.2. The model runtime will significantly increase for the complete flowsheet simulation. Therefore, approaches to improving the ACSL modelling efficiency are reported in Section 5.3.

As an initial investigation into the flexibility and robustness of the dynamic simulation, different LNG feedstocks will be introduced. These take the form of step changes in feed and set point conditions, representing a severe form of feedstock changeover. The results are presented in Section 5.4.

5.2 LINKING INDIVIDUAL MODELS

A closed-loop version of the flowsheet model was required to define the overall dynamic simulation. Thus, preliminary control loops were included in the flowsheet, and are illustrated in Figure 5.1. Proportional-integral (PI) controllers were mostly used except for the ratio control loops, which required only proportional controllers for their steady state models. A detailed control design study is reported in Chapter 6.

During the model implementation stage of Section 4.3, appropriate integration algorithms and integration step sizes were derived for each generic unit. This approach was impractical for the complete simulation as the ACSL code corresponding to each new integration algorithm and step size was defined within a dedicated modelling block. Since each block only communicates with other blocks once every communication step, this can lead to numerical delays in the system, and sequencing problems. Hence, the choice of integration algorithms was confined to distinct areas of the plant model containing the main unit groups, namely:

(i) Stream 1 (feed) to streams 4 and 6 - 1^{st}-order Runge-Kutta.
(ii) Flash unit - 4^{th}-order Runge-Kutta.
(iii) Distillation column - Gear's Stiff method.
(iv) Heavies processing section - 4^{th}-order Runge-Kutta.

The models for individual units were linked using the macro structure, and stream numbering system of Figure 4.1. However, a few inconsistencies occurred in compiling the simulation.

Many physical property values were calculated twice for a single stream, resulting in a duplication error. This occurred when an upstream operation calculated a physical property that was also calculated as an inlet condition to the next unit. However, physical property requirements now depended on the flowsheet arrangement, which remained unchanged during simulation. Thus, a form of logic statement was introduced for selective PP calculations, called a macro directive statement (MAGA, 1987). These statements are only accessed during ACSL model processing, prior to any simulation. So, logical statements could be implemented during ACSL

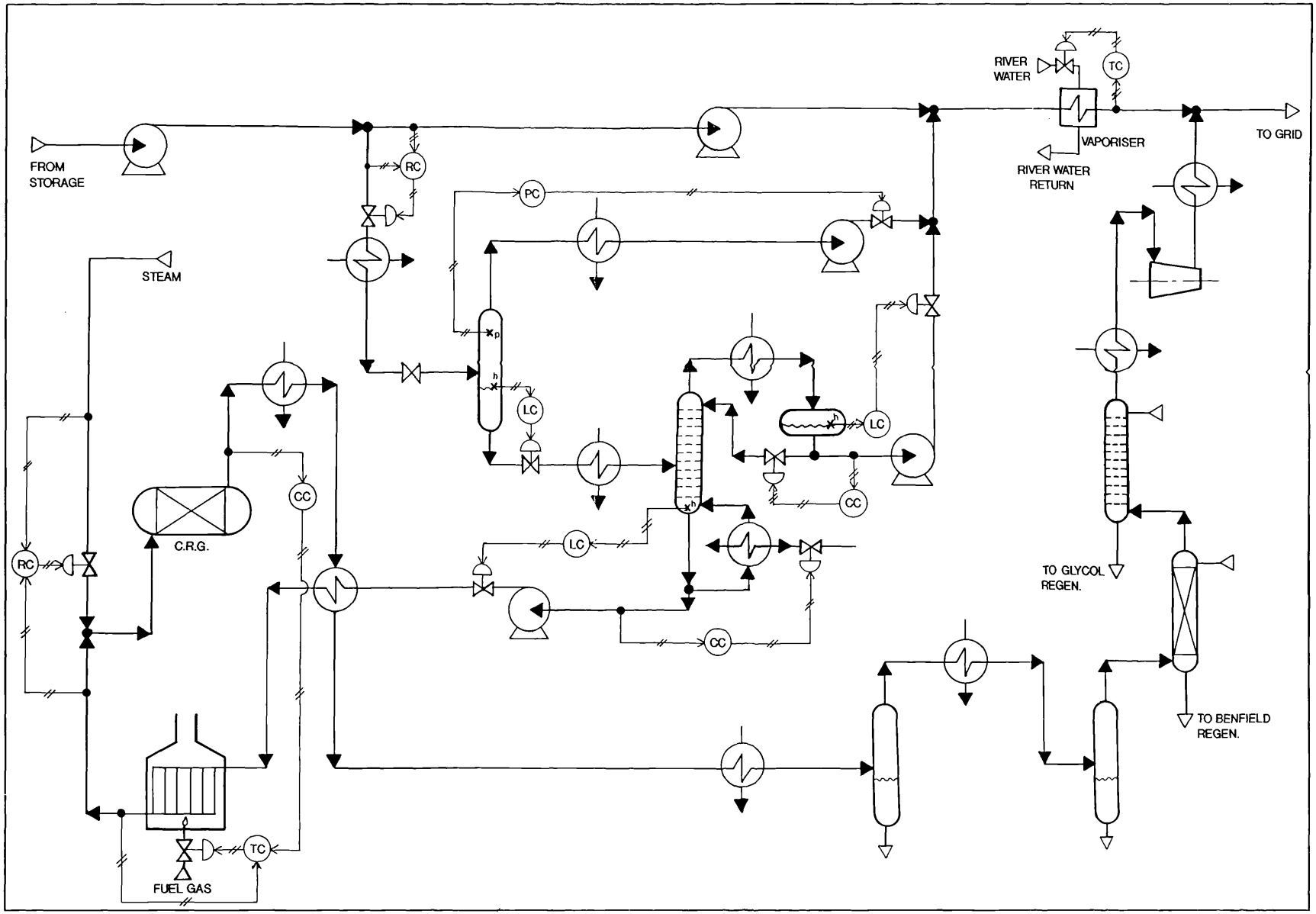

Figure 5.1 Preliminary control loop structure for the flowsheet

model processing to calculate selective physical properties data within macros.

Flags were included in the macro call statements to ensure only essential physical properties were calculated. The macro logic statements were incorporated in each drive macro. This reduced the memory allocation and runtime, primarily due to only essential physical properties data being calculated. The major drawback of this form of logic statement was that each *flag* had to be set before ACSL processing could begin. Hence, charts of the physical properties *flags* were derived for every unit combination in the flowsheet, which related a given unit to every other upstream unit. For example, a typical chart for a mixer requiring inlet enthalpy values would assign the relevant enthalpy flag ("YES" or "NO") to each inlet stream, in Table 5.1, according to the upstream macro.

"YES" flag *(enthalpy calculated in upstream macro)*	**"NO" flag** *(no enthalpy calculation in upstream macro)*
CRG reformer	Absorber
Distillation column	Compressor
Fired heater	Heater/cooler
Flash unit	ORV unit
Heat exchanger	Valve
Mixer	K.O. pot
Pump	

Table 5.1 Physical property flag for mixer call statement

When the individual model units were linked together, the counter-current heat exchanger in the heavies processing section formed an inherent feedback loop. Thus, the previous calculation step results for the returning feed stream, 28, were substituted into the heat exchanger model. This meant that the stream conditions for stream 28 were a calculation step behind, as they were updated at the end of each sequence.

5.3 FLOWSHEET MODEL RUNTIME

The complete flowsheet model was run to achieve a steady condition with the GL2Z feedstock settings. The results compared well with those of the steady state simulation package.

ACSL runtimes for the individual dynamic models were reasonably fast. However, the fully integrated system was significantly slower. Therefore, it was advantageous to reduce model runtime before any simulation studies of the flowsheet were pursued. Two areas were identified: upgrading the computer hardware and improving the ACSL model. Only the latter option was considered in this study, and concentrated on the following aspects:

(i) Optimising integration algorithms and time steps.
(ii) Removing any unnecessary calculations.
(iii) Investigating iterative loops.

These approaches were investigated and the findings are presented in the following subsections.

5.3.1 Numerical Integration Algorithms

There were originally four separate blocks in the ACSL model containing independent integration algorithms and step sizes. Besides computational delays arising from variables that crossed these block boundaries, ACSL statements could not be rearranged over the block boundaries, and so equation sorting was only possible within each block. Therefore, as implementing this technique could prove difficult during the control studies, it was decided to adopt a single integration algorithm and derivative block for the entire simulation.

Two integration algorithms were suitable for the fully integrated flowsheet model; the 4^{th}-order Runge-Kutta and Gear's Stiff method. As the former had a fixed step size, this would have to be set very small to maintain a stable model during disturbance conditions. Gear's Stiff method could take advantage of a variable step length to increase step size as the model achieved its steady state condition. However, there is a runtime overhead associated with this form of algorithm as a linearized state transition matrix has to be formed

and inverted to determine step size.

The choice of an appropriate integration algorithm was based on a comparison of ACSL runtimes. Gear's Stiff method required a very small maximum step size to start a simulation run, and hence its initial runtime was greater than for the Runge-Kutta algorithm. Overall runtimes favoured the fixed step algorithm. Thus, the 4^{th}-order Runge-Kutta algorithm was adopted, with an integration step size of 10^{-4} hr.

5.3.2 **Optimised Calculations**

Several areas were identified for optimising the ACSL model calculations and reducing runtime. For example, many calculations had been included for information purposes only. Intermediate calculations that were previously built up in steps were combined to form fewer expressions, and hence reduce the number of variables and memory allocation. Furthermore, those calculated variables that remained constant during a simulation (such as unit dimensions), were placed in the initial section of the ACSL code so that they were only calculated once at the start of a simulation.

In the original flowsheet model, stream composition was defined in both liquid and vapour phases, by prefixing X and Y, respectively. However, as mixed phase stream compositions were not represented, one phase composition was always redundant. Removing the redundant phase composition from each stream halved the number of variables required to describe each stream composition, and significantly reduced memory allocation.

The above improvements concentrated on eliminating redundancies from the model in an effort to improve runtime and memory allocation.

5.3.3 **Iterative Calculations**

Each iterative calculation in the flowsheet model was performed within a FORTRAN subroutine. The units requiring iterative calculations are listed in Table 5.2. The performance of each subroutine was investigated, and several areas for improving simulation runtime were identified.

Unit	Calculation
Pump	. Temperature
Flash	. Temperature . Pressure and vapour composition
Counter-current heat exchanger	. Enthalpy . Temperature
Fired heater	. Temperature
Mixer	. Temperature
CRG reformer	. CO conversion . Temperature

Table 5.2 Iterative calculations in the dynamic simulation

Most of the iterative calculations listed in Table 5.2 determined the stream temperature, given its composition, pressure, enthalpy and a temperature estimate. Within this iterative loop, the initial temperature gave a new enthalpy value that was compared with the actual stream enthalpy. If the enthalpy difference was below 0.05 kJ/kgmol, the estimated temperature was accepted and output. However, on converting the output to single precision for the ACSL environment, small changes in temperature became insignificant. Therefore, the error band was increased until an appropriate level of accuracy was identified. An enthalpy difference of 1.0 kJ/kgmol gave results within 0.1 K of the correct temperature. This corresponded to a maximum error of 0.05%.

It was found that most of the iterations in the dynamic simulation of the flowsheet had been calculated to an unnecessarily high degree of accuracy. So, the error bands were relaxed in most subroutines. A notable exception was the flash unit subroutine, which required two nested iterative calculations to determine the drum pressure and vapour product composition, as described in Section 3.2.3. However, the small reduction in runtime gained by reducing the error limits did not justify the corresponding loss in accuracy, and so the original settings were retained.

It was possible to increase the error limits to reduce model runtime, without compromising on accuracy and model stability. With each recommended error limit adopted in the flowsheet model, the original

model runtime was reduced by 25%. The recommended settings are summarised in Table 5.3.

Iterative calculation	Dynamic model	Error limit setting	% error (%)
Temperature	. Pump . Heat exchanger . Fired heater . Mixer . Flash unit . CRG reformer	1.0 kJ/kgmol	< 0.05
Enthalpy	. Heat exchanger	200 kJ/kgmol	0.011
CO conversion	. CRG reformer	α: 200 kgmol/hr β: 200 kgmol/hr	< 0.03 < 0.04

Table 5.3 Recommended settings for iterative calculations

5.3.4 Physical Properties

The ACSL simulation for the complete flowsheet was characterised by the following:

(i) *Differential equations* - 63 differential equations in total - 21 linear and 42 non-linear.

(ii) *Parameters* - 881 parameters, 735 of which constitute the 13 look-up tables in the distillation column model.

(iii) *Physical property values* - The PPD was used to calculate 166 physical property values.

(iv) *Variables* - There were over 2200 variables in the model.

(v) *Iterative loops* - The iterative loops, described in Section 5.3.3, were used in 17 different iterations.

(vi) *FORTRAN subroutines* - The model required 30 different FORTRAN subroutines, 9 of which included PPD programs.

The above breakdown suggested that the PPD played a major role in the simulation. However, tests showed that the PP values did not vary considerably between integration steps. Hence, a further means of reducing runtime was investigated by calculating the PP values at a regular interval, instead of each integration step. Logic statements were used to instruct ACSL to either carry-over or update the physical properties at each step.

This timer arrangement was assessed on a section of the flowsheet model that included the flash unit. Output responses and runtimes were compared for calculating physical properties at each integration step and with increasingly restricted access to the PPD. The addition of variables and logic statements for the timer mechanism did not detract from the improved runtime. A comparison of ACSL runtimes, in Table 5.4, showed a significant reduction in runtime when recalculating physical properties at selected intervals without compromising on accuracy. Therefore, the restricted access technique was adopted for the overall simulation model with a physical properties update once every 10 integration steps.

Number of Integration Steps (to next PP Recalculation)	**ACSL Model Runtime** (s)
1 (original)	4507
10	638
15	439
20	342
30	254

Table 5.4 Runtime results for frequency of calculating physical properties

This exercise demonstrated another means of reducing runtime, by the selective recalculation of physical properties at fixed intervals. A reduction to at least 15% of the original ACSL model runtime was realised using this technique, without compromising on accuracy or model stability, for the given simulation example.

5.4 FEEDSTOCK CHANGEOVER

5.4.1 Introduction

The preliminary flowsheet arrangement was designed to handle three different LNG feedstocks in steady state. However, the ability of the flowsheet to move between these design conditions had to be assessed to ensure that continuous operation was feasible. Thus, by introducing feedstock changeovers to the dynamic model its robustness and ability to move between operating conditions could be observed.

Feedstock changeovers were previously implemented on individual models during the validation exercise in Section 4.4. In the complete simulation, interaction effects would be expected to develop between the individual units and may even result in instability. So, the feedstock change was introduced as a step input to represent a disturbance that was more severe than would be anticipated on the actual plant.

The preliminary control loops in Figure 5.1 were retained for the changeover simulations, with preliminary PI controllers installed. A change in feedstock conditions for the complete flowsheet involved assigning new feed conditions and controller set points. These are listed in Table 5.5. As the simulation was originally set up for the intermediate feedstock, the changeovers were initiated from this condition. The feedstock changeovers investigated were:

(i) GL2Z (Medium) to GL1Z (Heavy), and back to GL2Z.

(ii) GL2Z (Medium) to GL1Z (Light), and back to GL2Z.

During a feedstock changeover, the deviation from product specifications and the dominant interaction effects between units were of particular interest. These responses would have implications on the local control loop designs and supervisory control. The ACSL simulation results are presented and discussed in the following subsections. A glossary of variable names associated with the ACSL simulation results is given in Table 4.2, and corresponds to the stream numbering in Figure 4.1.

Variable	LNG Feedstock		
	GL1K	GL2Z	GL1Z
Feed condition:			
Composition - CH_4	0.9315	0.9112	0.8820
C_2H_6	0.0540	0.0585	0.0727
C_3H_8	0.0050	0.0150	0.0261
nC_4H_{10}	0.0000	0.0035	0.0050
iC_4H_{10}	0.0020	0.0026	0.0041
nC_5H_{12}	0.0000	0.0012	0.0001
N_2	0.0075	0.0080	0.0100
Flow rate (kgmol/hr)	16375.60	15917.50	15522.80
Set point values:			
Split ratio, S-01	0.795	0.873	0.873
Flash preheater, H-01 (K)	201.57	205.53	209.71
Distillation column, D-01:			
Preheater, H-03 (K)	185.60	187.54	190.85
Light key to top product	0.9895	0.9903	0.9897
Light key to bottom product	0.5747	0.1158	0.0335
CRG reformer product methane composition	0.2556	0.2520	0.2514

Table 5.5 Feed conditions and set point changes for feedstock changeover

5.4.2 **Medium to Heavy Feedstock Changeover**

Selected simulation responses for the flash unit are plotted in Figure 5.2, for a step change in LNG feedstock and operating conditions. The flash unit responses were very oscillatory, due to either a high gain or small reset time for the pressure controller settings in the flash drum. This was demonstrated by disabling the pressure controller after 0.5 hr, which maintained the vapour flow rate, F8, at a constant flow rate. This resulted in the flash unit variables adopting smooth profiles. Generally, PI control with small integral action is recommended for pressure control (Shinskey, 1988). However, these settings were chosen for the preliminary simulation studies to:

(i) Speed up response time during model development.

(ii) Reduce pressure variations in the flash drum and hence avoid reaching critical operating conditions.

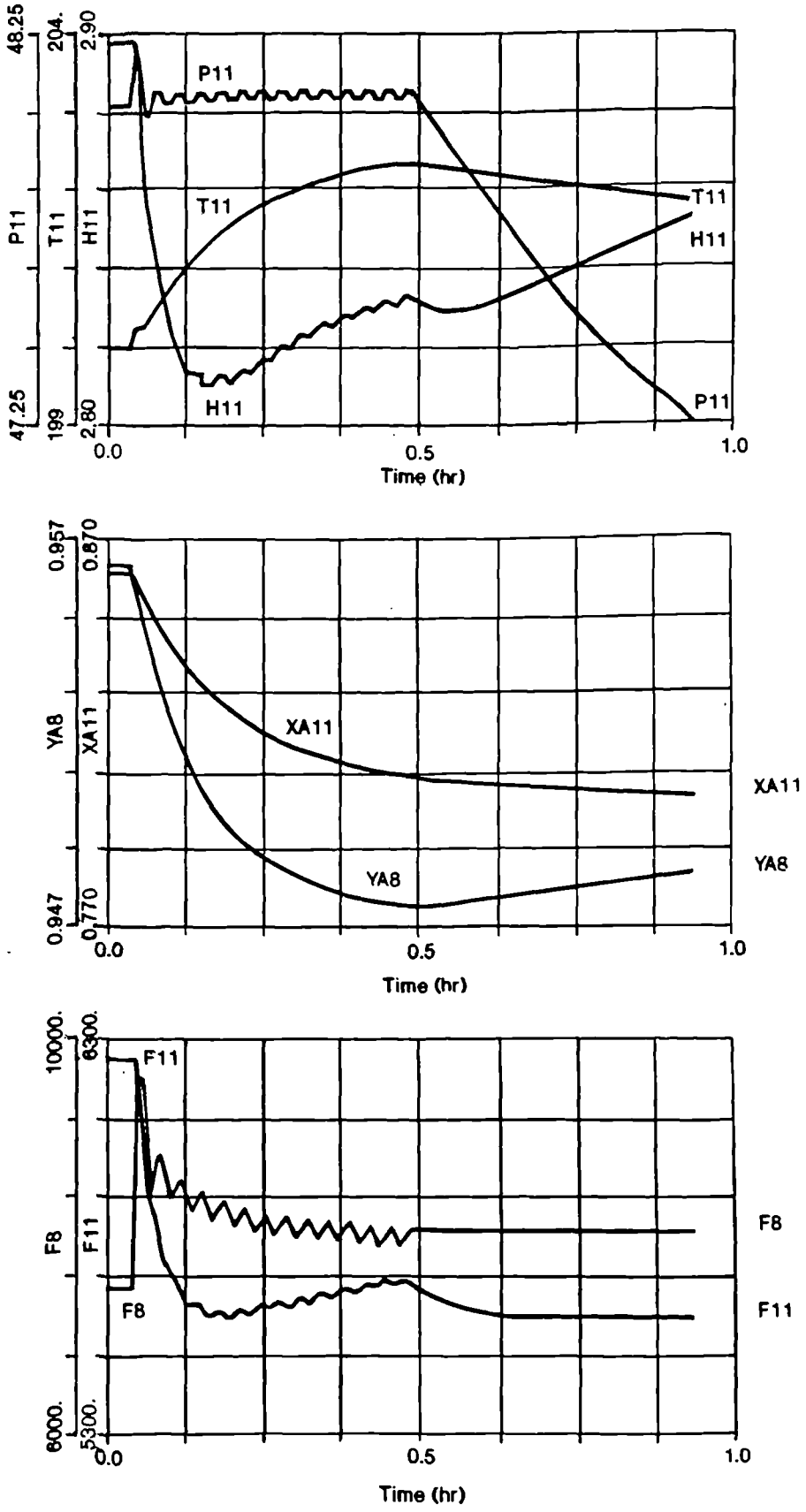

Figure 5.2 Step changeover from GL2Z to GL1Z feedstocks for the flash unit

The complete feedstock changeover responses are shown in Figure 5.3, over a 1 hour simulation period. The flash unit achieved its new GL1Z condition within 0.6 hr, with the oscillatory responses still present. The initial overshoots were caused by step changes in the set point values.

The effect of these step changes was more apparent in the distillation column set points for top and bottom product methane compositions, XA14 and XA21, respectively. This was due to the control action responding instantaneously, and the delay in feedstock changes reaching the column from the upstream flash unit. Thus, the significant reduction in set point for methane content in the bottom product, XA21, demanded a greater separation and removal of methane in the top product. The initial response of the controllers was to increase internal flows by raising boilup, via increasing heat to the reboiler. This resulted in a reduced F21 as the level controller attempted to maintain liquid level in the column base. At the top of the column, the increased vapour flow rate raised liquid level within the reflux drum, causing top product flow rate to increase. This dual effect quickly reduced the methane content in the bottom product, as the column feed gradually changed to the GL1Z feed condition. These extreme distillation column responses were again due to fast control action attempting to drive the unit to its new condition before the feed had changed sufficiently.

Two glitches originated within the distillation column. The first occurred at a methane feed composition midway between the medium and heavy feedstock conditions, for which there was no supporting steady state data in the model's look-up tables. This condition would adversely affect the 2-D tables used to calculate enthalpy gradient and multicomponent compositions on each tray. The second glitch occurred at a methane top product composition above the limits of the steady state data, and again suggested that the look-up tables were responsible.

These glitches were not present in the dynamic validation in Section 4.4. This was because the feed conditions remained unchanged during open-loop step responses that dealt with changes in the reflux

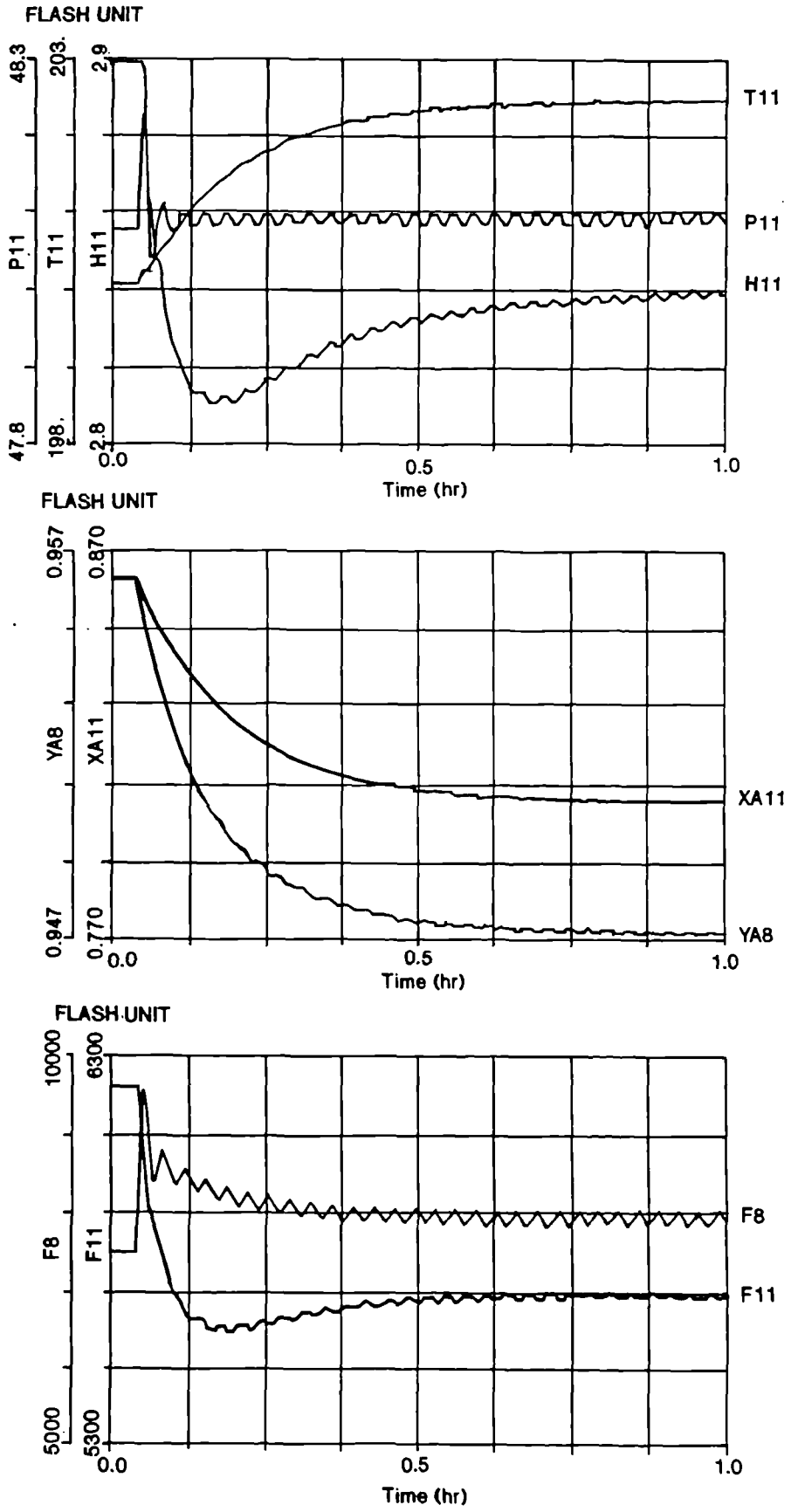

Figure 5.3 Step changeover from GL2Z to GL1Z feedstocks for the complete flowsheet simulation

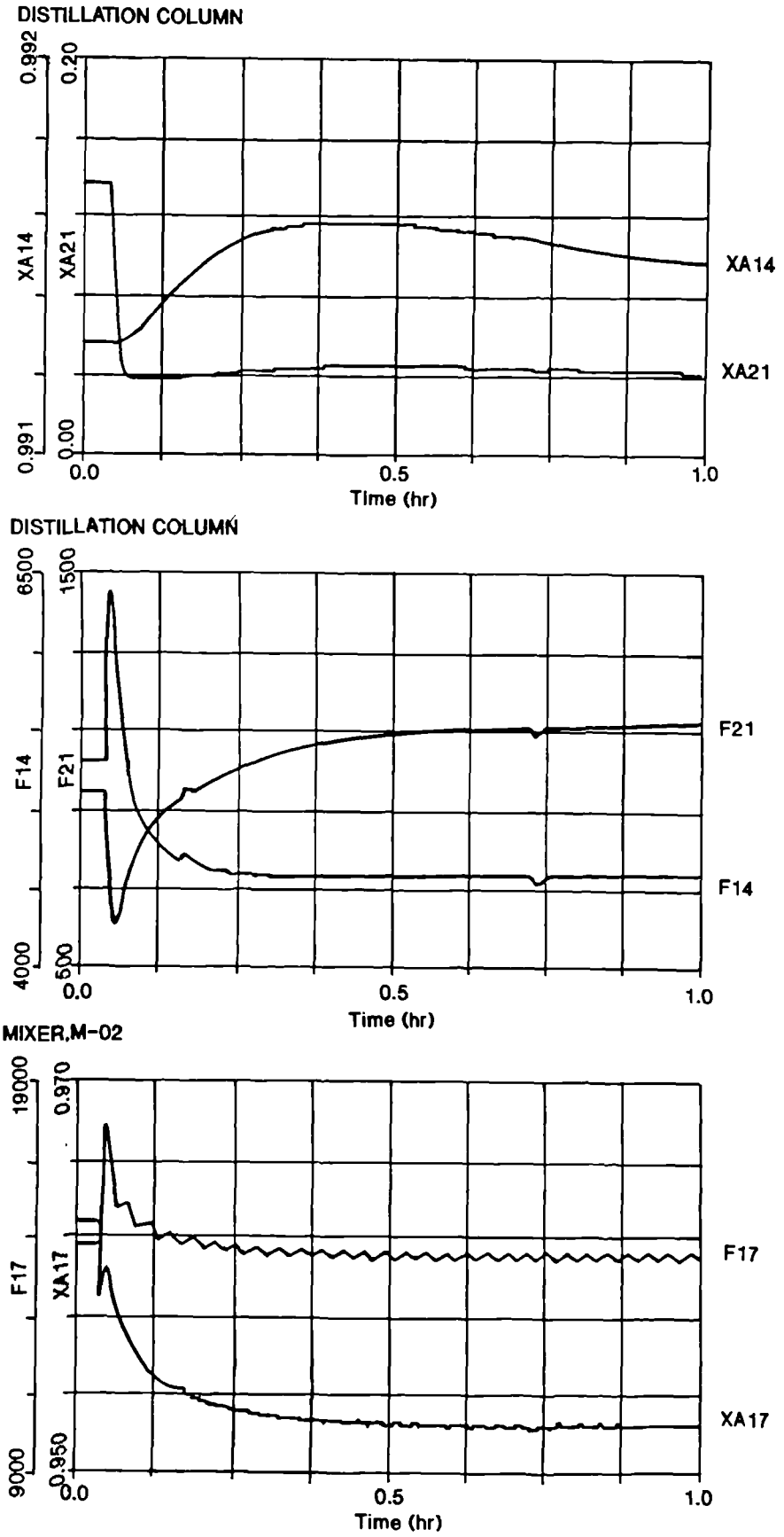

Figure 5.3 Step changeover from GL2Z to GL1Z feedstocks for the complete flowsheet simulation (contd.)

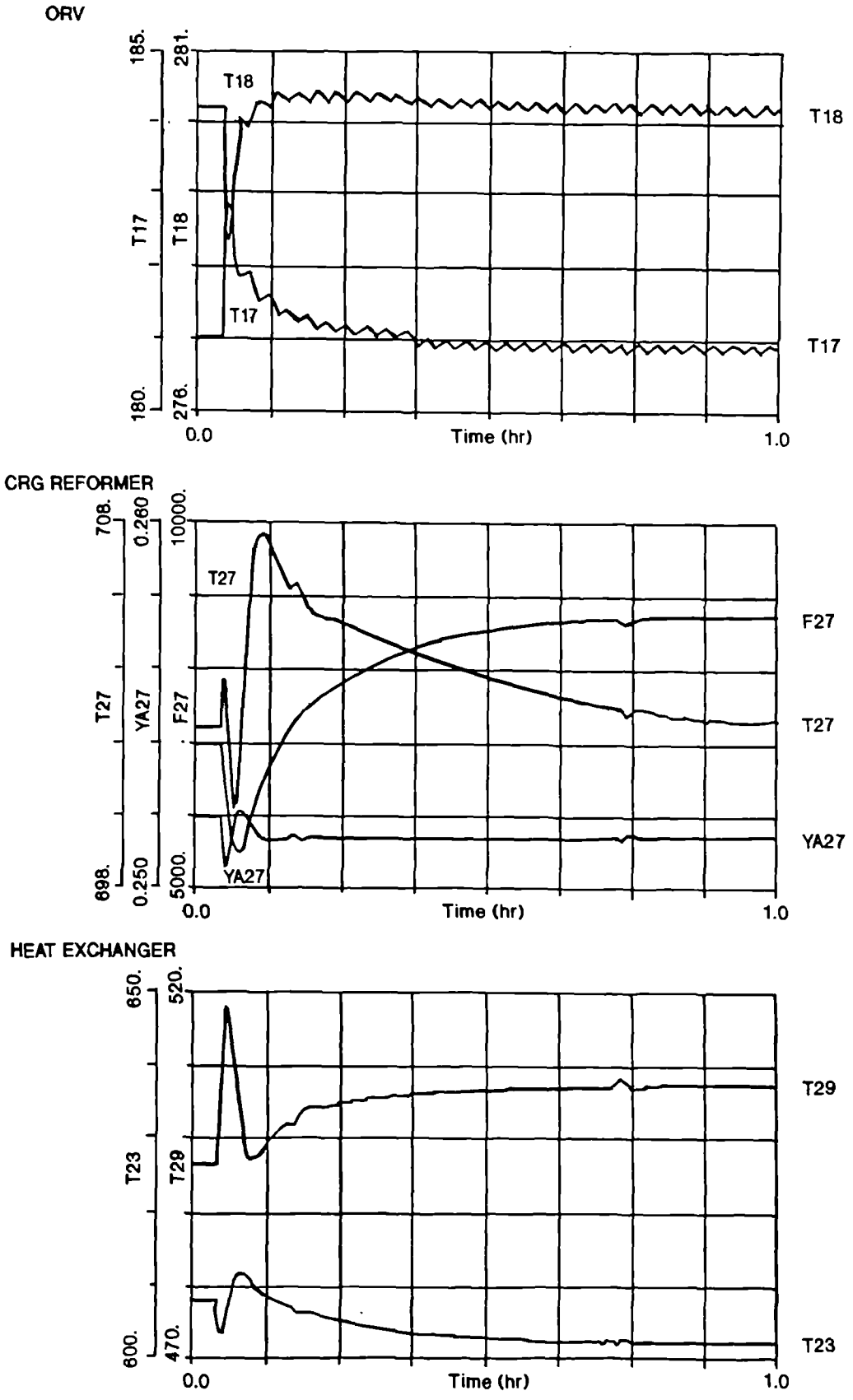

Figure 5.3 Step changeover from GL2Z to GL1Z feedstocks for the complete flowsheet simulation (contd.)

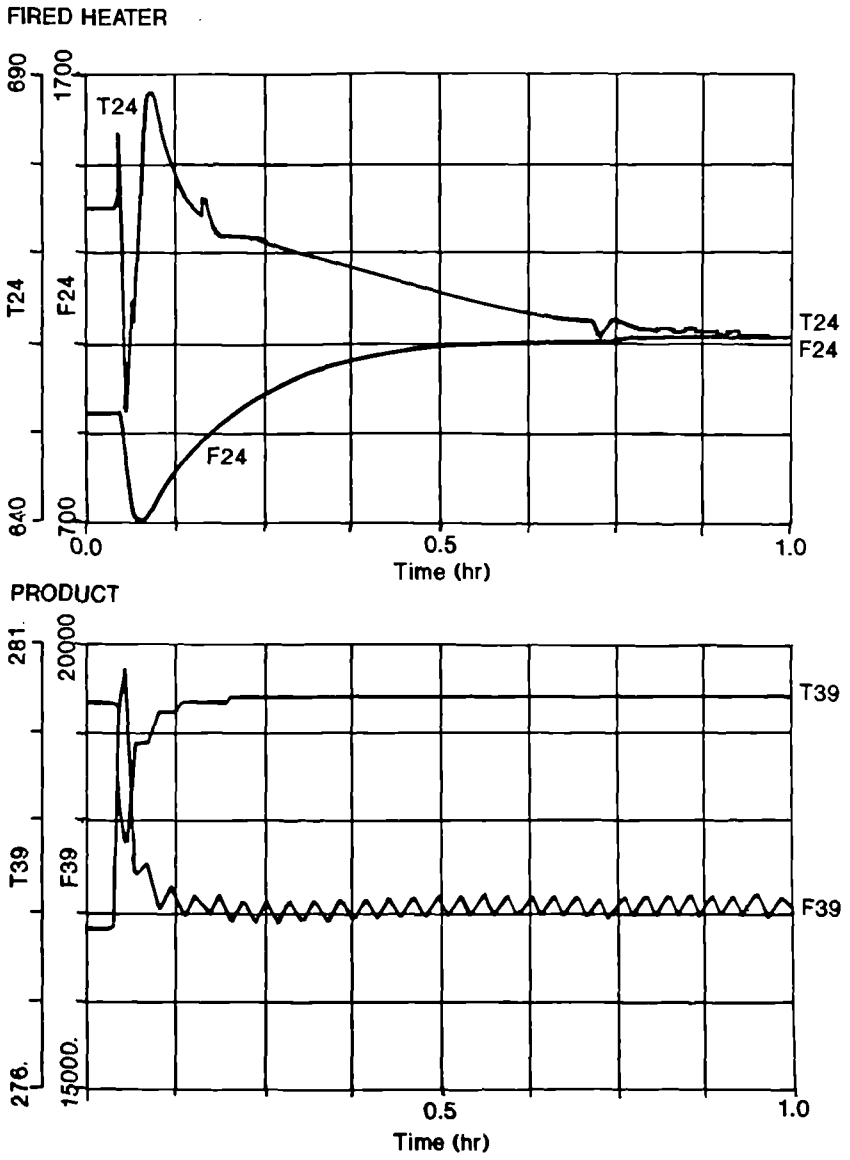

Figure 5.3 Step changeover from GL2Z to GL1Z feedstocks for the complete flowsheet simulation (contd.)

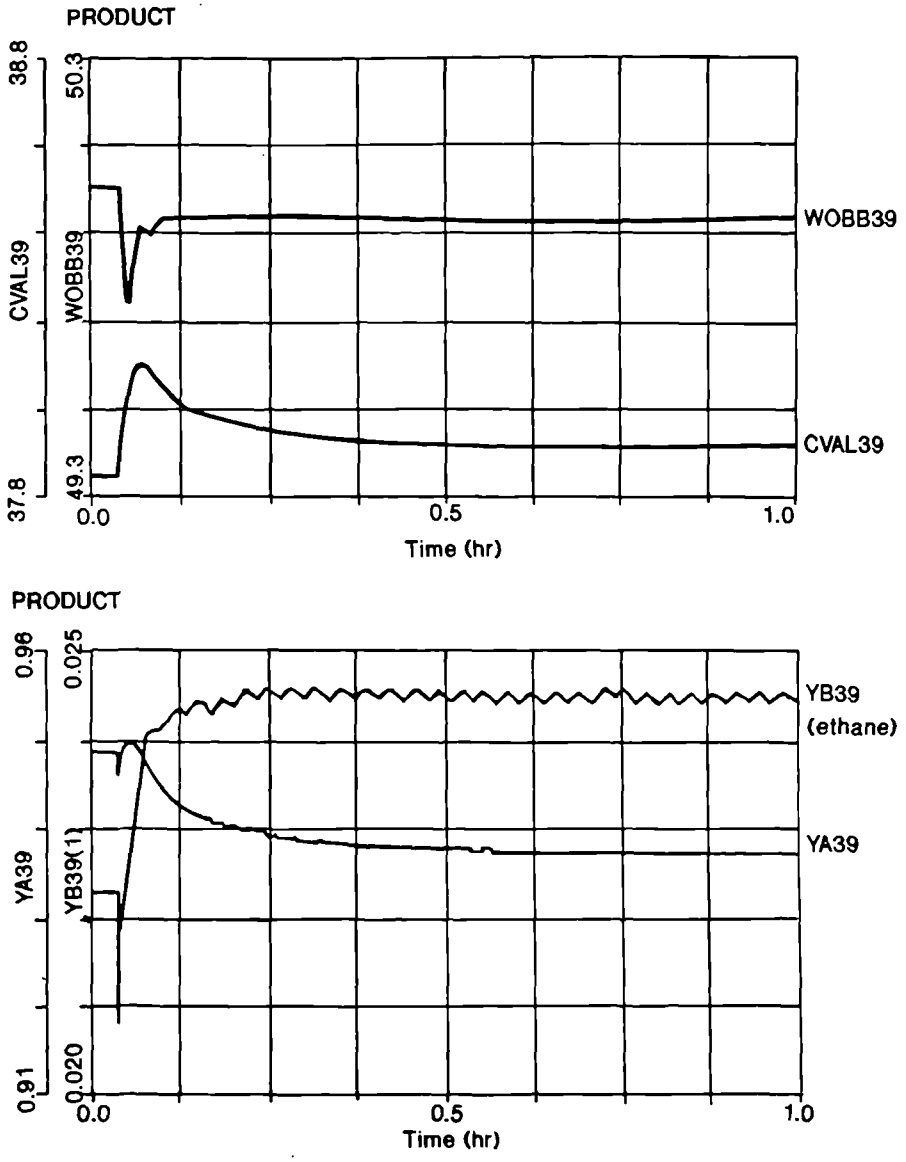

Figure 5.3 Step changeover from GL2Z to GL1Z feedstocks for the complete flowsheet simulation (contd.)

and boilup flow rates alone. Hence, the validation was effectively reduced to an assessment of the 1-D tables, relating to methane content on each tray.

The only set point change in the heavies processing section concerned a reduction in methane composition in the CRG reformer product, YA27. The subsequent control action caused an initial undershoot in YA27. Further upstream disturbances from the distillation column forced the fired heater and reformer feed temperatures, T24 and T27, to overshoot as methane composition attained its new set point. The overall temperature response was slower due to the dynamics associated with the fired heater and heat capacity within the catalyst pellets.

The unprocessed stream, 17 (combining the split stream with the top product of separation), exhibited an oscillatory response as it originated mostly from the flash unit, stream 8. This resulted in an oscillatory ORV unit temperature.

The product stream, 39, profiles in Figure 5.3 exhibited an initial step change. This was due to a proportion of the change in feed conditions to the flowsheet being instantly directed to the product stream via units with fast dynamic behaviour. These units, such as pumps and mixers, were approximated by steady state models and were described in Section 3.4. The responses were also affected by the upstream pressure controller action, with the flash unit top product now constituting 47% of total flow. This influenced the combustion characteristics, with calorific value, CVAL39, and Wobbe No., WOBB39, varying about their new steady values. However, both characteristics remained well within their prescribed ranges:

Calorific Value	36.9 - 42.4 MJ/m^3
Wobbe No.	47.3 - 51.2 MJ/m^3

throughout the changeover, with a maximum variation of 0.3 MJ/m^3. This may be attributed to the fast control action, which forced each unit to its new condition when a step change was instructed. The stepping effect in the product temperature response, T39, was due to an increased error band in the iterative calculation, as described in Section 5.3.3. This also affected stream density and WOBB39.

These responses have shown that product specifications were well maintained throughout most of the feedstock changeover. A comparison of the final changeover simulation results for the GL1Z condition with those of the preliminary flowsheet steady state data showed good agreement. Selected results are given in Table 5.6.

Variable	LNG Feedstock Condition			
	GL1Z		GL1K	
	Dynamic Model	Steady State	Dynamic Model	Steady State
Flash unit:				
F8 (kgmol/hr)	8007.06	8015.78	6454.33	6446.11
YA8	0.9471	0.9457	0.9572	0.9571
F11 (kgmol/hr)	5688.05	5445.60	6546.12	6572.48
XA11	0.8055	0.7874	0.9075	0.9064
Distillation column:				
F14 (kgmol/hr)	4580.44	4292.91	5264.49	5255.95
XA14	0.9900	0.9897	0.9900	0.9895
XB14(1) - ethane	0.0029	0.0038	0.0028	0.0039
F21 (kgmol/hr)	1110.78	1152.69	1331.78	1316.53
XA21	0.0382	0.0335	0.5779	0.5747
XB21(1) - ethane	0.5971	0.5956	0.3640	0.3655
Mixer (M-02):				
F17 (kgmol/hr)	14568.9	14370.1	15085.8	15059.1
XA17	0.9520	0.9501	0.9636	0.9627
CRG reformer:				
F27 (kgmol/hr)	8747.34	9150.96	6966.46	6836.59
T27 (K)	702.49	705.14	680.80	677.79
Product stream:				
F39 (kgmol/hr)	17146.5	17072.0	17072.0	17060.4
YA39	0.9376	0.9345	0.9522	0.9522
YB39(1) - ethane	0.0245	0.0259	0.0230	0.0236
CVAL39 (MJ/m^3)	37.92	38.00	37.83	37.94
WOBB39 (MJ/m^3)	49.93	50.44	49.99	50.49

Table 5.6 Selected simulation results for feedstock changeover

The most dominant interaction effects in the feedstock changeover, illustrated in Figure 5.3, concerned the flash unit and distillation column. As there was no vessel hold up between these two critical units in the separation section, any disturbances within the flash unit had a direct influence on the downstream distillation column. The feedstock changeover resulted in an initial step change in all units downstream of the flash unit. This suggested that the control loop design should be improved and a changeover mechanism devised to enable more gradual feedstock changeover. The existing control

action is generally too fast, and hence only 1 hour of real-time simulation was required to demonstrate a complete feedstock changeover.

The changeover was also initiated from the GL1Z to GL2Z feedstock conditions, resulting in a similar response to the original changeover.

5.4.3 Medium to Light Feedstock Changeover

Selected time responses for the GL2Z to GL1K feedstock changeover are shown in Figure 5.4. As before, a 1 hour simulation was sufficient to demonstrate feedstock changeover to a new condition, as the controller action was predominantly fast.

The oscillatory flash unit responses were more apparent than for the previous changeover in Figure 5.3. This suggests that even less integral action is required on pressure control for the GL1K feed condition. The step change in set points produced initially large variations in the distillation column responses. In particular, the top product flow rate, F14, dropped to 20% of its original value, before recovering to its final steady value. The sudden drop in F21 after 0.1 hr coincided with a peak XA21 value that was significantly above its upper steady state value of 0.58, and hence outwith the operating range of the look-up tables. Therefore, erroneous values were derived for the compositions, temperatures and vapour flow rates near the column base. This initiated a second disturbance downstream, in the heavies processing section.

In the product stream, the combustion characteristics deviated to a greater extent than in the previous changeover, in Figure 5.3, with a maximum variation of 0.55 MJ/m^3 in WOBB39. This was mainly due to significant changes in the distillation column product compositions and flow rates. However, the product specifications were still satisfied.

The final ACSL results at the new steady condition compared well with those obtained from the steady state simulation package. These results are also listed in Table 5.6. The reverse changeover from

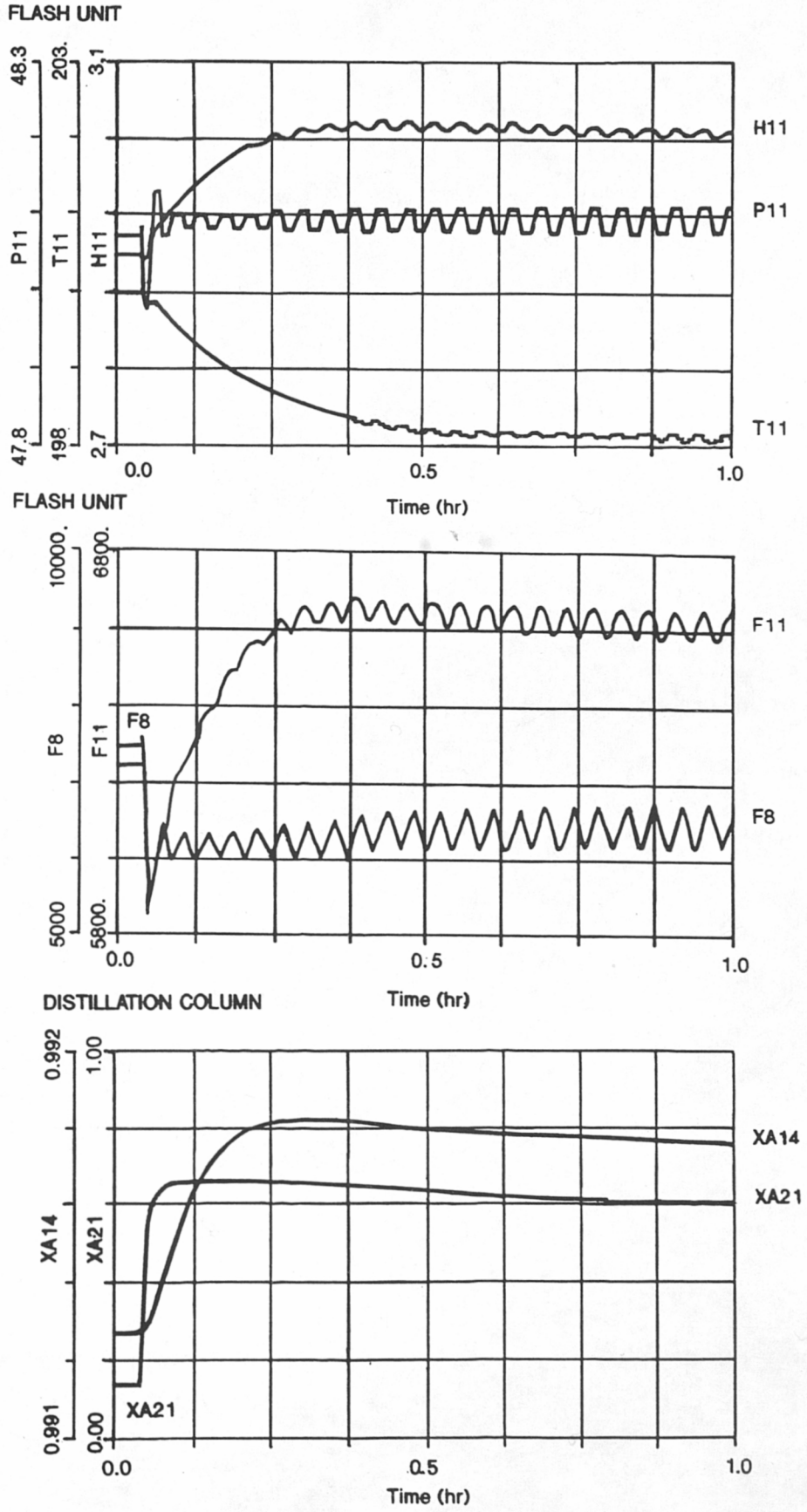

Figure 5.4 Step changeover from GL2Z to GL1K feedstocks for the complete flowsheet simulation

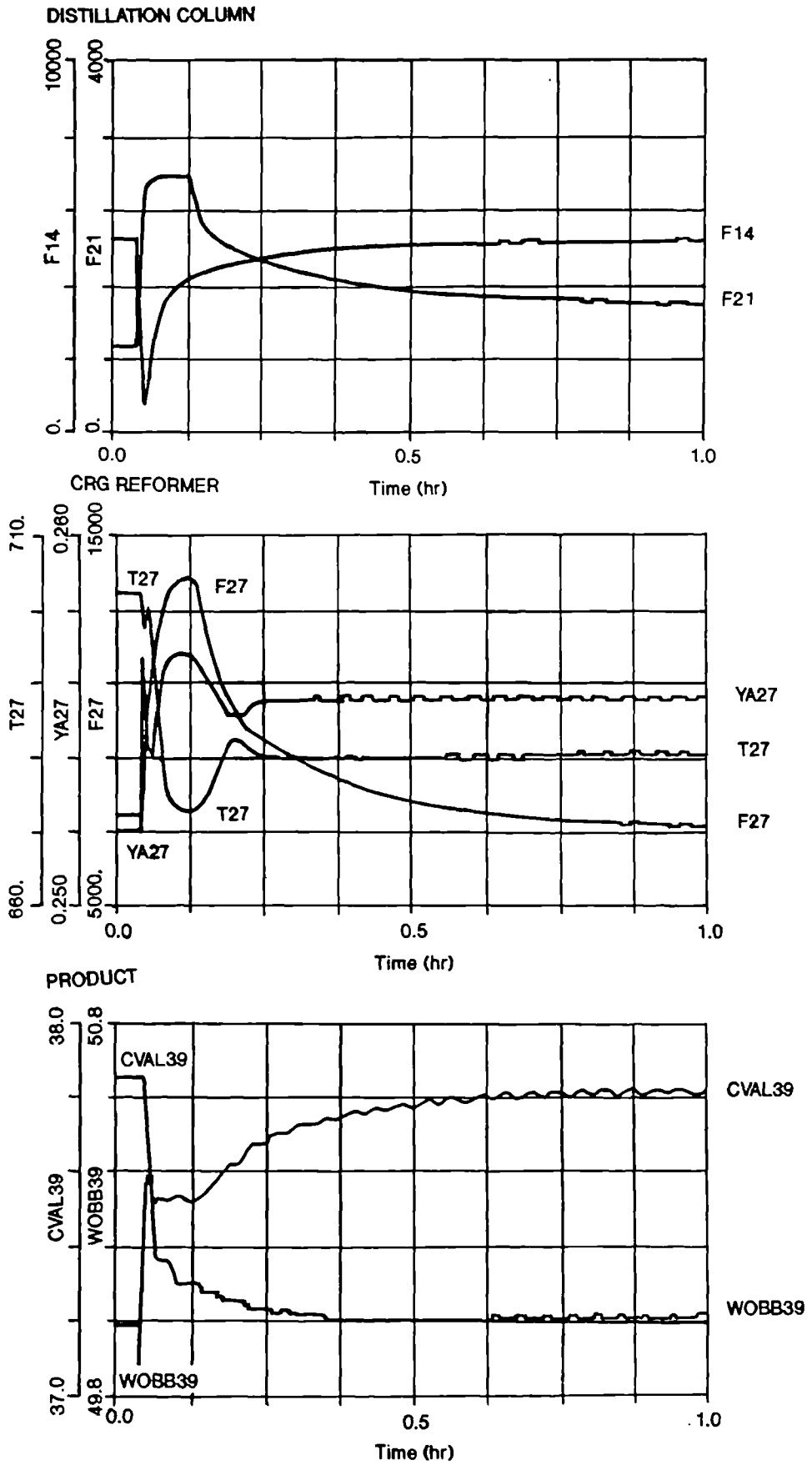

Figure 5.4 Step changeover from GL2Z to GL1K feedstocks for the complete flowsheet simulation (contd.)

GL1K to GL2Z feedstock was also successfully simulated, with similar results to those in Figure 5.4.

5.4.4 Heavy to Light Feedstock Changeover

A GL1Z to GL1K feedstock changeover represented the most severe step change in conditions. The ACSL model failed soon after the run was initiated, when the top product flow rate in the distillation column dropped to zero and flooding occurred. This was due to an increased demand on liquid down flow as methane flow rate in the bottom product was raised. The extreme response to a step change was first observed in the medium to heavy feedstock changeover in Figure 5.3, where the bottom product flow rate reduced to 60% of its initial value within 0.02 hour.

The reverse changeover from light to heavy feedstock also failed, as the lower column trays dried up. Here, the methane bottom product composition was forced to reduce, requiring a greater separation and more reboiler energy. These results further emphasise the need for a revised control loop structure for the distillation column and a suitable changeover mechanism for the complete flowsheet.

5.4.5 Changeover Implications

The feedstock changeover simulations represented a severe form of change from one to another feedstock by introducing step changes. The changeovers between neighbouring feedstocks were successful, with product specifications maintained within reasonable limits. However, several individual unit responses produced undesirable disturbances downstream. In particular, the oscillatory flash unit responses and rapid controller action on most units produced erratic behaviour when the step changes were initially introduced. These results also highlighted the interaction between units, in particular between the flash unit and distillation column.

The final simulation results at GL1Z and GL1K feedstock conditions gave good agreement with earlier steady state simulation data. This provided a further validation of the dynamic simulation models, and confirmed the robustness qualities of the overall simulation. The final changeover exercises between the outer feedstocks presented

severe changes in the operating conditions. As a result, the step changes in feedstock and set points placed too high a demand on the distillation column, and the simulation failed soon after initialisation. However, feedstock changeovers were successful from the intermediate to outer feeds, and in the reverse direction. These results were considered sufficient to demonstrate the ACSL model's ability to move between the feedstock conditions.

These changeover simulations have highlighted several areas for further development:

(i) The control loop structure should be addressed in detail.

(ii) The control loops require tuning to handle multiple operating conditions.

(iii) A changeover mechanism should be defined to simulate a gradual and realistic transition between feeds.

5.5 ACHIEVEMENTS AND CONCLUSIONS

This chapter has reported on two significant achievements:

(i) The development of a fully integrated simulation of the preliminary flowsheet, which represents plant behaviour for the range of feedstock conditions.

(ii) The ability of the ACSL model to simulate feedstock changeover.

The efficiency of the ACSL model structure has been improved in an effort to reduce simulation runtime and memory allocation, with encouraging results. The most significant improvement was to restrict the frequency of calculations in the PPD, which was equivalent to increasing the time step for physical properties calculations. This has greatly reduced runtime to 15% of its original value on a test section of the flowsheet model.

The feedstock changeovers have demonstrated the robustness of the dynamic simulation, and its ability to move between feedstock conditions in response to step changes. Interactions between the flash unit and distillation column were apparent during the changeovers. However, the combination of column feed conditions and control action often drove the distillation column outwith its operating envelope and resulted in unexpected behaviour. This will require management by a more sophisticated control system than has been initially applied here. As the product specifications were maintained within reasonable limits throughout the changeovers, this suggests that a supervisory control system should be more concerned with interaction effects than product specifications.

These initial simulation studies indicate that a detailed selection and tuning of individual control loops in the flowsheet will be required. In addition, a changeover mechanism to permit a gradual and controlled changeover between any of the LNG feedstocks will be necessary. These points will be addressed in Chapters 6 and 7.

CHAPTER 6

STRUCTURE AND DESIGN OF PROCESS CONTROL LOOPS

6.1 INTRODUCTION

A robust and reliable simulation of the proposed LNG reception terminal flowsheet has now been developed which will be employed as a design tool in the control studies in the following two chapters. This chapter describes the initial stages in developing a control system for the flowsheet. Regulatory control loop structures will be devised for individual blocks in the flowsheet to provide stable and robust operation during feedstock changeover and at multiple operating conditions.

A degrees-of-freedom analysis and qualitative arguments will be used to arrive at suitable control loop structures. This work is reported in Section 6.2. Single-input single-output, multiloop and multivariable sub-systems will all require control loops. Single loop and multiloop control designs will be described in Sections 6.3 and 6.4, respectively. Advanced control designs and supervisory control will be discussed in Chapter 7.

A detailed description of the controller design procedure is presented for each loop, assuming a unity feedback system. Controller reference signals have not been converted to electrical or pneumatic signals, so no signal conditioning is required.

6.2 REVIEW OF CONTROL LOOPS

The control loop design for individual units depends on the control loop objectives. These control objectives are strongly related to the overall plant objectives. For the LNG reception terminal flowsheet, the plant objectives are mainly concerned with handling a variety of LNG feedstocks while satisfying the following criteria:

(i) *Product specifications* - The C.V. and Wobbe No. must always be achieved, at a steady production rate and temperature.

(ii) *Operating constraints* - These describe the physical limitations on the various process units, to maintain safe and reliable operation.

These requirements may be used to identify suitable control loop set points for individual controllers.

Each control loop requires controlled (output) and manipulated (input) variables to be defined. The controlled variable should either be a direct measure of the output condition that is to be controlled, or a condition that is strongly related to it. For example, as composition is difficult to measure both accurately and quickly, the process stream temperature is often substituted. The corresponding manipulated variable should ideally be selected so that it has a direct and fast effect on the controlled variable.

Before the control loop configurations can be defined, the correct number of control loops has to be specified for each sub-system. The procedure adopted in this study is described in the following section.

6.2.1 Control Loop Configuration

A degrees of freedom analysis determines the correct number of loops for a given process by calculating the degrees of freedom, f, required to define the process. Thus, f describes the minimum number of independent variables and may be derived from a mathematical model of the process, where:

$$f = (\text{no. of variables}) - (\text{no. of equations})$$
$$= V - E$$

and, $f < 0$ describes a system that is over specified
$f > 0$ describes a system that is under specified.

The value of f is further reduced by introducing known disturbance variables, external to the sub-system. Thereafter, f indicates the required number of control loops for that sub-system to become fully specified ($f = 0$).

A degrees of freedom analysis was conducted on individual blocks in the flowsheet, containing one or more operations that share a common operational goal (Stephanopoulos, 1984). The flowsheet blocks are defined in Figure 6.1. The degrees of freedom analysis for each block is described in Appendix 7, in which suitable combinations of control loops are identified and selected using qualitative arguments. As an example, the analysis of Block 1 is described in Section 6.2.2. A summary of the resulting control loop structures is given in Table 6.1, and illustrated in Figures 6.2 to 6.7. It should be noted that implicit control loops were not considered.

Block No.	Figure No.	Control Loops		Control System
		No.	*Type*	
1	6.2	2	Flow, Ratio	SISO
2	6.3	4	Flow, Temperature, Pressure, Level	Multivariable
3	6.4	5	Flow, Temperature, Level	Multivariable
4	6.5	3	Flow	SISO
5	6.6	3	Flow, Ratio, Temperature	Multiloop
6	6.7	2	Flow, Temperature	SISO
7	---	2	Flow	SISO

Table 6.1 Control loop structure for flowsheet blocks

Each block in the degrees of freedom analysis was allocated sufficient control loops to be fully specified. Hence, when these blocks were recombined to form the complete flowsheet, the process was over specified. The revised control loop structure was obtained by eliminating surplus control loops, and is illustrated in Figure 6.8. It should be noted that the control loop configuration for the distillation column is the final arrangement, derived in Chapter 7.

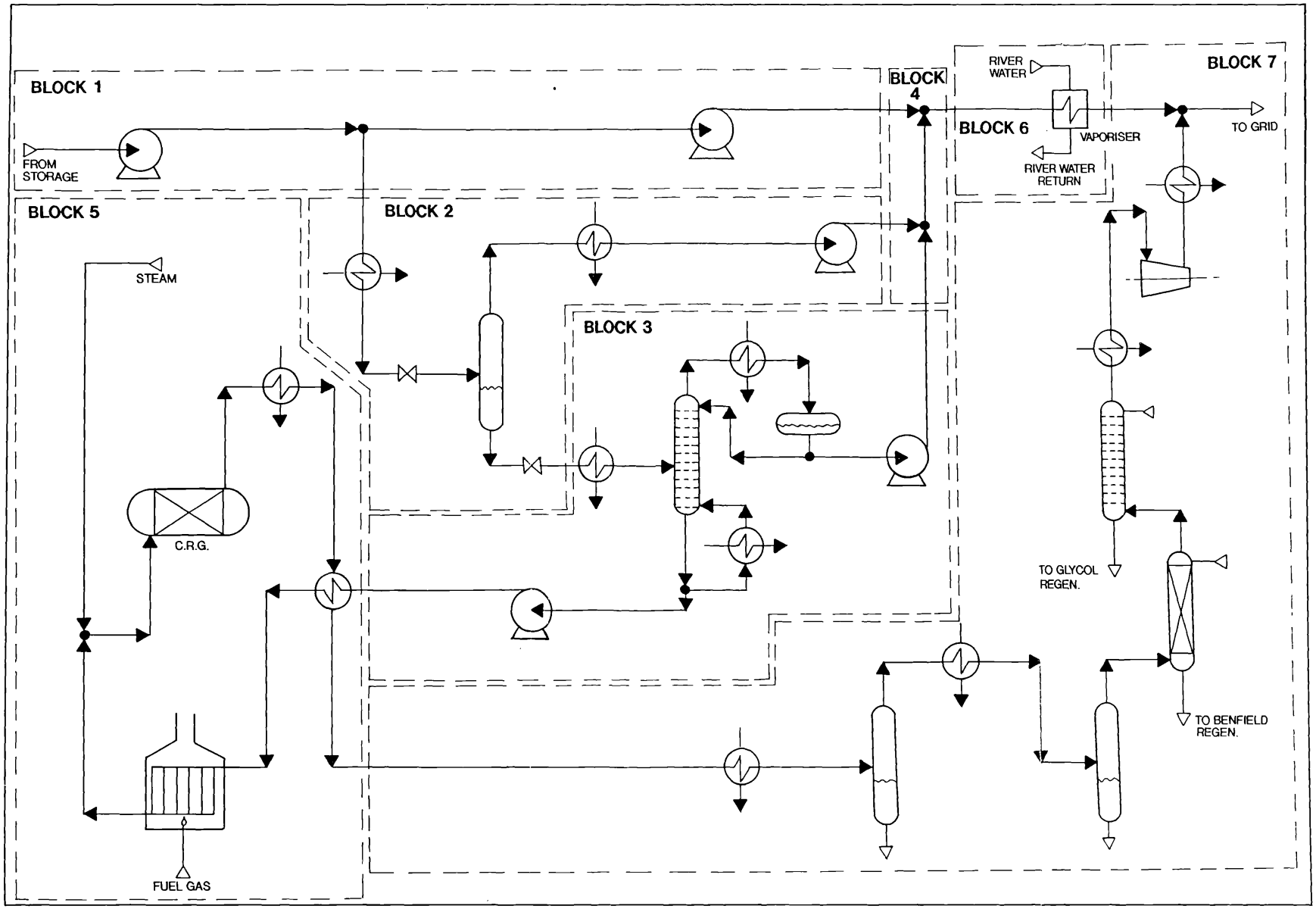

Figure 6.1 Flowsheet with control block boundaries

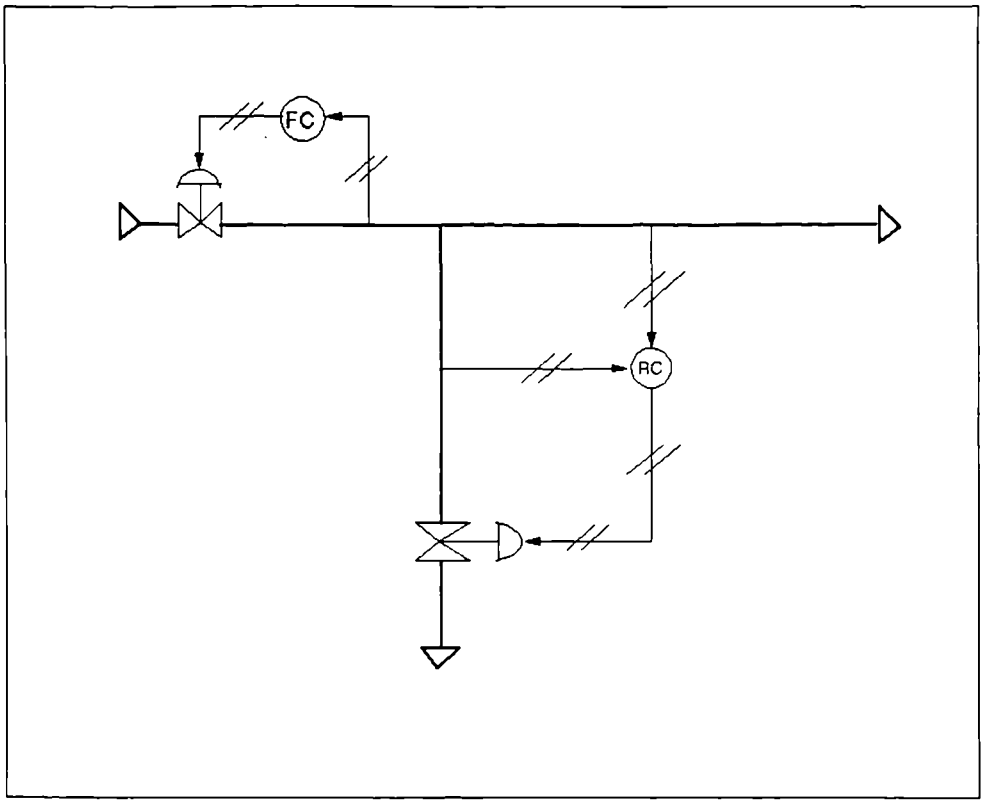

Figure 6.2 Control loop configuration for Block 1

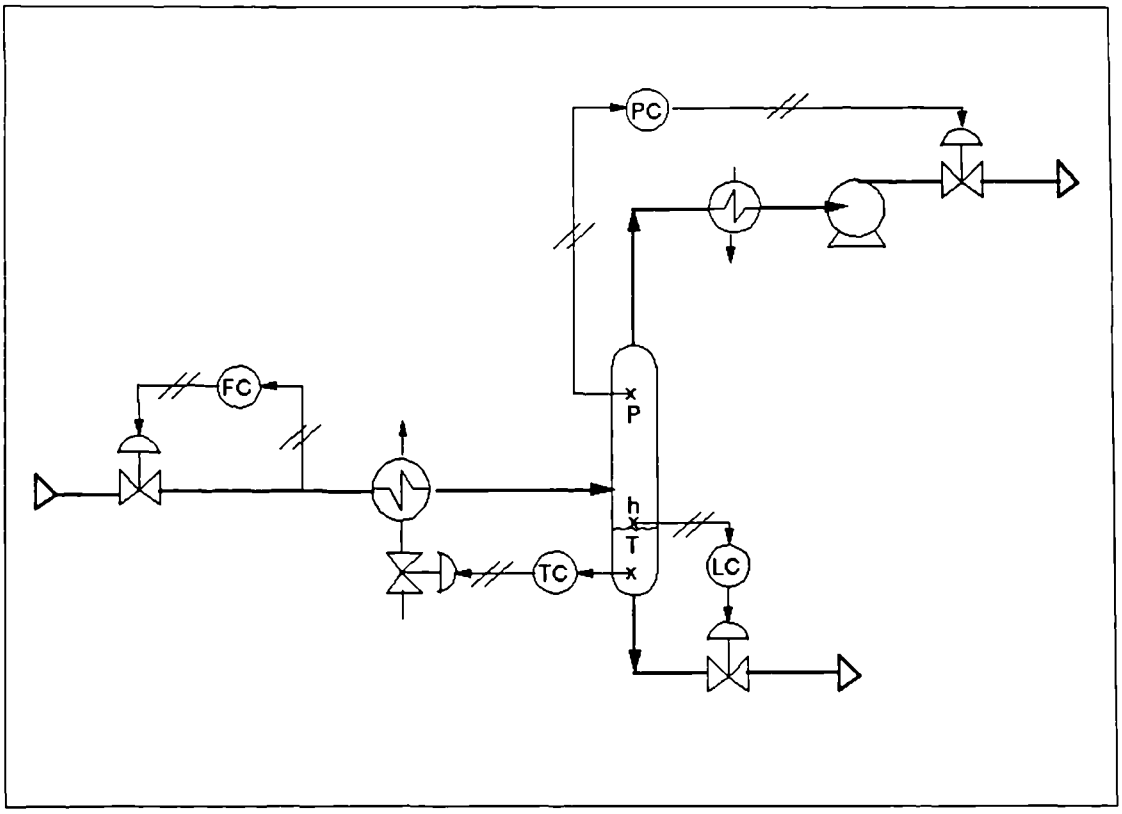

Figure 6.3 Control loop configuration Block 2

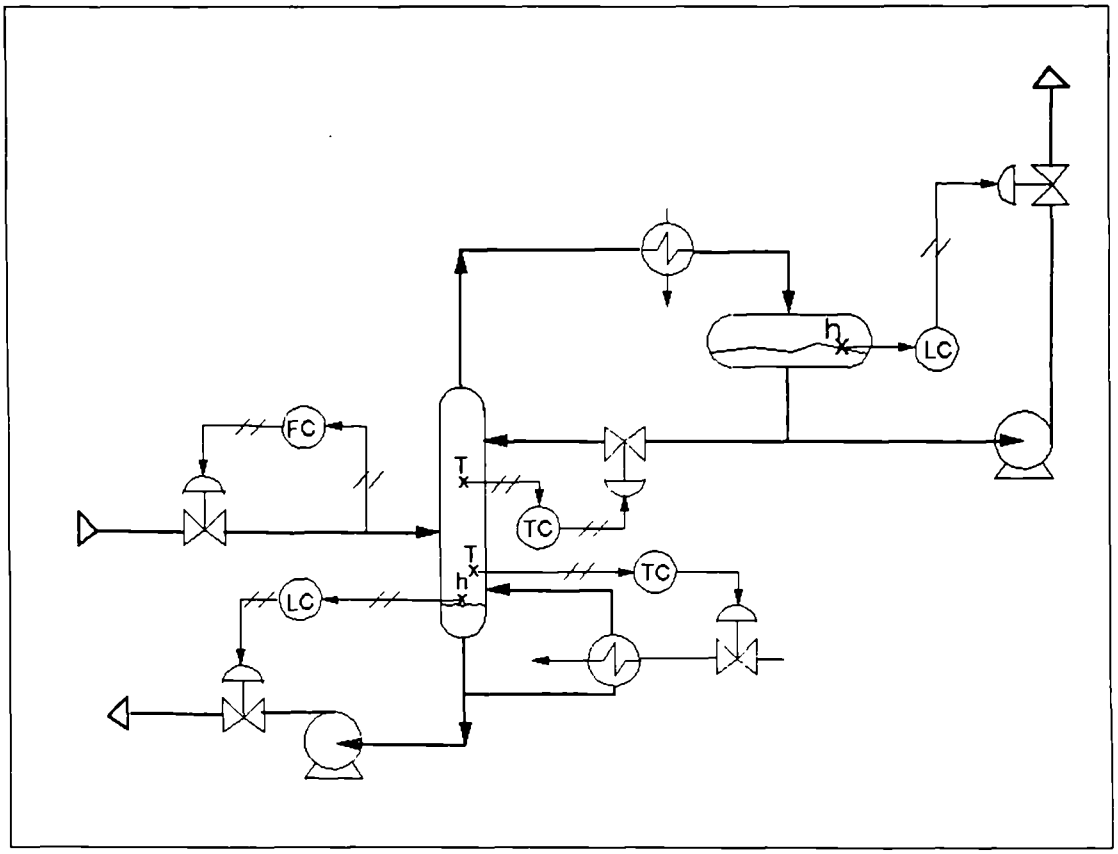

Figure 6.4 Control loop configuration for Block 3

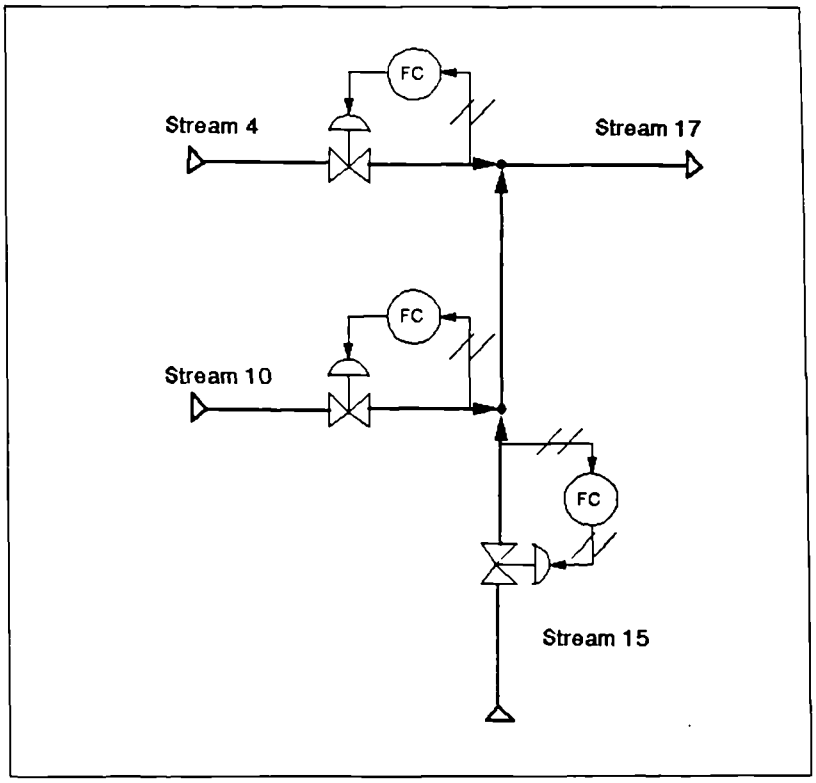

Figure 6.5 Control loop configuration for Block 4

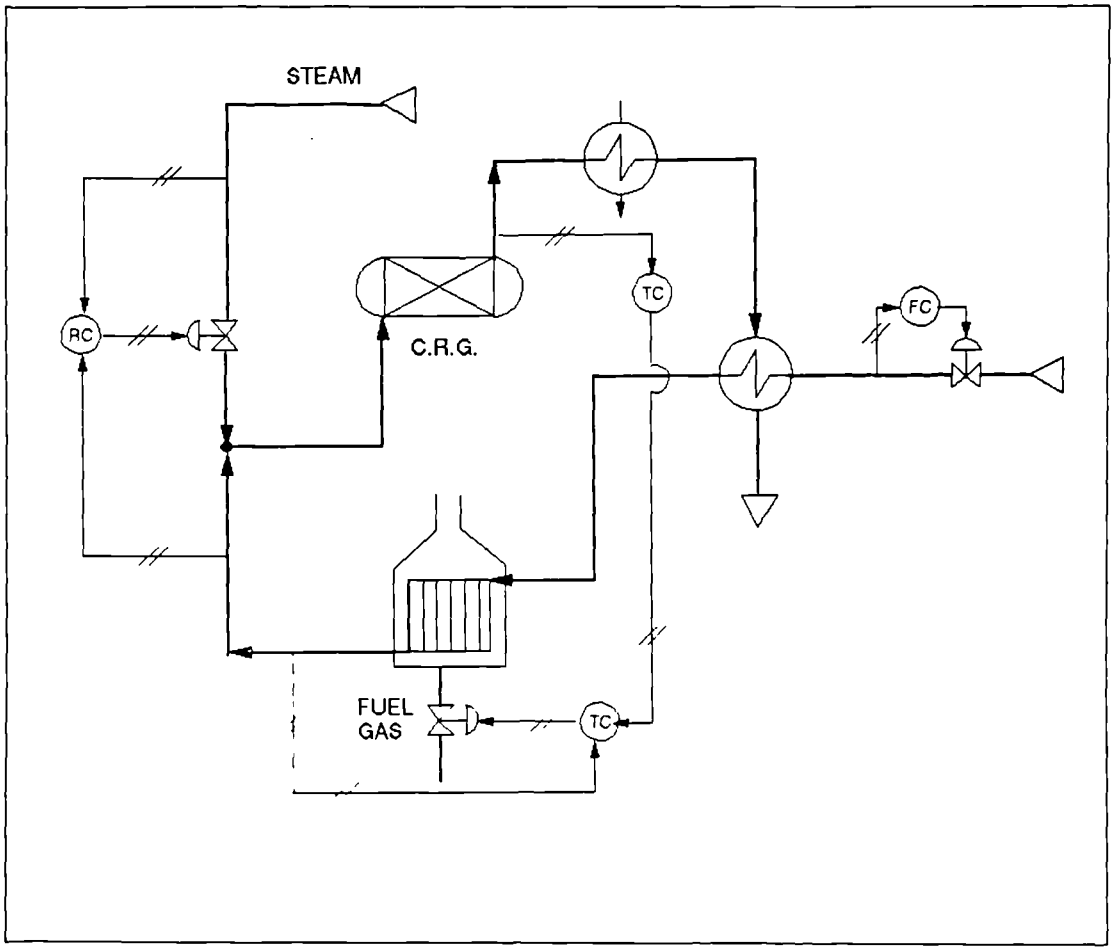

Figure 6.6 Control loop configuration for Block 5

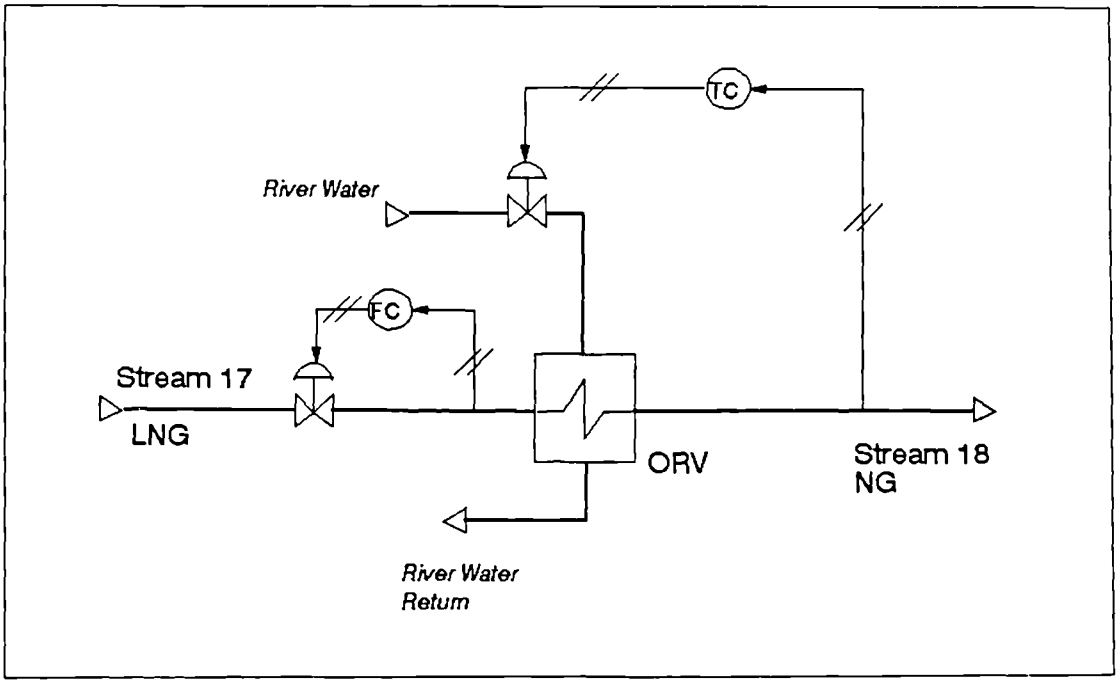

Figure 6.7 Control loop configuration for Block 6

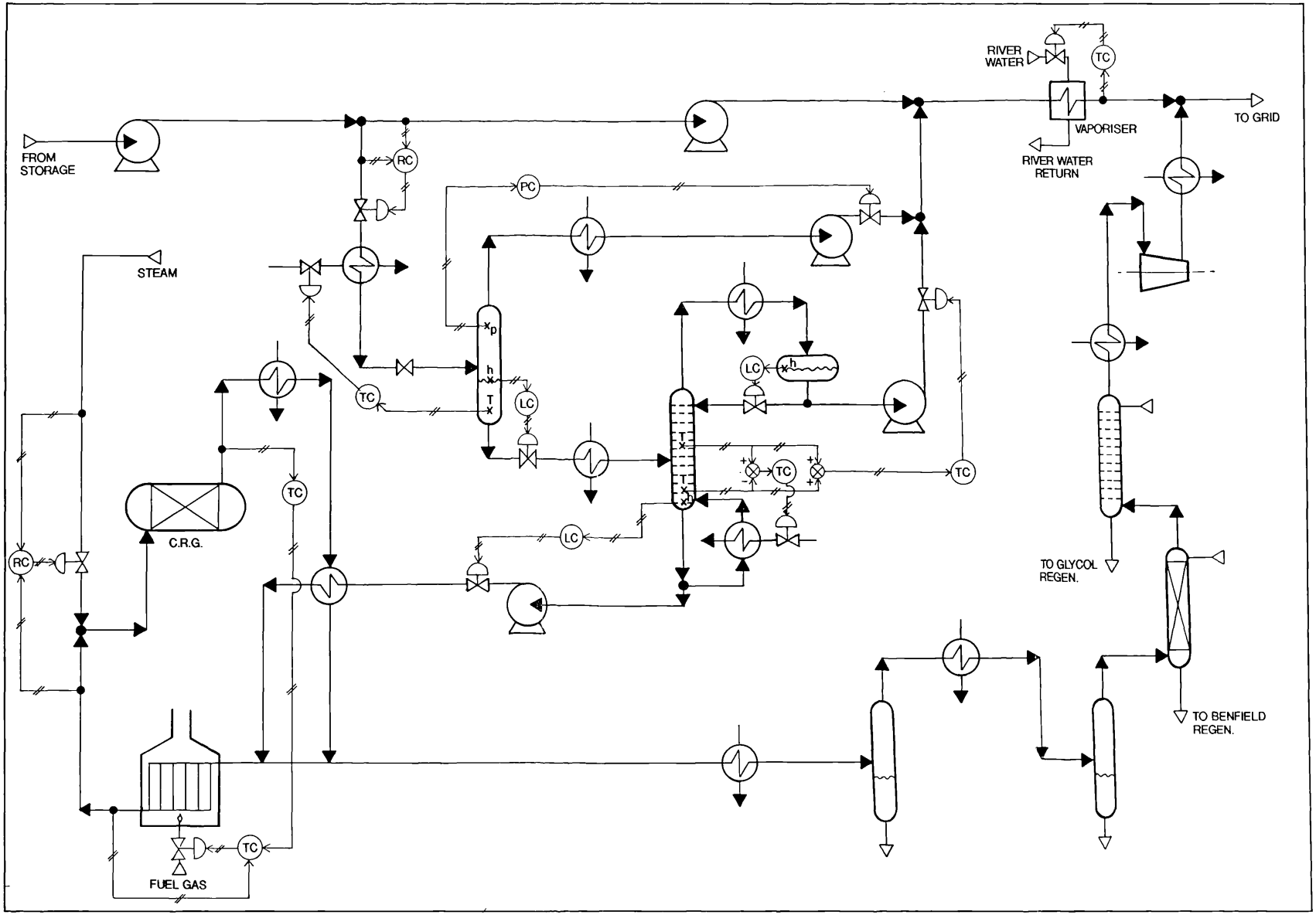

Figure 6.8 Recombined flowsheet with new control loop structure

A process with only one controlled output and one manipulated input requires single loop control. This is known as a single-input, single-output (SISO) system. For example, the control objective of the ORV unit in Figure 6.7 is to maintain natural gas outlet temperature at a desired value by manipulating the inlet water flow rate - a SISO system. Single loop controller design is the simplest to implement. Having identified the characteristics of the systems, and defined the performance specifications, an appropriate controller may be selected and tuned.

A multivariable system describes a system with more than one controlled variable and/or more than one manipulated variable. In cascade control, two or more control loops share a single manipulated variable. Thus, only one output can be controlled. This form of multiple loop control is used extensively in process control. In the heavies processing section, shown in Figure 6.6, cascade control is used to regulate the CRG reformer outlet temperature, with a secondary loop compensating for inlet stream temperature changes.

A multiple-input, multiple-output (MIMO) system has several outputs that require control and several manipulated inputs available to provide this control. Many feasible control loop configurations can be used to control a multivariable system (as demonstrated in Appendix 7) and are composed of several interacting control loops. This makes the control design of MIMO systems more difficult than for SISO and multiloop systems. The flash unit and distillation column are typical examples of operations requiring a MIMO control approach.

The control loop configurations used in this study fall into two main categories:

(i) *Feedback control* configurations, where directly measured controlled variables are used to adjust the manipulated variables.

(ii) *Inferential control* configurations, where secondary measurements (relating to the unmeasurable controlled variables) are used to adjust the manipulated variables.

Feedforward control, which anticipates the effect of independent variable change on the controlled variable, is not considered in this analysis. Every feedforward control loop must be used with a feedback control loop. Hence, the feedforward control does not affect the degrees of freedom analysis that identifies the number of feedback control loops required. Therefore, this control can be considered as a later addition to the control loop configuration.

The SISO and multiloop control loop structures were identified in Appendix 7, using qualitative arguments. The designs for these controllers are presented in the subsequent sections of this chapter. However, for the multivariable systems, only preliminary control loop structures were defined. This is because the interaction effects between each control loop have to be assessed in detail before appropriate control loops can be selected. Hence, interaction analyses were conducted on the flash unit and distillation column and are presented in Chapter 7.

6.2.2 Degrees of Freedom Analysis for Block 1

The sub-system considered in this degrees of freedom analysis extended from LNG storage to downstream of the splitter, S-01. As the LNG pumps were modelled as steady state units, with single inlet and outlet streams, they were not considered in this analysis. A simplified layout of the splitter is given below:

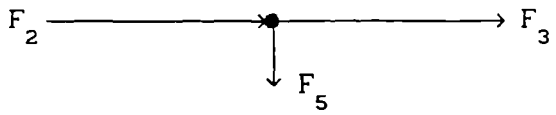

Three flow rates were considered in the steady state model of the splitter. As the steady state mass balance was the only expression describing the unit, this gave an f of 2. Hence, two feedback control loops were required to fully define this block as there were no externally specified variables.

F_2 and F_3 were selected as the controlled variables. F_2 was required for regulatory control, whereas the choice of F_3 as a controlled variable was arbitrary. Several manipulated variables were considered:

F_2, F_3, F_5, $F_3 + F_5$, F_3/F_5.

The possible control loop configurations for this block are listed in Table 6.2.

Configuration number	Loop configurations	
	F_2 control by	F_3 control by
1	F_2	F_3
2	F_2	F_5
3	F_2	F_3/F_5
4	$F_3 + F_5$	F_2

Table 6.2 Control loop configurations for Block 1

Using qualitative arguments, the effect of $(F_3 + F_5)$ on F_2 would be indirect, whereas self-regulation of F_2 is direct and fast. Hence, configuration 3 was selected, as ratio control is generally used to control the flow rate of two streams.

6.3 SINGLE LOOP CONTROL DESIGN

The SISO system control loops in the flowsheet consist of:

(i) Ratio control on the splitter, S-01.

(ii) Ratio control on the steam flow rate to the mixer, M-04.

(iii) Temperature control on the ORV unit, O-01.

Both ratio control loops act on operations with negligible dynamics, which are represented by steady state models. Hence, an open-loop step response would produce an instantaneous change in outlet conditions. However, the control valve is generally the slowest element in a flow control loop (Shinskey, 1988), as a step change in set point would not result in an immediate change in the valve position. This has been overcome in the dynamic simulation by ramping the set point ratio to its new demanded value with a maximum gradient of 0.1/5 secs.

The CRG reformer was designed for a high operating pressure, with a steam to hydrocarbon mass flow ratio of 3. If this ratio was identified as a controlled variable, a new degree of freedom would be introduced to the heavies processing section, to form a multivariable control system. Implications of varying the steam rate are discussed in Section 6.4.2. However, the control objectives would be adequately satisfied by varying feed temperature alone, without violating any operating constraints in the CRG reformer. Thus, the mass flow ratio was maintained at a constant value (assuming high pressure steam demand can be satisfied) with single loop ratio control. The remaining single loop control design for temperature control of the ORV has been investigated in detail in this section.

6.3.1 **ORV Control Loop Design**

The SISO control loop configuration for the ORV unit is illustrated in Figure 6.7. An equivalent block diagram arrangement, shown in Figure 6.9, was obtained from the transfer function description of the first-order system in Section 3.3.6. The block diagram identifies the manipulated and controlled variables for the control loop, with LNG inlet flow rate and temperature acting as disturbances. Water inlet temperature is assumed constant.

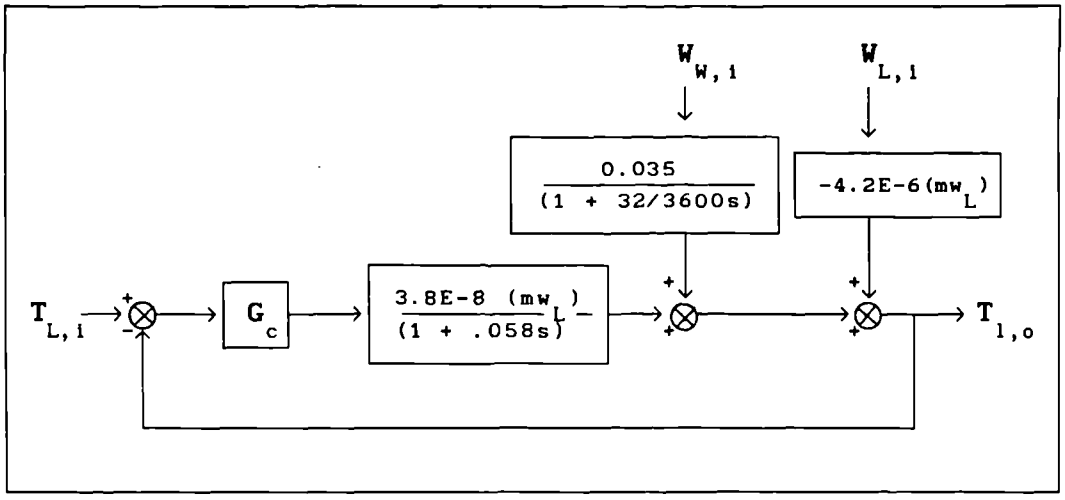

Figure 6.9 Block diagram of ORV unit

Performance criteria are generally used for the selection and tuning of a controller. These are based on the closed-loop response of a system. The *best* time-domain performance criteria for feedback control of the ORV outlet temperature were (Muir, 1987):

(i) No steady state error.

(ii) Maximum overshoot 10%.

(iii) Relatively fast rise time.

These criteria, illustrated in Figure 6.10, were used in the selection of a suitable SISO controller for the ORV unit.

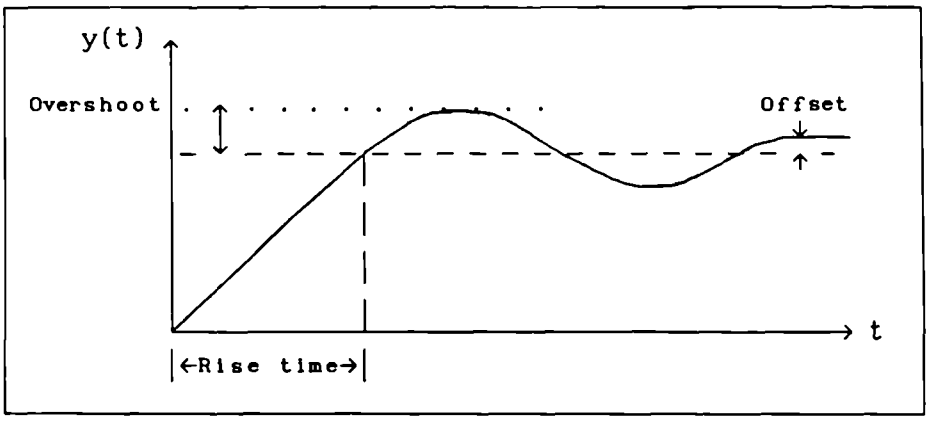

Figure 6.10 Time domain response criteria

Integral control action was essential to satisfy the performance requirement for zero steady state error. As integral control causes reduced response speed and stability degradation, this forms the basis for a proportional-integral (PI) controller. Shinskey

(1988) recommended a PID controller for temperature control, as the derivative term anticipates what the future error will be, and thus speeds up the response of the control action. Derivative action is most effective for systems with significant dead time. However, as the ORV unit was represented by a first-order system with no dead time, derivative action was unnecessary, and a PI controller was considered sufficient to satisfy the performance criteria. The transfer function for a PI controller is given by:

$$G_c(s) = K_c \left(1 + \frac{1}{\tau_I s} \right) \tag{6.1}$$

where K_c is the proportional gain of the controller, and τ_I is the integral time constant. The ORV unit is described by:

$$G_p(s) = \frac{K_p}{\tau s + 1} \tag{6.2}$$

where K_p is the steady state gain and τ is the time constant of the system. Thus, the closed-loop system in Figure 6.11 can be expressed in the general form:

$$Y(s) = \frac{G_c G_p}{(1 + G_c G_p)} R(s) + \frac{G_{d1}}{(1 + G_c G_p)} D_1(s) + \frac{G_{d2}}{(1 + G_c G_p)} D_2(s) \tag{6.3}$$

where

$Y(s)$ = natural gas output temperature (K)

$R(s)$ = natural gas set point temperature (K)

$D_1(s)$ = LNG inlet temperature disturbance (K)

$D_2(s)$ = LNG inlet flow rate disturbance (kgmol/hr).

There are various techniques available for tuning PI controllers, in the time- and frequency-domain (Åström and Haggland, 1988). As the performance criteria are defined in terms of the time-domain, tuning has been initially confined to these criteria. There are three basic approaches to SISO controller tuning in the time-domain:

(i) Applying trial and error settings to the process, to satisfy simple performance criteria.

(ii) Using time integral performance criteria to minimise system error, following a set point or disturbance (Ogata, 1990).

(iii) Using established rules, such as Ziegler-Nichols and Cohen-Coon methods (Stephanopoulos, 1984).

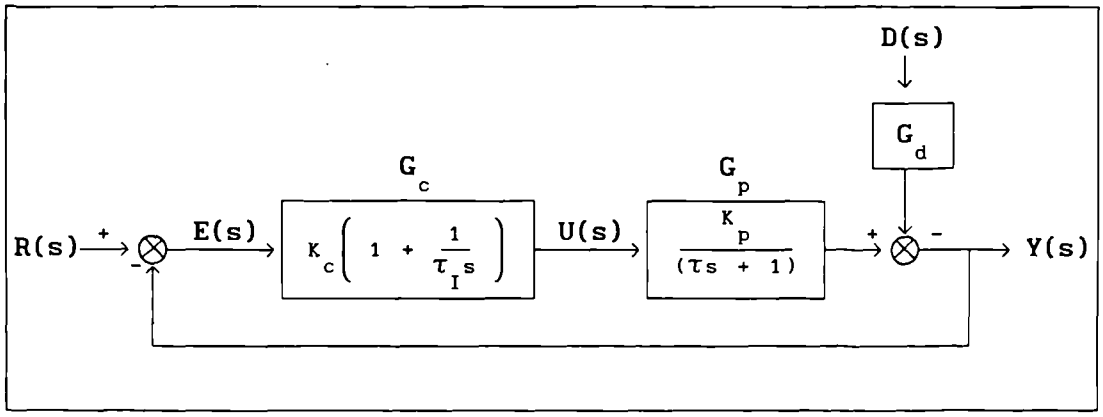

Figure 6.11 Block diagram of first-order system with PI control

6.3.2 SISO Control System Analysis

The control system analysis for the SISO control loop on the ORV unit has primarily investigated the response of the controlled variable to a set point change, to satisfy the time-domain performance criteria. However, other crucial factors have to be considered in the selection of the *best* controller settings. These include the response of the manipulated variable (water inlet valve) and disturbance rejection abilities of the PI controller. These aspects of controller tuning are considered in this section.

6.3.2.1 *Steady State Error Analysis*

Any control system exhibits steady state error in response to certain forms of inputs. The occurrence of this controller offset depends on the type of the open-loop transfer function. For the system configuration in Figure 6.11, the open-loop transfer function is:

$$G_c G_p(s) = \frac{K_p K_c (\tau_I s + 1)}{(\tau s + 1)\, \tau_I s} \qquad (6.4)$$

The s^1 term in the denominator represents a single pole at the origin. Hence, (6.4) is classified as a type 1 system (Ogata, 1990). The significance of the system type is illustrated in the following steady state error analysis.

The controller actuating error is the difference between the input and feedback signals in Figure 6.11, and is defined as:

$$E(s) = \frac{1}{1 + G_c G_p(s)} R(s) \qquad (6.5)$$

The final-value theorem can be used to compute the steady state actuating error, e_{ss}, given by:

$$e_{ss} = \lim_{t \to \infty} e(t) = \lim_{s \to 0} sE(s) \qquad (6.6)$$

Hence, the steady state actuating error of the ORV system for a **unit-step** input (R(s) = 1/s) is:

$$e_{ss} = \lim_{s \to 0} \frac{s}{1 + G_c G_p(s)} \frac{1}{s}$$

$$= \lim_{s \to 0} \frac{(\tau s + 1)\tau_I s}{(\tau s + 1)\tau_I s + K_p K_c (\tau_I s + 1)} = 0$$

As expected, the PI controller results in zero steady state error and satisfies one performance requirement.

The steady state error of the system to a **unit-ramp** input where $R(s) = 1/s^2$ is given by:

$$e_{ss} = \lim_{s \to 0} \frac{s}{1 + G_c G_p(s)} \frac{1}{s^2}$$

$$= \lim_{s \to 0} \frac{(\tau s + 1)\tau_I}{(\tau s + 1)\tau_I s + K_p K_c (\tau_I s + 1)} \frac{1}{s} = \frac{\tau_I}{K_p K_c}$$

These results are characteristic of a type 1 system, exhibiting a steady state error due to a ramp input. Thus, e_{ss} may be reduced by increasing gain, K_c, or reducing the integral time constant, τ_I.

6.3.2.2 *Overshoot Analysis*

In a detailed analysis of the ORV first-order system with PI control a relationship between controller settings and overshoot has been derived. The results are documented in Appendix 8. From this analysis, an algorithm has been developed that calculates the required controller gain for a given overshoot and integral time constant. As overshoot is limited to 10%, the algorithm has been used to predict controller settings for this specification.

For a given process, there is a range of PI controller settings that can satisfy a desired overshoot. This study initially considered a

selection of overshoots for the ORV system, at 5%, 10% and 15%. The results were plotted on a 2-dimensional graph of K_c vs. τ_I to form contours of equal overshoot. The Lotus 1-2-3 spreadsheet package was used to calculate controller parameters as it reduced computation time, and provided a graphical interpretation of controller settings, for a specified overshoot. The results in Figure 6.12 suggested that:

(a) The overshoot contours follow similar trends.

(b) For a given K_c, there is a unique value of τ_I which satisfies the required overshoot.

(c) For a given τ_I, two different values of K_c give the same percentage overshoot.

(d) The maximum allowable τ_I increases as overshoot decreases.

In a similar study, Schnelle and Miller (1988) noted that extending this analysis to a PID controller would require a complex, 3-dimensional plot.

In order to narrow the range of possible PI controller parameters giving 10% overshoot, an additional performance criterion was considered. Hence, an analysis of the rise time, T_r, of a first-order system with PI control was conducted and is included in Appendix 8. The findings were applied to a contour plot analysis of constant rise times. Selected contour plots, in Figure 6.13, showed that K_c and τ_I settings must be changed concurrently to maintain a constant rise time.

The contour plots for overshoot and rise time, in Figures 6.12 and 6.13, respectively, were superimposed to identify regions of acceptable controller performance. Results for the 10% overshoot and rise time contours are presented in Figure 6.14.

6.3.2.3 *Time Response Analysis*

The design and selection of a suitable PI controller has been based on satisfying the following performance specifications:

(i) *Steady state error* - eliminated by integral control action

(ii) *10% overshoot* - achieved using overshoot algorithm

(iii) *Fast response time* - relative

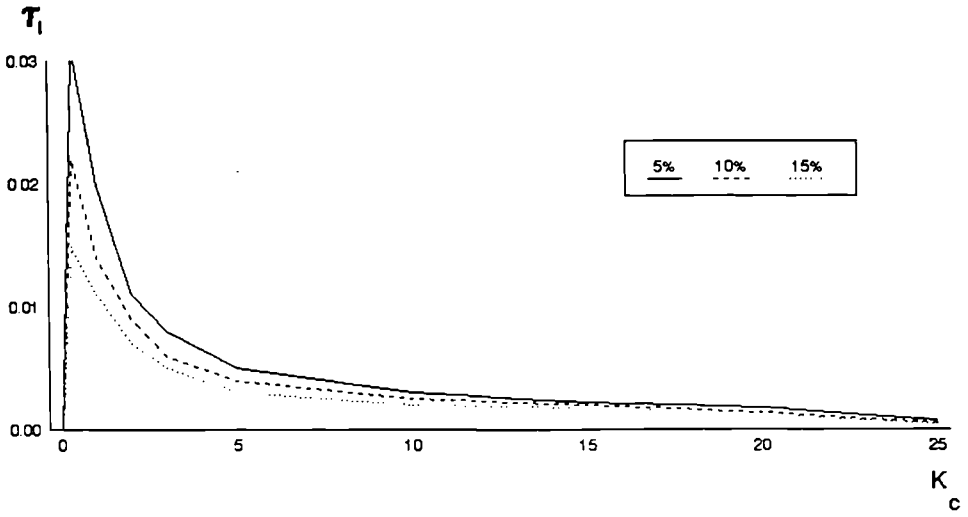

Figure 6.12 Overshoot contours for ORV unit controller design

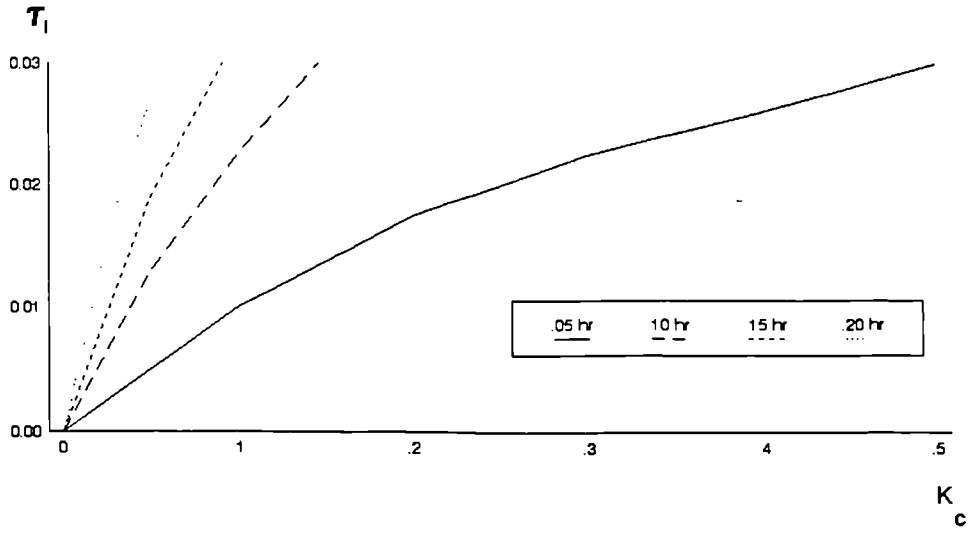

Figure 6.13 T_r contours for ORV unit controller design

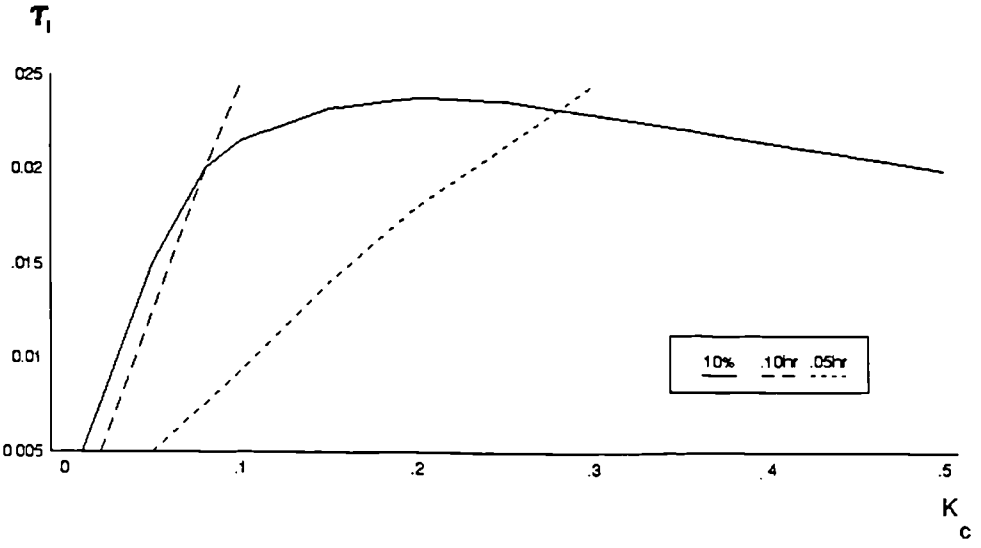

Figure 6.14 Combined contour plot for ORV unit controller design

In a similar controller design study (Muir, 1987), a rise time of approximately 0.05 hr was declared acceptable. However, the ORV unit has been scaled up to handle greater LNG flows. Hence, it seems reasonable to increase T_r to an upper limit of 0.10 hr.

Besides the above performance specifications other factors had to be addressed before the final controller settings could be selected.

a) *Control signal for set point change*

Following a step change in the set point, the proportional action of a PI controller reacts immediately to produce a large change in the control signal. (The conventional PI controller is proportional on error). In the ORV system, this signal takes the form of a control valve position. However, there are physical limitations placed on the control signal, permitting a maximum variation between 0.0 (closed valve) and 1.0 (fully open valve). Also, a control valve can become mechanically unstable when operated below 10% (Luyben, 1990), and excessive chatter should be avoided as this leads to wear. Hence, the control signal should be monitored to ensure the valve remains within its operating constraints.

The control signal, U(s), for a change in set point is defined as:

$$U(s) = G_c E(s) = \frac{G_c}{(1 + G_c G_p)} R(s)$$

For a first-order system with PI control this becomes,

$$U(s) = \frac{K_c(\tau_I s + 1)(\tau s + 1)}{\tau_I \tau s^2 + \tau_I(1 + K_p K_c)s + K_p K_c} R(s) \qquad (6.7)$$

The form of this transfer function allows U(s) to be inspected for step changes in R(s). Thus, from an initial control valve position of 0.5 (half open) the control signal can vary by ±0.4 before reaching any valve limits.

b) *Disturbance rejection*

The PI controller for the ORV system would be required to reject disturbances to a greater extent than set point changes within the plant, as the steady state set point is equivalent for each feed

condition. So, the regulator aspect of control design must also be considered. It should be noted that if only disturbance rejection was required, the controller could be more tightly tuned. In addition, the proportional action could be based on the process variable, which would allow a higher controller gain to be set. However, as the controller's performance criteria are based on set point response it is better to adopt the conventional proportional action on error, as this will give a faster approach to set point.

Of the anticipated disturbances to the ORV system, water inlet temperature is assumed constant, and water inlet flow rate acts as the manipulated variable. Thus, the remaining disturbances were LNG inlet flow rate and temperature. For disturbance rejection only with no set point change, the closed-loop transfer function from equation (6.3) becomes:

$$Y(s) = \frac{G_{d1}}{(1 + G_c G_p)} D_1(s) + \frac{G_{d2}}{(1 + G_c G_p)} D_2(s)$$

Replacing $G_{d1}(s)$ and $G_{d2}(s)$ by the LNG temperature and flow rate transfer functions, respectively, gives:

$$Y(s) = \frac{K_{d1}\tau_I s(\tau s + 1)}{(\tau_{d1} s + 1)\,(\tau_I s(\tau s + 1) + K_p K_c(\tau_I s + 1))} D_1(s)$$

$$+ \frac{K_{d2}\tau_I s(\tau s + 1)}{\tau_I s(\tau s + 1) + K_p K_c(\tau_I s + 1)} D_2(s) \qquad (6.8)$$

Only some time-domain performance criteria, relating to set point input in Figure 6.10, could be applied to disturbance rejection responses (Doebelin, 1985). The rise time was redefined in terms of the peak value, C_p, in Figure 6.15. The decay ratio, or number of cycles required to reduce to a given amplitude was also substituted.

It should be noted that time-domain analyses of a control system response are generally limited to step reference performance indices. Only a few sources extend the time-domain criteria to consider disturbance rejection performance (Doebelin, 1985). Even less suggest a validation of the resulting control signal.

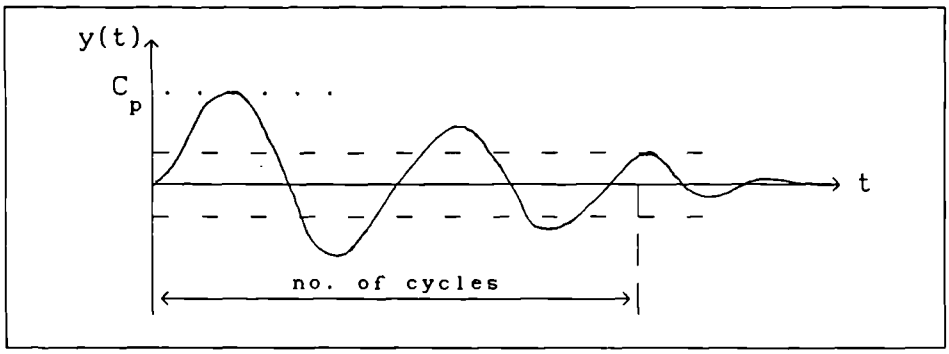

Figure 6.15 Time domain disturbance response criteria

In the preliminary feedstock changeover studies, in Section 5.4, step changes were introduced to feedstock and set point values, representing severe forms of changeover. Hence, the maximum step change in the ORV unit disturbances would not be expected to exceed those experienced during the changeovers:

(i) 16 K for inlet temperature.

(ii) 4500 kgmol/hr for inlet flow rate.

Thus, if satisfactory disturbance rejection could be achieved for the above disturbances, the controller settings would be acceptable.

c) *Control signal for disturbance rejection*

As with set point changes, the control signals for disturbance rejection must also be inspected to ensure the control valve limits are not exceeded. Thus, for a disturbance, D(s), to the ORV system, in Figure 6.11, the closed-loop transfer function becomes:

$$U(s) = -\frac{G_c G_d}{(1 + G_c G_p)} D(s) \qquad (6.9)$$

6.3.3 ORV Control Loop Tuning

A detailed time-domain analysis of the ORV system with PI control was conducted and reported in Section 6.3.2. By developing suitable algorithms, two of the performance specifications for controller design (percentage overshoot and rise time) have been presented in graphical form. The contour plot in Figure 6.12 shows a wide range of controller gains that satisfy the percentage overshoot.

The effect of gain on controller performance was studied by comparing

results for two extreme gain settings. For example, with τ_I = 0.002, K_c values of 0.0039 or 25.00 gave the desired 10% overshoot, in Figure 6.12. However, these controllers produce markedly different responses for set point change and disturbance rejection, when modelled using a linear control design package (PROGRAM CC). The results in Table 6.3 show that the high gain gave a faster response, with unacceptably large changes in the control signal (i.e. greater than 0.5). In addition, the control valve was expected to reach its new position in under 3s, which is unrealistic (Shinskey, 1988). These results demonstrated the possible range of responses for 10% overshoot, and illustrate the trends in T_r in Figure 6.14.

System Response	Variable	Criteria	PI Controller	
			Low gain	High gain
Set point Change	Outlet Temperature	Overshoot (%) T_r (hr)	10.19 0.179	10.01 0.001
	Control Signal	C_p at peak T_p (hr)	0.175 0.176	25.00 0.000
Disturbance Rejection (ΔT = 16 K)	Outlet Temperature	C_p (K) Cycles (10%)	0.508 0.800	0.016 0.5
	Control Signal	C_p at peak T_p (hr)	0.098 0.189	0.542 0.001

Table 6.3 System response for selected PI controllers

The performance criteria for a rise time, T_r, of 0.10 hr and 10% overshoot corresponded to a single point in Figure 6.14 at:

$$K_c = 0.0838, \qquad \tau_I = 0.0200.$$

The ORV system responses for these controller settings are presented in Figure 6.16. Unit-step results are given for set point change and disturbance rejection to LNG inlet temperature, with corresponding control signals. (The response to LNG inlet flow disturbance was significantly less). The disturbance rejection responses were well within the recommendations, with acceptable variations in control valve position. Therefore, as the PI controller gave good overall performance, these controller settings were adopted.

The steady state error analysis, in Section 6.3.2.1, revealed that for a first-order system with PI control the error to a ramp input is

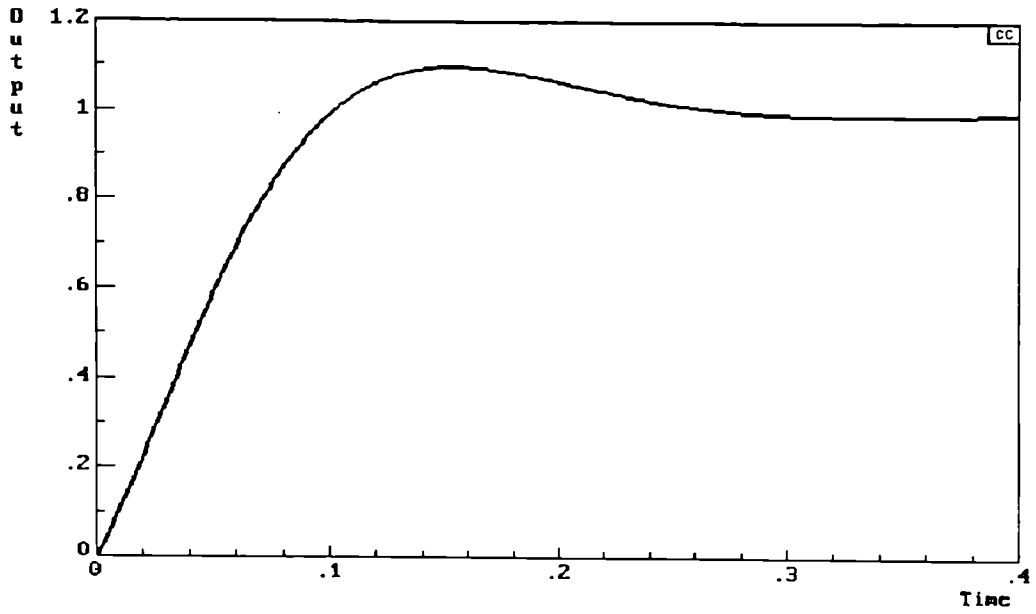

(a) temperature response for unit-step set point input

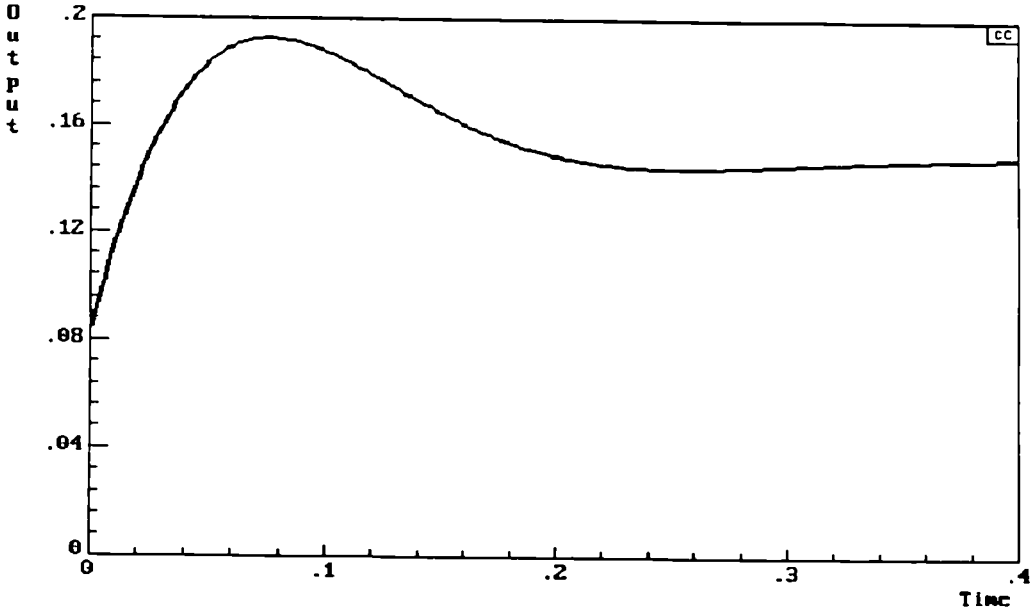

(b) control signal response for unit-step set point input

Figure 6.16 ORV system response for selected controller settings

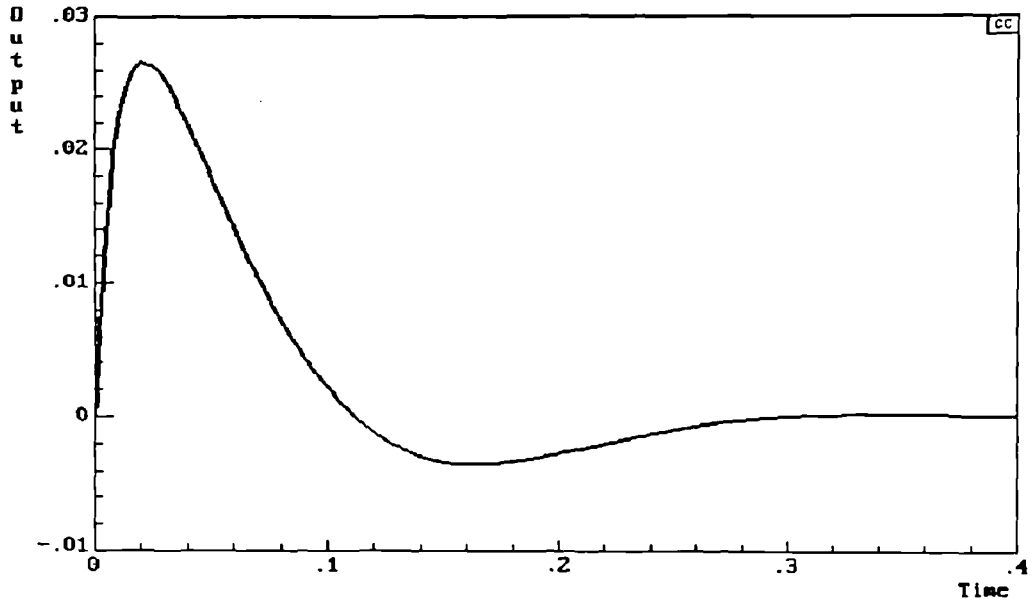

(c) temperature response for step disturbance input

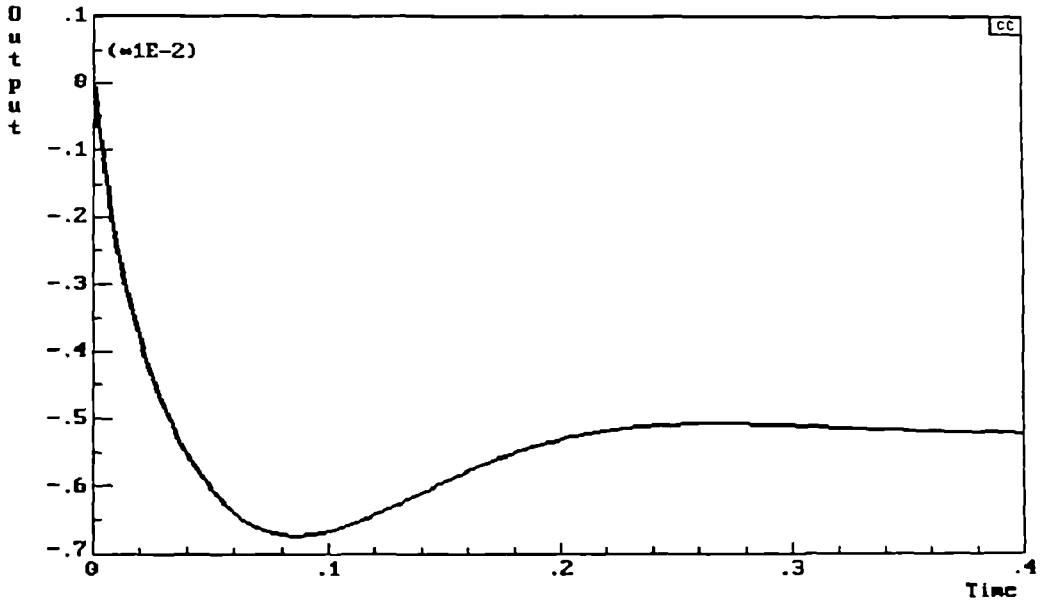

(d) control signal response for step disturbance input

Figure 6.16 ORV system response for selected controller settings (contd.)

proportional to τ_I/K_c. Thus, the steady state error for a ramp input would be reduced as K_c increases, as τ_I would decrease to maintain a 10% overshoot. Hence, improved performance to ramped set point changes could be obtained by speeding up controller response.

6.3.4 ORV Regulatory Control Achievements

A PI controller was selected for the single loop temperature control of the ORV unit. The performance specifications for the PI controller lead to a detailed time-domain analysis of the system. Set point change, disturbance rejection and control action responses were considered in the controller analysis. PROGRAM CC, a linear control design package, was used to investigate time-domain analyses for the control system. These results were included in the final selection of the PI controller parameters, which were:

$$K_c = 0.0838$$

$$\tau_I = 0.0200 \text{ hr.}$$

As the ACSL model for the ORV unit was also in transfer function form, the controller settings did not require further validation.

6.4 HEAVIES PROCESSING CONTROL DESIGN

The cascade control loop arrangement for the heavies processing section is illustrated in Figure 6.6. Two SISO feedback controllers required selection and design in this control arrangement.

The ACSL models used to describe each operation in the heavies processing section were essentially steady state models with associated time lags. The non-linear characteristics of this process made the design and assessment of a suitable controller difficult when considering several operating conditions. Hence, as the first step towards the design of a cascade control structure, the ACSL models were linearised. This approach has several advantages:

(i) Individual models may be analysed about their operating points, and compared for different operating points.

(ii) A standard block diagram of the process can help identify a suitable controller structure.

(iii) Linear control techniques may be applied.

(iv) A linear control design software package can be employed that produces simulation results much faster than ACSL.

The cascade control design began by identifying system variables for model linearisation. A block diagram of the heavies processing section was developed and assessed. The performance criteria were derived, based on a sensitivity analysis of the flowsheet. Various controller combinations were considered, and the final selection was implemented and tested on the corresponding non-linear ACSL models.

6.4.1 Control Objectives

To establish performance criteria for the heavies processing section, a number of sensitivity analyses were conducted. These were used to assess the impact of changes in the CRG reformer operating conditions on the product specifications.

The major control objective was to maintain methane production at a constant level. In addition, certain operating constraints were placed on the reformer. For example, carbon deposition is particularly damaging to catalyst activity, as characterised by the Boudouard temperature. This is further discussed in Appendix 1.

In earlier steady state and dynamic analyses of the complete flowsheet, the steam to hydrocarbon mass flow ratio was maintained at 3, for each operating condition. However, in practice this ratio would be expected to change as conditions dictate. The recommended operating conditions for such a CRG reformer (Monk, 1988) suggested a steam to hydrocarbon ratio of between 0.3 and 3.0. Clearly, the reformer would be operating with the highest possible excess steam.

The effect of varying the steam to hydrocarbon ratio was investigated using the ACSL simulation model. Results for the GL2Z feedstock condition, plotted in Figure 6.17, produced the following trends as the ratio was reduced from 3.0 to 0.5:

(i) Methane production increased by over 2%.

(ii) Both CO and CO_2 production increased significantly.

(iii) Product flow rate reduced to a third of its original value.

(vi) Outlet temperature increased by almost 100 K.

These results showed that reducing the steam to hydrocarbon ratio provided a steam utilities savings, reduced downstream operation sizing and produced more methane. However, several points should be noted. In a reformer, reducing the steam ratio would cause more heavy hydrocarbons to appear in the product stream. (Oversizing the catalyst tubes may help reduce this effect as it would create a greater opportunity for heavies conversion). However, the CRG reformer model used in the dynamic simulation assumed there was sufficient excess steam in the reformer to convert all the heavy hydrocarbons. Hence, the simulation results would become more inaccurate as the ratio reduced. In addition, the increased CO_2 production would place a greater load on the absorber, although this may be offset by the corresponding decrease in water removal and treatment. The increase in CO production would have to be carefully assessed as this represents a non-removable impurity that is limited by the product gas specifications in Table 2.2.

The effect of reducing the steam ratio was also considered in terms of the turndown ratio. A comparison of reformer product flow rates in Table 6.4, indicated that percentage turndown increased slightly as the ratio reduced, giving a small improvement in feedstock flexibility.

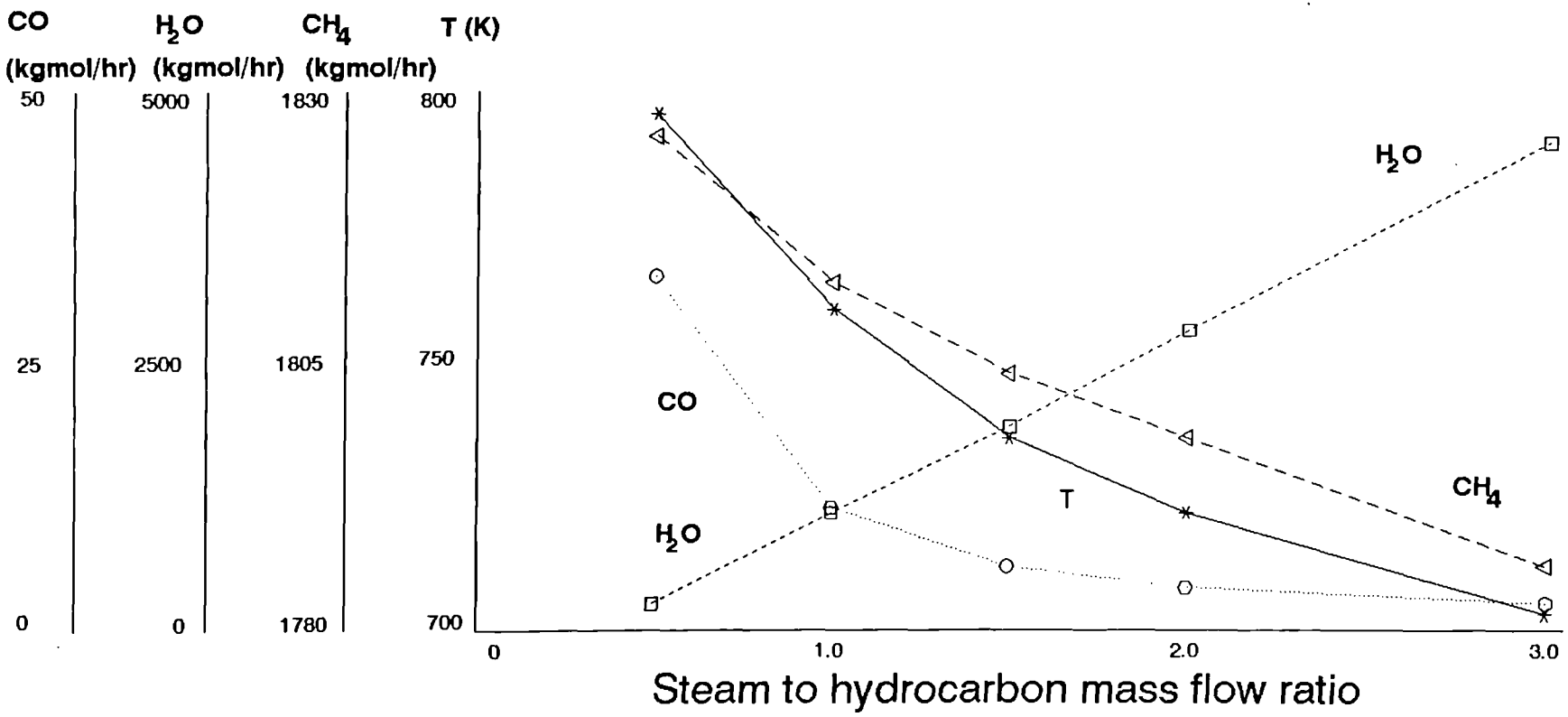

Figure 6.17 Effect of S/C ratio on CRG reformer product

Steam to Hydrocarbon Mass Flow Ratio	Product Flow Rate (kgmol/hr)			% Turndown
	GL1K	GL2Z	GL1Z	
3.0	6831	7088	9147	74.7
2.0	5121	5272	6796	75.3

Table 6.4 Turndown in CRG reformer product flow rate

The control implications of manipulating the steam ratio must also consider the CRG reformer product composition. As product composition cannot be accurately and quickly measured, temperature control was employed in manipulating fuel flow rate, as illustrated in Figure 6.6. If two manipulated variables (steam and fuel flow rates) influence one controlled variable (product temperature), a conflict of interest may arise. Manipulating the steam flow rate alone would affect the reformer inlet flow rate, composition and temperature. So, changes in the fired heater outlet temperature may be overridden by the steam flow rate, which is significantly greater. Also, using reformer outlet temperature for inferential composition control is not ideal, as the relationship between outlet temperature and degree of conversion, for the water-gas shift and methanation reactions, is based on an exponential relationship. Thus, introducing a variation in steam flow rate adds another dimension to product composition, rendering inferential control less effective.

The above discussion on varying steam flow rate, suggests that the steam flow rate and product composition should be monitored at regular intervals. In practice, the product temperature set point would be regularly updated by an on-line analyser. As analysers generally have a significant dead time, the update interval may be in the order of 5 to 10 minutes. Thus, a cascade control arrangement would be incorporated. For the remainder of this study, the steam flow ratio has been fixed at 3, to ensure total conversion of heavy hydrocarbons and avoid carbon deposition. Thus, only one manipulated variable has been retained for this process - the fuel flow rate.

Disturbance inputs to the heavies processing section would originate within the distillation column. These disturbances result in changes

in flow rate, composition and temperature. A secondary temperature disturbance would also arise from the feedback arrangement, via the counter-current heat exchanger.

6.4.2 **Linearised Models**

Linear approximations of the non-linear ACSL models were obtained directly from ACSL, as state space models.

Before linear approximations of the heavies processing section could be derived the overall block model structure was identified. This allowed linear approximations of the process to be developed, for either each unit or groups of units.

6.4.2.1 *State Space Models*

When a dynamic system is linearised about an operating state, it may be described by the following state space expressions:

$$\dot{\mathbf{x}}(t) = \mathbf{A}\mathbf{x}(t) + \mathbf{B}\mathbf{u}(t) \qquad (6.10)$$

$$\mathbf{y}(t) = \mathbf{C}\mathbf{x}(t) + \mathbf{D}\mathbf{u}(t) \qquad (6.11)$$

These consist of a linearised state equation (6.10) and output equation (6.11), involving three types of variables - input variables, $\{u_i(t)\}_{i=1}^{m}$, output variables, $\{y_i(t)\}_{i=1}^{r}$, and state variables, $\{x_i(t)\}_{i=1}^{n}$. Clearly there are m inputs, r outputs and n states. Four compatible matrices describe the state space model: $\mathbf{A}(t)$ is the state matrix, $\mathbf{B}(t)$ the input matrix, $\mathbf{C}(t)$ the output matrix and $\mathbf{D}(t)$ is the direct transmission matrix. Much of the recent control theory is based on the concept of state, which is essentially a time-domain approach.

The state of a dynamic system represents the smallest number of variables that must be defined to describe the system behaviour. These state variables make up the state vector $\mathbf{x}(t)$, which together with the input variables, $\mathbf{u}(t)$, at $t = t_o$ completely define the dynamic behaviour of the system. Since the system output, $\mathbf{y}(t)$, depends on its initial value and earlier input variable values, the system must include elements that memorise these input values (Ogata, 1990). In a continuous-time environment, integrators provide this function, and hence their outputs can serve as state variables.

Therefore, the number of state variables in a system is equivalent to the number of integrators describing the dynamic model. The inputs to a state space model are classified as either disturbances or manipulated variables. Both input and output variables can be defined as measurable or unmeasurable as illustrated in Figure 6.18.

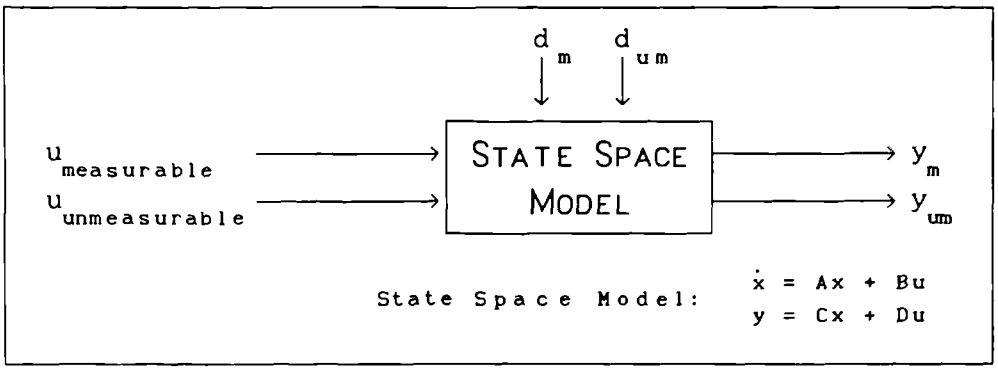

Figure 6.18 State space description of variables

State space models can be automatically generated by the ACSL simulation facility. The state space model structure requires the control and observable variables to be first identified. Having specified the size of perturbation on each input, ACSL calculates the Jacobian matrix about the current operating point, and then the **A**, **B**, **C** and **D** matrices are formed. (The Jacobian is the partial derivative of the state derivative vector with respect to the state variables).

6.4.2.2 *State Space Model Structure*

Before setting up the heavies processing section to obtain state space models, several questions must be addressed. For example, how many state space models are required to describe this process? This could range in number from one state space representation for each operation, to a single state vector containing all five operations. As cascade control has been implemented on this process, at least two state space models would be required.

The proposed state space model structure for the heavies processing section is illustrated in Figure 6.19. Disturbances entering the system at stream 22 were transmitted through each operation. The fuel flow rate manipulated variable was included in the fired heater model, with outlet stream changes passed on as disturbances to the CRG reformer. The resulting disturbances to the counter-current heat

exchanger did not include temperature, due to the intermediate cooler operation. The disturbance perturbations and number of states for each are described in Table 6.5.

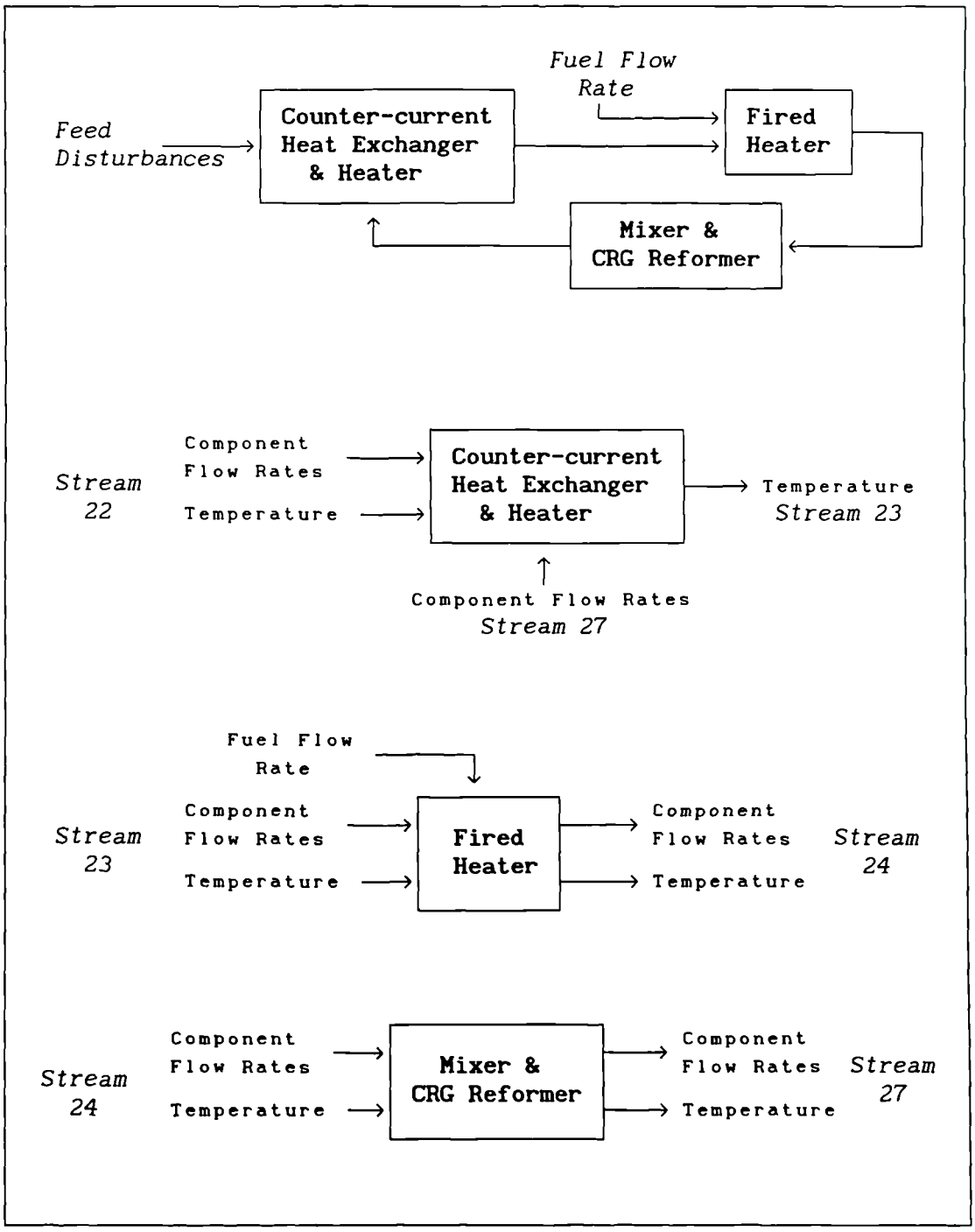

Figure 6.19 State space structure for the heavies processing section

State Space Model	Disturbance Input	Perturbation	No. of States
Counter-current heat exchanger & heater	$F_{i,22}$ $F_{i,27}$ $T_{i,22}$	10% 10% 5 K	2
Fired heater	$F_{i,23}$ T_{23} Q_{23}	10% 5 K 10%	8
Mixer & CRG reformer	$F_{i,24}$ T_{24}	10% 5 K	3

Table 6.5 State space models for heavies processing section

A set of state space models was obtained for each block, representing the three feedstock conditions. The state space representations, for the GL2Z feedstock, are archived in Appendix 9.

Transfer function relationships were then derived from the state-space models, using PROGRAM CC. The resulting block diagram structure is presented in Figure 6.20, with the associated transfer functions, for the GL2Z feedstock, given in Appendix 10.

As the state space representations for each block contained the same number of states, their transfer function structures were similar. The transfer functions shown in Table 6.6, relating fuel rate (G_4) and feed stream temperature (G_2) to outlet temperature for the fired heater, are good examples of this comparison.

Feedstock Condition	Manipulated input, fuel rate	Disturbance input, inlet temperature
GL1K	$\frac{1.931E7}{(s+1634)(s+60)}$	$\frac{92092.6}{(s+1634)(s+60)}$
GL2Z	$\frac{1.345E7}{(s+1162)(s+60)}$	$\frac{65495.6}{(s+1162)(s+60)}$
GL1Z	$\frac{1.269E7}{(s+1413)(s+60)}$	$\frac{79154.2}{(s+1413)(s+60)}$

Table 6.6 Transfer functions for fired heater outlet temperature

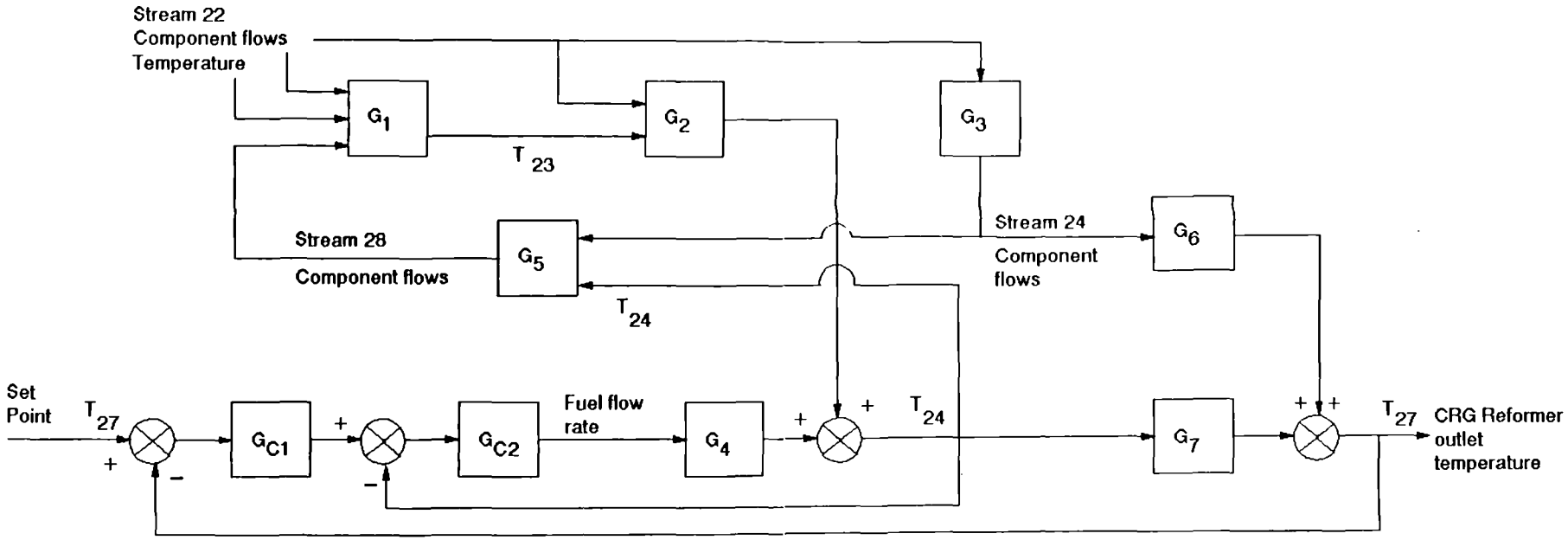

Transfer Function	Operation	Dimension
G_1	Heat Exchanger	11x1
G_2	Fired Heater	7x1
G_3	Fired Heater	6x6
G_4	Fired Heater	1x1
G_5	CRG Reformer	7x4
G_6	CRG Reformer	6x1
G_7	CRG Reformer	1x1

Figure 6.20 Block diagram of heavies processing section

The feedback loop in Figure 6.20, formed by the counter-current heat exchanger, was found to have a relatively small gain. The gain was defined as the combined effect of T24 on the transfer function product of G_5, G_1 and G_2. Thus, the feedback effect originated from the fired heater outlet temperature, which had a direct effect on the CRG reformer product composition and hence the counter-current heat exchanger outlet stream temperatures varied. This small effect was ignored in further cascade controller studies. The resulting block diagram was simplified and is shown in Figure 6.21.

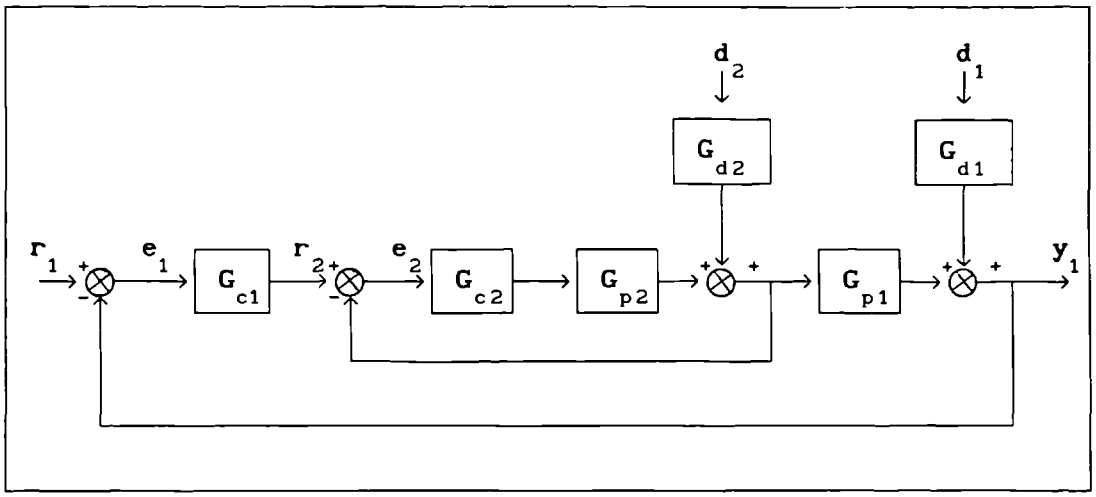

Figure 6.21 Simplified block diagram of cascade control loops

6.4.3 **Performance Criteria**

The performance criteria for cascade control of the heavies processing section are primarily concerned with the outer loop, which maintains the CRG reformer product temperature. Although guidelines for reformer operation do not state performance requirements, performance criteria must be established, as a basis for the comparison of alternate controller designs.

The performance criteria were derived from a sensitivity analysis of the system and its ability to achieve its control objectives. Only results for the GL2Z feedstock were considered. As the main control objective was to maintain methane production, the effect of this variable on the final product specifications was first assessed. ACSL simulation results for the GL2Z feedstock condition gave the final product stream conditions as:

C.V. = 38.38 MJ/m^3

Wobbe No. = 50.19 MJ/m^3

with product specification limits of:

$36.9 \leq$ C.V. ≤ 42.2 MJ/m^3

$47.3 \leq$ Wobbe No. ≤ 51.2 MJ/m^3

Hence, the combustion characteristics were positioned within 28% and 74% of their limiting ranges, respectively. As a target C.V. of 37.9 MJ/m3 was defined, only small variations in C.V. would be acceptable, of within say ±10% of the permitted range. This corresponded to a 37.4 to 38.4 MJ/m^3 range in C.V.

The ACSL simulation results for variation in the processed stream composition, in Table 6.7, indicates that significant changes in methane flow rate results in only small changes in product. This is because the processed stream constitutes only 12.3% of the final product flow rate, and methane has a lower C.V. than other hydrocarbons. These results suggest that the target C.V. could be better maintained by manipulating the separation process conditions.

Methane Flow Rate in heavies processed stream (kgmol/hr)	**Product Stream Combustion Characteristics**	
	C.V. (MJ/m^3)	Wobbe No. (MJ/m^3)
3000	38.24	50.20
2000	38.35	50.19
1786 (GL2Z condition)	38.38	50.19
1500	38.41	50.19
1000	38.48	50.19

Table 6.7 Combustion characteristics for variation in methane flow

The effect of changing CRG reformer inlet temperature by manipulating fuel flow rate was also investigated. The results in Table 6.8 indicated that large changes in the fired heater outlet temperature gave relatively small variations in methane production. The changes in reformer outlet temperature (a measured variable) were greater.

As expected, introducing the new product compositions from Table 6.8, into the final product stream, gave small variations in the combustion characteristics. Production rate varied by less than 2%.

Fired Heater Outlet Temperature (K)	CRG Reformer Product			
	Methane flow rate (kgmol/hr)		Temperature (K)	
	Actual	Δ	Actual	Δ
650	1790	+4	698	-5
673 (GL2Z condition)	1786	0	703	0
700	1781	-5	709	+6

Table 6.8 CRG reformer product condition for variation in inlet temperature

Although these sensitivity results suggested that large variations in CRG reformer operating conditions had little effect on product specifications, the results were obtained for isolated changes in selected conditions. So, although large fluctuations in methane production may be tolerated, reformer feed temperature must be constrained between 573 K and 800 K (Monk, 1988), and above the Boudouard temperature at reformer outlet.

The above sensitivity analyses enabled time-domain performance criteria to be determined. As inferential control of the CRG reformer product composition was governed by an exponential relationship (Appendix 1), and disturbances also affected the final product, it was desirable that the outer loop cascade controller achieved its set point temperature. For control design, percentage overshoot is usually set between 10% and 20% (Doebelin, 1985). Hence, the performance criteria for the outer control loop became:

(i) Zero offset.

(ii) 15% to 20% overshoot.

(iii) Reasonably fast response time.

Performance criteria for the inner loop were less critical, so a large overshoot, of say 20%, was acceptable. Moreover, it was not essential that the secondary controller achieved its set point value with no steady state error because the absolute value of the fired heater outlet temperature was not critical. Hence, performance specifications for the inner temperature control loop were concerned only with overshoot and a reasonable response time.

6.4.4 Controller Selection

The performance criteria in Section 6.4.3 were used to determine suitable classical controllers for the inner and outer loops.

Zero offset for the outer loop required integral action in the outer loop controller. Also, the sensitivity analysis showed that variations in CRG reformer outlet temperature had a small effect on methane production. This suggests that tight outer loop control was not essential, and hence a PI controller would suffice.

Temperature control on the inner loop was less important, as its set point is continually being readjusted by the outer loop control action. For a temperature on temperature cascade control arrangement, Shinskey (1988) recommended that the secondary controller was proportional only, so inner loop gain could be set high to give fast and responsive action. However, as this arrangement makes the primary controller susceptible to integral windup, PI control of the inner loop was also considered.

Hence, two controller arrangements were selected for cascade control of the heavies processing section:

(i) P inner loop / PI outer loop.

(ii) PI inner loop /PI outer loop.

The offset associated with each controller arrangement was determined from a steady-state error analysis. The transfer functions for the processes were represented in the general form:

$$G_{p2} = \frac{K_2}{(\tau_{a2}s + 1)(\tau_{b2}s + 1)}$$

$$G_{p1} = \frac{K_1(\tau_{a1}s + 1)}{(\tau_{b1}s^2 + \tau_{c1}s + 1)(\tau_{d1}s + 1)}$$

where G_{p2} and G_{p1} represent the inner and outer loop processes, respectively. The corresponding results for unit-step and ramp inputs are given in Table 6.9. These results show that the offset present in the inner loop for P/PI control is eliminated in the outer loop, due to integral action. Both configurations exhibit a steady state actuating error in response to a unit-ramp set point input.

Steady State Error	Input	Control Loop Arrangement	
		P / PI	PI / PI
Inner Loop	Step	$\frac{1}{(1 + K_{c2}K_2)}$	0
	Ramp	∞	$\tau_{I2} / K_{c2}K_2$
Outer Loop	Step	0	0
	Ramp	$\frac{\tau_I(1 + K_{c2}K_2)}{\tau_I(1+K_{c2}K_2) + K_{c1}K_{c2}K_1K_2}$	$\frac{\tau_{I1}K_{c2}K_2}{\tau_{I1}K_{c2}K_2 + K_{c1}K_{c2}K_1K_2}$

Table 6.9 Steady state errors for cascade control loop structures

6.4.5 Cascade Controller Tuning

The conventional procedure for tuning a cascade controller involves two stages (Stephanopoulos, 1984). First, the inner loop is designed with the outer loop open. Then, the outer control loop for the new system is designed, consisting of the closed inner loop and G_{p1}.

As a guide to controller settings, Shinskey (1988) recommended that the proportional band, PB, should be 10% for the inner loop and 25% for the outer. (PB is used to specify controller settings, where a certain change, PB%, in controller input causes a full-scale change in controller output, provided input and output signals are of the same type). Hence, the inner loop controller is 2.5 times more sensitive to input signal changes than the outer loop. The dynamics of the secondary loop must also be much faster than that of the primary loop. Furthermore, the higher gain in the secondary controller would make disturbance rejection more effective, without damaging overall system stability (Stephanopoulos, 1984).

In frequency-domain terms, the faster secondary control loop will have a smaller phase lag. Thus, the crossover frequency, ω_{co}, for the secondary loop will be higher. (Crossover frequency denotes the frequency at which the phase lag of an open-loop system is -180°. It is a measure of system stability and is proportional to the bandwidth of the closed-loop system).

6.4.5.1 *Inner Loop Proportional Control*

On tuning the P controller, system stability must be considered as it may impose a limitation on controller gain. The open-loop transfer function for the inner loop is:

$$G_{p2}G_{c2} = \frac{K_{c2}K_2}{(\tau_{a2}s + 1)(\tau_{b2}s + 1)} \qquad (6.12)$$

representing a second-order system. For this system, the phase lag approaches -180° as frequency reaches infinity. So, according to the Bode stability criterion, the system should always be stable, regardless of gain. However, Doebelin (1985) suggests that valid stability predictions can only be made when enough dynamics are included to describe at least a third-order system. Thus, some additional system component dynamics would have to be incorporated before a reasonable judgement could be made on stability.

A root-locus design criterion has been used to determine controller gain, K_c, by attaining a desired level of closed-loop stability (Doebelin, 1985). The root-locus gain-setting procedure positions the dominant root poles of the system at a specified damping ratio, ζ. A root-locus plot is ideal for this application as it represents the roots of the characteristic equation as gain is varied from zero to infinity. On the resulting complex plane plot, radial lines of constant damping ratio pass through the origin. For a second-order system, Doebelin (1985) recommends an initial ζ design value of 0.42. (A more stable system with less overshoot requires ζ to be increased to 0.6 or 0.8. A faster response is obtained by reducing ζ to 0.3).

A root-locus plot of the inner loop system, in Figure 6.22, indicates that ζ increases as K_c decreases. The results for a range of ζ are compared in Table 6.10. Set-point and disturbance step responses were then assessed for a variety of ζ values.

The unit-step results for $\zeta = 0.42$ demonstrated good stability, an acceptable overshoot and fast response time. Additional system responses for the GL1K and GL1Z feedstocks were also favourable. However, with a corresponding $K_c = 0.153$, a 1 K step change in set point would produce an initial proportional kick of 0.153. As this represents valve position, with an assumed steady state setting of

0.5, the controller could only handle step set point changes up to 3 K, before the valve reached its operating limits. In addition, the sensitivity analysis in Table 6.8 indicated that a 1 K change in reformer product temperature required over 4 K change in the fired heater set point, for the GL2Z feedstock condition. Hence, a lower proportional gain was selected for the inner loop controller, at:

$$K_c = 0.10.$$

Although offset increased as overshoot and response time were reduced, the more stable system (with $\zeta \simeq 0.5$) could handle a greater operating envelope.

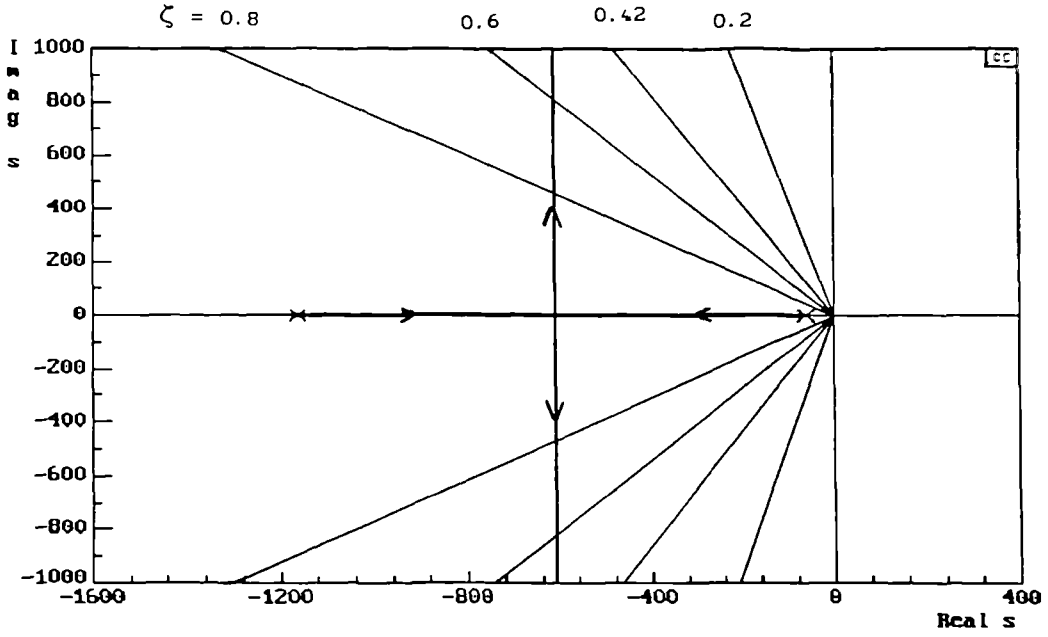

Figure 6.22 Root locus diagram for inner loop P control

Damping Ratio ζ	Natural Frequency ω_n (rad/hr)	Controller Gain K_c
0.3	2039	0.304
0.42	1458	0.153
0.5	1218	0.1052
0.6	1015	0.0715
0.707	871	0.0510
0.8	764	0.0383

Table 6.10 Proportional controller gain for selected damping ratios

6.4.5.2 *Inner Loop Proportional-Integral Control*

The open-loop transfer function for PI control of the inner cascade control loop is given by:

$$G_{p2}G_{c2} = \frac{K_{c2}(\tau_I s + 1)\,K_2}{\tau_{I2}(\tau_{a2}s + 1)(\tau_{b2}s + 1)} \frac{1}{s} \qquad (6.13)$$

which is a third-order, type 1 system. Tuning was based on a trial and error approach to satisfy the overshoot and response time criteria. From an initial investigation of integral time constants, the 0.001 to 0.01 range was selected. The corresponding gains at selected damping ratios, ζ, suggested that a ζ of at least 0.5 was required to reduce overshoot below 20%.

The root-locus plots in Figure 6.23, for τ_I values of 0.005 and 0.007, showed that a given damping ratio may be satisfied by more than one gain. For example, a controller with $\tau_I = 0.005$ achieved a 20% overshoot with $K_c = 0.005$ and 506. The higher gain gave an oscillatory and faster step response, due to a reduction in ζ from 0.60 to under 0.08. Also, unit-step responses produced a very oscillatory response for the GL1Z feed case due to a further reduction in ζ, indicating the control loop was too tightly tuned for this condition. By comparison, the lower gain controller behaved well, as illustrated in Figure 6.24, with only slight variation in performance. Hence, as fixed controller parameters were preferred, only low gain controllers were considered further.

An assessment of disturbance rejection performance was also conducted for step changes in feed temperature. Qualitative arguments were then applied to select the following PI controller settings:

$$K_c = 0.005$$
$$\tau_I = 0.005.$$

6.4.5.3 *Outer Loop Proportional-Integral Control*

The outer loops of both inner control loop configurations were tuned by trial and error. (As the performance criteria were developed within the time-domain, frequency-domain design methods could not be directly applied to the system. They could only be used to check the stability of the system once initial settings were obtained).

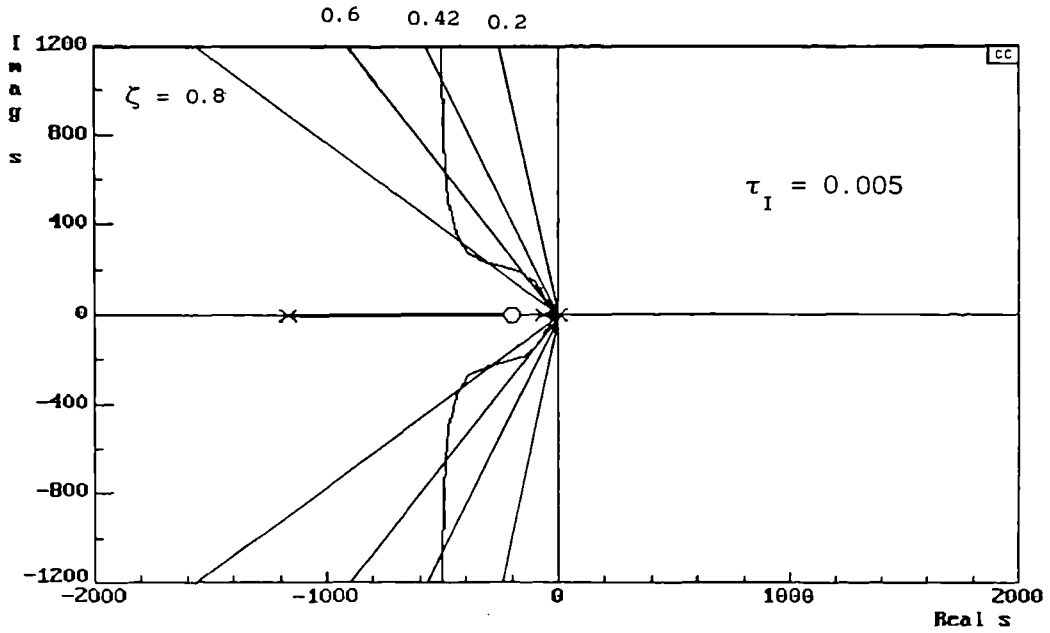

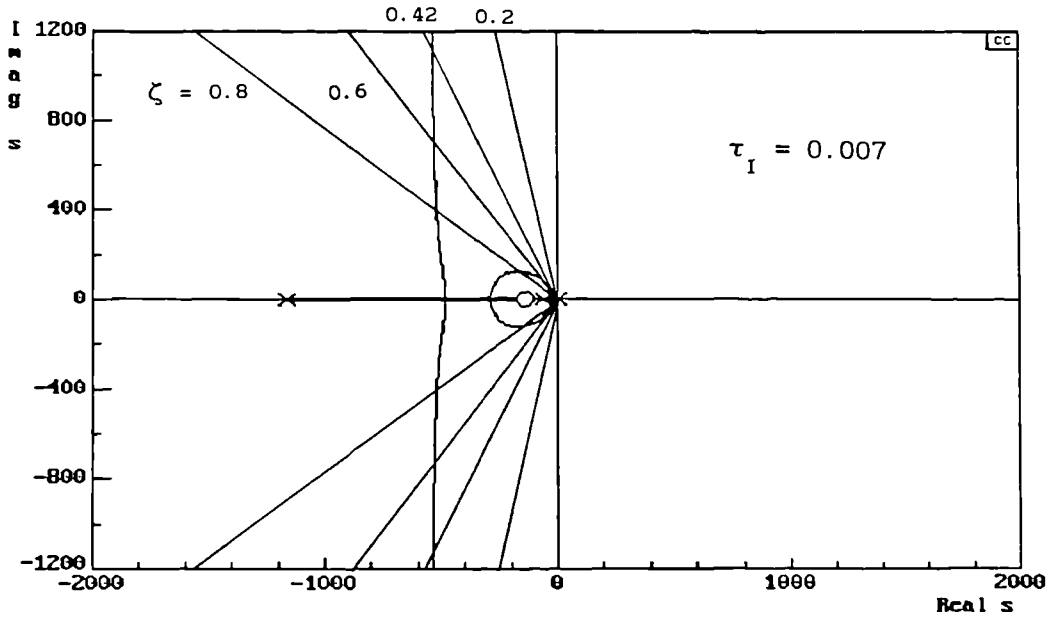

Figure 6.23 Root locus diagrams for inner loop PI control

(a) $\tau_I = 0.005$

(b) $\tau_I = 0.007$

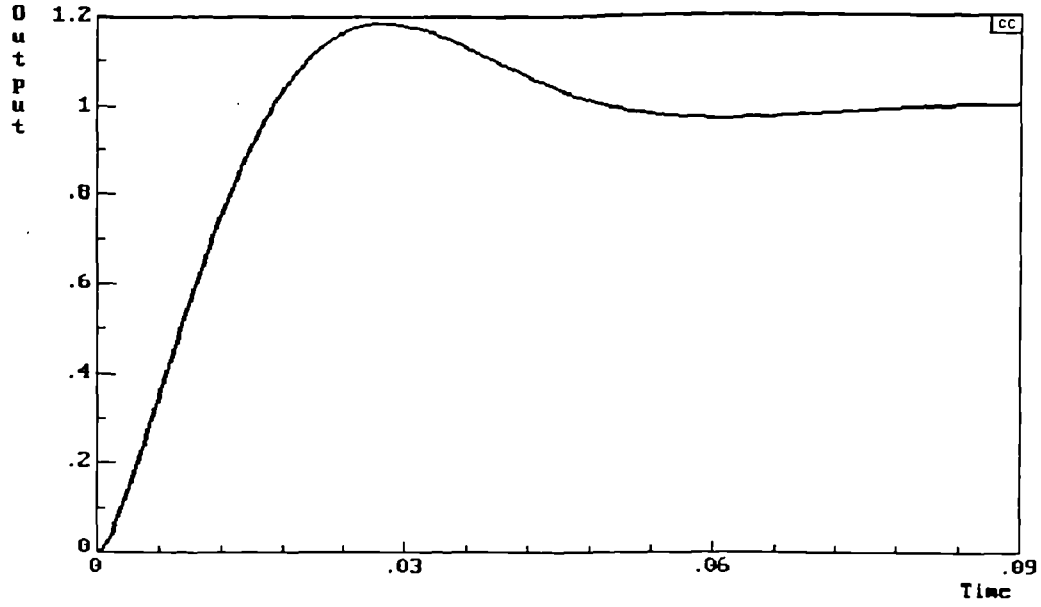

(a) temperature response for unit-step set point input

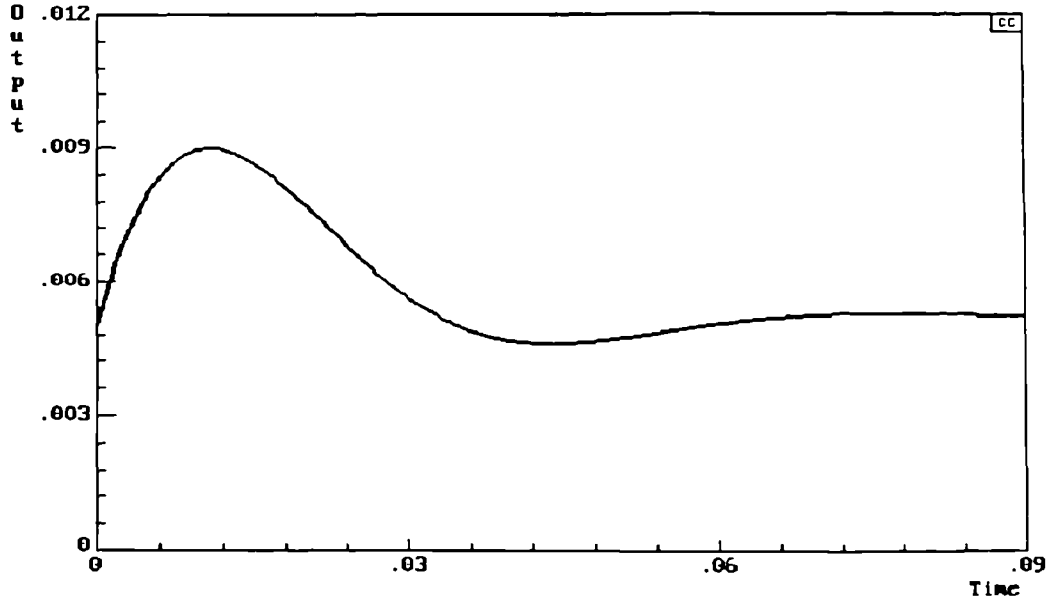

(b) control signal response for unit-step set point input

Figure 6.24 Inner loop response for selected PI controller

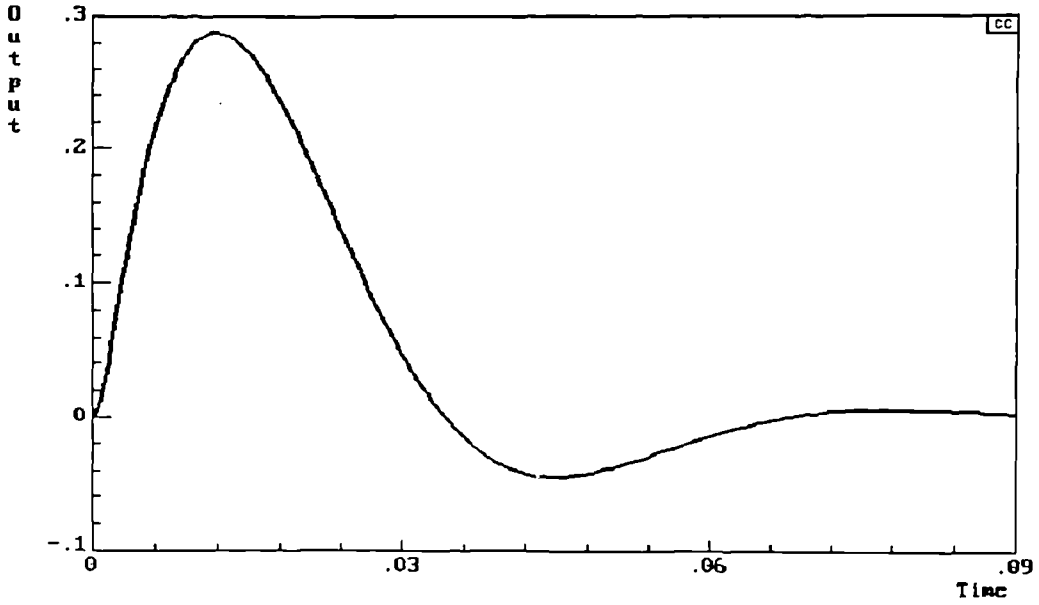

(c) temperature response for step disturbance input

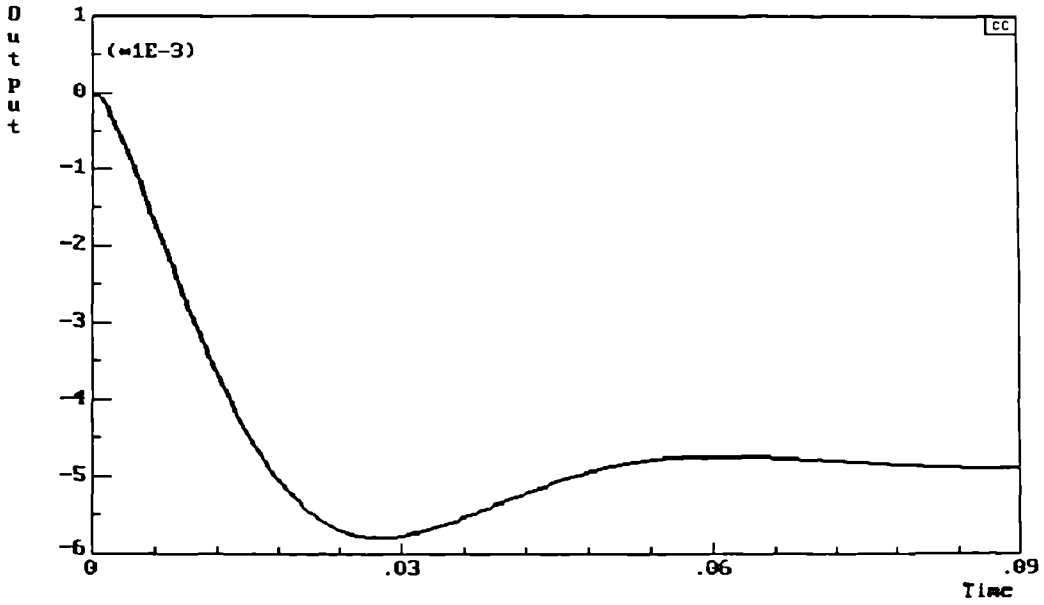

(d) control signal response for step disturbance input

Figure 6.24 Inner loop response for selected PI controller (contd.)

P inner/PI outer loop controllers:

PI outer loop controller settings were obtained for unit-step set point responses, which satisfied the 20% overshoot and response time criteria. Satisfactory closed-loop responses are illustrated in Figure 6.25 for the following outer loop controller settings:

$$K_c = 0.54$$
$$\tau_I = 0.003.$$

PI inner/PI outer loop controllers:

PI outer loop controller settings were selected that gave a maximum 20% overshoot (for the GL1Z feedstock condition) and a rise time of 0.045 hr. The results in Figure 6.26 replicated the P inner/PI outer loop controller responses, with outer loop controller settings of:

$$K_c = 1.25$$
$$\tau_I = 0.01.$$

The corresponding Bode plots for the inner and outer control loops in both arrangements are summarised in Table 6.11. These results indicated that ω_{co} was far greater for the inner control loop, as recommended by Shinskey (1988), and thus faster. However, it should be noted that the frequency response results for the inner loop in both controller arrangements, (6.12) and (6.13), corresponded to a second-order system. Hence, the phase lags did not exceed ~180°, and their stability measures were only approximate.

Frequency Response Results		**Gain Margin**	**Phase Margin (°)**	ω_{co} (rad/min)
P inner PI outer	Inner loop*	40.0	45.0	330.
	Outer loop	1.95	36.0	16.7
PI inner PI outer	Inner loop*	50.0	52.5	300.
	Outer loop	1.85	60.0	1.67

* approximate

Table 6.11 Bode plot results for P/PI and PI/PI

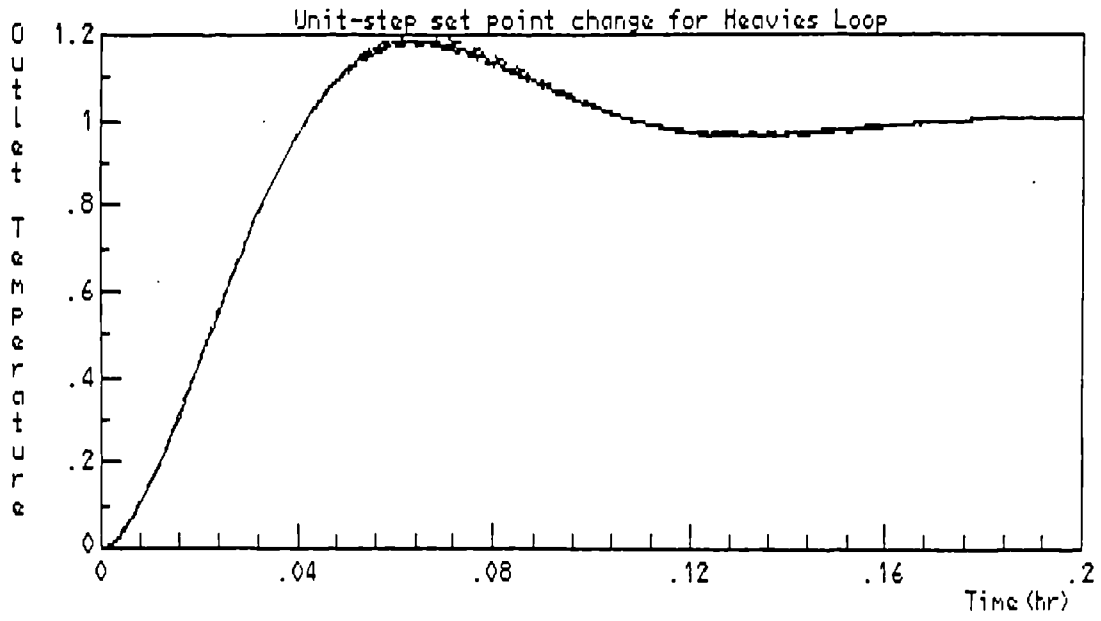

(a) outlet temperature response for unit-step set point input

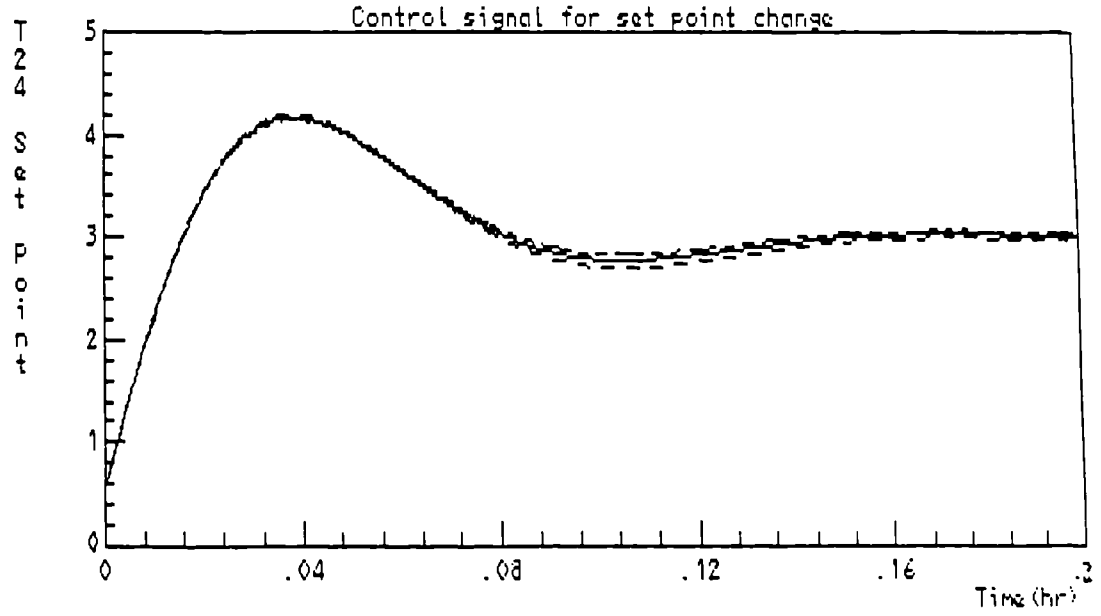

(b) inner set point response for unit-step set point input

Figure 6.25 Step responses for P inner/PI outer loop control

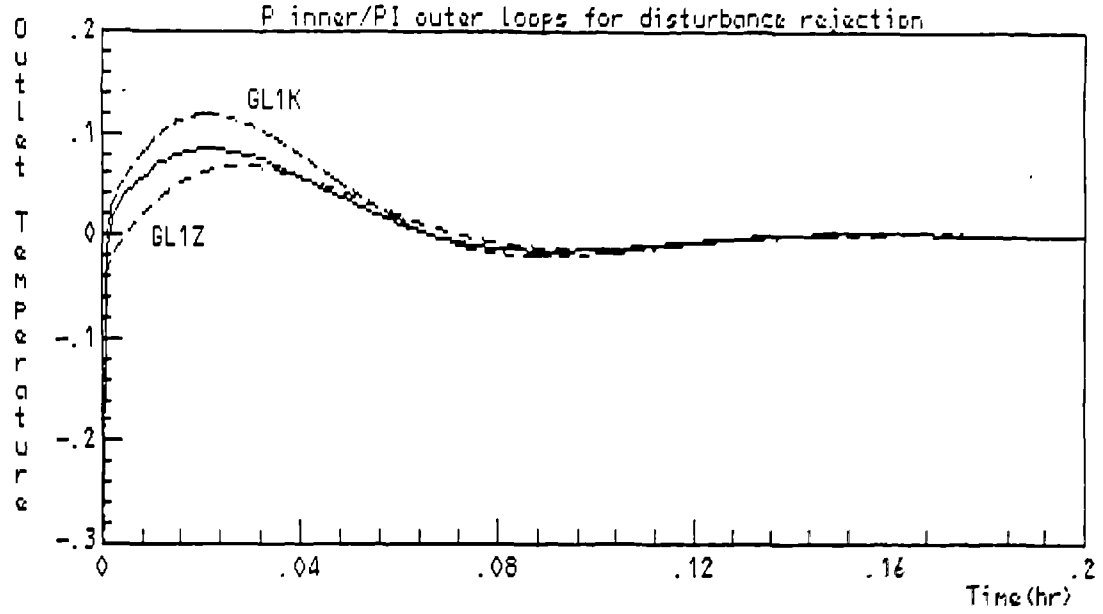

(c) outlet temperature response for step disturbance input

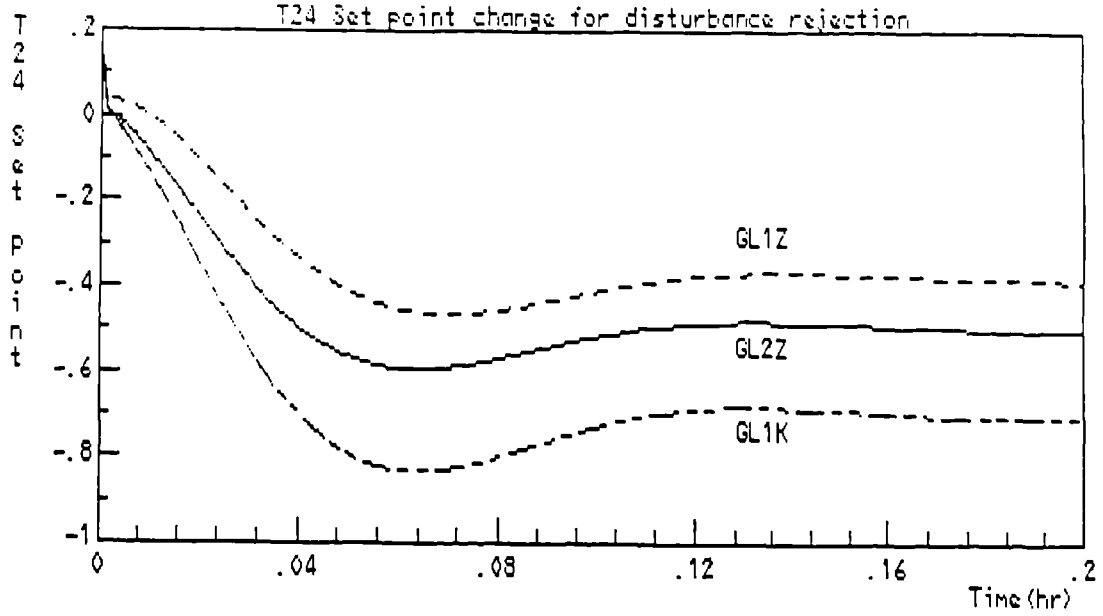

(d) inner set point response for step disturbance input

Figure 6.25 Step responses for P inner/PI outer loop control (contd.)

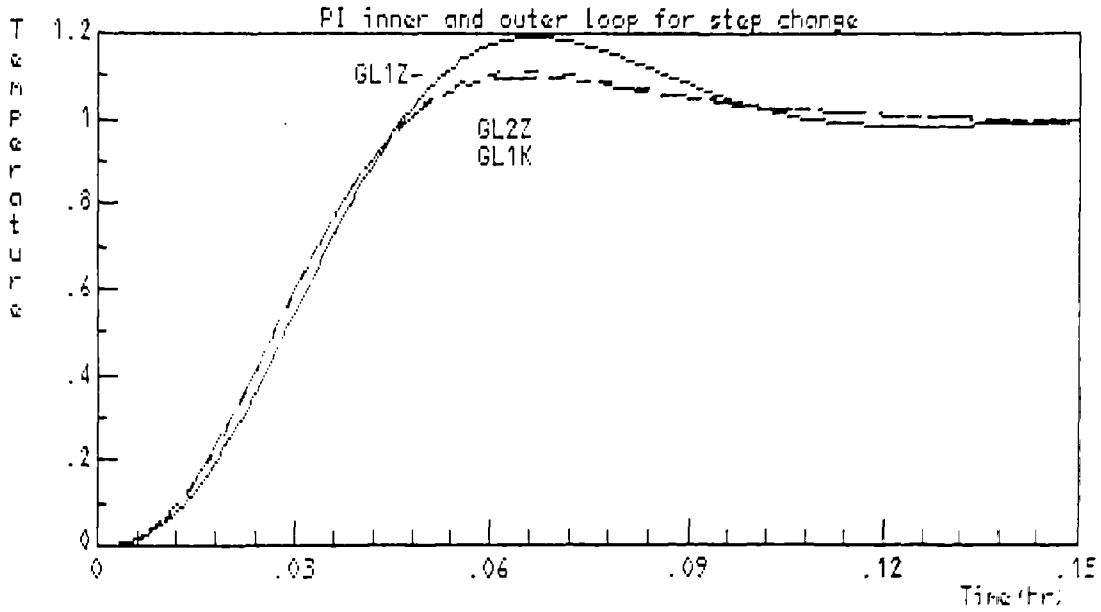

(a) outlet temperature response for unit-step set point input

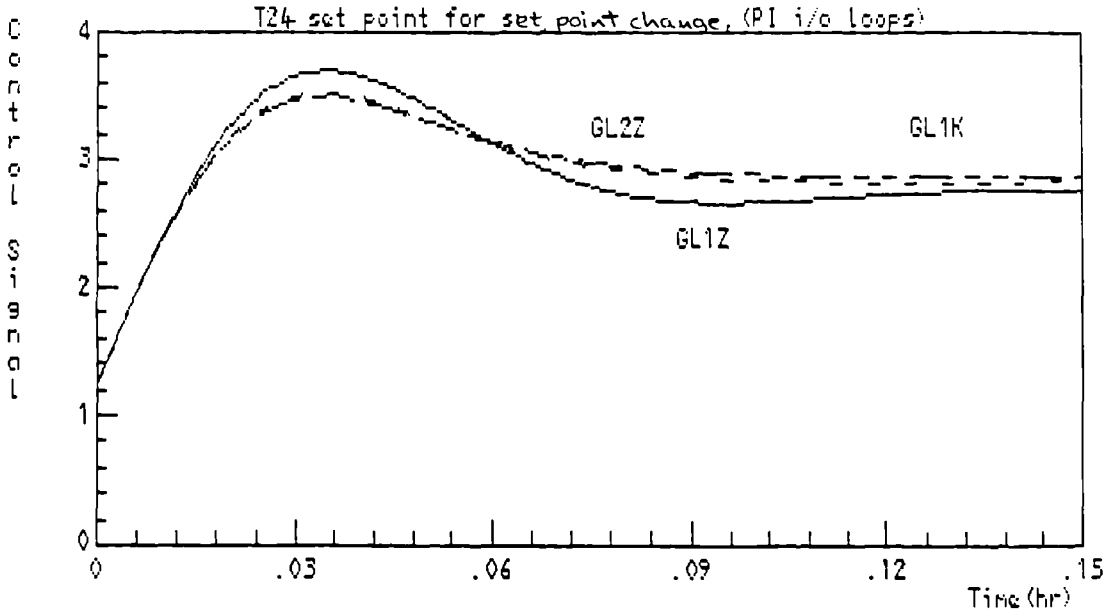

(b) inner set point response for unit-step set point input

Figure 6.26 Step responses for PI inner/PI outer loop control

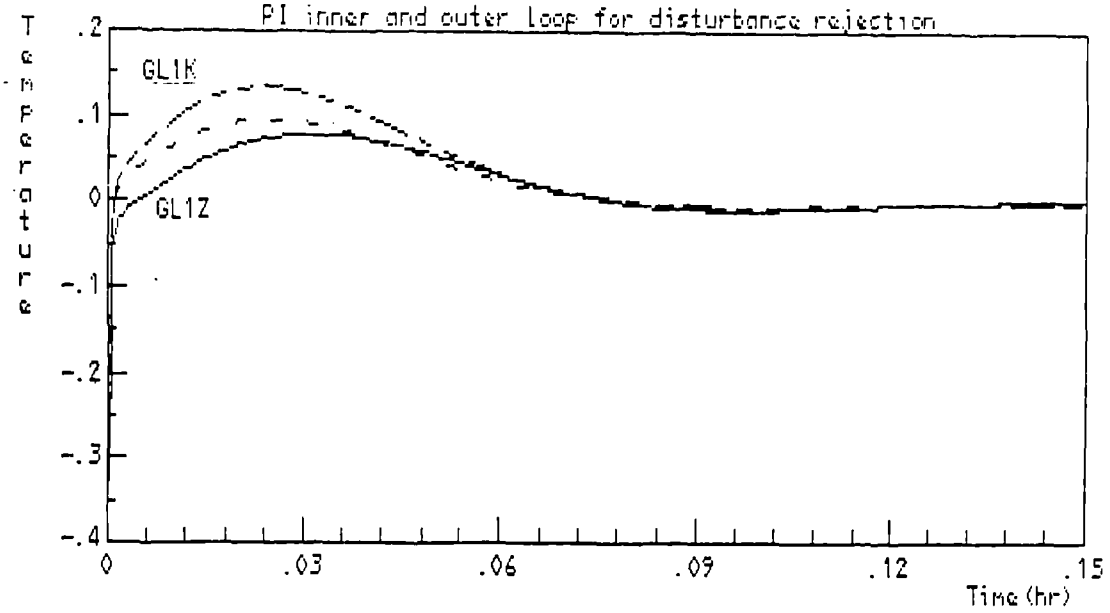

(c) outlet temperature response for step disturbance input

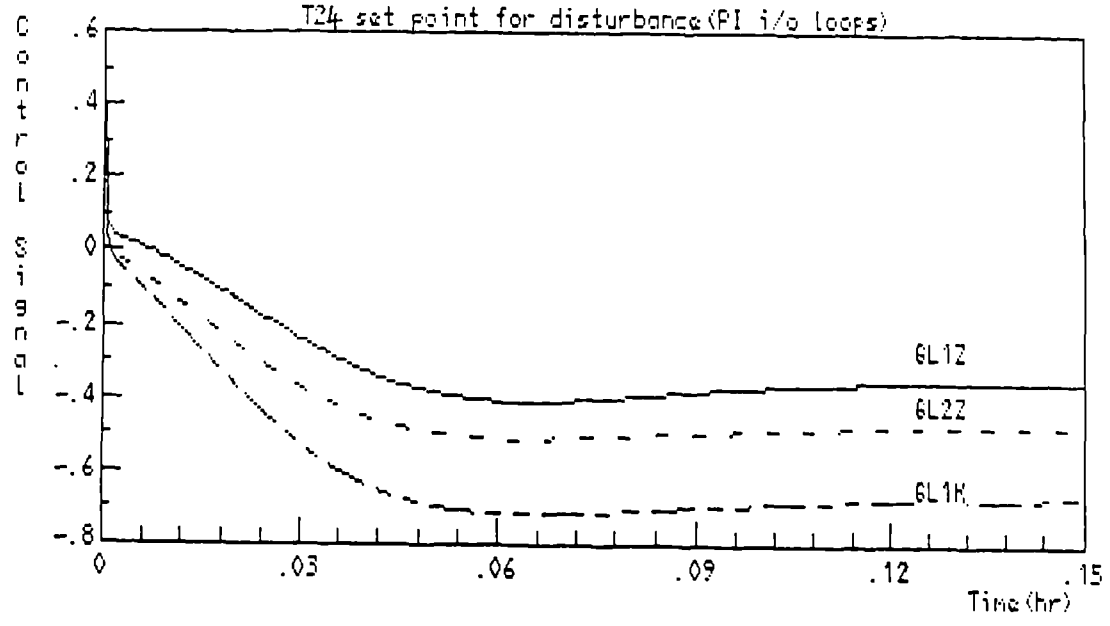

(d) inner set point response for step disturbance input

Figure 6.26 Step responses for PI inner/PI outer loop control (contd.)

The steady state actuating errors defined in Table 6.9 were calculated for the outer loop of each control loop arrangement. The recommended controller parameters are listed in Table 6.12. The results for a ramp change in set point indicated that the error associated with the P/PI arrangement was 75% of the corresponding error for the PI/PI arrangement. This suggests that the former control loop arrangement would be better at handling ramped set point changes for the linear model. However, as disturbances would also affect this process, the controllers should be assessed using the original non-linear model, with a typical operating scenario.

Controller Settings	P inner/PI outer	PI inner/PI outer
Inner loop	$K_{C2} = 0.1$	$K_{C2} = 0.005$ $\tau_{I2} = 0.005$
Outer loop	$K_{C1} = 0.54$ $\tau_{I1} = 0.003$	$K_{C1} = 1.25$ $\tau_{I1} = 0.01$

Table 6.12 Recommended cascade controller settings

6.4.6 Cascade Controller Performance for Non-linear Simulation

Linearised models of the heavies processing section were used to derive linear controller settings. Both types of fixed linear controllers showed good performance for both set point change and disturbance rejection. However, the final selection of a suitable cascade control arrangement must be validated with the original non-linear models. Hence, trials were conducted with ACSL, using the recommended controller settings in Table 6.12.

The trials were based on a combination of step responses for anticipated set point change and disturbance rejection. Intermediate points between the feedstock conditions were identified as the maximum anticipated disturbances. Selected ACSL simulation results for P inner/PI outer and PI inner/PI outer loop control are presented.

A step disturbance representing intermediate conditions between the initial GL2Z and GL1K conditions was introduced in Figure 6.27, and

included the methane molar flow rate response. (It should be noted that disturbance changes to the GL1K feedstock were selected as this presented the largest control signal variations in Figures 6.25 and 6.26). The responses indicated that P inner loop control performed better for disturbance rejection, as it limited the drop in CRG reformer product temperature, T27, to 6 K. The process also returned to a steady condition within 0.2 hr, whereas with PI inner loop control the settle time was above 0.3 hr. However, the fast controller action of the P inner loop resulted in an initial valve closure to 3%, which was well below the recommended 10% level (Luyben, 1990). This severe control action was further exhibited in the set point tracking and disturbance rejection responses in Figure 6.28, as the feedstock changed from GL2Z to GL1K. The P controller immediately closed the control valve while product temperature undershot towards its new set point value. Hence, the fired heater was allowed to change according to its own dynamics, with effectively no control active at the start of the simulation. The corresponding PI inner loop responses showed the temperature gradually moving to its new condition, and in a faster time.

Root-locus plots for the GL2Z feedstock condition indicated that both control arrangements were only conditionally stable. Increasing the outer loop K_c by a factor of three, for the PI/PI arrangement, would cause system instability. The P/PI arrangement exhibited a greater stability margin, indicating that its gain could be increased to a greater extent. These results were reflected in Table 6.11.

The above results identified advantages in both cascade controller arrangements, by taking control action before disturbances fully affected the reformer. However, the control system for the heavies processing section had to deal with large disturbances and changes in the operating conditions. Thus, a robust control system would be required to handle major upsets. The PI inner loop arrangement was preferred as it exhibited more stable performance for anticipated changes in operating conditions. This was validated when the PI/PI controllers were incorporated into the flowsheet model.

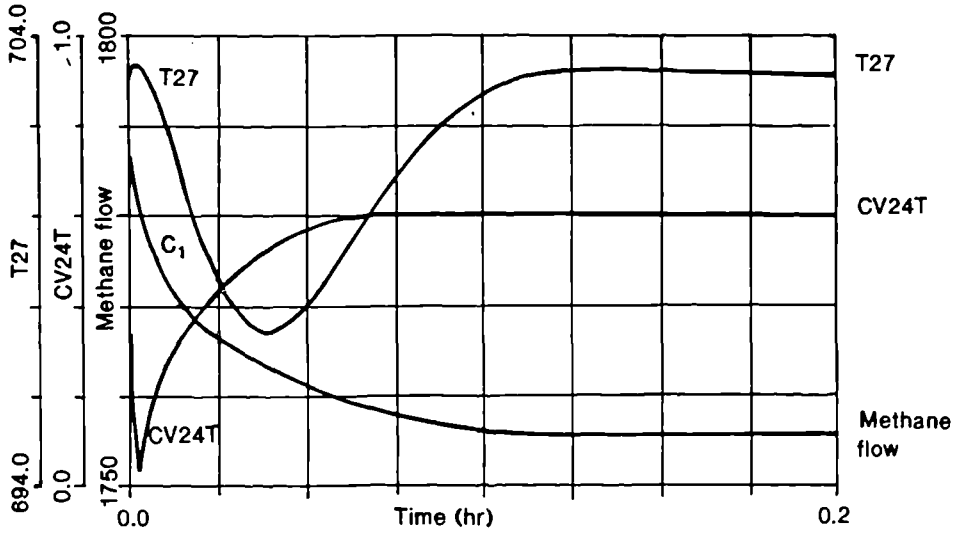

(a) P inner/PI outer loop controller

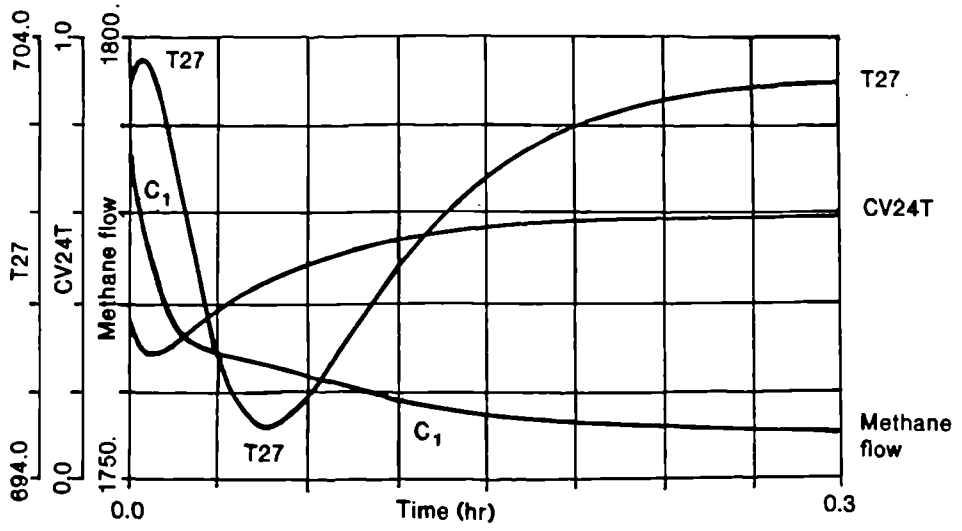

(b) PI inner/PI outer loop controller

Figure 6.27 Cascade control loop results for disturbance rejection

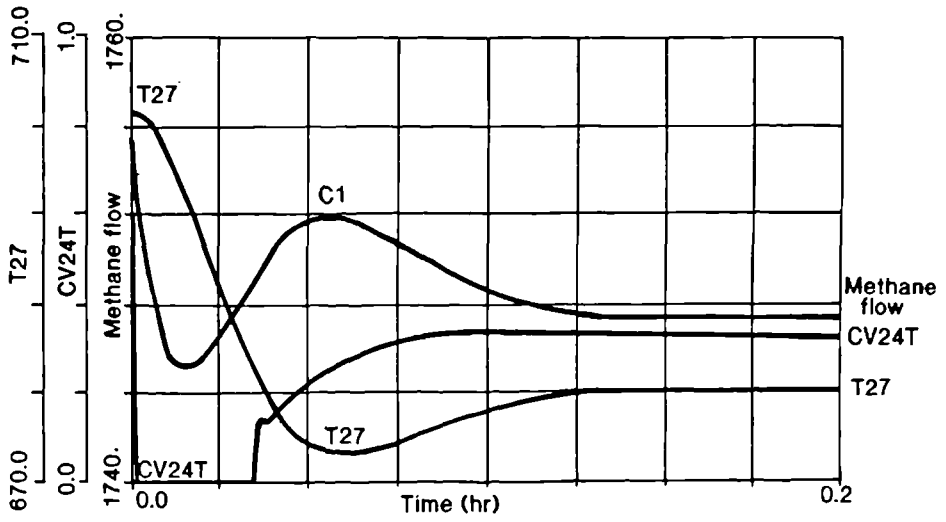

(a) P inner/PI outer loop controller

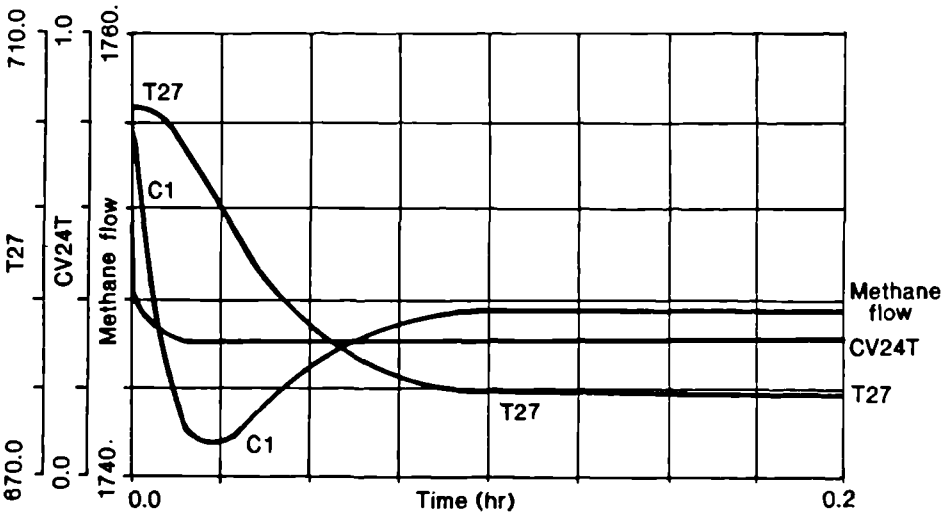

(b) PI inner/PI outer loop controller

Figure 6.28 Cascade control loop results for set point tracking and disturbance rejection

6.4.7 Modern Control Theory Implications

The ACSL model results for the heavies processing section differed from those defined in the performance criteria for a unit-step set point change. This was because a linear model approximation was used to design the linear controllers. Hence, a model mis-match arose as the model moved from its operating condition. In modern parlance, the extent of mis-match is termed *model uncertainty.* This is a fundamental problem in controller design as model identification is essentially of low order, often about a single operating condition, and inherently produces an uncertain description of the real process.

The model uncertainty, $\Delta G(s)$, can be defined as an additive perturbation, illustrated in Figure 6.29, and the model representation is defined as:

$$y(s) = [G(s)]\, u(s) = [G_o(s) + \Delta G(s)]\, u(s)$$

where $G_o(s)$ is the nominal process transfer function. Hence, in this control design study, $G_o(s)$ was the transfer function approximation obtained for a particular operating condition. The closed-loop transfer function is given by:

$$y(s) = \left[\frac{G(s)G_c(s)}{1 + G(s)G_c(s)}\right] r(s) + \left[\frac{1}{1 + G(s)G_c(s)}\right] d(s) \qquad (6.14)$$

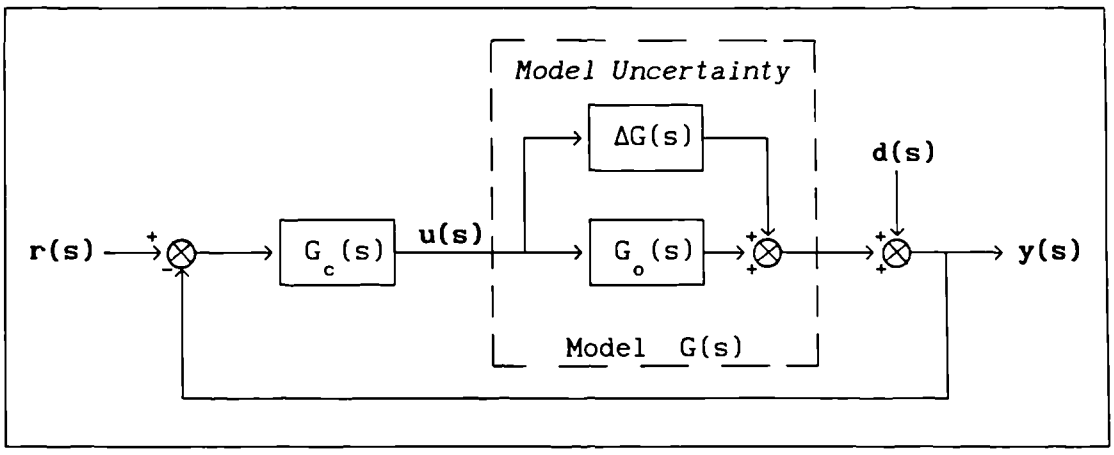

Figure 6.29 Control system configuration

The transfer function relationship in (6.14) can be used to quantify the performance and robustness qualities of a closed-loop system configuration. Hence, the *sensitivity function* and *complementary sensitivity function* are given by:

$$\left.\begin{aligned} \varepsilon(s) &= \frac{1}{1 + G(s)G_c(s)} \\ \text{and} \qquad \eta(s) &= \frac{G(s)G_c(s)}{1 + G(s)G_c(s)} \end{aligned}\right\} \quad (6.15)$$

respectively. There are two constraints which apply for the design of $G_c(s)$; the closed-loop system must be stable, and:

$$\eta(s) + \varepsilon(s) = 1 \quad (6.16)$$

where $\eta(s)$ and $\varepsilon(s)$ are shaped in the frequency domain by defining $G_c(s)$. The stability robustness of the closed-loop system is its ability to remain stable in the presence of model uncertainty. Performance robustness is the system's ability to provide good disturbance rejection and set point tracking. These properties are desirable and related through (6.15) and (6.16). Hence, good $\varepsilon(s)$ characteristics in a particular frequency range may lead to unsatisfactory characteristics in its complement, $\eta(s)$. Therefore, control design involves a compromise between performance robustness and stability robustness (Grimble and Johnson, 1991). These conditions exist for both single and multivariable design problems, and the need to accomplish this trade-off has formed the basis for many modern control design methods.

These phenomenon have been illustrated in the cascade control loop design in this section. Model uncertainty has been indicated by two factors; the approximation of a non-linear system by a transfer function model and the effect of changing operating conditions, as compared in Table 6.6. Fast controller action was attainable, but at the expense of model stability.

6.4.8 Conclusions for Cascade Control of the Heavies Processing Section

State space models were obtained from non-linear models representing the heavies processing section. These linear approximations were converted to transfer function form and compared for different feedstock conditions. Performance criteria were derived for the cascade controllers from a sensitivity analysis of the process.

Two combinations of proportional and proportional-integral controllers were investigated for the cascade control arrangement. Then, linear control design techniques were successfully applied to tune the classical controllers according to the performance criteria.

Controller performance was assessed using the original non-linear ACSL models and subjecting the process to severe set point and disturbance inputs. The simulation results indicated that proportional control on the inner loop generally gave a faster response. However, the PI inner/PI outer control loop arrangement was selected due to its robust qualities.

6.5 ACHIEVEMENTS AND CONCLUSIONS

Satisfactory control loop structures were developed for the preliminary LNG reception terminal flowsheet. A degrees-of-freedom analysis was conducted on blocks of the flowsheet, and the control loop configurations were derived from qualitative arguments. Control loops for SISO and multiloop systems were then successfully tuned.

A fixed proportional-integral controller was identified for the ORV system. However, to ensure that all the performance criteria were satisfied, a detailed time-domain analysis was conducted on this SISO system. This analysis graphically related percentage overshoot and rise time to the controller settings. Suitable settings were then identified and validated by assessing the system response to a series of set point changes and disturbance rejections. To ensure that realistic controller settings were chosen, the conventional time-domain criteria were extended to consider control valve action and disturbance rejection. This approach represented an unusually rigorous analysis for a SISO system.

A cascade control loop configuration was adopted for the heavies processing section. Linear approximations were obtained for each unit in the process, at each operating condition. Then, linear control design methods were successfully applied to the linearised models. Similar time-domain criteria to those considered in the SISO system were applied to this section. This was necessary to assess the impact of multiple feedstock conditions on controller settings. Of the two fixed controller arrangements considered for non-linear model validation, the PI inner/PI outer control loop arrangement was selected.

The remaining control loops for the multivariable systems will be discussed in Chapter 7.

CHAPTER 7

ADVANCED AND SUPERVISORY CONTROL

7.1 INTRODUCTION

The final stages in developing regulatory control loops and assessing plantwide control issues for a flexible LNG reception terminal are addressed in this penultimate chapter. This work will also enable the requirements for a supervisory control system for the plant to be identified.

An advanced control technique will be applied to the heavies processing section, whose initial control system was defined in Section 6.4. The outer PI controller will be replaced by a form of long-range predictive controller, using the Weighted Predictive Control (WPC) law. A detailed review of WPC and its application is discussed in Section 7.2.

The control of multivariable systems is addressed in relation to the flash unit and distillation column in Sections 7.3 to 7.5. Linear control design requires an open-loop linearised model approximation, relating each manipulated to controlled variable. This is discussed in Section 7.3. An interaction analysis on the open-loop systems will be described in Section 7.4. This will identify stable control loop pairings, with reduced interaction effects. Controller settings will then be derived for the multivariable systems in Section 7.5.

A series of changeover mechanisms will be derived for the complete flowsheet to give a gradual change from one to another LNG feedstock, using the revised and tuned control loop structures. This is presented in Section 7.6. Finally, the implications of adding a supervisory control system are discussed in this concluding section.

7.2 ADVANCED CONTROL DESIGN FOR THE HEAVIES PROCESSING SECTION

The cascade control loop arrangement selected for the heavies processing section employed classical controller designs, and was reported in Section 6.4. The outer loop of the cascade controller has been considered for further development to investigate an advanced control technique, without changing the controller structure. Hence, the original PI inner loop control settings were retained, and the outer loop was replaced by a digital controller.

The theoretical development of the Weighted Predictive Control (WPC) law is discussed in the following section. The WPC algorithm has been applied to linear model approximations, with careful selection of design parameters. The final non-adaptive WPC controller settings have been validated for set-point change and disturbance rejection, using the original non-linear ACSL simulation.

7.2.1 Introduction to Long-range Predictive Controllers

A move towards more complex controller tuning than PID, was initiated by Åström and Wittenmark (1973), who proposed the Minimum Variance control algorithm. Since then, several variations on this algorithm have been developed, notably the Generalized Minimum Variance controller (Clarke and Gawthrop, 1975). These control laws were based on single-step minimisation of a fixed step ahead prediction error of the process outputs. By a general selection of the prediction horizon, De Keyser et al. (1988) derived the long-range predictive control (LRPC) law. Essentially, LRPC projects the future outputs from the currently available data up to a prediction horizon, and is based on assumptions about present and future control action. Generalized Predictive Control (GPC) is a recent extension of the Generalized Minimum Variance algorithm, encompassing LRPC (Clarke et al., 1987) that involves the multi-step minimisation of output prediction errors. The GPC controller has demonstrated robust performance even for variations in the dead-time and model order of a process (Clarke, 1988). However, for non-minimum phase processes, GPC does not guarantee stabilizing control laws.

A new version of GPC called Weighted Predictive Control (WPC) has

been proposed by Grimble (1990). This control algorithm retains many features of GPC, and is also successful in controlling non-minimum phase processes. The WPC algorithm was considered appropriate in the heavies processing section as the family of long-range predictive controllers has been successfully applied to industrial processes with model variations (Clarke, 1988; Fujiwara and Miyakawa, 1990).

7.2.2 **Weighted Predictive Control Law**

Process Model

For regulation about a particular operating point, it is first necessary to approximate the non-linear process by a locally-linearised model. GPC adopts a controlled auto-regressive and integrated moving average (CARIMA) model (Clarke, 1988):

$$A(q^{-1})y(t) = B(q^{-1})\,u(t-1) + \frac{C(q^{-1})}{\Delta}\,\zeta(t) \qquad (7.1)$$

where q^{-1} is the backward-shift operator and Δ is the differencing operator $(1 - q^{-1})$. In (7.1), u(t) is the control output, y(t) is the process output, and $\zeta(t)$ is an uncorrelated random sequence describing the disturbance. A, B and C are polynomials of the form:

$$\begin{aligned} A(q^{-1}) &= 1 + a_1 q^{-1} + \ldots + a_{na} q^{-na} \\ B(q^{-1}) &= b_0 + b_1 q^{-1} + \ldots + b_{nb} q^{-nb} \\ C(q^{-1}) &= 1^{o} + c_1 q^{-1} + \ldots + c_{nc} q^{-nc} \end{aligned}$$

The time-varying nature of the parameters of $C(q^{-1})$ often makes identification difficult. Hence, as a further extension to GPC, Duan and Grimble (1990) introduced a well-posed polynomial $T(q^{-1})$ as a design parameter in (7.1) to give:

$$A(q^{-1})y(t) = B(q^{-1})\,u(t-1) + \frac{T(q^{-1})}{\Delta}\,\xi(t) \qquad (7.2)$$

where $\xi(t) = [C(q^{-1})/T(q^{-1})]\zeta(t)$. The inclusion of $T(q^{-1})$ is claimed to improve system robustness to unmodelled dynamics. The corresponding block diagram is illustrated in Figure 7.1.

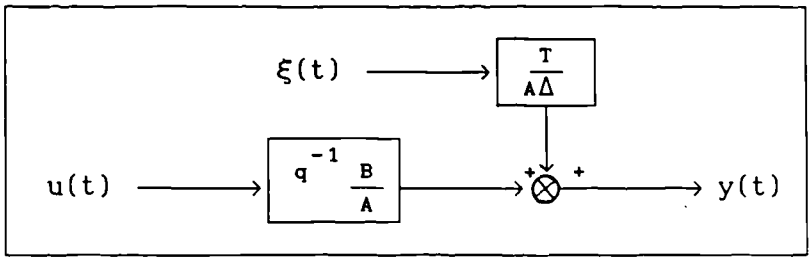

Figure 7.1 Block diagram of CARIMA model

WPC Cost Function

The optimal controller settings for a process are obtained by minimising a performance criterion representing the cost of the system error signal. The performance criterion for WPC is a multi-step cost function, which includes pseudo-tracking error and control weighting, given by:

$$J_{WPC} = E\left\{ \sum_{j=N_o}^{N_1} [\phi(t+j+1|_t) - w(t+j+1|_t)]^2 + \sum_{j=0}^{N_2} \lambda(j)[\Delta u(t+j)]^2 \right\} \qquad (7.3)$$

where

E(.) denotes the conditional expectation on all observations up to and including time t,
N_o and N_1 define the prediction horizon
N_2 defines the control horizon
$\phi(t)$ is an auxiliary output
w(t) is the set point
$\lambda(j)$ is the control weighting function.

By factoring the $B(q^{-1})$ polynomial in (7.2) into stable and unstable parts, the auxiliary output, $\phi(t)$, may be expressed in terms of an auxiliary output filter:

$$\phi(t) = M(q^{-1})y(t)$$

where $M(q^{-1})$ is defined in terms of the stable part of $B(q^{-1})$ and design weighting functions $M_n(q^{-1})$ and $M_d(q^{-1})$. These functions are used to shape the system response, providing M_n/M_d is stable and its norms are scaled to unity. One difference between WPC and GPC is in factoring the $B(q^{-1})$ polynomial.

Prediction Equations

WPC is based on a prediction algorithm over the auxiliary output observations $\{\phi(t + N_o), \ldots, \phi(t + N_1)\}$ in LRPC. The predicted output $\phi(t+j)$ is decomposed by LPRC into *free* and controlled plant responses, consisting of past and present outputs and past, present and future control signals. As the future control signals are unknown at the current time t, they are decomposed by a series of Diophantine equations and a prediction equation is formed:

$$\hat{\Phi} = \mathbf{G}\,\tilde{\mathbf{U}} + \mathbf{P} \qquad (7.4)$$

where the elements of **G** represent points on the plant step response, and **P** is a vector of intermediate prediction signals, in terms of past outputs and controls. Hence, recalling (7.3) and (7.4), the

prediction and control horizons require vectors of the form:

$$\hat{\Phi} = [\, \hat{\phi}\,(t+N_o+1|_t),\ \hat{\phi}\,(t+N_o+2|_t),\ldots,\ \hat{\phi}\,(t+N_1+1|_t)\,]^T \qquad (7.5)$$

$$\tilde{U} = [\, \Delta u(t),\ \Delta u(t+1),\ldots,\ \Delta u(t+N_2)\,]^T \qquad (7.6)$$

$$P = [\, P_{N_o}(t),\ P_{N_o+1}(t),\ldots,\ P_{N_1}(t)\,]^T \qquad (7.7)$$

$$w = [\, w(t+N_o+1),\ w(t+N_o+2),\ldots,\ w(t+N_1+1)\,]^T \qquad (7.8)$$

G is of dimension $(N_1 - N_0 + 1) \times (N_2 + 1)$. Hence, for $N_o = 0$ and $N_1 = N_2$, a lower triangular matrix of dimension $(N_1 + 1) \times (N_1 + 1)$ is formed for G:

$$G = \begin{bmatrix} g_0 & 0 & \ldots & 0 \\ g_1 & g_0 & \ldots & 0 \\ . & & & \\ . & & & \\ g_{N_1} & g_{N_1-1} & \ldots & g_0 \end{bmatrix} \qquad (7.9)$$

The prediction equation is fundamental to the WPC control law. An important feature of Dynamic Matrix Control that has been retained in WPC (Duan and Grimble, 1990) is the assumption concerning future control actions. This states that beyond the control horizon, N_2, the control increments, $\Delta u(t)$, are set to zero. Therefore, this limits $\tilde{U}$, and the dimensions of the prediction equation (7.4).

WPC Control Law

The cost function (7.3) can be rewritten in vector form as:

$$J_{WPC} = E\{\, (\hat{\Phi} - W)^T(\hat{\Phi} - W) + \tilde{U}^T \Lambda\, \tilde{U}|_t \,\} \qquad (7.10)$$

where $\Lambda = \text{Diag}\,\{\lambda_0,\ \lambda_1,\ldots,\ \lambda_{N_2}\}$. Assuming no constraints on future controls, the minimisation of J_{WPC} gives:

$$\tilde{U} = (\, G^TG + \Lambda\,)^{-1}\, G^T(\, W - P\,) \qquad (7.11)$$

As the first element of $\tilde{U}$ is $\Delta u(t)$ in (7.6), the current control is:

$$u(t) = u(t-1) + \Delta u(t) = u(t-1) + \bar{g}^T(W - P) \qquad (7.12)$$

where $\bar{g}^T$ is the first row of $(G^TG + \Lambda)^{-1}G^T$.

WPC Model

An important assumption in WPC is that the future set-point is equal to the current set-point w(t), thus:

$$\mathbf{W} = [1 \quad 1 \quad \ldots \quad 1]^T w(t) \tag{7.13}$$

The closed-loop transfer function for a set-point input has been derived as (Duan and Grimble, 1990):

$$y(t) = \frac{k\, q^{-1} \frac{B}{A\Delta}}{\left\{ 1 + q^{-1} \frac{H^o}{T} + q^{-1} \frac{BF^o}{AM_d T} + k\, q^{-1} \frac{B}{A\Delta} \right\}} w(t)$$

$$= \frac{k\, q^{-1} B M_d}{A\Delta M_d + q^{-1} L^o} \; w(t) \tag{7.14}$$

where

$$k = \sum_{i=N_0}^{N} \bar{g}(i) \qquad F^o = \sum_{i=N_0}^{N} \bar{g}(i) F_i \qquad H^o = \sum_{i=N_0}^{N} \bar{g}(i) H_i$$

$$L^o = \sum_{i=N_0}^{N} \bar{g}(i) [(A\Delta M_d H_i + BF_i)/T]$$

k is the open-loop gain and F and H are polynomial expressions introduced by diophantine equations. It should be noted that the numerator polynomial $B(q^{-1})$ is unchanged by the closed-loop, and hence the open-loop zeros are unaffected. Also, the disturbance filter $T(q^{-1})$ is absent in (7.14) and thus has no effect on the set-point response of the process. The corresponding block diagram for a set-point input is illustrated in Figure 7.2.

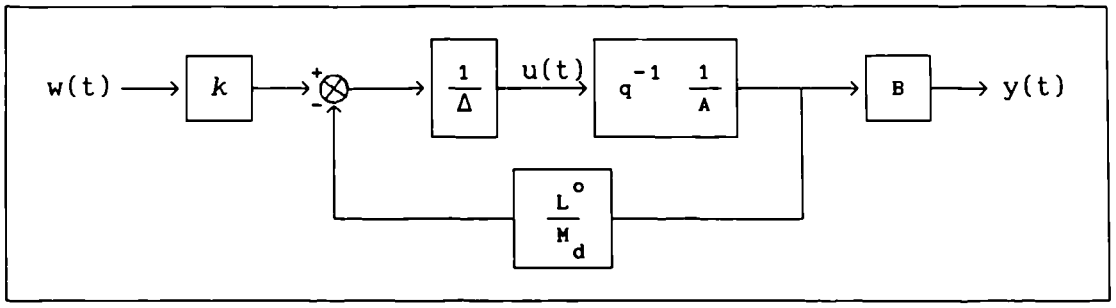

Figure 7.2 WPC controller block diagram for set point input

The process model in (7.2) has a disturbance signal given by:

$$v(t) = \frac{T}{A\Delta} \xi(t)$$

Therefore, the corresponding closed-loop transfer function for a

disturbance input is:

$$y(t) = \frac{A\Delta M_d}{A\Delta M_d + q^{-1}L^o}\, v(t) + \frac{q^{-1}A\Delta M_d H^o}{(A\Delta M_d + q^{-1}L^o)T}\, v(t) \qquad (7.15)$$

As the disturbance filter $T(q^{-1})$ is only present in the second term of (7.15), this imposes a limitation on the possible improvement in disturbance rejection performance. Comparing (7.14) and (7.15) shows that every design parameter except $T(q^{-1})$ contributes to both set point and disturbance responses. The complete block diagram for set point and disturbance inputs is illustrated in Figure 7.3.

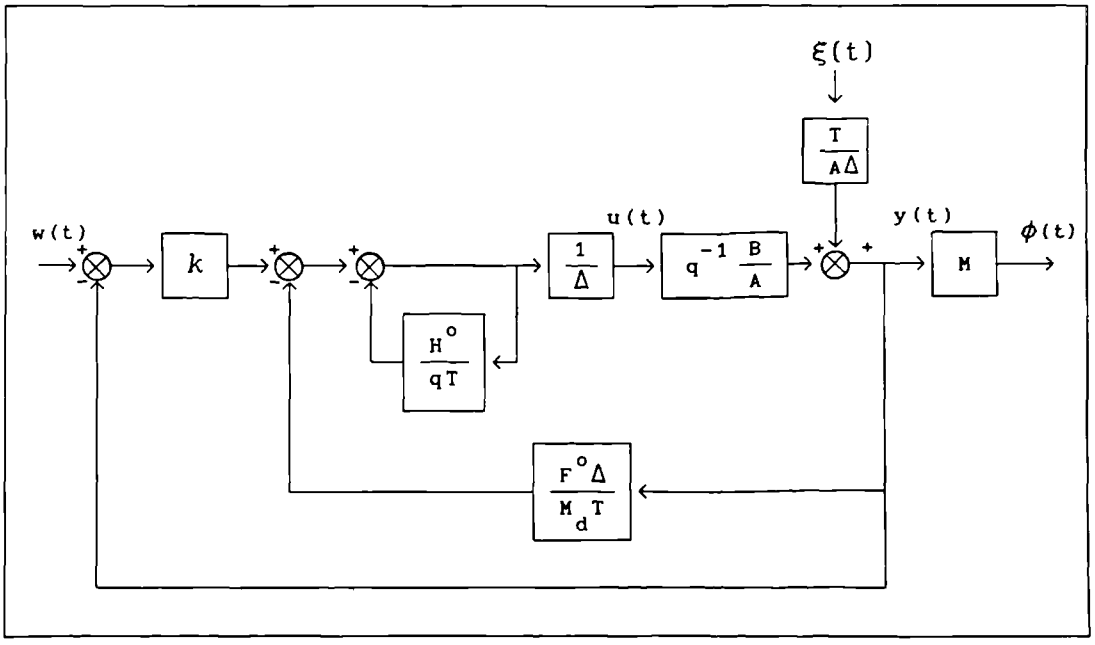

Figure 7.3 Closed-loop block diagram of WPC controller

WPC Design Parameters

Many control objectives can be satisfied with WPC, based on the control and predictive horizons (in (7.3)), design parameters and weighting functions. To examine the effect of these parameters on the system response, the closed-loop transfer functions (7.14) and (7.15) can be expressed as a function of the design parameters where:

$$y(t) = f_s(M_n, M_d, T_s, n_A, n_B)\, w(t) + f_d(M_n, M_d, T_s, n_A, n_B, T)\, v(t) \qquad (7.16)$$

The form of the cost function (7.3) also affects the optimal controller settings, where:

$$J_{WPC} = f\{ N_o, N_1, N_2, \lambda \} \qquad (7.17)$$

Thus the following parameters may be used to alter the system response in WPC:

(i) M_n *and* M_d - If the numerator and denominator of the auxiliary output filter, $M_n(1)/M_d(1)$, is not scaled to unity, a steady state offset results.

(ii) T_s - The sampling period of the system is critical to digital controller performance. A T_s of 1/4 to 1/10 of the settling time of the process is generally selected.

(iii) n_A *and* n_B - The degree of polynomials A and B have a direct impact on the degrees of the WPC control element.

(iv) $T(q^{-1})$ - The observer polynomial has all its roots outside the unit circle in the q^{-1} plane, and only affects disturbance rejection.

(v) N_o *and* N_1 - These parameters define the prediction horizon of WPC. N_o is generally set to zero. In GPC, N_o is equivalent to the number of sampling intervals in the process dead time. However, with $B(q^{-1})$ factored in WPC, the dead time is included in the stable polynomial. N_1 is usually a small value similar to process rise time. Increasing the prediction horizon slows system response.

(vi) N_2 - The control horizon is always less than or equal to the maximum prediction horizon (Clarke, 1988). For an open-loop stable process, with $N_o = 0$ and $N_2 \leq N_1$, N_2 has little effect on system response.

(vii) λ - The control weighting sequence is generally set at a constant value, where $0 < \lambda < 1$.

WPC Algorithm

Having derived a linearised model of the process, the following steps can be applied to design a WPC non-adaptive controller:

1. Choose suitable values for each design parameter:
   M_n, M_d, T_s, N_o, N_1, N_2, λ.
2. Obtain a deterministic CARIMA model of the process (7.2).
3. Factorise $B(q^{-1})$ into stable and unstable parts.
4. Evaluate the elements of matrix **G** in (7.4), from the polynomials of the process, and the auxiliary filter.
5. Compute the polynomial matrices, F_j and H_j, from the diophantine equations.

6. Compute the auxiliary signals, $P_j(t)$, in (7.4).
7. Compute $(G^TG + \Lambda)^{-1}$ in (7.11) for the design weighting function.
8. Evaluate k, F^o and H^o in (7.14).
9. Evaluate non-adaptive WPC controller settings.

7.2.3 WPC Implementation

The WPC law was applied to the cascade control outer loop in the heavies processing section. The transfer function model of the process, with PI inner loop control, in Section 6.4, was adopted. Only the GL2Z feedstock condition was considered in the subsequent WPC design. For the GL2Z feedstock condition, the combined 6^{th}-order plant model was given by:

$$G_p(s) = \frac{2.81\times10^9\ (s+2575)\ (s+200)}{(s+45.4)\ (s^2+5190s+6.74\times10^6)\ (s^3+1222s^2+1.37\times10^5s+1.35\times10^7)} \quad (7.18)$$

The WPC algorithm produces a 6^{th}-order controller for the original model (7.18). Hence, to design a more flexible controller, a reduced 3^{rd}-order model was obtained. From the recommended sampling period, T_s, of between 0.01 and 0.025 hr (Duan and Grimble, 1990) a lower T_s of 0.01 hr was chosen. The remaining WPC design parameters were based on the plant characteristics for an open-loop stable system. The initial design values are listed in Table 7.1.

Parameter	Value
M_n	1.
M_d	1.
T	1.
N_0	0
N_1	2
N_2	0
λ	0.1

Table 7.1 Initial design parameter settings

Steps 4 to 9 of the WPC algorithm were automated as a design package using PROGRAM CC (Duan and Grimble, 1990). The design program evaluated fixed controller settings and a corresponding set point response for the plant. As disturbance rejection was important, a linearised ACSL model of the plant was set up to simulate both set point change and load disturbances. The simulation was run in

continuous (plant model) and discrete (digital controller) time, using a continuous block time step of 0.0001 hr, and discrete block sampling period of 0.01 hr. The general ACSL model structure is illustrated in Figure 7.4. The original 6^{th}-order model was adopted for these ACSL simulations. Load disturbance was represented by a single disturbance from the ethane flow rate as this was considered the most likely and severe disturbance input.

With set point and disturbance responses available for a linear plant using WPC, the final validation involved setting up the digital controller on the non-linear ACSL model.

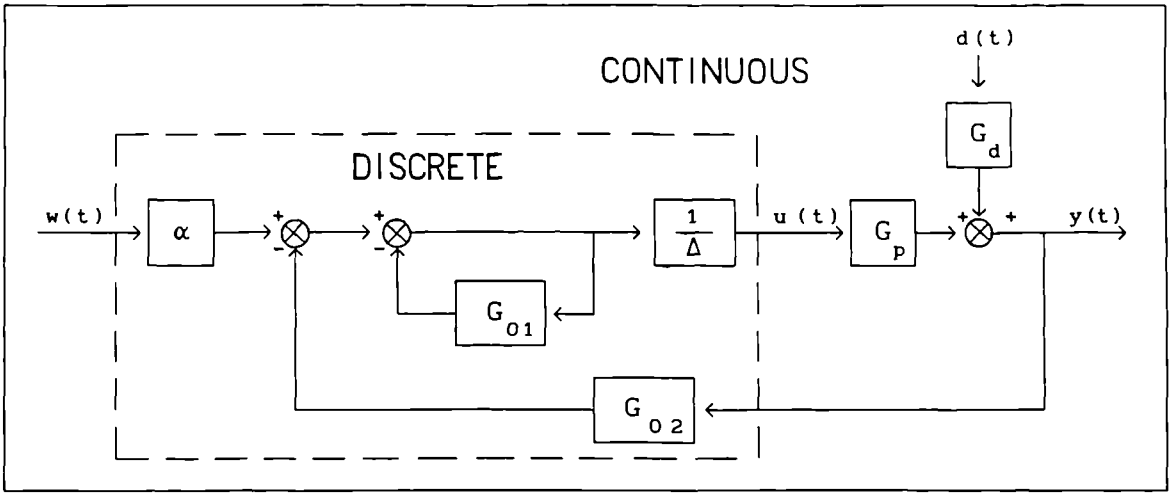

Figure 7.4 ACSL interpretation of WPC controller structure

7.2.3.1 *WPC Design Parameters*

The choice of suitable design parameters for WPC was based on an iterative procedure, whereby set point and disturbance responses were compared using the linear ACSL simulation.

The original prediction and control horizons in Table 7.1 were retained, and the effect of varying three parameter settings was investigated; λ, $M(q^{-1})$ and $T(q^{-1})$. The results in Table 7.2 show that both increasing λ and incorporating $M(q^{-1})$ gave a slower system response with reduced overshoot, and reduced set point deviation. Hence, their original settings in Table 7.1 were retained.

Design Parameter		Set Point Input		Disturbance Input	
		Overshoot (%)	Rise Time (hr)	Peak (K)	Settling Time (hr) (to within 0.05 K)
λ	0.05	3.8	0.041	0.28	0.032
	0.10†	1.6	0.050	0.25	0.037
	0.30	1.9	0.089	0.24	0.059
$\frac{M_n}{M_d}$	1†	1.6	0.050	0.25	0.037
	$\frac{1-0.5q^{-1}}{0.5}$	0.0	0.083	0.25	0.039

† - base condition

Table 7.2 Linear ACSL mode step response results for selected parameter variations

The disturbance model $T(q^{-1})$ was varied to assess its impact on the disturbance rejection response. As expected, the WPC step responses in Figure 7.5 show that $T(q^{-1})$ did not influence set point change (7.14). The results for the linear 6^{th}-order ACSL model, in Table 7.3, indicate that as the zeros of $T(q^{-1})$ approach the unit circle, the peak output reduces at the expense of settling time. The corresponding open-loop frequency results show that the gain and phase margins increase, providing greater relative stability and thus more sluggish closed-loop performance. Recommended gain and phase margins depend on the application, although they generally exceed 2.0 and 30°, respectively. Hence, this indicated that the original $T(q^{-1})$ of $1 - 0.2q^{-1}$ should be retained as a design parameter.

Disturbance Model $T(q^{-1})$	**Peak Output** y_p (K)	**Settling Time** (hr) (to within 0.05 K)	**Gain Margin**	**Phase Margin** (°)
$1 - 0.2q^{-1}$	0.250	0.037	2.86	55.6
$1 - 0.4q^{-1}$	0.225	0.047	3.70	58.2
$1 - 0.6q^{-1}$	0.195	0.053	4.35	66.2
$1 - 0.8q^{-1}$	0.169	0.077	7.14	79.4

Table 7.3 Disturbance model effects on linear ACSL model

The corresponding closed-loop frequency response results for the $T(q^{-1})$ parameter are presented in Figure 7.6. The complementary sensitivity function, $\eta(s)$, relating the set point to the output, is identical for each $T(q^{-1})$ condition. The sensitivity function, $\varepsilon(s)$,

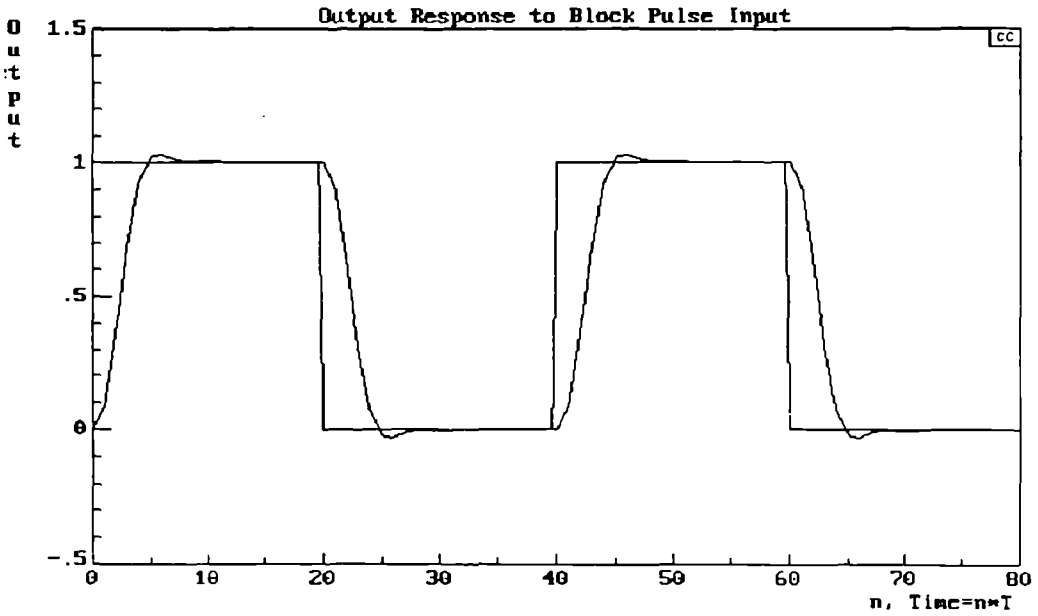

(a) reformer outlet stream temperature

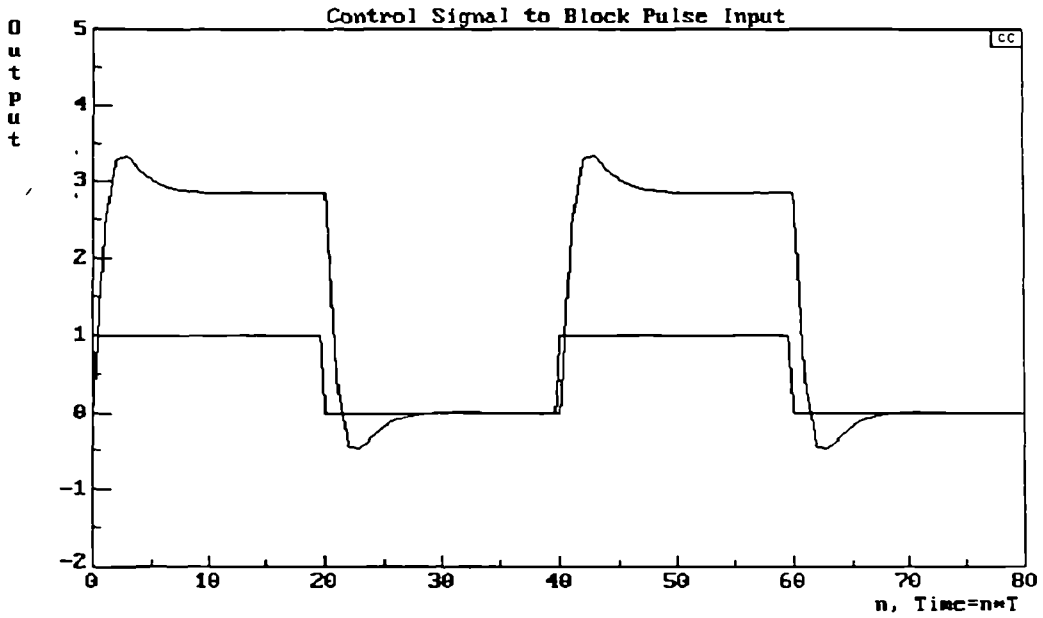

(b) stream 24 set point temperature

Figure 7.5 Unit-step set point response for base WPC settings with linear plant model

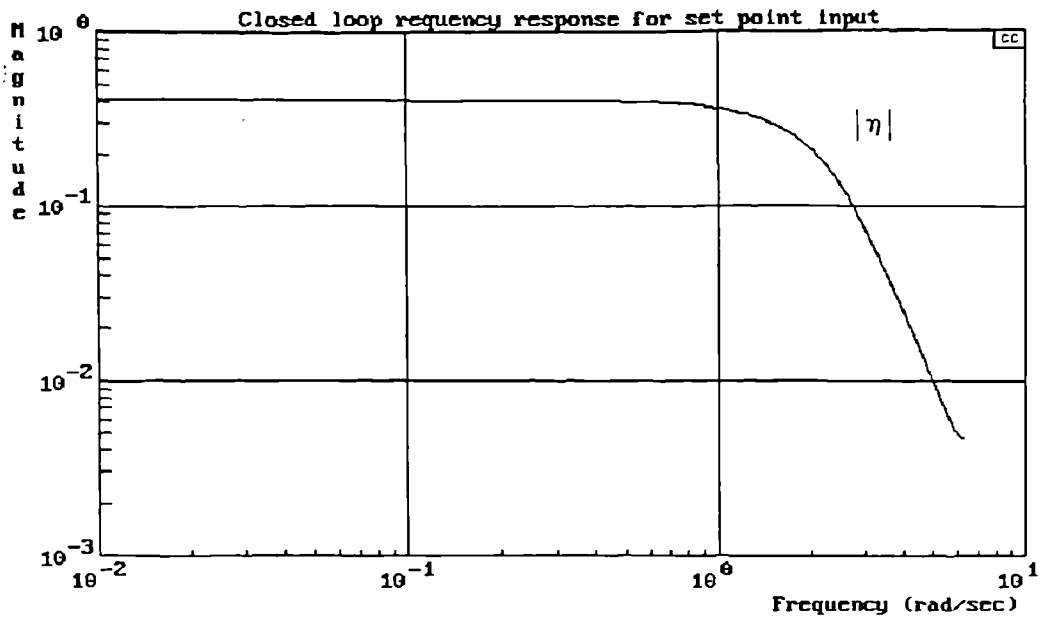

(a) complementary sensitivity plot

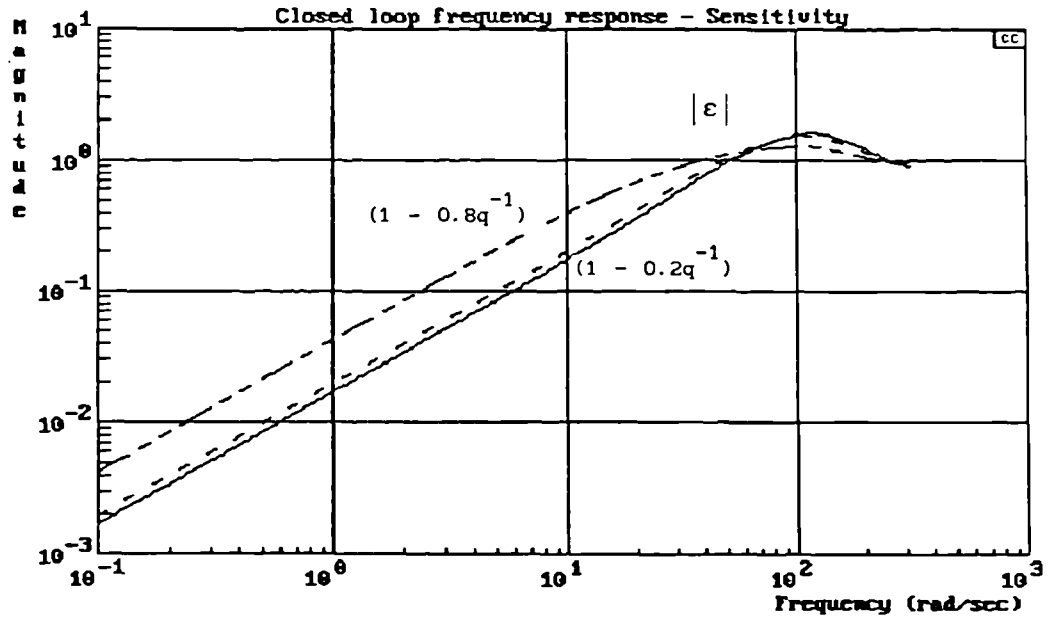

(b) sensitivity plot

Figure 7.6 Closed-loop frequency response results for WPC

$$\text{for } T(q^{-1}) = \begin{cases} (1 - 0.2q^{-1}) \\ (1 - 0.4q^{-1}) \\ (1 - 0.8q^{-1}) \end{cases}$$

shows the effect of the disturbance on the output.

Controller performance has been measured in terms of $|\varepsilon|$, system bandwidth, ω_B, and resonant frequency, ω_R. A small $|\varepsilon|$ value at low frequencies indicates that the feedback controller has good low frequency disturbance rejection qualities (Williams, 1991). ω_B represents a break point (when $|\varepsilon|$ equals $1/\sqrt{2}$) beyond which control action becomes ineffective, although the process is still responsive. The $|\varepsilon|$ peak occurs at ω_R, which is a measure of the speed of response, where a higher ω_R represents a faster system. Also, the peak $|\varepsilon|$ value is a relative stability criterion, where an increased peak height indicates poorer relative stability. These measures were used to assess the results in Figure 7.6 and suggested that the original controller settings gave the fastest system responses, at the expense of relative stability. Conversely, the $T(q^{-1}) = 1 - 0.8q^{-1}$ condition was slower with better relative stability.

As a final validation, the non-adaptive WPC controller settings were incorporated in the original non-linear ACSL model. The disturbance rejection exercise in Section 6.4 was repeated for each controller. Results for a step change in the GL2Z initial conditions towards the GL1K feedstock condition are compared in Table 7.4.

Disturbance Model $T(q^{-1})$	**Peak Output** y_p(K)	**Settling Time** (hr) (to within 0.05 K)
$1 - 0.2q^{-1}$	6.875	0.201
$1 - 0.4q^{-1}$	7.375	0.232
$1 - 0.6q^{-1}$	7.813	0.283
$1 - 0.8q^{-1}$	8.625	0.525

Table 7.4 Disturbance model effects on non-linear ACSL model

The above results reflected the frequency response plots in Figure 7.6, with more effective controller performance from the original disturbance model. However, these results conflicted with the earlier disturbance rejection responses for the linear model approximation, in Table 7.3. This difference has been attributed to several factors:

(i) *Model mis-match* - The linear model's accuracy reduces as the process moves from its original operating point at which the model parameters were identified.

(ii) *Disturbance input* - Linear disturbance was represented by a single input. However, up to eight disturbances have been identified in the non-linear model. Thus, a representative disturbance input would have to consider model order reduction of the disturbance transfer functions.

(iii) $T(q^{-1})$ - This design parameter has been used to approximate the actual disturbances to the system. Hence, the improved controller performance for the original $T(q^{-1})$ model suggested that this polynomial more closely resembled the actual disturbance inputs.

From the above simulation and frequency response results, the recommended design parameters in Table 7.2, with $T(q^{-1}) = 1 - 0.2q^{-1}$, were preferred. The final non-adaptive WPC controller settings, corresponding to Figure 7.4, were:

$$\alpha = 2.437615$$

$$G_{01}(q^{-1}) = \frac{0.39465q^{-1} - 3.38310\times10^{-2}q^{-2} - 1.47\times10^{-3}q^{-3}}{1 - 0.2q^{-1}} \quad (7.19)$$

$$G_{02}(q^{-1}) = \frac{7.10028 - 8.81545q^{-1} + 4.90846q^{-2} - 1.24337q^{-3}}{1 - 0.2q^{-1}} \quad (7.20)$$

It should be noted that the denominators of (7.19) and (7.20) correspond to the disturbance model, $T(q^{-1})$.

The performance of the non-adaptive WPC algorithm was finally compared with the original classical PI controller selected in Section 6.4. ACSL simulation results in Figure 7.7 were surprisingly similar to those in Figures 6.27 and 6.28, for PI inner/PI outer loop control. This was partly because:

(i) Only the outer loop of the cascade controller was replaced. This limited possible improvement, as the multiloop system was reduced to a SISO control design problem.

(ii) The classical PI controller was operated in continuous mode. Hence, in the ACSL dynamic simulation environment,

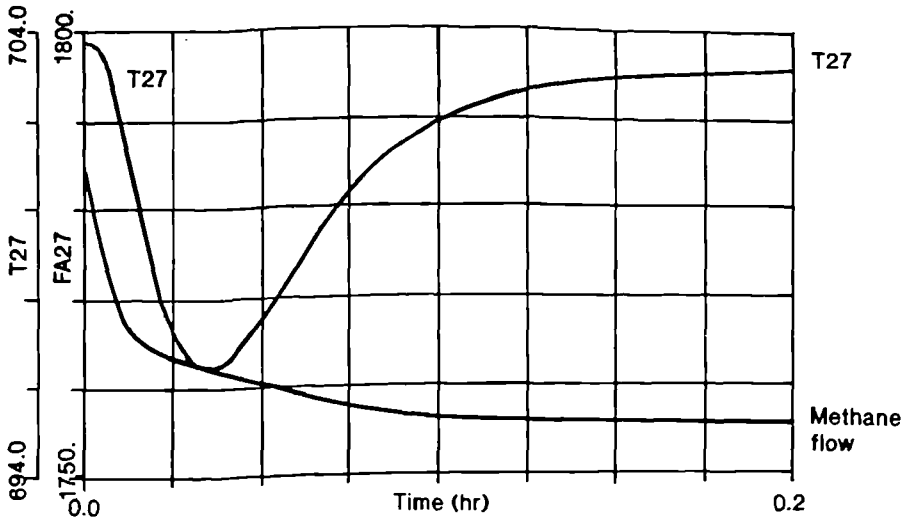

(a) disturbance rejection

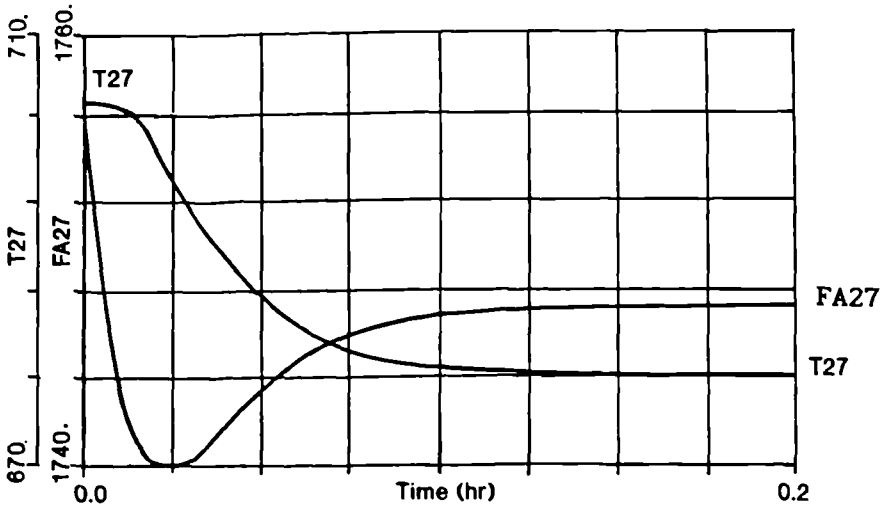

(b) set point tracking and disturbance rejection

Figure 7.7 WPC controller responses with PI inner loop control

the sampling period of the PI controller was equivalent to the time step of the integration algorithm, 10^{-4} hr, whereas the digital WPC controller was set at 10^{-2} hr.

7.2.4 General Comments on WPC Application

The WPC design procedure for the heavies processing section has differed from previous SISO controller designs because an existing software package has been employed to develop a digital controller. The various design steps and parameter values have therefore been based on those recommended by experienced users.

The open-loop heavies processing section was described by a 6^{th}-order transfer function model (7.18). Model order reduction techniques, in PROGRAM CC, were used to remove fast dynamics from the continuous time model. Then, a discrete time model was derived for the WPC design study and a reduced order controller was obtained. However, why not design a controller based on the original plant, and then reduce the order of the resulting WPC controller?

There are several reasons for initially reducing the plant order. Firstly, the WPC calculations in PROGRAM CC become faster, and there is less chance of numerical inaccuracy (resulting from very fast and slow dynamics within the plant). In addition, this method allows the WPC controller to be designed for an approximate model that is more representative of the plant dynamics at its various operating points.

The design parameters available for shaping the system response were given in (7.16) and (7.17). Although, at first glance, there appeared to be a variety of options for each controller design, most parameter values were dictated by the type of system to be controlled. Many recommended parameter values listed in Table 7.1 remained unchanged in the final WPC controller design. However, further analysis of the WPC design would have considered variations in the weighting function, λ, offset by the auxiliary filter settings, M_n/M_d.

As disturbance rejection was more important than set point tracking, the effect of the disturbance model, $T(q^{-1})$, was investigated more

rigorously. The closed-loop frequency results in Figure 7.6 demonstrated the potential of $T(q^{-1})$ to improve disturbance rejection. Usually, if a controller is designed for disturbance rejection, it is too tightly tuned for set point tracking and a compromise is reached. However, $T(q^{-1})$ has been shown to enhance disturbance rejection without influencing the set point tracking.

7.2.5 Concluding Remarks on WPC

The main accomplishments of this application have been:

(i) An investigation of a recent advanced control algorithm.

(ii) The introduction of a digital controller to the dynamic simulation.

(iii) A comparison of the performance of classical and an advanced control design techniques.

(iv) An illustration of the importance of good linear model representations in process control design.

The virtues of Weighted Predictive Control lie in the number of design parameters that can be employed in shaping the system response. These design parameters influence both the set point tracking and disturbance rejection.

The heavies processing section has been successfully controlled using a non-adaptive WPC controller. The inconsistency in step response results between linear and non-linear models has been attributed to the inherent non-linearities in the process and the simplified representation of disturbance inputs. Although the non-linear simulation results have been similar to those obtained using classical control methods, this does not represent a reasonable comparison. Further improvements to system response may be realisable by simply reducing the sampling period and retuning the controller. Introducing a self-tuning version of WPC should certainly improve system performance as operating conditions change.

7.3 MULTIVARIABLE SYSTEM CONTROL DESIGN

The LNG terminal flowsheet includes MIMO processes, in which there is more than one manipulated and controlled variable. This implies that there is more than one possible control loop configuration. In addition, interactions may arise whereby one manipulated variable affects more than one controlled variable in the process. These interaction effects may be minimised by careful selection and combination of the control loop variables.

The design procedure adopted in this chapter for a MIMO process control design can be described by the following general steps:

(i) Identify suitable variables for the control configuration.
(ii) Obtain linear model approximations relating each manipulated variable to each controlled variable.
(iii) Assess the interaction effects.
(iv) Select the input and output pairings with least interaction.
(v) Choose suitable controller designs.
(vi) Derive controller settings using a MIMO tuning method.

The flash unit and distillation column require three and four control loops, respectively. These processes have been used to illustrate the steps involved in designing and tuning controllers for a multivariable system. This work is documented in Sections 7.3 to 7.5.

In this section the controlled and manipulated variables will be identified for the distillation column arrangement. As control loop interaction and tuning is based on linear model data, difficulties encountered in deriving a useful linear model approximation will also be addressed in this section. The distillation column work illustrates this problem.

7.3.1 Control Loop Variable Selection for the Distillation Column

In MIMO control systems, there are several possible control loop configurations. Various criteria are used to select the *best* among all possible loop configurations, involving factors such as:

(i) Choosing the input variable that has a direct and fast

effect on a controlled variable.

(ii) Choosing couplings with little dead time between every input and its corresponding output.

(iii) Selecting couplings with the least interaction.

The selection of controlled and manipulated variables is based on a consideration of the process and control objectives. These issues are discussed for each process in Appendix 7. Usually, the appropriate variables are readily apparent. The controlled variables either represent the variables that are to be controlled or are an indirect measure of those variables. The manipulated variables have been chosen to give a fast and effective response.

In the distillation column, only two of the controlled variables were immediately obvious; liquid levels in the reflux drum and column base. The remaining controlled variables were identified as tray temperatures, from a selection of 11 possible trays, to control the cut and separation. The most suitable trays for temperature control occur in a region with high temperature gradients (Wozny et al., 1987) as this requires lower controller gain. The temperature profiles for the three feedstock conditions are illustrated in Figure 7.8. These plots indicated that the greatest variation in temperature occurred on trays towards the base of the column, corresponding to the less pure bottom product composition. Hence, the base tray, Tray 1, was selected for temperature control of the stripping section.

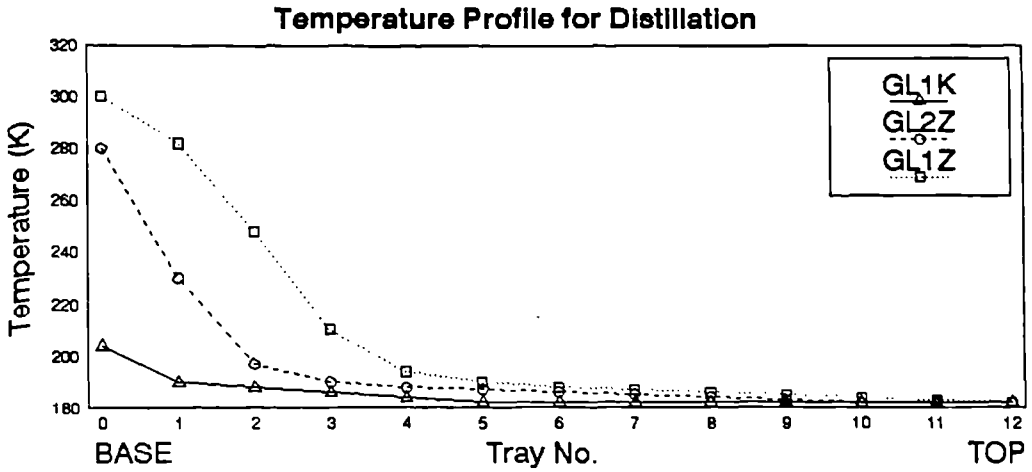

Figure 7.8 Temperature profiles for the distillation column

Temperature variations in the rectifying section were small. Hence, a sensitivity analysis was conducted to ascertain which tray's temperature was most affected by a change in a manipulated input. Open-loop step response results in Table 7.5, for a ±5% change in reflux valve position, indicated that Tray 6 responded most favourably. (The variation in temperature on Tray 1 was significantly greater than on any other tray). Hence, Trays 1 and 6 were selected as controlled variables, representing the stripping and rectifying sections, respectively (Ryskamp, 1982).

Tray No.	Reflux Valve Position			
	Step Increase		*Step Decrease*	
	Temperature Change (K)	Scaled Temperature Change ($\times 10^{-3}$)	Temperature Change (K)	Scaled Temperature Change ($\times 10^{-3}$)
11	-0.809	-4.40	0.626	3.43
10	-1.694	-9.25	0.913	4.98
9	-2.524	-13.70	0.950	5.16
8	-3.167	-17.13	1.408	7.62
7	-3.563	-19.19	1.707	9.19
6	**-3.742**	**-20.04**	**1.912**	**10.24**
5	-3.150	-16.79	1.876	10.00
4	-1.061	-5.62	1.253	6.64
1	-44.628	-184.60	47.850	207.20

Table 7.5 Open-loop step response results for tray temperatures

7.3.2 **Linear Model Approximation**

An open-loop linearised description of a process is required for linear controller design and tuning. For a multivariable system, the complete linear model relates each manipulated variable and disturbance input to the controlled variables. These models are generally presented in state space or transfer function form.

There are numerous process identification techniques available. On-line methods include linear regression from step response and frequency response data. For the SISO systems in Chapter 6, state space models were generated using ACSL. This approach has been adopted for the distillation column, to assess its performance and flexibility.

The non-linear distillation column model was linearised, about three operating points, first using ACSL and then a linear control design package in an attempt to derive a *workable* model. Although the linearisation was unsuccessful, it has been documented to illustrate subtle problems that can adversely affect model approximation. This work also highlights the vulnerability of the control engineer who might assume that these linear approximations accurately represent the process. Although the distillation column is non-linear, several assumptions were made to simplify the dynamic model. Hence, this model is a simplification of the real process, and as such is partially linearised.

7.3.2.1 *Distillation Column State Space Representation*

State space models for the distillation column were obtained directly from ACSL, using valve positions to disturb the process, on the following process streams:

(i) Top product, D.
(ii) Reflux, L.
(iii) Boilup, V.
(iv) Bottom product, B.

The output (controlled) variables included temperatures on Trays 1 and 6, and liquid levels in the condenser and column base. The ACSL generated results were repeatable for a selection of perturbations, suggesting a reliable linear model representation could be obtained for the three feedstock conditions.

Each state space model contained 26 states - 2 per tray, and 2 each for the condenser and column base. A comparison of the state matrix **A** for each condition revealed that there were inconsistencies in the element values, in either sign or magnitude. Thus, a general trend relating the three matrices could not be identified. Eigenvalues, λ_i, were also obtained from ACSL, as these indicate the natural modes of the state matrix **A**, in terms of the roots of the characteristic equation. The results are summarized in Table 7.6.

LNG feedstock condition	No. of poles close to origin	Unstable modes (positive λ_i)	
		No.	*Value*
GL1K	2	2	3.1×10^{-6}, 4.3×10^{-5}
GL2Z	2	3	$0.2\times10^{-5}\pm4.1\times10^{-6}$ i, +36.0
GL1Z	2	0	--

Table 7.6 Unstable modes in distillation column state space model

As most of the positive values of λ_i occur close to the origin, in Table 7.6, the unstable modes may be initially attributed to numerical inaccuracies within ACSL. However, the largest positive λ_i for the GL2Z feedstock condition was of comparable frequency to the stable modes, and hence could not be dismissed as readily. One possible source of model instability could have been the magnitude of the input disturbances. Further tests showed this did not effect the **A** matrix elements. As the GL1Z feedstock condition contained no unstable modes, the model order reduction exercise was initially investigated with this model.

7.3.3 Model Order Reduction

Reducing the number of states within the distillation column system was investigated because:

(i) The λ_i values suggested that most of the modes were very fast.

(ii) A smaller scale model would be more easily assessed and compared.

(iii) The reduced order model could be converted into a manageable transfer function form.

The linear control system design package previously employed, PROGRAM CC, was unsuitable for large scale systems, as its reliability was only guaranteed up to 10 states. Hence, a more extensive design package was employed for this model, namely MATLAB.

Normalising

The MATLAB Reference Manual (TMWI, 1987) recommended that state matrices which exhibit severe variation in their element values should be normalised to prevent ill-conditioning. This does not

affect the λ_i values of **A**. In the distillation column model, the state matrix elements varied significantly because the state variables for each tray represented either molar composition or molar hold up. Hence, these state space matrices were normalised within MATLAB.

The normalising matrices were derived from the original state space description in Section 6.4.2 by expressing the state vector, **x**, in terms of a revised state vector $\mathbf{x}_n$, where:

$$\mathbf{x} = \mathbf{N}_x \mathbf{x}_n$$

and $\mathbf{N}_x$ is a similarity transformation. With **u** similarly expressed, $\mathbf{u} = \mathbf{N}_u \mathbf{u}_n$, this gives

$$\dot{\mathbf{x}} = \mathbf{N}_x \dot{\mathbf{x}}_n = \mathbf{A}(\mathbf{N}_x \mathbf{x}_n) + \mathbf{B}(\mathbf{N}_u \mathbf{u}_n) \qquad (7.21)$$

Rearranging (7.21):

$$\dot{\mathbf{x}}_n = \mathbf{N}_x^{-1}\mathbf{A}\mathbf{N}_x \mathbf{x}_n + \mathbf{N}_x^{-1}\mathbf{B}\mathbf{N}_u \mathbf{u}_n$$
$$= \mathbf{A}_n \mathbf{x}_n + \mathbf{B}_n \mathbf{u}_n \qquad (7.22)$$

where $\mathbf{A}_n$ and $\mathbf{B}_n$ are the normalised matrices of **A** and **B**. In completing the state space model description, in normalised terms:

$$\mathbf{y} = \mathbf{N}_y \mathbf{y}_n = \mathbf{C}\mathbf{x} = \mathbf{C}\mathbf{N}_x \mathbf{x}_n$$

Hence,

$$\mathbf{y}_n = \mathbf{N}_y^{-1}\mathbf{y} = \mathbf{N}_y^{-1}\mathbf{C}\mathbf{N}_x \mathbf{x}_n$$

This results in the following similarity transformations:

$$\mathbf{A}_n = \mathbf{N}_x^{-1}\mathbf{A}\mathbf{N}_x \qquad \mathbf{B}_n = \mathbf{N}_x^{-1}\mathbf{B}\mathbf{N}_u \qquad \mathbf{C}_n = \mathbf{N}_y^{-1}\mathbf{C}\mathbf{N}_x \qquad 7.23$$

The similarity transformations (7.23) were diagonal for the distillation column, with elements represented by the maximum anticipated value of each state. These are listed in Table 7.7.

Similarity Transformation	Element	Value
$\mathbf{N}_x$	Molar composition of methane	1.0
	Molar hold up in reflux drum (kgmol)	600.0
	Molar hold up in column base (kgmol)	100.0
$\mathbf{N}_u$	Control valve position	1.0
$\mathbf{N}_y$	Tray temperature (K)	300.0
	Molar composition of methane	1.0
	Liquid level in reflux drum (m)	2.0
	Liquid level in column base (m)	1.0

Table 7.7 Similarity transformation elements

Having normalised the model, the next logical step was to reduce the number of states from 26 in state space form. As the model was both controllable and observable (Barnett and Cameron, 1985), the balanced realisation form of model reduction was recommended. However, attempts to employ this technique failed as the **A** matrix was not positive definite (TMWI, 1987). The MATLAB-generated λ_i values revealed that the model was also numerically unstable, with three previously undetected unstable modes. Hence, model order reduction could only be achieved by partitioning the matrix into stable and unstable parts, and reducing the stable part. (There were no automatic facilities in MATLAB to partition a matrix).

Alternatively, the state space model could be converted directly into its transfer function form. This would allow:

(i) The steady state gain of selected transfer function relationships to be validated with open-loop step response data from ACSL.

(ii) The relevant transfer functions to be identified.

(iii) Alternate forms of model-order reduction techniques to be pursued.

However, the resulting transfer function matrix did not give good agreement with the ACSL results. This may have been because the state space representation is the most reliable form of linear, time-invariant model to use for computer analysis. Also, numerically accurate calculations are more likely if the system is well-conditioned.

Condition Number

The number of decimal places that can be lost due to round off errors is indicated by the condition number, γ, of the system. Comparing the original and normalised forms of the system, respectively:

$$\gamma_{orig.} = 3.3 \times 10^{11} \qquad \gamma_{norm.} = 2.9 \times 10^{8}$$

shows that numerical accuracy has improved with normalisation. The corresponding loss in decimal places is a function of $\log_{10}\{\gamma(\mathbf{A})\}$, resulting in approximately 11 and 8 decimal places, respectively.

The procedure adopted in the model order reduction exercise for the distillation column is summarised in Figure 7.9.

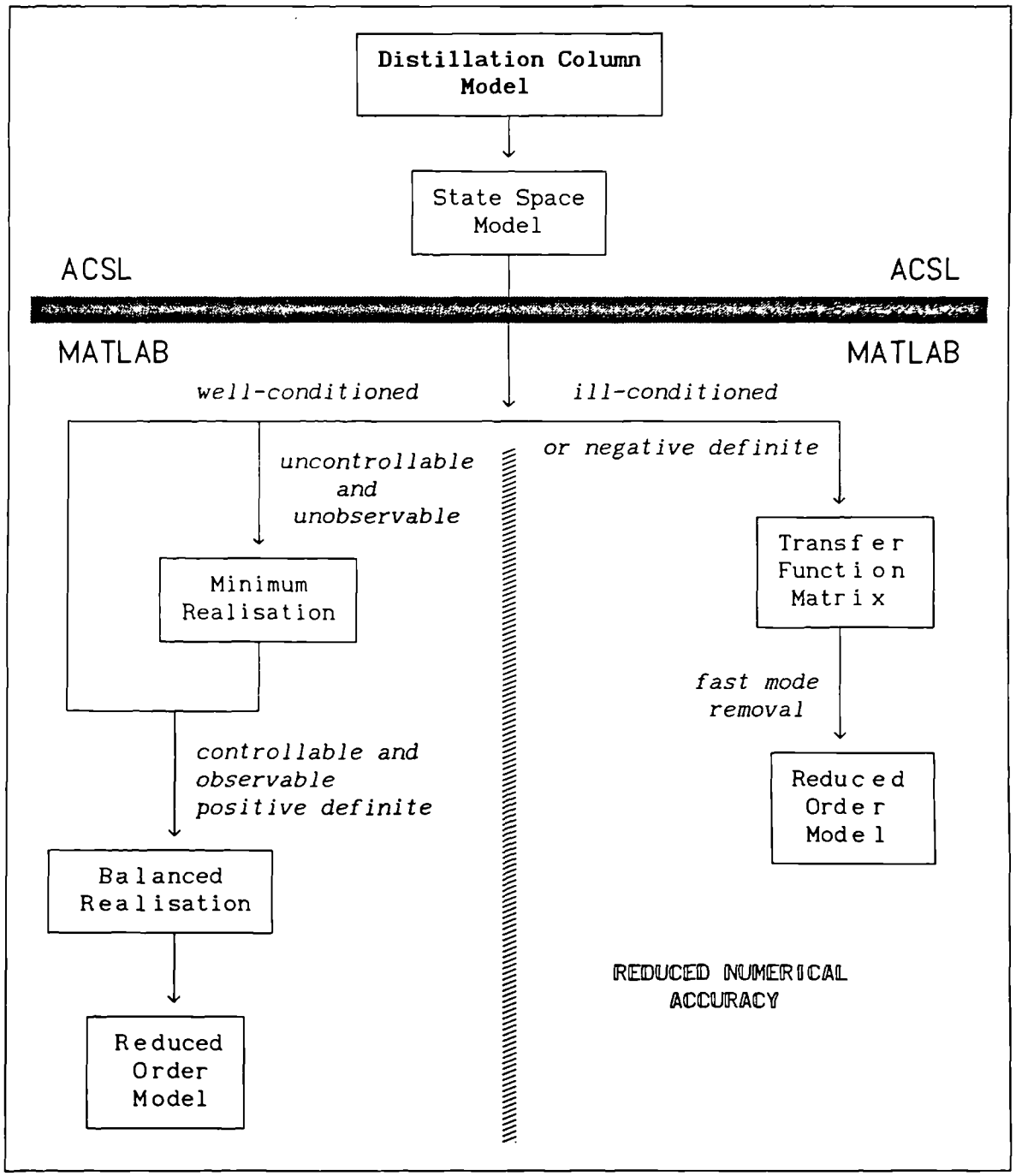

Figure 7.9 Model order reduction procedure for distillation column

7.3.4 Concluding Remarks on Linear Model Approximation

The linear approximation exercise for the distillation column identified several problems that were not apparent in previous linearisation procedures. These are due to several factors:

(i) The distillation column had a large number of states.

(ii) The state space model was ill-conditioned, although this was improved by normalising the **A** matrix.

(iii) The model contained unstable modes that limited the number of appropriate model order reduction techniques.

(iv) There were inherent numerical inaccuracies within ACSL-generated state space models, which made conversion to the transfer function form difficult.

Hence, it was decided to adopt a conventional on-line process identification technique.

First- and second-order plus dead time transfer functions were obtained from ACSL generated step response data, using a graphical fitting technique (Seborg et al., 1989). It was found that the magnitude of the step change affected the steady state gain and response of the system. Thus, a realistic step change was derived by anticipating that the maximum valve range, about any feedstock condition, would be midway between the valve positions for neighbouring feedstock conditions. The typical change in valve position was approximated by half that value. This enabled valve position increments to be standardised for step changes in the manipulated variables. Open-loop step response tests were successfully conducted on the control loop arrangement in Figure 6.5. A further discussion and results are included in Section 7.4.4.

7.4 INTERACTION ANALYSES FOR MULTIVARIABLE PROCESSES

A characteristic of multivariable systems is that more than one control loop arrangement can be derived. Thus, having identified potential controlled and manipulated variables, each control loop arrangement has to be assessed to identify the *best* arrangement for a given system. An inherent degree of interaction exists between control loops. Thus, the effective control action can be improved by reducing this interaction. An interaction analysis is used to eliminate unworkable control loop pairings and identify the control loop arrangement with the least interaction. These interactions are compared by calculating various indices, some of which are described and implemented in this section.

A steady state interaction analysis requires open-loop steady state gain information, relating each controlled to manipulated variable. The flash unit system has been given as an example of how steady state gain data is derived from a non-linear multivariable system, as it exhibits interesting phenomena. Interaction analyses were conducted on both the flash unit and distillation column. These results are discussed in Sections 7.4.3 and 7.4.4.

7.4.1 **Steady State Gain Data for the Flash Unit**

Step changes were introduced to the control valve positions (manipulated variables) of the flash unit shown in Figure 7.10. However, it was found that liquid level did not achieve a new steady state condition following each input, and instead adopted a steady rate of change. This was because liquid level is an integrating element. This behaviour had an adverse effect on other controlled variables, especially when the drum level dropped to zero, producing unreliable results.

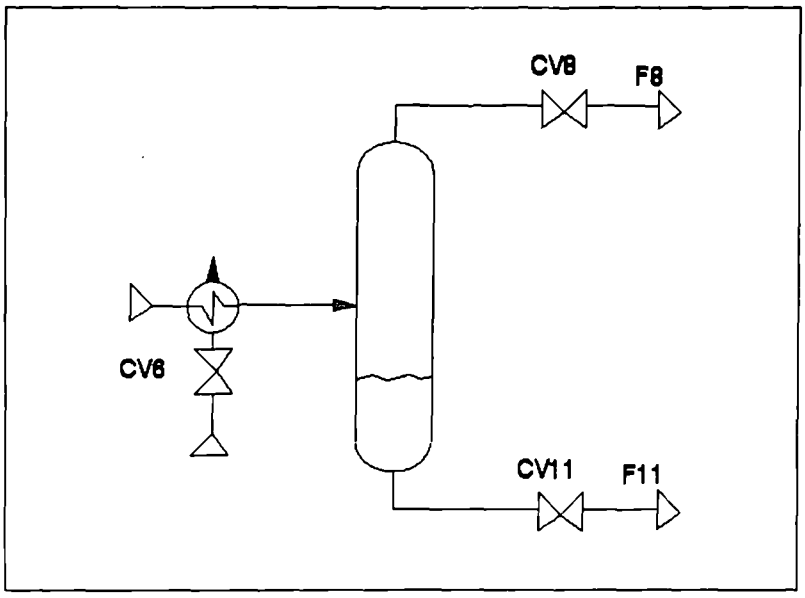

Figure 7.10 Open-loop flash unit system

An alternate procedure derives the open-loop steady state gains of a system from its corresponding closed-loop responses, with preliminary control loops active (McAvoy, 1983a). For an n-loop process, the open-loop gain matrix is given by:

$$\mathbf{x} = \mathbf{G}(0)\mathbf{m} \tag{7.24}$$

where $\mathbf{x}$ and $\mathbf{m}$ are vectors of the controlled and manipulated variables, respectively, and $\mathbf{G}(0)$ is the nxn steady state gain matrix. For a closed-loop system, the closed-loop gain matrix, $\mathbf{G}(0)^{-1}$, is obtained from (7.24):

$$\mathbf{G}(0)^{-1}\mathbf{x} = \mathbf{m} \tag{7.25}$$

Hence, for a control system with n loops paired and x_i controlled by m_i, new m_i values are recorded after a step change is introduced to each set point in turn. Thus, a single loop test for loop i would result in changes for each manipulated variable, such that:

$$\mathbf{x} = \begin{bmatrix} 0 \\ 0 \\ . \\ \Delta x_i \\ 0 \end{bmatrix} \qquad \text{gives} \qquad \mathbf{m} = \begin{bmatrix} \Delta m_1 \\ \Delta m_2 \\ . \\ . \\ \Delta m_n \end{bmatrix}$$

which, for a single loop test, results in:

$$\begin{bmatrix} g(0)^{-1}_{1i} \\ g(0)^{-1}_{2i} \\ . \\ . \\ g(0)^{-1}_{ni} \end{bmatrix} = \begin{bmatrix} \Delta m_1/\Delta x_i \\ \Delta m_2/\Delta x_i \\ . \\ . \\ \Delta m_n/\Delta x_i \end{bmatrix}$$

This represents column i of $G(0)^{-1}$. When n loop tests have been conducted on the closed-loop system, the complete $G(0)^{-1}$ matrix can be inverted to give the open-loop steady state gain matrix, $G(0)$.

The resulting closed-loop step response data for the flash unit, in Table 7.8, highlighted several points of note. It was found that closed-loop gains were greater for a step increase in pressure set point, P11, than a step decrease, for each control valve. The opposite effect was observed for step changes in set point temperature, T11 and level, H11. These gain variations highlighted the non-linearities present in the flash unit model, which were related to both the initial steady state condition and the perturbation size.

Set Point Perturbation, Δx_i	**Variation in Manipulated Variable, Δm_i**		
	CV8	*CV6*	*CV11*
Pressure, P11			
+0.25 bar	-4.2671	-0.9489	+4.1773
-0.25 bar	+3.0287	+0.7633	-2.6825
Average Gain	-3.6479	-0.8561	+3.4299
Temperature, T11			
+0.50 K	+15.7736	-18.0593	+4.1224
-0.50 K	-21.6837	+36.5887	-5.0391
Average Gain	+18.7287	-27.3240	+4.5807
Liquid Level, H11			
+0.10m	+0.0025	+0.0003	**+0.0170**
-0.10m	-0.0870	-0.0171	**+0.1157**
Average Gain	+0.0452	+0.0087	**?0.0664**

Table 7.8 Closed-loop steady state gains for the flash unit

The most noticeable inconsistency occurred in the liquid level on CV11, where both an increase and decrease in level set point resulted in the valve opening further. (The average gain is marked ? in

Table 7.8). Thus, for an increase in liquid level, the feed temperature and product flow rates all increased. However, for the same decrease, bottom product flow rate (manipulated by CV11) continued to increase. This suggests that feed temperature had the greatest influence on operating conditions, indicated by its large gains. By comparison, CV11 had the least effect, and was dominated by the other control actions. As it was unclear whether a positive or negative value of the (H11, CV11) gain was correct, both values were considered in the subsequent interaction analyses.

7.4.2 **Interaction Analysis**

Process interactions arise from interconnected networks of mechanical, fluid or electrical components. Control loop interaction results from the regulatory action on one control loop affecting other loops in the same process. This initiates a control action in the remaining loops that disturbs the output from the original loop. Interaction can occur in transient or steady state form, or a combination of both.

7.4.2.1 *Interaction Indices*

A selection of interaction measures has been applied to the flash unit and distillation column processes based on the steady gain matrix of the plant, **G**(0). Five different interaction measures have been considered for the multivariable systems. These indices are used to eliminate unworkable loop pairings, and are described below.

Relative Gain Array

The relative gain array (RGA) was developed by Bristol (1966) to analyse steady state interaction between control loops. This method enables the best pairing of input and output variables to be selected, by quantifying the degree of interaction on each control loop. The relative gain is the ratio of two open-loop gains:

$$\lambda_{ij} = \frac{(\delta x_i/\delta m_j)\big|_{\text{(all loops off)}}}{(\delta x_i/\delta m_j)\big|_{\substack{\text{(all loops but } m_j\text{-}x_i \\ \text{perfect)}}}} \qquad (7.26)$$

for an output x_i and manipulation m_j. The numerator represents the open-loop static gain, and the denominator is the steady state gain

when all other inputs and outputs are under perfect control.

The value of λ_{ij} determines the level of interaction, such that:

(i) If $\lambda_{ij} < 0$, the system is either unstable or inverse responding.

(ii) If $\lambda_{ij} = 0$, then m_j has no influence on x_i, and (x_i, m_j) should not be paired.

(iii) If $0 < \lambda_{ij} < 1$, then an interaction exists that is smaller for greater values of λ_{ij}.

(iv) If $\lambda_{ij} = 1$, then there is no interaction and the control loops are completely decoupled.

(v) If $\lambda_{ij} \gg 1$, the system may be sensitive to changes in parameter values.

Thus, relative gains between all the inputs and outputs of a system can be determined to assess the degree of interaction. As the RGA is scale-invariant, λ_{ij} values are unaffected by normalising. In its simplest form, for a 2x2 system, the summation properties of the RGA require only one relative gain element to be defined. The RGA is given by:

$$\Lambda = \begin{array}{c} \begin{matrix} m_1 & m_2 \end{matrix} \\ \begin{bmatrix} \lambda & 1-\lambda \\ 1-\lambda & \lambda \end{bmatrix} \end{array} \begin{matrix} x_1 \\ x_2 \end{matrix}$$

The RGA elements can alternatively be determined by matrix methods, using the *open-loop* steady state gain matrix, **G**(0). Hence, an individual RGA element is defined as:

$$\lambda_{ij} = [\mathbf{G}(0)]_{ij} \, [\{\mathbf{G}(0)^{-1}\}^T]_{ij}$$

The most extensive application of RGA is in distillation column control (Yang et al., 1991), as an initial step in control loop selection. It should be noted that the RGA does not guarantee that the *dynamic* interaction between loops is also minimal (McAvoy, 1983b).

Niederlinski Index

The stability of control loop pairings may be assessed using the Niederlinski Index (N.I.) (Niederlinski, 1971). This index is a *necessary but not sufficient* condition for stability of a closed-loop system with integral action. It states that a system is unstable for any controller settings, with integral control action, if N.I. is negative, such that:

$$N.I. = \frac{|\,G(0)\,|}{\prod_{i=1}^{n} g(0)_{ii}} < 0 \qquad (7.27)$$

where $|G(0)|$ is the determinant of $G(0)$ and the denominator represents the product of diagonal $G(0)$ elements.

Morari Index of Integral Controllability (MIC)

This interaction measure is presented by Grosdidier et al. (1985) as:

$$MIC = \lambda[G^{+}(0)] \qquad (7.28)$$

where $\lambda[G]$ represents the eigenvalues of G and $G^{+}(0)$ is the adjusted steady state gain matrix with positive diagonal elements. A negative value of any of the system eigenvalues indicates a closed-loop unstable system. Hence, loop pairings with negative MIC values should be eliminated.

Morari Resiliency Index (MRI)

MRI compares the inherent resilience of alternate control structures (Morari and Zafiriou, 1989), and is defined as:

$$MRI = \underline{\sigma}\,[\,G(j\omega)\,] \qquad (7.29)$$

which is the minimum singular value of $G(j\omega)$. In this study, only the steady state gains have been considered, at zero frequency. As the MRI is a measure of the ability of the system to deal with disturbances and changes in the operating conditions, a larger value of MRI indicates a more resilient control loop structure. (A larger $\underline{\sigma}$ value means that the G matrix is further from being singular, and finding the inverse of G is a better conditional operation. As a perfect feedback controller would represent the inversion of the process it controls, a well conditioned inverse reflects good controllability). MRI requires dimensionless steady state gain data.

Condition Number

The condition number, $\gamma(G)$, is the ratio between maximum and minimum singular values of a system, defined as:

$$\gamma(G) = \frac{\bar{\sigma}\,[\,G(0)\,]}{\underline{\sigma}\,[\,G(0)\,]} \qquad (7.30)$$

If $\gamma(G)$ is large then the plant is more sensitive to uncertainty (Morari and Zafiriou, 1989). Thus, a low $\gamma(G)$ is preferred.

7.4.3 **Control Loop Pairing for the Flash Unit**

The RGA and N.I. have been applied to derive the *best* multivariable control loop structure for the flash unit. This process has three manipulated and control variables, which can be configured to give 3! different control loop arrangements.

7.4.3.1 *Flash Unit Interaction Analysis*

Closed-loop step response data for the 3×3 flash unit was derived in Section 7.4.1. The corresponding $G(0)^{-1}$ matrix was represented by two different matrices, with either a positive or negative (m_3, x_3) element, as the correct sign was unknown:

$$G(0)^{-1} = \begin{array}{c} \begin{matrix} x_1 & x_2 & x_3 \end{matrix} \\ \begin{bmatrix} -3.6479 & +18.7287 & +0.0452 \\ -0.8561 & -27.3240 & +0.0087 \\ +3.4299 & +4.5807 & \pm 0.0664 \end{bmatrix} \end{array} \begin{matrix} m_1 \\ m_2 \\ m_3 \end{matrix} \qquad (7.31)$$

The RGA matrix corresponding to a positive (m_3, x_3) element (7.31), has been derived as:

$$\Lambda_+ = \begin{array}{c} \begin{matrix} m_1 & m_2 & m_3 \end{matrix} \\ \begin{bmatrix} 267.9 & -287.0 & 20.1 \\ -219.9 & 246.1 & -25.2 \\ -47.0 & 41.9 & 6.1 \end{bmatrix} \end{array} \begin{matrix} x_1 \\ x_2 \\ x_3 \end{matrix} \qquad (7.32)$$

For a negative (m_3, x_3) element, the RGA becomes:

$$\Lambda_- = \begin{array}{c} \begin{matrix} m_1 & m_2 & m_3 \end{matrix} \\ \begin{bmatrix} 2.879 & -0.072 & -1.807 \\ -6.095 & 4.833 & 2.262 \\ -4.216 & -3.761 & 0.545 \end{bmatrix} \end{array} \begin{matrix} x_1 \\ x_2 \\ x_3 \end{matrix} \qquad (7.33)$$

As negative RGA elements should be avoided for control loop pairing, only diagonal RGA element selection would be feasible for (7.32) and (7.33). Although there was a sign change in the $g(0)^{-1}_{3,3}$ element, the same control loop pairings were recommended, such that:

(x_1, m_1)		(P11, CV8)
(x_2, m_2)	or, in flash unit terms:	(T11, CV6)
(x_3, m_3)		(H11, CV11)

which represents the conventional control loop structure for a flash unit arrangement.

The RGA elements in (7.33) were far smaller than in (7.32), which indicated a reduced interaction between control loops. As this arose

from a sign change on a closed-loop steady state gain, it suggested that the effects of interaction may become more dominant when liquid level rises as a result of increasing CV11, and vice versa. This was further illustrated by considering the condition number, $\gamma(G)$, of the open-loop step response matrices for positive and negative (m_3, x_3) elements, respectively:

$$\gamma_+ = 1.7E5 \qquad \gamma_- = 1.5E4$$

The magnitude of the above γ's suggests both matrices may be ill-conditioned, with γ_+ to a greater extent. The N.I. gave positive values for both matrices, from which no conclusion can be drawn.

Three indices were employed to assess the suitability of 6 different control loop configurations for a 3x3 system. The RGA method helped eliminate unworkable control loop pairings. Thus, the conventional control loop structure selected in Appendix 7 has been validated using interaction analysis techniques. The recommended control loop pairings are illustrated in Figure 6.3.

7.4.4 Control Loop Pairing for the Distillation Column

A distillation column may be described as a 5x5 plant. During dynamic model development of the multicomponent column in Section 3.2, perfect pressure control was assumed, reducing the degrees of freedom of the system to 4. A further simplification was introduced to the column model by assuming perfect level control in the reflux drum and column base, as level is a less critical control variable in the system. This is a common assumption (Skogestad and Morari, 1987a) that reduces the control problem to a 2x2 system. In practice, few columns are controlled with a full 5x5 complement of controllers, and a decentralised system is often adopted with single loop control (Skogestad et al., 1990). Hence, the pressure and level control loops are generally designed first, resulting in a 2x2 composition control problem.

The control design involved identifying a suitable control loop structure for inferential dual composition control of the column.

7.4.4.1 *Control Loop Structures for the Distillation Column*

Potential control loop configurations have been identified based on the controlled and manipulated variables for the distillation column, in Section 7.3.1. These are defined in terms of the two independent variables used in composition control, namely cut and separation.

The conventional L-V control loop configuration is illustrated in Figure 7.11. Its name is derived from the use of L and V as manipulated variables for composition control of the top and bottom products, with level and pressure control. This arrangement suffers from interaction effects between the composition control loops (Waller, 1986), which may be alleviated by adopting the sum and difference of tray temperatures as the controlled variables, rather than their absolute values. Hence, an alternate control loop structure is illustrated in Figure 7.12.

Bequette and Edgar (1986) investigated design methods to reduce the interaction between control loops, with the controlled variables represented by the sum and difference of two tray temperatures. Their study concentrated on a D-V configuration, and is illustrated in Figure 7.13. There are many forms of dual composition control that could be adopted for the system (Waller, 1986). This control loop design study was confined to and investigated three contrasting schemes - two L-V configurations and one D-V configuration, which are illustrated in Figures 7.11 to 7.13. For each set of two controlled and two manipulated variables, two arrangements were possible. Hence, six potential control loop configurations were investigated.

7.4.4.2 *Interaction Analysis for the Distillation Column*

The interaction analysis was applied to the six possible configurations to identify the structure with least interaction. The analysis was confined to the GL2Z feedstock condition only.

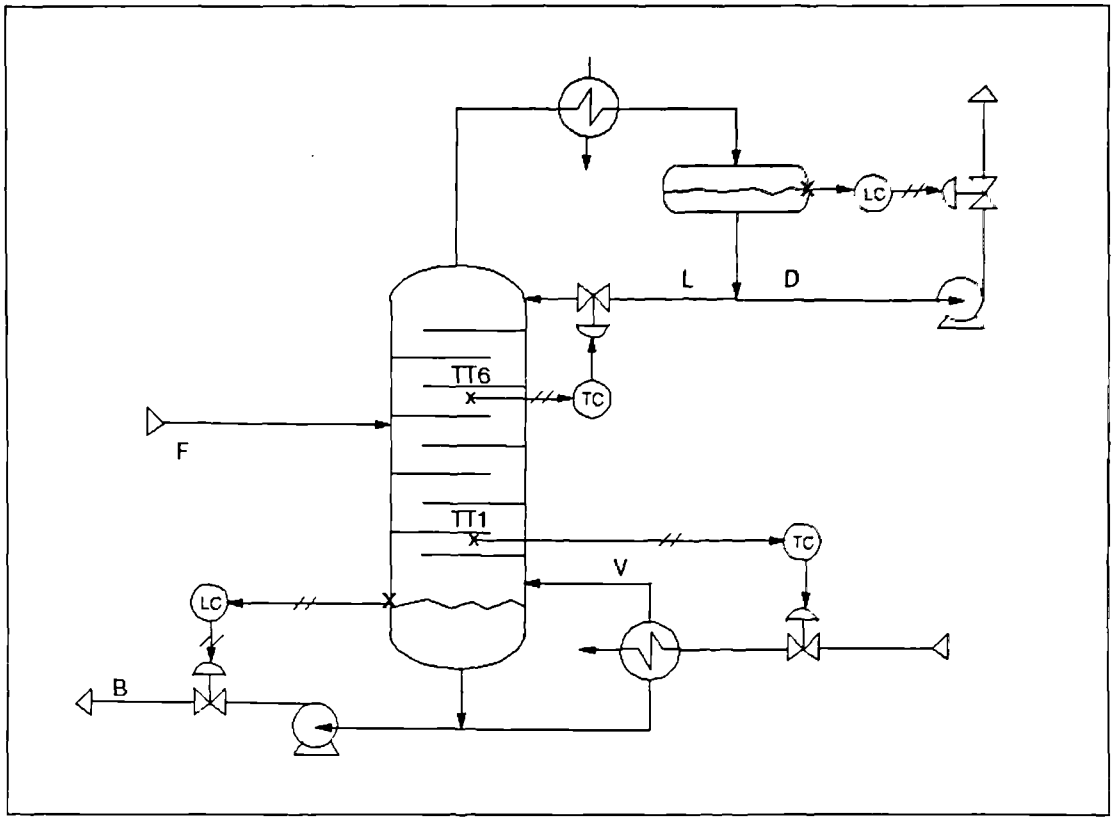

Figure 7.11 Control of distillation column with L-V configuration

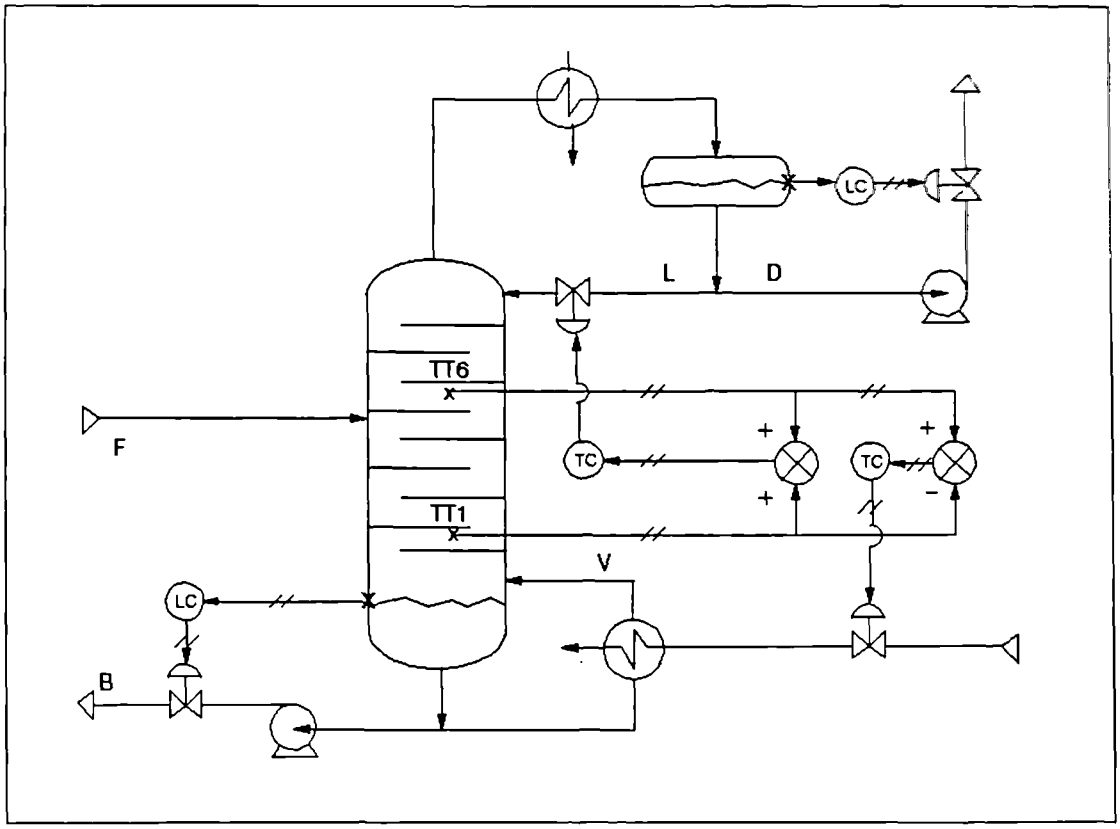

Figure 7.12 An alternate L-V configuration

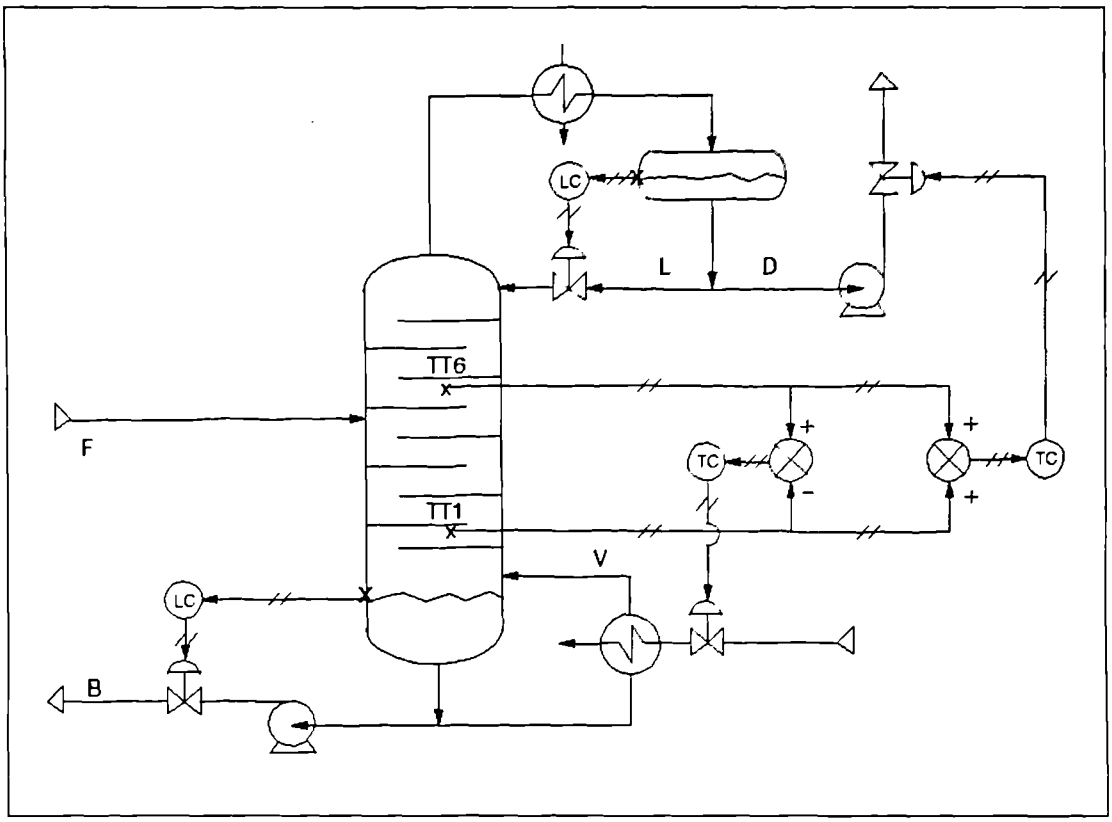

Figure 7.13 Control of distillation column with D-V configuration

Open-loop steady state gain information for the L-V configurations was derived from recommendations in Section 7.3.4 using step response data. As the D-V configuration was open-loop unstable, the closed-loop procedure described in Section 7.4.1 was adopted, to give $G(0)^{-1}$. The open-loop steady state gains for each control loop configuration, relating control valve positions to tray temperatures, are presented in Table 7.9. Similar work in the open literature presented differing results for several reasons:

(i) Tray compositions were adopted as the controlled variables (Skogestad and Morari, 1987b).

(ii) The distillation column was described by a crude dynamic model (Morari and Zafiriou, 1989).

(iii) The actual flow rates were manipulated rather than control valve positions (Yu and Luyben, 1986).

The interaction indices described in Section 7.4 were derived for each control structure, and are presented in Table 7.10.

Gain Matrix G(0)	Control Loop Configuration		
	L-V[1]	L-V[2]	D-V[2]
g_{11}	-73.73	-1348.86	-11749.40
g_{12}	+69.23	+1106.24	-1114.81
g_{21}	-1275.12	+1201.37	+13903.40
g_{22}	+1037.01	-967.78	+1535.57

[1] Tray 6 and Tray 1 temperatures as controlled variables
[2] Sum and difference of Tray 6 and Tray 1 temperatures as controlled variables

Table 7.9 Open-loop steady state gain matrices

Control Loops	Variable Pairing	MRI $\underline{\sigma}G(0)$	$\gamma(G)$	RGA λ_{11}	N.I.	MIC $\lambda[G^{+}(0)]$
L-V	L-V-1: (L-T6)(V-T1)	7.2	229	-6.5	-1/6.5	+1121.3 -10.5
	L-V-2: (L-T1)(V-T6)	7.2	229	+7.5	+1/7.5	+1335.5 +8.8*
L-V	L-V-3: (L-sum)(V-dif)	10.1	230	-55.3	-1/55.3	+2326.8 -10.1
	L-V-4: (L-dif)(V-sum)	10.1	230	+56.3	+1/56.3	+2297.3 +10.3*
D-V	**D-V-1: (D-sum)(V-dif)**	**130.8**	**140**	**+7.1**	**+1/7.1**	**+13090.8** **+194.2***
	D-V-2: (D-dif)(V-sum)	130.8	140	-6.1	-1/6.1	+15185.6 -167.4

sum - sum of Tray 6 and Tray 1 temperatures
dif - difference between Tray 6 and Tray 1 temperatures
* - closed-loop stable pairing

Table 7.10 Steady state analysis of alternative control structures

Unworkable variable pairings were eliminated using the interaction indices, which showed that:

(i) *MRI* - The D-V control structure had the highest MRI value, and hence could most easily handle disturbances and changes in operating conditions. By comparison, the L-V structures had low MRI values, and could be inherently sensitive.

(ii) *Condition Number* - The small value of $\gamma(G)$ for the D-V structure indicated that it was least sensitive of the three to model uncertainty.

(iii) *RGA* - The conventional L-V-1 loop pairing gave negative RGA elements, indicating a possibly unstable system (Yu and Luyben, 1986). This may have been due to the multicomponent nature of the system. It was also noted that the reflux, L, has a greater effect on the temperature of Tray 1 than boilup, V!

(iv) *N.I. and MIC* - These values confirmed that each control structure had only one closed-loop stable pairing

From the above discussion relating to the results in Table 7.10 the D-V-1 control loop pairing was selected:

$$(D, \quad (T_{T6} + T_{T1}))$$
$$(V, \quad (T_{T1} - T_{T6}))$$

as illustrated in Figure 7.13 (Bequette and Edgar, 1986). Although, the L-V-2 and L-V-4 loop pairings (Ryskamp, 1982) were also closed-loop stable, they gave less favourable interaction measures. In particular, a low MRI value rendered L-V-2 inherently sensitive, and the large RGA for L-V-4 indicated an ill-conditioned plant (Skogestad and Morari, 1987b).

As a further extension of the steady state analysis, Morari and Zafiriou (1989) stated that a stable 2x2 plant is Decentralized Integral Controllable (DIC) if:

$$\lambda_{11}(0) > 1/2$$

Satisfying this condition meant that a closed-loop system with integral control action was stable, and stable closed-loop performance could be achieved by tuning each loop separately. Hence, each closed-loop stable system in Table 7.10 was DIC.

7.4.5 Concluding Remarks on Interaction Analyses

Five interaction indices were used in the interaction analyses on the flash unit and distillation column. The conventional control loop structure was selected for the flash unit as it represented the arrangement with least interaction. In the distillation column analysis, RGA values indicated that the conventional L-V control loop structure was potentially unstable. Although the D-V configuration was selected, it was open-loop unstable as variations in the liquid

levels would be reintroduced into the system as disturbances. It was also noted that for a 2x2 system, the RGA, N.I. and MIC indices gave the same information (Yu and Luyben, 1986).

These interaction analyses were based on the steady state gains and thus considered only steady state effects of interaction on the control loops. However, McAvoy (1983a) stated that if the RGA elements are greater than one, which is the case for both flash unit and distillation column in this study, then dynamic interactions are far more important. Hence, a detailed study of the control loop configurations should also have considered dynamic interaction effects, using the dynamic RGA. The difficulty with this type of RGA is that a net disturbance effect has to be identified. This may lead to the model mis-match problems encountered with disturbances to the heavies processing section, discussed in Section 7.2.

7.5 MULTIVARIABLE CONTROL LOOP TUNING

Although SISO tuning methods can be used to tune a controller for a MIMO system, they may not be effective due to the inherent interaction between control loops. This could be overcome by detuning the control loops to reduce interaction effects. The major difference between SISO and multivariable system tuning is that control loops cannot be considered in isolation.

A MIMO control system would consider every manipulated and controlled variable and design a matrix controller that related each variable. The control structure complexity for such a system can be reduced by considering a series of SISO controllers that interact, to form a multiloop system. This approach has been adopted for both the flash unit and distillation column processes.

A complete example of multivariable control system design is given for the flash unit process, from performance specifications through to controller tuning. The tuning method adopted in this example was for a multiloop control system structure and based on conventional SISO controller tuning methods.

7.5.1 Multi-loop Controllers

An open-loop process with n manipulated and n controlled variables, and no disturbance input, can be described in the Laplace domain by:

$$\begin{aligned} x_1 &= G_{11}m_1 + G_{12}m_2 + \ldots + G_{1n}m_n \\ x_2 &= G_{21}m_1 + G_{22}m_2 + \ldots + G_{2n}m_n \\ &\vdots \\ x_n &= G_{n1}m_1 + G_{n2}m_2 + \ldots + G_{nn}m_n \end{aligned}$$

The process is represented by an n×n transfer function matrix:

$$\mathbf{x} = \mathbf{G}\,\mathbf{m} \qquad (7.34)$$

where **x** is the vector of n controlled outputs and **G** is the open-loop transfer function. When feedback control is added, the closed-loop process can be described by the block diagram arrangement of Figure 7.14.

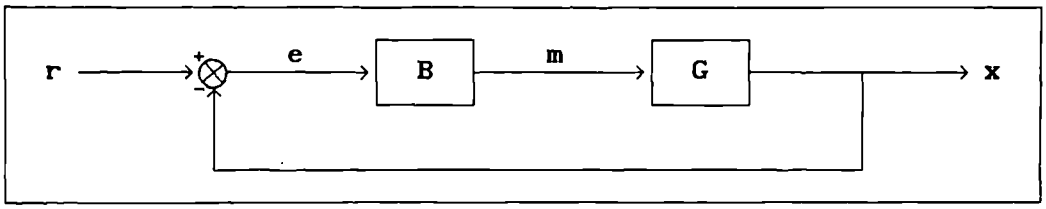

Figure 7.14 Multivariable control loop block diagram

The feedback controllers are represented by the **B** matrix of dimension n×n. Most industrial processes adopt conventional SISO feedback controllers, so that each loop controls one controlled variable by varying one manipulated variable. The corresponding **B** matrix is diagonal in structure, with zero off diagonal elements:

$$\mathbf{B} = \begin{bmatrix} B_1 & . & . & 0 \\ . & B_2 & . & . \\ . & & & . \\ 0 & . & . & B_n \end{bmatrix} \qquad (7.35)$$

B_1 through to B_n represent the individual controllers for each control loop in the process, hence the term *diagonal controller* structure. A multivariable controller structure would have elements in each position in the **B** matrix. The **B** matrix relates the manipulated variables and the error signal:

$$\mathbf{m} = \mathbf{B}\,\mathbf{e}$$
$$= \mathbf{B}\,[\,\mathbf{r} - \mathbf{x}\,]$$

Hence, (7.34) becomes:

$$\mathbf{x} = \mathbf{G}\,\mathbf{B}\,[\,\mathbf{r} - \mathbf{x}\,] \qquad (7.36)$$

Due to the interactions between control loops in a multivariable system, traditional SISO tuning techniques (Stephanopoulos, 1984; Åström and Haggland, 1988) cannot be readily applied. Generally, multiloop SISO control loops (7.35) require detuning or decoupling to overcome interaction effects.

7.5.2 **The BLT Method**

A simple tuning method has been proposed for the flash unit, based on the classical SISO design techniques, and adapted by Luyben (1986) to form a multivariable tuning method. The BLT (biggest log-modulus tuning) method offers a simple design procedure for obtaining reasonable controller settings for n multiloop SISO controllers. It

is limited to open-loop stable systems, and requires an open-loop transfer function representation.

The BLT method is based on the Ziegler-Nichols tuning method for SISO control loops. For PI multiloop controller tuning, requiring 2n controller settings, the first step is to derive SISO controller settings from the diagonal transfer function elements in G(s) (Åström and Haggland, 1988). The BLT method has been used to detune these controller settings. The basic principles of BLT for n multiloop PI controllers are described below.

A relationship between SISO and multivariable tuning methods has been developed from the closed-loop stability criteria applied to SISO systems. These are briefly defined in Table 7.11.

	SISO		Multivariable
Closed-loop Transfer Function	$\frac{GB}{1 + GB}$		$[I + GB]^{-1}GB$
Nyquist Diagram	Plot	$(\text{characteristic equation}) - 1 = (1 + GB) - 1 = GB$	$W(s) = -1 + \det[I + GB]$
	Instability:	Encirclement of (-1,0)	
Closed-loop Log Modulus	Plot	$\frac{GB}{1 + GB}$	$\frac{W}{1 + W}$
	L_c	$20 \log_{10}\left\lvert \frac{GB}{1 + GB} \right\rvert$	$20 \log_{10}\left\lvert \frac{W}{1 + W} \right\rvert$
	L_c^{max}	$L_c^{max} = +2$ dB	$L_{cm}^{max} = +2n$ dB

Table 7.11 Cosed-loop stability criterion for SISO and MIMO systems

The Nyquist stability criterion can be applied to a multivariable system, using the closed-loop characteristic equation to check for instability. The multivariable Nyquist plot in Table 7.11 has been derived to indicate closed-loop instability by encirclements of the (-1,0) point, similar to the SISO case.

This frequency response analogy has been used to consider robustness of the closed-loop transfer functions in terms of the log modulus. The peak value of the log modulus plot for SISO systems is termed the *maximum closed-loop log modulus*, L_C^{max}. This is a measure of the proximity of the GB(s) curve to the (-1,0) point, at all frequencies. For SISO systems, an L_C^{max} value of +2 dB corresponds to good controller settings (Luyben, 1990). This has been extended to the multivariable case via the Nyquist plot relationship as shown in Table 7.11. The multivariable closed-loop log modulus is:

$$L_{cm} = 20 \log_{10} \left| \frac{W}{1 + W} \right| \tag{7.37}$$

Based on the +2 dB L_C^{max} for SISO systems, Luyben (1986) recommended:

$$L_{cm}^{max} = 2 n \tag{7.38}$$

for multivariable systems with n control loops.

On the frequency response plot, the L_{cm}^{max} value of 2n dB is achieved by detuning the original SISO controller settings for each control loop in the multivariable system using a detuning factor, F. The revised Ziegler-Nichols settings are defined as:

$$K_{ci} = \frac{K_{ZN_i}}{F} \qquad \tau_{Ii} = \tau_{ZN_i} F \tag{7.39}$$

and

$$B_i(s) = K_{ci}\left\{ 1 + \frac{1}{\tau_{Ii} s} \right\}$$

where K_c and τ_I are the controller gain and integral time constant, respectively, and suffix i refers to the control loop. The effect of F is to give a more stable and sluggish response as F is increased and the control loops are detuned.

The BLT tuning algorithm is as follows:

(i) Obtain PI controller settings for n control loops using the Ziegler-Nichols method.

(ii) Estimate F, and detune the 2n controller settings (7.39).

(iii) Plot the frequency response of W/(1+W), where W = -1 + det[I + **GB**].

(iv) Compare L_{cm}^{max} with 2n. If the tuning criterion (7.38) is not satisfied, repeat steps (ii) to (iv).

As this tuning method has been successfully applied to several multivariable examples (Yu and Luyben, 1986; Monica et al., 1988;

Hsie and McAvoy, 1991), it was adopted in the flash unit control study, to select PI multiloop SISO controllers

7.5.3 Control Loop Design for the Flash Unit

7.5.3.1 *Performance Specifications for the Flash Unit*

During the model validation exercise in Section 4.4 pressure was identified as the most important controlled variable as the flash unit operated close to critical conditions. Hence, an upper limit of 1 bar has been imposed on pressure variation about the set point necessitating tight control requirements. Temperature control was less critical than pressure, but should also achieve zero set point offset. Liquid level need only be maintained within operating limits. Hence, a variation of 0.1 m from the set point value of 2.9 m was declared acceptable.

Suitable feedback controllers were selected from classical controller designs. Skinskey (1988) recommended a PI controller for vapour pressure control, and a PID controller for temperature control to speed up control loop action by anticipating the future control error. However, it should be recalled that the feed preheater in Figure 6.3 was described by a steady state model with no dynamic effects. Thus, any dead time associated with the feed temperature response will be small, reducing the benefits of derivative control action. Hence, a PI controller was adopted for the temperature control. A proportional controller is generally adopted for level control applications.

Only the temperature set point changes during feedstock changeovers. Therefore, the pressure and level controllers would primarily be concerned with disturbance rejection. Hence, the interaction between control loops, identified in Section 7.4.4, is not necessarily detrimental - each controller would help maintain the process at its set point condition during load disturbances (Luyben, 1990).

7.5.3.2 *Level Controller Tuning for the Flash Unit*

A proportional controller would be sufficient to maintain liquid level in the flash drum as set point offset is acceptable. Hence, there were two options available:

(i) A 3x3 flash unit system is tuned with PI controllers.

(ii) Level control is derived independently, and the remaining 2x2 flash unit system is tuned with level control active.

The latter was adopted as it simplified the multivariable system tuning requirements, and allowed a suitable level controller to be selected. Hence, with preliminary control loops installed for pressure and temperature control, two types of level controller were investigated - P and PI.

Both controllers were tuned by trial-and-error, and the closed-loop ACSL model subjected to a series of disturbance and set point changes. The corresponding closed-loop responses for P and PI control are shown in Figure 7.15. Although most disturbances had only slight effects on liquid level, a set point change in drum temperature produced an immediate drop in liquid level for both controllers. As liquid level was maintained well within ±0.1m, a reverse acting proportional control was selected for the flash unit level controller, with controller gain set at $K_c = 3.0$.

7.5.3.3 *Multivariable Flash Unit Tuning Using the BLT Method*

An open-loop linear representation of the 2x2 flash unit was obtained by graphical fitting of step response data, with level control active. The corresponding open-loop transfer function about the GL2Z feedstock condition for:

$$\mathbf{x} = \mathbf{G}(s)\,\mathbf{m}$$

was defined as

$$\begin{bmatrix} P11 \\ T11 \end{bmatrix} = \begin{bmatrix} g_{11} & g_{12} \\ g_{21} & g_{22} \end{bmatrix} \begin{bmatrix} CV8 \\ CV6 \end{bmatrix}$$

where:

$$g_{11} = \frac{-261.6\, e^{-0.04s}}{(0.57s + 1)} \qquad g_{12} = \frac{+1079.0\, e^{-0.03s}}{(0.50s + 1)}$$

$$g_{21} = \frac{-215.0}{(0.57s + 1)} \qquad g_{22} = \frac{+925.0\, e^{-0.01s}}{(0.50s + 1)}$$

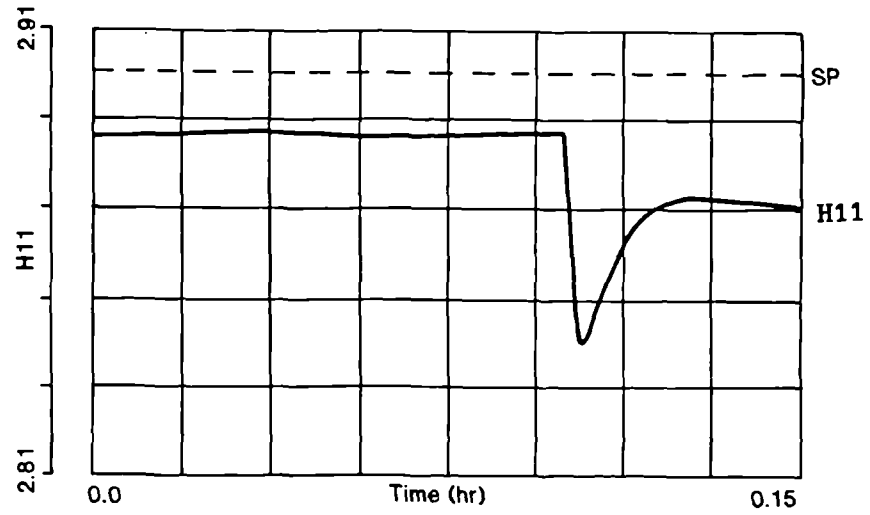

(a) proportional controller

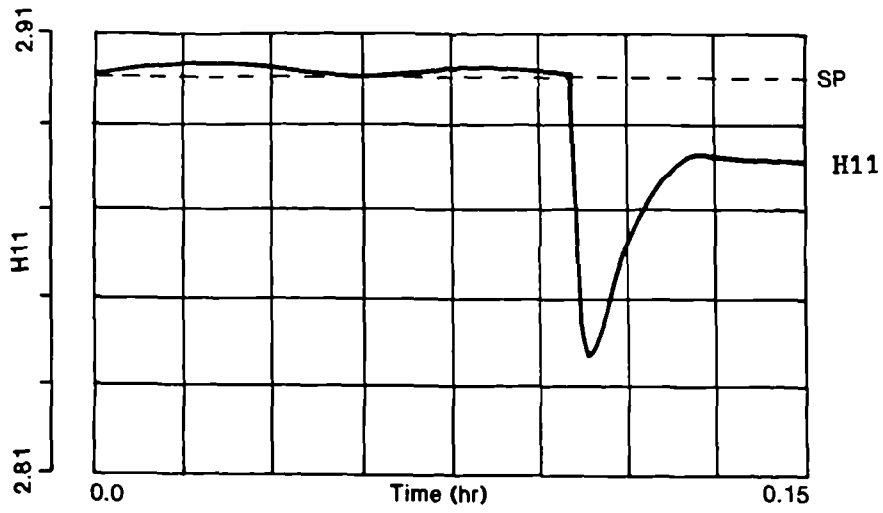

(b) proportional-integral controller

Figure 7.15 Closed-loop responses for level control in flash unit

The corresponding Ziegler-Nichols settings for g_{11} and g_{22} were:

	K_{ZN}	τ_{ZN}
B1:	0.04	0.130
B2:	0.04	0.033

with B_1 inverse responding. The log modulus plot of W(s) for the Ziegler-Nichols settings gave L_{cm}^{max} = 9.30 dB. However, from Table 7.11, the multivariable closed-loop tuning criterion would be satisfied by reducing L_{cm}^{max} to +4 dB, for a 2x2 system. Hence, F was increased from unity to detune the SISO controllers, as illustrated in Figure 7.16. The stability criterion was satisfied with F = 1.33, for a diagonal controller matrix given by:

$$B(s) = \begin{bmatrix} 0.03\left(1 + \frac{1}{0.173s}\right) & \cdot \\ \cdot & 0.03\left(1 + \frac{1}{0.044s}\right) \end{bmatrix}$$

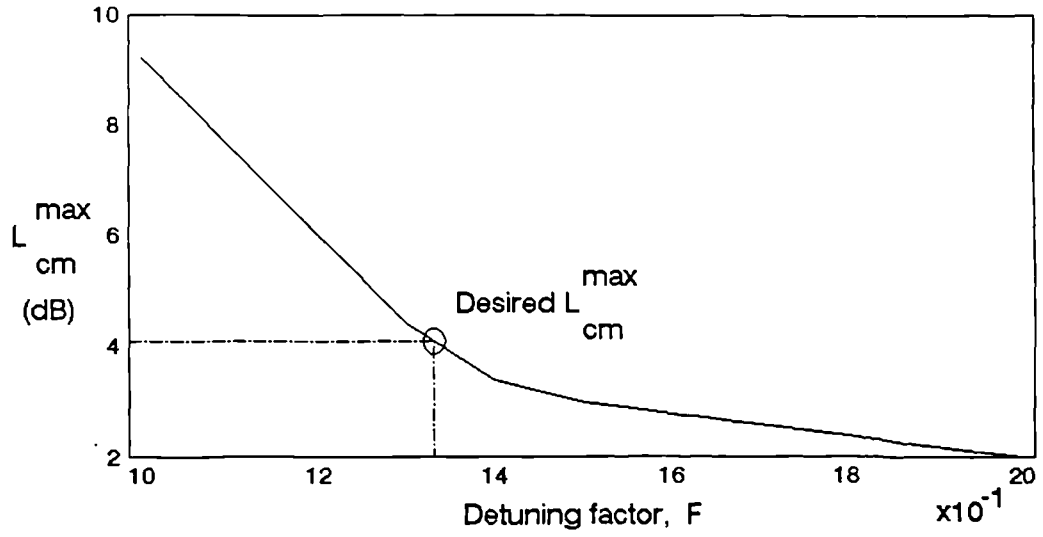

Figure 7.16 Effect of detuning factor F on L_{cm}^{max}

Equal importance was assumed for both control loops. However, as drum pressure required tighter control, controller weighting was introduced to the BLT method, by assigning an independent detuning factor for each controller, F_1 and F_2. Two conditions were considered, and the results are summarised in Table 7.12.

The above PI controller settings were assessed by introducing a series of step disturbances to the non-linear flash unit model. The corresponding ACSL responses in Figure 7.17 showed that upgrading B_1 at the expense of B_2 gave a better performance, as the initial pressure kick was reduced and easily maintained within tight limits. The recommended controller settings for the flash unit are listed in Table 7.13, with reverse acting pressure and level controllers.

PI Controller Settings	Degree of Controller Weighting		
	Equal Weighting	Detune B_2 only	Upgrade B_1 Detune B_2
Pressure Control			
$F_{B_1^1}$	1.33	1.00	0.50
K_{c1}	0.030	0.040	0.080
τ_{I1}	0.1729	0.1300	0.0650
Temperature Control			
$F_{B_2^2}$	1.33	1.36	1.50
K_{c2}	0.030	0.0294	0.0267
τ_{I2}	0.0439	0.0449	0.0495

Table 7.12 PI controller settings for the 2x2 flash unit system

Controller	K_c	τ_I
Pressure	0.080	0.0650
Temperature	0.0267	0.0495
Level	3.0	---

Table 7.13 Controller settings for the flash unit

7.5.3.4 *Concluding Remarks on BLT Tuning for the Flash Unit*

The control structure for the 3x3 flash unit multivariable system was simplified to a multiloop SISO control system. The BLT method was selected for controller tuning as it was based on the classical Ziegler-Nichols SISO tuning method and was relatively easy to apply. The method was further simplified by initially tuning the level controller separately, by trial-and-error. This reduced the plant to a 2x2 multivariable system, with level control active.

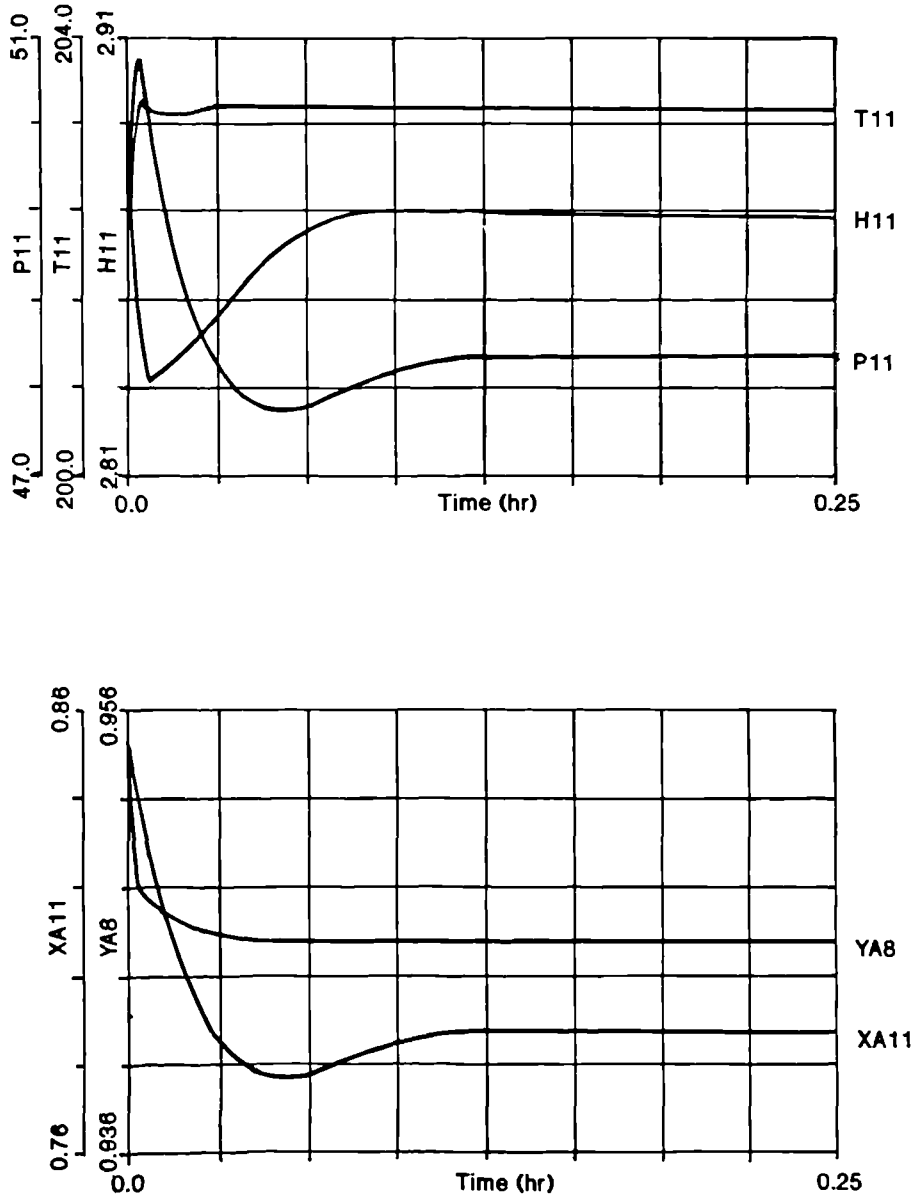

Figure 7.17 Closed-loop response of flash unit

(a) Original Ziegler-Nichols settings

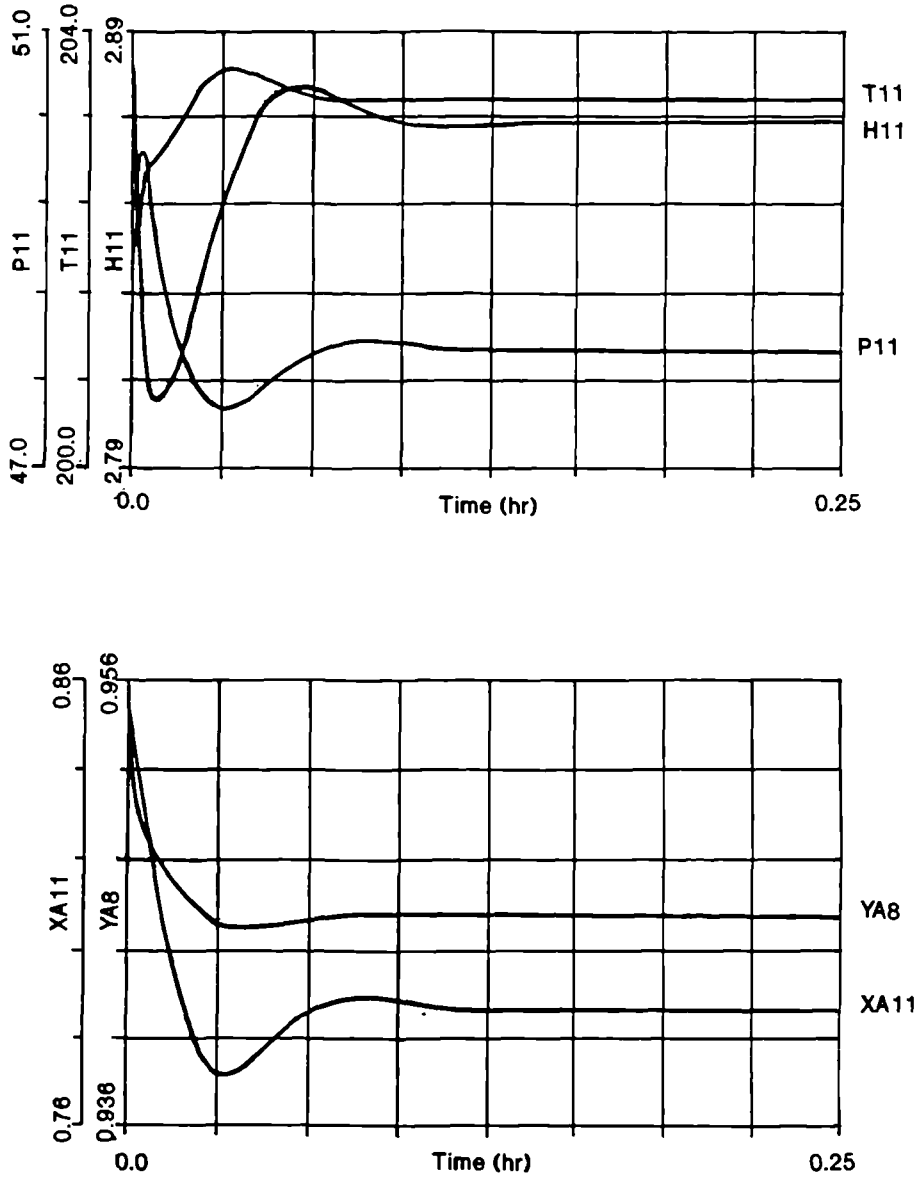

Figure 7.17 Closed-loop response of flash unit (contd.)
(b) Detuned BLT settings

The original BLT method of equal weighting on both control loops was unsatisfactory as tight pressure control was essential for the flash unit. Hence, selective controller weighting was applied to further detune the temperature controller. This allowed a suitable combination of non-adaptive PI controller settings to be derived for the GL2Z feedstock condition.

It should be noted that significant nonlinearities existed in the system, and the linearised data represented approximations about a single operating point. Thus, if the controller design had been initiated about another operating point, different controller settings probably would have resulted. However, as the time constants for the open-loop transfer functions were similar, this suggested that reasonably good values were obtained for the controller settings (Luyben, 1986).

The BLT tuning method was recommended as a benchmark for comparing multivariable controller performance (Luyben, 1986). Thus, the next step in the multiloop SISO controller tuning would be to consider introducing derivative action to the temperature controller (Monica et al., 1988). However, it should be noted that this may adversely affect the pressure response and introduce the need for decoupling.

7.5.4 Multivariable System Tuning Considerations for the Distillation Column

Most process identification techniques in the literature are based on open-loop systems, or lead directly to self-tuning control design from a closed-loop assessment. Closed-loop response data has been used to estimate parameters in a simple process model (Yuwana and Seborg, 1982) but the application has been confined to SISO systems.

The distillation column represents a multivariable system with a D-V control loop configuration, as shown in Figure 7.13. As the system was open-loop unstable, its open-loop steady state gains for the interaction analysis in Section 7.4.4 were obtained indirectly from closed-loop results.

Open-loop instability may be overcome by interpreting the existing

closed-loop control configuration as a new *open-loop* condition, and replacing the controllers with proportional action only. Then, to remove set point offset, outer control loops would be introduced with integral action. This would effectively give cascade control, with proportional control on each inner loop and PI control on the outer loops. The proposed control structure is illustrated in Figure 7.18. With this arrangement, the outer control loops may be disabled, leaving a stable *open-loop* system. This would allow conventional process identification to be conducted on the *open-loop* system.

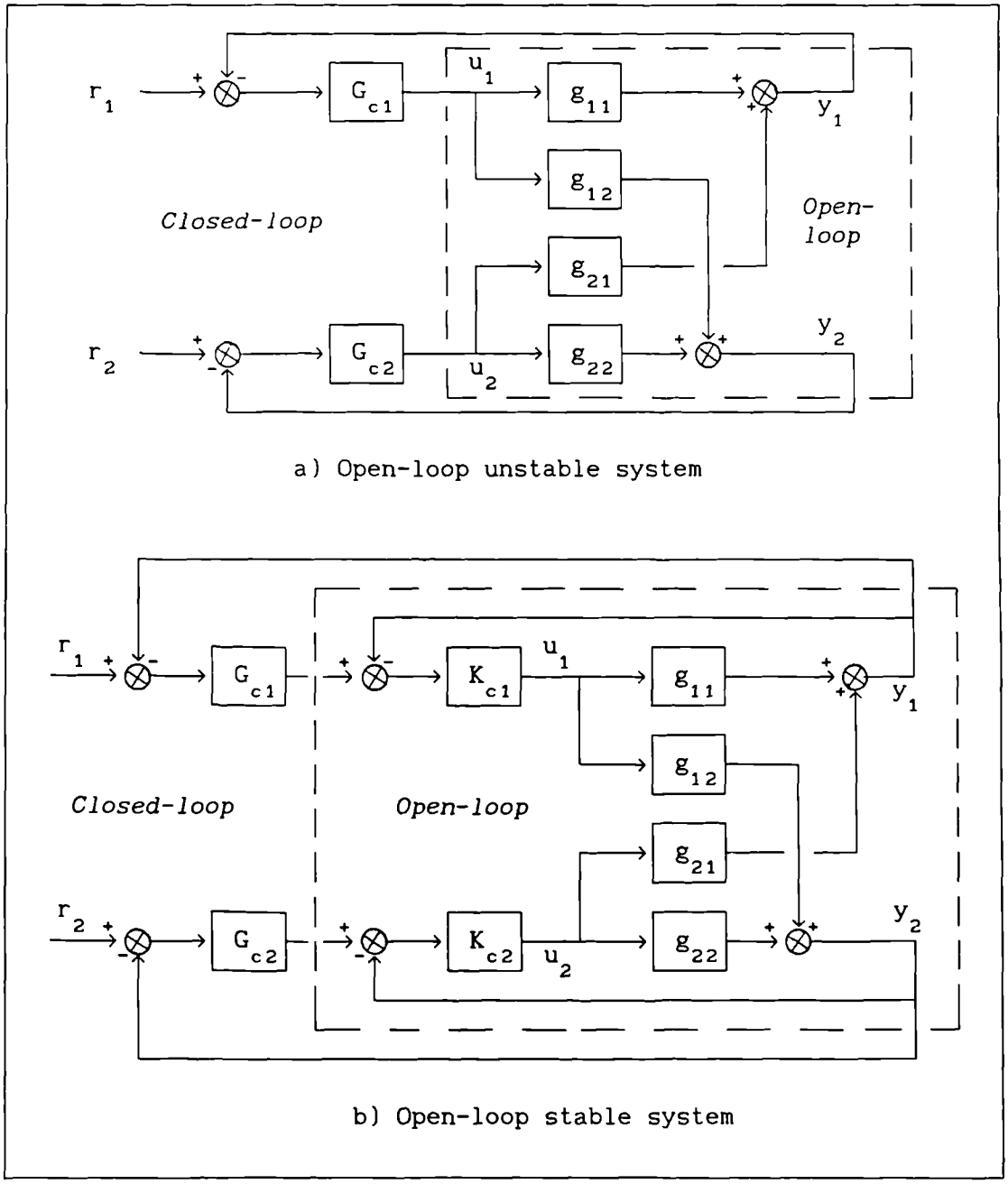

Figure 7.18 Proposed control loop structure for distillation column

Initial tests have been conducted on this system. The resulting open-loop step responses for the diagonal elements of G(s) were simply represented by a first-order plus dead time transfer function. However, step responses for the off-diagonal elements were oscillatory with small steady state gains, due to the proportional controller action. This response would be represented by:

$$g_{ij} = \frac{Ks}{s^2 + \tau_1 s + \tau_2} \quad , \; i \neq j$$

which would make process identification more complicated. If this cascade control arrangement was adopted, the control loop pairing would have to be reassessed, as in Section 7.4.

For the purposes of this study, PI controllers were installed on the D-V loop pairings, and tuned using a trial-and-error approach.

7.5.5 Multivariable Control Loop Tuning Achievements

A multivariable control loop tuning method was successfully applied to the flash unit process. The derivation of the BLT method from SISO tuning enabled controller settings to be directly manipulated and so more readily tuned to satisfy the performance specifications. By prioritising the control loops, the control problem was reduced to a 2×2 system, with a greater weighting placed on the pressure controller. The flexibility of this method was crucial to its success as the flash unit model was inherently non-linear.

The recommended control loop pairings for the distillation column in Section 7.4.4 resulted in an open-loop unstable system. This highlighted the disparity between linear control techniques and the processes they control. As conventional process identification methods were not appropriate, some form of on-line self-tuning would have to be considered in further studies. Thus, the controller settings were derived by trial-and-error.

7.6 PLANTWIDE CONTROL

The regulatory control loop designs for individual units were derived and tuned for SISO, multiloop and multivariable systems. These are illustrated in the LNG terminal flowsheet in Figure 6.8. In each case, the processes were considered individually and designed without considering interaction with neighbouring units. However, each controller will ultimately be acting as part of a team of controllers, either within a larger process, or directly affecting the overall operation of the flowsheet. Hence, these implications should also be addressed on a plantwide scale, where the performance of each controller is assessed in the plant environment.

The plantwide scenario considers control development from the regulatory to supervisory control system domain, and is concerned with the overall performance of the flowsheet, during both steady state and feedstock changeover conditions. The role of a supervisory control system in the LNG reception terminal is addressed at the beginning of this section.

This section is devoted to formulating a supervisory control system by considering overall plant performance and the implications of feedstock changeover on:

(i) Regulatory controller performance.
(ii) A changeover mechanism for each feedstock condition.
(iii) Supervisory control issues.

7.6.1 Supervisory Control System

A supervisory control system is used to optimise the plant performance by coordinating the activities of processes and individual control loops. The function of the supervisory control computer is to gather plant data, and periodically instruct set point changes. The use of computer systems for on-line process control has gained wide acceptance. This is reflected by the number of generalised supervisory control software packages on the market (Tsai et al., 1986). Consequently, supervisory control systems have become more accessible and easier to implement.

In this study, a supervisory control system would be required to maintain plant performance during two different operating conditions; steady state operation for multiple operating conditions, and intermediate conditions during feedstock changeover.

7.6.1.1 *Overall Plant Sensitivity*

A major requirement of a supervisory control system will be to maintain product specifications. Hence, two effects on the product conditions need investigating:

(i) Corrective action required when product specifications are not being attained - trouble shooting strategy.

(ii) The effect of changing operating conditions.

This would constitute a *cause and effect* sensitivity analysis, whereby key controllers are manipulated to achieve the desired product. The most effective manipulated variables in the regulatory control structure are the split ratio at S-01 (which directly varies the processed and unprocessed stream flow rates) and the LNG feed flow rate.

7.6.1.2 *Supervisory Control Requirements*

It is anticipated that the feedstock changeover would be a gradual process whereby a new feedstock is introduced as another LNG storage tank is brought on-stream. A pseudo-step change would probably only occur during emergency conditions.

For the purposes of a supervisory control system, set points and controller settings need to be identified for each operating condition. Then, a mechanism can be developed to change set points and controller parameters as the feedstock changes. Subgroups of units may be identified from a database of settings. Hence, controller scheduling should consider:

(i) The timing of each event.

(ii) The changeover mechanism, i.e. schedule, ramp or on-line adaptation.

Supervisory control algorithm

An algorithm would need to be developed in the final stages of a supervisory control assessment to identify the key objectives and

functions of the plant, and to provide a structured programme of events. The main items in this algorithm would be to:

(i) Identify set point and controller setting changes.

(ii) Define a timing mechanism for changeover of units.

(iii) Select appropriate supervisory control methods - material and energy balance control and comparison with relevant industrial applications.

(iv) Supply supervisory actions during steady state condition - split ratio control.

(v) Supply supervisory actions to enable feedstock changeover - calculation procedure for new set points and controller settings, algorithm for timing mechanism.

(vi) Contain a hierarchy of levels for the plant operation, illustrated in Figure 7.19, which considers:

. Individual operations and their regulators within a *Process Actuator-Sensor Level*

. Supervisors dedicated to one or more operations, with a *Supervisor Level.*

. An upper level concerned with plant scheduling for the intermediate level supervisors.

7.6.1.3 *Feedstock Changeover*

A major requirement of the supervisory control system would be to maintain product specifications during feedstock changeover, while ensuring safe operation of each unit. The implications of this may be observed during a series of controlled feedstock changeovers, with only regulatory controllers installed. The remainder of this section will concentrate on deriving suitable operating procedures for feedstock changeover scenarios, and analysing the model responses with a view to formulating a higher level control system.

The regulatory controllers for the flowsheet are illustrated in Figure 6.8. The classical control design derived for the heavies processing section has been adopted, as the digital WPC controller restricted simulation practices. The settings for each controller, derived in Chapters 6 and 7, were non-adaptive and hence remained constant for each feedstock condition.

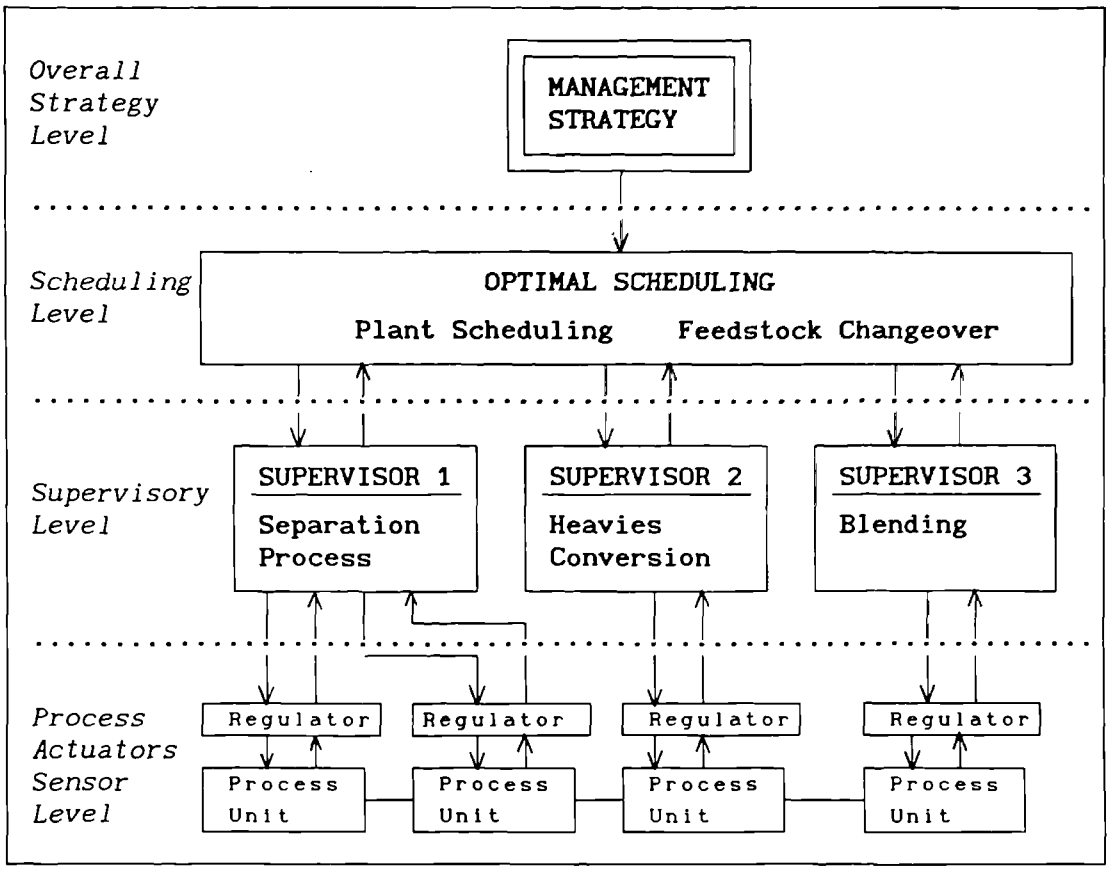

Figure 7.19 Supervisory control hierarchy

7.6.2 Changeover Mechanism

The difference in operating conditions for each feedstock consisted of feed stream component flow rates and set points. These values were obtained directly from steady state simulation results, and are listed in Table 7.14.

The change in feedstock was envisaged as a gradual transition whereby the exit valve from one tank was closed as another opened, when an LNG storage tank emptied. This was simulated by ramping from the initial to final compositions listed in Table 7.14. As a preliminary investigation, the same ramping period was adopted for both the feed and set point values. This simplified changeover mechanism would be ideal if each process experienced the feed changes instantaneously. However, as there are significant delays, the feedstock changeover responses would also show interaction effects between processes.

Settings	LNG Feedstock		
Feed stream component flow rates (kgmol/hr):	GL1K	GL2Z	GL1Z
CH_4	15253.87	14504.03	13691.11
C_2H_6	884.28	931.17	1128.51
C_3H_8	81.88	238.76	405.15
nC_4H_{10}	0.00	55.71	77.61
iC_4H_{10}	32.75	41.39	63.64
nC_5H_{12}	0.00	19.10	1.55
N_2	122.82	127.34	155.23
Set points:			
Split ratio, S-01	0.795	0.873	0.873
Flash unit temperature (K)	198.20	200.33	203.36
Distillation column:			
Feed temperature (K)	185.60	187.54	190.85
Sum of tray temperatures (K)	374.30	415.01	469.82
Difference of tray temperatures (K)	-4.14	-42.94	-93.28
CRG reformer product temperature (K)	677.88	703.15	705.99

Table 7.14 Feedstock changeover conditions

The following feedstock changeovers were investigated:

(i) GL2Z to GL1Z

(ii) GL2Z to GL1K

(iii) GL1Z to GL1K

Each changeover mechanism was developed by trial-and-error, to derive suitable ramping periods and a controlled transition. Various ramping periods were investigated, ranging from 0.1 hr to 1.0 hr.

It was found that a simulation failure would usually originate in the distillation column. A **fast** set point ramp increased the boilup demand and liquid withdrawal from the base of the distillation column. As perfect level control was assumed, this resulted in a negative bottom product flow rate to maintain liquid level. In practice, the column would be flooding. Conversely, a **slow** ramp caused both distillation column controlled variables (sum and

difference of tray temperatures) to differ increasingly from their set point temperatures as the simulation progressed. The increased demand on the top product flow rate reduced reflux to such an extent that the trays in the rectifying section emptied, and flooding would result in the column.

These results suggest that the distillation column was being forced to new operating conditions that could not be easily attained. This was attributed to:

(i) The interaction between the flash unit and distillation column, whereby the upstream feed was dependent on flash conditions.

(ii) The linear variation in set point values during a feedstock changeover, for which there may be no steady state condition.

A presentation and discussion of the ACSL model results follow. A glossary of variable names associated with the ACSL plots is given in Table 4.2, and corresponds to the stream numbering in Figure 4.1.

7.6.2.1 *Medium to Heavy Feedstock Changeover*

The changeover mechanism from GL2Z to GL1Z LNG feedstocks consisted of two ramps, and are defined in Table 7.15. In the first ramp, each variable was moved to its new value in a 1.0 hr period, except the two distillation column set points, which attained 90% of their final values. The second ramp moved the distillation column set points to their final values in 0.5 hr. The ACSL simulation results are presented in Figure 7.20.

The flash unit responses in Figure 7.20 demonstrated how temperature closely tracked its set point over the 1 hr period. The gradual changing conditions gave a 0.2 bar overshoot in drum pressure, which inflected at the ramp end. The proportional controller adequately maintained liquid level, to within 0.03 m. After the first ramp, no further disturbances entered the flash unit, and so the controlled variables moved immediately in the direction of their set points. As a result, the product flow rates inverted to reduce the internal disturbances.

Ramp	*Period* (hr)	**Final Settings**		
		Feed Condition and Set Points	$(T_{T6} + T_{T1})$ *set point* (K)	$(T_{T6} - T_{T1})$ *set point* (K)
I	1.0	GL1Z conditions (in Table 7.14)	464.34	-88.24
II	0.5	Unchanged	469.82	-93.28
Feed Condition and Set Points 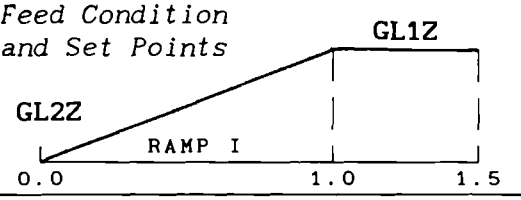			*Distillation Column Set Points* 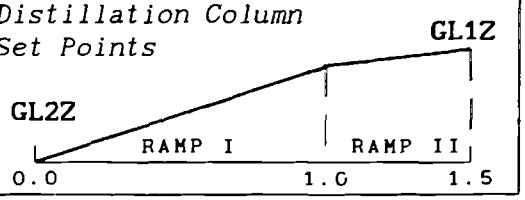	

Table 7.15 Changeover mechanism for GL2Z to GL1Z feedstock condition

Both distillation column controlled variables, TPT6 (sum of tray temperatures) and BMT1 (tray temperatures difference) followed their dual ramp set point profiles in opposite directions. This was because they represented the sum and difference of two tray temperatures that were extracted from a temperature profile table. Thus, if both controlled variables became greater than their set point values (as occurred at the end of the first ramp), any corrective action would be at the expense of one control variable. Hence, introducing a second set point ramp of reduced gradient allowed the controllers sufficient time to remove any offset.

Several quirks originated within the distillation column model that may be attributed to a combination of indirect manipulation of the boilup (via heat to the reboiler), a violation of the model's operating envelope and sub-optimal controller tuning. (This model could be enhanced by incorporating two additional sets of steady state data in the look-up tables, to extend the upper and lower limits of the operating envelope; super-light and super-heavy LNG feedstocks). The variations in distillation column product flow rates, F14 and F21, were reflected downstream. The PI controller on the ORV unit adequately maintained outlet temperature close to its set point of 280.15 K, throughout the changeover, with a deviation of under 1 K. This response demonstrated the disturbance rejection capabilities of the temperature controller.

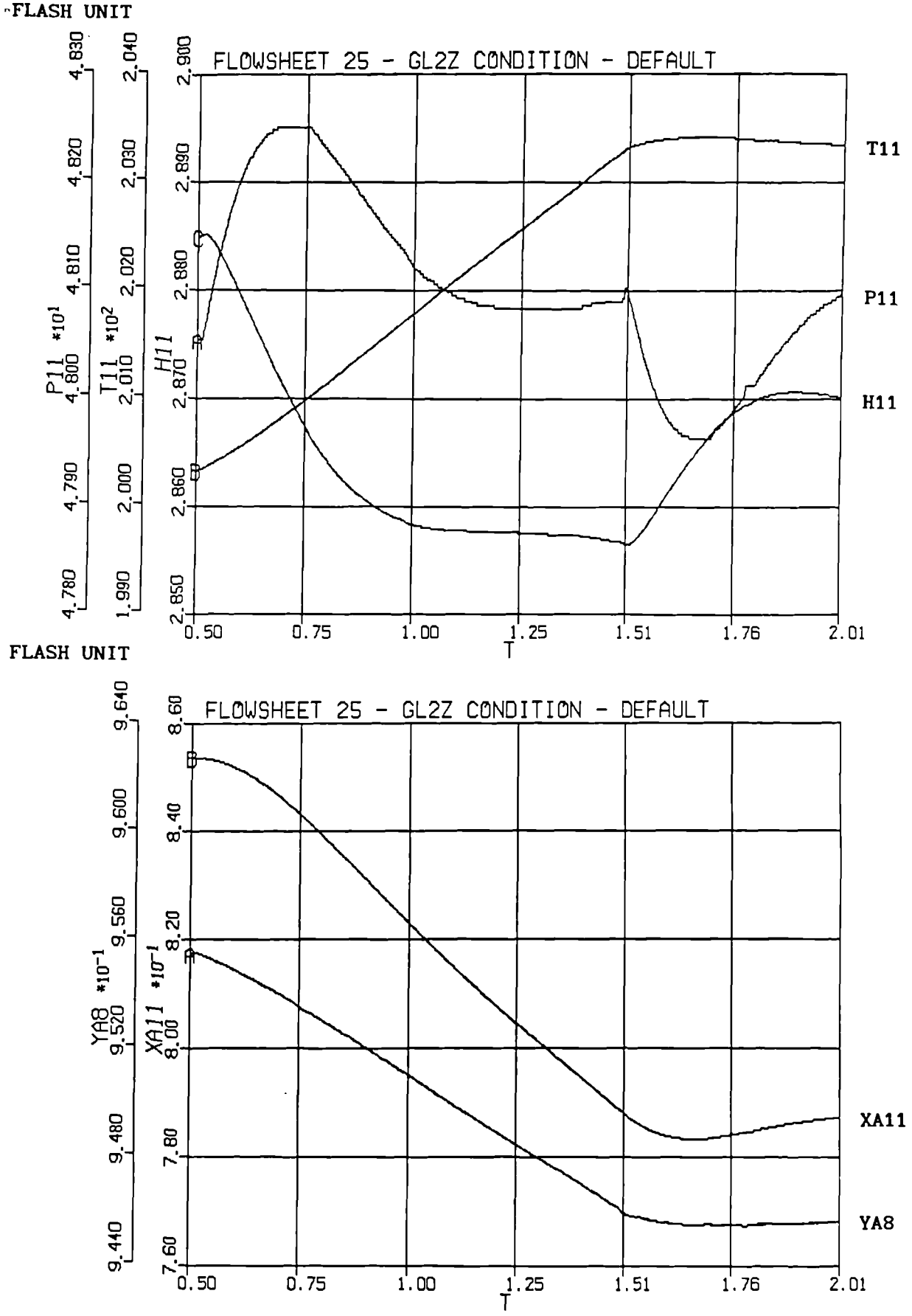

Figure 7.20 Feedstock changeover from GL2Z to GL1Z

FLASH UNIT

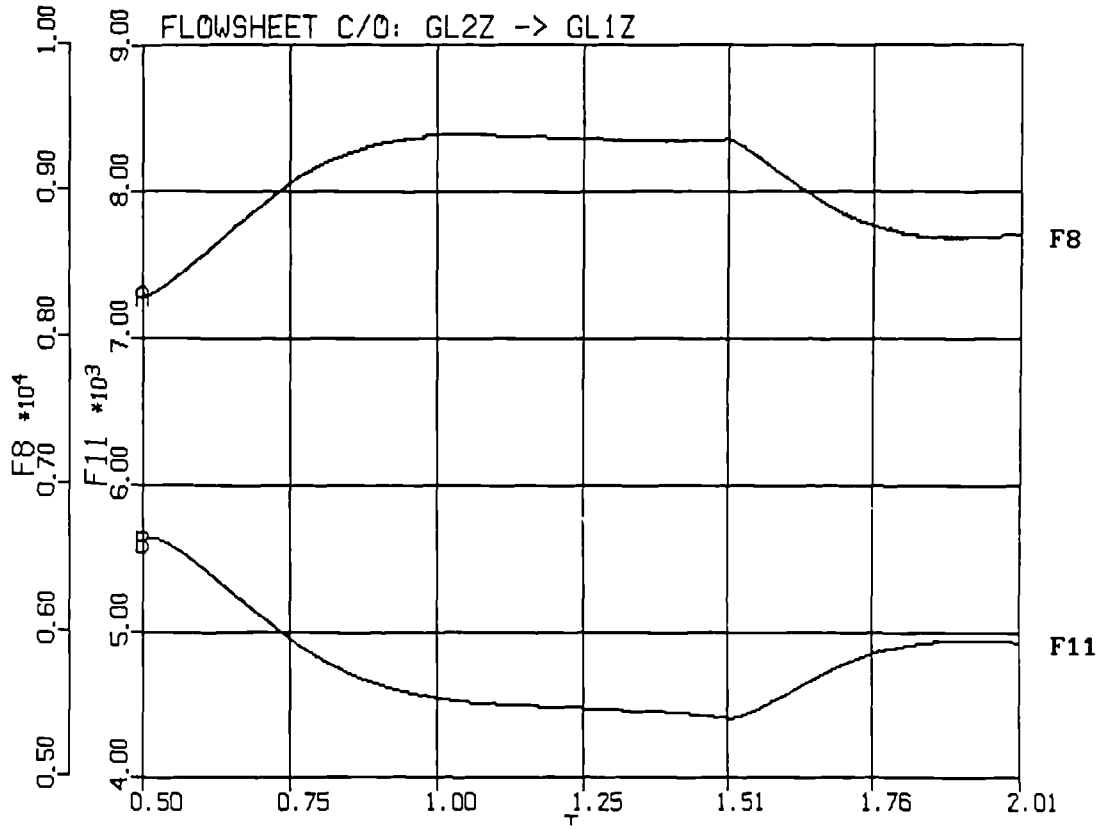

DISTILLATION COLUMN

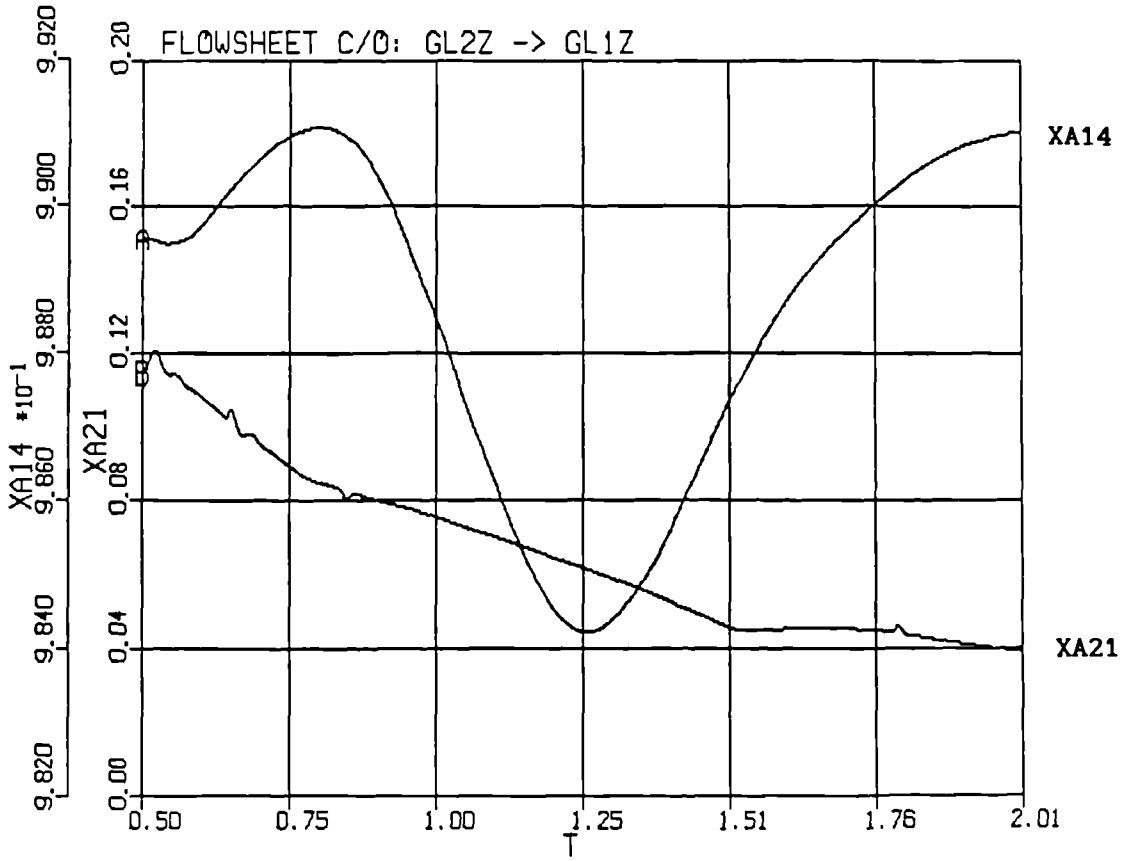

Figure 7.20 Feedstock changeover from GL2Z to GL1Z (contd.)

DISTILLATION COLUMN

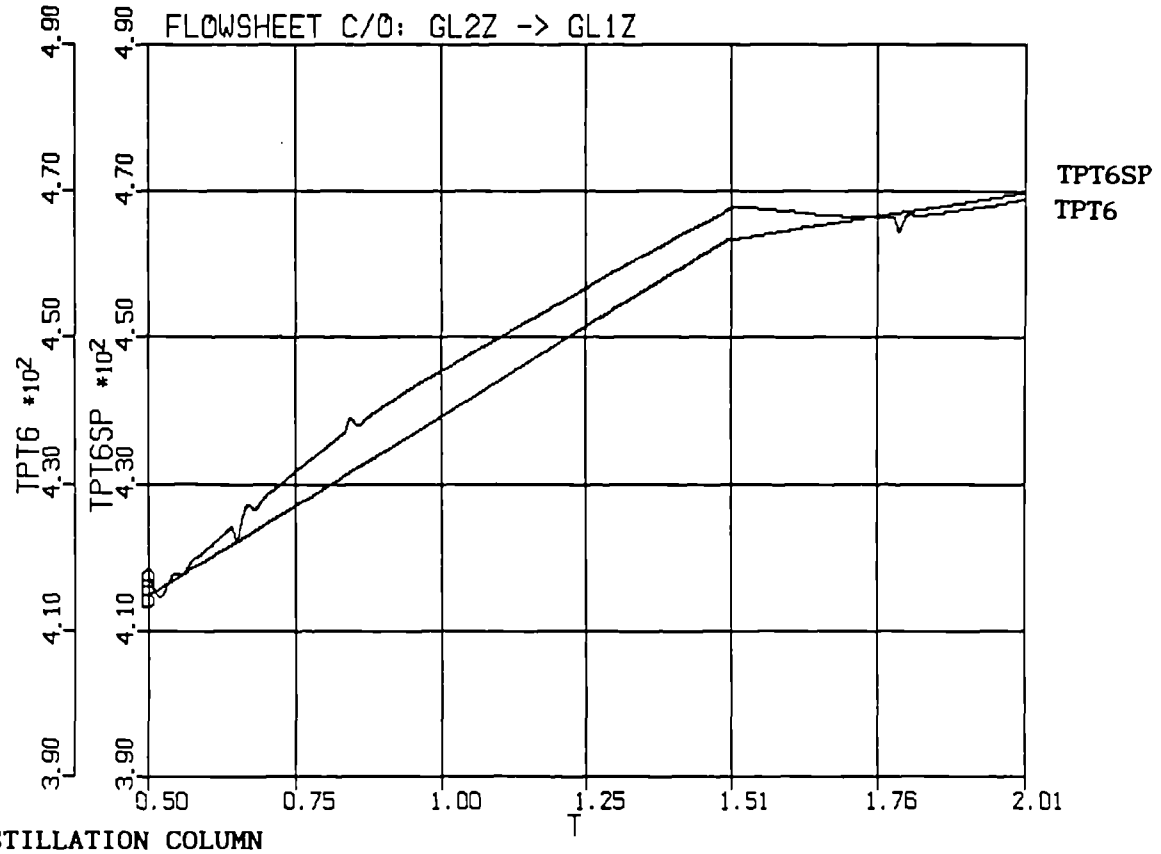

DISTILLATION COLUMN

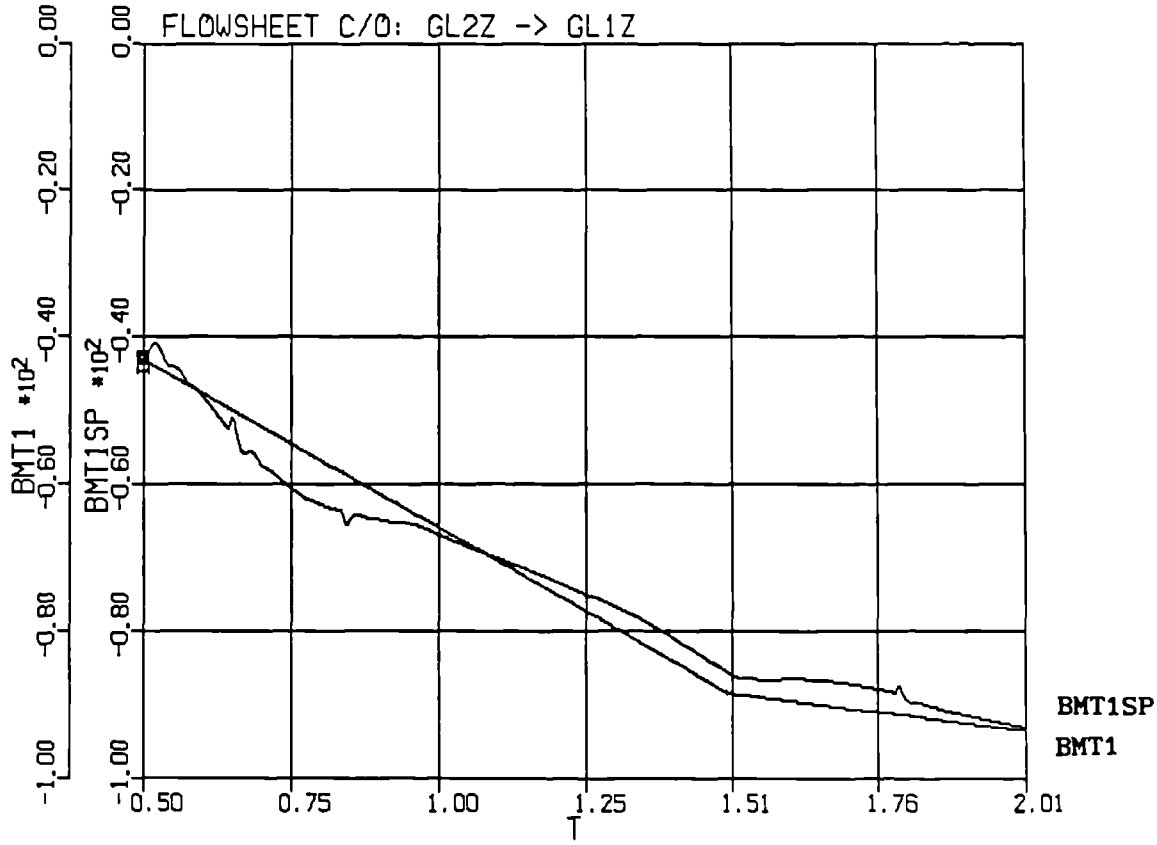

Figure 7.20 Feedstock changeover from GL2Z to GL1Z (contd.)

DISTILLATION COLUMN

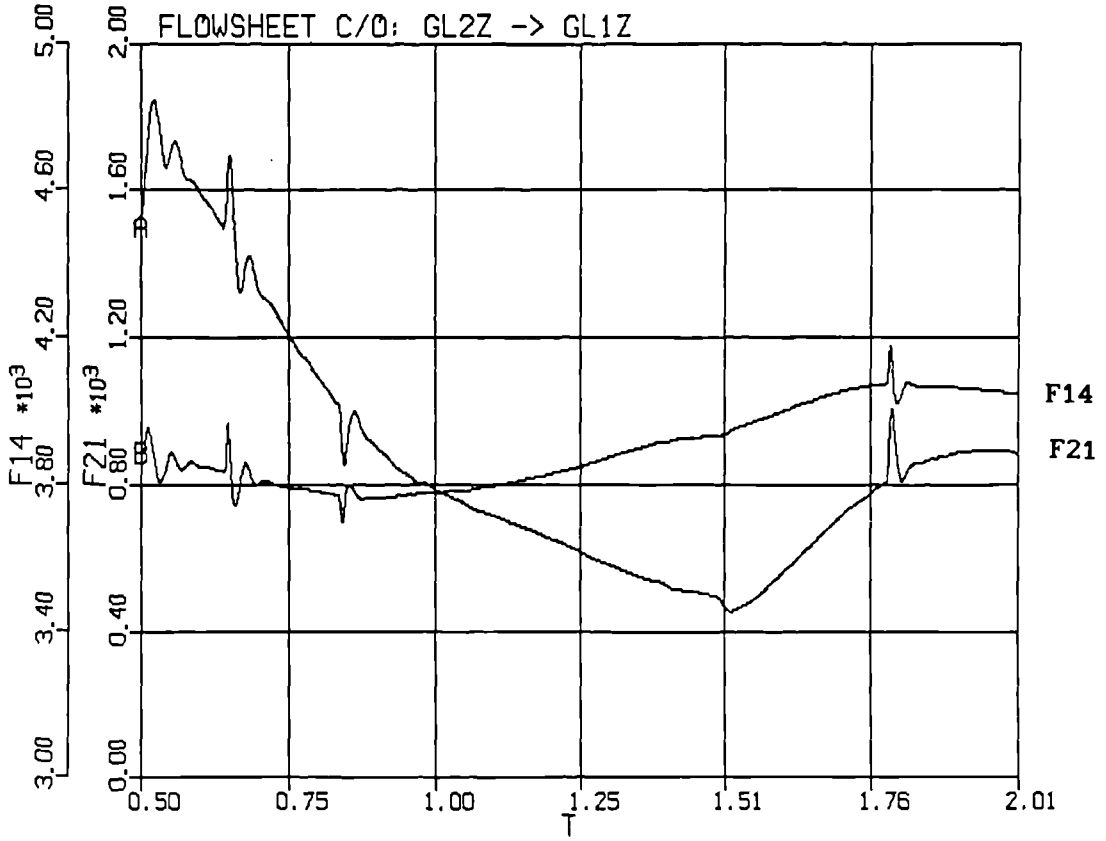

ORV UNIT

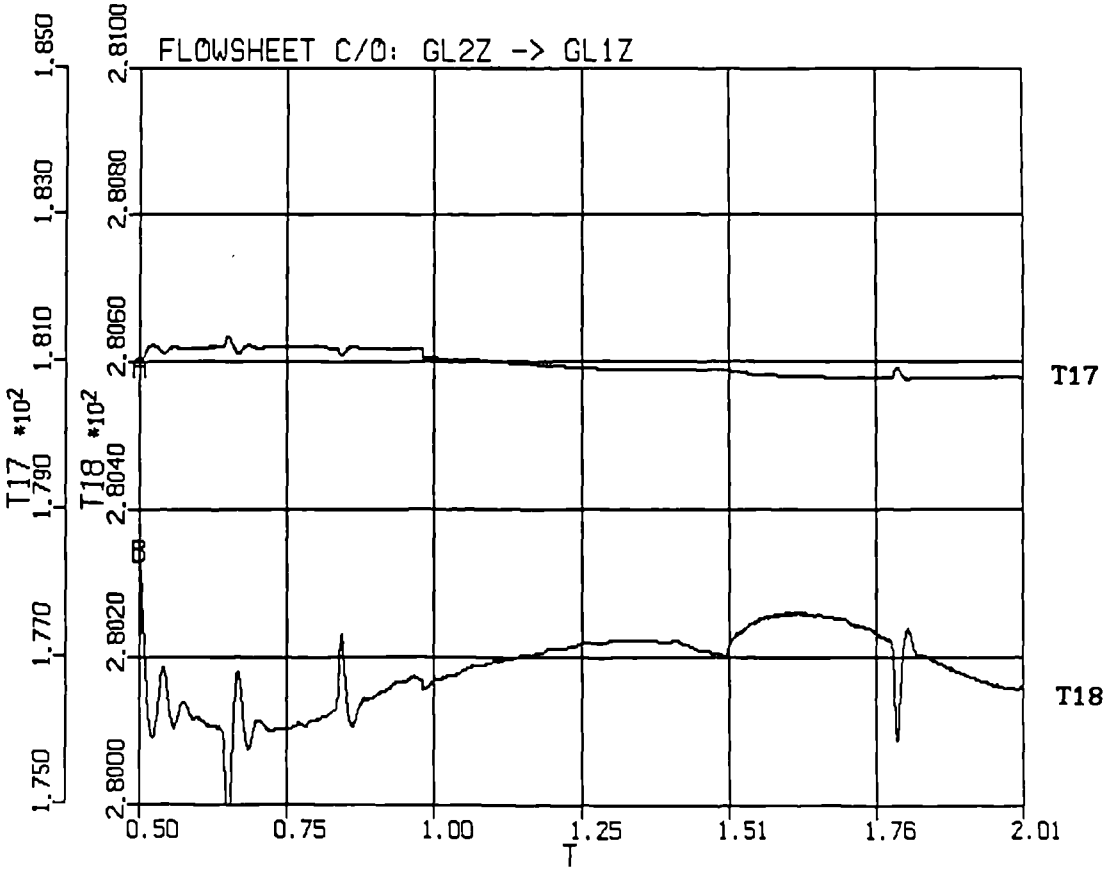

Figure 7.20 Feedstock changeover from GL2Z to GL1Z (contd.)

CRG REFORMER

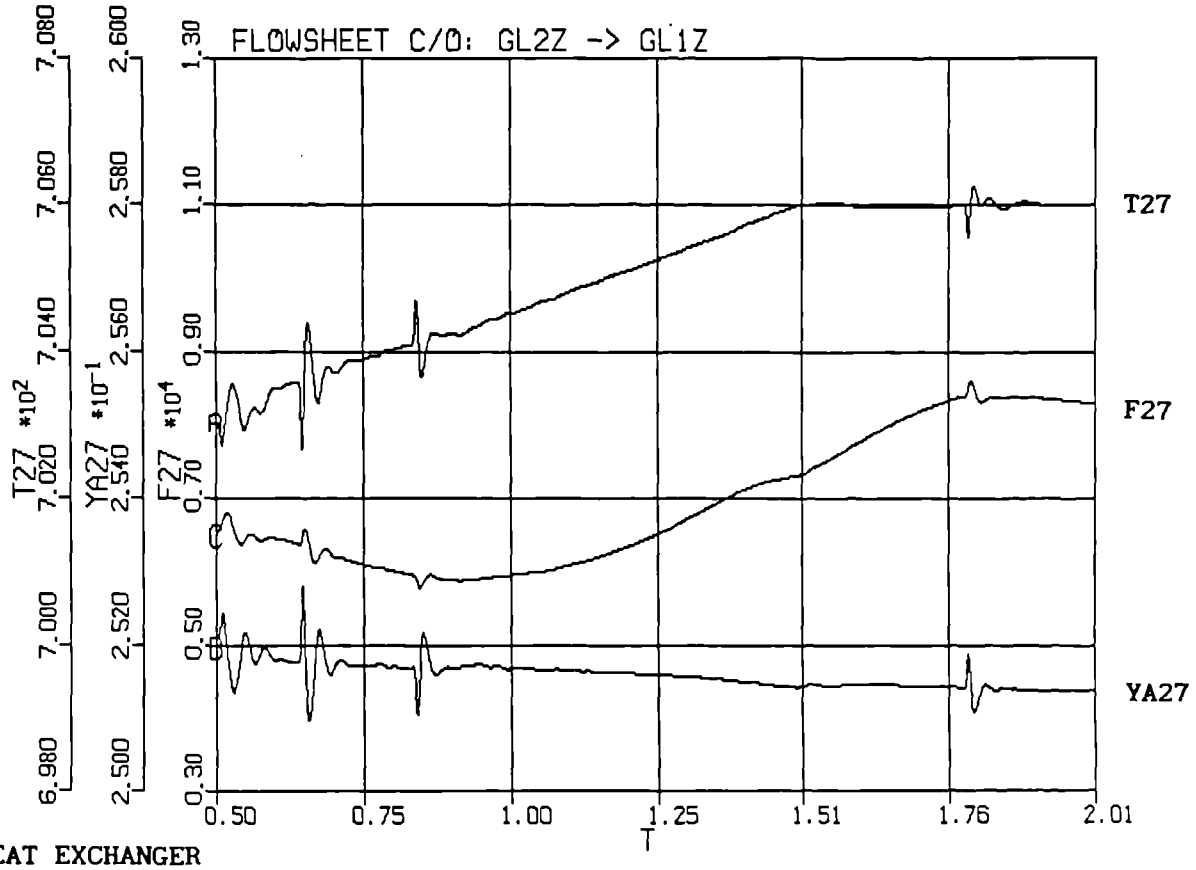

HEAT EXCHANGER

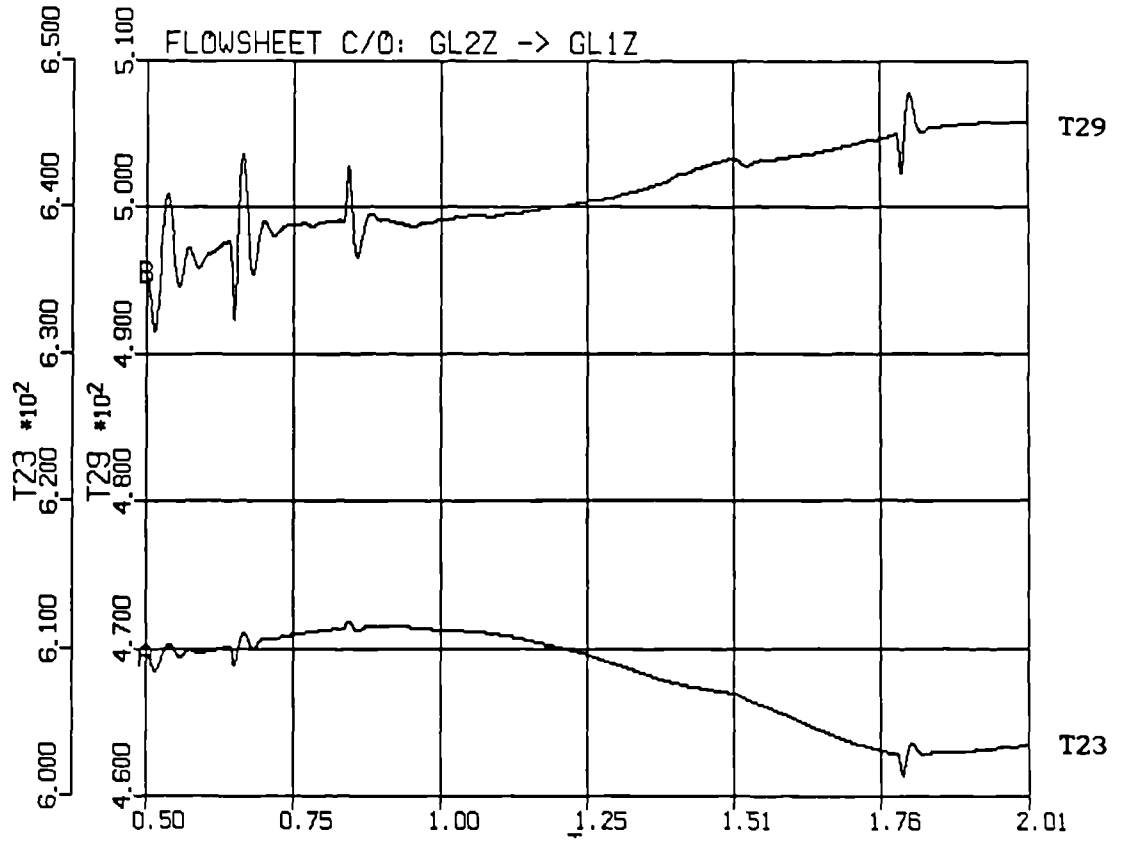

Figure 7.20 Feedstock changeover from GL2Z to GL1Z (contd.)

FIRED HEATER

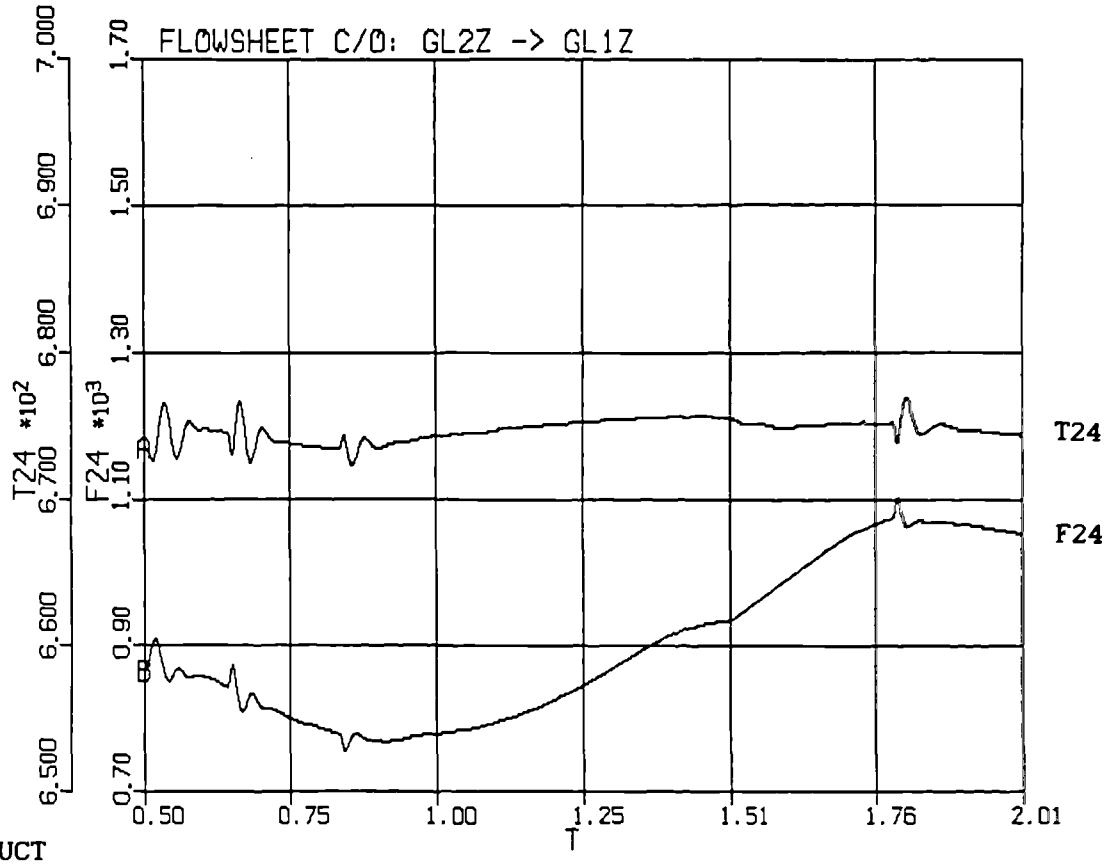

PRODUCT

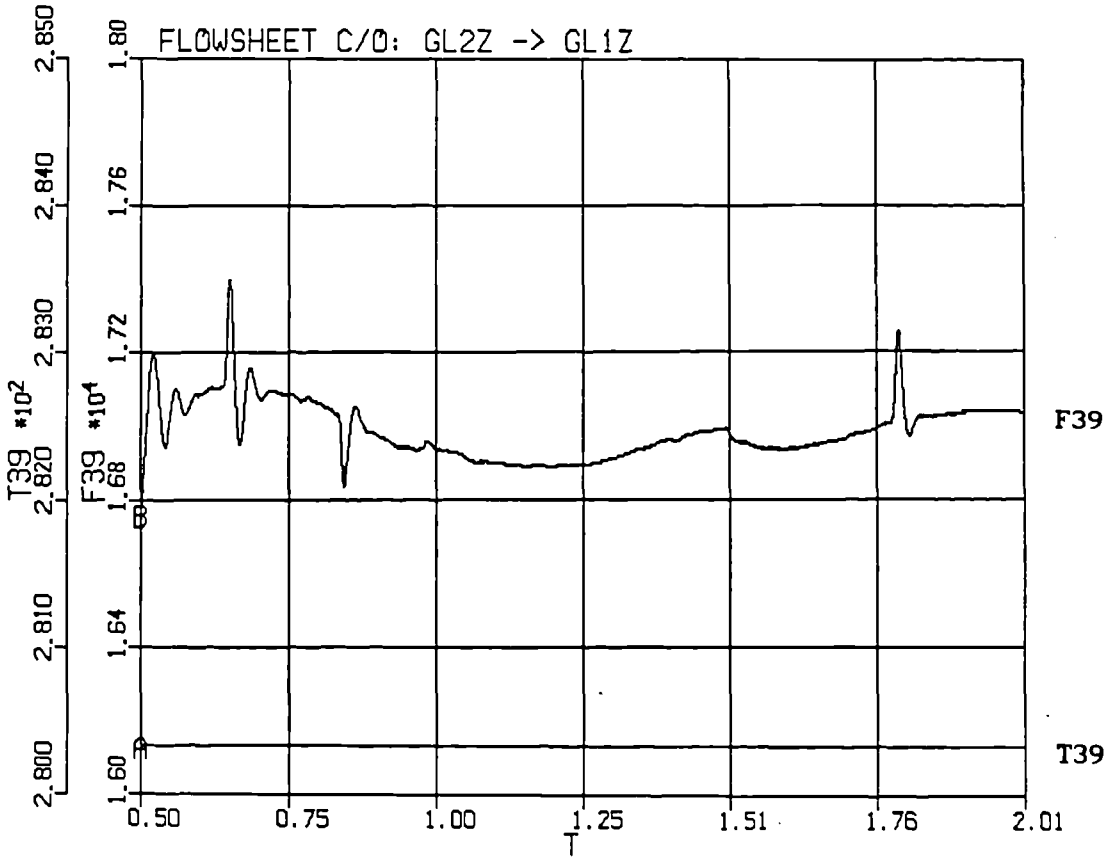

Figure 7.20 Feedstock changeover from GL2Z to GL1Z (contd.)

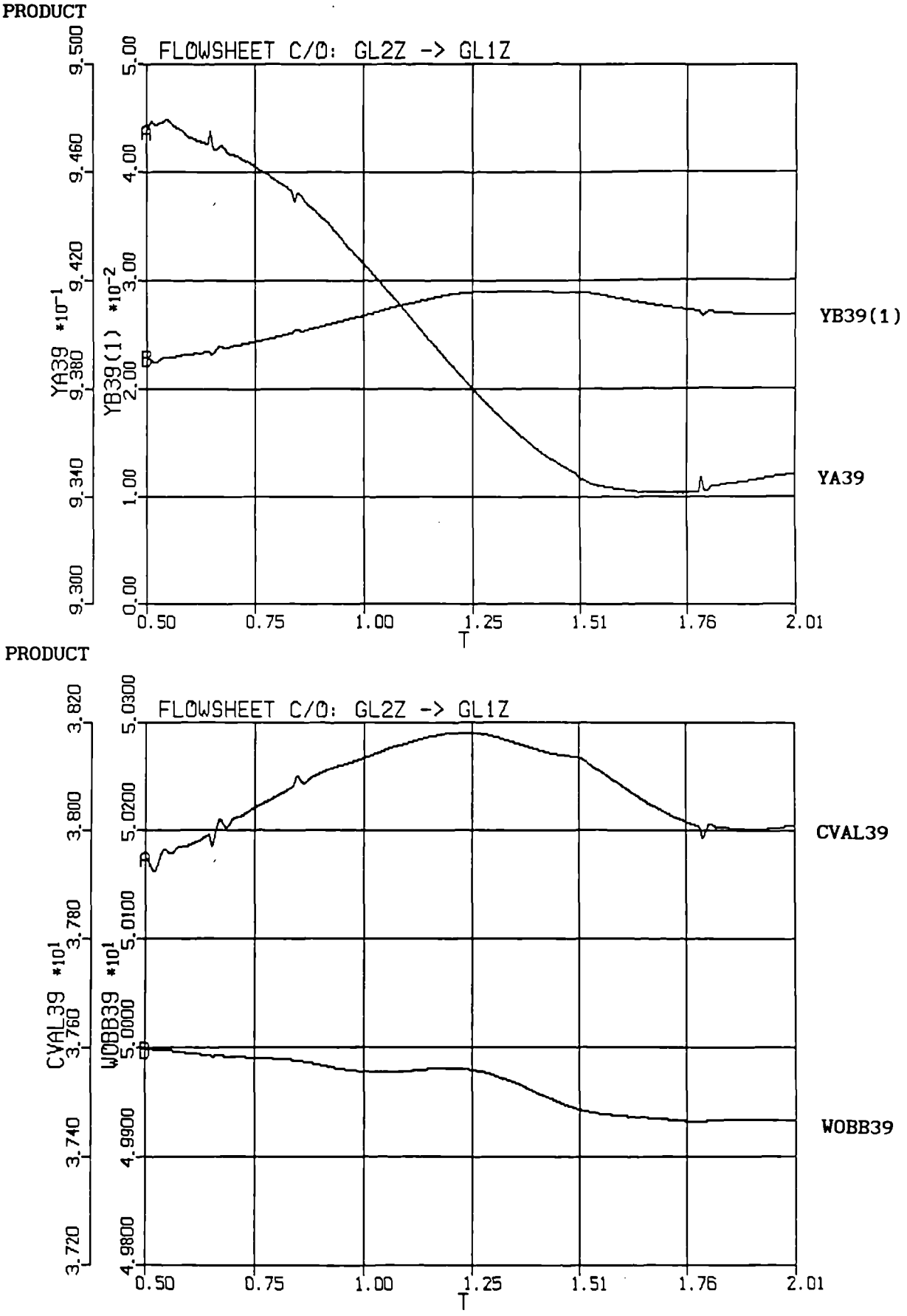

Figure 7.20 Feedstock changeover from GL2Z to GL1Z (contd.)

In the heavies processing section, the set point tracking ability of the cascade control loop was upset by upstream disturbance glitches in flow rate and composition from the distillation column. However, these glitches were dampened in the product flow rate by the addition of steam at a fixed mass flow ratio. Methane composition in the reformer stream remained fairly steady throughout the changeover.

Export gas production, F39, remained within 3% of its target value (approximately 17000 kgmol/hr), with disturbances originating mainly from the distillation column. The steady product stream temperature was attributed to good temperature control in the ORV unit. (Perfect temperature control was assumed on the final heater in the processed stream, H-09). Product composition remained fairly steady throughout, and this was reflected in the combustion characteristics. Calorific value of the export gas, CVAL39, varied by only 0.2 MJ/m^3, while the Wobbe number, WOBB39, steadily reduced by under 0.1 MJ/m^3. After 1.0 hr of simulation, the end of the first ramp had little effect on the export gas quality, compared to the upstream responses.

The overall results for ramped changeover from GL2Z to GL1Z feedstocks were significantly improved on the earlier step change responses in Section 5.4. Gradual ramping of the LNG feedstocks and set points removed initially severe overshoot responses, especially in the product stream. In addition, the previously oscillatory behaviour propagated within the flash unit was eliminated by the multiloop controller tuning method adopted in Section 7.5. Severe product flow rate variations were also avoided in the distillation column, providing a stable and credible operating environment.

7.6.2.2 *Medium to Light Feedstock Changeover*

A single ramping period of 1.0 hr for both feed condition and set points in Table 7.14, gave a successful changeover from GL2Z to GL1K feedstocks. The ACSL simulation results are plotted in Figure 7.21, and include a 1.0 hr settling period after completion of the ramp. Only significant points concerning the results have been noted.

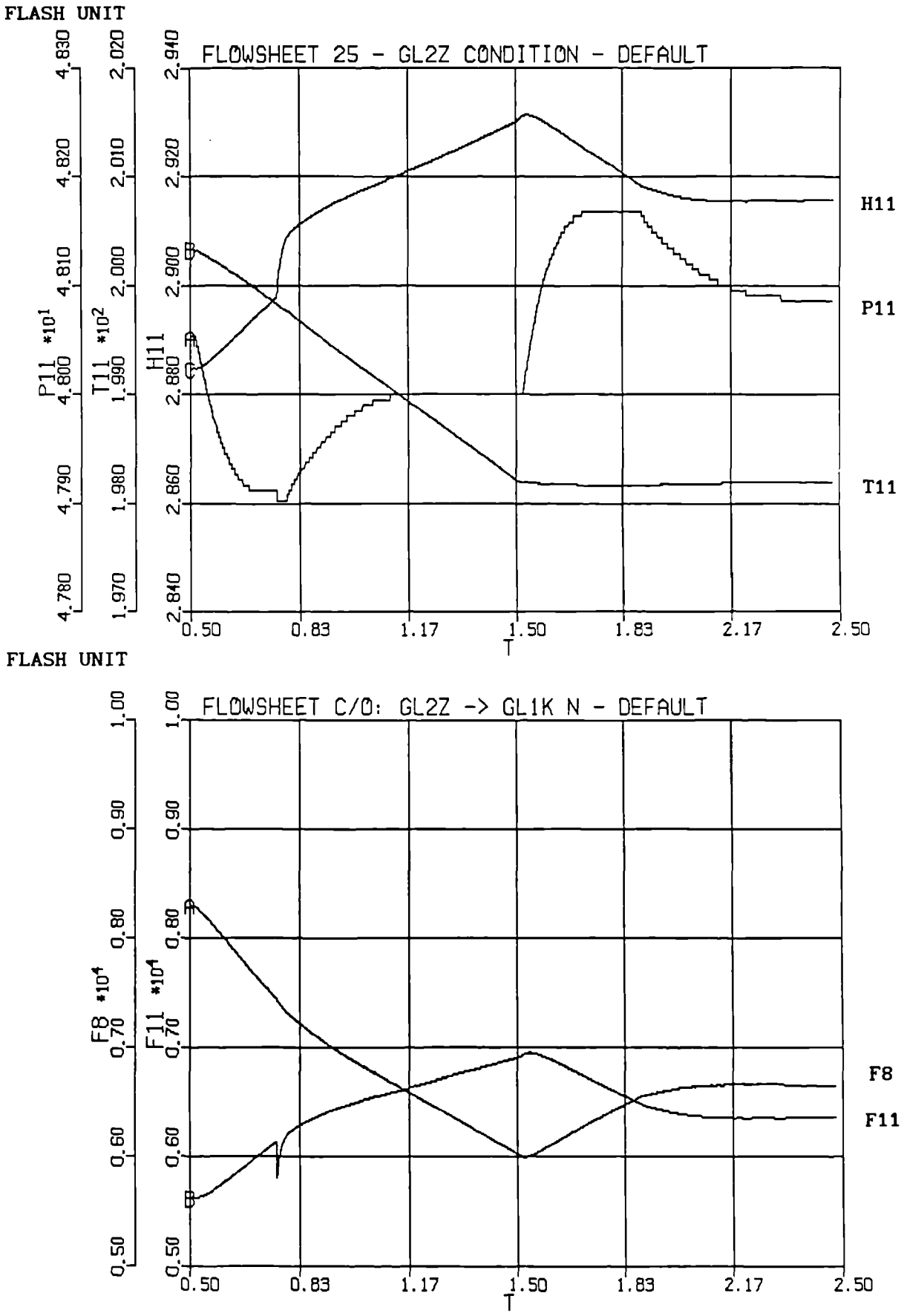

Figure 7.21 Feedstock changeover from GL2Z to GL1K

DISTILLATION COLUMN

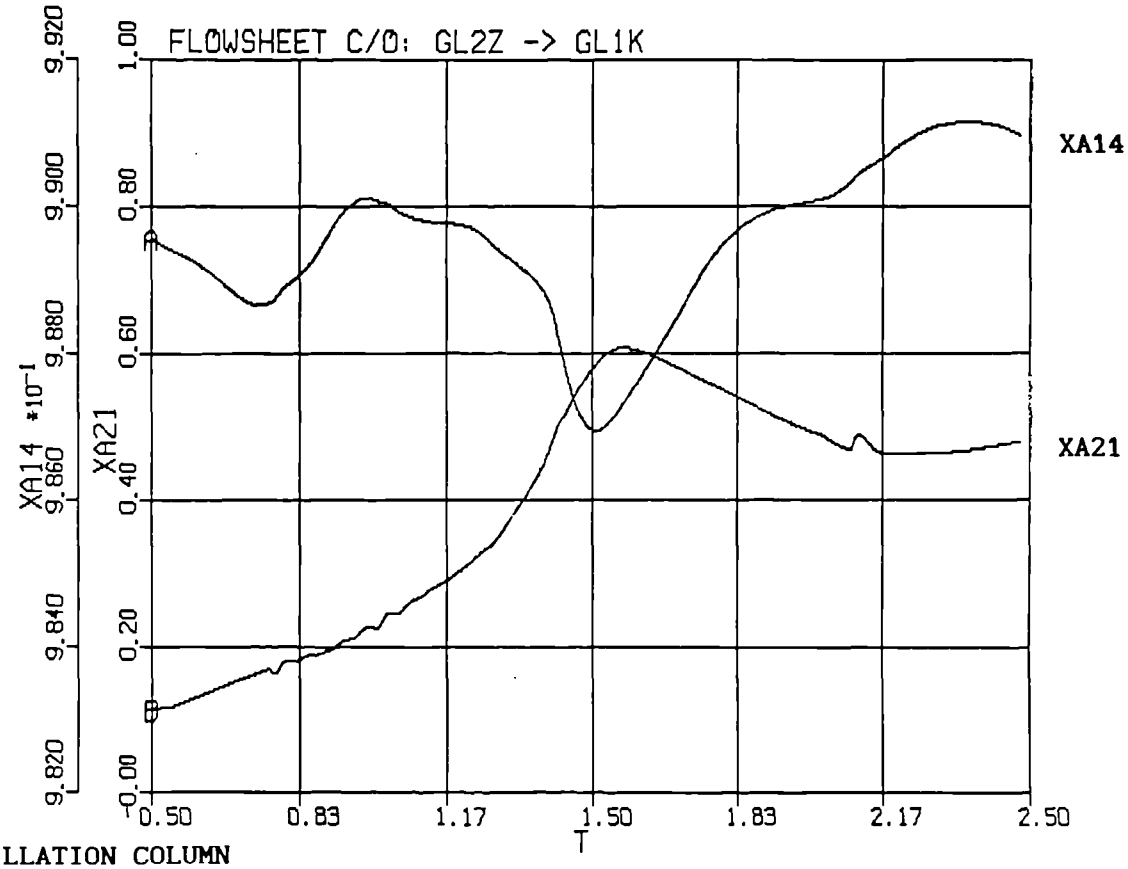

DISTILLATION COLUMN

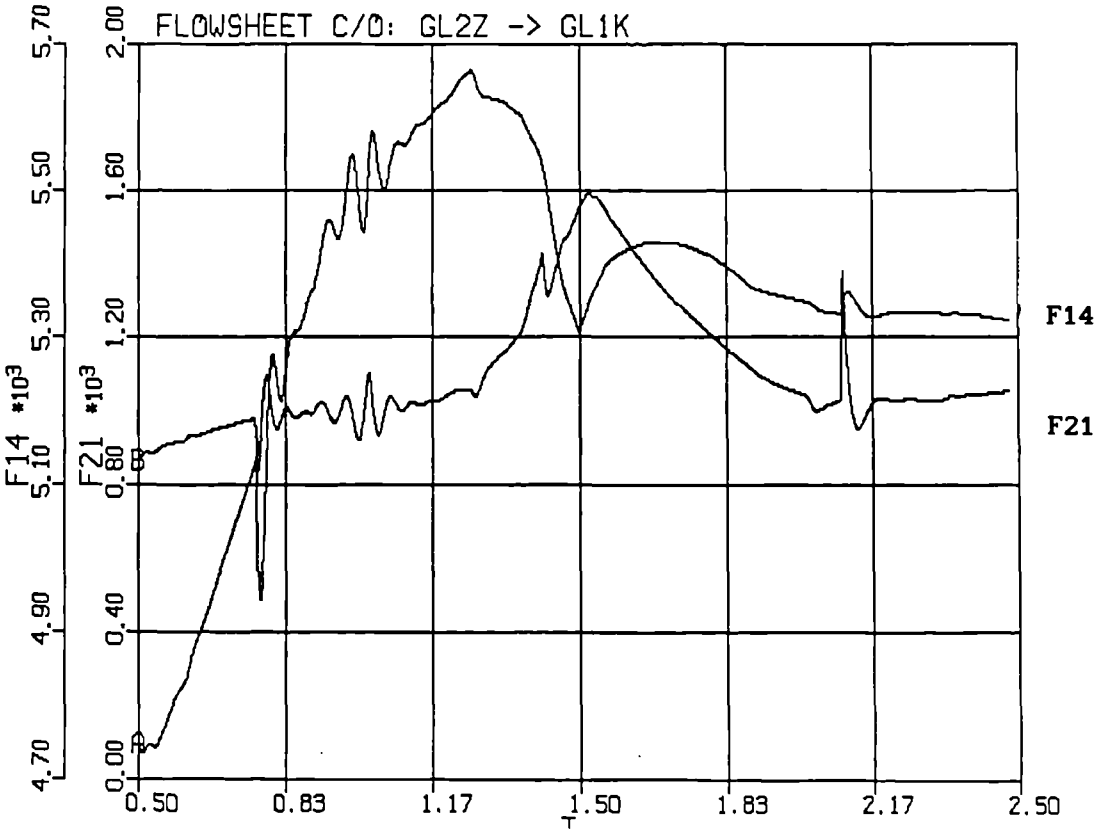

Figure 7.21 Feedstock changeover from GL2Z to GL1K (contd.)

DISTILLATION COLUMN

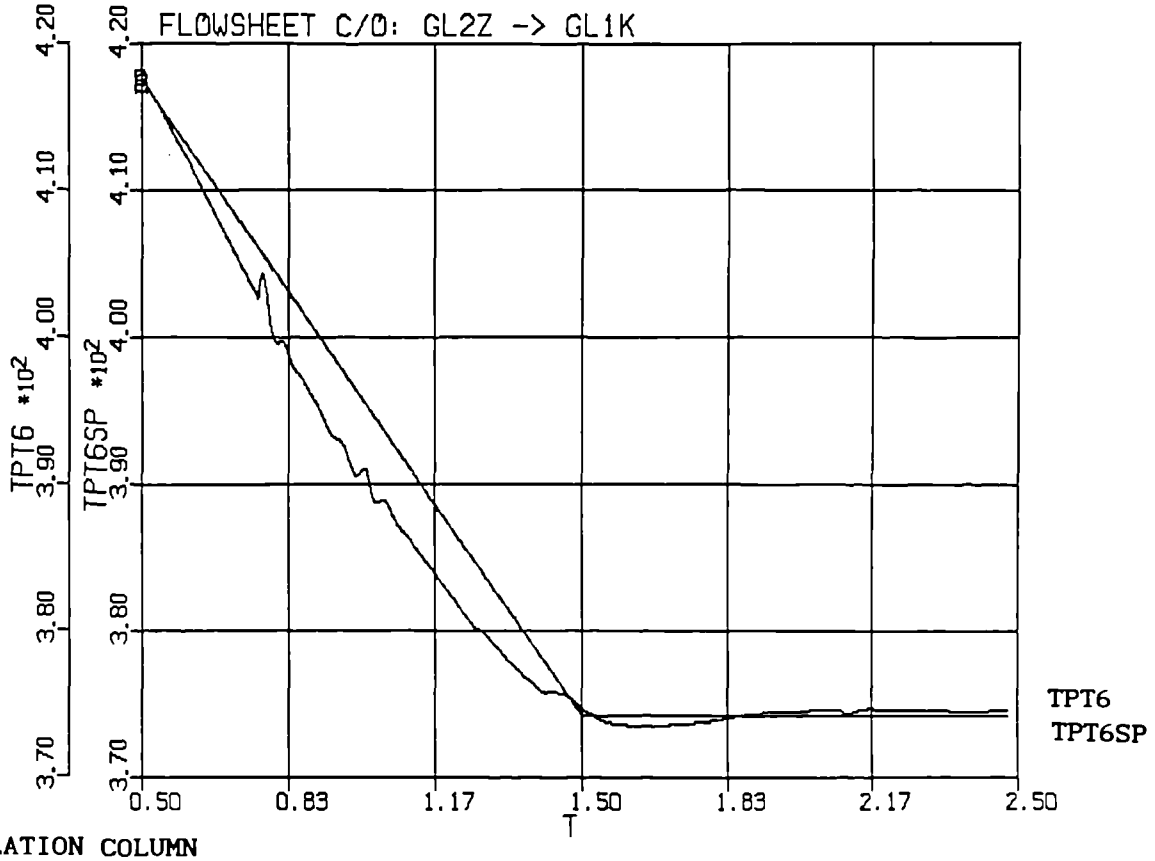

DISTILLATION COLUMN

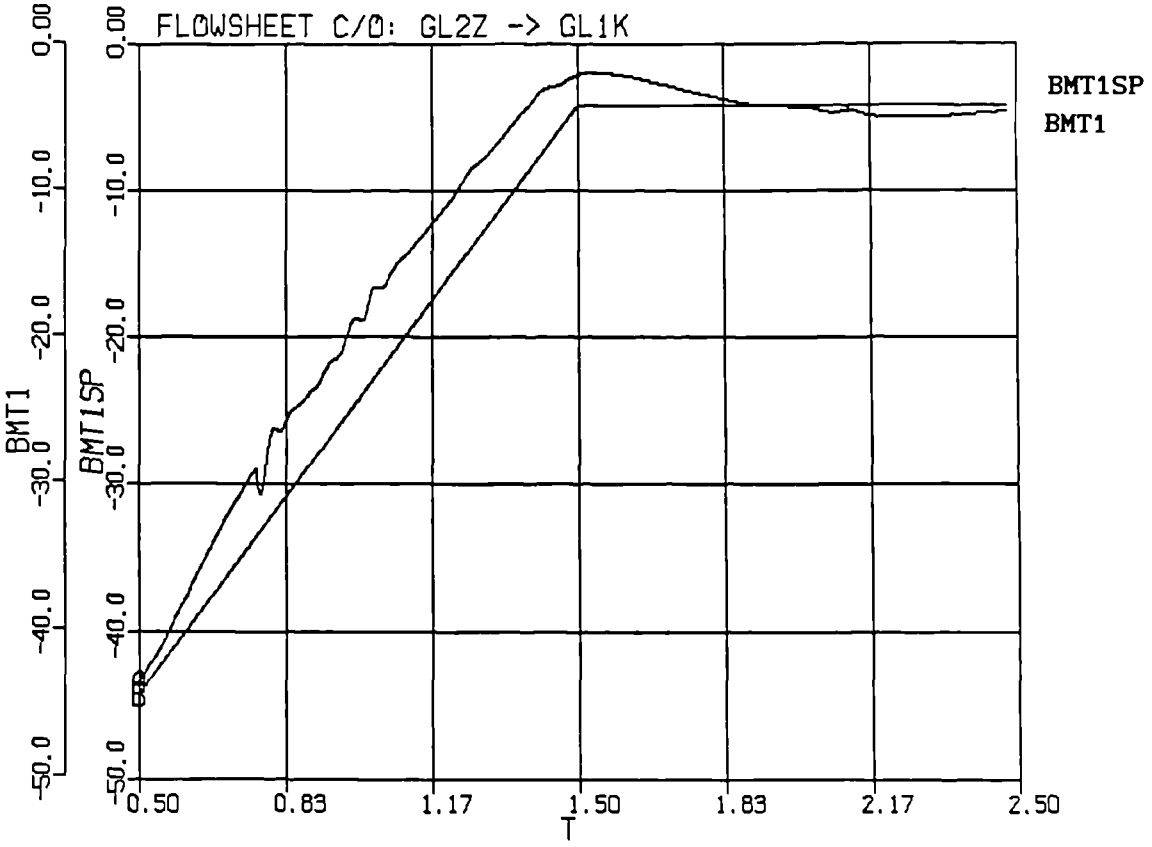

Figure 7.21 Feedstock changeover from GL2Z to GL1K (contd.)

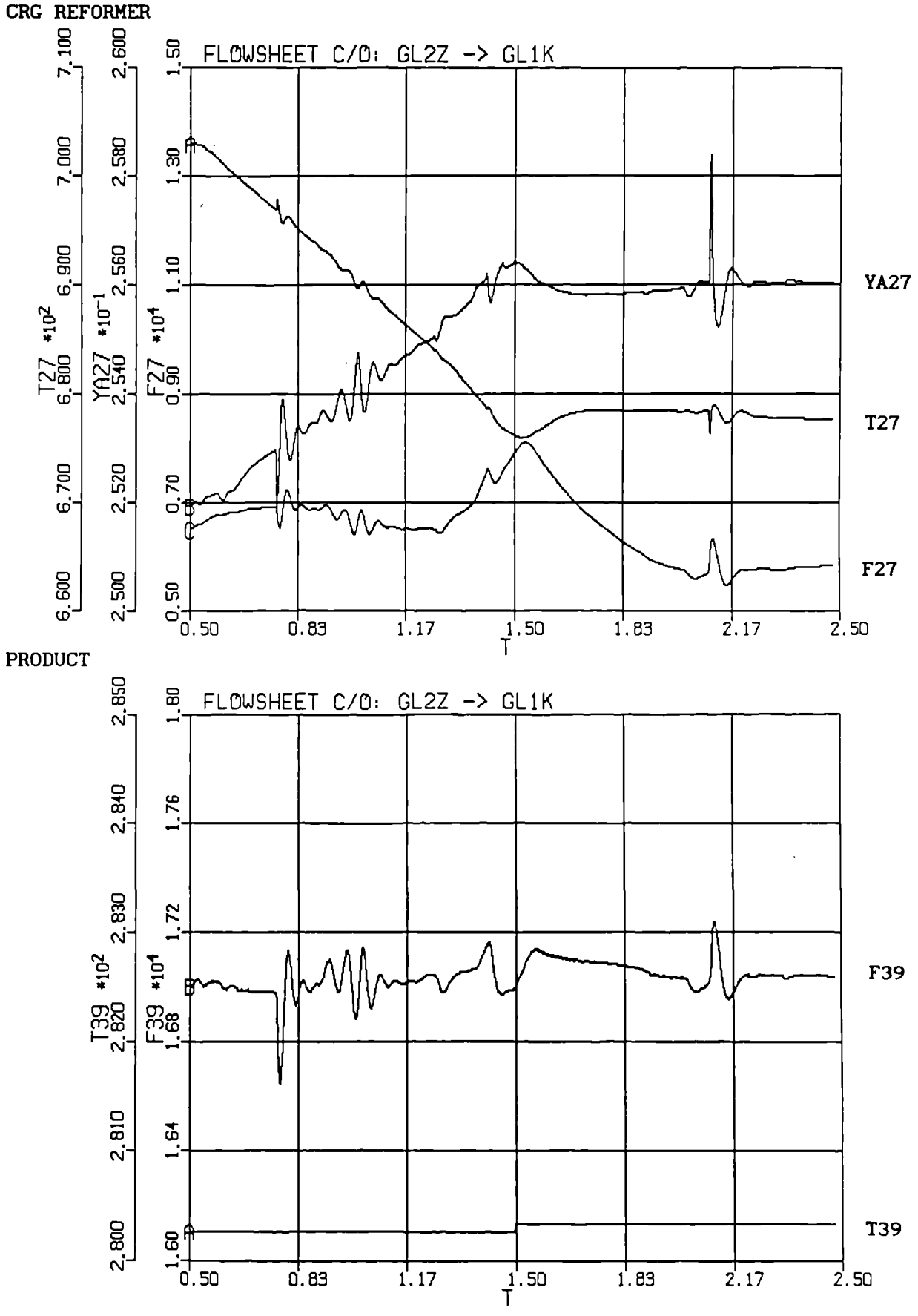

Figure 7.21 Feedstock changeover from GL2Z to GL1K (contd.)

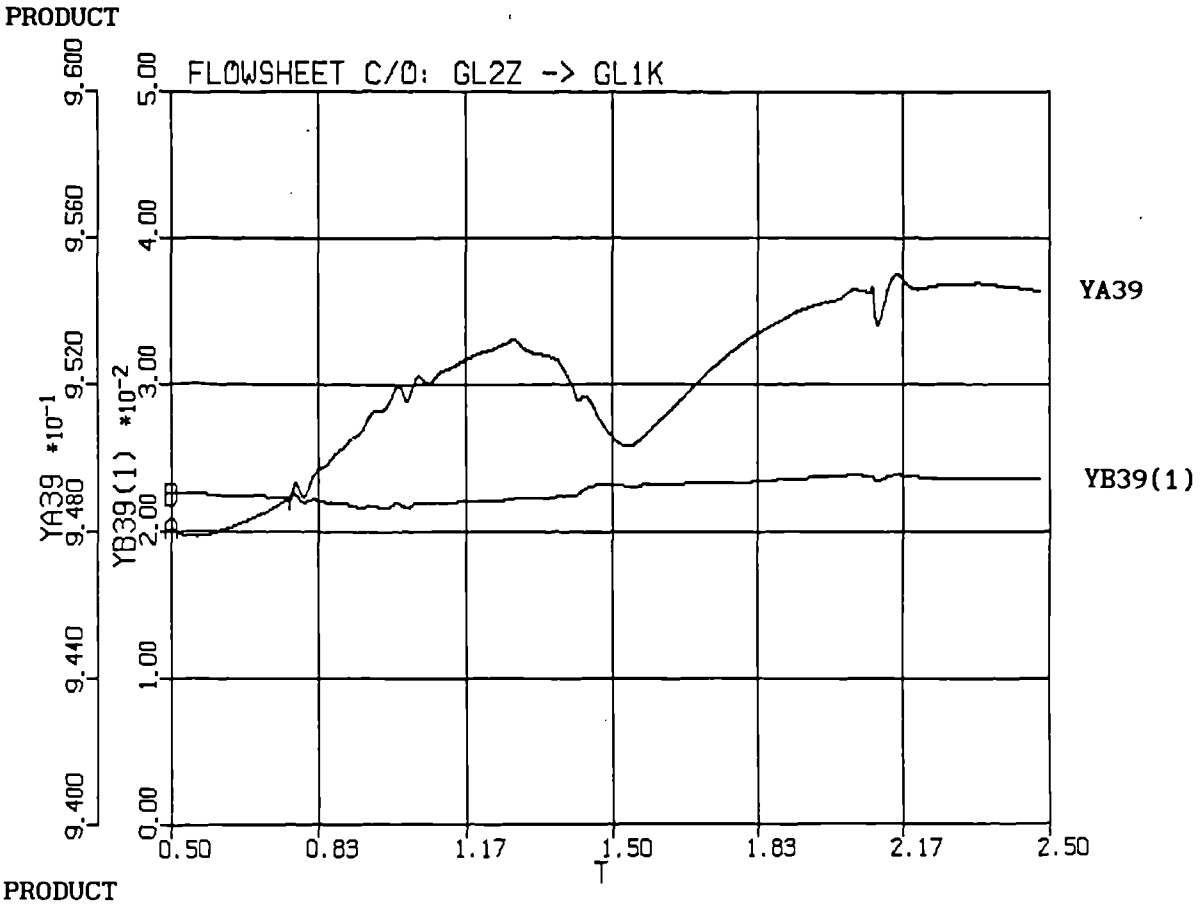

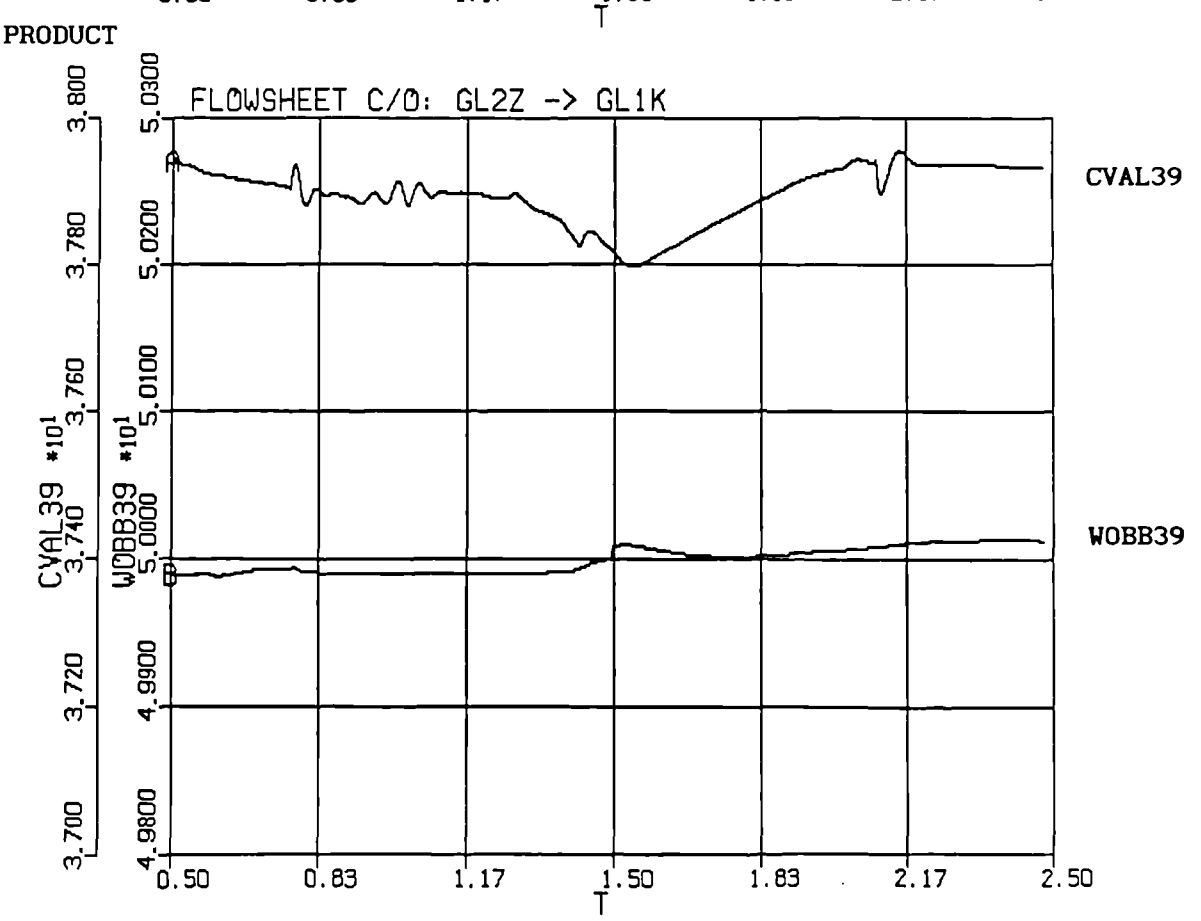

Figure 7.21 Feedstock changeover from GL2Z to GL1K (contd.)

The flash unit responses showed similar trends to those in Figure 7.20 with drum temperature closely following its set point ramp. Pressure, P11, and liquid level, H11, were maintained well within their recommended operating limits. The glitch in bottom product flow rate, F11, during the ramping period, originated from a small step in drum pressure that reduced density and caused a sudden increase in liquid level. The stepping behaviour of the pressure response was attributed to the limiting tolerances used in the iterative calculations for pressure and vapour composition and the narrow plotting range.

Both controlled variables within the distillation column, TPT6 (sum of tray temperatures) and BMT1 (difference in tray temperatures), changed at a faster rate than their set points. This produced a marked error in the control signals. However, the corrective action of TPT6 shortly before the ramp end resulted in a gradual column transition, and allowed the feed condition and set point values to be ramped together. The large offset in BMT1 at the end of the ramp was highlighted by the high methane composition in the bottom product XA14, peaking at over 60% methane. The distillation column was operating beyond its steady state envelope in this region.

In the heavies processing section, the cascade controller showed good set point tracking and disturbance rejection performance. At the end of the ramp, T27 overshot before recovering to its set point value. This overshoot resulted from upstream disturbances propagated in the distillation column.

The export gas responses demonstrated that production, F39, was maintained close to its target flow rate, and temperature, T39, requirements. The increase in methane composition, YA39, resulted from the raised methane content in the feed stream, coupled with a reduced split ratio (see Table 7.14). Although the variations in combustion characteristics were small, they were adversely affected when the ramping period ended. This suggests that a further feedstock changeover mechanism should consider splitting the single ramp into two, with a reduced gradient on the second ramp.

7.6.2.3 *Heavy to Light Feedstock Changeover*

Two 1.0 hr ramping periods were required for the GL1Z to GL1K changeover, with an intermediate settling period of 0.5 hr. This allowed sufficient time for the distillation column controlled variables to approach their set point values, before the ramping continued. The changeover mechanism is described in Table 7.16.

Settings	**Flowsheet Condition**		
	Initial GL1Z Condition	Ramp I Intermed. Condition	Ramp II GL1K Condition
Feed stream component flow rates (kgmol/hr):			
CH_4	13691.11	14472.49	15253.87
C_2H_6	1128.51	1006.39	884.28
C_3H_8	405.15	243.52	81.88
nC_4H_{10}	77.61	38.80	0.00
iC_4H_{10}	63.64	48.19	32.75
nC_5H_{12}	1.55	0.78	0.00
N_2	155.23	139.02	122.82
Set points:			
Split ratio, S-01	0.873	0.873	0.795
Flash unit temperature (K)	203.36	200.33	198.20
Distillation column:			
Feed temperature (K)	190.85	187.54	185.60
Sum of tray temperatures (K)	469.82	415.01	374.30
Difference of tray temperatures (K)	-93.28	-42.94	-4.14
CRG reformer product temperature (K)	705.99	703.15	677.88
Feed Condition and Set Points			

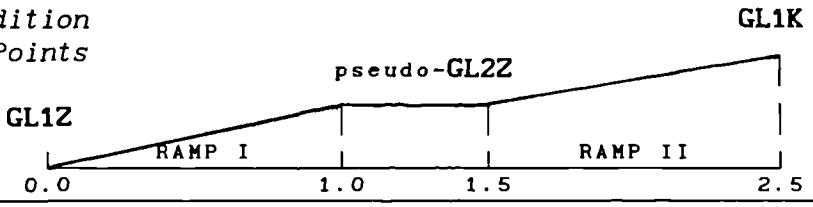

Table 7.16 Changeover mechanism for GL1Z to GL1Z feedstocks

The first ramp in Table 7.16 moved the feedstock composition to an intermediate condition, equivalent to both tank exit valves being 50% open. As this condition was similar to the GL2Z feedstock, most of the set points adopted the GL2Z settings in Table 7.14. The ACSL

simulation results for a complete GL1Z to GL1K feedstock changeover are given in Figure 7.22, with two settling periods - after 1.0 hr and 2.5 hr. The main results are described below.

The responses for each ramp in Figure 7.22 could be compared to the previous results for feedstock changeovers between neighbouring feeds. The first ramp was similar to the GL2Z to GL1Z changeover in Figure 7.20, except in reverse. The second ramp more closely reflected the GL2Z to GL1K changeover as the simulation ended.

As expected when the first ramp began, pressure in the flash drum dropped in a reverse reaction to Figure 7.20. However, it failed to recover before the first ramp ended. This was probably because the flash unit was being moved towards the GL2Z operating condition, with a feed that differed from the GL2Z composition. Thus, a conflict of interest arose as the control loops strived to achieve their set point values. The glitch in F11 corresponded to a sharp rise in pressure after the ramp ended. The responses during the second ramp were very similar to those in Figure 7.21 as the GL1K condition was attained.

As the intermediate feed to the distillation column did not comply with the GL2Z condition, the composition and temperature profiles within the column also changed. Hence, the GL2Z set points were not achieved. This was illustrated by the response of the controlled variables (TPT6 and BMT1) as they attempted to track their set points. By the end of the first ramp, sizeable control signal errors had developed. In the intermediate settling period, only TPT6 was satisfied, suggesting that a steady condition may not be achievable. The flash unit disturbance propagated by F11 had a larger impact on the distillation column, taking 0.15 hr to pass. The next glitch in column product streams, just before the second ramp began, may have resulted from the base controller's attempts to increase BMT1. This further demonstrated the disparity between distillation column conditions and the GL2Z set points. Further disturbances were related to the set point offsets when the second ramp began, with a large rise in BMT1 to overtake its increasing set point. At the end of the second ramp a large error was again associated with BMT1.

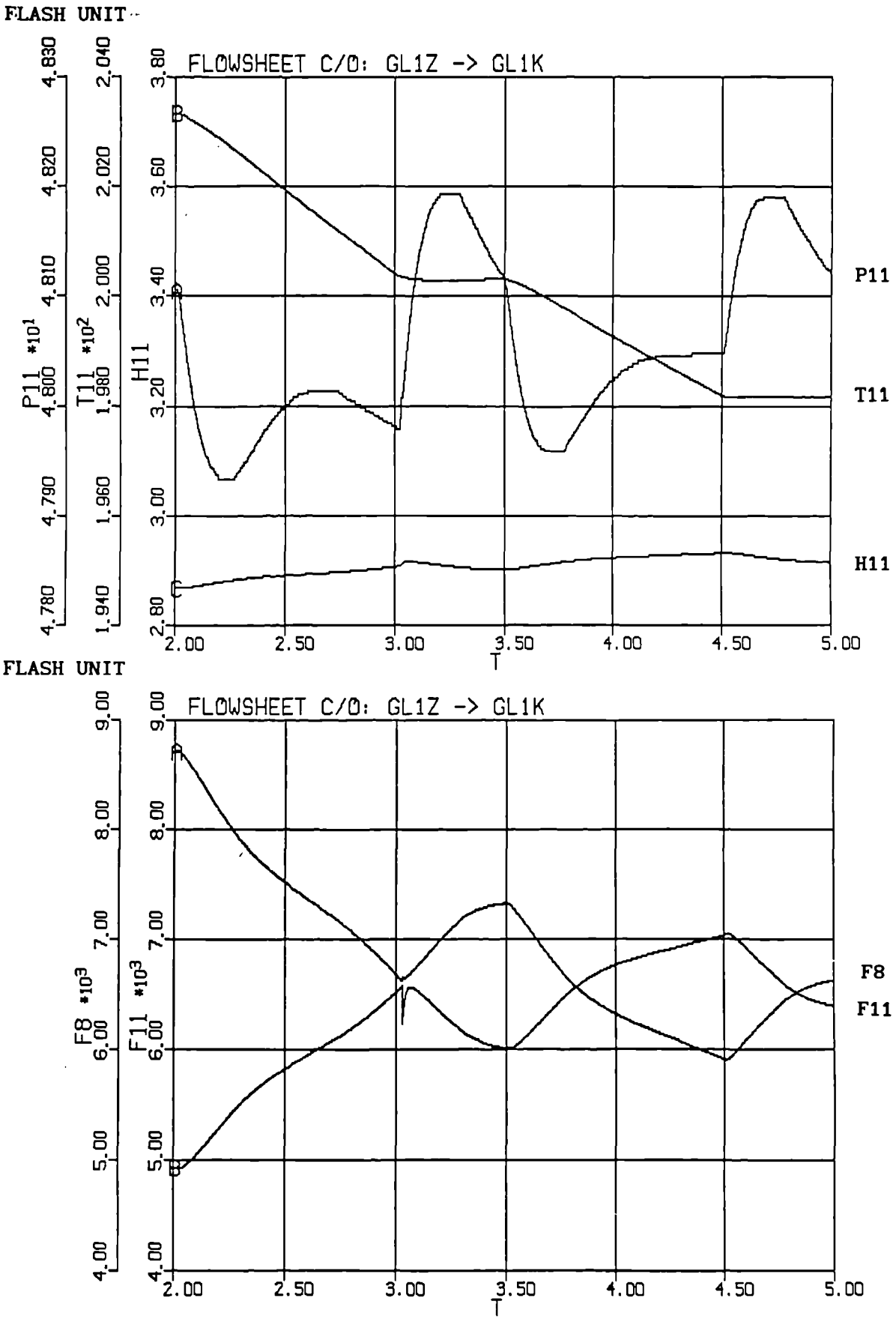

Figure 7.22 Feedstock changeover from GL1Z to GL1K

DISTILLATION COLUMN

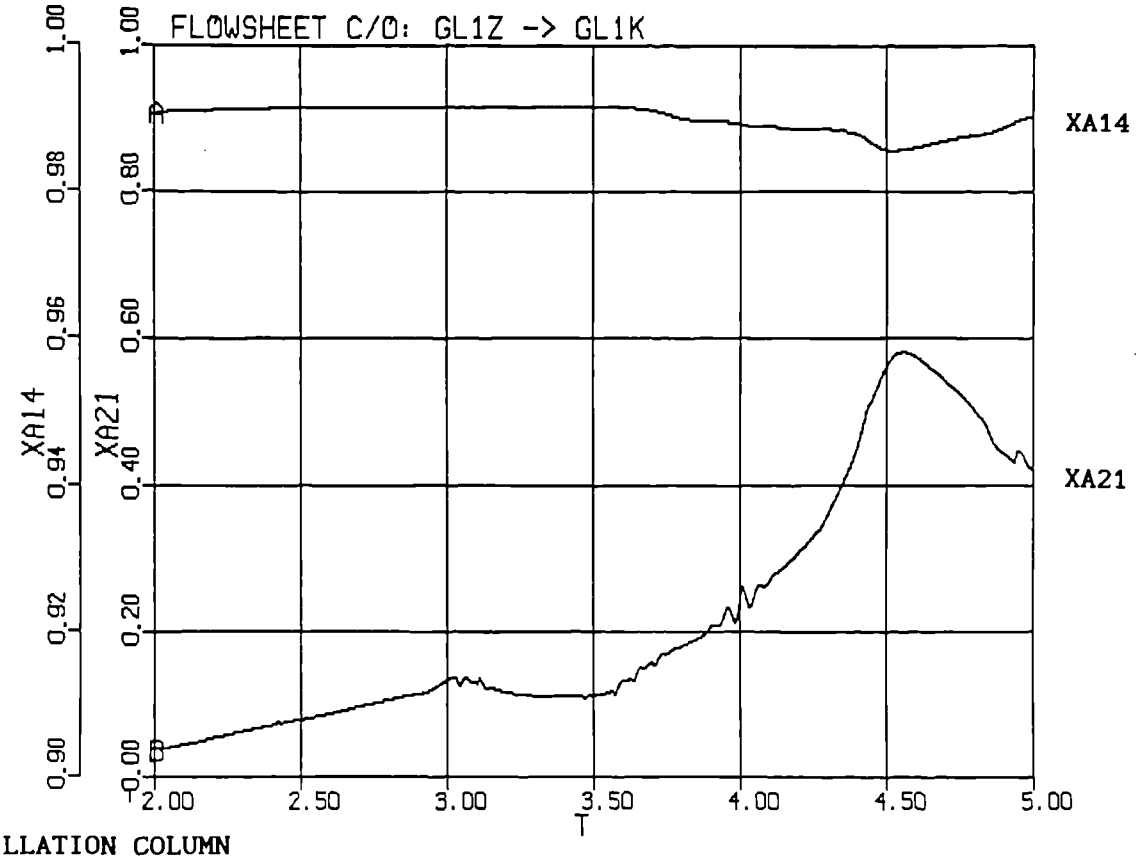

DISTILLATION COLUMN

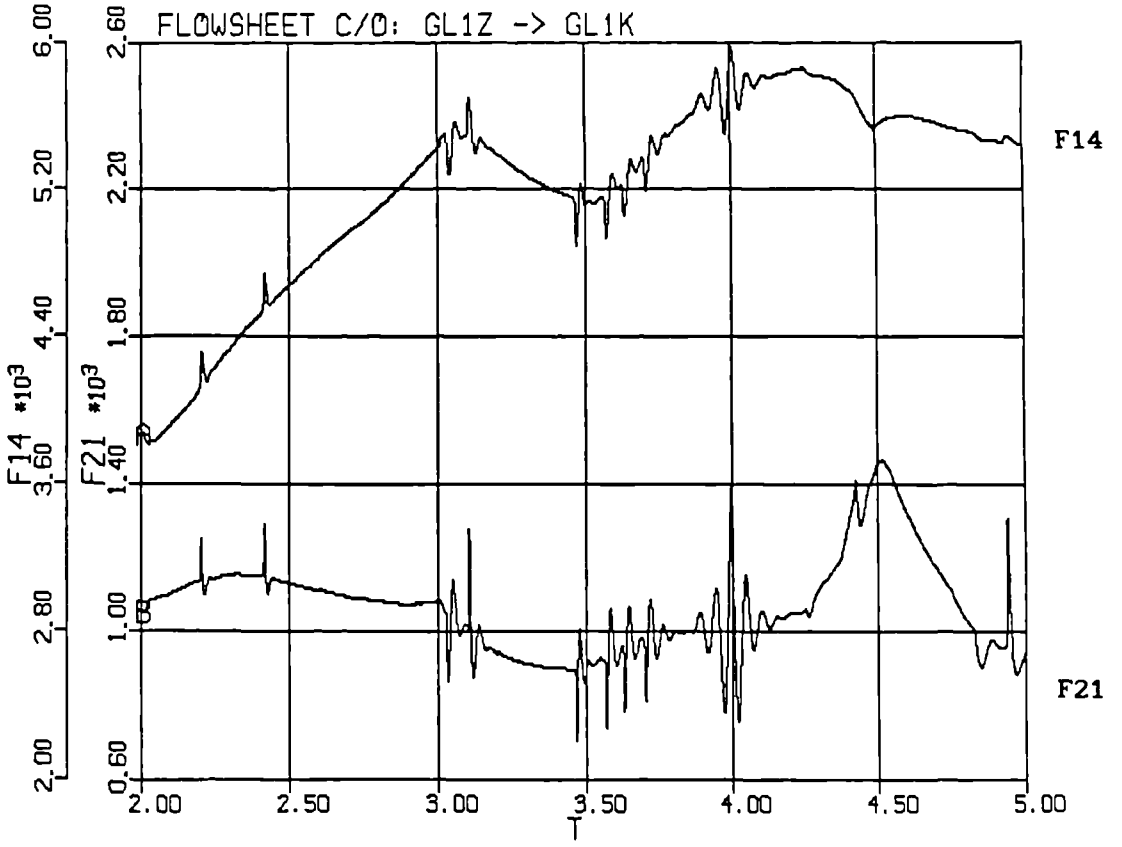

Figure 7.22 Feedstock changeover from GL1Z to GL1K (contd.)

DISTILLATION COLUMN

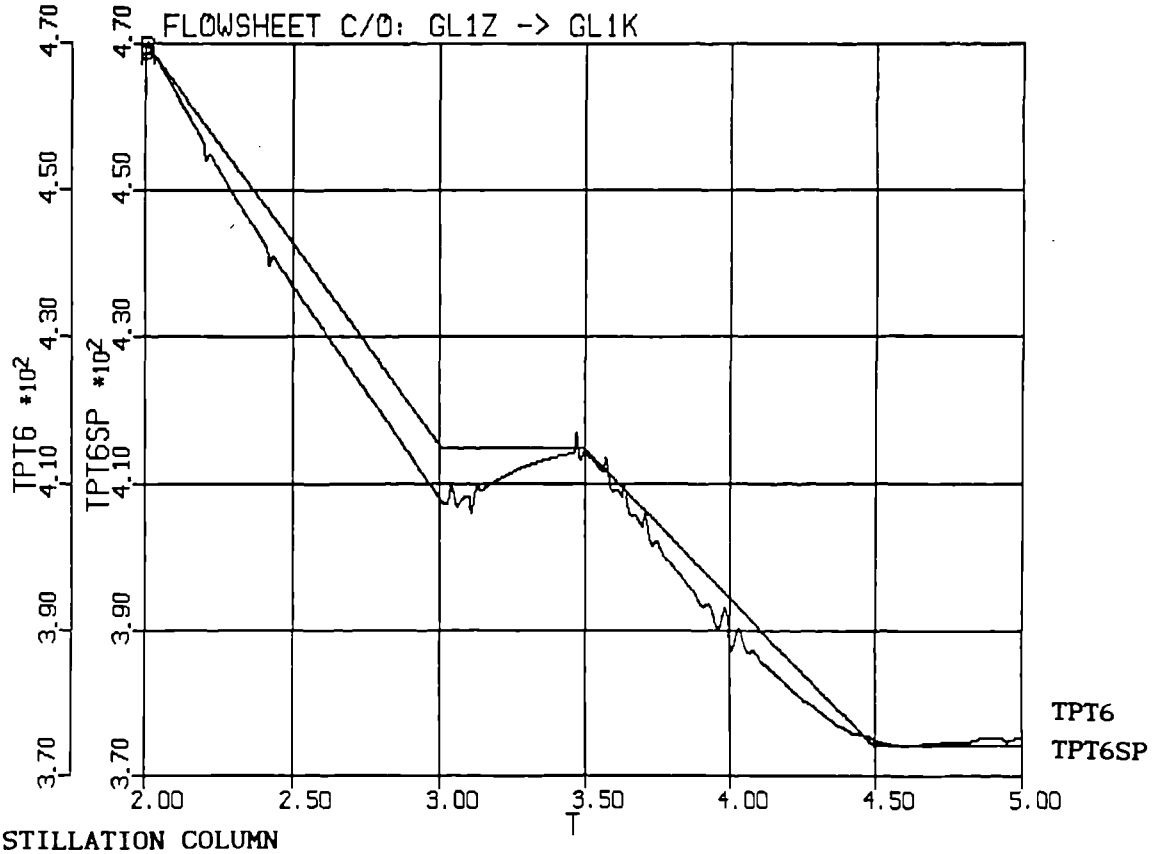

DISTILLATION COLUMN

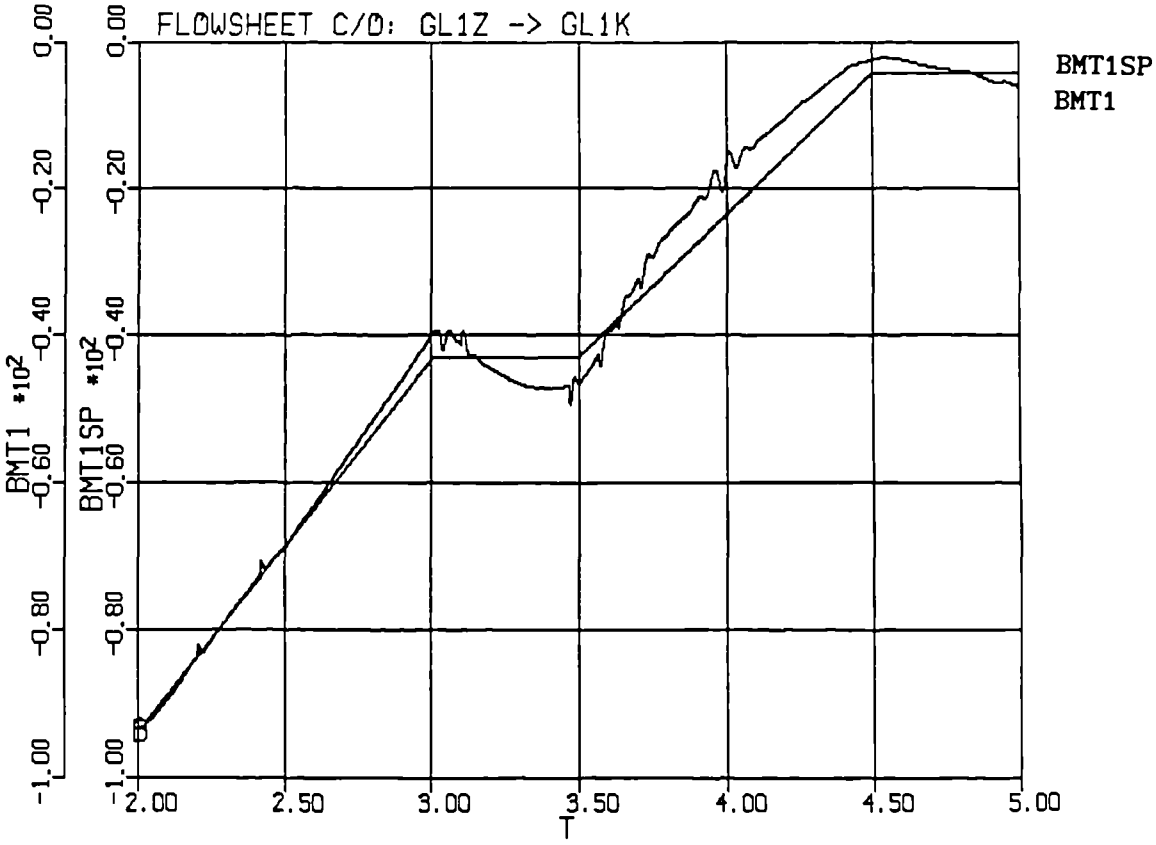

Figure 7.22 Feedstock changeover from GL1Z to GL1K (contd.)

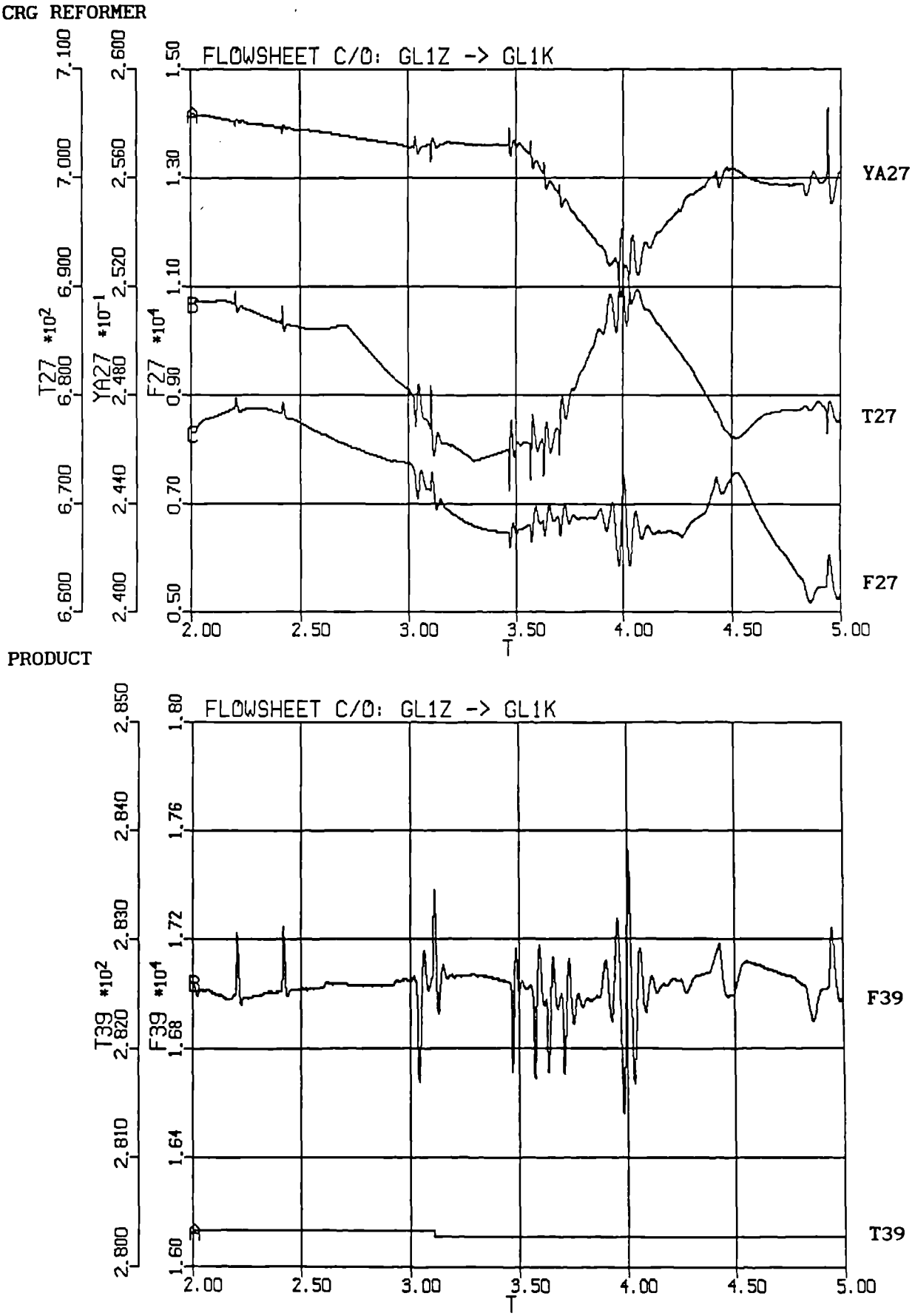

Figure 7.22 Feedstock changeover from GL1Z to GL1K (contd.)

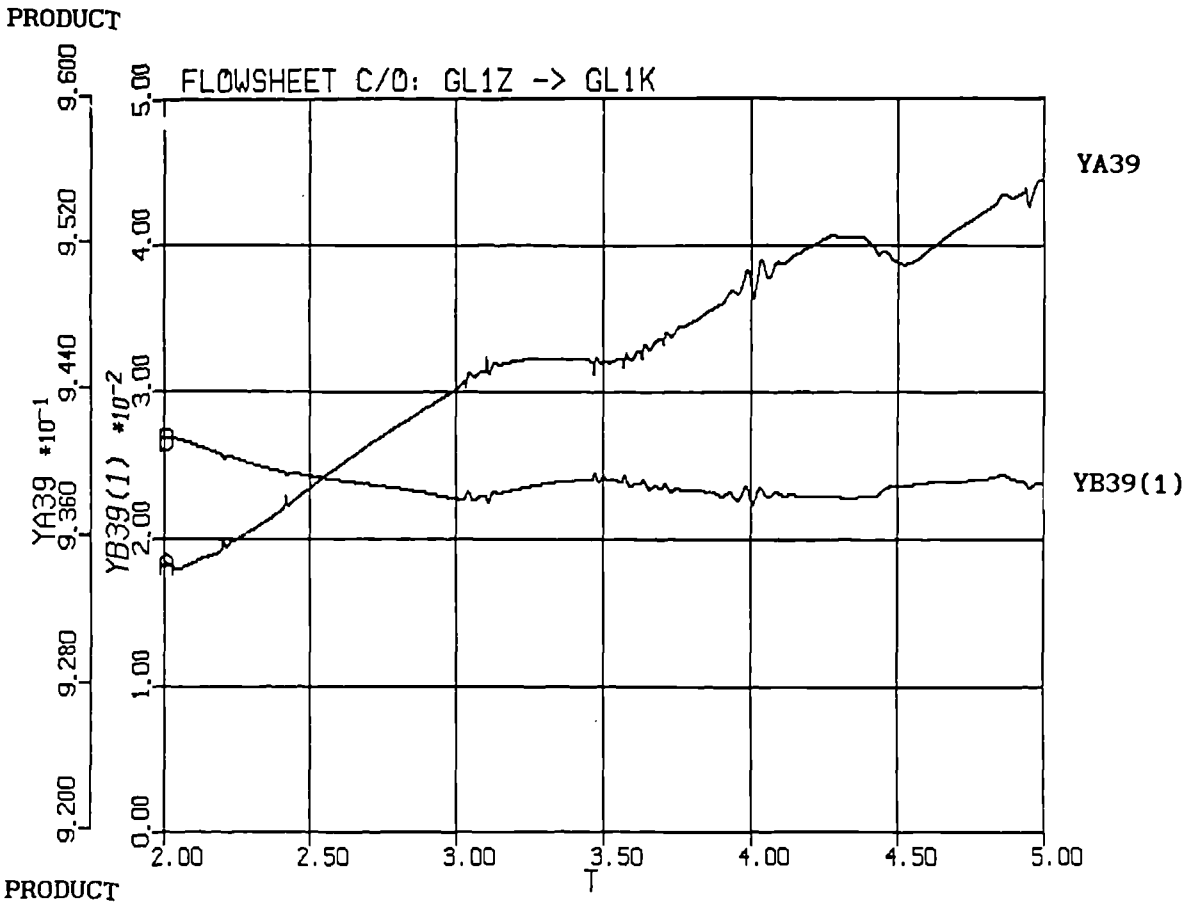

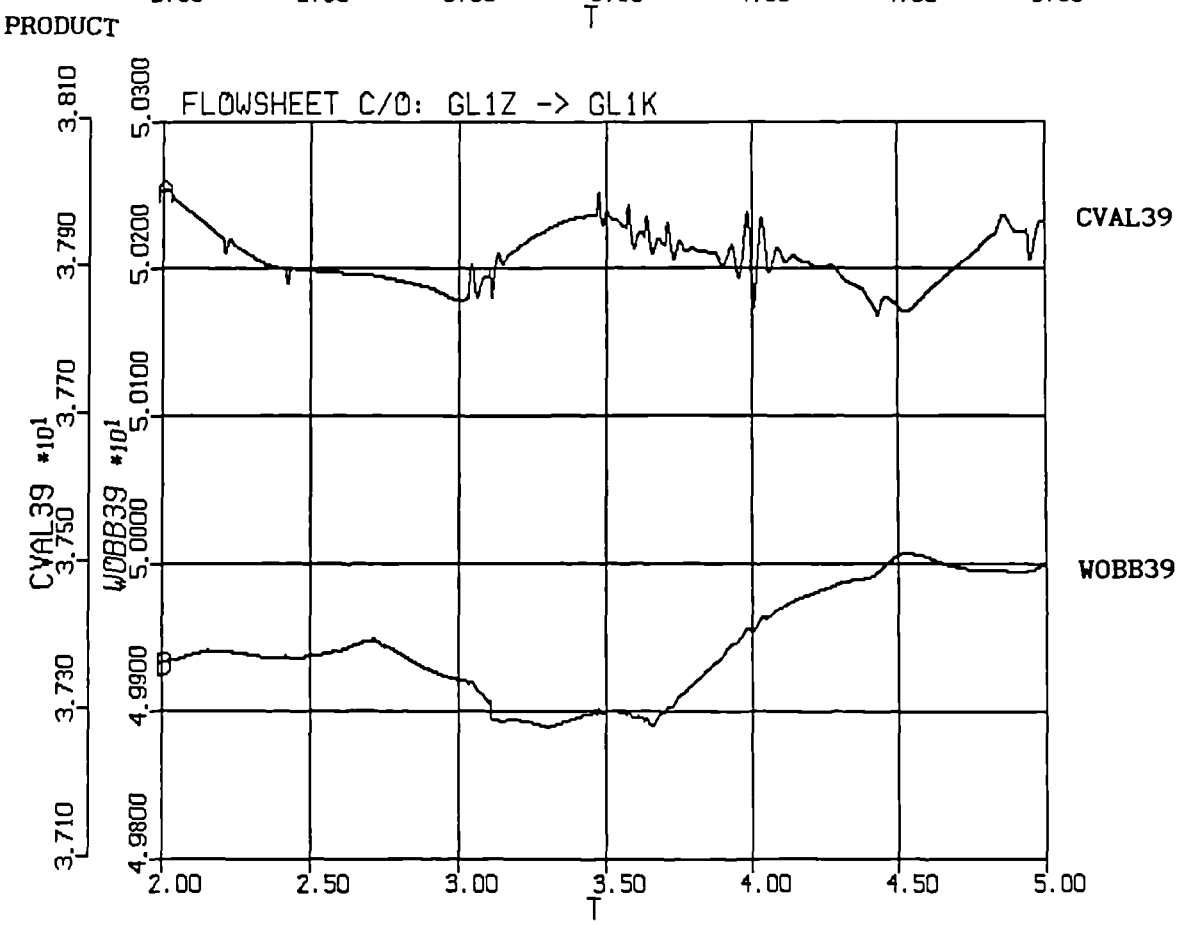

Figure 7.22 Feedstock changeover from GL1Z to GL1K (contd.)

The disparity in intermediate feed conditions was also reflected in the heavies processing section where methane production reached a minimum during the intermediate settling period. This was because the distillation column bottom product, stream 21, contained more methane and lighter hydrocarbons than the original GL2Z condition, and hence fewer carbon components were available for reforming. This was overcome as the GL1K feed was blended into the plant, and the set points moved towards the GL1K condition.

Export gas responses were reasonably steady until the end of the first ramp. Then, as a series of disturbances filtered through the flowsheet, from the flash unit and distillation column the production rate varied by up to 6%. The CVAL39 response was also unsteady, with a relatively large variation in WOBB39. Disturbances generated during the second ramp were not apparent in the original GL2Z to GL1K feedstock changeover, in Figure 7.21. This suggests that the intermediate settling period should have been extended to achieve a better interim steady condition. This may have improved subsequent distillation column responses as the settling period was essential to overcome set point tracking problems.

The reverse feedstock changeover, from GL1K to GL1Z feedstocks, was not simulated. However, it is envisaged that a similar settling period would be required, with a dual ramp from the intermediate to heavy feedstock condition, as described in Section 7.6.2.1.

7.6.2.4 *Changeover Patterns and Restrictions*

The combination of effective controller tuning and a gradual changeover mechanism gave a reasonably smooth transition between LNG feedstocks. The responses in Figures 7.20 to 7.22 represented an improvement over the original step change results in Section 5.4.

The improved flash unit controller tuning eliminated oscillatory behaviour throughout the plant. Although there were marked variations in product flow rates from the distillation column, these would be less likely to cause operational problems. (In the previous study, in Section 5.4, F14 dropped to 15% of its original value). In particular, the product specifications were successfully maintained

throughout the changeover. This illustrates the improvement possible with good controller tuning and a workable changeover mechanism, and helps define supervisory control system requirements. However, these results for regulatory control action may represent a *best* case, as fast dynamic behaviour has been neglected and pressure variations have generally not been simulated. The latter has significant implications on control valve operation.

The changeover simulations have also highlighted the limitations of incorporating a pseudo-binary distillation column model within a multicomponent system. Each changeover mechanism was dictated by this model as it was prone to failure. During a changeover near the GL1Z or GL1K feedstock conditions, the distillation column feed could move outwith the boundaries defined by the steady state operating conditions. At this point, the operating envelope is violated, the data becomes unreliable and model instability might result.

Operational problems may exist in the choice of a suitable distillation column control structure. The controlled variables represented the sum and difference of two tray temperatures, which were obtained from a constant look-up table, as a function of methane. In effect, the methane compositions on two trays are being controlled. Furthermore, these control loop pairings were selected from open-loop steady state gains, which related manipulated to controlled variables about one operating point. This effectively reduced each 2-D table to a 1-D investigation, as the feed condition remained unchanged and only reflux and boilup varied. With hindsight, disturbance rejection should have been included in the control loop assessment.

These changeover investigations identified modelling and control limitations in the distillation column model in particular. Key issues in the changeover strategy were also addressed, enabling an overall supervisory control structure to be recommended.

7.6.3 Supervisory Control Structure Recommendations

The feedstock changeover simulations demonstrated the need for a gradual change in operating conditions, using some form of ramping. Ideally, each set point should ramp independently to a new condition.

The single ramp mechanism has not caused many simulation problems. This may be attributed to the regulatory loop controllers which were designed with significant disturbance rejection capabilities. However, in a real plant, the dynamically faster units and interconnecting pipework may generate appreciable dynamic behaviour. This would introduce more significant delays between the processed and unprocessed streams, whereby a feedstock changeover would affect the product in a series of disturbance waves; from the flash unit, distillation column and finally the processed stream.

Individual ramps for each set point would also be required from a safety viewpoint. The simulation studies identified the distillation column as the most susceptible unit to model failure. Hence, separate ramps would permit a delay in varying the column conditions, and enable a longer ramping period to be adopted.

The next requirement for defining a supervisory control system would be to maintain the product specifications, by manipulating the split ratio and LNG feed rate. However, the changeover responses showed that the product specifications were reasonably well maintained and the main application of a supervisory control system would be to coordinate the flash unit and distillation column. This is because significant interaction exists between the units.

The changeover studies have prompted several recommendations for a changeover mechanism, namely:

(i) All feed conditions, set points and controller settings should be ramped.

(ii) The LNG feedstock and flash unit operating conditions should be ramped simultaneously.

(iii) There should be a delay before distillation column conditions change, to take account of flash unit dynamics. The ramping period should also be extended.

(iv) The remaining set points should be given by independent ramps, and act on changes in the distillation column operating conditions.

The supervisory control system would be employed in this capacity to instruct set point changes. However, its primary task during both feedstock changeover and steady operating conditions would be to reduce the interaction effects within the separation process, and thus limit downstream disturbances to the heavies processing section and product gas.

A supervisory control system has not been implemented on the flowsheet simulation as set point changes have been instructed before events occur, by trial-and-error. Ideally, the supervisory system would monitor conditions to avoid hazardous situations and maintain product specifications, then change the set points accordingly. A hierarchy of levels would be devised from the vertical integration of sensors and controllers, through advanced controls to higher level processing (Thompson and Wilkins, 1989). These simulation studies have provided a basis for structuring the control tasks, and illustrated the interdependency of process design and control design within a multi-unit environment.

7.7 ACHIEVEMENTS AND CONCLUSIONS

A non-adaptive form of the Weighted Predictive Control algorithm was successfully applied to the cascade control arrangement on the heavies processing section. WPC included design parameters to shape system responses, which were dictated by the system characteristics. Although this type of algorithm has been developed primarily for set point tracking, disturbance rejection was important in the control design requirements for the flexible LNG reception terminal. Hence, WPC tuning focused on the disturbance model parameter, $T(q^{-1})$. Although the WPC controller gave comparable performance to the analog PI controller developed in Section 6.4, disturbance rejection was shown to be enhanced without impacting on the set point response.

Difficulties were encountered in obtaining linearised models of the flash unit and distillation column due to inherent non-linearities, and model complexity. As the multivariable systems had several possible control loop configurations, and inherent loop interaction, several interaction indices were used to eliminate unworkable loop pairings, based on open-loop gain data. A multiloop SISO controller tuning method was then adopted to give satisfactory controller settings for the flash unit.

With the completion of the multivariable control loops for the flash unit and distillation column models, all regulatory control loops have been defined and tuned to provide stable and robust unit operation during feedstock changeover and multiple operating conditions.

A series of ramping mechanisms were devised to achieve feedstock changeovers for the complete flowsheet simulation, which ensured stable and robust plant operation and maintained product specifications. On simulating these mechanisms, the results showed that satisfactory performance could be achieved, but demonstrated that attention had to be paid to the interaction between various process units, particularly the flash unit and distillation column.

Finally, a number of recommendations were made for the supervisory control system for the proposed flexible LNG reception terminal. The simulation results indicated that the interaction of individual process units during feedstock changeover was of greatest importance to a supervisory control system. The maintenance of product specifications was originally considered to be the primary concern.

CHAPTER 8

CONCLUSIONS AND RECOMMENDATIONS FOR FURTHER WORK

8.1 INTRODUCTION

This thesis has documented the development of a flexible LNG reception terminal that is capable of handling a variety of LNG feedstocks, without modifications to the process plant. The dynamic simulation of the preliminary flowsheet design has been used as a design tool to develop a control system design for the complete plant, and investigate the impact of feedstock changeovers. General conclusions which can be drawn from the completed work are summarised in this chapter.

The objectives of this thesis were categorised into four main research work areas: process design, dynamic simulation, control studies and plantwide control. The achievements and novel aspects in the study are discussed in Section 8.2. In Section 8.3, the main conclusions relating to the overall design of a flexible LNG reception terminal are addressed, and recommendations for future development work are given in Section 8.4.

8.2 ACHIEVEMENTS AND NOVEL ASPECTS

This section highlights the major achievements and novel aspects of the research work documented in this thesis. The major objective of this work has been achieved in that a preliminary design for a flexible LNG reception terminal has been developed.

Process Design:

(i) A preliminary flowsheet design with the requisite flexibility was developed for an LNG reception terminal. A unique set of *selection criteria*, based on plant utilities and available turndown, was developed to identify the *best* process design.

Dynamic Simulation:

(ii) Mathematical models were developed from first principles to describe each process unit for the full range of LNG feedstock and multicomponent stream conditions. In the case of the distillation column, an original *pseudo-binary* model was devised that greatly simplified modelling complexity whilst maintaining the required degree of accuracy.

(iii) An interactive *physical properties database* was modified and incorporated into the dynamic simulation. This provided continuous, accurate and varying physical property values for each stream. The incorporation of this database was essential to successfully simulate the range of operating and feedstock conditions encountered in the proposed LNG reception terminal.

(iv) As plant data was not available, the *individual dynamic models* were validated in the steady state and dynamic sense by comparison with existing literature examples. The model responses conformed to expected behavioural patterns.

(v) The individual models were integrated to form an efficient and reliable *dynamic simulation of the plant* over its full operating envelope. Simulation of feedstock changeovers predicted that significant interactions would occur between certain process units in the proposed LNG reception terminal.

Control Studies:

(vi) *Linearised model representations* of selected process units

were obtained for control system design using a variety of procedures. Difficulties arose in deriving linear approximations of highly non-linear models. Where the region of applicability of the linear model was greatly reduced, reversion to practical linearisation techniques was necessary.

(vii) *Regulatory control loops* were developed and tuned to provide stable and robust process unit operation during feedstock changeover and at multiple operating conditions. A detailed time-domain analysis was conducted on the ORV system which produced a distinctive graphical representation of the controller parameters. Control system performances were evaluated for disturbance rejection, and control valve action. This is supplementary to the conventional controller tuning practice. This analysis was used to assess the impact of multiple feedstock conditions and to select realistic controller settings.

(viii) An *advanced control technique* was applied to the heavies processing section and a non-adaptive digital controller was developed. This enabled the disturbance rejection to be improved without impacting on the set point response.

(ix) A series of *indices* were employed in the multivariable control system design to eliminate unworkable control loop pairings. The results generally conformed with conventional control loop structures, although open-loop instability was identified in some schemes.

Plantwide Control:

(x) The dynamic simulation with tuned control loops was successfully used to develop a *changeover mechanism* for the plant. This enabled a smooth transition between LNG feedstocks and involved a gradual change to the new feedstock condition, and ramping of set point values.

(xi) The changeover mechanism was employed to successfully simulate the proposed range of *feedstock changeovers.* This identified that the distillation column would be most susceptible to changes in operating conditions, and hence would dictate the changeover period. It also identified the requirements of a supervisory control system.

8.3 CONCLUSIONS

The major conclusion of this thesis is that feedstock flexibility in process plant design can be successfully simulated if each phase of the design addresses this as a primary objective. This has been exemplified in the particular case of a flexible LNG reception terminal. The conclusions specific to each of the design phases are categorised below.

Process Design:

(i) A preliminary flowsheet design which demonstrates good turndown features and handles a specified range of feedstocks can be chosen by the application of selection criteria based on steady state simulation data.

Dynamic Simulation:

(ii) A pseudo-binary distillation column model can be used to accurately simulate a range of feedstock conditions without the additional complexity of a multicomponent representation, provided the operating envelope of the model is not exceeded.

(iii) Accurate physical property data is essential to successfully simulate a range of feedstock conditions in a flexible plant. This can be achieved by the use of an interactive physical properties database.

(iv) Dynamic simulation of feedstock changeover has shown that interaction effects may occur between individual process units.

Control Studies:

(v) Linear control design methods require a linearised representation of the unit before any tuning techniques can be applied. This creates problems with highly non-linear systems, and leads to a conservative tuning margin.

(vi) Control studies show that adoption of a fixed controller design applicable at all operating conditions will give satisfactory control system performance in a flexible plant. However, it is anticipated that tighter tuning would be possible with adaptive controllers on the more non-linear

systems. Also, disturbance rejection and control valve response are shown to be important requirements in the tuning of regulatory control loops for a flexible plant.

Plantwide Control:

(vii) Dynamic simulation indicates that feedstock changeovers can be achieved by ramping feed and set point changes over a suitable time period.

(viii) The main objective of this supervisory control scheme would be to monitor the interaction effects between the flash unit and distillation column whilst maintaining product specifications.

8.4 RECOMMENDATIONS FOR FURTHER WORK

Process Design:

(i) Conduct a capital investment appraisal to assess and optimise the economic viability of the various flowsheet designs.

(ii) Consider heat integration in the flowsheet design, to reduce utility costs. At present, no optimisation has been involved.

Dynamic Simulation:

(iii) Further upgrade the distillation column model by incorporating additional steady state simulation data for extra-light and extra-heavy LNG feedstock conditions. This would extend the operating envelope of the dynamic model.

(iv) Incorporate pressure variations in the complete dynamic simulation. This would provide more realistic flow rate changes through valves and pipework.

(v) Validate the dynamic simulation of process units using real plant data.

Control Studies:

(vi) Investigate a means of obtaining reliable linear representations of non-linear models.

(vii) Investigate the implications of different operating conditions on the multivariable control loop structures.

(viii) Assess dynamic interaction on the multivariable structures and compare results with the original interaction analyses.

(ix) Assess the flash unit controller settings for the remaining LNG feedstock conditions, GL1Z and GL1K, in detail.

(x) Investigate the feasibility of obtaining an open-loop system by introducing cascade control loops, as discussed in Section 7.6.

Plantwide Control:

(xi) Develop and implement a supervisory control system, to monitor the product quality and automatically change set points to satisfy the product specifications and demand.

(xii) Develop an integrated approach to flowsheet design, dynamic simulation, regulatory and supervisory control system design which addresses feedstock flexibility.

REFERENCES

1. Åström K.J. and Haggland T., 1988, Automatic tuning of PID regulators, ISA, Research Triangle Park, N.C., USA.
2. Åström K.J. and Wittenmark B., 1973, On self-tuning regulators, Automatica, **9**, pp. 185-199.
3. Barnett S. and Cameron R.G., 1985, Introduction to Mathematical Control Theory, Oxford University Press, UK.
4. Bequette B.W. and Edgar T.F., 1986, The equivalence of non-interacting control system design methods in distillation, Proc. ACC, Seattle, WA, USA, pp. 31-38.
5. BPCL, 1972, Gas Making and Natural Gas, British Petroleum Company Limited, BP Trading Ltd., UK.
6. BPCP, 1991, BP statistical review of world energy, British Petroleum Company plc, UK, June.
7. Bristol E.H., 1966, On a new measure of interaction for multivariable process control, IEEE Trans. Autom. Control, **AC-11**, pp. 133-134.
8. Burton M.J., 1990, Pace of low temperature work warms up, Professional Engineering, **3** (6), pp. 18-20.
9. Carberry J.J., 1976, Chemical and Catalytic Reaction Engineering, McGraw-Hill Book Co., New York, USA.
10. Cho Y.S. and Jospeh B., 1983a, Reduced-order steady-state and dynamic models for separation processes, Part I: Development of the model reduction procedure, AIChE Journal, **29** (2), pp. 261-269.
11. Cho Y.S. and Joseph B., 1983b, Reduced-order steady-state and dynamic models for separation processes, Part II: Application to nonlinear multicomponent systems, AIChE Journal, **29** (2), pp. 270-276.
12. Choe Y-S. and Luyben W.J., 1987, Rigorous dynamic models of distillation columns, Ind. Eng. Chem. Res., **26**, pp. 2158-2161.
13. Clarke D.W., 1988, Application of generalized predictive control, IFAC Adaptive Control of Chemical Processes, Denmark.

14. Clarke D.W. and Gawthrop P.J., 1975, Self-tuning controllers, Proc. IEE, **122**, pp. 929-934.
15. Clarke D.W., Mohtadi C. and Tuffs P.S., 1987, Generalized predictive control - Parts 1 and 2, Automatica, **23** (2), pp. 137-160.
16. Craig D.F. and Burklow B.W., 1980, Effect of primary reformer steam-to-carbon ratios on ammonia plant efficiency, Ammonia Plant Safety - CEP, **22**, pp. 131-139.
17. De Keyser R.M.C., Van de Velde G.A. and Dumortier F.A.G., 1988, A comparative study for self-adaptive long-range predictive control methods, Automatica, **24** (2), pp. 149-163.
18. De Leye L. and Froment G.F., 1986, Rigorous simulation and design of columns for gas absorption and chemical reaction - I, Comp. & Chem. Eng., **10** (5), pp. 493-504.
19. Doebelin E.O., 1985, Control System Principles and Design, John Wiley & Sons Inc., New York, USA.
20. Douglas J.M., 1988, Conceptual Design of Chemical Processes, McGraw-Hill book Co., New York, USA.
21. Duan J. and Grimble M.J., 1990, Self-tuning weighted predictive control, Industrial Control Unit, Univ. Strathclyde, Glasgow, UK, submitted ACC, Boston, 1991.
22. Eigenberger G. and Ruppel W., 1986, Problems of mathematical modelling of industrial fixed-bed rectors, Ger. Chem. Eng., **9** (2) pp. 74-83.
23. Foss B.J., 1983, Composition control of binary distillation columns using multivariable optimal control, Modeling, Identification and Control, **4** (4), pp. 195-216.
24. Fuentes C. and Luyben W.L., 1982, Comparison of energy models for distillation, Ind. Eng. Chem. Fundam., **21** (3), pp. 323-325.
25. Fuentes C. and Luyben W.L., 1983, Control of high-purity distillation columns, Ind. Eng. Chem. Process Des. Dev., **22** (3), pp. 361-366.
26. Fujiwara T. and Miyakawa H., 1990, Application of predictive adaptive control system for steam temperature control in boiler plant, Proc. 29th Conference on Decision and Control, Honolulu, Hawaii, December.

27. Gani R., Ruiz C.A. and Cameron I.T., 1986, A generalized model for distillation columns- I: Model description and applications, Comp. & Chem. Eng., **10** (3), pp. 181-198.
28. Georgiou A., Georgakis C. and Luyben W.L., 1988, Nonlinear dynamic matrix control for high-purity distillation columns, AIChE Journal, **34** (8), pp.1287-1298.
29. Grimble M.J., 1990, Long range predictive optimal control law with guaranteed stability for process control applications, ICU/293/June, Industrial Control Unit, Univ. Strathclyde, Glasgow, UK.
30. Grimble M.J. and Johnson M.A., 1991, H_∞ robust control design - A tutorial review, Computing and Control Engineering Journal, November, pp. 275-282.
31. Grosdidier P., Holt B.R. and Morari M., 1985, Closed loop properties from steady state gain information, Ind. Eng. Chem. Fundam., **24**, pp. 221-235.
32. Guy J.K., 1982a, Modelling heat-transfer systems, Chemical Engineering, May 3, pp. 93-98.
33. Guy J.K., 1982b, Modelling the phase equilibria in dynamic systems, Chemical Engineering, Nov. 29, pp. 75-79.
34. Häggblom K.E and Waller K.V., 1990, Control structures for disturbance rejection and decoupling of distillation, AIChE Journal, 36(7), pp. 1107-1113.
35. Heat Exchanger Design Handbook, 1983, Hemisphere Publishing Corporation, USA.
36. Hearfield L., 1984, Decommissioning LNG inground storage at Canvey, Gas Engineering & Management, June, pp. 219-225.
37. Henley E.J. and Seader J.D., 1981, Equilibrium Stage Separation Operations in Chemical Engineering, John Wiley & Sons Inc., New York, USA.
38. Hill G.H., 1977, An Introduction to Chemical Engineering Kinetics and Reactor Design, John Wiley & Sons, Inc., New York, USA.
39. Hsie L. and McAvoy T.J., 1991, Comparison of single loop and QDMC-based control of crude oil distillation towers, J. Proc. Contr., **1**, pp. 15-21.
40. Jensen J.T., 1985, Gas resources and gas markets: A global view, Energy, 10 (2), pp. 139-149.

41. Johnson M.A., 1984, Visit Report: Tokyo Gas, ICU/54/Sept., Industrial Control Unit, Univ. Strathclyde, Glasgow, UK.

42. Oil and Gas Journal, 1990, Worldwide Report, OGJ, December 31, pp. 41-45.

43. Kapoor N., McAvoy T.J. and Marlin T.E., 1986, Effect of recycle structure on distillation tower time constants, AIChE Journal, **32** (3), pp. 411-418.

44. Kapoor N. and McAvoy T.J., 1987, An analytical approach to approximate dynamic modeling of distillation towers, Ind. Eng. Chem. Res., **26** (12), pp. 2473-2482.

45. Keen D., 1983, Calorific value control in the vaporisation of heavy LNG, King-Wilkinson correspondence.

46. Kinoshita M., 1986, Simple model for dynamic simulation of stage separation processes with very volatile components, AIChE Journal, **32** (5), pp. 872-874.

47. Krishnamurthy R. and Taylor R., 1985, Simulation of packed distillation and absorption columns, IEE Proc. Des. & Dev., **24** (3), pp. 513-524.

48. Lau H., Alvarez J. and Jensen K.F., 1985, Synthesis of control structures by singular value analysis: Dynamic measures of sensitivity and interaction, AIChE Journal, **31** (3), pp. 427-439.

49. Lechat J.F. and Caudron S., 1986, Reception of different qualities of LNG in large storage tanks, GASTECH '86 Proceedings, LPG/LNG Conference, Hamburg, Nov. 25-28.

50. Leibson I., Davenport S.T. and Muenzier M.H., 1987, Costs to transport natural gas, Hydrocarbon Processing, April, pp. 47-50.

51. Lom W.L. and Williams A.F., 1976, Substitute Natural Gas, Applied Science Publishers Ltd., London, UK.

52. Luyben W.L., 1973, Process Modeling, Simulation and Control for Chemical Engineers, McGraw-Hill Book Co., New York, USA.

53. Luyben W.L., 1986, Simple method for tuning SISO controllers in multivariable systems, Ind. Eng. Chem. Process Des. Dev., **25**, pp. 654-660.

54. Luyben W.L., 1990, Process Modeling, Simulation and Control for Chemical Engineers, McGraw-Hill Book Co., New York, USA.

55. MAGA, 1987, Advanced Simulation Control Language (ACSL) Reference Manual, Mitchell and Gauthier Associates, Concord, Mass., USA.

56. Mandler J.A., Morari M. and Seinfeld J.H., 1986, Control system design for a fixed-bed methanation reactor, Chemical Engineering Science, **41** (6), pp. 1577-1597.
57. McAvoy T.J., 1983a, Interaction Analysis, Instrument Society of America, Research Triangle Park, N.C., USA.
58. McAvoy T.J., 1983b, Some results on dynamic interaction analysis of complex control systems, Ind. Eng. Chem. Des. Dev., **22** (1), pp. 42-49.
59. Monica T.J., Yu C-C., Luyben W.L., 1988, Improved multiloop single-input/single output (SISO) controllers for multivariable processes, Ind. Eng. Chem. Res., **27**, pp. 969-973.
60. Monk P., 1988, BG Internal Memo, CRG reformer design, 19th September.
61. Morari M. and Zafiriou E., 1989, Robust Process Control, Prentice-Hall International, Inc., NJ, USA.
62. Muir L.J., 1987, Simulation and Control System Design for a Liquefied Natural Gas Vaporiser, PhD Thesis, Industrial Control Unit, Univ. Strathclyde, Glasgow, UK.
63. Müller E. and Hofmann H., 1987, Dynamic modelling of heterogeneous catalytic reactions - I: Theoretical considerations, C.E.S., **42** (7), pp. 1695-1704.
64. Murray A.P and Snyder T.S., 1985, Steam-methane reformer kinetic computer model with heat transfer and geometry options, IEC Proc. Des. Dev., **24** (2), 286-294.
65. Niederlinski H., 1971, A heuristic approach to the design of linear multivariable interacting control systems, Automatica, **7**, pp. 691-701.
66. Ogata K., 1990, Modern Control Engineering, Prentice-Hall International, Inc., NJ, USA.
67. Ovenston A. and Walls J.R., 1980, Chemical thermodynamic study of the conversion of fossil fuels to prime chemical feedstocks with steam, C.E.S., **35**, pp. 627-633.
68. Peiser A.M. and Grover s.S., 1962, Dynamic simulation of a distillation tower, CEP, **58** (9), pp. 65-70.
69. Peters M.S. and Timmerhaus K.D., 1968, Plant Design and Economics for Chemical Engineers, McGraw-Hill Book Co., New York, USA.
70. PROCESS Manual, 1987, SimSci Inc., USA.

71. Raman R., 1985, Chemical Process Computations, Elsevier Applied Science Publishers Ltd., London, UK.
72. Reid R.C., Prausnitz J.M. and Poling B.E., 1987, The Properties of Gases and Liquids, McGraw-Hill Book Co., New York, USA.
73. Roffel B., and Rijnsdorp J.E., 1982, Proccess Dynamics, Control and Protection, Ann Arbor Science Publishers, Ann Arbor.
74. Ryskamp C.J., 1982, Explicit versus implicit decoupling in distillation control, CPC-II, Eds. Seborg D.E. and Edgar. T.F, Engineering Foundation/AIChE, pp. 361-375.
75. Schnelle P.D. and Miller D.L., 1988, Graphical interpretations of PI tuning performance and robustness, Proceedings of ISA/88 International Conference, Houston, USA, 16-21 October.
76. Schnitzlein K. and Hofmann H., 1987, An alternative model for catalytic fixed bed reactors, C.E.S., **42** (11), pp. 2569-2577.
77. Schwarz H.R., 1989, Numerical Analysis, Volume 6, Pergammon Press, Chichester, UK.
78. Seborg D.E., Edgar T.F. and Mellichamp D.A., 1989, Process Dynamics and Control, John Wiley & Sons, Inc., New York, USA.
79. Shinskey F.G., 1988, Process-Control Systems, McGraw-Hill Book Co., New York, USA.
80. Sinnott R.K., 1983, Chemical Engineering, Volume 6, Pergamon Press, Oxford, UK.
81. Skogestad S. and Morari M., 1987a, Control configuration selection for distillation columns, AIChE Journal, **33** (10), pp. 1620-1635.
82. Skogestad S. and Morari M., 1987b, Implications of large RGA elements on control performance, Ind. Eng. Chem. Res., **26**, pp. 2323-2330.
83. Skogestad S. and Morari M., 1988, Understanding the dynamic behaviour of distillation columns, Ind. Eng. Chem. Res., **27** (10), pp. 1848-1862.
84. Skogestad S., Lundstrom P. and Jacobsen E.W., 1990, Selecting the best distillation control configuration, AIChE Journal, **36** (5), pp. 753-764.
85. Stephanopoulos G., 1984, Chemical Process Control - An Introduction to Theory and Practice, Prentice-Hall International, Inc., NJ, USA.

86. Subramanian T.K:, 1967, Estimate reformer gas composition, Hydrocarbon Processing, **46** (9), pp. 169-172.

87. Suenson M.M., Georgakis C. and Evans L.B., 1985, Steady-state and dynamic modelling of a gas absorber-stripper system, Ind. Eng. Chem. Fundam., **24** (3), pp. 288-295.

88. Thompson C.B. and Wilkins M.J., 1989, Choosing an industrial control system for the 1990's, Collected Papers: Two Day Symposium, Inst. of M & C, London, UK, 24-25 October.

89. TMWI, 1987, PC-MATLAB User's Guide, The Math Works Inc., Version 3.2-PC, June 8, 1987.

90. Tsai T.H., Lane J.W. and Lin C.S., 1986, Modern Control Techniques for the Processing Industries, Marcel Dekker, Inc., USA.

91. Ulrich G.D., 1984, A Guide to Chemical Engineering Process Design and Economics, John Wiley & Sons, New York, USA.

92. Van Doesburg H. and de Jong W.A., 1976, Transient behaviour of a fixed-bed methanator - I, C.E.S., **31** (1), pp. 45-51.

93. Van Meerbeke R.C., 1982, Accident at the Cove Point LNG facility, CEP, January, pp. 39-45.

94. Vortmeyer D., and Schaefer R.J., 1974, Equivalence of one- and two-phase models of heat transfer processes in packed beds: one dimensional theory, C.E.S., **29**, pp. 485-491.

95. Waller K.V., 1986, Distillation control system structures, IFAC Control of Distillation Columns and Chemical Reactors, Bournemouth, UK.

96. Williams S.J., 1991, H_∞ for the layman, Measurement and Control Journal, **24**, pp. 18-21.

97. Wimpress N., 1978, Generalized method predicts fired-heater performance, Chemical Engineering, May 22.

98. Wolfs P. and Hoornstra R., 1982, Combination of an LNG terminal and a coal gasification plant at Eemshaven - The Netherlands, 15^{th} World Gas Conference, IGU/H52-82.

99. Wozny G., Witt W. and Jeromin L., 1987, Dynamics of distillation with high product purities, Chem. Eng. Technol., **10**, pp. 338-348.

100. Xu J. and Froment G.F., 1989, Methane steam reforming, methanation and water-gas shift, AIChE Journal, 35-1, pp. 88-103.

101. Yang D.R., Seborg D.E. and Mellichamp D.A., 1991, Combined balance control structure for distillation columns, Ind. Eng. Chem. Res., **30**, pp. 2159-2168.

102. Yu C-C. and Luyben W.L., 1986, Design of multiloop SISO controllers in multivariable processes, Ind. Eng. Chem. Process Des. Dev., **25**, pp. 498-503.

103. Yuwana M., and Seborg D.E., 1982, A new method for on-line controller tuning, AIChE Journal, **28** (3), pp. 434-440.

APPENDIX 1

HEAVY HYDROCARBON CONVERSION

The reaction between a hydrocarbon feedstock and steam, in the presence of a catalyst, can produce hydrogen, ammonia synthesis gas, lean gas or town gas, depending on the operating conditions of the reactor. There are several processing techniques available for converting heavy hydrocarbons; reforming, partial oxidation and methanation. Only steam reforming and methanation processes will be considered here. These process units are fixed bed reactors, with catalyst pellets packed into vertical or horizontal tubes through which the reactants pass.

The general reaction for heavy hydrocarbon conversion is:

$$C_nH_{2(n+1)} + nH_2O \longrightarrow nCO + (2n+1)H_2 \qquad \text{(A1.1)}$$

This is an endothermic reaction and constitutes the first stage in heavies conversion. The extent to which conversion occurs depends on a number of factors; in particular, the steam to carbon (S/C) ratio, reactant temperature, pressure and catalyst performance. The next stage in the conversion process involves the remaining hydrocarbons, excess steam, CO and H_2 as reactants. On reaching equilibrium, the product contains CH_4, H_2, CO_2, CO and H_2O. The product is controlled by the notional complete reaction (A1.1) and by subsequent simultaneous equilibria of any two reactions (Lom and Williams, 1976) provided they are independent and between them contain every component in the final product. The following reactions represent a typical combination:

$$CH_4 + H_2O \rightleftharpoons CO + 3H_2 \qquad \text{(A1.2)}$$

$$CO + H_2O \rightleftharpoons CO_2 + H_2 \qquad \text{(A1.3)}$$

referred to as the methanation and water gas shift reactions, respectively. However, every gasification reaction may occur in the course of the overall conversion from feed to final product. The reaction data in Table A1.1 indicates that two extreme product compositions are possible, depending on operating conditions. Hydrogen-rich gas production is highly endothermic, requiring a

source of heat input to the reactor, to sustain (A1.2). This type of reaction is favoured by a high inlet temperature and low operating pressure. A steam methane reformer is often employed for this process.

Reaction	ΔH at 25°C (kcal/kgmol)	Volume change ΔV	Equilibrium constant K_p
A1.2	+49243	2 to 4	$(CO)(H_2)^3 / (CH_4)(H_2O)$
A1.3	-9847	2 to 2	$(CO_2)(H_2) / (CO)(H_2O)$

Table A1.1 Equilibrium in Gasification Reactions

In methane gas production, the overall reaction is exothermic, and so no external heat source is required. This type of reactor is typically adiabatic and operates at low temperature and high pressure. The Catalytic Rich Gas (CRG) reformer, which was originally developed by the British Gas Council to produce H_2 for town gas, can also be used for methane production. The methanation process is often employed as a continuation of the reforming process, particularly the CRG reformer, to break the reaction down into more controllable stages and further increase methane production.

The final gas composition may be predicted using nomographs (Subramanian, 1967) or equilibrium constants, K_p. Equilibrium constants are dependent on reaction temperature alone, and are expressed in terms of the ratio of partial pressures, as defined in Table A1.1.

The reactivity of different components is considerably affected by the presence of a catalyst. The operating conditions for a reactor are also dictated by a safe temperature region for the catalyst. Carbon deposition occurs below the Boudouard temperature, according to the exothermic reaction:

$$2CO \rightleftharpoons CO_2 + C \qquad \text{(A1.4)}$$

Too high an operating temperature causes sintering and reduces the catalyst surface area. Hence, upper and lower temperature limits must be observed. As the catalyst becomes less active, the inlet temperature has to be raised further to maintain the outlet

temperature conditions. This is apparent from the progressive change in temperature profile in the catalyst bed (BPCL, 1972). Reaction (A1.4) can also results from a low S/C ratio (Craig and Burklow, 1980).

Reformer Modelling

The choice of (A1.2) and (A1.3) to describe the methanation reactions within a heavy hydrocarbon conversion unit is borne out in many steady state simulations of the steam methanation reactor and CRG reformer (Ovenston and Walls, 1980; Murray and Snyder, 1985). Common assumptions in mathematical modelling include plug flow of the reformer gases, axial temperature changes, and negligible carbon formation. Distributed parameter systems are generally developed to predict the temperature profile and product composition. Dynamic modelling of fixed-bed reformers is discussed in detail in Section 3.3.2.

APPENDIX 2

FLOWSHEET SIMULATION RESULTS

Family 1: Scheme 10

CRITERION	Feedstock			Turndown (%)
	GL1K	GL2Z	GL1Z	
Production				
Feed (kg/s)	47.48	59.37	68.84	69.0
kg Product/kg Feed	1.010	1.016	1.023	98.7
Wobbe No. position	0.733	0.665	0.624	85.1
Heavies Processing				
Process Stream Flow (kg/s)	1.320	2.752	4.339	30.4
Steam Flow (kg/s)	3.697	7.374	11.868	31.2
Effluent Flow (kg/s)	2.68	5.58	8.93	30.0
Operating Costs				
Total Power (kW)	4193.27	6860.04	9880.84	42.4
Compression Power (kW)	2310.52	4561.99	7272.49	31.8
Expansion Power (kW)	209.49	400.62	620.18	33.8
Nett Heating (MW)	95.31	136.16	178.25	53.5
Nett Cooling (MW)	17.53	34.72	55.54	31.6
Cryogenic Heat (MW)	0.00	0.00	0.00	--
Fired Heat (MW)	22.50	44.37	70.66	31.8
Process Heat (MW)	3.07	6.06	9.67	31.8
Cryogenic Cooling (MW)	0.00	0.00	0.00	--
Process Cooling (MW)	17.53	34.72	55.54	31.6

Family 1: Scheme 12

CRITERION	Feedstock			Turndown (%)
	GL1K	GL2Z	GL1Z	
Production				
Feed (kg/s)	52.67	52.93	52.86	99.5
kg Product/kg Feed	1.010	1.016	1.023	98.7
Wobbe No. position	0.735	0.668	0.615	83.7
Heavies Processing				
Process Stream Flow (kg/s)	0.790	1.270	1.797	44.0
Steam Flow (kg/s)	2.212	3.493	4.969	44.5
Effluent Flow (kg/s)	1.64	2.70	3.76	43.6
Operating Costs				
Total Power (kW)	5913.26	6489.22	7093.81	83.3
Compression Power (kW)	4786.65	5380.86	6012.82	79.6
Expansion Power (kW)	89.01	129.68	167.57	53.1
Nett Heating (MW)	58.22	66.23	74.60	78.0
Nett Cooling (MW)	16.37	22.84	29.79	55.0
Cryogenic Heat (MW)	24.20	32.06	31.64	75.5
Fired Heat (MW)	13.24	20.68	28.62	46.2
Process Heat (MW)	9.09	2.74	3.80	30.2
Cryogenic Cooling (MW)	0.00	0.00	0.00	--
Process Cooling (MW)	16.38	22.84	29.79	55.0

Family 1: Scheme 14

CRITERION	Feedstock			Turndown (%)
	GL1K	GL2Z	GL1Z	
Production				
Feed (kg/s)	52.68	52.92	52.90	99.5
kg Product/kg Feed	1.010	1.016	1.022	98.8
Wobbe No. position	0.743	0.666	0.616	82.9
Heavies Processing				
Process Stream Flow (kg/s)	0.785	1.275	1.746	45.0
Steam Flow (kg/s)	2.924	3.212	4.920	59.4
Effluent Flow (kg/s)	1.61	2.73	3.73	43.2
Operating Costs				
Total Power (kW)	2450.15	3249.29	4043.68	60.6
Compression Power (kW)	1324.90	2137.97	3056.03	43.4
Expansion Power (kW)	86.40	130.18	167.69	51.5
Nett Heating (MW)	56.60	65.25	61.50	86.7
Nett Cooling (MW)	11.39	18.62	25.88	44.0
Cryogenic Heat (MW)	0.69	1.29	1.81	38.3
Fired Heat (MW)	12.89	20.76	16.34	62.2
Process Heat (MW)	1.71	2.75	3.80	44.9
Cryogenic Cooling (MW)	0.20	0.45	0.68	29.6
Process Cooling (MW)	11.19	18.18	25.20	44.4

Family 2: Scheme 20

CRITERION	Feedstock			Turndown (%)
	GL1K	GL2Z	GL1Z	
Production				
Feed (kg/s)	51.26	50.49	49.26	96.1
kg Product/kg Feed	0.994	0.989	0.986	99.2
Wobbe No. position	0.840	0.813	0.820	96.8
Heavies Processing				
Process Stream Flow (kg/s)	14.968	20.146	23.743	63.0
Steam Flow (kg/s)	45.109	60.588	71.427	63.2
Effluent Flow (kg/s)	45.21	60.75	72.27	62.5
Operating Costs				
Total Power (kW)	2844.93	3407.57	3756.43	75.6
Compression Power (kW)	1756.17	2360.41	2765.46	63.5
Expansion Power (kW)	948.31	1233.98	2091.09	45.4
Nett Heating (MW)	58.93	63.87	67.19	87.7
Nett Cooling (MW)	133.89	180.60	212.01	63.2
Cryogenic Heat (MW)	0.00	0.00	0.00	--
Fired Heat (MW)	12.65	16.94	7.62	45.0
Process Heat (MW)	5.63	7.56	21.73	25.9
Cryogenic Cooling (MW)	0.00	0.00	0.00	--
Process Cooling (MW)	133.89	180.60	212.01	63.2

Family 2: Scheme 22

CRITERION	Feedstock			Turndown (%)
	GL1K	GL2Z	GL1Z	
Production				
Feed (kg/s)	52.76	52.89	53.29	99.0
kg Product/kg Feed	0.994	0.989	0.986	99.2
Wobbe No. position	0.834	0.798	0.810	95.7
Heavies Processing				
Process Stream Flow (kg/s)	13.084	15.788	17.426	75.1
Steam Flow (kg/s)	39.306	47.420	52.384	75.0
Effluent Flow (kg/s)	40.03	47.05	53.65	74.6
Operating Costs				
Total Power (kW)	5768.78	5632.83	5606.64	97.2
Compression Power (kW)	4648.68	4534.03	4524.85	97.3
Expansion Power (kW)	107.63	119.20	121.50	88.6
Nett Heating (MW)	58.19	60.58	61.98	93.9
Nett Cooling (MW)	121.40	144.74	158.91	76.4
Cryogenic Heat (MW)	31.59	32.08	31.90	98.5
Fired Heat (MW)	10.20	12.16	13.32	76.6
Process Heat (MW)	4.68	5.59	6.14	76.3
Cryogenic Cooling (MW)	0.00	0.00	0.00	--
Process Cooling (MW)	121.40	144.74	158.91	76.4

Family 2: Scheme 24

CRITERION	Feedstock			Turndown (%)
	GL1K	GL2Z	GL1Z	
Production				
Feed (kg/s)	52.54	52.73	52.95	99.2
kg Product/kg Feed	0.994	0.989	0.986	99.2
Wobbe No. position	0.836	0.798	0.812	95.5
Heavies Processing				
Process Stream Flow (kg/s)	13.082	15.661	17.315	75.6
Steam Flow (kg/s)	39.247	47.193	52.05	75.4
Effluent Flow (kg/s)	39.71	47.59	52.77	75.2
Operating Costs				
Total Power (kW)	2771.48	3110.54	3294.02	84.1
Compression Power (kW)	1534.17	1830.26	2009.98	76.3
Expansion Power (kW)	107.71	188.77	194.33	55.4
Nett Heating (MW)	59.52	63.62	65.92	90.3
Nett Cooling (MW)	119.75	144.81	159.86	74.9
Cryogenic Heat (MW)	11.61	15.85	17.77	65.3
Fired Heat (MW)	10.19	12.10	13.23	77.0
Process Heat (MW)	4.68	5.57	6.10	76.7
Cryogenic Cooling (MW)	2.68	4.49	5.49	48.9
Process Cooling (MW)	117.06	140.32	154.37	75.8

Family 3: Scheme 30

CRITERION	Feedstock			Turndown (%)
	GL1K	GL2Z	GL1Z	
Production				
Feed (kg/s)	51.11	50.15	48.81	95.5
kg Product/kg Feed	0.994	0.989	0.986	99.2
Wobbe No. position	0.837	0.816	0.823	97.5
Heavies Processing				
Process Stream Flow (kg/s)	13.800	18.656	22.111	62.4
Steam Flow (kg/s)	41.399	56.168	66.382	62.4
Effluent Flow (kg/s)	41.71	56.72	67.27	62.0
Operating Costs				
Total Power (kW)	5759.59	7171.45	8144.93	70.7
Compression Power (kW)	4240.09	5715.60	6757.26	62.7
Expansion Power (kW)	1962.62	2565.17	2940.31	66.7
Nett Heating (MW)	58.52	63.24	65.93	88.8
Nett Cooling (MW)	125.90	170.24	201.52	62.5
Cryogenic Heat (MW)	0.00	0.00	0.00	--
Fired Heat (MW)	12.80	17.14	20.15	63.5
Process Heat (MW)	5.19	6.99	8.27	62.7
Cryogenic Cooling (MW)	0.00	0.00	0.00	--
Process Cooling (MW)	125.90	170.24	201.52	62.5

Family 3: Scheme 32

CRITERION	Feedstock			Turndown (%)
	GL1K	GL2Z	GL1Z	
Production				
Feed (kg/s)	52.47	52.85	52.98	99.0
kg Product/kg Feed	0.994	0.990	0.986	99.2
Wobbe No. position	0.835	0.811	0.815	97.1
Heavies Processing				
Process Stream Flow (kg/s)	11.596	14.005	16.106	72.0
Steam Flow (kg/s)	34.840	42.069	48.370	72.0
Effluent Flow (kg/s)	35.17	42.59	49.09	71.6
Operating Costs				
Total Power (kW)	8804.47	8527.88	8386.73	95.3
Compression Power (kW)	7457.04	7168.05	7046.34	94.5
Expansion Power (kW)	2572.08	2060.62	1873.90	72.9
Nett Heating (MW)	66.90	69.28	71.20	94.0
Nett Cooling (MW)	115.11	141.13	159.50	72.2
Cryogenic Heat (MW)	24.12	24.25	24.36	99.0
Fired Heat (MW)	10.02	11.88	13.47	74.4
Process Heat (MW)	7.69	7.22	7.39	93.4
Cryogenic Cooling (MW)	6.96	8.43	9.07	76.8
Process Cooling (MW)	108.15	132.70	150.43	71.9

Family 3: Scheme 34

CRITERION	Feedstock			Turndown (%)
	GL1K	GL2Z	GL1Z	
Production				
Feed (kg/s)	77.52	78.09	78.54	98.7
kg Product/kg Feed	0.994	0.990	0.986	99.2
Wobbe No. position	0.824	0.799	0.813	97.0
Heavies Processing				
Process Stream Flow (kg/s)	18.992	22.178	24.662	77.0
Steam Flow (kg/s)	58.140	66.376	73.828	78.8
Effluent Flow (kg/s)	57.45	67.34	75.13	76.5
Operating Costs				
Total Power (kW)	7638.82	8631.29	9377.68	81.5
Compression Power (kW)	5826.40	6763.37	7501.36	77.7
Expansion Power (kW)	1717.07	1844.49	1906.95	90.0
Nett Heating (MW)	89.82	103.30	100.04	87.0
Nett Cooling (MW)	177.85	209.20	232.94	76.4
Cryogenic Heat (MW)	16.84	29.97	25.29	56.2
Fired Heat (MW)	16.39	18.81	20.65	79.4
Process Heat (MW)	6.78	7.85	8.68	78.2
Cryogenic Cooling (MW)	4.74	7.62	9.19	51.5
Process Cooling (MW)	173.12	201.57	223.75	77.4

Family 2: Scheme 25

CRITERION	Feedstock			Mean Value	Turndown (%)
	GL1K	GL2Z	GL1Z		
Production					
Feed (kg/s)	75.67	78.27	78.92	77.62	95.9
kg Product/kg Feed	0.994	0.990	0.987	0.990	99.3
Wobbe No. position	0.863	0.861	0.848	0.857	98.3
Heavies Processing					
Process Stream Flow (kg/s)	8.172	9.001	11.601	9.591	70.4
Steam Flow (kg/s)	24.820	26.925	34.883	28.876	71.2
Effluent Flow (kg/s)	25.28	27.57	35.86	29.57	70.0
Operating Costs					
Total Power (kW)	3346.88	3580.85	3829.99	3585.91	87.4
Compression Power(kW)	951.17	1026.12	1326.65	1101.30	71.7
Expansion Power (kW)	--	--	--	--	--
Nett Heating (MW)	86.66	90.73	93.01	90.13	93.2
Nett Cooling (MW)	91.07	99.22	122.13	104.14	74.6
Cryogenic Heat (MW)	27.65	31.24	31.69	30.19	87.2
Fired Heat (MW)	1.83	2.83	2.71	2.46	64.7
Process Heat (MW) (with reboiler duty)	14.03	17.97	21.13	17.71	66.4
Cryogenic Cooling(MW) (with condenser duty)	18.02	20.47	20.42	19.63	88.0
Process Cooling (MW)	73.05	78.76	101.71	84.51	71.8

APPENDIX 3

OPERATING CONDITIONS FOR FLOWSHEET

Flowsheet No. 25, Rev.1;

Average of GL1K, GL2Z, and GL1Z feedstock conditions

Item No.	P-01	P-02	H-01	V-01	F-01	H-02	P-03
Description	Pump	Pump	Heat Exchanger	Valve	Flash	Heat Exchanger	Pump
Rate, Capacity or Heat Load	596 m^3/hr	91 m^3/hr	11079 MJ/hr	490 m^3/hr		29693 MJ/hr	396 m^3/hr
Temperature (K)	-170	-169	-169 → -72	-72	-72	-72 → -90	-86
Pressure (bar)	1 → 52	52 → 70	52	52 → 48	48	48	48 → 70
Approximate Dimensions	η = 90%	η = 90%			d=2.7m h=14.5m		η = 90%
Notes	Centrifugal	Centrifugal					Centrifugal
Power (kW)	938	51					274

Item No.	V-02	H-03	D-01	P-04	O-01	P-05	H-04
Description	Valve	Condenser	Distillation Column	Pump	ORV	Pump	Heat Exchanger
Rate, Capacity or Heat Load	381 m^3/hr	-7031 MJ/hr	-6037 MJ/hr -30472 MJ/hr	413 m^3/hr	140200 MJ/hr	85 m^3/hr	33570 MJ/hr
Temperature (K)	-72	-85	-83 / +21	-83	-107 → +10	21	21 → 320
Pressure (bar)	48 → 35	35	35	35 → 70	70	35 → 46	46
Approximate Dimensions			11 trays (theoretical)	η = 90%	3504 tubes	η = 90%	
Notes			Total condenser	Centrifugal		Centrifugal	
Power (kW)				325		58	

Item No.	B-01	R-01	H-05	H-04	H-06	K-01	H-07
Description	Fired Heater	CRG Reformer	Cooler	Heat Exchanger	Cooler	Knock-out pot	Cooler
Rate, Capacity or Heat Load	8866 MJ/hr	139432 MJ/hr	27394 MJ/hr	33570 MJ/hr	218431 MJ/hr	139432 kg/hr	19729 MJ/hr
Temperature (K)	320 → 400	400 → 422	422 → 342	342 → 235	235 → 127	127	127 → 20
Pressure (bar)	46	44.5	43.5	43	43	43	43
Approximate Dimensions		Tube bundle Area=1.5m2 Height=2.5m					
Notes							
Power (kW)							

Item No.	K-02	A-01	A-02	H-08	C-01	H-09	
Description	Knock-out pot	Absorber	Absorber	Cooler	Compressor	Cooler	
Rate, Capacity or Heat Load	51464 kg/hr	48193 kg/hr	32110 kg/hr	1178 MJ/hr	1367 m^3/hr	4668 MJ/hr	
Temperature (K)	20	20 → 23	23 → 24	24 → 10	10 → 60	60 → 10	
Pressure (bar)	42	42	42	43	42 → 70	70	
Approximate Dimensions					Single stage centrifugal		
Notes		CO_2-removal	H_2O-removal		$\eta(pol)=75\%$		
Power (kW)					1055		

APPENDIX 4

DYNAMIC SIMULATION ENVIRONMENT

There are many commercially available packages for dynamic simulation, mainly concerned with continuous systems. Some are specific to the chemical process industry, but the majority are for general application. The performance of a selection of these packages was assessed against several performance criteria, using information extracted from software manuals, sales literature and published papers. Those packages considered could be run on a mainframe, personal computer or work station. No benchmark test was included in the assessment.

Dynamic Simulation Packages

Nine simulation packages were initially considered. A summary of each is given in Table A4.1.

Dynamic Simulation Package	Base Language	Structure	Model Size Limit	Additional Features
ACSL	FORTRAN	Equation	Large	
EASE+ACSL	FORTRAN	Block	Yes	
ISIM	FORTRAN	Equation	Yes	
ESL	FORTRAN	Equation	Large	
KBCSIM	FORTRAN	Block	Small	Limited icons
MATRIX$_X$	Unknown	Block	Large	Control design applications
Modelworks	Modula-2	Unknown	Small	
muPSI	FORTRAN	Unknown	Small	
SIMNON	Unknown	Equation	Large	
SPEEDUP	PASCAL FORTRAN	Unknown	Large	Library of process models Physical property and thermodynamic data

Table A4.1 Dynamic simulation packages

Selection Criteria

The dynamic simulation package is required to handle a large scale model of the entire LNG reception terminal flowsheet. Thus, an initial screening of the available packages in Table A4.1 identified and eliminated those packages that restricted model size, namely

EASE+ACSL, ISIM, KBCSIM, Modelworks and muPSI. Also, as the dynamic simulation will be employed as a tool for control system design, it is essential that the model has a fast runtime. This suggests that a mainframe or workstation computer platform would be most suitable.

Selection criteria were developed to assess the five remaining simulation packages, and are grouped into three main sections:

(i) Model development
(ii) Runtime features
(iii) Environmental features

A points system was adopted to assess selected parameters:

I Poor
II Adequate
III Good

Package list prices were compared using the following price bands (prices applicable in March, 1989):

£200 < M < £600, H > £600.

Comparison of Available Packages

The results of the selection criteria are presented in Table A4.2. Those packages available at Strathclyde University (ACSL and SIMNON) were initially compared. **ACSL** is available on a VAX platform, and offers a choice of eight integration routines. It also includes a greater range of modelling facilities than **SIMNON**, and has control system design functions. ACSL has faster run times and is also the preferred simulation package within the University.

Of the external packages considered, **SPEEDUP** is the most applicable as it was developed for the process industry, and is block structured. Many of the flowsheet's operations are available in an extensive process model library. SPEEDUP also has access to physical properties and thermodynamics calculation systems. However, SPEEDUP was the most expensive package in this assessment.

MATRIX$_x$ is a state-of-the-art simulation and control design package, which employs a simple command language. On the workstation version, runtime is fast and results may be displayed in a variety of forms. However, cost is also a major factor with MATRIX$_x$. Although the PC

version is less expensive, it has fewer facilities and may not handle the size of model anticipated. **ESL** was also worthy of consideration as it is designed to handle large scale systems, with diverse applications.

Dynamic Simulation Package	**ACSL**	**ESL**	**MATRIX$_X$**	**SIMNON**	**SPEEDUP**
Model Development					
Ease of implementation	II	II	III	II	III
Software documentation	II	II	II	III	III
Access to user-written routines	Y	Y	Unknown	N	Y
Choice of integration algorithms	Y	Y	Y	N	Y
Library models	N	N	N	N	Y
Runtime Features					
Compilation time	II	II	III	II	II
Calculation speed	III	II	III	II	II
Debug facility	N	Y	Unknown	N	Y
On-line *help* facility	N	N	Y	Y	Y
Access to results	III	II	III	II	III
Graphics display	Y	Y	Y	Y	Y
Model linearisation	Y	Y	Y	N	Y
Environmental Features					
Machine	VAX	IBM/VAX	PC/WS	IBM PC	IBM/VAX
Operating system	VMS	DOS/VMS	DOS/Unix	MS DOS	DOS/VMS
Commercial cost	H	Unknown	H	H	H
External contact	Rapid Data	Univ. Salford	Scientific Computers Ltd.	Lund Inst.of Tech.	Imperial College

Table A4.2 Assessment of dynamic simulation packages

Selected Package

Obviously, a more comprehensive assessment of the available packages would require bench marking, as it is impossible to compare runtimes from sales literature alone. Hence, the selection criteria remarks only provide a relative indication of the performance of each package. The following comments provide the rationale for the selection of **ACSL** as the simulation package for this study.

To ease model implementation, it would be advisable to adopt a simulation package that is already available at both sites. The

availability of on-site support would help in gaining familiarity with the chosen package and in identifying any modelling constraints. Of the two internal packages, only ACSL was available at both sites.

As the flowsheet consists of individual process units, it would be useful to adopt a block structured package. This would allow the units to be independently analysed and linked together more easily than with an equation-based model. Although SPEEDUP at first appeared to be the most suitable for this application, with library models specific to process modelling, neither party had ready access to this simulation package.

Of the remaining externally available packages, MATRIX$_x$ offered the most widespread applications. MATRIX$_x$ had already been employed locally, suggesting that a user-support group would be available. However, the model requirements suggest that the workstation version of this package would be more appropriate, presenting additional hardware costs.

In conclusion, **ACSL** was selected as the most appropriate package. ACSL is FORTRAN-based and allows additional user supplied subroutines to be accessed. In particular, it is familiar to both parties, and has been successfully applied in previous research projects. In this study, Level 8L1/8P of ACSL was adopted on the Digital VAX 8250 machine, with the VMS Version 4.5 operating system.

APPENDIX 5

UNIT SIZING

Reflux Drum Sizing

For a horizontal reflux drum (Henley and Seader, 1981) the optimum length to diameter ratio is given by:

$$L/D = 4 \qquad \text{(A5.1)}$$

For a recommended liquid residence time of at least 5 minutes, with the drum half full of liquid, drum volume is given by:

$$V = \frac{2\ Wt}{\rho_L} \qquad \text{(A5.2)}$$

where W is the liquid mass flow rate. Substituting (A5.1) gives:

$$V = \frac{\pi D^2}{4} L = \pi D^3 \qquad \text{(A5.3)}$$

The corresponding reflux drum dimensions for each LNG feedstock are given in Table A5.1. The largest drum sizing was selected for the distillation column.

Feedstock	**GL1Z**	**GL2Z**	**GL1K**
Diameter (m)	2.64	2.76	2.72
Length (m)	10.57	11.03	10.90

Table A5.1 Reflux drum sizing

A rectangular cross section was assumed, whilst retaining the calculated length and volume. Thus, for a reflux drum of vertical cross sectional area, A_v, of 6 m^2, the breadth and depth are 2 m and 3 m, respectively. Hence, the horizontal cross-sectional area became:

$$A_h = B \times L = 22.06\ m^2$$

CRG Reformer Tube Sizing

The method adopted for tube sizing was based on British Gas information (Monk, 1988) with steady state data extracted from the preliminary flowsheet design. The summarised results are given in Table A5.2.

CRG Reformer Conditions	LNG Feedstock		
	GL1K	GL2Z	GL1Z
Mean molecular weight	19.06	20.43	20.61
Natural gas flow rate (kgmol/hr)	1316.53	945.50	1152.69
Flow rate (lb/hr)	55330.2	42593.0	52384.1
Required tube area (ft^2)	13.83	10.65	13.10
Required diameter (ft)	4.18	3.68	4.08
Design diameter (ft)	4.5	4.0	4.0
Maximum depth of bed (ft)	10	10	10
Minimum depth of bed (ft)	8	8	8

Table A5.2 CRG reformer tube diensions for each feed condition

To ensure the CRG reformer could handle each feedstock condition, the largest recommended design diameter and minimum bed depth were selected:

$$\text{Tube bundle area, } A_t = \frac{\pi d^2}{4} = \frac{\pi}{4}(4.5)^2 = 15.90 \text{ ft}^2 = 1.478 \text{ m}^2$$

$$\text{Tube bundle length, } L_t = 8\text{ft} = 2.438 \text{ m}$$

ORV Sizing

The ORV unit was scaled in relation to a previous study by Muir (1987). The steady state simulation results for the medium feedstock, GL2Z, were used as this represented the intermediate operating conditions. (Inlet flow rates for the remaining feedstock conditions varied between +0.5% and -4% which were well within the 20% flow disturbances which were applied to develop Muir's transfer function model).

The original water to LNG mass flow ratio for the type B ORV was given by:

$$\frac{W_W}{W_L} = \frac{0.6925 \text{ kg/s/tube}}{0.01978 \text{ kg/s/tube}} = 35.01 \qquad \text{(A5.4)}$$

Thus, the corresponding water flow rate for the GL2Z condition with an LNG inlet flow rate of 14971.97 kgmol/hr, was:

$$F_W = 35.01 \times 14971.97 \times mw_L / mw_W$$
$$= 484780.38 \text{ kgmol/hr}$$

The required LNG outlet temperature of 10°C could only be achieved with a greater water inlet temperature. As it is unlikely that UK river or sea water will exceed this value, a nominal water inlet temperature of 10°C was assumed for the purposes of unit sizing. An approach temperature of 3°C corresponded to a NG outlet temperature of 7°C. Hence, the steady state energy balance gave the water outlet temperature, T_{Wo}, as:

$T_{Li} = 180.444$ K $\qquad T_{Wi} = 283.15$ K

$T_{Lo} = 280.15$ K $\Rightarrow \qquad T_{Wo} = 279.464$ K

and an overall change in water temperature,

$$\Delta T_W = 3.7 \text{ K}$$

This satisfied the following environmental constraints:

(i) The change in water temperature between entering and leaving the ORV should not exceed 5 K.

(ii) The water outlet temperature should not fall below 273 K.

Adopting dimensions for the type B ORV tube, the ORV unit was scaled up to accommodate the LNG flow rate for the GL2Z condition, by increasing the number of vaporiser tubes. Hence, for an overall mass flow rate of 69.29 kg/s;

$$\text{Total number of tubes} = \frac{69.29 \ \text{kg/s}}{0.01978 \ \text{kg/s/tube}} = 3504 \text{ tubes}$$

The transfer function matrix was also adapted because:

(i) The revised ORV linear model simulates the complete unit, as opposed to one tube in the original study.

(ii) The units of flow rate are kgmol/hr.

Hence, the following factors were incorporated in the transfer functions:

$$\left\{ \frac{mw_L}{3504 \times 3600} \right\} \quad \text{for flow rate gains}$$

$$\left\{ \frac{1}{3600} \right\} \quad \text{for time constants}$$

giving the revised transfer function matrix:

$$\begin{bmatrix} T_{wi} \\ W_{wi} \end{bmatrix} = G(s) \begin{bmatrix} T_{Li} \\ W_{Li} \\ T_{wi} \\ W_{wi} \end{bmatrix}$$

where

$$G(s) = \begin{bmatrix} \dfrac{0.035}{[1 + (32/3600)]} & -4.2\times10^{-6}(mw_L) & 1.5 & \dfrac{3.8\times10^{-8}(mw_L)}{(1 + 0.058s)} \\ 0.029 & -1.9\times10^{-6}(mw_L) & 0.94 & 6.8\times10^{-8}(mw_L) \end{bmatrix}$$

APPENDIX 6

STEADY STATE VALIDATION OF SELECTED DYNAMIC MODELS

Distillation Column: Operating pressure = 35.0 bar
No. of theoretical trays = 11
Total condenser and reboiler

Variable	LNG Feedstock		
	GL1Z	GL2Z	GL1K
Stream 14: (Top)			
Flow rate (kgmol/hr)	4293.07 (4292.91)	5156.58 (5154.50)	5253.71 (5255.95)
Temperature (K)	181.65 (182.19)	181.62 (182.25)	181.66 (182.19)
Composition: C_1	0.9897 (0.9897)	0.9903 (0.9903)	0.9895 (0.9895)
C_2	0.0038 (0.0038)	0.0041 (0.0040)	0.0038 (0.0039)
N_2	0.0065 (0.0065)	0.0057 (0.0057)	0.0066 (0.0066)
Reflux (kgmol/hr)	2002.19 (1830.71)	1901.41 (1780.35)	1581.04 (1486.56)
Stream 21: (Bottom)			
Flow rate (kgmol/hr)	1152.44 (1152.69)	943.49 (945.50)	1318.77 (1316.53)
Temperature (K)	305.75 (305.75)	280.17 (279.22)	204.02 (204.01)
Composition: C_1	0.0335 (0.0335)	0.1158 (0.1158)	0.5752 (0.5747)
C_2	0.5901 (0.5956)	0.5933 (0.5939)	0.3659 (0.3655)
C_3	0.2699 (0.2675)	0.1895 (0.1892)	0.0409 (0.0409)
nC_4	0.0574 (0.0563)	0.0487 (0.0487)	-- --
iC_4	0.0465 (0.0458)	0.0358 (0.0358)	0.0179 (0.0179)
nC_5	0.0024 (0.0013)	0.0168 (0.0166)	-- --
N_2	-- --	-- --	0.0001 (0.0010)
Boilup (kgmol/hr)	3537.11 (3256.52)	2699.16 (2678.89)	4625.70 (4570.86)

( ) - steady state simulation results

CRG Reformer: Operating pressure = 45.5 bar

Variable	LNG Feedstock		
	GL1Z	GL2Z	GL1K
Stream 25: (Steam)			
Flow rate (kgmol/hr)	6962.49 (6968.71)	5379.75 (5384.28)	5060.58 (5064.91)
Stream 26: (Feed)			
Flow rate (kgmol/hr)	8115.14 (8121.40)	6325.25 (6329.78)	6377.11 (6381.45)
Temperature (K)	670.12 (670.73)	670.13 (670.68)	669.25 (669.84)
Stream 27: (Product)			
Flow rate (kgmol/hr)	9146.20 (9150.96)	7088.26 (7091.78)	6830.91 (6836.59)
Temperature (K)	705.99 (705.14)	703.15 (702.45)	677.88 (677.79)
Composition: CH_4	0.2514 (0.2514)	0.2519 (0.2519)	0.2558 (0.2556)
CO	0.0004 (0.0004)	0.0004 (0.0004)	0.0002 (0.0002)
CO_2	0.0559 (0.0558)	0.0534 (0.0533)	0.0332 (0.0332)
H_2	0.0433 (0.0429)	0.0425 (0.0422)	0.0365 (0.0365)
H_2O	0.6489 (0.6494)	0.6517 (0.6517)	0.6744 (0.6744)

( ) - steady state simulation results

Flash Unit: Operating pressure = 48.09 bar

Variable	LNG Feedstock		
	GL1Z	GL2Z	GL1K
Stream 8: (Vapour)			
Flow rate (kgmol/hr)	7946.29 (8015.78)	7693.84 (7795.96)	6413.05 (6446.11)
Temperature (K)	202.47 (203.36)	199.97 (200.33)	198.12 (198.20)
Composition: C_1	0.9472 (0.9457)	0.9561 (0.9555)	0.9573 (0.9571)
C_2	0.0331 (0.0348)	0.0288 (0.0296)	0.0310 (0.0312)
C_3	0.0053 (0.0055)	0.0037 (0.0038)	0.0017 (0.0017)
nC_4	0.0003 (0.0003)	0.0003 (0.0003	-- --
iC_4	0.0003 (0.0003)	0.0003 (0.0003)	0.0004 (0.0004)
nC_5	0.0000 (0.0000)	0.0000 (0.0000)	-- --
N_2	0.0133 (0.0133)	0.0108 (0.0105)	0.0097 (0.0096)
Stream 11: (Liquid)			
Flow rate (kgmol/hr)	5705.35 (5445.60)	6251.01 (6100.00)	6610.02 (6572.48)
Temperature (K)	202.47 (203.36)	199.97 (200.33)	198.12 (198.20)
Composition: C_1	0.8056 (0.7874)	0.8620 (0.8547)	0.9078 (0.9064)
C_2	0.1191 (0.1290)	0.0910 (0.0955)	0.0752 (0.0764)
C_3	0.0506 (0.0566)	0.0274 (0.0293)	0.0080 (0.0082)
nC_4	0.0105 (0.0119)	0.0070 (0.0076)	-- --
iC_4	0.0085 (0.0097)	0.0051 (0.0056)	0.0035 (0.0036)
nC_5	0.0002 (0.0003)	0.0025 (0.0026)	-- --
N_2	0.0055 (0.0051)	0.0050 (0.0048)	0.0055 (0.0054)

( ) - steady state simulation results

APPENDIX 7

DEGREES OF FREEDOM ANALYSIS FOR FLOWSHEET BLOCKS

BLOCK 2

Operation: Flash Unit

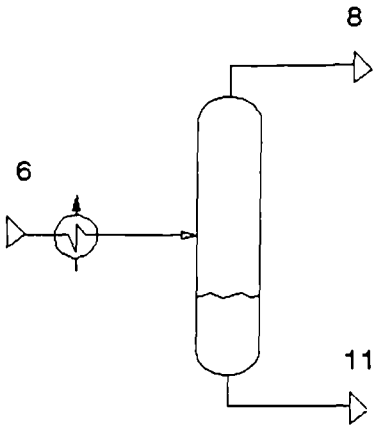

Variables:

No	Type
(3N+6)	F_6, F_8, F_{11}, T_6, T_{11}, h_{11}, p_{11}, $y_{i,8}$, $x_{i,11}$ (for i = 1,.., N) $x_{i,6}$ (for i = 1,.., N-1)

Parameters:

No.	Type
(N + 8)	h_6, h_8, h_{11}, mw_6, mw_8, mw_{11}, ρ_{11}, A_6, $K_i = fn(T,p)$ (for i=1,.., N)

Equations:

No.	Type
1	Total mass balance
(N-1)	Component balance
1	Energy balance
N	Vapour-liquid equilibrium relationship
2	Consistency constraint

Total: (2N + 3)

Degrees of Freedom:

$$f = V - E$$
$$= (3N+6) - (2N+3) = (N + 3)$$

Externally Specified Variables:

No.	Type
(N - 1)	$x_{i,6}$ (for i = 1,..., N-1)

Number of Controlled Variables:

f - (no. of externally specified variables) = (N+3) - (N-1)

= 4

Control Loop Configurations:

Four control variables must be identified in this multivariable control system. The drum temperature and pressure should be maintained to give the desired separation, while constant production is ensured by maintaining feed flow rate. In addition, liquid level should remain within certain operating limits. Assuming the feed flow rate is self-regulating, there are 3! possible control loop configurations, as shown below.

Controlled variables: p_{11}, h_{11}, T_{11}

Manipulated variables: F_8, F_{11}, T_6

Configuration Number	Loop Configurations		
	p_{11} Control by	h_{11} Control by	T_{11} Control by
1	F_8	F_{11}	T_6
2	F_8	T_{11}	F_6
3	F_{11}	F_6	T_{11}
4	T_{11}	T_8	F_6
5	T_6	F_6	F_8
6	T_6	F_8	F_{11}

From qualitative reasoning, manipulating the top product flow rate, F_8, to vary liquid level in the drum would have less effect than if the bottom product flow rate, F_{11}, was varied. Varying feed stream temperature would also have little effect. Thus, pairing F_{11} with h_{11} suggests the most direct combination - this leaves two possible configurations, 1 and 5.

As pressure quickly reacts to changes in the vapour flow rate, the first configuration was selected as a preliminary control loop structure. This is a conventional form of control loop arrangement for a flash unit. However, due to inherent interaction effects within a multivariable system, a detailed study of the control loop structure has been conducted in Chapter 7.

Key:

N - number of components

BLOCK 3

Operation: Distillation Column

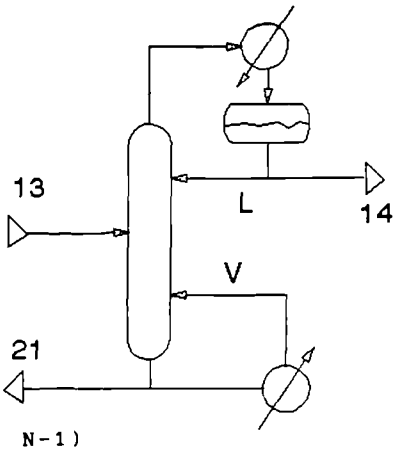

Variables:

No.	Type
(N+1)	F_{13}, T_{13}, $x_{i,13}$ (for i = 1,.., N-1)
(n+2)N	Liquid composition on each tray and product streams
(n+1)N	Vapour composition on each tray and vapour boilup
(n+2)	Molar hold up on each tray, reflux drum and column base
2n	Liquid and vapour flows per tray
(n+2)	Tray temperature
4	F_{14}, L, F_{21}, V

Total: (2nN + 4N + 4n + 9)

Parameters:

- Liquid and vapour enthalpies
- Liquid densities
- Look up tables for tray composition, tray temperature and ethalpy gradient
- Column and drum dimensions
- Francis weir constant

Equations:

No.	Type
(n+2)	Total mass balance
(n+2)	Component balance
(n+1)	Rearranged energy balance
n	VLE relationship
n	Francis Weir formula
(n+2)(N-1)	Heavies balance - Liquid phase
(n+1)(N-1)	Heavies balance - Vapour phase
(n+2)	Temperature relationship

Total: (2nN + 3N + 4n + 4)

Degrees of Freedom:

$$f = V - E$$
$$= (2nN + 4N + 4n + 9) - (2nN + 3N + 4n + 4)$$
$$= (N + 5)$$

Externally Specified Variables:

No.	Type
N	T_{13}, $x_{i,13}$ (for i = 1,.., N-1)

Number of Controlled Variables:

f - (no. of externally specified variables) = (N+5) - N
= 5

Control Loop Configurations:

Five control loops are required to fully specify this multivariable system, including perfect pressure control. A constant production rate is maintained by self-regulation of the feed. Of the four remaining loops, two are required to maintain liquid levels in the reflux drum and column base. The choice of control variables for the remaining two loops depends on the control objectives and measurability of the variables.

Two-point composition control has been considered for this system as maintaining both product compositions would result in less feed variation in the downstream units. However, due to the inherent dead time associated with composition monitoring, tray temperature is typically used to estimate stream composition, in the form of inferential control. Therefore, the following preliminary control structure was adopted (Skogestad et al., 1990):

(i) Top product flow rate, F_{14} - Condenser liquid level
(ii) Reflux, L - Upper tray temperature
(iii) Boilup, V - Lower tray temperature
(iv) Bottom product flow rate, F_{21} - Column base liquid level

In practice, the temperature set point would be regularly updated using cascade control from a composition analyser. Hence, this arrangement represents a worst case as the set point is not being regulated.

The final control loop configuration was based on a detailed interaction analysis of several structures. The control loop variable selection and analysis is documented in Chapter 7.

Key:

N - number of components n - number of trays

BLOCK 4

Process: Mixer arrangement

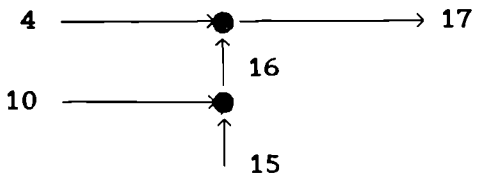

Variables:

No.	Type	
5(N + 1)	Flow rate, F Composition, x_i Temperature, T^i	for Streams 4, 10, 15, 16, 17

Parameters:

No.	Type
5	Stream enthalpy

Equations:

No.	Type
2	Enthalpy balance
2	Steady state mass balance
2(N-1)	Steady state component balance

Total: 2(N + 1)

Degrees of Freedom:

$$f = V - E$$
$$= 5(N + 1) - 2(N + 1)$$
$$= 3(N + 1)$$

Externally Specified Variables:

No.	Type
3N	T_4, $x_{i,4}$, T_{10}, $x_{i,10}$, T_{15}, $x_{i,15}$ (for i = 1,.., N-1)

Number of Controlled Variables:

$$3(N+1) - 3N = 3$$

Control Loop Configurations:

Controlled variables: F_4, F_{10}, F_{15}

Manipulated variables: F_4, F_{10}, F_{15}

The simplest and most direct loop configuration is to self-regulate each stream, as follows.

F_4 Control by	F_{10} Control by	F_{15} Control by
F_4	F_{10}	F_{15}

BLOCK 5

Process: Heavies processing loop

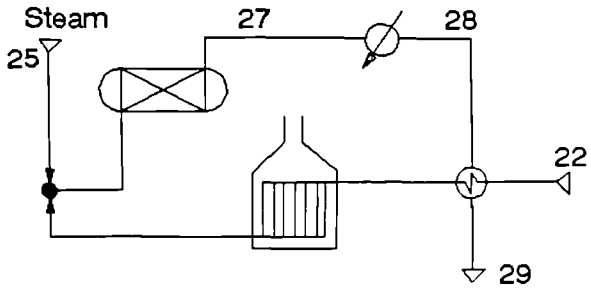

Variables:

No.	Type	
8	Flow rate, F	for streams 22 to 29
8(N-1)	Composition, x_i (for i=1,.., N-1)	
8	Temperature, T	
1	Heat input to fired heater, Q	

Total: (8N + 9)

Parameters:

- Stream enthalpies, densities and molecular weights
- Volume of fired heater, V23
- Heats of reaction for CRG reformer
- Reaction equilbrium, K_i (= ℓ(T))
- CRG reformer tube dimensions

Equations:

No.	Type
2(2N+1)	Enthalpy, mass and component balances in counter-current heat exchanger
(N+1)	Enthalpy, mass and component balances in fired heater
(N+1)	Enthalpy, mass and component balances in mixer
(N+1)	Enthalpy, mass and component balances in CRG reformer
N	Steady state mass and component balances in cooler

Total: (6N + 5)

Degrees of Freedom:

$$f = V - E$$
$$= (8N+9) - (6N+5) = (2N + 4)$$

Externally Specified Variables:

No.	Type
N	T_{22}, $x_{i,22}$ (for i = 1,.., N-1)
N	T_{25}, $y_{i,25}$ (for i = 1,.., N-1)
1	T_{28}

Total: (2N + 1)

Number of Controlled Variables:

(2N+4) - (2N+1) = 3

Control Loop Configurations:

The product stream composition and flow rate depend on the degree of conversion within the CRG reformer. As the reformer is isothermal, reaction rates are related to feed stream temperature, composition and S/C ratio. Self-regulation of the feed flow rate ensures a constant hydrocarbon feed to the reformer. Similarly, ratio control on the steam inlet flow rate maintains a constant feed ratio. Thus, only one control loop remains to be specified.

The main control objective is to maintain high methane production in the CRG reformer. As composition analysis is not a continuous measurement, the product stream temperature is substituted. This provides an indirect measure of conversion in the form of inferential control, as it determines rates of reaction within the CRG reformer.

The reformer product temperature is controlled by manipulating fuel flow to the upstream fired heater, and hence the reformer preheat temperature. However, the counter-current heat exchanger forms a regenerative preheating system as any variation in the reformer product stream would generate a disturbance in the fired heater feed stream temperature. (The open-loop step responses in Section 4.4.3 illustrate this phenomenon). Hence, cascade control is required to maintain product temperature, with two measured variables (reformer product and fired heater outlet temperatures), and one manipulated variable (fuel rate). Therefore, disturbances arising within the secondary loop are corrected before they can affect the primary controlled output. Some form of composition analysis would normally be employed in this control loop arrangement, to update the temperature set point in the primary loop at regular intervals. The selected control loop configuration for the heavies processing section is given below.

Measured	Variables Manipulated	Controlled
F_{22}	F_{22}	F_{22}
F_{24}	F_{25}	F_{25}
T_{27}, T_{24}	Fuel Rate	Methane Production

BLOCK 6

Operation: ORV

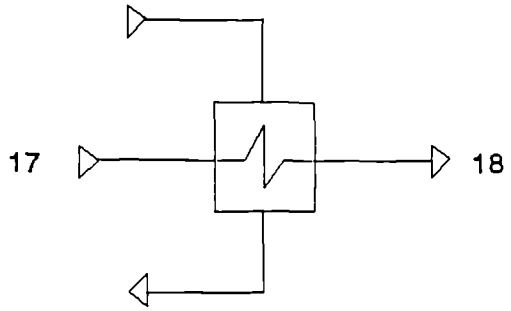

Variables:

No.	Type
2(N + 2)	F_{17}, T_{17}, T_{18}, $x_{i,17}$, F_W, $T_{W,f}$, $T_{W,o}$, $x_{i,W}$ (for i = 1,.., N-1)

Parameters:

No.	Type
	Number and length of ORV tubes
4	Feed stream densities

Equations:

No.	Type
2	Natural gas and water outlet temperatures

Degrees of Freedom:

$$f = V - E$$
$$= 2(N + 2) - 2 = 2(N + 1)$$

Externally Specified Variables:

No.	Type
2N	T_{17}, $x_{i,17}$, $T_{W,f}$, $x_{i,W}$ (for i = 1,.., N-1)

Number of Controlled Variables:

$$2(N+1) - 2N = 2$$

Control Loop Configurations:

Controlled variables: F_{17} and T_{18}

Manipulated variables: F_{17} and $F_{W,f}$

Configuration number	F_{17} Control by	T_{18} Control by
1	F_{17}	$F_{W,f}$
2	$F_{W,f}$	F_{17}

Configuration 1 is better as self-regulation of F_{17} is direct, whilst T_{18} can be maintained by either $F_{W,f}$ or F_{17}.

BLOCK 7

Process: Drying and Clean-up sections

Variables:

No.	Type
5(N+1)	Flow rate, composition and temperature for streams 20, 30, 34, 35 and 39
2N	F_{31}, $y_{i,31}$, F_{40}, $x_{i,40}$ (for all i = 1,.., N-1)
(2N+1)	T_{32}, F_{33}, $y_{i,33}$, F_{41}, $x_{i,41}$
(N+1)	p_{42}, F_{42}, $x_{i,42}$
(N+1)	p_{35}, F_{43}, $x_{i,43}$
3	T_{36}, T_{37}, T_{38}

Total: 11(N + 1)

Parameters:

. Stream enthalpies, heat capacities
. Absorber volumes, V33 and V34
. Compressor efficiency and Gas constant

Equations:

No.	Type
4N	Equilibrium relationships and mass balance for KO pots
2(2N+1)	Mass, component, temperature and pressure balances in absorber units
1	Temperature balance in compressor unit
(N+1)	Enthalpy, mass and component balances in mixer

Total: (9N + 4)

Degrees of Freedom:

$$f = V - E$$
$$= 11(N + 1) - (9N + 4) = 2N + 7$$

Externally Specified Variables:

No.	Type
(2N+3)	T_{30}, $y_{i,30}$, T_{32}, T_{36}, T_{38}, T_{20}, $y_{i,20}$ (for i = 1,.., N-1)
2	Degree of impurity absorption

Total: (2N + 5)

Number of Controlled Variables:

(2N+7) - (2N+5) = 2

Control Loop Configuration:

The two controlled variables, F_{20} and F_{30}, would be best maintained at their desired values by self-regulation control.

APPENDIX 8

SISO Control System Analysis

Consider a first-order process with PI control. The closed-loop response for a step change in set point (where $R(s) = r/s$) is described by the following transfer function relationship:

$$Y(s) = \frac{G_c G_p}{1 + G_c G_p} R(s)$$

$$= \frac{K_c K_p (\tau_I s + 1)}{\tau_I \tau s^2 + (\tau_I + K_c K_p \tau_I) s + K_c K_p} \left(\frac{r}{s} \right)$$

$$= \frac{\frac{K_c K_p}{\tau_I \tau} (\tau_I s + 1)}{s^2 + (1 + K_c K_p) \frac{s}{\tau} + \frac{K_c K_p}{\tau_I \tau}} \left(\frac{r}{s} \right)$$

$$= \frac{\frac{K_c K_p}{\tau} s + \frac{K_c K_p}{\tau_I \tau}}{\left(s + \frac{1}{2\tau} (1 + K_c K_p) \right)^2 + \left(\frac{K_c K_p}{\tau_I \tau} - \frac{1}{4\tau^2} (1 + K_c K_p^2) \right)} \left(\frac{r}{s} \right)$$

$$= \frac{as + b}{[(s + \alpha)^2 + \beta^2]} \left(\frac{r}{s} \right) \qquad \text{(A8.1)}$$

where $a = K_c K_p / \tau$ (A8.2)

$b = K_c K_p / \tau_I \tau$ (A8.3)

$\alpha = (1 + K_c K_p) / 2\tau$ (A8.4)

$\beta^2 = \frac{K_c K_p}{\tau_I \tau} - \frac{1}{4\tau^2} (1 + K_c K_p)^2$ (A8.5)

The standard transfer function for a second-order system (A8.1) may be rewritten as:

$$Y(s) = \frac{as + b}{[(s + \zeta\omega_n)^2 + \omega_d^2]} \left(\frac{r}{s} \right) \qquad \text{(A8.6)}$$

where ζ is the damping factor, and $\omega_d = \omega_n \sqrt{(1 - \zeta)}$ is the damped natural frequency. For overshoot to occur, the system must be underdamped ($0 < \zeta < 1$), with positive values of ω_d and $\zeta\omega_n$. Thus,

from (A8.1) and (A8.6), overshoot occurs when:

$$\alpha > 0 \quad \text{and} \quad \beta^2 > 0$$

Time Response Analysis

The dynamic behaviour of a second-order system can be analysed in the time-domain. This requires the inverse Laplace transform of (A8.1), which is solved by partial fractions expansion. The Laplace transform is rearranged as follows:

$$Y(s) = \frac{as + b}{(s + \alpha)^2 + \beta^2} \left(\frac{r}{s} \right)$$

$$= r \left\{ \frac{1}{s} + \frac{A(s + \alpha)}{\left[(s + \alpha)^2 + \beta^2\right]} + \frac{B}{\left[(s + \alpha)^2 + \beta^2\right]} \right\}$$

Equating the numerators gives:

$$Y(s) = r \left\{ \frac{1}{s} - \frac{(s + \alpha)}{\left[(s + \alpha)^2 + \beta^2\right]} + \frac{(a - \alpha)}{\left[(s + \alpha)^2 + \beta^2\right]} \right\} \qquad \text{(A8.7)}$$

Each term in (A8.7) is now inverted to the time domain, yielding:

$$y(t) = r \left[1 - e^{-\alpha t} \cos \beta t + \frac{(a-\alpha)}{\beta} e^{-\alpha t} \sin \beta t \right] \qquad \text{(A8.8)}$$

Overshoot Analysis

In a unit step response of an underdamped system, the overshoot represents the first peak in the response, characterised by the first turning point. Hence, the overshoot occurs when the output response has zero gradient, corresponding to:

$$\frac{1}{r} \frac{dy}{dt} = - e^{-\alpha t}(-\beta \sin \beta t) - \left[-\alpha e^{-\alpha t} (\cos \beta t) \right]$$

$$+ \frac{(a - \alpha)}{\beta} \left[e^{-\alpha t} \beta \cos \beta t - \alpha e^{-\alpha t} \sin \beta t \right]$$

$$= e^{-\alpha t} \left[\left(\beta - \frac{(a - \alpha)}{\beta} \alpha \right) \sin \beta t + (\alpha + a - \alpha) \cos \beta t \right]$$

$$= e^{-\alpha t} \left[\frac{(\beta^2 + \alpha^2 - a\alpha)}{\beta} \sin \beta t + a \cos \beta t \right] \qquad \text{(A8.9)}$$

From earlier definitions, it can be shown that $b = \alpha^2 + \beta^2$. Hence, (A8.9) becomes:

$$\frac{1}{r} \frac{dy}{dt} = e^{-\alpha t} \left[\frac{(b - a\alpha)}{\beta} \sin \beta t + a \cos \beta t \right] \qquad \text{(A8.10)}$$

At the first turning point, t_1, the gradient of the response is zero,

and (A8.10) can be reduced to:

$$\frac{(b - a\alpha)}{\beta} \sin \beta t_1 + a \cos \beta t_1 = 0 \qquad \text{(A8.11)}$$

The following trignometric identity can now be applied to solve the expression, where (A8.11) is equated to:

$$\sin A \cos B - \cos A \sin B = \sin (A - B) \qquad \text{(A8.12)}$$

with the identity in terms of:

$$\sin \beta t_1 \cos \phi - \cos \beta t_1 \sin \phi = \sin (\beta t_1 - \phi) \qquad \text{(A8.13)}$$

the angle ϕ is defined as

$$\cos \phi = \frac{(b - a\alpha)}{\beta} \qquad \sin \phi = - a$$

The right hand side of (A8.12) is then equated to zero and,

$$\beta t_1 - \phi = n\pi, \qquad \text{for } n = 0,1,\ldots$$

which gives:

$$\beta t_1 = n\pi + \phi$$

However, the ϕ angle is negative, so the first turning point at $\beta t_1 > 0$ occurs at n = 1, which gives:

$$\beta t_1 = \pi - \phi$$

Thus, the overshoot occurs at time,

$$t_1 = \frac{\pi - \phi}{\beta} \qquad \text{(A8.14)}$$

Overshoot Height

As an expression for the time at the overshoot is known, this can be introduced to the closed-loop time domain equation, to calculate the actual overshoot. Rearranging the condition for zero response gradient at the overshoot (A8.11):

$$\sin \beta t_1 = \frac{-a\beta}{(b - a\alpha)} \cos \beta t_1 \qquad \text{(A8.15)}$$

and substituting into (A8.8) gives:

$$y(t_1) = r \left[1 - e^{-\alpha t_1} \cos \beta t_1 \left(1 + \frac{(a - \alpha)a\beta}{(b - a\alpha)\beta} \right) \right]$$

$$= r \left[1 - e^{-\alpha t_1} \cos \beta t_1 \frac{(b - 2a\alpha + a^2)}{(b - a\alpha)} \right] \qquad \text{(A8.16)}$$

Now, from (A8.15) defining

$$\tan \beta t_1 = \frac{\sin \beta t_1}{\cos \beta t_1} = \frac{a\beta}{(a\alpha - b)}$$

gives the trignometric relationship where:

$$\cos \beta t_1 = \frac{(a\alpha - b)}{d}$$

and,

$$d = \left(a^2\beta^2 + (a\alpha - b)^2 \right)^{1/2}$$

Finally, substituting into equation (A8.16) gives:

$$y(t_1) = r \left[1 - e^{-\alpha t_1} \frac{(a\alpha - b)}{d} \frac{(b - 2a\alpha^2 + a)}{(b - a\alpha)} \right]$$

$$= r \left[1 - \frac{(2a\alpha - a^2 - b)}{d} e^{-\alpha t_1} \right]$$

Hence, the percentage overshoot is defined as:

$$\% \text{ Overshoot} = \frac{(y(t_1) - r)}{r} \times 100\%$$

$$= - \frac{(2a\alpha - a^2 - b)}{d} e^{-\alpha t_1} \times 100\% \qquad \text{(A8.17)}$$

Algorithm for Calculating Overshoot

The above time-domain analysis can be applied to a first-order system with PI cntrol to satisfy overshoot performance specifications. The algorithm predicts the overshoot size and time, t_1, for given PI controller settings, as follows:

1. Select first-order plant parameters : K_p, τ
2. Select PI controller parameters : K_c, τ_I
3. Calculate:

$$\beta^2 = \frac{K_c K_p}{\tau_I \tau} - \frac{1}{4\tau^2} (1 + K_c K_p)^2$$

If $\beta^2 \leq 0$, no overshoot will occur, so reselect controller parameters K_c, τ_I.

4. Calculate:

(i) $\beta = \sqrt{\beta^2}$

(ii) $a = K_c K_p / \tau$

(iii) $b = K_c K_p / \tau_I \tau$

(iv) $\alpha = (1 + K_c K_p) / 2\tau$

(v) $d = [a^2 \beta^2 + (a\alpha - b)^2]^{1/2}$

5. Solve for

$$\phi = \tan^{-1}\left(\frac{a\beta}{b - a\alpha}\right)$$

$$\text{then,} \quad t_1 = \frac{(\pi - \phi)}{\beta}$$

6. Calculate:

$$\% \text{ Overshoot} = -\frac{(2a\alpha - a^2 - b)}{d} e^{-\alpha t_1} \times 100\%$$

Rise Time Analysis

The rise time, T_r, of a system is defined as the time required for the transient response to a unit-step input to rise from between either 10% to 90%, or 0% to 100% of its final value (Ogata, 1990). For an underdamped system, the 0% to 100% rise time is more common.

An expression for T_r may be obtained from the system time response (A8.8),

$$y(t) = 1 - e^{-\alpha t}(\cos \beta t - \frac{(a-\alpha)}{\beta} \sin \beta t) \qquad \text{(A8.18)}$$
$$= 1, \quad \text{at } t = T_r$$

for a unit-step change. Since $e^{-\alpha t} \neq 0$, (A8.18) reduces to:

$$\cos \beta T_r - \frac{(a - \alpha)}{\beta} \sin \beta T_r = 0$$

From the trignometric identity in (3.22), the angle is defined by:

$$\cos \gamma = \frac{(a - \alpha)}{\beta} \qquad \sin \gamma = 1$$

which gives,

$$\sin (\beta T_r - \gamma) = 0$$
$$\Rightarrow (\beta T_r - \gamma) = n\pi, \quad \text{for } n = 0, 1, ..$$

Hence, the rise time is defined as:

$$T_r = (\pi + \gamma) / \beta \qquad \text{(A8.19)}$$

where,

$$\gamma = \tan^{-1}\left(\frac{\beta}{a - \alpha}\right) \qquad \text{(A8.20)}$$

This rise time analysis can be developed into an algorithm, in conjunction with the earlier overshoot study, and used to satisfy performance criteria for a first-order system with PI control.

APPENDIX 9

STATE SPACE REPRESENTATION FOR THE HEAVIES PROCESSING SECTION

The following state space matrices describe a linear representation of the three main blocks in the heavies processing section, for the GL2Z feedstock condition. The input variable, u, defines both manipulated input variables and disturbances to the system, as the disturbances were introduced as inputs to each ACSL model.

The state and output equations are defined as:

$$\dot{\mathbf{x}} = \mathbf{Ax} + \mathbf{Bu}$$
$$\mathbf{y} = \mathbf{Cx} + \mathbf{Du}$$

(i) Counter-Current Heat Exchanger Block

INPUTS			OUTPUTS
Disturbances			
FA_{22}	Methane	flow rate	T_{23}
$FB^{22}(1)$	Ethane		
$FB^{22}(2)$	Propane		
T_{22}			
FA_{27}	Methane	flow rate	
FE^{27}	Hydrogen		
FF^{27}	Steam		

States: Product stream enthalpies

Vectors:

$$\mathbf{x} = \begin{bmatrix} enth_{29} \\ enth_{23} \end{bmatrix} \quad \mathbf{u} = \begin{bmatrix} FA_{22} \\ FB^{22}(1) \\ FB^{22}(2) \\ T_{22} \\ FA^{27} \\ FE^{27} \\ FF^{27} \end{bmatrix} \quad \mathbf{y} = \begin{bmatrix} T_{22} \end{bmatrix}$$

State matrix:

$$\mathbf{A} = \begin{bmatrix} -111.1 & 0 \\ 0 & -111.1 \end{bmatrix}$$

Input matrix:

$$\mathbf{B} = \begin{bmatrix} -218 & -474 & -698 & 1683 & 129 & 60 & 55 \\ -1433 & -721 & 161 & 257 & 19 & 10 & 16 \end{bmatrix}$$

State output matrix:

$$\mathbf{C} = \begin{bmatrix} 0.01 \end{bmatrix}$$

Output matrix:

$$\mathbf{D} = \begin{bmatrix} 0.107 & 0.28 & -0.062 & \ldots \end{bmatrix}$$

(ii) **Fired Heater Block**

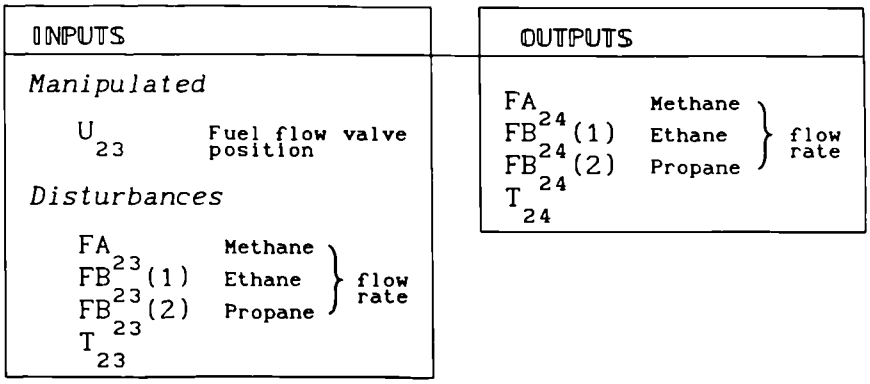

States:

- Final and intermediate enthalpies
- Component flow rates

Vectors:

$$\mathbf{x} = \begin{bmatrix} enth_{24f} \\ enth_{24} \\ FA_{24} \\ FB_{24}(1) \\ FB_{24}(2) \\ FB_{24}(3) \\ FB_{24}(4) \\ FB_{24}(5) \end{bmatrix} \quad \mathbf{u} = \begin{bmatrix} U_{23} \\ FA_{23} \\ FB_{23}(1) \\ FB_{23}(2) \\ T_{23} \end{bmatrix} \quad \mathbf{y} = \begin{bmatrix} FA_{24} \\ FB_{24}(1) \\ FB_{24}(2) \\ T_{24} \end{bmatrix} \begin{matrix} \} \text{ unmeas-urable} \\ \text{measurable} \end{matrix}$$

State Matrix:

$$\mathbf{A} = \begin{bmatrix} -1162 & 4 & -209 & -127 & -109 & -30 & 16 & 72 \\ 60 & -60 & . & . & . & . & . & . \\ . & . & -60 & . & . & . & . & . \\ . & . & . & -60 & . & . & . & . \\ . & . & . & . & -60 & . & . & . \\ . & . & . & . & . & -60 & . & . \\ . & . & . & . & . & . & -60 & . \\ . & . & . & . & . & . & . & -60 \end{bmatrix}$$

Input matrix:

$$\mathbf{B} = \begin{bmatrix} 1.227E5 & -21739 & -12214 & -1116 & 1.227E5 \\ . & . & . & . & . \\ . & . & . & . & . \\ . & . & . & . & . \\ . & . & . & . & . \\ . & . & . & 60 & . \\ . & . & 60 & . & . \\ . & 60 & . & . & . \end{bmatrix}$$

State Output Matrix:

$$\mathbf{C} = \begin{bmatrix} . & . & . & . & . & . & . & 1 \\ . & . & . & . & . & . & 1 & . \\ . & . & . & . & . & 1 & . & . \\ . & 9E-3 & -0.45 & -0.28 & -0.25 & -0.06 & 0.03 & 0.17 \end{bmatrix}$$

Output matrix:

$$\mathbf{D} = 0$$

(iii) **CRG Reformer Block**

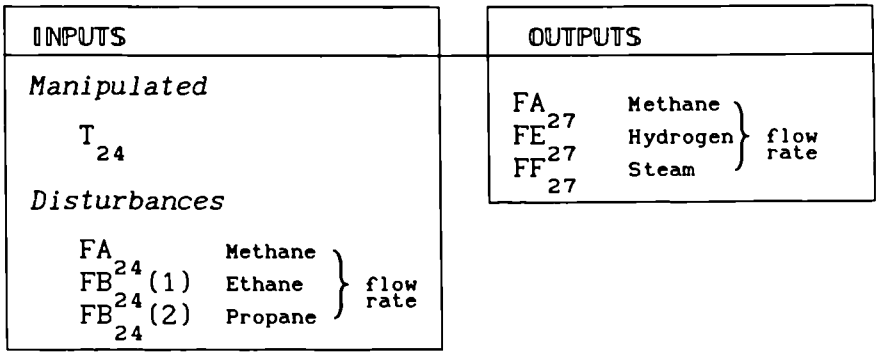

States:

. Final and intermediate enthalpies
. Product flow rate

Vectors:

$$\mathbf{x} = \begin{bmatrix} enth_{27f} \\ enth_{27} \\ F_{27} \end{bmatrix} \qquad \mathbf{u} = \begin{bmatrix} T_{24} \\ FA_{24} \\ FB_{24}(1) \\ FB_{24}(2) \end{bmatrix} \qquad \mathbf{y} = \begin{bmatrix} FA_{27} \\ FE_{27} \\ FF_{27} \end{bmatrix}$$

State matrix:

$$\mathbf{A} = \begin{bmatrix} -2595 & 121 & -5522 \\ 48 & -48 & . \\ . & -8 & -2592 \end{bmatrix}$$

Input matrix:

$$\mathbf{B} = \begin{bmatrix} 38822 & 134 & 51935 & 88935 \\ . & . & . & . \\ . & 10417 & 15867 & 21754 \end{bmatrix}$$

State Output Matrix:

$$\mathbf{C} = \begin{bmatrix} . & 1.6E\text{-}3 & -7.8E\text{-}4 \\ . & -4.8E\text{-}3 & 2.2E\text{-}3 \\ . & 1.6E\text{-}3 & -6.9E\text{-}4 \end{bmatrix}$$

Output Matrix:

$$\mathbf{D} = \begin{bmatrix} . & 0.77 & 1.95 & 2.98 \\ 1.5E\text{-}5 & 0.69 & -0.84 & -1.94 \\ . & 2.39 & 4.96 & 7.33 \end{bmatrix}$$

APPENDIX 10

TRANSFER FUNCTION MODELS FOR THE HEAVIES PROCESSING SECTION

The following transfer functions have been derived from the state space models in Appendix 9, for the GL2Z feedstock condition. They relate to the block diagram in Figure 6.20.

(i) $G_1(s)$

$$T_{23}(s) = G_1(s) \; [\; FA_{22}(s) \;\; FB_{22}(1)(s) \;\; FB_{22}(2)(s) \;\; T_{22}(s) \;\; FA_{28}(s) \;\; FE_{28}(s) \;\; F_{28}(s)\;]^T$$

where,

$$G_1(s) = \begin{bmatrix} \frac{0.107(s - 16.0)}{(s + 111.1)} & \frac{0.028(s - 129.2)}{(s + 111.1)} & \frac{0.062(s + 86.5)}{(s + 111.1)} \\ \frac{2.442}{(s + 111.1)} & \frac{0.181}{(s + 111.1)} & \frac{0.095}{(s + 111.1)} & \frac{0.152}{(s + 111.1)} \end{bmatrix}$$

(ii) $G_2(s)$

$$T_{24}(s) = G_2(s) \; [\; FA_{22}(s) \;\; FB_{22}(1)(s) \;\; FB_{22}(2)(s) \;\; T_{23}(s) \;]^T$$

where,

$$G_2(s) = \begin{bmatrix} \frac{10.032(s + 59.6)(s + 3.7)}{den(2)(s + 60.0)} & \frac{2.088(s - 1961.7)}{den(2)} \\ \frac{-3.888(s + 1312.9)}{den(2)} & \frac{65495.6}{den(2)} \end{bmatrix}$$

and $den(2) = (s + 1162.2)(s + 59.8)$

(iii) $G_3(s)$

$$\begin{bmatrix} FA_{24} \\ FB_{24}(1) \\ FB_{24}(2) \end{bmatrix} = \begin{bmatrix} \frac{60}{(s + 60)} & \cdot & \cdot \\ \cdot & \frac{60}{(s + 60)} & \cdot \\ \cdot & \cdot & \frac{60}{(s + 60)} \end{bmatrix} \begin{bmatrix} FA_{22} \\ FB_{22}(1) \\ FB_{22}(2) \end{bmatrix}$$

(iv) $G_4(s)$

$$T_{24}(s) = \frac{1.344E7}{(s + 1162.2)(s + 59.8)} U_{23}(s)$$

(v) $G_5(s)$

$$\begin{bmatrix} FA_{28} \\ FE_{28} \\ FF_{28} \end{bmatrix} = G_5(s) \begin{bmatrix} FA_{24} \\ FB_{24}(1) \\ FB_{24}(2) \\ T_{24} \end{bmatrix}$$

where,

$$G_5(s) = \begin{bmatrix} \frac{0.775(s^2 + 5180.9s + 6.79E6)(s + 44.5)}{den(G5)} \\ \frac{0.691(s + 2693.1)(s + 48.3)(s + 2527.8)}{den(G5)} \\ \frac{2.386(s^2 + 5187.7s + 6.73E6)(s+ 45.1)}{den(G5)} \end{bmatrix}$$

$$\frac{1.947(s^2 + 5183.8s + 6.72E6)(s + 45.6)}{den(G5)}$$

$$\frac{-0.839(s^2 + 5146.5s + 6.63E6)(s + 47.3)}{den(G5)}$$

$$\frac{4.956(s^2 + 5188.2s + 6.73E6)(s + 45.5)}{den(G5)}$$

$$\frac{2.976(s^2 + 5184.3s + 6.72E6)(s + 45.8)}{den(G5)}$$

$$\frac{-1.942(s^2 + 5163.6s + 6.67E6)(s + 47.3)}{den(G5)}$$

$$\frac{7.3295(s^2 + 5188.2s + 6.73E6)(s + 45.5)}{den(G5)}$$

$$\begin{bmatrix} \frac{2962.895(s + 2596.8)}{den(G5)} \\ \frac{1.526E-5(s + 25588.7)(s - 22949.5)(s + 2596.6)}{den(G5)} \\ \frac{3037.4(s + 2596.2)}{den(G5)} \end{bmatrix}$$

and $den(G5) = (s^2 + 5190.4s + 6.7E6)(s + 45.4)$